

AD A057466

AFFDL-TR-77-83
Volume I

LEVEL

2

**EXTENDED STUDY OF FLAW GROWTH
AT FASTENER HOLES**

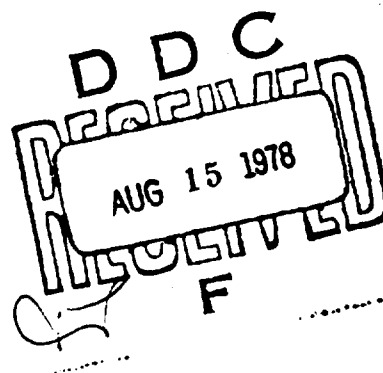
LOCKHEED-GEORGIA COMPANY
MARIETTA, GEORGIA 30063

APRIL 1978

TECHNICAL REPORT AFFDL-TR-77-83, Volume I
Final Report for June 1975 - June 1977

Approved for public release; distribution unlimited.

AIR FORCE FLIGHT DYNAMICS LABORATORY
AIR FORCE WRIGHT AERONAUTICAL LABORATORIES
AIR FORCE SYSTEMS COMMAND
WRIGHT-PATTERSON AIR FORCE BASE, OHIO 45433



78 08 07 021

AD NO. _____
DDC FILE COPY

NOTICE

When Government drawings, specifications, or other data are used for any purpose other than in connection with a definitely related Government procurement operation, the United States Government thereby incurs no responsibility nor any obligation whatsoever; and the fact that the Government may have formulated, furnished, or in any way supplied the said drawings, specifications, or other data, is not to be regarded by implication or otherwise as in any manner licensing the holder or any other person or corporation, or conveying any rights or permission to manufacture, use, or sell any patented invention that may in any way be related thereto.

This report has been reviewed by the Information Office (OI) and is releasable to the National Technical Information Service (NTIS). At NTIS, it will be available to the general public, including foreign nations.

This technical report has been reviewed and is approved for publication.

James L. Rudd

JAMES L. RUDD
Project Engineer

R.M. Bader

ROBERT M. BADER, Chief
Structural Integrity Branch
Structural Mechanics Division

FOR THE COMMANDER

Ralph L. Kuster, Jr.

RALPH L. KUSTER, JR., Colonel, USAF
Chief, Structural Mechanics Division

Copies of this report should not be returned unless return is required by security considerations, contractual obligations, or notice on a specific document.

REPORT DOCUMENTATION PAGE		READ INSTRUCTIONS BEFORE COMPLETING FORM									
1. REPORT NUMBER AFFDL TR-77-83, Vol. 1 - Vol. 4		3. PRECEDENCE CATALOG NUMBER									
2. TITLE (and Subtitle) EXTENDED STUDY OF FLAW GROWTH AT FASTENER HOLES		4. AUTHOR(s) T. M. Hsu, W. M. McGee, and J. A. Aberson									
5. PERFORMING ORGANIZATION NAME AND ADDRESS Lockheed-Georgia Company A Division of Lockheed Aircraft Corporation Marietta, Georgia 30063		6. PROGRAM ELEMENT, PROJECT, TASK AND A WORK UNIT NUMBER Project No.: 486U Task No.: 486U02 Work Unit No.: 486U0212									
7. CONTROLLING OFFICE NAME AND ADDRESS Air Force Flight Dynamics Laboratory (AFFDL/FBE) Wright Patterson AFB, Ohio 45433		8. REPORT DATE April 1978									
9. MONITORING AGENCY NAME & ADDRESS (if different from Controlling Office) (12) 347p.		9. SECURITY CLASS. (of this report) Unclassified									
10. DISTRIBUTION STATEMENT (of this Report) A, proved for public release; distribution unlimited.		10. DECLASSIFICATION DOWNGRADING SCHEDULE									
11. DISTRIBUTION STATEMENT (of the abstract entered in Block 20, if different from Report)											
12. SUPPLEMENTARY NOTES											
13. KEY WORDS (Continue on reverse side if necessary and identify by block number) <table border="0"> <tr> <td>Stress Intensity Factors</td> <td>Fastener System</td> </tr> <tr> <td>Fastener Hole Flaws</td> <td>Spectrum Loads</td> </tr> <tr> <td>Fatigue Crack Growth</td> <td>2219-T851 Aluminum</td> </tr> <tr> <td>Natural Crack</td> <td>6AL-4V BA(ELI) Titanium</td> </tr> </table>				Stress Intensity Factors	Fastener System	Fastener Hole Flaws	Spectrum Loads	Fatigue Crack Growth	2219-T851 Aluminum	Natural Crack	6AL-4V BA(ELI) Titanium
Stress Intensity Factors	Fastener System										
Fastener Hole Flaws	Spectrum Loads										
Fatigue Crack Growth	2219-T851 Aluminum										
Natural Crack	6AL-4V BA(ELI) Titanium										
14. ABSTRACT (Continue on reverse side if necessary and identify by block number) <p>An analytical and experimental investigation was conducted to characterize the fracture and cyclic-growth behavior of cracks emanating from various types of fastener holes, such as open, close-tolerance, interference-fit, and cold-worked fastener holes. An analytical approach was developed for estimating stress intensity factors for through cracks emanating from these types of fastener holes. Approximate stress intensity factors for quarter-elliptical cracks emanating from a corner of the same types of fastener holes were derived from corresponding through-crack solutions. Two alloy plates (2219-T851 aluminum and</p>											

DD FORM 1 JAN 73 1473

EDITION OF 1 NOV 63 IS OBSOLETE

UNCLASSIFIED

SECURITY CLASSIFICATION OF THIS PAGE (When Data Entered)

210 065

10

Unclassified

SECURITY CLASSIFICATION OF THIS PAGE (When Data Entered)

6AL-4V (ELI) beta annealed titanium) with and without intentional initial flaws were tested under constant amplitude cyclic load and flight-by-flight fighter and bomber spectrum loads. Two initial flaw shapes corresponding to a quarter-circular corner crack and a through-the-thickness crack and three initial crack lengths (small, intermediate and large) were used in the test program. Three levels of cold working and interference and one level of fastener load transfer were included for each alloy. The amount of load transferred through the loaded fastener was maintained uniformly at the level which produced a bearing stress equal to the far-field stress.

Correlations between calculated stress intensities and those reduced from fatigue crack growth data were good, except for very small cracks growing from the cold-worked holes. Also, the natural cracks initiated in the fatigue tests were most commonly corner and embedded types whose shapes corresponded quite closely to the quarter- and semi-elliptical shapes used in the analyses.

Test growth rates for holes with residual strains (cold-worked or interference-fit fasteners) were significantly slower than for straight reamed holes without any conditioning - especially for small initial cracks. This benefit decayed as crack length increased.

Data scatter was most apparent in fighter-spectrum tests and in the tests of short initial cracks propagating from cold-worked and interference-fit holes. Another important feature observed was how the initial corner flaw shapes changed during their growth: for straight reamed holes with or without cold working, the final dimension on the hole wall was almost always larger than the final dimension on the plate surface, especially for the cold-worked hole; for interference-fit fastener holes without fastener load transfer, the final flaw shape was close to quarter-circular; for interference-fit fastener holes with fastener load transfer, the final dimension on the hole wall was less than that on the plate surface.

Lastly, a review of experimental results and numerical predictions indicated the possibility that the beneficial residual compressive strains induced by cold-working operations were relaxed during the subsequent application of cyclic loads.

FOREWORD

This report describes results of work performed by the Lockheed-Georgia Company on Air Force Contract F33615-75-C-3099, "Extended Study of Flaw Growth at Fastener Holes." The effort was sponsored by the Air Force Flight Dynamics Laboratory as part of the Advanced Metallic Structures - Advanced Development Program, Project No. 486U. Mr. James L. Rudd of AFFDL/FBE was the Air Force Project Engineer.

This program was conducted within the Engineering Branch of the Lockheed-Georgia Company, Marietta, Georgia, under the direction of Chief Engineer - Research and Technology, Mr. H. B. Allison. The Project Engineer was Dr. T. M. Hsu of the Advanced Structures Department. The experimental work was performed under the supervision of W. M. McGee who was assisted by H. R. Michael. The unflawed stress analysis was performed by Dr. J. A. Aberson. The stress intensity factor analysis and data evaluation were performed by Dr. T. M. Hsu.

This report was submitted by the authors on June 10, 1977.

ACCESSION NO.	
NTIS	6-11-77
DOC	6-11-77
FORM NO. 0	10
DISPATCHED TO: AFRL/AFH	
TOTAL	
A	

TABLE OF CONTENTS

<u>Section No.</u>		<u>Page</u>
I	INTRODUCTION	1
II	SCOPE	4
	1. EXPERIMENTAL PROGRAM	4
	1.1 Material Characterization and Failure Criterion Tests	4
	1.2 Fatigue Tests for Fastener Holes without Intentional Flaws	5
	1.3 Constant Amplitude Tests for Cracked Fastener Holes	5
	1.4 Spectrum Loading Tests for Cracked Fastener Holes	6
	2. ANALYTICAL PROGRAM	6
III	EXPERIMENTAL PROGRAM	7
	1. MATERIALS	7
	2. TEST SPECIMENS	7
	3. HOLE PREPARATION AND FASTENER INSTALLATION	9
	4. PRECRACKING PROCEDURES	10
	5. TESTING PROCEDURES	12
	5.1 Tensile and Compressive Tests	12
	5.2 K_c Tests	12
	5.3 Failure Criterion Tests	12
	5.4 Crack Growth and Fatigue Tests	12
IV	RESULTS AND DISCUSSION OF EXPERIMENTAL PROGRAM	16
	1. MATERIAL CHARACTERIZATION TESTS	16
	2. UNFLAWED FATIGUE TESTS	17
	2.1 Constant Amplitude Load Tests	17
	2.2 Spectrum Load Tests	18
	3. CRACK GROWTH TESTS	20
	3.1 Constant Amplitude Load Tests	20
	3.2 Bomber Spectrum Load Tests	27
	3.3 Fighter Spectrum Load Tests	30
	4. FRACTURE TESTS OF FLAWED COLD-WORKED HOLES	33
	5. THRESHOLD CRACK LENGTHS	34

TABLE OF CONTENTS - Continued

<u>Section No.</u>		<u>Page</u>
V	ANALYTICAL PROGRAM	38
	1. STRESS ANALYSIS FOR UNFLAWED FASTENER HOLES	38
	2. APPROXIMATE STRESS INTENSITY FACTOR SOLUTIONS	43
	2.1 Introduction	43
	2.2 Through Cracks Emanating from Fastener Holes	45
	2.3 Corner Cracks Emanating from Fastener Holes	56
	2.4 Embedded Cracks Emanating from Fastener Holes	64
	3. FAILURE CRITERION FOR FLAWED COLD-WORKED HOLES	66
	4. CRACK GROWTH PREDICTIONS FOR SPECTRUM LOADING	69
VI	OBSERVATIONS AND CONCLUSIONS	71
VII	RECOMMENDATIONS	75
	REFERENCES	312

LIST OF FIGURES

<u>Figure No.</u>		<u>Page</u>
1	Types of Cracks Considered in the Analytical Program	76
2	Photomicrographs of Test Materials - Mag. - 500X	77
3	Test Specimen Configurations for Material Characterization and Failure Criterion Tests	78
4	Test Specimen Configurations for Fatigue Tests with Intentional Flaws	79
5	Test Specimen Configurations for Fatigue Tests without Intentional Flaws	80
6	Detail of Fastener Load Transfer Arrangement	81
7	Detail of Test Setup	81
8	Fighter Spectrum	82
9	Bomber Spectrum	83
10	Constant Amplitude Crack Growth Rate Data for 2219-T851 Aluminum Alloy Plates	84
11	Constant Amplitude Crack Growth Rate Data for 6Al-4V Beta Annealed Titanium Alloy Plates	85
12	Fatigue Behavior of Various Types of Fastener Holes in 2219-T851 Aluminum Alloy Plates Subjected to Constant Amplitude Loading (18 ksi and $R = 0.1$)	86
13	Typical Surfaces of Natural Cracks Due to Constant Amplitude Fatigue Loading for 2219-T851 Aluminum Alloy	87
14	Fatigue Behavior of Various Types of Fastener Holes in 6Al-4V Beta Annealed Titanium Plates Subjected to Constant Amplitude Loading (40 ksi and $R = 0.1$)	88
15	Fatigue Behavior of Various Types of Fastener Holes in 2219-T851 Aluminum Alloy Plates Subjected to Bomber Spectrum Loading	89
16	Fatigue Behavior of Various Types of Fastener Holes in 2219-T851 Aluminum Alloy Plates Subjected to Fighter Spectrum Loading	90
17	Typical Surfaces of Natural Cracks Due to Spectrum Fatigue Loading for 2219-T851 Aluminum Alloy	91
18	Fatigue Behavior of Various Types of Fastener Holes in 6Al-4V Beta Annealed Titanium Plates Subjected to Bomber Spectrum Loading	92
19	Fatigue Behavior of Various Types of Fastener Holes in 6Al-4V Beta Annealed Titanium Plates Subjected to Fighter Spectrum Loading	93

LIST OF FIGURES (Continued)

Figure No.		Page
20	Growth Behavior of Small Corner Cracks from Open and Close Tolerance Fastener Holes with and without Fastener Load Transfer in 2219-T851 Aluminum Plates Subjected to 18 ksi Constant Amplitude Loading	94
21	Growth Behavior of Intermediate Corner Cracks for Various Levels of Interference for Interference-Fit Fastener Holes in 2219-T851 Aluminum Plates Subjected to 18 ksi Constant Amplitude Loading	95
22	Growth Behavior of Intermediate Corner Cracks from Level 2 Interference-Fit Fastener Holes with and without Fastener Load Transfer in 2219-T851 Aluminum Alloy Plates Subjected to Constant Amplitude Loading ($\sigma = 18$ ksi, $R = 0.1$)	96
23	Growth Behavior of Intermediate Corner Cracks from Cold-Worked Fastener Holes with and without Load Transfer in 2219-T851 Aluminum Plates Subjected to 18 ksi Constant Amplitude Loading	97
24	Comparison of Growth Behavior of Intermediate Corner Cracks for Various Levels of Cold Working for Open Holes in 2219-T851 Aluminum Alloy Plates Subjected to Constant Amplitude Loading ($\sigma = 18$ ksi, $R = 0.1$)	98
25	Comparison of Growth Behavior of Intermediate Corner Cracks from Various Types of Fastener Holes in 2219-T851 Aluminum Alloy Plates Subjected to Constant Amplitude Loading ($\sigma = 18$ ksi, $R = 0.1$)	99
26	Surfaces of Corner Cracks Emanating from Various Types of Level 1 Cold-Worked Holes in 2219-T851 Aluminum Plates Subjected to Constant Amplitude Far-Field Loading ($\sigma_{\max} = 18$ ksi, $R = 0.1$)	100
27	Growth Behavior of Small Thru Cracks from Open and Close Tolerance Fastener Holes in 2219-T851 Aluminum Alloy Plates Subjected to Constant Amplitude Loading	101
28	Growth Behavior of Small Thru Cracks from Open and Close Tolerance Fastener Holes in 2219-T851 Aluminum Alloy Plates Subjected to Constant Amplitude Loading ($\sigma = 18$ ksi, $R = 0.1$)	102
29	Growth Behavior of Small Thru Cracks from Interference-Fit Fastener Holes with and without Load Transfer in 2219-T851 Aluminum Plates Subjected to Constant Amplitude Loading ($\sigma = 18$ ksi, $R = 0.1$)	103

LIST OF FIGURES (Continued)

<u>Figure No.</u>		<u>Page</u>
30	Growth Behavior of Intermediate Thru Cracks from Interference-Fit Fastener Holes for Various Levels of Interference in 2219-T851 Aluminum Alloy Plates Subjected to Constant Amplitude Loading ($\sigma = 18$ ksi, $R = 0.1$)	104
31	Growth Behavior of Thru Cracks from Interference-Fit Fastener Holes for Various Levels of Interference in 2219-T851 Aluminum Plates Subjected to Constant Amplitude Loading ($\sigma = 21$ ksi, $R = 0.1$)	105
32	Growth Behavior of Small and Intermediate Thru Cracks from Level 3 Interference-Fit Fastener Holes in 2219-T851 Aluminum Plates Subjected to Constant Amplitude Loading ($\sigma = 18$ ksi, $R = 0.1$)	106
33	Growth Behavior of Small Thru Cracks from Cold-Worked Fastener Holes in 2219-T851 Aluminum Plates Subjected to Constant Amplitude Loading ($\sigma = 18$ ksi, $R = 0.1$)	107
34	Growth Behavior of Intermediate Thru Cracks from Open and Filled Cold-Worked Fastener Holes in 2219-T851 Aluminum Alloy Plates Subjected to Constant Amplitude Loading ($\sigma = 18$ ksi, $R = 0.1$)	108
35	Growth Behavior of Intermediate Thru Cracks from Level 1 Cold-Worked Holes with and without Fastener Load Transfer in 2219-T851 Aluminum Plates Subjected to Constant Amplitude Loading ($\sigma = 18$ ksi, $R = 0.1$)	109
36	Growth Behavior of Large Thru Cracks from Level 1 Cold-Worked Holes in 2219-T851 Aluminum Plates Subjected to Constant Amplitude Loading ($\sigma = 18$ ksi, $R = 0.1$)	110
37	Growth Behavior of Large Thru Cracks from Cold-Worked Open Holes for Various Levels of Cold Working in 2219-T851 Aluminum Alloy Plates Subjected to Constant Amplitude Loading ($\sigma = 18$ ksi, $R = 0.1$)	111
38	Comparison of Growth Behavior of Large Thru Cracks from Cold-Worked and Interference-Fit Fastener Holes in 2219-T851 Aluminum Alloy Plates Subjected to Constant Amplitude Loading ($\sigma = 18$ ksi, $R = 0.1$)	112
39	Growth Behavior of Small Corner Cracks from Open and Close Tolerance Fastener Holes in 6Al-4V Beta Annealed Titanium Alloy Plates Subjected to Constant Amplitude Loading ($\sigma = 40$ ksi, $R = 0.1$)	113

LIST OF FIGURES (Continued)

<u>Figure No.</u>		<u>Page</u>
40	Growth Behavior of Intermediate Corner Cracks from Open and Close Tolerance Fastener Holes in 6Al-4V Beta Annealed Titanium Alloy Plates Subjected to Constant Amplitude Loading ($\sigma = 40$ ksi, $R = 0.1$)	114
41	Growth Behavior of Intermediate Corner Cracks from Interference-Fit Fastener Holes for Various Levels of Interference in 6Al-4V Beta Annealed Titanium Plates Subjected to Constant Amplitude Loading ($\sigma = 40$ ksi, $R = 0.1$)	115
42	Growth Behavior of Intermediate Corner Cracks from Interference-Fit Fastener Holes with and without Fastener Load Transfer in 6Al-4V Beta Annealed Titanium Plates Subjected to Constant Amplitude Loading ($\sigma = 40$ ksi, $R = 0.1$)	116
43	Growth Behavior of Intermediate Corner Cracks from Level 1 Cold-Worked Holes in 6Al-4V Beta Annealed Titanium Plates Subjected to Constant Amplitude Loading ($\sigma = 40$ ksi, $R = 0.1$)	117
44	Comparison of Growth Behavior of Intermediate Corner Cracks from Various Types of Fastener Holes in 6Al-4V Beta Annealed Titanium Alloy Plates Subjected to Constant Amplitude Loading ($\sigma = 40$ ksi, $R = 0.1$)	118
45	Growth Behavior of Small Thru Cracks from Open and Close Tolerance Fastener Holes in 6Al-4V Beta Annealed Titanium Alloy Plates Subjected to Constant Amplitude Loading ($\sigma = 40$ ksi, $R = 0.1$)	119
46	Growth Behavior of Small and Intermediate Thru Cracks from Interference-Fit Fastener Holes in 6Al-4V Beta Annealed Titanium Alloy Plates Subjected to Constant Amplitude Loading ($\sigma = 40$ ksi, $R = 0.1$)	120
47	Growth Behavior of Small Thru Cracks from Level 2 Interference-Fit Fastener Holes with and without Fastener Load Transfer in 6Al-4V Beta Annealed Titanium Alloy Plates Subjected to Constant Amplitude Loading ($\sigma = 40$ ksi, $R = 0.1$)	121
48	Growth Behavior of Thru Cracks from Level 1 Cold-Worked Open Holes in 6Al-4V Beta Annealed Titanium Alloy Plates Subjected to Constant Amplitude Loading	122
49	Growth Behavior of Small Thru Cracks from Level 1 Cold-Worked Filled Holes in 6Al-4V Beta Annealed Titanium Alloy Plates Subjected to Constant Amplitude Loading	123

LIST OF FIGURES (Continued)

<u>Figure No.</u>		<u>Page</u>
50	Growth Behavior of Small Thru Cracks from Level 1 Cold-Worked Loaded Holes in 6Al-4V Beta Annealed Titanium Alloy Plates Subjected to Constant Amplitude Loading	124
51	Growth Behavior of Thru Cracks from Level 2 Cold-Worked Open Holes in 6Al-4V Beta Annealed Titanium Alloy Plates Subjected to Constant Amplitude Loading ($\sigma = 40$ ksi, $R = 0.1$)	125
52	Growth Behavior of Thru Cracks from Level 3 Cold-Worked Open Holes in 6Al-4V Beta Annealed Titanium Alloy Plates Subjected to Constant Amplitude Loading ($\sigma = 40$ ksi, $R = 0.1$)	126
53	Crack Growth Behavior of Corner Cracks from Open and Close Tolerance Holes with and without Fastener Load Transfer in 2219-T851 Aluminum Alloy Plates Subjected to Bomber Spectrum Loading.	127
54	Growth Behavior of Intermediate Corner Cracks from Various Levels of Interference-Fit Fastener Holes in 2219-T851 Aluminum Alloy Plates Subjected to Bomber Spectrum Loading	128
55	Growth Behavior of Intermediate Corner Cracks from Level 2 Interference-Fit Fastener Holes with and without Fastener Load Transfer in 2219-T851 Aluminum Alloy Plates Subjected to Bomber Spectrum Loading	129
56	Growth Behavior of Intermediate Corner Cracks from Various Types of Level 1 Cold-Worked Holes in 2219-T851 Aluminum Alloy Plates Subjected to Bomber Spectrum Loading	130
57	Growth Behavior of Intermediate Corner Cracks from Level 1 and Level 2 Cold-Worked Open Holes in 2219-T851 Aluminum Alloy Plates Subjected to Bomber Spectrum Loading	131
58	Comparison of Growth Behavior of Small Corner Cracks from Level 1 Cold-Worked and Interference-Fit Fastener Holes in 2219-T851 Aluminum Alloy Plates Subjected to Bomber Spectrum Loading	132
59	Comparison of Growth Behavior of Intermediate Corner Cracks from Level 2 Interference-Fit Fastener Holes and Level 2 Cold-Worked Open Holes in 2219-T851 Aluminum Alloy Plates Subjected to Bomber Spectrum Loading	133
60	Comparison of Growth Behavior of Intermediate Corner Cracks from Various Types of Fastener Holes in 2219-T851 Aluminum Alloy Plates Subjected to Bomber Spectrum Loading	134

LIST OF FIGURES (Continued)

<u>Figure No.</u>		<u>Page</u>
61	Growth Behavior of Small Thru Cracks from Open and Close Tolerance Fastener Holes in 2219-T851 Aluminum Alloy Plates Subjected to Bomber Spectrum Loading	135
62	Growth Behavior of Intermediate Thru Cracks from Interference-Fit Fastener Holes for Various Levels of Interference in 2219-T851 Aluminum Alloy Plates Subjected to Bomber Spectrum Loading	136
63	Growth Behavior of Intermediate Thru Cracks from Level 2 Interference-Fit Fastener Holes with and without Fastener Load Transfer in 2219-T851 Aluminum Alloy Plates Subjected to Bomber Spectrum Loading	137
64	Growth Behavior of Thru Cracks from Level 1 Cold-Worked Open Holes in 2219-T851 Aluminum Alloy Plates Subjected to Bomber Spectrum Loading	138
65	Growth Behavior of Thru Cracks from Level 1 Cold-Worked Filled Holes in 2219-T851 Aluminum Alloy Plates Subjected to Bomber Spectrum Loading	139
66	Growth Behavior of Thru Cracks from Level 1 Cold-Worked Holes Having Fastener Load Transfer in 2219-T851 Aluminum Alloy Plates Subjected to Bomber Spectrum Loading	140
67	Growth Behavior of Large Thru Cracks from Cold-Worked Open Holes for Various Levels of Cold Working for 2219-T851 Aluminum Alloy Plates Subjected to Bomber Spectrum Loading	141
68	Comparison of Growth Behavior of Intermediate Thru Cracks from Level 2 Interference-Fit and Cold-Worked Fastener Holes in 2219-T851 Aluminum Alloy Plates Subjected to Bomber Spectrum Loading	142
69	Comparison of Growth Behavior of Small Thru Cracks from Various Types of Fastener Holes in 2219-T851 Aluminum Alloy Plates Subjected to Bomber Spectrum Loading	143
70	Growth Behavior of Corner Cracks from Open and Close Tolerance Holes in 6Al-4V Beta Annealed Titanium Alloy Plates Subjected to Bomber Spectrum Loading	144
71	Growth Behavior of Intermediate Corner Cracks from Level 1 Interference-Fit Fastener Holes in 6Al-4V Beta Annealed Titanium Alloy Plates Subjected to Bomber Spectrum Loading	145
72	Growth Behavior of intermediate Corner Cracks from Interference-Fit Fastener Holes for Various Levels of Interference in 6Al-4V Beta Annealed Titanium Alloy Plates Subjected to Bomber Spectrum Loading	146

LIST OF FIGURES (Continued)

<u>Figure No.</u>		<u>Page</u>
73	Growth Behavior of Intermediate Corner Cracks from Level 1 Cold-Worked Fastener Holes in 6Al-4V Beta Annealed Titanium Alloy Plates Subjected to Bomber Spectrum Loading	147
74	Growth Behavior of Intermediate Corner Cracks from Cold-Worked Open Holes for Various Levels of Cold Working in 6Al-4V Beta Annealed Titanium Alloy Plates Subjected to Bomber Spectrum Loading	148
75	Comparison of Growth Behavior of Intermediate Corner Cracks from Level 1 Cold-Worked and Interference-Fit Fastener Holes in 6Al-4V Beta Annealed Titanium Alloy Plates Subjected to Bomber Spectrum Loading	149
76	Comparison of Growth Behavior of Intermediate Corner Cracks from Level 2 Cold-Worked and Interference-Fit Fastener Holes in 6Al-4V Beta Annealed Titanium Alloy Plates Subjected to Bomber Spectrum Loading	150
77	Growth Behavior of Small Thru Cracks from Open and Close Tolerance Fastener Holes in 6Al-4V Beta Annealed Titanium Alloy Plates Subjected to Bomber Spectrum Loading	151
78	Growth Behavior of Intermediate Thru Cracks from Interference-Fit Fastener Holes for Various Levels of Interference in 6Al-4V Beta Annealed Titanium Alloy Plates Subjected to Bomber Spectrum Loading	152
79	Growth Behavior of Intermediate Thru Cracks from Level 2 Interference-Fit Holes in 6Al-4V Beta Annealed Titanium Alloy Plates Subjected to Bomber Spectrum Loading	153
80	Growth Behavior of Thru Cracks from Cold-Worked Open Holes in 6Al-4V Beta Annealed Titanium Alloy Plates Subjected to Bomber Spectrum Loading	154
81	Growth Behavior of Thru Cracks from Level 1 Filled Cold-Worked Fastener Holes in 6Al-4V Beta Annealed Titanium Alloy Plates Subjected to Bomber Spectrum Loading	155
82	Growth Behavior of Thru Cracks from Level 1 Loaded Cold-Worked Fastener Holes in 6Al-4V Beta Annealed Titanium Alloy Plates Subjected to Bomber Spectrum Loading	156
83	Growth Behavior of Large Thru Cracks from Cold-Worked Holes for Various Levels of Cold Working in 6Al-4V Beta Annealed Titanium Alloy Plates Subjected to Bomber Spectrum Loading	157
84	Comparison of Growth Behavior of Intermediate Thru Cracks from Level 2 Interference-Fit Fastener Holes and Cold-Worked Open Holes in 6Al-4V Beta Annealed Titanium Alloy Plates Subjected to Bomber Spectrum Loading	158

LIST OF FIGURES (Continued)

<u>Figure No.</u>		<u>Page</u>
85	Growth Behavior of Corner Cracks from Open and Close Tolerance Fastener Holes in 2219-T851 Aluminum Alloy Plates Subjected to Fighter Spectrum Loading	159
86	Growth Behavior of Small and Intermediate Corner Cracks from Interference-Fit Fastener Holes for Various Levels of Interference in 2219-T851 Aluminum Alloy Plates Subjected to Fighter Spectrum Loading	160
87	Growth Behavior of Intermediate Corner Cracks from Level 1 Cold-Worked Holes in 2219-T851 Aluminum Alloy Plates Subjected to Fighter Spectrum Loading	161
88	Comparison of Growth Behavior of Intermediate Corner Cracks from Level 1 Cold-Worked and Interference-Fit Fastener Holes in 2219-T851 Aluminum Alloy Plates Subjected to Fighter Spectrum Loading	162
89	Comparison of Growth Behavior of Intermediate Corner Cracks from Various Types of Fastener Holes in 2219-T851 Aluminum Alloy Plates Subjected to Fighter Spectrum Loading	163
90	Growth Behavior of Intermediate Thru Cracks from Open and Close Tolerance Fastener Holes in 2219-T851 Aluminum Alloy Plates Subjected to Fighter Spectrum Loading	164
91	Growth Behavior of Intermediate Thru Cracks from Interference-Fit Fastener Holes for Various Levels of Interference in 2219-T851 Aluminum Alloy Plates Subjected to Fighter Spectrum Loading	165
92	Growth Behavior of Small Thru Cracks from Level 3 Interference-Fit Fastener Holes in 2219-T851 Aluminum Alloy Plates Subjected to Fighter Spectrum Loading	166
93	Growth Behavior of Thru Cracks from Level 1 Cold-Worked Open Holes in 2219-T851 Aluminum Alloy Plates Subjected to Fighter Spectrum Loading	167
94	Growth Behavior of Thru Cracks from Level 1 Cold-Worked Filled Holes in 2219-T851 Aluminum Alloy Plates Subjected to Fighter Spectrum Loading	168
95	Growth Behavior of Thru Cracks from Level 1 Cold-Worked Holes with Fastener Load Transfer in 2219-T851 Aluminum Alloy Plates Subjected to Fighter Spectrum Loading	169
96	Typical Crack Surfaces of Thru Cracks (Having Various Initial Crack Lengths) Emanating from Level 1 Cold-Worked Open Holes Subjected to Fighter Spectrum Loading	170

LIST OF FIGURES (Continued)

<u>Figure No.</u>		<u>Page</u>
97	Growth Behavior of Thru Cracks from Level 2 Cold-Worked Open Holes in 2219-T851 Aluminum Alloy Plates Subjected to Fighter Spectrum Loading	171
98	Growth Behavior of Small Corner Cracks from Open and Close Tolerance Fastener Holes in 6Al-4V Beta Annealed Titanium Alloy Plates Subjected to Fighter Spectrum Loading	172
99	Growth Behavior of Intermediate Corner Cracks from Interference-Fit Fastener Holes for Various Levels of Interference in 6Al-4V Beta Annealed Titanium Alloy Plates Subjected to Fighter Spectrum Loading	173
100	Growth Behavior of Intermediate Corner Cracks from Level 2 Interference-Fit Fastener Holes with and without Fastener Load Transfer in 6Al-4V Beta Annealed Titanium Alloy Plates Subjected to Fighter Spectrum Loading	174
101	Growth Behavior of Intermediate Corner Cracks from Various Types of Level 1 Cold-Worked Holes in 6Al-4V Beta Annealed Titanium Alloy Plates Subjected to Fighter Spectrum Loading	175
102	Growth Behavior of Small Corner Cracks from Cold-Worked Open Holes for Various Levels of Cold Working in 6Al-4V Beta Annealed Titanium Alloy Plates Subjected to Fighter Spectrum Loading	176
103	Growth Behavior of Small Thru Cracks from Open and Close Tolerance Fastener Holes in 6Al-4V Beta Annealed Titanium Alloy Plates Subjected to Fighter Spectrum Loading	177
104	Growth Behavior of Intermediate Thru Cracks from Level 2 Interference-Fit Fastener Holes with and without Fastener Load Transfer in 6Al-4V Beta Annealed Titanium Alloy Plates Subjected to Fighter Spectrum Loading	178
105	Growth Behavior of Small and Intermediate Thru Cracks from Level 3 Interference-Fit Fastener Holes in 6Al-4V Beta Annealed Titanium Alloy Plates Subjected to Fighter Spectrum Loading	179
106	Growth Behavior of Small to Large Thru Cracks from Level 1 Cold-Worked Open Holes in 6Al-4V Beta Annealed Titanium Alloy Plates Subjected to Fighter Spectrum Loading	180
107	Growth Behavior of Small to Large Thru Cracks from Level 1 Cold-Worked Filled Holes in 6Al-4V Beta Annealed Titanium Alloy Plates Subjected to Fighter Spectrum Loading	181

LIST OF FIGURES (Continued)

<u>Figure No.</u>		<u>Page</u>
108	Growth Behavior of Small to Large Thru Cracks from Level 1 Cold-Worked Holes with Fastener Load Transfer in 6Al-4V Beta Annealed Titanium Alloy Plates Subjected to Fighter Spectrum Loading	182
109	Growth Behavior of Intermediate Thru Cracks from Level 2 Cold-Worked Open Holes in 6Al-4V Beta Annealed Titanium Alloy Plates Subjected to Fighter Spectrum Loading	183
110	Finite Element Model	184
111	Cyclic Stress-Strain Curve	185
112	Unflawed Stress Distribution Along the x-Axis in 2219-T851 Aluminum Plate Caused by 2% Cold Working and Subsequent Far-Field Loading	186
113	Stress Distribution Along the x-Axis in 2219-T851 Aluminum Plate Caused by 2% Cold Working and Subsequent Far-Field Loading ($a_i = 0.1025"$)	187
114	Stress Distribution Along the x-Axis in 2219-T851 Aluminum Plate Caused by 2% Cold Working and Subsequent Far-Field loading ($a_i = 0.0525"$)	188
115	Unflawed Stress Distribution Along the x-Axis in 2219-T851 Aluminum Alloy Plate Caused by 4% Cold Working and Subsequent Far-Field Loading	189
116	Unflawed Stress Distribution Along the x-Axis in 2219-T851 Aluminum Plate Caused by 5% Cold Working and Subsequent Far-Field Loading	190
117	Unflawed Stress Distribution Along the x-Axis in 2219-T851 Aluminum Plates Caused by 2%, 4%, and 5% Cold-Working and Subsequent 18 Ksi Far-Field Loading	191
118	Unflawed Stress Distribution Along the x-Axis in Various Types of 2% Cold-Worked Holes in 2219-T851 Aluminum Plates Subjected to 18 Ksi Far-Field Loading	192
119	Unflawed Stress Distribution Along the x-Axis in 2219-T851 Aluminum Plates Caused by 2%, 4% and 5% Cold Working and Subsequent 18 Ksi Far-Field Loading and 10% Fastener Load Transfer	193
120	Unflawed Stress Distribution Along the x-Axis in 6Al-4V Beta Annealed Titanium Plate Caused by 2% Cold Working and Subsequent Far-Field Loading	194

LIST OF FIGURES (Continued)

<u>Figure No.</u>		<u>Page</u>
121	Unflawed Stress Distribution Along the x-Axis in 6Al-4V Beta Annealed Titanium Plate Caused by 4% Cold Working and Subsequent Far-Field Loading	195
122	Unflawed Stress Distribution Along the x-Axis in 6Al-4V Beta Annealed Titanium Plate Caused by 5% Cold Working and Subsequent Far-Field Loading	196
123	Unflawed Stress Distribution Along the x-Axis at 2% Cold-Worked Holes with and without Fastener Load Transfer in 6Al-4V Beta Annealed Titanium Plates Caused by 40 Ksi Far-Field Loading	197
124	Unflawed Stress Distribution Along the x-Axis in 6Al-4V Beta Annealed Titanium Plates Caused by 2%, 4% and 5% Cold Working and Subsequent 40 Ksi Far-Field and 10% Fastener Loads	198
125	Unflawed Stress Distribution Along the x-Axis in 2219-T851 Aluminum Alloy Plate Caused by 0.0024 Inches Diametrical Interference and Subsequent Far-Field Loading	199
126	Unflawed Stress Distribution Along the x-Axis in 2219-T851 Aluminum Alloy Plate Caused by 0.0038 Inches Diametrical Interference and Subsequent Far-Field Loading	200
127	Unflawed Stress Distribution Along the x-Axis in 2219-T851 Aluminum Alloy Plate Caused by 0.0060 Inches Diametrical Interference and Subsequent Far-Field Loading	201
128	Unflawed Stress Distribution Along the x-Axis in 6Al-4V Beta Annealed Titanium Plate Caused by 0.0034 Inches Diametrical Interference and Subsequent Far-Field Loading	202
129	Unflawed Stress Distribution Along the x-Axis in 6Al-4V Beta Annealed Titanium Plate Caused by 0.0042 Inches Diametrical Interference and Subsequent Far-Field Loading	203
130	Unflawed Stress Distribution Along the x-Axis in 6Al-4V Beta Annealed Titanium Plate Caused by 0.0050 Inches Diametrical Interference and Subsequent Far-Field Loading	204
131	Unflawed Stress Distribution Along the x-Axis in 2219-T851 Aluminum Alloy Plates Due to the Installation of Three Different Levels of Interference-Fit Fastener	205
132	Unflawed Stress Distribution Along the x-Axis in 2219-T851 Aluminum Alloy Plates Due to the Application of 18 Ksi Far-Field Loading for Three Different Levels of Interference-Fit Fastener Holes	206
133	Unflawed Stress Distribution Along the x-Axis in 2219-T851 Aluminum Alloy Plates After Removal of the Far-Field Loading for Three Different Levels of Interference-Fit Fastener Holes	207

LIST OF FIGURES (Continued)

<u>Figure No.</u>		<u>Page</u>
134	Schematic of Linear Superposition Method	208
135	A Straight Crack Subjected to Two Pairs of Concentrated Forces on the Crack Surfaces	208
136	A Double Radial Crack Emanating from a Circular Hole Subjected to Two Pairs of Concentrated Forces on the Crack Surfaces	209
137	Idealization of the Hole as a Portion of a Straight Crack When the Applied Forces Are Close to the Crack Tip	209
138	Normalized Stress Intensity Factors for a Double Crack Emanating from an Open Hole	210
139	Normalized Stress Intensity Factors for a Single Crack Emanating from an Open Hole	211
140	Normalized Stress Intensity Factors for Thru Cracks from an Open Hole in 2219-T851 Aluminum Plates Subjected to High Far-Field Loading (Accounting for Plasticity Effect)	212
141	Illustration of Superposition Method	213
142	Normalized Unflawed Stress Distribution Along x-Axis in the Plate with Various Amounts of Fastener Load Transfer	214
143	Normalized Stress Intensity Factors for a Double Crack Emanating from Neat-Fit Hole with Fraction of Fastener Load Transfer	214
144	Normalized Stress Intensity Factors for Double Thru Cracks Emanating from an Open and Close Tolerance Fastener Holes With and Without Fastener Load Transfer in 2219-T851 Aluminum Plates	215
145	Normalized Stress Intensity Factors for Double Thru Cracks Emanating from an Open and Close Tolerance Fastener Holes With and Without Fastener Load Transfer in 6Al-4V Beta Annealed Titanium Plates	216
146	Stress Intensity Factors for a Single Thru Crack Emanating from a Close Tolerance Fastener Hole in 6Al-4V β A Titanium Plate Subjected to 40 Ksi Far-Field Loading	217
147	Stress Intensity Factors for a Single Thru Crack Emanating from a Close Tolerance Fastener Hole Having 10% Fastener Load Transfer in 6Al-4V β A Titanium Plate Subjected to 40 Ksi Far-Field Loading	218
148	Stress σ at $y = 0$ in an Aluminum Plate with a Steel Interference-Fit Fastener Caused by Interference, Edge Loading and Unloading	219

LIST OF FIGURES (Continued)

<u>Figure No.</u>		<u>Page</u>
149	Stress Intensity Factors for a Double Crack Emanating from an Interference-Fit Fastener Hole	219
150	Normalized Stress Intensity Factors for Double Thru Cracks Emanating from Interference-Fit Fastener Holes in 2219-T851 Aluminum Plates Subjected to 18 Ksi Far-Field Loading and Subsequent Unloading	220
151	Stress Intensity Factors for Single Thru Cracks Emanating from Interference-Fit Fastener Holes for Various Levels of Interference in 2219-T851 Aluminum Alloy Plates Subjected to 18 Ksi Far-Field Loading and Subsequent Unloading	221
152	Normalized Stress Intensity Factors for Double Thru Cracks Emanating from Interference-Fit Fastener Holes in 6Al-4V Beta Annealed Titanium Plates Subjected to 40 Ksi Far-Field Loading and Subsequent Unloading	222
153	Stress Intensity Factor for Single Thru Cracks Emanating from Interference-Fit Fastener Holes for Various Levels of Interference in 6Al-4V Beta Annealed Titanium Plates Subjected to 40 Ksi Far-Field Loading and Subsequent Unloading	223
154	Effective Stress Intensity Factor Ratios for Single Thru Cracks Emanating from Interference-Fit Fastener Holes for Various Levels of Interference in 2219-T851 Aluminum Plates Subjected to Constant Amplitude 18 Ksi and $R = +0.1$ Far-Field Loading	224
155	Effective Stress Intensity Factor Ratios for Single Thru Cracks Emanating from Interference-Fit Fastener Holes for Various Levels of Interference in 6Al-4V Beta Annealed Titanium Plates Subjected to Constant Amplitude 40 Ksi and $R = +0.1$ Far-Field Loading	225
156	Crack Growth from 0.0024 Inch Diametrical Interference-Fit Fastener Holes in 2219-T851 Aluminum Alloy Plates Subjected to Constant Amplitude Far-Field Loading ($\sigma = 18$ Ksi and $R=0.1$)	226
157	Crack Growth from 0.0038 Inch Diametrical Interference-Fit Fastener Holes in 2219-T851 Aluminum Alloy Plates Subjected to Constant Amplitude Far-Field Loading ($\sigma = 18$ Ksi and $R=0.1$)	227
158	Crack Growth from 0.0060 Inch Diametrical Interference-Fit Fastener Holes in 2219-T851 Aluminum Alloy Plates Subjected to Constant Amplitude Far-Field Loading ($\sigma = 18$ Ksi and $R=0.1$)	228
159	Stress at the Region of 4.4% Cold-Worked Hole in 7075-T6 Aluminum Plate Caused by 16 Ksi Edge Loading and Subsequent Unloading	229
160	Stress Intensity Factors for a Single Thru Crack Emanating from Cold-Worked Hole	230

LIST OF FIGURES (Continued)

Figure No.		Page
161	Normalized Stress Intensity Factors for Double Thru Cracks Emanating from Cold-Worked Open Holes in 2219-T851 Aluminum Plates Subjected to 18 ksi Far-Field Loading	231
162	Stress Intensity Factors for a Single Thru Crack Emanating from Level 1 Cold-Worked Open Hole in 2219-T851 Aluminum Plate Subjected to Uniform Far-Field Loading	232
163	Stress Intensity Factors for a Single Thru Crack Emanating from Level 2 Cold-Worked Open Hole in 2219-T851 Aluminum Plate Subjected to Uniform Far-Field Loading ($\sigma = 18$ ksi)	233
164	Stress Intensity Factors for a Single Thru Crack Emanating from Level 3 Cold-Worked Open Hole in 2219-T851 Aluminum Plate Subjected to Uniform Far-Field Loading (18 ksi)	234
165	Stress Intensity Factors for a Single Thru Crack Emanating from Level 1 Cold-Worked Hole in 2219-T851 Aluminum Plate Subjected to 18 ksi Far-Field Loading and 10% Fastener Load Transfer	235
166	Normalized Stress Intensity Factors for Double Thru Cracks Emanating from Cold-Worked Open Holes in 6Al-4V Beta Annealed Titanium Plates Subjected to 40 ksi Far-Field Loading	236
167	Stress Intensity Factors for A Single Thru Crack Emanating from Level 1 Cold-Worked Open Hole in 6Al-4V Beta Annealed Titanium Alloy Plate Subjected to Uniform Far-Field Loading	237
168	Stress Intensity Factors for a Single Thru Crack Emanating from Level 2 Cold-Worked Open Hole in 6Al-4V Beta Annealed Titanium Plate Subjected to 40 ksi Uniform Far-Field Loading	238
169	Stress Intensity Factor for a Single Thru Crack Emanating from Level 3 Cold-Worked Hole in 6Al-4V Beta Annealed Titanium Plate Subjected to 40 ksi Uniform Far-Field Loading	239
170	Stress Intensity Factor for a Single Thru Crack Emanating from Level 1 Cold-Worked Hole in 6Al-4V Beta Annealed Titanium Plate Subjected to 18 ksi Far-Field Loading and 70% Fastener Load Transfer	240
171	Stress Intensity Factors for Single Thru Cracks Emanating from Various Types of Level 1 Cold-Worked Holes in 2219-T851 Aluminum Plates Subjected to 18 ksi Far-Field Loading	241
172	Stress Intensity Factors for a Single Thru Crack Emanating from Level 1 Cold-Worked Hole in 2219-T851 Aluminum Plate Subjected to Various Levels of Far-Field Loading	242
173	Flaw Shape Parameter Φ	243
174	Front Free Surface Correction Factors, M_1	244

LIST OF FIGURES (Continued)

<u>Figure No.</u>		<u>Page</u>
175	Factor M_1' / ϕ For $a/c \leq 1$	245
176	Factor M_1' / ϕ For $a/c \geq 1$	246
177	Relationship Between Parametric Angle β and Geometric Angle θ	247
178	Nondimensional Factor F at the Edge of a Hole	248
179	Normalized Stress Intensity Factors Along the Periphery of a Double Corner Crack Emanating from an Open Hole ($a/c = 0.75$)	249
180	Normalized Stress Intensity Factors Along the Periphery of a Double Corner Crack Emanating from an Open Hole ($a/c = 1.0$)	250
181	Normalized Stress Intensity Factors Along the Periphery of a Double Corner Crack Emanating from an Open Hole ($a/c = 1.5$)	251
182	Normalized Stress Intensity Factors Along the Periphery of a Double Corner Crack Emanating from an Open Hole ($a/c = 2.0$)	252
183	Comparisons of the Normalized Stress Intensity Factors for Double Corner Crack Emanating from an Open Hole	253
184	Comparisons of Estimated Magnification Factors for a Single Quarter-Ellipse Corner Crack Emanating from an Open Hole	254
185	Fracture Surface of Test Specimen No. 1	255
186	Change of Flaw Shape on Fracture Surface of Corner Crack Specimen (Test No. 1)	255
187	Correlation of Data and Prediction for a Corner Crack Emanating from an Open Hole in 7050-T73 Aluminum Plate Subjected to Constant Amplitude Loading (Test Specimen No. 1)	256
188	Correlation of Data and Prediction for a Corner Crack Emanating from an Open Hole in 7050-T73 Aluminum Plate Subjected to Constant Amplitude Loading (Test Specimen No. 2)	257
189	Correlations of Data and Predictions for Corner Cracks Emanating from Open Holes in PMMA Polymer Plates Subjected to Constant Amplitude Loading	258
190	Normalized Stress Intensity Factors at the Intersection of Plate Surface and the Border of Single Corner Cracks Emanating from Interference-Fit Fastener Holes for Various Levels of Interference in 2219-T851 Aluminum Plates Subjected to Constant Amplitude Far-Field Loading ($a/c = 0.75$)	259

LIST OF FIGURES (Continued)

<u>Figure No.</u>		<u>Page</u>
191	Normalized Stress Intensity Factors at the Intersection of Plate Surface and the Border of Single Corner Cracks Emanating from Interference-Fit Fastener Holes for Various Levels of Interference in 6Al-4V Beta Annealed Titanium Plates Subjected to Constant Amplitude Far-Field Loading ($a/c = 0.75$)	260
192	Correlation of Data and Predictions for Corner Cracks Emanating from Interference-Fit Fastener Holes in 2219-T851 Aluminum Plates Subjected to Constant Amplitude Loading ($\sigma_o = 18$ Ksi and $R = 0.1$)	261
193	Correlation of Data and Predictions for Corner Cracks Emanating from Interference-Fit Fastener Holes in 6Al-4V Beta Annealed Titanium Plates Subjected to Constant Amplitude Loading ($\sigma_o = 40$ Ksi and $R = 0.1$)	262
194	Flaw Shape Factor, $M \Phi$	263
195	Crack Surface of a Double Embedded Crack at Open Hole in 7075-T651 Aluminum Plate Subjected to Constant Amplitude Loading ($\sigma_{max} = 15$ Ksi, $R = 0.1$)	264

LIST OF TABLES

<u>Table No.</u>		<u>Page</u>
1	SUMMARY OF FATIGUE AND CRACK GROWTH TEST HOLES	265
2	SUMMARY OF MATERIAL CHARACTERIZATION AND FAILURE CRITERION TESTS	266
3	SUMMARY OF CONSTANT AMPLITUDE FATIGUE TESTS ON 2219-T851 ALUMINUM SPECIMENS WITH $\sigma_o = 18$ ksi AND $R = 0.1$	267
4	SUMMARY OF CONSTANT AMPLITUDE FATIGUE TESTS ON 6Al-4V BETA ANNEALED TITANIUM SPECIMENS WITH $\sigma_o = 40$ ksi AND $R = 0.1$	268
5	SUMMARY OF INITIAL CRACKS (OR ORIGINS) OF ALL CONSTANT AMPLITUDE FATIGUE TESTS ON BOTH ALUMINUM AND TITANIUM SPECIMENS	269
6	SUMMARY OF SPECTRUM FATIGUE TESTS ON 2219-T851 ALUMINUM SPECIMENS	270
7	SUMMARY OF INITIAL CRACKS (OR ORIGINS) OF ALL SPECTRUM FATIGUE TESTS ON 2219-T851 ALUMINUM SPECIMENS	271
8	SUMMARY OF SPECTRUM FATIGUE TESTS ON 6Al-4V BETA ANNEALED TITANIUM SPECIMENS	272
9	SUMMARY OF INITIAL CRACKS (OR ORIGINS) OF ALL SPECTRUM FATIGUE TESTS ON 6Al-4V BETA ANNEALED TITANIUM SPECIMENS	273
10	SUMMARY OF CRACK GROWTH OF PART-THRU CRACKS FROM FASTENER HOLE TESTS FOR 2219-T851 ALUMINUM ALLOY PLATES SUBJECTED TO CONSTANT AMPLITUDE LOADING	274
11	SUMMARY OF CRACK GROWTH OF THRU CRACKS FROM FASTENER HOLE TESTS FOR 2219-T851 ALUMINUM ALLOY PLATES SUBJECTED TO CONSTANT AMPLITUDE LOADING	275
12	SUMMARY OF CRACK GROWTH OF PART-THRU CRACKS FROM FASTENER HOLE TESTS FOR 6Al-4V BETA ANNEALED TITANIUM ALLOY PLATES SUBJECTED TO CONSTANT AMPLITUDE LOADING	277
13	SUMMARY OF CRACK GROWTH OF THRU CRACKS FROM FASTENER HOLE TESTS FOR 6Al-4V BETA ANNEALED TITANIUM ALLOY PLATES SUBJECTED TO CONSTANT AMPLITUDE LOADING	278
14	DIMENSIONS DURING COLD-WORKING OPERATION	280
15	DIMENSIONS OF INTERFERENCE-FIT FASTENER HOLES	281

LIST OF TABLES (Continued)

<u>Table No.</u>		<u>Page</u>
16	SUMMARY OF CRACK GROWTH OF PART-THRU CRACKS FROM FASTENER HOLE TESTS FOR 2219-T851 ALUMINUM ALLOY PLATES SUBJECTED TO BOMBER SPECTRUM LOADING	282
17	SUMMARY OF CRACK GROWTH OF THRU CRACKS FROM FASTENER HOLE TESTS FOR 2219-T851 ALUMINUM ALLOY PLATES SUBJECTED TO BOMBER SPECTRUM LOADING	283
18	SUMMARY OF CRACK GROWTH OF PART-THRU CRACKS FROM FASTENER HOLE TESTS FOR 2219-T851 ALUMINUM ALLOY PLATES SUBJECTED TO FIGHTER SPECTRUM LOADING	284
19	SUMMARY OF CRACK GROWTH OF THRU CRACKS FROM FASTENER HOLE TESTS FOR 2219-T851 ALUMINUM ALLOY PLATES SUBJECTED TO FIGHTER SPECTRUM LOADING	285
20	SUMMARY OF CRACK GROWTH OF PART-THRU CRACKS FROM FASTENER HOLE TESTS FOR 6A2-4V BETA ANNEALED TITANIUM ALLOY PLATES SUBJECTED TO BOMBER SPECTRUM LOADING	286
21	SUMMARY OF CRACK GROWTH OF THRU CRACKS FROM FASTENER HOLE TESTS FOR 6A2-4V BETA ANNEALED TITANIUM ALLOY PLATES SUBJECTED TO BOMBER SPECTRUM LOADING	287
22	SUMMARY OF CRACK GROWTH OF PART-THRU CRACKS FROM FASTENER HOLE TESTS FOR 6A2-4V BETA ANNEALED TITANIUM ALLOY PLATES SUBJECTED TO FIGHTER SPECTRUM LOADING	288
23	SUMMARY OF CRACK GROWTH OF THRU CRACKS FROM FASTENER HOLE TESTS FOR 6A2-4V BETA ANNEALED TITANIUM ALLOY PLATES SUBJECTED TO FIGHTER SPECTRUM LOADING	289
24	SUMMARY OF ANALYTICAL PROGRAM	290
25	CHEMICAL COMPOSITIONS OF TEST MATERIALS	291
26	MECHANICAL PROPERTIES OF MATERIALS	292
27	SUMMARY OF TEST PROGRAM FASTENERS	293
28	FIGHTER SPECTRUM - STANDARD SEVERITY	294
29	BOMBER SPECTRUM - STANDARD SEVERITY	295
30	FRACTURE TOUGHNESS FOR 2219-T851 ALUMINUM AND 6A2-4V β ANNEALED TITANIUM	296
31	INITIAL AND FINAL DIMENSIONS OF CORNER CRACK TESTED SPECIMENS	297

LIST OF TABLES (Continued)

<u>Table No.</u>		<u>Page</u>
32	RESULTS OF FRACTURE TESTS ON FLAWED ALUMINUM AND TITANIUM COLD-WORKED OPEN HOLES	301
33	THRESHOLD CRACK LENGTHS FOR VARIOUS FASTENER-HOLE COMBINATIONS IN 2219-T851 ALUMINUM PLATES SUBJECTED TO 18 KSI CONSTANT AMPLITUDE FAR-FIELD LOADING	302
34	THRESHOLD CRACK LENGTHS FOR VARIOUS FASTENER-HOLE COMBINATIONS IN 6Al-4V BETA ANNEALED TITANIUM PLATES SUBJECTED TO 40 KSI CONSTANT AMPLITUDE FAR-FIELD LOADING	303
35	GREEN'S FUNCTION FOR A DOUBLE CRACK EMANATING FROM AN OPEN HOLE IN AN INFINITE PLATE	304
36	SUMMARY OF STRESS INTENSITY FACTOR SOLUTIONS FOR THRU CRACKED FASTENER HOLES	305
37	COMPARISON OF STRESS INTENSITY FACTOR SOLUTIONS FOR CORNER CRACKS EMANATING FROM OPEN HOLES IN PLATES LOADED IN TENSION NORMAL TO CRACK SURFACES	306
38	SUMMARY OF STRESS INTENSITY FACTOR SOLUTIONS FOR CORNER CRACKED FASTENER HOLES	307
39	COMPARISON OF STRESS INTENSITY FACTOR SOLUTIONS FOR A DOUBLE SEMI-ELLIPTICAL EMBEDDED CRACK EMANATING FROM AN OPEN HOLE IN 7075-T651 ALUMINUM ALLOY PLATE	308
40	SUMMARY OF STRESS INTENSITY FACTOR SOLUTIONS FOR EMBEDDED-CRACKED FASTENER HOLES	309
41	CORRELATIONS OF TESTED AND PREDICTED CRACK GROWTH LIVES FOR CONSTANT AMPLITUDE LOADED SPECIMENS	310
42	CORRELATIONS OF TESTED AND PREDICTED CRACK GROWTH LIVES FOR SPECTRUM LOADED SPECIMENS	311

LIST OF SYMBOLS

All symbols are defined in the text where they first appear and the major symbols are listed below:

a	Crack length for thru crack or crack depth for part-thru crack
a_{th}	Threshold crack length
B_1, B_2	Bowie's normalized stress intensity factor solutions for single and double radial cracks, respectively
c	Crack length on the surface of the plate for corner crack or half crack length on the hole wall for embedded flaw
E	Young's modulus
F_{cy}, F_{ty}	Compression and tension yield strengths of material, respectively
f_{OP}, f_{CT}	Normalized unflawed stress distributions at the edges of open holes and close tolerance fastener holes, respectively
f_{CW}, f_{IF}	Normalized unflawed stress distributions at the edges of cold-worked holes and interference-fit fastener holes, respectively
G	Green's function
H	Normalized stress intensity factor for a thru crack emanating from an open hole having significant local yielding
K or K_I	Opening mode stress intensity factor
K_c	Critical stress intensity factor
K_{max}	Maximum cyclic stress intensity factor
K_{min}	Minimum cyclic stress intensity factor
K_{th}	Peak cyclic threshold stress intensity factor for fatigue crack growth
ΔK_{th}	Threshold stress intensity factor range for fatigue crack growth
M	Flaw shape factor
M_1	Front surface correction factor
M_2	Back surface correction factor
M_c	Curvature correction factor at the edge of the hole

LIST OF SYMBOLS (Continued)

M'_1	$M'_1 = M \cdot M_1$
P	Far-field applied load
R	Stress ratio = $\sigma_{\min} / \sigma_{\max}$
β	Elliptical angle measured from the minor axis
β_{CT}	Total correction factor for a thru crack emanating from close tolerance fastener hole
β_{CW}	Total correction factor for a thru crack emanating from cold-worked fastener hole
β_{IF}	Total correction factor for a thru crack emanating from interference-fit fastener hole
β_{OP}	Total correction factor for a thru crack emanating from an open hole
β_T	Total correction factor
ν	Poisson's ratio
σ	Stress
σ_o	Far-field applied stress
σ_{ys}	0.2% offset yield strength of material
Φ	Elliptical integral of the second kind

SUMMARY

An analytical and experimental investigation was conducted to characterize the fracture and cyclic growth behavior of small cracks emanating from various types of fastener holes.

An analytical procedure was developed for estimating the stress intensity factor for a given crack length, hole condition, and load combination. It consists of two major steps. First, a nonlinear finite element solution for the elastic-plastic stress field appropriate to the unflawed hole was generated. In the second step, a crack was introduced in this stress field by removing the tractions on the crack faces and computing the corresponding stress intensity factors using the Green's function approach.

The developed Green's function approach was used to calculate the stress intensity factors for throughcracks emanating from open, close tolerance, interference-fit, and cold-worked fastener holes subjected to uniform far-field loading and, in some cases, attendant fastener loading. The approximate stress intensity factors for quarter-elliptical cracks emanating from the corner of the same types of fastener holes were derived from the corresponding thru crack solutions. The stress intensity factor for a double, semi-elliptical embedded crack originating at same types of fastener holes was derived from the modification of a surface flaw solution.

Experimental data in the form of crack length versus number of load cycles (or flights) resulting from applications of constant amplitude loading and flight-by-flight spectrum loading were obtained for 370 different test holes on two different alloys, namely, 2219-T851 aluminum and 6Al-4V standard E11 beta annealed titanium. Seventy-four constant amplitude and spectrum fatigue tests of unflawed specimens were also conducted to provide information for comparing the effective life of a nominally unflawed specimen with that of a specimen containing a small initial flaw, and for determining the location and initial shape of naturally induced cracks.

The stress level used in the constant amplitude load tests was approximately equal to one third of the material yield strength. Two different spectra representing bomber and fighter operations were employed in the spectrum load tests. Two initial flaw shapes

corresponding to a quarter-circular corner crack and a through-the-thickness crack and three initial crack lengths (small, intermediate and large) were used in the test program. The test holes, including open, close tolerance, interference-fit, and cold-worked fastener holes, were subjected to remote loading as well as fastener loading when applicable. Three levels of cold working and interference were included for each alloy. The amount of load transferred through the loaded fastener was maintained uniformly at a level which produced a bearing stress equal to the far-field stress.

Based upon the analytical study, it was found that when the applied far-field stress exceeded about one third of the material yield strength, local plastic deformation occurred at the edge of an open hole, and the computed normalized stress intensity factors were lower than the Bowie factors obtained for the purely elastic case. As local yielding proceeded, the normalized factors decreased as the far-field applied stress increased. When the crack length was longer than one hole radius, this plasticity effect became negligible.

For the cases in which cracks emanated from interference-fit fastener holes in both aluminum and titanium alloy plates subjected to constant amplitude far-field loading, the computed effective stress intensity factor ranges, $K_{\max} - K_{\min}$, were essentially constant and independent of the level of diametrical interference. However, the effective stress intensity factor ratio, $R_{\text{eff}} = K_{\min} / K_{\max}$, did depend upon the level of interference. For a crack length less than one radius, R_{eff} decreased rapidly as the amount of interference increased. When $a/r \geq 1$, R_{eff} remained almost constant as the amount of fastener hole interference increased.

For cracks emanating from cold-worked fastener holes, the stress intensity factors corresponding to a given crack length increased as the amount of cold working decreased. The stress intensity factors at cracked cold-worked open and close tolerance fastener holes were practically the same. However, with a small amount of fastener load transfer, the corresponding stress intensity factors increased significantly.

The correlations between the computed stress intensity factors and those reduced from tests using the fatigue crack growth method of calibrating K were good, except for small cracks emanating from cold-worked holes.

Results of tests showed that for a conditioned fastener hole (such as diametrical interference or cold working), the crack growth rates, in general, were significantly lower than those for a straight reamed hole without conditioning, especially for small initial cracks.

The crack growth rates decreased with increasing amounts of cold working or interference. The beneficial effect of the residual strains (created during the installation of interference-fit fasteners or during the cold working operation) on retarding fatigue crack growth was most significant when the crack length was small. The benefit decayed as the crack length increased. For initially intermediate and large cracks emanating from interference-fit fastener holes subjected to the same type of far-field loading, within the levels of interference studied during this program, the associated growth rates were almost the same for each level of interference. Although cold working did retard crack growth, the fatigue life of the cold-worked hole was no better than that of the close tolerance fastener hole for the same amount of fastener load transfer. Both corner cracks and embedded flaws were the most common types of natural cracks initiated due to fatigue cycling. The shapes of these natural cracks were very close to quarter- and semi-elliptical, respectively, as assumed in most of the analyses.

Data scatter obtained from the fighter spectrum tests was larger than that corresponding to the bomber spectrum tests, while the results of the constant amplitude tests showed least scatter. For the same far-field loading, data scatter was large in the tests of cracks emanating from cold-worked and interference-fit fastener holes, with such scatter decreasing rapidly as the crack length increased. For a given initial crack size, if the applied load was very low (resulting in an effective ΔK being approximately equal to ΔK threshold), the growth behavior of the crack was essentially the same as that of a fatigue test without an intentional flaw.

Another important feature observed was the change in flaw shape during the growth of corner cracks. For straight reamed holes with or without cold working, the final dimension on the hole wall was almost always larger than the final dimension on the plate surface, especially for cold-worked holes. For interference-fit fastener holes without fastener load transfer, the final flaw shape was close to quarter-circular. However, for interference-fit fastener holes with fastener load transfer, the final dimension on the hole wall was less than that on the plate surface.

Theoretically speaking, if the crack length is smaller than the compressive zone resulting from the cold-working operation and the application of the maximum cyclic load, the crack should not propagate under constant amplitude cyclic loading. However, the experimental data generated during this program negated such a conclusion. It is suspected that relaxation of the residual compressive strains due to cold working occurred, and after a period of fatigue cycling, the net hoop stress reverted to tension upon the application of the maximum cyclic load. The existing methodology is not capable of taking such relaxation into account. The interactions of the overloads and compressive loads in the spectrum with the residual compressive hoop stress around the fastener hole resulting from the cold-working operation should be investigated in more detail. Limited data available to date seems to indicate that these interactions might negate any beneficial effects gained from the cold-working operation.

SECTION I

INTRODUCTION

The influence of fracture mechanics on the design, manufacture, and maintenance of military aircraft has steadily increased during the past decade. The continuing search for greatly improved research methods in this area has largely stemmed from the need for a better understanding of the growth characteristics of minute crack-like defects. A review of U. S. Air Force aircraft structural failures^{(1)*} revealed that cracks emanating from fastener holes represent the most common origin of these failures. Cracks in fastener holes have been observed in a variety of shapes and lengths, but practically all of these have two common historical features. They initiated or were introduced somewhere on the boundary of the hole and their initial dimensions were quite small in comparison with the radius of the hole. Therefore, in the interest of the widest possible application of the results, it is appropriate to study small and intermediate size** fastener-hole cracks in sufficient detail to assess their growth characteristics.

The principal difficulties in such an analytical study relate to the comparative smallness of the crack. Generally, the plane deformation stress intensity factors, K_I and K_{II} , are primarily functions of the remote stress level and the crack length. However, for a small fastener hole crack, K_I and K_{II} are expected to be additionally sensitive to the particular combination of the following conditions:

- 1) whether the hole is open or filled
- 2) load transferred by the fastener
- 3) degree of fastener interference
- 4) severity and extent of prior hole conditioning procedures such as cold working and reaming.

A crack that has grown to a length comparable to the radius of the hole is influenced much less by hole conditions, and its stress intensity factor can be estimated from available and uncluttered closed form solutions.

* Numbers in superscript parentheses indicate the references listed at the end of this report.

** In this report, the crack size definitions are as follows:

Small: $0.005" \leq a < 0.050"$
Intermediate: $0.050" \leq a < 0.150"$
Large: $a \geq 0.150"$

The objective of this program was to analyze and experimentally characterize the fracture and cyclic growth behavior of small flaws originating at fastener holes. The program was intended to extend the investigation beyond that of a previous study.⁽²⁾ The purpose of the analytical study was to provide solutions for stress intensity factors appropriate to fastener hole cracks, as shown in Figure 1, in order to determine whether the routine procedures of fracture mechanics are applicable for assessing the residual strengths and predicting the cyclic growth patterns for these cracks. The results of the experimental program were used to evaluate the capability of the analytical solution to predict the growth patterns of flaws from fastener holes in 2219-T851 aluminum and 6Al-4V β -annealed titanium. Additionally, the test results were used to determine whether fracture mechanics methods furnish a suitable failure criterion for flawed, cold-worked holes.

An analytical procedure was developed for estimating the stress intensity factor for a given crack length, hole condition, and load combination. It consists of two major steps. First, a nonlinear finite element solution for the elastic-plastic stress field appropriate to an unflawed hole was generated. In the second step, a crack was introduced in this stress field by removing the tractions on the crack faces and computing the corresponding stress intensity factors using the Green's function approach.

The unflawed elastic-plastic stress solution considered strain-hardening plastic deformation and elastic unloading. It accounted for the practical order of loading (e.g., cold working followed by the application of remote loading and possible fastener reaction) and included the effects of geometrical nonlinearities, such as the loss of contact between the hole wall and a close-tolerance fastener during the deformation process.

The tractions removed in the second step reflected the combined effect of hole conditioning procedures and applied loads. The stress intensity solution was fully elastic. This was appropriate for material behind the crack tip, but any additional plastic deformation of material ahead of the tip was replaced by an elastic equivalent. Such an approximation was necessary to preserve the notion of a stress intensity factor and was consistent with what is routinely done in applying the principles of linear fracture mechanics; i.e., a plastic zone just ahead of and peculiar to the crack tip is quantitatively ignored.

The analytical program, though extensive and reasonably comprehensive, was intended to complement a parallel experimental program. The main thrust of the experimental program was to provide baseline data for assessing the growth characteristics under constant-amplitude cyclic loading and flight-by-flight spectrum loading of small-and intermediate-size fastener hole cracks for two different alloys, namely, 2219-T851 aluminum and 6Al-4V standard ELI beta annealed titanium. The stress level used in the constant amplitude load tests was approximately equal to one third of the material yield strength. Two different spectra representing the bomber and fighter operations were employed in the spectrum load tests. Two initial flaw shapes corresponding to a quarter-circular corner crack and a through-the-thickness crack and three initial crack lengths (small, intermediate and large) were used in the test program. The hole conditions and types of applied loading included practical combinations of the four conditions previously listed. Three levels of cold working and interference were included for each alloy. The amount of load transferred through the loaded fastener was maintained uniformly at a level which produced a bearing stress equal to the far-field stress.

A limited number of constant amplitude and spectrum fatigue tests of unflawed specimens were also conducted to provide information for

- 1) Comparing the effective life of a nominally unflawed specimen with that of a specimen containing a small initial flaw;
- 2) Determining the location and initial shape of naturally induced cracks.

In recognition of the relatively broader scatter of the growth of small cracks and fatigue-test results, two specimens were employed for each condition. The total number of flawed and unflawed test holes in the experimental program is 444, and they are summarized in Table 1.

Wherever possible, the computed stress intensity factors were validated with the experimental data.

SECTION II

SCOPE

Scopes of both experimental and analytical programs are discussed in this section.

1. EXPERIMENTAL PROGRAM

The scope of the experimental program was established to extend the large flaw evaluation program reported in Reference (2). Consequently, a commonality exists in those details considered to be important in making the two programs complementary. Commonality between the two programs was maintained for the following variables:

- Alloys, tempers, and thicknesses
- Specimen thicknesses and grain orientations
- Fastener types, diameters, and moduli
- Preparation of tapered and cold-worked holes
- Levels of interference and cold work
- Load profiles
- Bomber and fighter test spectra
- Test environments
- Ratio of far-field to bearing stress for load transfer

The scope of this program was structured into four elements as outlined below:

- Material characterization and failure criterion
- Constant-amplitude crack growth evaluations
- Spectrum load crack growth evaluations
- Fatigue evaluations of specimens without intentional flaws

Complete details of the technical items common to each program as well as a complete definition of each scope element are presented in the subsequent sections of this report.

1.1 Material Characterization and Failure Criterion Tests

The scope of the material characterization and failure criterion test program is summarized in Table 2. Tensile and compressive tests were performed for the long transverse grain direction to characterize the mechanical properties and generate stress-strain curves. The stress-

strain curves were used to derive strain hardening coefficients necessary to support the analytical treatment of cold-worked and interference-fit fastener holes. K_c was determined for one thickness of each alloy using the center crack specimen configuration. The thicknesses selected correspond to those used for the subsequently described crack growth and fatigue evaluations. The da/dN tests were performed for the same thicknesses. For purposes of this program, the da/dN tests were performed for the slow growth rate region (10^{-8} to 10^{-5} inch per cycle). Such tests also included the determination of a ΔK threshold value. All da/dN testing was performed for a center crack specimen configuration, a load ratio of 0.10 and a frequency of 10 cycles per second. Three failure criterion tests per alloy were performed to evaluate a possible failure criterion for cold-worked holes. All three specimens for a given alloy contained the same level of cold work. Prior to cold working, each respective specimen was precracked to produce small, intermediate and large through flaws. Testing of these was performed without fasteners installed.

1.2 Fatigue Tests for Fastener Holes without Intentional Flaws

Baseline fatigue tests were performed on specimens without intentional flaws to obtain natural crack origins, shapes and lives. These were performed for constant amplitude and spectrum load conditions. The constant amplitude test program is detailed in Table 3 for the aluminum alloy and in Table 4 for the titanium alloy. Each alloy required eight (8) specimens to obtain fatigue data on eighteen (18) test holes. The variables were selected duplications of ones employed in constant amplitude tests on specimens with cracked holes, but only one level of cold work and one level of interference were used in the unflawed fatigue tests. Tables 6 and 8 detail the spectrum test variables. Combined, these spectrum tests required thirty (30) specimens to obtain fatigue data for thirty-eight test holes. These also were selected duplications of conditions contained in the respective test plans for holes having intentional cracks. Only one level of cold work and one level of interference were included for these and the levels selected for each were the dominant ones in the test program.

1.3 Constant Amplitude Tests for Cracked Fastener Holes

The scope of the constant amplitude tests for cracked fastener holes in 2219-T851 aluminum alloy is detailed in Table 10 for part-through cracks and in Table 11 for through-the-thickness cracks, respectively. Similar details for 6A4-4V beta annealed titanium alloy are contained in Tables 12 and 13, respectively. In most cases, a duplicate test for each test hole condition was included for both aluminum and titanium alloys. A total of eighty-six (86)

test holes were specified for the aluminum alloy and were distributed in thirty-one (31) specimens. For the titanium alloy there were seventy-two (72) test holes distributed in twenty-five (25) specimens. In this program, corner crack evaluations were limited to small and intermediate size cracks only. However, large size cracks were included in the through crack evaluations. Three levels of cold working and three levels of fastener hole interference, presented in Tables 14 and 15, respectively, were used in these tests.

1.4 Spectrum Loading Tests for Cracked Fastener Holes

The scope of both the bomber and fighter spectra load evaluations for 2219-T851 aluminum alloy and 6 Al-4V beta annealed titanium alloy is presented in Tables 16 to 19 and 20 to 23, respectively. A total of one hundred and nine (109) test holes were defined for the aluminum alloy and were distributed in forty (40) specimens. For the titanium alloy, there were one hundred and three (103) test holes distributed in thirty-five (35) specimens. The detailed test plan was generally structured to evaluate the effectiveness of different levels of cold work and interference under spectrum loading. The plan for thru cracks also evaluated the relationship between crack size and loss of beneficial effects of interference and cold working. The same three levels of cold work and interference were used for both the constant amplitude and spectrum tests.

Duplicate tests were performed for all interference-fit fastener holes and cold-worked holes having small and intermediate initial flaw sizes.

2. ANALYTICAL PROGRAM

The purpose of the analytical program was to provide solutions for stress intensity factors appropriate to fastener hole cracks in order to judge whether the routine procedures of fracture mechanics are applicable for assessing the residual strengths and predicting the cyclic growth patterns of the cracks. Such a judgement was based on the results generated by the experimental program. The analytical program isolated the parameters significantly influencing the stress intensity factors for the flaw types shown in Figure 1, subject to the fastener hole conditions and loading conditions summarized in Table 24.

SECTION III EXPERIMENTAL PROGRAM

1. MATERIALS

Two different materials in plate form were employed in the experimental program, 2219-T851 aluminum alloy and 6Al-4V beta annealed titanium alloy. These alloys were selected to provide results complementing those obtained on a previous program⁽²⁾. The aluminum alloy plates had a nominal thickness of one-inch, a width of 72 inches and a length of 120 inches. Two plates were used and both were from Kaiser Lot Number 484881 with specified conformance to MIL-A-8920. The titanium alloy plates had a nominal thickness of 0.60 inch, a width of 55 inches and a length of 129 inches. The titanium plates were furnished by the Air Force and were reported to have been manufactured from the same heat by RMI. Also, the titanium was from the same heat used on a previously related program⁽²⁾ where the titanium was reported to be an extra low interstitial grade and annealed above the beta transus temperature. Three plates were used on the program reported herein.

A standard chemical analysis was performed on a sample of each alloy with the results in Table 25 showing the compositions to be within specification limits. Photomicrographs characterizing the microstructure of each alloy were also made and are shown in Figure 2. These were made in the plane of the plates. The Ti-6Al-4V microstructure showed a normal beta annealed basket weave structure of relatively coarse transformed beta while the 2219-T851 microstructure showed a normal solution treated and aged structure with an insignificant amount of dark undissolved Cu-Mg-Al constituent and several light Al-Cu-Mg particles. Rockwell hardnesses of both materials were also acceptable, $R_{\alpha} = 67$ for the Ti-6Al-4V and $R_{\beta} = 79.5$ for the 2219-T851. Additionally, standard tensile and compressive data in the LT grain direction were obtained for each alloy. This grain direction was selected to be compatible with all subsequent testing and was the one employed in Reference 2. These data are contained in Table 26. Both the tensile and compressive data for 2219-T851 exceeded MIL-HDBK-5 "B" values. The tensile data for Ti-6Al-4V was between MIL-HDBK-5 "A" and "B" values and the compressive yield strength was approximately equal to the "B" value.

2. TEST SPECIMENS

To evaluate the various combinations of variables contained in the experimental program, several different, but in many cases similar, test specimen configurations were required.

Configurations required for material characterization and failure criterion tests are shown in Figure 3. Those for evaluating flow growth at fastener holes are shown in Figure 4 and configurations for fatigue tests without intentional flaws are shown in Figure 5. All specimens were rectangular (except tensile and compression tests) with reduced test sections and had their longest dimensions or loading direction parallel to the longitudinal grain direction of the rolled plate material. Test section thicknesses were 0.375 and 0.450 inch for the titanium alloy and aluminum alloy, respectively. These thicknesses correspond to the ones used in the Reference 2 program. A unique serialization was established for each specimen and all variables associated with each specimen serialization were identified. This serialization was maintained throughout all operations, from a locational lay-out plan on the uncut plate material to the reporting of final data. The locational lay-out plan identified the location of each specimen and was used for cutting specimen blanks. The blanks then were machined to the desired lengths and widths. Next, a machining cut was made on each face of the blanks to produce the flatness necessary for precision machining of the test section and a straight specimen for testing. Once test section machining was complete, the specimens were prepared in accordance with their serialization. Except for material characterization specimens, this further preparation consisted of producing the various hole conditions described in the following section.

Two different specimen widths were used for the flow growth evaluations. The 4-inch-wide specimens were used for the small and intermediate size flaws and the 6-inch-wide specimens were used for large flaws. In order to minimize the test time and cost, and to gather the maximum amount of useful data, almost all specimens contained two or three test holes. To avoid interaction effects between cracks⁽³⁾, hole spacing was 3 inches in the 4-inch wide specimens used for evaluating small and intermediate cracks. Similarly, a 5-inch spacing was used for the holes having large cracks in the 6-inch-wide specimens.

The general philosophy used in combining more than one test hole in a specimen was comprised of the following principles:

- A particular specimen contained flaws of the same size.
- A particular specimen contained flaws of the same shape.
- A particular specimen contained fasteners of the same type.
- As-reamed open holes were only mixed with as-reamed holes filled with close-tolerance fasteners.
- Cold-worked holes were mixed with interference-fit fastener holes.

This philosophy was originally expected to ensure the collection of useful data from each hole contained in a particular specimen and to reduce the number of specimens required.

In fatigue tests without intentional flaws, the specimen configurations shown in Figure 5 were employed. Two of these configurations contain more than one test section. When one section failed, it was removed and testing was continued on the remaining specimen or specimens.

3. HOLE PREPARATION AND FASTENER INSTALLATION

Five different hole-fastener combinations were included in the experimental program as follows:

- 1) Reamed hole - open.
- 2) Reamed hole - filled with close-tolerance fastener.
- 3) Cold-worked hole - open.
- 4) Cold-worked hole - filled with close-tolerance fastener.
- 5) Tapered hole - filled with Taper-Lok fastener.

In addition to the above hole and fastener variables, three different levels of cold work were employed as well as three different Taper-Lok fastener interference levels.

Alloy steel fasteners having a nominal diameter of 3/8 inch were used in the aluminum alloy specimens. For the titanium alloy specimens, 5/16 diameter fasteners of Ti-6Al-4V STA were used. Fastener details are contained in Table 27. The fastener selection with respect to size and material was based on previous work reported in Reference 2.

Reamed holes for a given specimen alloy had the same final reamed diameter, which was that required to produce a close-fitting fastener without interference. Where close-tolerance fasteners were required, the fasteners were installed without preload.

Cold-worked holes were produced using the process referred to as the "Boeing Split Sleeve Method," in which a hole smaller than that required was drilled and then fitted with a split, steel sleeve. A mandrel larger than the hole was then drawn through the sleeve to cold-expand the hole to a larger diameter. The sleeve was then removed, followed by reaming the hole to final size. Current practice allows from 0.004 to 0.010 inch of

diametrical increase by the final reaming operation. Different amounts of cold work are produced by varying initial hole size and/or mandrel size. Three different levels of cold work were used, two of which were the same as the ones used in Reference 2. These two were approximately 5 percent and 4 percent, respectively. A lower value of 2 percent was selected as the third level. This lower level was selected since 5 percent is approaching the upper limit of the process with respect to allowable thickness variation in the hole vicinity and probability of circumferential cracking in some alloys. The detail dimensions of fastener holes during the cold-working operation are tabulated in Table 14 which include the initial hole diameter, mandrel diameter, sleeve wall thickness, diameter after relaxation and diameter after final reaming. In all cases this split in the sleeve was oriented 90 degrees away from the crack zone. Where close tolerance fasteners were required, the fastener was installed without preload as was done for the as-reamed holes.

The preparation of tapered holes was performed using standard cutters designed for use with the Taper-Lok fastener system. Final reaming was performed using a positive stop to ensure uniformity in size from hole to hole. The hole was sized such that, with the fastener installed, there was gripping area extending from each side of the specimen. This was required for cases specified to have load transfer. The fasteners were first pushed into the holes with finger-tight pressure. Installation was then accomplished using nut torque while monitoring axial movement with a dial indicator. When axial movement reached a value equivalent to the desired interference level, no further torque was applied. The nut was then loosened to relieve preload followed by re-tightening to a nominally low value. The dial indicator was monitored during this operation to ensure that no change in interference occurred. Three different interference levels covering the range generally used in production were employed for each material. These levels are defined in Table 15.

Since optical monitoring was to be performed during subsequent testing, in many cases the fastener heads were removed to enhance visibility of the test area. Since there was no fastener preload involved in the program, this was considered to have no influence on the results. In all cases a new fastener was used in each test hole requiring a fastener.

4. PRECRACKING PROCEDURES

Precracking of holes was performed by applying constant amplitude axial fatigue loads to the specimens in electrohydraulic servo controlled fatigue machines. In the selection

of precracking loads, specimen test requirements were always considered to ensure that the result of precracking would not retard the crack growth under the subsequent test conditions. The program encompassed small, intermediate, and large initial cracks of two different shapes: single symmetrical thru-the-thickness cracks and single quarter-circular part-thru cracks. Nominal initial sizes of these cracks were as follows:

Small	= 0.005 inch
Intermediate	= 0.050 inch
Large	= 0.150 inch

Various combinations of these initial crack sizes were produced for as-reamed straight shank holes, cold-worked holes, and tapered holes. For all thru-cracks, electrical discharge machining (EDM) was used to produce fatigue starter slots. For the intermediate and large sizes not requiring cold work, EDM was performed on the final reamed hole wall. Where small cracks were required, EDM was performed on a pilot hole. The pilot hole then was precracked to a length such that when the pilot was reamed to final size, the desired small flaw remained. This procedure was considered necessary to produce a short crack having reasonable symmetry through-the-thickness.

EDM also was used to produce starters for the intermediate and large corner flaws. Where cold working was not required, the starters were machined on the corner of final reamed holes. The size of the EDM starter was controlled to allow approximately 0.020 to 0.030 inch of precrack to produce the desired initial crack size. Since control and sharpness of the EDM are insufficient for the small corner flaws, an alternate method was used to produce crack starters on finished holes. Sharp notches were diamond ground in the hole edge at an angle of approximately 45 degrees. Grinding was accomplished using a razor blade in a slurry of 5-micron diamond paste. The total length of the notch was controlled to between 0.001 and 0.002 inch as measured on the surface. For all Taper-Lok installations requiring corner cracks, the crack was located on the fastener head side representing the largest hole diameter.

Where cold working was required, the crack starter was located on the hole to be cold worked, and precracking was accomplished prior to cold working. Initial precrack lengths were controlled to compensate for the final ream after cold working. The amount

of compensation required was determined during cold working of trial holes. All corner cracks for cold worked holes were located on the mandrel entrance side which would be the back surface with respect to the mandrel pull gun.

When precracking multiple hole specimens, fatigue cycling was initiated with all holes open or unfilled. All cracks did not initiate from the starters at the same time. The faster growing crack or cracks were retarded by filling the holes. In this manner reasonable control of initial crack size was accomplished.

5. TESTING PROCEDURES

5.1 Tensile and Compressive Tests

Tensile and compressive tests were performed using the appropriate standards recommended by ASTM. Testing was accomplished using a calibrated universal testing machine and extensometers were employed to measure specimen deformation under load in order to produce a recorded load versus deformation curve. For the tensile tests, these curves were determined to failure. From these tests, F_{cy} , F_{ty} , F_{tu} , and stress-strain curves were derived. Strain hardening coefficients, percent elongation and percent area reduction were also determined.

5.2 K_C Tests

Triplicate fracture toughness tests were performed for one thickness for each alloy. Center crack specimens were employed with the center crack being produced by fatigue from a through-the-thickness EDM slot. Testing was accomplished using a universal testing machine and the specimen was instrumented with a clip gage for recording crack opening displacement. K_C values were derived using the stress intensity factor solution for a center crack in a finite plate and validated using F_{ty} determined from the tensile tests.

5.3 Failure Criterion Tests

The failure criterion tests for cold-worked holes were conducted in the same manner previously described for the K_C tests. Specimens containing a single through crack emanating from level 1 cold-worked open holes were used in the tests.

5.4 Crack Growth and Fatigue Tests

The following procedures apply to crack growth and fatigue tests performed which include da/dN tests, fastener hole crack growth tests with intentional flaws and fatigue tests on fastener holes without intentional flaws.

All crack growth and fatigue tests were performed using electrohydraulic servo controlled test systems manufactured by the MTS Systems Corporation. Each system contained the necessary elements properly integrated to control the servo loop, program loads, monitor loads and perform failsafe functions. For constant amplitude tests, load monitoring was performed using a system calibrated amplitude measurement unit. A sine wave function generator was used to provide load command to the servo loop. Each test system was also interfaced to a digital computer which was used to provide load commands for the fighter and bomber test spectra.

All four inch wide specimens were loaded through hydraulically operated grips and the six-inch-wide specimens were loaded through fittings bolted to the ends. Specimens subject to buckling under compressive loads were fitted with lateral support bars to provide stability. These bars had Teflon film on the specimen side to minimize friction and fretting and were attached to prevent load transfer.

Where fastener load transfer was required, a beam arrangement was used to load the fastener in double shear as illustrated in Figure 6. The beams were connected to one grip through load reaction columns, which were instrumented with electrical-resistance strain gages to allow monitoring of load transfer. The effective stiffness of the beams could be varied to adjust load transfer to the desired amount. The amount of load transfer was held constant to provide a ratio of far-field to fastener bearing stress of approximately 1.0. This corresponds to a load transfer of approximately 10 percent for the aluminum specimens and 7 percent for the titanium specimens. This amount of fastener load transfer typifies the fasteners located at a spanwise splice in wing structures, a stringer run-out area, and a spar web to spar cap joint. An overall view of the test arrangement is shown in Figure 7.

The test sections of all fatigue and crack growth specimens were enclosed in clear, acrylic chambers to allow testing in dessicated air at ambient temperature, 70-80°F. The cyclic frequency was 10 Hz for all constant amplitude tests except the aluminum fatigue tests which were cycled at 15 Hz. The cyclic frequency was varied with load layer in the spectrum tests and ranged from 10 Hz for the low amplitude cycles to 1 Hz for the high amplitude cycles. The cyclic frequency for the da/dN tests was 20 Hz.

Crack length measurements were made on one surface using optical techniques. Filars and reference grills were used in conjunction with microscopes to provide measurement

sensitivities of 0.0002 inch and 0.001 inch, respectively. For constant amplitude tests, crack length measurements were made while holding at the mean load level. Measurements were made while holding at the end of flight mean level during the spectrum load tests.

If the far-field applied stress used in the constant-amplitude tests was maintained constant for the testing of all hole conditions, direct comparisons could be made from the test data. In order to grow a crack from a high level of interference or cold-worked fastener hole within a reasonable test time, a relatively high far-field stress was required. However, if the level of applied stress were too high, cracks may grow too fast at the open holes or close tolerance fastener holes with and without fastener load transfer. Also, a relatively high far-field stress may create a large yield zone around such holes which may affect the load redistribution and produce interactions between the cracked holes. In order to determine the optimum load level to be used in the constant amplitude load tests, several load levels were evaluated on through-cracked aluminum specimens. The final maximum load used for all constant amplitude load tests was 18 ksi for 2219-T851 aluminum specimens and 40 ksi for 6Al-4V beta annealed titanium specimens. The applied stress ratio, $R = \sigma_{\min} / \sigma_{\max}$, was 0.1. Those applied maximum stresses were about one-third of the yield strength of each material. Marker loads were applied periodically during the tests of the first two constant amplitude specimens by changing the applied load ratio ($R = 0.85$) and cyclic frequency, but maintaining the same maximum test load. Since the total growth band for the small and intermediate flaws was so narrow, the growth during each marking was limited to a very small amount, 0.0002 inch to 0.0005 inch. These marker loads did not produce a clear marking on the fracture surface. Therefore, no marker loads were applied in the remaining tests.

For the spectrum load evaluations, test spectra typical for a fighter and bomber were used. Table 28 defines the spectrum for the fighter and that for the bomber is defined in Table 29. The fighter profile for a flight is shown in Figure 8 as programmed by the Lockheed test system. Also shown is the sixth and eighteenth flight occurrences of load layers 65 and 66, respectively. The profile for the bomber is shown in Figure 9 for a standard flight along with the occurrences of load layers two and three. Layers 18, 28, and 29 were inserted in a similar fashion. These spectra were the same as those used in the Reference 2 program.

In addition to providing crack growth data, measurements of surface crack lengths during testing were used to control the test with respect to intentionally retarding the fast growing cracks and test termination. For test termination purposes the small, intermediate, and large flaws were grown to approximately 0.050 inch, 0.150 inch and 0.50 inch, respectively. Tests without intentional flaws were either fatigue tested to failure or testing was terminated when a natural crack was detected.

SECTION IV

RESULTS AND DISCUSSION OF EXPERIMENTAL TESTS

The original test plan was established to extend the large flaw evaluation program reported in Reference 2 to include small and intermediate flaws. The original plan included constant amplitude load tests, periodic overload tests and spectrum load tests. Since data scatter was anticipated, especially for small cracks emanating from inelastic regions, the periodic overload tests were replaced by the duplication of constant amplitude load tests and spectra load tests to allow an in-depth understanding of the growth behavior of small and intermediate cracks emanating from interference-fit fastener holes and cold-worked holes.

During the course of the test program, it was observed that one of the cracks grew much faster than the others in some multiple test hole specimens. During such tests, when the data in the desired range had been taken for the fastest growing crack, a small hole (1/8" - 3/16") was drilled at the crack tip and a Taper-Lok fastener was installed in an attempt to stop the growth of the fastest crack in order to collect more data from cracks at the other holes. Upon recycling, in most of the cases, the specimen failed at the section containing the fastest growing crack before all the desirable data at the other holes could be collected. To enhance the chance of collecting all the desired test data for those specimens where the test holes had not yet been prepared, the distribution of fastener-hole conditions was rearranged. Even so, only limited success was achieved. Extra specimens (those with specimen numbers ending in x) were defined to collect the desired test data.

The results of all tests are presented in this section. Wherever possible, data scatter of duplicate tests is shown and a comparison of the different types of fasteners and/or hole conditions is described and discussed in detail.

1. MATERIAL CHARACTERIZATION TESTS

The mechanical properties of each test material are presented in Table 26. The ultimate tensile strength, yield strength, and elongation (2 in. for aluminum and 1 in. for titanium), respectively, were 67.4 ksi, 54.3 ksi, and 11.3% for aluminum, and 135.6 ksi, 126.5 ksi, and 12.8% for titanium. The compressive yield strength was 58.4 ksi for aluminum and 138.2 ksi for titanium. Table 30 summarizes the results of the fracture toughness tests. The apparent fracture roughness was 46.3 ksi/ $\sqrt{\text{in.}}$ for aluminum, and 141.3 ksi/ $\sqrt{\text{in.}}$ for

titanium. However, it should be noted that the net section stress at fracture for the titanium specimens exceeded 80% of the yield strength of the material.

The baseline crack growth rate data for the T-L direction at $R = 0.1$ obtained from the constant amplitude tests are shown in Figure 10 for aluminum and in Figure 11 for titanium. The threshold ΔK obtained during the tests ranged from 1.03 to 1.99 $\text{ksi}\sqrt{\text{in.}}$ for aluminum and 2.77 to 3.69 $\text{ksi}\sqrt{\text{in.}}$ for titanium. The average threshold value of the maximum stress intensity factor, $(K_{\text{max}})_{\text{th}}$, was 1.7 $\text{ksi}\sqrt{\text{in.}}$ for aluminum and 3.7 $\text{ksi}\sqrt{\text{in.}}$ for titanium. The solid curves in Figures 10 and 11 are the least-square-mean line representations of all the data points shown. The curves are used in the subsequent analytical-experimental correlations.

2. UNFLAWED FATIGUE TESTS

2.1 Constant Amplitude Load Tests

The results of constant amplitude unflawed fatigue tests of aluminum specimens are contained in Table 3. These results are also shown in Figure 12. For aluminum specimens, nine (9) out of eighteen (18) test holes failed before any crack was observed. Two out of these nine failed in the grip section. Cracks were detected in the other nine test holes. These consisted of five (5) single corner cracks, two (2) double corner cracks, one (1) embedded flaw, and one (1) double corner crack located on the same side of the fastener hole. Post-test examination on seven failure surfaces indicated that the initial cracks (or origins) of these failures were three corner cracks, three embedded cracks and a surface crack away from the hole wall. The typical shape and origin of a natural crack originating at a close tolerance fastener hole and a natural crack originating at the surface away from an interference-fit hole are shown in Figure 13. Both test holes have about 10 percent fastener load transfer. Similar results for titanium specimens are tabulated in Table 4 and also Figure 14. For titanium specimens, twelve (12) out of eighteen (18) test holes failed before any crack was observed. One of these twelve failed in the grip section. The six detected cracks included four (4) single corner cracks and one (1) single and one (1) double thru crack. The number of cycles applied to each specimen and the dimensions of the cracks observed at the time the test was terminated are also included in the tables. Post-test examination on eleven failure surfaces showed that the initial cracks of these failures were six corner cracks and five embedded cracks. Table 5 summarizes the initial cracks of all constant amplitude fatigue tests on both aluminum and titanium specimens. From Table 5, it can be seen that for the fastener-plate combinations

considered in this program, the corners of unloaded fastener holes are the most common origins of natural cracks initiated due to fatigue, the shape of the observed natural cracks being approximately quarter elliptical with the major and minor axes coinciding with the hole wall and plate surface, respectively. The other common origins of natural cracks due to fatigue cycling are the hole wall surfaces of holes filled with close tolerance fasteners having fastener load transfer. The plate surface away from the hole for interference-fit fasteners is also a possible origin of natural crack.

For both the aluminum and titanium specimens subjected to identical loading conditions, the interference-fit fastener hole had the longest fatigue life. This may be because a higher level of interference (level 2) was used. The reason this level of interference was chosen is because it was the dominant one in the crack growth tests. For aluminum, the cold-worked hole shows a longer fatigue life than that of the close tolerance fastener hole. However, for titanium, the fatigue life of the cold-worked hole is comparable to that of the close tolerance fastener hole.

2.2 Spectrum Load Tests

The results of the unflawed fatigue tests for the 2219-T851 aluminum specimens subjected to the bomber spectrum loading are summarized in Table 6 and Figure 15. Similar results for the aluminum specimens subjected to the fighter spectrum loading are also summarized in Table 6 and Figure 16. Except for the reamed open holes, all test holes had fastener load transfer. Six (6) out of ten (10) test holes subjected to the bomber spectrum loading and five (5) out of eight (8) test holes subjected to the fighter spectrum loading failed before any crack was observed. The seven (7) observed natural cracks include two (2) single corner cracks, two (2) double corner cracks, one (1) single thru crack, and two (2) double thru cracks. These thru cracks were believed to have originated from embedded cracks. Six out of eleven failure surfaces subjected to both the bomber and the fighter spectra loading examined after the test showed that embedded flaws appeared to be the origin of such failures. The other five origins were at the corners of the fastener holes. The initial cracks (or origins) of all spectrum fatigue tests on aluminum specimens are summarized in Table 7. As seen from Table 7, both the corners and the hole wall surfaces of the fastener holes were the most common origins of observed natural cracks initiated due to spectrum fatigue tests.

The typical surfaces of natural cracks originating at a close tolerance fastener hole subjected to the bomber spectrum and cold-worked holes subjected to both the bomber and fighter spectra are shown in Figure 17. Table 6 indicates that for specimens having about 10 percent fastener load transfer, the level 1 cold-worked holes show fatigue lives comparable to those with close tolerance fastener holes. The test results of the same aluminum specimens subjected to 18 ksi constant amplitude loading (Table 3) indicated that the fatigue lives of the level 1 cold-worked holes with fastener load transfer were longer than those with close tolerance fastener holes having the same amount of fastener load transfer. Even longer fatigue lives were observed for the interference-fit fastener holes. This is partially because a higher level (level 2) of interference was used in the test program.

Similar fatigue test results on 6Al-4V beta annealed titanium specimens are summarized in Table 8 and Figure 18 for the bomber spectrum loading and in Table 8 and Figure 19 for the fighter spectrum loading.

Six (6) out of twelve (12) test holes subjected to the bomber spectrum loading and five (5) out of eight (8) test holes subjected to the fighter spectrum loading failed before any crack was detected. All observed natural cracks due to the bomber spectrum loading were either single or multiple corner cracks. The three observed cracks due to the fighter spectrum loading included two (2) single corner cracks and one (1) double thru crack. This double thru crack was found to have originated from a double embedded crack. Post-test examination on eleven failure surfaces indicated that the possible initial cracks (or origins) of these failures were nine corner cracks and two embedded cracks. Table 9 summarizes the initial cracks of all spectrum fatigue tests on titanium specimens. As seen from Table 9, the corners of the fastener holes are the most common origins of natural cracks initiated due to spectrum fatigue. From Table 8, it can be seen that the interference-fit fastener holes consistently gave longer fatigue lives than other types of tested holes. Level 1 cold-worked holes having fastener load transfer showed fatigue lives which were comparable to those for the same type of holes without cold working when they were subjected to the bomber spectrum loading. However, when the level 1 cold-worked holes were subjected to the fighter spectrum loading, their fatigue lives were significantly shorter than those for close tolerance fastener holes without cold working.

3. CRACK GROWTH TESTS

The results of the growth of intentional flaws tested on both 2219-T851 aluminum and 6Al-4V beta annealed titanium materials are presented and discussed in this section. For each material, the results were obtained for a combination of the following variables:

- 1) Loading profile: Constant amplitude, bomber spectrum, and fighter spectrum
- 2) Hole condition: Open, close tolerance, interference-fit, and cold-worked
- 3) Fastener load: with and without fastener load transfer
- 4) Level of interference or cold working: three each
- 5) Initial crack shape: quarter-elliptical corner cracks and through-the-thickness cracks
- 6) Initial crack size: small, intermediate, and large.

Since each specimen contained different fastener hole conditions with different initial crack lengths, a direct comparison of the results for the same type of specimen may not be meaningful. Therefore, key experimental results are rearranged and normalized to the same initial crack length according to each fastener hole condition.

Wherever possible, data scatter of duplicate tests are shown and the effects of the key variables are isolated and described in detail.

3.1 Constant Amplitude Load Tests

2219-T851 Aluminum Corner Crack Tests - The results of the corner crack tests for the 2219-T851 aluminum specimens are shown in Figures 20 through 25. Figure 20 shows the growth behavior of small corner cracks from open holes and close tolerance fastener holes with and without fastener load transfer in aluminum plates subjected to 18 ksi constant amplitude far-field loading. The differences between the values of the solid and open symbols represent the data scatter obtained from two duplicate tests. The pair of numbers shown inside the parentheses at the end of each set of data represent the final lengths of the crack. The first number corresponds to the crack length along the hole wall, a , and the second number corresponds to the crack length on the plate surface, c . These values were measured from the crack surfaces which were opened after testing. The final lengths of some fast growing cracks could not be measured because the crack surfaces were destroyed when the growth of these cracks was intentionally retarded in an attempt to collect more data from the slower growing

cracks in the same specimen. As seen from Figure 20, the growth rate at the hole having fastener load transfer is considerably higher than the growth rates of the other holes. The growth rates are about the same at an open hole and close tolerance fastener hole without fastener load transfer. Growth characteristics of intermediate corner cracks for three different levels (0.0024, 0.0038 and 0.0060 inch diametral) of interference for interference-fit fastener holes are presented in Figure 21. Based on the limited final flaw shapes obtained in the experimental program, it was found that the final flaw shape of all corner cracks emanating from interference-fit fastener holes without fastener load transfer was very close to quarter circular. In other words, the crack growth rates along the hole wall and the plate surface were about the same. However, with fastener load transfer, the crack growth rate along the plate surface becomes higher than that along the hole wall as reflected in the final dimensions shown in Figure 22 and Table 31. One may conclude, from Figures 21 and 22, that the test data scatter obtained from the tests of crack growth from interference-fit fastener holes is very large. The average data trend, however, indicates that the higher the amount of diametral interference, the slower the fatigue crack growth rate. The crack growth rate does not show any significant change when about 10 percent of the far-field applied load is reacted through the fastener. Figure 23 shows the similar growth behavior of intermediate corner cracks from various types of 2.2 percent cold-worked holes. There is no significant difference in the growth rate at cracked cold-worked open and close tolerance fastener holes. However, with fastener load transfer, its associated growth rate is higher than that of unloaded holes having the same amount of cold-working. The final flaw shape of corner crack emanating from cold-worked holes is very similar to that of straight reamed holes without cold-working. Figure 24 compares the growth of intermediate corner cracks from various levels of cold working. The detail dimensions during the cold-worked operation have been given in Table 14.

Figure 25 shows a comparison of the growth behavior of intermediate corner cracks from various types of fastener holes in 2219-T851 aluminum alloy plates subjected to 18 ksi constant amplitude loading. The data shown for the interference-fit fastener holes is the fastest growing one of duplicate tests. In general, with the preconditioning of a fastener hole, such as diametral interference or cold working, the crack growth rate is significantly lower than that of a straight reamed hole without preconditioning. The growth rate on the plate surface of a cold-worked hole is much less than that of an interference-fit fastener hole.

Another important observation involves the change in flaw shapes during the growth of corner cracks. For a straight reamed hole with or without cold working, the final dimension on the hole wall is almost always larger than the final dimension on the plate surface, especially for the cold-worked holes presented in Figure 26, which shows the typical surfaces of corner cracks emanating from a level 1 cold-worked open hole and level 1 cold-worked close tolerance fastener holes with and without fastener load transfer. For interference-fit fastener holes without fastener load transfer, the final flaw shape is close to quarter circular. For interference-fit fastener holes having fastener load transfer, the final dimension on the hole wall is less than that on the plate surface.

2219-T851 Aluminum Thru Crack Tests - During the course of selecting the optimum far-field stress to be used in the constant amplitude load tests, each of two specimens containing small thru cracks at three different types of straight reamed holes (open, close tolerance with and without fastener load transfer) were loaded at $R = 0.1$ and $\sigma_{max} = 28$ and 24 ksi, respectively. The results of these tests are shown in Figure 27. When the first specimen was loaded at 28 ksi, the crack at an open hole grew significantly slower than the one located at the close tolerance fastener hole without having fastener load transfer. This was somewhat unexpected. It is suspected that the high applied load created large yield zones around the test holes which may have affected the load redistribution and produced interactions between cracked holes. When the second specimen was loaded at 24 ksi, the pattern of crack growth was what one would anticipate based upon a linear analysis. However, there is still sizeable yielding around each test hole. To avoid such plasticity effects and after the examination of both the fighter and bomber spectra (the maximum root-mean-square stress of the fighter and bomber spectra are 14.18 and 17.84 ksi, respectively), 18 ksi was chosen as the far-field stress for all constant amplitude load tests for aluminum specimens.

The results of the constant amplitude load tests for the thru cracked aluminum specimens are shown in Figures 28 through 38. Figure 28 shows that the crack at a loaded fastener hole grew much slower than that of an open hole and unloaded close tolerance fastener hole. After the test, it was found that the fastener used in the one-hole specimen containing the loaded fastener hole (specimen no. A-CA-3x) gave a much tighter fit than was expected of the near-fit fastener hole. Due to this small amount of interference, its associated growth rate was reduced significantly.

Figure 29 shows the growth behavior of small thru-cracks emanating from three interference-fit fastener holes in a 2219-T851 aluminum specimen subjected to 18 ksi constant amplitude loading. The levels of interference were 0.0024" and 0.0038" with and without fastener load transfer. This specimen was designed to generate growth data over the range of small to large flaws. As can be seen from this figure, after 70,000 of the more than one-quarter million cycles were applied, all specimen flaws experienced practically no further growth. The initial growth increment shown may occur only on the surface due to the tunneling of the crack front during precracking and installation of an interference-fit fastener. This specimen was recycled later and after 770,000 cycles were applied, no crack extension was observed in any of the three holes. At 810,000 cycles, a crack at the 0.0024-inch interference-fit fastener hole grew to 0.55" on one surface of the plate but not on the other surface. At 822,000 cycles, it became a uniform thru crack and the specimen failed at 835,500 cycles while the cracks at the remaining two holes showed no growth at all. The results of the corresponding unflawed fatigue tests are also shown in the figure. It is believed that the effective maximum stress intensity factors at 0.0038" interference-fit fastener holes are below the threshold K_{max} . Therefore, these two test holes behaved like those of fatigue tests without intentional flaws.

Figures 30 and 31 compare the growth behavior of intermediate thru cracks from interference-fit fastener holes for three different levels of interference in 2219-T851 aluminum alloy plates subjected to constant amplitude 18 and 21 ksi far-field loadings, respectively. There were no significant differences in fatigue crack growth rates as a result of the introduction of the different diametrical interferences.

The growth behavior of intermediate thru cracks from level 3 interference-fit fastener holes in aluminum plate superimposed on the corresponding growth behavior for small thru cracks is shown in Figure 32. The transition from small thru cracks to intermediate thru cracks appears to be very smooth.

Figure 33 typifies the growth behavior of a small thru-crack emanating from a cold-worked hole. From this figure, it can be seen that the growth of the crack is far from uniform through the thickness of the plate. The crack grows much faster on the entrance side of the mandrel. In most cases, the crack growth on the exit side of the mandrel is completely retarded due to cold-working. The growth pattern of a small thru-crack emanating from a

cold-worked hole is very similar to that of a corner crack with a very large a/c ratio. This phenomenon was not observed in tests of large thru cracks emanating from cold-worked holes. One possible explanation is that, during the cold-working operation, the lip of the sleeve is pulled up against the edge of the hole on the exit side of the mandrel by the cold-working gun. Such an operation produces a higher than nominal residual compressive stress in the area where the lip of the sleeve makes contact with the plate. For a smaller flaw, the crack tip falls within this area. Therefore, the crack growth is retarded on the exit side of the mandrel. For a longer crack, the crack tip is located outside the affected region and the crack grows more or less uniformly through the thickness.

Figures 34 and 35 show the growth behavior of intermediate thru cracks from a 2.2% cold-worked open hole and 2.2% cold-worked close tolerance fastener holes with and without fastener load transfer in aluminum alloy plates subjected to 18 ksi far-field loading. Similar results for large initial cracks are presented in Figure 36. From Figures 34 through 36, one can see that the growth of a thru crack emanating from a 2.2% cold-worked open hole is slightly slower than the corresponding growth from the corresponding cold-worked hole having a close tolerance fastener. The effect of the 10% fastener load transfer on crack growth decreases with increasing crack length. When the crack length is beyond 0.15", the load transfer effect is completely negligible.

Figure 37 compares the growth rates of large thru cracks from 2.2%, 3.6% and 5.4% cold-worked open holes. As seen, the higher the level of cold working, the slower the fatigue crack growth rate. Figure 38 presents a comparison of the growth behavior of large thru cracks from various types of fastener holes in 2219-T851 aluminum alloy plates subjected to 18 ksi constant amplitude loading.

6Al-4V Beta Annealed Titanium Corner Crack Tests - The results of titanium corner-cracked specimens tested under constant amplitude 40 ksi far-field loading are presented in Figures 39 through 44. Figure 39 shows the growth behavior of small corner cracks from an open and close tolerance fastener holes. The experimental data scatter of two duplicate tests for the open hole specimen looks fairly large. However, most of the difference occurs in the region of small crack length only. When the crack length extends from small to intermediate size, such scatter becomes very small and the growth behavior is exactly what one would expect from the linear elastic fracture mechanics point of view, i.e., a crack at a loaded fastener hole grows faster than the corresponding ones at an open hole and on an

loaded close tolerance fastener hole as shown in Figure 40. Figure 41 shows the growth patterns of intermediate corner cracks from three different levels of diametrical interference (0.0034", 0.0042" and 0.0050") in titanium plate. Based upon surface measurements and the final crack dimensions measured from the opened crack surfaces, one may conclude that the level of interference (between 0.0034" and 0.0050") does not have a significant influence on the crack growth from interference-fit fastener holes. This phenomenon has also been observed for the aluminum material. The effect of fastener load transfer on the growth of intermediate corner cracks from 0.0042" and 0.0050" interference-fit fastener holes is shown in Figure 42. As can be seen, with fastener load transfer, the growth of the crack is slightly slower on the plate surface. The same behavior was observed in the test of aluminum specimen A-CA-3. Results for intermediate corner cracks emanating from 1.6% cold-worked holes with various types of fastener-hole conditions are shown in Figure 43. With fastener load transfer, the crack growth rate is higher as anticipated. Cracks at cold-worked open holes grew practically at the same rate as their counterparts in holes with the same level of cold work but filled with close tolerance fasteners.

Similar to the aluminum material, all titanium corner crack test holes were opened after the tests and the final dimensions (both surface and hole wall) of the cracks were measured. These measured values have been included in the appropriate figures. The final crack lengths of all the available test holes, which include both aluminum and titanium materials, are also tabulated in Table 31.

One unique feature observed from Table 31 is that for almost all interference-fit fastener holes, the final dimension on the surface is consistently larger than the corresponding one on the hole wall. However, for cold-worked and straight reamed holes, the final crack length on the surface is smaller than the corresponding one on the hole wall.

Figure 44 compares the growth behavior of intermediate corner cracks from various types of fastener holes in 6AL-4V beta annealed titanium alloy plates subjected to a constant amplitude loading of 40 ksi and $R = 0.1$. As seen from the figure, the growth of a corner crack is the slowest at an interference-fit fastener hole, followed by a cold-worked hole, close tolerance fastener hole and open hole.

6Al-4V Beta Annealed Titanium Thru Crack Tests - The experimental results for the titanium thru crack specimens tested under 40 ksi constant amplitude loading and $R = 0.1$ are presented in Figures 45 through 52. Figure 45 shows the growth characteristics of small thru cracks from an open and close tolerance fastener holes with and without fastener load transfer in 6Al-4V beta annealed titanium alloy plates. As previously mentioned, the amount of fastener load transfer was chosen so that the ratio of the resulting bearing stress and the far-field applied stress was about 1.0. Therefore, the percentage of the applied load which was transferred through the fastener was dependent upon the fastener hole diameter and the width of the specimen. For a 4" wide specimen, the amount of load transferred through the fastener was about 10% in each loaded aluminum specimen and 7% in each loaded titanium specimen due to the difference in hole diameters. Therefore, the effect of fastener load transfer on the crack growth rates in the titanium specimens was not as severe as in the aluminum specimens. This is reflected in the results shown in Figure 45. Figure 46 shows the growth of small and intermediate thru cracks from levels 1 and 3 (0.0034" and 0.0050") interference-fit fastener holes in titanium plates subjected to 40 ksi constant amplitude loading. For crack lengths larger than 0.05 inch, the growth rates are practically the same for both levels of interference-fit fastener holes. Figure 47 shows the growth behavior of small thru cracks from level 2 interference-fit fastener holes with and without fastener load transfer in titanium plates. The results of these tests indicate that the crack growth rate decreases considerably with fastener load transfer. After reexamination of the test records, it was found that both load transfer specimens (T-CA-11 and T-CA-12), each containing three interference-fit fastener holes (see Table 15), failed in the grip section. Because of the damage in the grip section, the effective load the crack tip experienced could be far less than planned, resulting in much slower crack growth. The crack growth rates of level 2 interference-fit fastener holes without fastener load transfer are very comparable to those shown in Figure 46 for levels 1 and 3 interference-fit holes.

The results of the constant amplitude tests for the titanium specimens containing thru-cracked cold-worked holes are presented in Figures 48 through 52. Figure 48 shows the crack growth of six thru cracks from level 1 cold-worked open holes in titanium plates subjected to 40 ksi constant amplitude far-field loading. The initial crack lengths used in these tests included small, intermediate and large cracks. The origins of each data set having initially intermediate and large cracks are so located that the estimated time required to grow the crack

from small initial size to the largest crack length obtained during these tests will be conservative. Similar results for thru cracks from level 1 cold-worked close tolerance fastener holes with and without fastener load transfer are given in Figures 50 and 49, respectively. As seen from Figures 48 through 50, the effect of initial crack size on the growth behavior of thru cracks from various types of level 1 cold-worked holes is fairly small. For a neat-fit hole having fastener load transfer, the crack grew somewhat faster than the corresponding crack at a neat-fit hole without fastener load transfer. However, the crack at an open and neat-fit cold-worked hole shows practically no difference in growth rate. Figures 51 and 52 show the growth behavior of thru cracks for two higher levels of cold working for open holes. For a large initial crack, the growth rate of the first small increment of growth is considerably smaller than the corresponding growth rate extended from a small initial crack. This growth characteristic was not observed in the tests of the lowest level of cold-worked holes.

3.2 Bomber Spectrum Load Tests

2219-T851 Aluminum Corner Crack Tests - The results of the corner crack tests for the aluminum specimens subjected to standard severity bomber spectrum loading are presented in Figures 53 through 60. Figure 53 shows the growth behavior of small corner cracks from an open hole and close tolerance fastener holes with and without fastener load transfer. Similar data obtained from the testing of large initial cracks reported in Reference 2 are also included in the figure. These large crack data extend the small crack data generated under this program quite well. As anticipated, the crack grew faster from the loaded fastener hole than those from an open hole and close tolerance fastener hole without fastener load transfer. Figure 54 compares the crack growth of intermediate corner cracks for three different levels of interference-fit fastener holes in 2219-T851 aluminum alloy plates subjected to the bomber spectrum loading. The levels of diametrical interference used in the bomber spectrum load tests are exactly the same as those used in the constant amplitude load tests. Two data points reported in Reference 2 from the testing of a large corner crack emanating from a level 2 interference-fit fastener hole are also included in Figure 54. The trend of the data clearly shows that the larger the amount of interference, the slower the fatigue crack growth rates. Figure 55 shows the effect of fastener load transfer on the crack growth behavior of intermediate corner cracks from level 2 interference-fit

fastener holes in aluminum specimens subjected to the bomber spectrum loading. One set of test data generated in Reference 2 is also shown as solid star symbols in the figure. The growth characteristics of intermediate corner cracks from various types of level 1 cold-worked holes in 2219-T851 aluminum alloy plates subjected to the bomber spectrum loading are shown in Figure 56. The crack at the loaded cold-worked hole grew the fastest, followed by the neat-fit cold-worked hole and then the cold-worked open holes. A similar trend was observed in the constant amplitude tests of cold-worked fastener holes. Figure 57 compares the crack growth of intermediate corner cracks from level 1 and level 2 cold-worked open holes. Comparisons of the growth behavior of corner cracks from two different levels of cold-worked open holes and compatible levels of interference-fit fastener holes are shown in Figures 58 and 59. Considering the scatter of experimental test data, the growth rates are practically the same for intermediate corner cracks from the same level of cold-worked hole and interference-fit fastener hole. These growth rates are slower than the corresponding rates at straight shank reamed holes without preconditioning as given in Figure 60.

2219-T851 Aluminum Thru Crack Tests - The results of the tests for thru-cracked aluminum specimens subjected to the bomber spectrum loading are given in Figures 61 through 69. Figure 61 shows the growth behavior of small thru cracks from an open hole and close tolerance fastener holes with and without fastener load transfer in aluminum plates subjected to the bomber spectrum loading. The growth of intermediate thru cracks from interference-fit fastener holes for three different levels of interference is shown in Figure 62, in which the growth of a crack at a level 3 interference-fit fastener hole grew somewhat faster than the corresponding crack at a level 2 interference-fit hole obtained from a different specimen. Figure 63 compares the crack growth of intermediate thru cracks from level 2 interference-fit fastener holes with and without fastener load transfer.

Figures 64 through 66 present the results of five similar tests on aluminum specimens containing level 1 cold-worked open and close tolerance fastener holes with and without fastener load transfer, respectively, subjected to the bomber spectrum loading. Data scatter is largest when fastener load transfer is present. In general, for a same type of fastener-hole condition, data scatter increases with decreasing initial crack length. The growth rates for cracks originating at cold-worked open and close tolerance fastener holes

are practically the same, while cracks at loaded fastener holes have faster growth rates. Figure 67 compares the crack growth of large thru cracks from three different levels of cold working for open holes in 2219-T851 aluminum alloy plates subjected to the bomber spectrum loading. As seen from the figure, when the level of cold working increases, the crack growth life increases. The crack growth of intermediate thru cracks from level 2 interference-fit and level 2 cold-worked holes are compared in Figure 68. Figure 69 summarizes a comparison of the growth characteristics of small thru cracks from various types of fastener holes in 2219-T851 aluminum alloy plates subjected to the bomber spectrum loading. It is clear that both cold working and diametrical interference have offered a significant benefit by retarding the fatigue crack growth under the bomber spectrum loading, especially when the crack length is less than 0.15 inch.

6Al-4V Beta Annealed Titanium Corner Crack Tests - Figures 70 through 76 show the growth behavior of corner cracks from various types of fastener holes in 6Al-4V beta annealed titanium plates subjected to the bomber spectrum loading. During the testing of specimen no. T-B5-1, which contains an open hole and close tolerance fastener both with and without fastener load transfer, the crack at the loaded close tolerance fastener hole grew much faster than the other two holes after the crack extended from 0.01 inch to about 0.1 inch. The test results of large cracks reported in Reference 2 are also included in Figure 70 for straight reamed holes and in Figure 71 for level 1 (0.0034 inch diametrical) interference-fit fastener holes. Figure 72 compares the growth behavior of intermediate corner cracks from interference-fit fastener holes for three different levels of interference in titanium alloy plates subjected to the bomber spectrum loading. As seen from Figure 72, the cracks for the two higher levels of interference grew much slower than the corresponding cracks for the level 1 interference which showed a large amount of data scatter. The results of duplicate tests for intermediate corner cracks from level 1 cold-worked open holes and close tolerance fastener holes with and without fastener load transfer are shown in Figure 73. The cracks grew fastest for the loaded fastener holes. The cracks at the cold-worked open and close tolerance fastener holes without fastener load transfer showed comparable growth rates. When the amount of cold working increases, the fatigue crack growth rates decrease. This is reflected in Figure 74, which shows the growth of intermediate corner cracks from cold-worked open holes for three different levels of cold working in titanium alloy plates subjected to the bomber spectrum loading. Comparisons of the

crack growth behavior of intermediate corner cracks from the comparable cold-worked holes and interference-fit fastener holes are shown in Figures 75 and 76. In general, data obtained from the testing of cracks from interference-fit fastener holes show a larger amount of scatter than data for cold-worked holes.

6Al-4V Beta Annealed Titanium Thru Crack Tests - The results of the thru crack tests for titanium specimens subjected to the bomber spectrum loading are presented in Figures 77 through 84. Figure 77 shows the crack growth behavior of small thru cracks from an open hole and close tolerance fastener holes with and without fastener load transfer in 6Al-4V beta annealed titanium alloy plates. Figure 78 compares the growth behavior of intermediate thru cracks from both level 2 and level 3 interference-fit fastener holes. The test data show that the cracks at the higher level of interference grew slower than the corresponding cracks at lower level of interference. Specimen No. T-85-10 contained intermediate thru cracks at three level 2 interference-fit fastener holes. One of the holes had fastener load transfer. When this specimen was subjected to the bomber spectrum load, the crack at the loaded hole grew slower than the cracks at the other holes, as illustrated in Figure 79. The other two test holes show practically no difference in growth rates. Figures 80 to 82 show the results of four similar tests on titanium specimens containing small to large initial through cracks at a level 1 cold-worked open hole and close tolerance fastener holes with and without fastener load transfer, respectively. The data scatter is relatively small in comparison to that of interference-fit fastener holes. From these three figures, one can see that the cracks at the cold-worked holes having fastener load transfer grew faster than the corresponding cracks at the cold-worked open holes, while the cracks at the neat-fit cold-worked holes grew the slowest. The growth behavior of large thru cracks from three different levels of cold working in titanium plates subjected to the bomber spectrum loading is shown in Figure 83. The trend of the crack growth behavior is exactly as anticipated, i.e., the higher level of cold working results in the slower fatigue crack growth rates. Figure 84 compares the growth of intermediate thru cracks from level 2 cold-worked open holes and level 2 interference-fit fastener holes in titanium alloy plates subjected to the bomber spectrum loading. The growth rates for these two different types of preconditioned fastener holes are practically the same.

3.3 Fighter Spectrum Load Tests

2219-T851 Aluminum Corner Crack Tests - The results of the tests for the aluminum corner cracked specimens subjected to a standard severity fighter spectrum loading are presented

in Figures 85 through 89. Figure 85 shows the growth behavior of small corner cracks from an open hole and close tolerance fastener holes with and without fastener load transfer. Data obtained from the testing of initial large corner cracks reported in Reference 2 are also included in the figure. The growth rates of the cracks at the open hole and the close tolerance fastener hole having about 10% fastener load transfer are about the same, while the crack at the close tolerance fastener hole without fastener load transfer shows significantly slower growth rates than the other two. Figure 86 shows the crack growth behavior of small and intermediate corner cracks from interference-fit fastener holes for three different levels of interference in aluminum plates subjected to the fighter spectrum loading. These test results include two intermediate corner cracks from level 2 interference-fit fastener holes having about 10% fastener load transfer. As seen from this figure, the higher the amount of diametrical interference, the slower the fatigue crack growth rate. Also, a small amount of fastener load transfer results in faster growth rates. Figure 87 shows the growth characteristics of intermediate corner cracks from various types of level 1 cold-worked fastener holes in aluminum plates subjected to the fighter spectrum loading. Figure 88 compares the test results of intermediate corner cracks from level 1 cold-worked holes and level 1 interference-fit fastener holes. The growth rates obtained from the tests of cracks at these two different types of preconditioned fastener holes are approximately equal. However, these growth rates are considerably slower than the corresponding rates at straight reamed open holes as shown in Figure 89.

2219-T851 Aluminum Thru Crack Tests - The results of the tests of aluminum thru crack specimens subjected to the fighter spectrum loading are presented in Figures 90 through 97. Figure 90 shows the growth behavior of intermediate thru cracks from an open hole and close tolerance fastener holes with and without fastener load transfer. The cracks at the open hole and unloaded neat-fit fastener hole show practically the same growth rates, while the crack at the loaded neat-fit hole grew much faster than the others. The crack growth behavior of intermediate thru cracks from interference-fit fastener holes for three different levels of interference in aluminum plates subjected to the fighter spectrum loading is shown in Figure 91. When the amount of diametrical interference increases, the fatigue crack growth rates decrease rapidly. The data scatter obtained from the tests of four level 3 interference-fit fastener holes is fairly large as can be seen from Figure 92. Similar results obtained from five separate tests of initially small to large thru cracks from various types of level 1 cold-worked holes are shown in Figures 93 through 95. In general,

this data scatter is considerably larger than that from all other tests. After the testing was completed, the crack surfaces were opened. Typical markings on the crack surfaces are shown in Figure 96. Based on the examination of the fracture surfaces, it is believed that, when the initial crack length is small (well within the residual compressive zone resulting from cold working the hole), the influence of the residual compressive stresses is stronger than the retardation effect created by the tensile overload during the application of the fighter spectrum load. However, when the initial crack length is large, some acceleration occurs during the first few increments of crack growth, followed by slower growth. The markings of the crack surface for the initially large crack (Figure 96) clearly show that the spacings of the first three markings, corresponding to the first three blocks of flights of the fighter spectrum loads, are wider than the subsequent ones. Each block consists of six flights. After the application of the first 18 flights, the retardation effect due to the high overload plays more and more an important role than the residual compressive stresses created during the cold working operations. After the first few increments of crack growth, the subsequent growth of the crack becomes stable, and the growth behavior is more or less what one would anticipate. Such growth behavior was not observed during the bomber spectrum load tests. This may be because the fighter spectrum has a higher overload ratio than that of the bomber spectrum. Figure 97 shows the growth behavior of small thru cracks from three level 2 cold-worked open holes in aluminum specimens subjected to the fighter spectrum loading.

6Al-4V Beta Annealed Titanium Corner Crack Tests - The results of the corner crack tests for 6Al-4V beta annealed titanium alloy plates subjected to the fighter spectrum loading are presented in Figures 98 through 102. During the testing of specimen T-FS-1, the crack at the loaded close tolerance fastener hole grew much faster than the cracks at the other two test holes. The specimen failed through the first test hole before enough data could be obtained on the other test holes. The results of this test are shown in Figure 98. Figure 99 shows the growth behavior of intermediate corner cracks from interference-fit fastener holes for three different levels of interference and Figure 100 shows similar results of intermediate corner cracks from level 2 interference-fit fastener holes with and without fastener load transfer in titanium alloy plates subjected to the fighter spectrum loading. The data presented in these two figures show a fairly large amount of scatter and no consistent relationship can be established between the level of interference and its associated fatigue crack growth rate. Test results obtained from the testing of corner cracks from various

cold-worked fastener holes are shown in Figures 101 and 102. For the same level of cold working, the crack at a loaded hole grew consistently faster than the corresponding cracks at an open hole and unloaded neat-fit hole. The results shown in Figure 102 indicate that, when the amount of cold working increases, the associated fatigue crack growth rates decrease.

6Al-4V Beta Annealed Titanium Thru Crack Tests - Figures 103 through 109 present the results of thru crack tests on titanium specimens subjected to the fighter spectrum loading. Figure 103 shows the growth behavior of small thru cracks from an open hole and close tolerance fastener holes with and without fastener load transfer. After the application of 325 flights on specimen T-FS-9, which contained three interference-fit fastener holes having initially small thru cracks, all three cracks showed practically no growth. It is believed that the maximum effective stress intensity factors for these small cracks was below the threshold K_{max} . Figure 104 compares the crack growth of intermediate thru cracks from level 2 interference-fit fastener holes with and without fastener load transfer, while Figure 105 presents the results of four tests of small to intermediate thru-cracks from level 3 interference-fit fastener holes in titanium alloy plates subjected to the fighter spectrum loading.

The crack growth behavior of small to large initial cracks from level 1 cold-worked holes in 6Al-4V beta annealed titanium alloy plates subjected to the fighter spectrum loading is shown in Figure 106 for open holes and in Figures 107 and 108 for close tolerance fastener holes with and without fastener load transfer, respectively. The amount of data scatter is large, but it is not as large as the scatter obtained from the fighter spectrum loading tests on the aluminum specimens. Figure 109 shows the growth behavior of intermediate thru cracks from two level 2 cold-worked open holes. By comparing this figure with Figure 106, it is clear that increasing the amount of cold working leads to substantially slower growth rates.

4. FRACTURE TESTS OF FLAWED COLD-WORKED HOLES

A failure criterion which could accurately predict the failure of flawed structures would be a useful engineering tool for the evaluation of structural integrity and the selection of materials. Linear elastic fracture mechanics provides a one-parameter failure criterion, K_{IC} , for cracked structures with small-scale yielding. However, for a crack emanating from a cold-worked hole, due to the presence of the large plastic strains induced during cold-working process,

It may be that the failure cannot be characterized completely by linear elastic fracture mechanics.

Three specimens, each containing various initial crack lengths at level 1 cold-worked open holes, were tested in the same manner as those used in the K_{IC} tests, for both the 2219-T851 aluminum and 6Al-4V beta annealed titanium materials. The results of these tests are tabulated in Table 32.

5. THRESHOLD CRACK LENGTHS

It is generally accepted that the stress intensity factor controls the rate of propagation of a fatigue crack. Any cracked structure can be expected to respond in a predictable manner to a given load cycle if its associated stress intensity factor is available. Such a response usually is in the form of an increment of crack growth. Therefore, for predictive purposes, the basic constant amplitude crack growth rate data is presented in the form of the instantaneous crack propagation rate, da/dN , as a function the stress intensity range, ΔK . In this relationship, there is a threshold value of ΔK , say ΔK_{th} , below which a cracked structure does not have measurable crack extension due to fatigue cycling.

Normally, the crack growth rate data show some scatter, and the least-square mean line representation of all the test data is used to establish the da/dN vs. ΔK relationship. For a given ΔK , the scatter of its associated growth rate normally will increase as the value of ΔK decreases, especially when ΔK approaches ΔK_{th} . This is illustrated in Figures 10 and 11. The value of ΔK_{th} observed during the baseline crack growth rate tests ranged from 1.1 to 1.9 $\text{ksi}\sqrt{\text{in.}}$ for the aluminum alloy, and from 2.8 to 3.7 $\text{ksi}\sqrt{\text{in.}}$ for the titanium alloy.

In the crack growth tests, if the crack size is so small or the applied load is so low that the stress intensity factor range is smaller than ΔK_{th} , one would anticipate that the crack will not grow, and the growth behavior of such a crack would be essentially the same as that of a fatigue test without any intentional flaw. In the duplication of such a test, the data scatter would be very large. Conversely, if the resulting stress intensity factor range is much larger than ΔK_{th} , the data scatter in the duplicate tests would be small. The amount of data scatter increases as ΔK decreases and approaches ΔK_{th} . If the resulting ΔK is close to ΔK_{th} , one may anticipate that

two identical cracks under the same loading condition might show a completely different growth behavior, e.g., one crack might grow in the same manner as a crack with a large ΔK value while the other identical crack might show practically no growth.

Based upon the above discussion, one may conclude that the stress intensity factor range is the primary parameter which controls the growth patterns of small cracks (small cracks normally result in small ΔK values unless the applied load is abnormally high). This is clearly reflected in the data generated under the present test program. As discussed in the previous section, some cracks grew much faster than the others in the multiple-test-hole specimens. Although efforts were taken to collect more data from these slower growing cracks, only limited success was achieved. Instead of eliminating these very limited growth data, they are used in this section to establish the minimum flaw size such that, under the same loading condition, the crack will not grow. From these data, one can qualitatively correlate the different fastener hole combinations tested with the approximate stress intensity factor solutions.

The stress intensity factor for a given cracked geometry normally depends upon the geometry, the size of the crack and the applied load. However, for cracks emanating from inelastic fields such as cold-worked or interference-fit fastener holes, K also depends upon the level of cold work or interference, δ/d , the material yield strength, σ_y , Young's modulus, E , and Poisson's ratio, ν . For a given crack geometry, the stress intensity factor can be written in the following general form:

$$K = \sigma \sqrt{\pi a} \beta_T \quad (1)$$

where β_T is the total correction factor which, in general, is comprised of the linear product of a series of correction factors. For a given fastener hole configuration, the β_T factor only varies with the crack length a .

For a given fastener hole configuration and applied load, when the crack extends a small increment Δa , its associated stress intensity factor can be determined from that of the previous increment by using Equation (1), or

$$K_{a+\Delta a} = \sqrt{\frac{a+\Delta a}{a}} \frac{\beta_T(a+\Delta a)}{\beta_T(a)} \cdot K_a \quad (2)$$

If an increment Δa is small in comparison to the crack length a , then one may assume that the change of the total correction factor is negligible, and Equation (2) can be reduced and rearranged as

$$K|_a = \left(\frac{a}{a + \Delta a} \right)^{1/2} \cdot K|_{a + \Delta a} \quad (3)$$

If the crack length a is close to the "threshold a " for a given constant amplitude load spectrum, then Equation (2) can be used to estimate the "threshold a " with a knowledge of K_{th} and the approximate K solution at crack length a_m from the following equation:

$$a_{th} = a_m \left(\frac{K_{th}}{K_m} \right)^2 \left(\frac{\beta_T(a_m)}{\beta_T(a_{th})} \right)^2 \quad (4)$$

If the difference between a_{th} and a_m is very small, then the difference in the total correction factor, β_T , can be neglected and Equation (4) is reduced to

$$a_{th} = a_m \left(\frac{K_{th}}{K_m} \right)^2 \quad (5)$$

The stress intensity factor K_m may be estimated from very slow crack growth test data by using the fatigue-crack-growth method of calibrating the measured crack growth rate, da/dN , and the stress intensity factor range, ΔK .

Table 33 shows the estimated threshold crack lengths using Equation (5) for both corner cracks and through cracks at various types of fastener holes in 2219-T851 aluminum alloy plates subjected to 18 ksi far-field loading. Similar results for 6Al-4V beta annealed titanium alloy plates subjected to 40 ksi far-field loading are shown in Table 34. The threshold values of the maximum stress intensity factors used in the calculations are 1.7 ksi $\sqrt{\text{in.}}$ for aluminum, and 3.7 ksi $\sqrt{\text{in.}}$ for titanium. The computed stress intensity factors for a through crack from an open hole using the estimated threshold crack lengths and Bowie's hole correction factors are 1.85 ksi $\sqrt{\text{in.}}$ for the aluminum specimens and 5.31 ksi $\sqrt{\text{in.}}$ for the titanium specimens. The computed K_{th} agrees very well with the test data for the aluminum material, but is too high for the titanium material. This is because a_m (0.022") measured in the test for the titanium material is much larger than a_{th} . If the Bowie factors, $B_1(a_m) \cdot B_1(a_{th})$, were used to account

for the large difference in the crack lengths, then the new computed a_{th} would be 0.0027" which results in the stress intensity factor of 3.90 ksi $\sqrt{\text{in.}}$. This value agrees very well with the data.

Based on the computed threshold crack lengths for the far-field stresses used in the test program, the following conclusions may be drawn:

- 1) For the same fastener hole configuration, values of a_{th} for through cracks are smaller than those for part-through cracks.
- 2) For the same type of crack, values of a_m for fastener holes having residual strains, such as interference-fit or cold-worked holes, are larger than those for reamed holes without residual strains. Values of a_{th} increase with an increase in the amount of fastener-hole interference or cold working, especially for aluminum specimens.
- 3) For the aluminum specimens, the cold-working operation retards the propagation of small cracks more efficiently than interference-fit fastener holes. However, for titanium specimens, the interference-fit fastener holes perform slightly better than cold-worked holes in retarding the growth of small cracks.

It should be noted that a_{th} does not depend upon the fastener-hole configuration alone, but also upon the level of the applied load. Therefore, it may not be too meaningful to define a_{th} without coupling it with the applied loading.

If a procedure can be developed to represent a spectrum loading with constant amplitude loading which produces an equivalent damage (crack growth), then the aforementioned approach can be used to determine the threshold crack length for any fastener hole configuration subjected to spectrum loading. For any flawed fastener hole, if the initial flaw size is smaller than the threshold crack length for a given load spectrum, then one may anticipate that the flawed fastener hole will behave practically in the same manner as a fastener hole without an intentional flaw when subjected to same spectrum fatigue loading.

SECTION V

ANALYTICAL PROGRAM

This section contains two steps for estimating an opening mode stress intensity factor for a given crack geometry, hole condition, and load combination. The first step describes and illustrates the procedures used for obtaining the unflawed elastic-plastic stress field for interference-fit fasteners and cold-worked holes subsequently subjected to uniform far-field stress with and without fastener loading. The second step summarizes the stress intensity factor solutions for cracks emanating from fastener holes presented in Figure 1. Possible failure criteria for cracked cold-worked holes and crack growth predictions are also presented.

1. STRESS ANALYSIS FOR UNFLAWED FASTENER HOLES

Cracks or crack precipitating flaws will be introduced in aircraft structure either during manufacturing or service which, later on, create fatigue problems. The majority of such structural problems can be traced to fastener joints where high stress concentrations are located. In order to improve the fatigue (or crack initiation) life, fastener systems using the concept of beneficial residual stresses have been used in more sophisticated aircraft design practices. The concept is that sometime during the fastener installation and hole preparation processes, some form of interference is introduced to induce fatigue improving residual stresses around the fastener hole. Such fatigue improvement fastener systems can generally be classified in one of the following two classes:

- 1) Interference-fit fasteners in which the fastener shank is pressed into a hole smaller in diameter than the shank, and
- 2) Cold-worked holes in which an oversized mandrel is pulled through a fastener hole, cold working the hole in the process.

The finite element displacement method was principally used to obtain the unflawed stress distributions for the test specimens containing such interference-fit and cold-worked fastener holes used in this program. The computer program, INLAP, a modified version of the one reported in Ref. 4, analyzes a structural model for plane stress plastic deformation

occurring as a result of concentrated forces applied at the joints of the finite element model and/or imposed joint displacements. The nonlinear (plastic) behavior is approximated by an incremental iterative scheme described fully in the referenced report.

Briefly, this scheme consists of the following:

- (a) an increment of load (and/or displacement) is applied to the model;
- (b) all model joint displacements are computed and element stresses found;
- (c) each element is then checked (von Mises energy-of-distortion) to determine if yield (plastic deformation) has initiated, or if once initiated is continuing;
- (d) plastic strains are estimated for those elements past yield from either bi-linear (see Figure 111), Ramberg-Osgood or Goldberg-Richard uniaxial stress-strain curves and the Prandtl-Reuss flow law,
- (e) with the load increment held constant and with the new estimated values of the plastic strains, the analysis is iterated through steps (b), (c), and (d) until the changes in plastic strains from the previous iteration all are smaller than a user-set convergence tolerance.
- (f) the load increment is increased (decreased if unloading of applied loads/displacements is studied) and steps (a) through (e) are repeated.

Step (f) is continued until all loads/displacements are applied (or removed) from the finite-element model.

For the analyses of the specimens tested during the period of this contract, the computer program, INLAP, was changed to allow an analyst to apply a sequence of sets of loads and/or displacements to the structural model of the test. Thus, analyses which closely corresponded to the laboratory sequences were performed. For instance, the single program execution sequence used to calculate the stresses for the cold-worked hole tests consisted of three distinct steps. In the first step, a radial expansion, representing the insertion of the cold-working mandrel/sleeve combination, was imposed onto the joints defining the hole in the finite-element model of the doubly symmetric test specimen as shown in Figure 110 which consisted of 232 nodes and 397 constant strain triangular

elements. In the second step, the equivalent radial forces necessary to produce the hole expansion (including plastic deformation) were computed, the hole displacements imposed in step 1 were removed, and the equivalent forces (applied to the appropriate joints around the hole) were then relaxed (unloaded) to zero. Steps 1 and 2 simulated the expansion-relaxation sequence of a hole in a typical specimen. In the third and last analysis step, with the hole edge unloaded, upward-vertical loads were applied and then relaxed along the top edge of the model of Figure 110 to represent the application of uniform uniaxial tension fatigue cycles to the specimen. At convenient increments in all three steps of the analysis sequence, model element stresses were computed and printed. The cyclic stress-strain relationship used for the aluminum alloy models is given by the curve on Figure 111. The actual bilinear representation used in the analyses is indicated by the dashed lines on that figure. For the titanium models, a similar curve was used with an initial elastic modulus of 21.08×10^6 psi, a plastic modulus of 8.733×10^4 psi, and a yield stress of 125,300 psi. The unloading branch of the titanium curve was assumed to have the same moduli with reverse yielding occurring at -125,300 psi.

For both the aluminum and titanium specimens, the extent of the residual compressive tangential stress zone existing around the hole as a result of the cold-expansion/relaxation sequence and the effect of the applied uniaxial tension fatigue cycles onto that zone were established for three cold expansion levels. These results are summarized in Table 14.

Two important test modifications to the cold-work uniaxial stress sequence were to insert either an unloaded neat-fit (close tolerance) fastener or a loaded (i.e., 10% load transfer for aluminum specimens, 7% load transfer for titanium specimens) neat-fit fastener into the specimen hole prior to the application of the axial load fatigue cycles. To account for these inclusions, bar (axial) elements linking the geometric center of the hole and the nodes defining the hole edge were added to the finite element model. Also, to analyze the load transfer cases, which are not doubly-symmetric, a new model, constructed by adding a mirrored-reflection lower-half to the model of Figure 110, was used. For both loaded and unloaded fastener cases, trial analyses were made to establish which bars were in compression. All those in tension were removed from the model, and, therefore, only fastener bearing was characterized in the stress distributions. The analysis sequence used

to study the neat-fit fastener specimens was identical to that used for the open-hole specimens, as described above, except in the following two ways. During the application of the uniaxial stress, the joint at the center of the hole, where all the bars intersected, was (1) restrained horizontally (symmetric displacement condition), and, for the load transfer cases, was (2) loaded with a downward vertical force equal to half of the total load transferred. Results of these analyses are shown on Figures 112 through 124.

The last sequence studied was that in which the test specimen had an interference-fit fastener installed followed by the application of uniform axial stress fatigue cycles. To simulate the interference-fit fastener, and to determine the resulting residual stresses, the model of Figure 110 was modified in a manner similar to that reported in Ref. 5. The fastener was represented in the model by a double ring of elastic triangular elements lining the inside of the hole. The stiffnesses of these elements were collectively chosen to be equivalent to the stiffness of the solid fastener. As the first step in the analysis sequence, an internal pressure sufficient to expand the ring - if it were externally unrestrained - to the original diameter of the uninstalled fastener was applied incrementally to the inner edge of the ring. Holding the internal pressure fixed at its full value, the second step was then to apply and relax a uniform uniaxial stress across the model's top edge. Three different levels of interference were studied for each aluminum and titanium alloy in the above manner. The results are shown in Figures 125 through 133.

The following, are comments concerning the significant trends and conclusions derived from the results of the unflawed stress analyses.

Figures 112 to 124 present the results of the unflawed and flawed stress distributions computed using the elastic-plastic finite element procedure described above for various types of cold-worked holes. Similar unflawed results are presented in Figures 125 to 133 for interference-fit fastener holes for variable levels of interference. Figure 112 shows the unflawed stress distribution along the x-axis in 2219-T851 aluminum plate caused by 2% cold working and subsequent 1.8 Ksi and 18 Ksi far-field loadings. Figures 113 and 114 show similar stress distributions at a 2% cold-worked hole with initial crack lengths of 0.0125" and 0.0525", respectively, before cold working. These stress distributions show almost no change with the introduction of an initial crack (0.05") before cold working, except in the small region next to the hole wall. The magnitude of the

compressive residual hoop stress decreases slightly if a crack is introduced before the cold working operation. Similar stress distributions for 4% and 5% cold-worked open holes, without an initial crack, are shown in Figures 115 and 116, respectively. As seen from these figures, the extent of the compressive zone is increased with an increase in the percentage of cold working. Figure 117 compares the unflawed stress distributions along the x-axis in aluminum plates caused by 2%, 4% and 5% cold working with the subsequent application of 18 ksi far-field uniaxial tension loading. Figure 118 shows the similar stress distributions at various types of 2% cold-worked holes (i.e. open, close tolerance fastener holes both with and without fastener load transfer). Figure 119 shows the effect of the level of cold working on the stress distributions of loaded cold-worked fastener holes.

As seen from these figures, when the amount of cold-working increases, the extent of the compressive zone in the vicinity of the hole increases and the maximum tensile stress is located farther away from the edge of the hole. However, the magnitude of the maximum tensile stress does not change. Similar results obtained in the titanium plates caused by 2%, 4% and 5% cold workings and subsequent 4 ksi and 40 ksi far-field loading are shown in Figures 120 through 122. Except for the magnitude of the stress, the trend of these distributions is very similar to that of the aluminum material. Figure 123 compares the unflawed stress distribution at various types of 2% cold-worked holes (i.e. open, close-tolerance fastener holes both with and without fastener load transfer) in titanium plates subjected to 40 ksi uniaxial tension far-field loading. There is practically no difference in stress distribution at cold-worked open and unloaded neat-fit holes. However, when 10% of the far-field applied load is reacted through the fastener, the maximum and the minimum stresses increase slightly. Figure 124 shows the stress distribution along the x-axis in 6Al-4V beta annealed titanium plates caused by 2, 4 and 5 percent cold working with subsequently applied 40 ksi far-field tension and 10% fastener load transfer.

The unflawed stress distributions obtained from the elastic-plastic finite element analyses for the levels of diametrical interference used in the test program are presented in Figures 125 through 127 for the aluminum material, and 128 through 130 for the titanium material.

The results obtained for the aluminum material are replotted in Figures 131 to 133 to show the effect of the level of interference on the stress distribution.

Based on the current unflawed stress analyses, the following 3 observations are made:

- 1) Due to the installation of an interference-fit fastener alone, the tangential residual stress at the edge of the hole decreases as the level of interference increases. The peak tangential stress is the same for each level of interference but is located farther away from the hole as the level of interference increases.
- 2) When the far-field load is applied subsequent to the installation of an interference-fit fastener, the peak resultant tangential stress is located farther away from the hole and the peak remains practically the same for each level of interference.
- 3) When the far-field loading is removed, the residual tangential stress at the edge of the hole is nearly the same as the one caused by the interference alone. However, the peak tangent residual stress decreases slightly and is located farther away from the hole than the one caused by the interference only. This phenomenon is considerably different from those obtained using an elastic-perfectly plastic analysis, which predicts a sizeable decrease in the residual tangential stress at the edge of the hole (17,20).

2. APPROXIMATE STRESS INTENSITY FACTOR SOLUTIONS

2.1 Introduction

The stress intensity factor, which generally depends upon crack length, remote loading and structural geometry, has been employed to characterize the severity of the crack-tip stress field. To date, there has been much useful work done on the problem of determining reliable stress intensity factors for cracks emanating from fastener holes. Almost all of these analytical determinations are based upon modifications of a solution obtained by Bowie⁽⁶⁾ for cracks emanating from a circular hole in an infinite elastic sheet. For cracks emanating from an inelastic field near a fastener hole, such as produced by an interference-fit fastener or a cold-worked hole, the stress intensity factors could be estimated by using the weight function approach as discussed by Bueckner⁽⁷⁻¹⁰⁾ or the reciprocal theorem proposed by Rice⁽¹¹⁾. Both techniques require a knowledge of the unflawed stress distribution in the region of the hole. Paris et al⁽¹²⁾ has combined these techniques with the finite element method to develop a weight function for the single edge cracked strip.

The closed form expressions for the weight function for edge cracks^(8,13), center cracks⁽¹⁴⁾ and collinear cracks⁽¹⁰⁾ in a wide panel are available. But, the closed form weight function for cracks emanating from a fastener hole is not available. Development of such a function is very difficult, if not impossible. Therefore, the weight function for a straight crack has sometimes been used to estimate the stress intensity factor for radial cracks emanating from a circular hole,⁽¹⁵⁻¹⁷⁾. For a large crack, where the influence of a fastener hole on the stress intensity factor is small, such an approximation gives good results. However, for the case of a small crack, say $c/r \leq 1.0$, such an approximation could be significantly in error. Grandt⁽¹⁸⁾ used the reciprocal theorem due to Rice⁽¹¹⁾ to develop the following equation which estimates the Mode I stress intensity factor, K_I , for cracks emanating from any type of circular fastener hole:

$$K_I = \int_{\Gamma} p \cdot h \, d\Gamma = \frac{E'}{K_B} \int_0^a p(x) \frac{\partial \eta}{\partial a} \, dx \quad (6)$$

where p is the stress vector on the boundary; h is the weight function; η is the y -component of the crack surface displacements; K_B is the Bowie solution for the stress intensity factor; and E' is an appropriate elastic modulus: $E' = E/(1 - \nu^2)$ for plane strain and E for generalized plane stress. Since the closed form expression for η as a function of the crack length a is not available, it was determined by fitting an equation to the discrete displacements computed using the finite element method for a series of crack lengths ranging from $a/r = 0.4$ to $a/r = 2.8$. The stresses and strains computed using the conventional finite element method may be fairly accurate. But the differentiation of an approximate expression obtained by curve fitting finite element results may result in inaccuracies.

Two high-order singularity elements have been developed at Lockheed-Georgia. One takes only the symmetric terms in the Williams' series and, hence, is applicable only to symmetric problems ($K_{II} = 0$); the other makes use of both symmetric and antisymmetric terms and is applicable to unsymmetric or mixed mode (K_I and K_{II}) problems. The efficiency and accuracy of these elements has been demonstrated in reference⁽¹⁹⁾. In order to obtain more accurate solutions for cracks emanating from a hole, the high-order singularity element for symmetric problems was used to compute the Mode I stress-intensity factor for a double-radial crack emanating from an open hole and subjected to concentrated loads on and perpendicular to the crack surface. The computed stress intensity factor was

used to develop the Green's function (equivalent to a nondimensional stress intensity factor) for a double-radial crack emanating from a circular hole. Once the Green's function is available, the Mode I stress intensity factors for cracks emanating from any type of fastener hole can be calculated from a knowledge of the unflawed stress distribution in the region of the hole.

2.2 Thru Cracks Emanating from Fastener Holes

Figure 134 shows the scheme of the linear superposition method. The stress intensity factor of problem a is equivalent to the sum of those of problems b and c. Since problem b is crack free, the stress intensity factor of problem a is equivalent to that of problem c.

By idealizing the loading in problem c as N discrete loads, P_1, \dots, P_N , the stress intensity factor for a given crack length a can be computed from the following equation:

$$K(a) = \sum_{i=1}^N K_i = \sum_{i=1}^N k_i(x_i, a) P_i(x_i) \quad (7)$$

where $k_i(x_i, a)$ is the normalized stress intensity factor due to the i^{th} unit load applied at location x_i . For arbitrary distributed stress, σ , instead of discrete forces, P_i , Equation (7) becomes

$$K(a) = \int_0^a k(x, a) \cdot \sigma(x) dx \quad (8)$$

By defining $G = k(a/\pi)^{1/2}$ and $\xi = x/a$ and substituting them into Equation (8), one obtains

$$K(a) = \sigma_0 \sqrt{\pi a} \int_0^1 \bar{\sigma}(\xi) G(a, \xi) \cdot d\xi \quad (9)$$

where σ_0 is the uniform far-field stress and $\bar{\sigma} = \sigma'/\sigma_0$ is the normalized unflawed stress distribution on the prospective crack surface.

For a straight crack subjected to two pairs of concentrated forces on the crack surface as shown in Figure 135, the corresponding Green's function, G , is

$$G(a, \frac{b}{a}) = \frac{K}{P} \left(\frac{a}{r} \right)^{1/2} = \left[\left(\frac{a+b}{a-b} \right)^{1/2} + \left(\frac{a-b}{a+b} \right)^{1/2} \right] / \pi \quad (10)$$

The Green's function G , for a double radial crack emanating from a circular hole and subjected to two pairs of concentrated forces on the fracture surfaces, as shown in Figure 136, can be obtained from the computed stress intensity factor using finite-element analysis with inclusion of the singularity element for various crack lengths a/r and b/a ratios as follows:

$$G\left(\frac{a}{r}, \frac{b}{a}\right) = \frac{K}{P} \sqrt{\frac{a}{\pi}} \quad (11)$$

Due to the limitation of finite element methodology, when the concentrated forces were applied close to the crack tip, say $b/a > 0.9$, the corresponding Green's function was obtained using the central crack solution in Figure 137. The Green's function corresponding to this case is

$$G\left(\frac{a}{r}, \frac{b}{a}\right) = \left[\frac{4(1 + \frac{r}{a})}{(1 - \frac{b}{a})(1 + \frac{b}{a} + \frac{2r}{a})} \right]^{1/2} / \pi \quad (11a)$$

The computed Green's function were then tabulated as a function of a/r and b/a in Table 35. For any a/r ratio different from those tabulated values, an interpolation or extrapolation technique was used to obtain the corresponding Green's functions.

With a knowledge of the Green's functions, G , and the stress, σ , on the prospective crack surface with the crack absent, one can compute from Equation (9) the corresponding stress intensity factor for any radial crack from a hole.

When crack face overlapping occurs or the applied force P_i is in compression, the computed K_i in Equation (7) will become negative. Physically, it means the crack surfaces are closed and react against each other.

For a case where there is only one crack emanating from a hole, instead of redeveloping the associated Green's function, it was found that the following equation will give a good estimate of the stress intensity factor:

$$K_I \Big|_{\text{one crack}} = \frac{B_1}{B_2} K_I \Big|_{\text{two cracks}}, \quad (12)$$

where B_1 and B_2 are Bowie's factors for single and double cracks, respectively.

Open Holes

To check the validity and accuracy of the present solution, Bowie's closed-form solution⁽⁶⁾ for a double radial crack emanating from an open hole in an infinite plate was employed. By approximating the unflawed stress distribution as

$$\sigma = \sigma_0 \left[1 + \frac{1}{2} \left(\frac{r}{r+x} \right)^2 + \frac{3}{2} \left(\frac{r}{r+x} \right)^4 \right] \quad (13)$$

the computed nondimensional stress intensity factors using Equation (9) for a double crack emanating from an open hole subjected to uniaxial and biaxial uniform far-field loading are presented in Figure 138. The corresponding Bowie's solutions are also included in the figure. As can be seen, the current results are within 2 percent of Bowie. Similar results computed using Equations (9) and (12) for a single crack emanating from an open hole subjected to uniaxial and biaxial uniform far-field loading are presented in Figure 139. As seen from this figure, estimation of the stress intensity factor for a single crack from that of a double crack and Equation (12) agrees excellently with that of Bowie.

For the case when the applied far-field stress exceeds about one third of the material yield strength, plastic deformation will begin at the edge of an open hole. The extent of local yielding depends upon the applied stress. The stress intensity factor computed, using Bowie's solution based on the purely elastic analysis, will be too high. In such a case, the stress intensity factor can be estimated from the unflawed stresses obtained from an elastic-plastic analysis and Equation (9).

Let f_{op} be the normalized unflawed stress distribution on the prospective crack surface obtained from an elastic-plastic analysis. Then the stress intensity factor of a through crack can be written as

$$K = \sigma_0 \sqrt{\pi a} H \quad (14)$$

where

$$H = \frac{B_1}{B_2} \int_0^1 f_{op}(\xi) G(a, \xi) d\xi, \quad i = 1, 2 \quad (15)$$

The factor H , equivalent to the Bowie factor in the purely elastic case, accounts for the hole effect when the local yielding occurs. Unlike Bowie's factor B , this factor depends upon the far-field stress. Figure 140 shows the non-dimensional factor H for three different levels of applied far-field stresses. As seen from the figure, when the far-field stress increases, the corresponding nondimensional stress intensity factor H decreases, especially for a very short crack.

Close Tolerance Fastener Holes with and without Fastener Load Transfer -

The stress distribution of an unloaded close tolerance fastener hole in a plate subjected to uniform far-field loading has been studied by many investigators. So has the problem of a close tolerance fastener hole having 100% fastener load transfer. For a case where the close tolerance fastener only transfers a fraction of the remote loading, the corresponding stress distribution has been calculated from those of the aforementioned two cases via the superposition method illustrated in Figure 141.

The idealized problem of a remotely loaded strip with a neat-fit rigid insert (fastener) is an inherently nonlinear problem. This is most easily demonstrated through the observation that the contact surface cannot be prescribed in advanced but depends rather on the solution and is usually determined by trial. The same nonlinear characteristics apply when the strip is loaded at only one end and the load is reacted at the rigid insert (100% load transfer). The contact surface is more extensive in the latter case and occupies a different portion of the hole boundary. In view of these observations, any solution for fractional load transfer obtained via the superposition of these two cases must

be regarded as approximate at best. When the fastener is deformable, the validity of superposition is all the more suspect and moreover any such approximation is likely to give poorest results on or near the hole boundary.

A detailed finite element model was used to compute the unflawed circumferential stress distributions along the plane perpendicular to the load in a hole of a 7075-T6 aluminum plate fitted with a 6Al-4V titanium fastener for various percentages of fastener load transfer at Lockheed-Georgia. The width of the plate was 1.15 inches and the hole diameter was 0.1875 inches (or a hole diameter to width ratio of 0.16). The computed dimensionless stress distribution is shown in Figure 142. The estimated unflawed stress at the edge of the hole using the superposition method is higher than the stress using the finite element method by about 2% for a 30% load transfer case and 13% for a 75% load transfer case.

Let f_{CT} be the normalized unflawed stresses on the prospective crack surface. Then the stress intensity factor for a through crack emanating from a close tolerance fastener hole can be written as

$$K = \sigma_0 \sqrt{\pi a} \cdot \beta_{CT} \quad (16)$$

where

$$\beta_{CT} = \frac{B_1}{B_2} \int_0^1 f_{CT}(\xi) G(a, \xi) d\xi, \quad i = 1, 2 \quad (17)$$

The nondimensional factor β_{CT} is a function of crack length and the percentage of fastener load transfer.

The computer β_{CT} using the unflawed stresses shown in Figure 142 for a double crack emanating from close tolerance fastener hole having various percentages of fastener load transfer are shown in Figure 143. Bowie's solution for an open hole is also shown in the figure as a dotted line. From this figure, one can see that the stress intensity factor for a close tolerance fastener hole without load transfer is lower than that of an open hole. However, when the amount of load transfer increases, the stress intensity

factor increases rapidly, especially for short crack lengths. The computed nondimensional stress intensity factor at the edge of the hole is approximately 1.12 times the normalized unflawed stress at that location. This agrees very well with the edge-crack solution.

The computed nondimensional stress intensity factors for a double through crack emanating from an open and close tolerance fastener hole with and without 10% fastener load transfer are shown in Figure 144 for a 4-inch wide aluminum specimen and in Figure 145 for a 4-inch wide titanium specimen. The computed stress intensity factors for a single through crack emanating from a close tolerance fastener hole with and without fastener load transfer are shown in Figures 146 and 147, respectively for titanium specimens. Test data reduced using the fatigue crack growth method of calibrating K are also shown in the figures as symbols for comparison.

For the case in which the local yielding occurs at the edge of the fastener hole due to high far-field applied loading, the corresponding stress intensity factors can be obtained by using the previously described approach and the unflawed stresses determined from an elastic-plastic analysis.

Interference-Fit Fastener Hole - Slightly oversized fasteners are commonly employed in structural applications to improve fatigue life. When a hole is filled with an interference-fit fastener, substantial plastic yielding will occur around the hole. The extent of plastic yielding depends upon the level of interference and the magnitude of the remotely applied loading. Based on the elastic-plastic finite element analysis, one finds that the unflawed stress distribution along the x-axis near the fastener for a plate-fastener material combination is dependent upon the material yield stress σ_{ys} , Young's modulus E , Poisson's ratio ν , interference level (δ/d) and the remote load σ . For the case of a crack emanating from an interference-fit fastener hole, a sizeable residual stress intensity factor may exist even in the absence of the remote load. Therefore, instead of the remote loading σ_o , the yield strength of the plate material, σ_{ys} , should be used in the stress intensity factor expression which may be written as

$$K = \sigma_{ys} \sqrt{\pi a} \beta_{IF} \quad (18)$$

where

$$R_{IF} = \frac{B_1}{B_2} \int_0^1 f_{IF}(\xi) G(a, \xi) d\xi, \quad i = 1, 2 \quad (19)$$

The f_{IF} factor in Equation (19) represents the unflawed stresses on the prospective crack surface normalized by the plate material yield strength. For a given material, the nondimensional factor β_{IF} is a function of the crack length, far-field load, and the amount of fastener-hole interference.

Figure 148 shows the unflawed stress distributions for a 7075-T6 aluminum plate with a steel interference-fit fastener caused by 0.004" interference and subsequent edge loading and unloading⁽²⁰⁾. The computed stress intensity factors using these unflawed stresses and Equations (18) and (19) are shown in Figure 149. From this figure, one sees that for $a/r < 0.5$, when the far-field loading (25 ksi) is removed, the computed K is less than zero. Physically, it means that the fracture surfaces are completely closed and compress each other. The effective stress intensity factor range equals the difference between curves 2 and 3. For a similar plate with an open hole subjected to 25 ksi far-field loading, the corresponding K (also ΔK) is plotted in the same figure as dotted lines for comparison purposes. For small crack lengths, the computed ΔK is much smaller for an interference-fit fastener hole than an open hole. This explains why the crack emanating from an interference-fit fastener hole grows much slower than a corresponding crack in an open hole when the crack length is small. When the crack length is longer than one half of the radius of the fastener hole, the computed stress intensity factor becomes positive after the far-field applied load is removed. The effective cyclic-load ratio experienced by the crack tip is no longer the same as the far-field applied load ratio (which is zero in this case). When the crack length is longer than 3 times the radius of fastener hole, the effective stress intensity factor ranges are about the same as those for an open hole. Based upon these computed stress intensity factors, one may conclude that the beneficial effect of an interference-fit fastener on retarding fatigue crack growth is the most significant when the crack length is small. This beneficial effect decays as the crack length increases until the interference-fit fastener hole no longer retards the fatigue crack growth. Such a limit depends upon the amount of interference and the magnitude of the far-field applied load. For the particular example shown here, this limit crack length is about 3 times the hole radius.

The unflawed stress distributions for interference-fit fastener holes for three levels of interference in both aluminum and titanium plates caused by uniform far-field loading have been presented and discussed in Section V, paragraph 1. The normalized stress intensity factors, β_{IF} , computed using these unflawed stresses and Equation (19) are presented as a function of crack length in Figure 150 for double through cracks emanating from 0.0024", 0.0038" and 0.0060" interference-fit fastener holes in aluminum plates subjected to 18 ksi far-field uniform loading. The corresponding stress intensity factors computed using Equation (18) are shown in Figure 151. Three curves, K_{max} , K_{min} and $K_{max} - K_{min}$, are shown in each figure. They are the computed stress intensity factors corresponding to an 18 ksi far-field applied load, the removal of such load and the difference between these load cases, respectively. As seen from the figures, there are sizeable residual stress intensity factors remaining upon the removal of the far-field applied load. Although the far-field applied load is constant in amplitude, the effective stress intensity factor ratio, $R_{eff} = K_{min}/K_{max}$, at the crack tip is not constant. This ratio varies with the crack length. The computed β_{IF} and stress intensity factors corresponding to the application and removal of the 40 ksi far-field loading for double through cracks emanating from interference-fit fastener holes having 0.0034", 0.0042" and 0.0050" interferences in titanium plates are shown together in Figures 152 and 153, respectively. These results are similar to those for the aluminum material. One important feature observed here is that, for the far-field load applied in the tested specimens, the effective stress intensity factor ranges, $K_{max} - K_{min}$, are essentially the same for each level of interference. However, the effective stress intensity factor ratio, R_{eff} , does depend upon the level of interference, as shown in Figures 154 and 155, which present the effective stress intensity factor ratio as a function of the nondimensional crack length, a/r , for three levels of interference. From these figures, one can easily see that for a crack whose length is less than about one radius of the fastener hole, R_{eff} decreases rapidly as the amount of interference increases. When the crack length is greater than one radius of the fastener hole, R_{eff} increases as the amount of interference increases. However, such an increase is very small. For a given far-field loading, the implication is that when $a/r < 1$, an increase in the amount of fastener hole interference will result in a slower fatigue crack growth rate, especially for a very short crack. When $a/r > 1$, the fatigue crack growth rate will be practically the same within the levels of interference studied here.

For the purpose of validating the analytical solution, a crack emanating from an interference-fit fastener hole in a plate subjected to constant amplitude far-field loading was treated as a crack emanating from a fastener hole having no residual stress and subjected to varying amplitude loads which produce the same ΔK_{eff} and R_{eff} . The predicted crack growth histories, using the computed ΔK_{eff} and R_{eff} , are compared with test data in Figures 156 to 158 for single through-the-thickness cracks emanating from 0.0024, 0.0038, and 0.0040 inch diametral interference-fit fastener holes, respectively, in 2219-T851 aluminum alloy plates subjected to constant amplitude 18 ksi and $R = 0.1$ far-field loading. The following crack growth equation⁽²⁾ was used in the predictions:

$$\frac{da}{dN} = c (K_{max} - K_{th})^m (\Delta K)^n \quad (20)$$

where $c = 0.34 \times 10^{-8}$, $m = 0.84$, $n = 2.40$, and $K_{th} = 1.5$. The units of the crack growth rate and the stress intensity factors are inch/cycle and $\text{ksi}\sqrt{\text{in}}$, respectively. As seen from these figures, data scatter is fairly large in the tests of cracks emanating from interference-fit fastener holes and the predictions are well within the scatter of the test data.

Cold-Worked Holes - Procedures used in obtaining the unflawed stress distribution produced by the two steps of mandrel hole enlargement were presented in Section V, paragraph 1. The analysis shows that the cold-working operation causes hoop compression adjacent to the edge of the fastener hole and residual tension in the outer field. Due to the high residual compressive hoop stresses around the hole, to ensure that the resultant stresses remain tensile over the crack length, the remote applied stress must be high. Otherwise, the crack surface may not completely open and no crack growth results.

Let f_{CW} be the unflawed stresses on the prospective crack surface normalized by the plate material yield strength. The stress intensity factor for a through crack emanating from a cold-worked fastener hole can be written as

$$K = \sigma_{ys} \sqrt{\pi a} \beta_{CW} \quad (21)$$

where

$$\beta_{CW} = \int_0^1 f_{CW}(\xi) G(a, \xi) d\xi, \quad i = 1, 2 \quad (22)$$

For a given material, the nondimensional factor β_{CW} is a function of crack length, far-field applied load, and level of cold working.

As discussed earlier, the hoop stress in the vicinity of a cold-worked hole would be in compression if the far-field applied load is not high enough. In such a case, the computed stress intensity factor using the Green's function approach could become negative, especially for a small crack length. Physically, it means that the crack surfaces are closed and react against each other. Therefore, the computed negative K should be set equal to zero.

Figure 159 shows the unflawed stress distributions in the region of a 4.4% cold-worked hole in a 7075-T6 plate caused by 16 ksi edge loading and subsequent unloading⁽²¹⁾. After the edge loading is removed, a residual compressive tangential stress remains at the edge of the hole ($a/r < 1$). The computed stress-intensity factor ranges, $K_{\max} - K_{\min}$, using Equations (21) and (22) are presented in Figure 160 as dashed line. K_{\min} was computed using the unflawed stress corresponding to 0.8 ksi edge loading. For the same level of cold-working (4.4%) and edge loadings ($\sigma_{\max} = 16$ ksi, $\sigma_{\min} = 0.8$ ksi), the stress intensity factor ranges obtained from the crack growth tests reported in References 22 and 23 and the maximum stress intensity factor K_{\max} , predicted using the linear superposition method⁽¹⁸⁾, are also included in the figure. As can be seen, the current analysis gives an excellent correlation with the experimental data.

The unflawed stress distributions of cold-worked holes for three levels of cold working in both 2219-T851 aluminum plate and 6Al-4V beta annealed titanium plate subjected to by constant amplitude far-field loading have been presented and discussed in Section V, paragraph 1. The normalized stress intensity factors, β_{CW} , computed using these unflawed stresses and Equation (22) are presented as a function of crack length in Figure 161 for double thru cracks emanating from 2%, 4% and 5% cold-worked open holes in aluminum plates subjected to 18 ksi far-field uniform loading. The corresponding stress intensity factors computed using Equations (21) and (12) for single thru cracks emanating from cold-worked open holes are presented in Figures 162 and 164. Figure 165 shows the computed stress intensity factors for a single thru crack emanating from a 2% cold-worked hole having 10% fastener load transfer. The stress intensity factors reduced from test data for large cracks using the fatigue crack growth method of calibrating the crack

growth rate, da/dN , and the stress intensity factor range, ΔK , are also included in the figures. As can be seen from these figures, the computed stress intensity factors are in good agreement with that reduced from test data. Similar results for titanium plates containing 2%, 4% and 5% cold-worked open holes are presented in Figures 166 to 169. Figure 170 shows similar results for a 2% cold-worked hole having 10% fastener load transfer. The actual amount of fastener load transfer in the tested specimen was about 6 percent of the total far-field applied load. The stress intensity factors shown in Figure 170 were computed using the unflawed stress distribution obtained for a fastener having 10% load transfer. Had correct amount of fastener load transfer been accounted for, the computed stress-intensity factors would decrease slightly and correlate even better with the test data.

Figure 171 compares the computed stress intensity factors for single through cracks emanating from a 2% cold-worked open hole and close tolerance fastener holes with and without fastener load transfer in 2219-T851 aluminum plates subjected to 18 ksi far-field loading. The stress intensity factors at cracked cold-worked open and close tolerance fastener holes show practically no difference. However, with a small amount of fastener load transfer, the corresponding stress intensity factors increase significantly.

Figure 172 shows the stress intensity factors for single through cracks emanating from 2% cold-worked open holes in aluminum plate subjected to various levels of far-field loading. Since the stress intensity factor at a cracked cold-worked hole does not depend linearly on the far-field applied load, the computed K values are presented as a function of a , where a is measured from the edge of the hole. From this figure, one sees that when the far-field loading increases, the corresponding stress intensity factor increases, and the region of negative K (which has been set equal to zero in the plots) decreases.

It should be noted that the unflawed stress distributions computed here are based on a static analysis (or first few cycles under repeated loading). Theoretically speaking, if the crack length is smaller than the compressive zone, resulting from the cold working operation and the application of the maximum cyclic load, the crack will not propagate under cyclic loads. However, during the course of the experimental program, it was found that an intentional fatigue crack, which is much smaller than the computed negative K region, does propagate after the application of a large number of repeated load cycles.

It is suspected that the relaxation of beneficial residual strains due to cold working occurs, and after a certain period of fatigue cycling, the net hoop stress results in tension upon reapplication of the maximum cyclic load. The current analysis is not capable of accounting for such relaxation.

Table 36 summarizes all available stress intensity factor solutions for through cracks emanating from the types of fastener holes studied under this program.

2.3 Corner Cracks Emanating From Fastener Holes

One of the most common types of flaws for which there exists no closed form analytical solution is the corner crack at a circular fastener hole. To date, several approximate methods have been proposed for computing the stress intensity factors along the periphery of a quarter-elliptical crack emanating from the corner of an open hole. Based on K_c values obtained from standard specimens and failure stresses of specimens with corner cracks, Hall and Finger⁽²⁴⁾ derived an empirical equation for computing such stress intensity factors. Gran et. al.⁽²⁵⁾ modified the solution for an embedded elliptical flaw to account for hole and free surface effects. Hsu and Liu⁽²⁶⁾, used a similar approach to modify the half-elliptical surface flaw solution to account for the hole effect. Kobayashi and Eneranya⁽²⁷⁾ extended an alternating method by using appropriate fictitious pressure on the fictitious three-quarter part of the elliptical crack which protrudes into three-quarter space to solve the corner flaw problem in a quarter-infinite solid. Kobayashi et. al.⁽²⁸⁾ used the same three-dimensional alternating technique to estimate the stress intensity factor of a corner crack at a hole in a rotating disk. Shah⁽¹⁷⁾ used similar procedures of prescribing a fictitious pressure on the crack surface to simulate the cylindrical front surface intersecting a double embedded semicircular crack at a fastener hole to compute the nondimensionalized factor F_S for a/c ratios ranging from 0.1 to 1.0 and c/r values ranging from 0.1 to 10.0 from which he concluded that F_S could be assumed to be independent of a/c ratio. However, the final nondimensionalized factors F_S used in his analysis are the ones obtained from the integration of unflawed stresses and the Green's functions derived by Smith et. al.⁽²⁹⁾ for a circular crack embedded in an infinite solid without a hole. A constant front surface correction, independent of the location on the crack border, was assumed. Smith and Kullgren⁽³⁰⁾ performed a sequence of iterations between an analytical solution for an elliptical crack embedded in an infinite solid and a finite element alternating solution for

a finite thickness uncracked plate with a fastener hole to obtain the stress intensity factors along the periphery of a part-elliptical crack emanating from a fastener hole in a finite thickness plate. McGowan and Smith⁽³¹⁾ used a combination of stress-freezing photoelasticity and a numerical method to obtain the stress intensity factors at the intersection of a corner crack, hole and plate surfaces. Snow⁽³²⁾ used the fatigue crack growth method of calibrating the measured crack growth rate, da/dN , and the stress intensity factor range, ΔK , to determine the stress intensity factors of corner cracks from which an empirical equation was developed. Fujimoto⁽³³⁾ used the slicing technique to idealize the part-through crack as a series of through-the-thickness radial cracked slices with springs attached to the crack faces to represent the shear coupling between the slices. Similar to Shah's analysis, the Green's functions for a circular crack embedded in an infinite solid without a hole were used in the determination of a series of spring forces transmitted across the crack faces. Other numerical methods, such as finite-element⁽³⁴⁾ and boundary-integral-equation approaches,⁽³⁵⁾ have also been used to solve the problem of a quarter-elliptical crack in a quarter-infinite solid.

All aforementioned solutions are approximate. There is no exact solution available which could be used to assess the accuracy of any individual solution.

Experimentally, the fatigue crack growth method of calibrating da/dN and ΔK (which, in general, is derived from the testing of through cracked specimens having known K solutions) can be used to estimate the stress intensity factor of the tested crack geometry. Considering the data scatter from which the da/dN vs. ΔK relationship is established, it is very difficult to assess the accuracy of K values obtained based on the measured growth rate of certain increments. To date, the three-dimensional alternating technique has been used most often to estimate the stress intensity factor for a quarter-elliptical corner crack from a hole. However, there are several sources of numerical errors that might be introduced in the analysis using the alternating technique, especially during the process of zeroing out the fictitious residual tractions acting on the free surfaces (including the crack face). The other error is in the least squares fitting of the crack pressure distribution with a polynomial. In addition, the computer time required to execute one such problem is significantly large.

In this section, the approximate stress intensity factor solutions derived from the modification of the Hsu and Liu⁽²⁶⁾ solution for a quarter-elliptical crack emanating from the corner of an open hole is presented. Wherever possible, the solutions are compared with other approximate solutions. The stress intensity factor solutions for a quarter-elliptical crack emanating from the corner of close tolerance, cold-worked, and interference-fit fastener holes are also presented.

Open Hole

The shape of a corner crack at a fastener hole is generally assumed to be quarter-elliptical with the semi-major and semi-minor axes coinciding with the hole wall and the plate surface. Let a and c represent the crack lengths measured along the hole wall and the plate surface, respectively. The approximate stress intensity factor solution for a quarter-elliptical crack emanating from the corner of an open hole proposed by Hsu and Liu⁽²⁶⁾ may be written as

$$K\left(\frac{a}{c}, \beta\right) = \sigma_0 \sqrt{\pi a} \cdot \beta_{op}\left(\frac{x}{r}\right) \cdot \frac{M\left(\frac{a}{c}, \beta\right) \cdot M_1\left(\frac{a}{c}, \beta\right)}{\Phi\left(\frac{a}{c}\right)} \text{ for } a/c \leq 1 \quad (23)$$

and

$$K\left(\frac{c}{a}, \beta\right) = \sigma_0 \sqrt{\pi a} \cdot \beta_{op}\left(\frac{x}{r}\right) \cdot \sqrt{\frac{c}{a}} \cdot \frac{M\left(\frac{c}{a}, \beta\right) \cdot M_1\left(\frac{c}{a}, \beta\right)}{\Phi\left(\frac{c}{a}\right)} \text{ for } a/c > 1$$

where $\beta_{op}\left(\frac{x}{r}\right)$ is the Bowie hole correction factor evaluated at the normalized distance from the edge of the hole, x/r ; Φ is the complete elliptical integral of the second kind presented in Figure 173 as a function of the ratio of the minor and major axes of the ellipse; β is an elliptical angle measured from the hole wall; M is defined as

$$M = \left[\left(\frac{a}{c}\right)^2 \sin^2 \beta + \cos^2 \beta \right]^{1/4}, \text{ for } a/c \leq 1 \quad (24)$$

and

$$M = \left[\left(\frac{c}{a}\right)^2 \cos^2 \beta + \sin^2 \beta \right]^{1/4}, \text{ for } a/c > 1$$

and M_1 is the front surface correction factor determined by interpolating the known solutions for the following three cases: (1) $a/c = 0$, (2) $a/c = 1$, and (3) $a/c = \infty$.

For $a/c = 0$, the crack geometry is similar to that of an edge crack for which the front surface correction factor is 1.12. For $a/c = \infty$, the crack geometry is similar to that of a center crack for which M_1 is equal to 1.0. For $a/c = 1$, M_1 has been obtained numerically and presented as a function of an elliptical angle β by Smith et al. (30). Values of M_1 are presented in Figure 174 in a ten-degree (elliptical angle) increments from the hole wall to the plate surface for all possible a/c ratios.

For the convenience of application, the front surface correction factor and flaw shape factors in Equation (23) are combined as follows:

$$K\left(\frac{a}{c}, \beta\right) = \sigma_0 \sqrt{\pi a} \beta_{op}\left(\frac{x}{r}\right) \cdot \frac{M_1'}{\Phi}\left(\frac{a}{c}, \beta\right) \text{ for } a/c \leq 1 \quad (25)$$

and

$$K\left(\frac{c}{a}, \beta\right) = \sigma_0 \sqrt{\pi a} \sqrt{\frac{c}{a}} \beta_{op}\left(\frac{x}{r}\right) \cdot \frac{M_1'}{\Phi}\left(\frac{c}{a}, \beta\right) \text{ for } a/c > 1$$

The normalized $\frac{M_1'}{\Phi}$ factor is plotted in Figure 175 as a function of a/c for $a/c \leq 1$ and in Figure 176 as a function of c/a for $a/c > 1$.

For the convenience of visualizing the variation of the stress intensity factor along the crack border, the geometric angle θ is defined as the angle measured from the hole wall to a specific point on the periphery of an elliptical crack. Figure 177 shows the relationship between the angles β and θ for the ratios of the minor to major axes ranging from 0.001 to 1.0.

Equation (25), proposed by Hsu and Liu, is modified in the following manner. For a corner crack with a small c/r ratio, the entire crack surface is located in the region of elevated stress and the unflawed stress variation within the crack surface is small. For this case, Equation (25) normally results in good estimates of the stress intensity factors. However, when the c/r ratio becomes large, the crack surface extends into the region of lower stress. Because the stress intensity factors are sensitive to the local stress field in the vicinity of the crack, the actual stress intensity factor at the edge of the hole for this case is expected to be lower than the stress intensity factor computed from Equation (25). Also, when the crack is deep, the hole acts to restrict the crack opening

which tends to reduce the actual stress intensity factor at the edge of the hole, again resulting in a computed stress intensity factor which is too large. To account for these effects, Equation (25) is modified as follows:

$$K\left(\frac{a}{c}, \beta\right) = \sigma_0 \sqrt{\pi a} \beta_{op}\left(\frac{x}{r}\right) \cdot \frac{M_1'}{\Phi}\left(\frac{a}{c}, \beta\right) \cdot M_c\left(\frac{c}{r}, \frac{x}{c}\right) \text{ for } a/c \leq 1 \quad (26)$$

and

$$K\left(\frac{c}{a}, \beta\right) = \sigma_0 \sqrt{\pi a} \left(\frac{c}{a}\right)^{1/2} \beta_{op}\left(\frac{x}{r}\right) \cdot \frac{M_1'}{\Phi}\left(\frac{c}{a}, \beta\right) \cdot M_c\left(\frac{c}{r}, \frac{x}{c}\right) \\ \text{for } a/c > 1$$

where

$$M_c = F + \frac{x}{c} (1-F) \quad (27)$$

in which the factor F , presented in Figure 178 as a function of c/r , is obtained from the stress intensity factors Shah⁽¹⁷⁾ estimated at the location where the crack and hole wall intersect and x is the distance from the hole wall to the particular point of interest on the crack periphery.

Normalized stress intensity factors ($K/\sigma_0\sqrt{\pi a}$) for a double corner crack emanating from an open hole were computed using Equations (26) and are presented in Figures 179 to 182 as a function of the geometric angle θ for a/c ratios of 0.75, 1.0, 1.5, and 2.0, respectively. Solutions were also obtained from Equation (26) for an a/c ratio of 0.5 and are correlated in Figure 183 with other approximate solutions proposed by Smith⁽³⁰⁾ and Shah⁽¹⁷⁾. Similarly, solutions for a single corner crack emanating from an open hole were obtained from Equation (26) for an a/c ratio of 1.0 and are correlated in Figure 184 with other approximate solutions proposed by Kobayashi et.al.⁽²⁸⁾ and Shah⁽¹⁷⁾. The magnification factors presented in Figure 184, were obtained by normalizing the stress intensity factors by dividing by K_{I0} (the stress intensity factor for an elliptical crack in an infinite body subjected to a uniform tensile stress $3\sigma_0$).

Because there is no closed form (exact) stress intensity factor solution for a quarter-elliptical corner crack emanating from an open hole with which to compare the current solution presented in Equation (26), correlations were also made of predictions using the current solution with experimental test data. Two sets of test data were generated under

carefully controlled laboratory conditions. The specimens were made of 7050-T73 aluminum plate with a thickness of 0.25 inch, a width of 3 inches, and a hole diameter of 0.26 inch. An electro discharge machine was used to introduce the initial notch at the corner of the hole (one crack only). Fatigue crack propagation tests were then conducted under a high-humidity environment (90-95% relative humidity), at room temperature, with a loading frequency of 10 cycles per second. The specimens were subjected to constant amplitude loading with a maximum stress of 15 ksi and a stress ratio of 0.1. Crack lengths (both a and c) were recorded using a macromechanic device. During the test, the "marker" loads were occasionally applied to produce bench marks on the fracture surfaces. These bench marks provided a record of the actual shape of the crack during crack propagation and also served to verify the macromechanic readings on the crack length measurements. The maximum stress level for the "marker" load cycles was also 15 ksi, but the stress ratio R was increased to 0.85. Photograph showing the etch cut and the bench marks resulting from application of the "marker" loads on the crack surface of the first specimen is presented in Figure 185. Figure 186 shows the actual flaw shape on the fracture surface of one of the specimens resulting from the application of the marker loads and the result of fitting a quarter-elliptical curve through two readings observed on the surfaces: a and c . The figure indicates the accuracy of assuming that the corner crack is quarter-elliptical in shape.

Correlations of analytical predictions using Equation (26) and the experimental test data for the two previously mentioned test specimens are presented in Figures 187 and 188. The figures present the number of cycles versus crack length for both the front surface and the hole wall. It was assumed in the predictions that for a given number of applied load cycles, the extension of the quarter-elliptical crack border was controlled by the stress intensity factors at the intersections of the crack periphery and both the hole wall and the plate surface, (i.e., K_A and K_C). In general, the stress intensity factors at these two locations are different, resulting in different crack growth rates. Therefore, the new flaw shape aspect ratio after each crack growth increment differed from the previous one. The new flaw shape aspect ratio was computed using the new crack lengths on both the hole wall and plate surface. The process was repeated until the crack length along the hole wall was equal to the plate thickness. At that time, the crack was assumed to be a through crack with a crack length equal to c . This assumption was made based upon the experimental observation that after the crack penetrates the back surface and the cyclic load

application continues, the back surface crack length increases much faster than that of the front surface until the front of the through crack becomes stable. Figures 187 and 188 indicate that good correlations were obtained between the analytical predictions and the experimental test data. Figure 189 shows correlations of predictions using Equation (26) and two sets of Snow's test data⁽³²⁾ generated using PMMA polymer material. Comparisons between the computed normalized stress intensity factors, using Equation (26) and other approximate solutions, and data obtained by Snow⁽³²⁾ using the fatigue crack growth method of calibrating the measured crack growth rate, da/dN , and the stress intensity factor range, ΔK , are tabulated in Table 37. As seen from all these comparisons, good correlations between the analytical predictions and the test data have been obtained. For the case when the applied far-field stress exceeds about one third of the material yield strength, local yielding occurs at the vicinity of the hole. In such a case, the stress intensity factor for a corner crack located at an inelastic hole can be estimated from that of a thru crack solution by replacing the Bowie factor β_{op} in Equation (26) by the factor H as shown in Figure 140.

Close Tolerance Fastener Holes with and without Fastener Load Transfer - With the knowledge of a through crack solution β_{CT} , the stress intensity factor for quarter elliptical cracks emanating from the corner of a close tolerance fastener hole with or without fastener load transfer can be estimated from Equation (26) by replacing the Bowie factor β_{op} by the factor β_{CT} . Values of β_{CT} can be computed using Equation (17) and some typical values are given in Figures 143 to 145. These β_{CT} values are valid for the width to hole diameter ratios considered.

Interference-Fit Fastener Holes - As previously mentioned, substantial plastic yielding occurs around a hole due to the installation of an interference-fit fastener and a sizeable residual stress intensity factor remains after the removal of the far-field applied load. Similar to a close tolerance fastener hole, the stress intensity factor for quarter-elliptical cracks emanating from the corner of an interference-fit fastener hole can be estimated from Equation (26) by replacing the factor β_{op} by the factor β_{IF} .

Typical β_{IF} factors for a through crack emanating from an interference-fit fastener hole are presented in Figure 150 for 2219-T851 aluminum plate and in Figure 152 for 6Al-4V beta annealed titanium plate. The computed normalized stress intensity factor at the

intersection of plate surface and the border of a single corner crack emanating from interference-fit fastener holes for three levels of interference for each material studied are presented in Figures 190 and 191 for an a/c ratio of 0.75. This ratio was chosen because it represents the average flow shape seen on the fracture surface of such fastener holes. As discussed earlier, the stress intensity factor for a crack emanating from an interference-fit fastener hole is not linearly proportional to the far-field applied load. It depends also upon the level of interference, the material yield strength, Young's modulus, and Poisson's ratio. For the purpose of validating the analytical solution, a crack emanating from an interference-fit fastener hole in a plate subjected to constant amplitude far-field loading was treated as a crack emanating from a fastener hole having no residual stress and subjected to varying amplitude loads which produce the same ΔK_{eff} and R_{eff} .

The predicted crack growth histories are compared with test data in Figure 192 for a single corner crack emanating from 0.0024, 0.0038, and 0.0060 inch diametric interference-fit fastener holes in 2219-T851 aluminum plates subjected to constant amplitude 18 ksi and $R = 0.1$ far-field loading. Similar analytical-experimental correlations for a single corner crack emanating from 0.0034, 0.0042, and 0.0050 inch diametric interference-fit fastener holes in 6Al-4V beta annealed titanium plates subjected to 40 ksi and $R = 0.1$ far-field loading are shown in Figure 193. Both Forman's⁽³⁶⁾ and Hall's⁽²⁾ crack growth rate equations were used in the predictions. The predictions using Forman's equation show considerably shorter lives than those using Hall's equation. As seen from these figures, the predictions are well within the scatter of the test data.

Cold-Worked Holes - With a knowledge of the through crack solution β_{CW} , the stress intensity factor for quarter elliptical cracks emanating from the corners of the cold-worked fastener holes with or without fastener load transfer can be estimated from Equation (26) by replacing the factor β_{op} with the factor β_{CW} . Values of β_{CW} are given by Equation (22) and in Figures 161 and 166. As discussed previously, if the crack length is smaller than the compressive zone, resulting from the cold working operation and the application of the maximum cyclic load, the crack will not propagate under cyclic loads. However, during the course of the experimental program, it was found that an intentional corner crack, which is much smaller than the computed negative K region, does propagate after the application of a large number of repeated load cycles. It is suspected that the relaxation

of beneficial residual strains due to cold working occurs, and after a certain period of fatigue cycling, the net hoop stress results in tension upon reapplication of the maximum cyclic load. The current analysis is not capable of accounting for such relaxation.

For convenience, the available stress intensity factor solutions for corner cracks emanating from the types of fastener holes studied during this program are summarized in Table 38.

2.4 Embedded Cracks Emanating from Fastener Holes

The stress intensity factor for semi-elliptical embedded cracks emanating from opposite sides of an open hole has been estimated by many investigators. Hsu and Liu⁽²⁶⁾ modified the surface flaw solution by using Bowie's through crack solution to account for the hole effect to obtain the stress intensity factor for such an embedded crack. Shah⁽¹⁷⁾ obtained an approximation by solving the equivalent problem of a pressurized penny shaped crack in a solid without a hole. The pressure he applied on the crack surface was the two dimensional stress distribution adjacent to a hole in an infinite plate. Kobayashi⁽³⁷⁾ used a superposition method based upon removing residual crack surface tractions obtained by a linear approximation of the prescribed stress distribution in an uncracked plate. Correction is then made to the through crack stress intensity to produce corresponding values for semi-elliptical embedded cracks and surface effects are neglected. Smith⁽³⁰⁾ used the modified finite element alternating method to compute solutions for two-hole-diameters-to-plate thickness ratios. Similar to corner cracks, there is no exact stress intensity factor solution available for an embedded crack in a hole to assess the accuracy of the aforementioned approximations.

For engineering application purposes, the stress intensity factor solution for an embedded crack emanating from an open hole proposed by Hsu and Liu⁽²⁶⁾ is modified and presented in this section. The solution is used to correlate with available experimental data. Comparisons between the current solution and other approximate solutions are also made. The solution is then extended to the case where the embedded crack is emanating from other types of fastener holes.

Open Holes - The approximate stress intensity factor solution for two semi-elliptical cracks, symmetrically embedded in the edge of an open hole, proposed by Hsu and Liu,⁽²⁶⁾ may be written as:

$$K_I = \sigma \sqrt{\pi a} \cdot B_{op} \cdot M \Phi . \quad (28)$$

The function M/Φ for any crack aspect ratio is given in Figure 194. The free-curved-surface effect due to the presence of an open hole was not properly accounted for in the above equation. Hence, similar to the corner crack discussed in the previous section, the stress intensity factor at the hole wall estimated by Equation (28) is too high, because Equation (28) does not account for the restraint of the hole. Therefore, Equation (28) should be modified as

$$K = \sigma \sqrt{\pi a} \beta_{op} \frac{M}{\Phi} \cdot M_c \quad (29)$$

where M_c has been defined in Equation (27).

Experimental data for semi-elliptical embedded cracks emanating from fastener holes are very limited. Figure 195 shows the growth pattern of a double embedded crack originating at a 5/16" open hole in 4 inches wide 7075-T651 aluminum alloy plate. The growth pattern was established using marker loads. The thickness of the specimen was 0.45". The test was conducted under Lockheed's IRAD program. The specimen was subjected to a constant amplitude far-field load of 15 ksi and $R = 0.1$ at room temperature and a lab air environment. To create markers on the fracture surface, 10,000 cycles of marker loads were applied between every 1000 cycles of normal far-field loading by changing the applied load ratio to 0.85 but maintaining the same maximum load (15 ksi). The crack growth during each application of the marker loads was small. The stress intensity factors at the hole wall and in the depth direction (intersection of crack front and semi-minor axis) were reduced from the test data, using the fatigue crack growth method of calibrating K , and are tabulated in Table 39. The corresponding stress intensity factors computed using Equation (29) and Shah's ⁽¹⁷⁾ solution are also included in the table. Since the growth increments due to the marker loads have been neglected in the data reduction, K values reduced from the data are slightly higher as reflected in the table. In general, the correlation is fairly good.

Close Tolerance Fastener Holes with and Without Fastener Load Transfer - With a knowledge of the through crack solution β_{CT} , the stress intensity factor for semi-elliptical embedded cracks emanating from a close tolerance fastener hole with or without fastener load transfer can be estimated from Equation (29) by replacing the factor β_{op} with the factor β_{CT} . Values of β_{CT} are given by Equation (17) and in Figures 143 to 145.

Interference-Fit Fastener Holes - Similar to a close tolerance fastener hole; the stress intensity factor for semi-elliptical embedded cracks emanating from an interference-fit fastener hole can be estimated from Equation (29) by replacing the factor β_{op} with the factor β_{IF} . Typical β_{IF} factors for thru cracks emanating from the interference-fit fastener holes are given in Figures 150 and 152.

Cold-Worked Holes - Theoretically speaking, the stress intensity factor for semi-elliptical embedded cracks emanating from a cold-worked hole can be estimated from Equation (29) by replacing the factor β_{op} with the factor β_{CW} . However, it is suspected that the beneficial residual strains due to cold working may be relaxed after a certain period of fatigue cycling. The current analysis is not capable of accounting for such relaxation.

For convenience, the available stress intensity factor solutions for embedded cracks emanating from the types of fastener holes studied during this program are summarized in Table 40.

3. FAILURE CRITERION FOR FLAWED COLD-WORKED HOLES

A failure criterion which could accurately predict failure of flawed structures would be a useful engineering tool for the evaluation of structural integrity and the selection of materials. Linear elastic fracture mechanics provides a one-parameter failure criterion, K_{IC} , for cracked structures with small-scale yielding. However, for a crack emanating from a cold-worked hole, due to the presence of the large plastic strains induced during the cold-working process, the failure may not be characterized completely by linear elastic fracture mechanics.

The recent attention given to the J integral as a failure criterion is partly due to the fact that the path-independent J integral can be calculated through regions where the stress and strain states can be determined with sufficient accuracy. For linear elastic behavior, the J integral is identical to G, the strain-energy release rate per unit crack extension. Therefore, a J integral failure criterion for the linear elastic case is identical to the K_{IC} failure criterion. The use of the J integral as a failure criterion would provide a means of directly extending fracture-mechanics concepts from linear elastic behavior to elastic-plastic behavior.

The path-independent integral discovered and designated J by Rice⁽³⁸⁾ is defined by

$$J = \int_{\Gamma} W dy - \bar{T} \frac{\partial \bar{u}}{\partial x} ds, \quad (30)$$

where x and y are cartesian coordinates measured tangent and normal to the crack at the tip, ds is an element of arc length along any path Γ circumscribing the crack tip, W is the strain-energy density and \bar{T} and \bar{u} are respectively the stress and displacement vectors appropriate to material just inside Γ . The promise of the J integral as a meaningful measure of propensity for crack propagation when large scale yielding* is apparent springs from two observations: the path independence of the integral can be established without specifying a linearly responding material; if however a linearly responding material is specified, J can be shown to reduce to the plane-strain energy-release rate. Notwithstanding these, an elastic material response is required to evaluate J because of the appearance of W in its definition. Consequently, J can be computed without ambiguity for a nonlinearly elastic response but not for an inelastic one. Thus, in any application where the material nonlinearity arises due to the onset of plastic deformation, the value of J can be tracked only up to the point where the distinction between nonlinear elasticity and plasticity is manifest; i.e., when some part of the region under consideration begins to unload.

With regard to the cold-work process, the beneficial residual stress field is, of course, the direct result of unloading following an expansion severe enough to carry material near the edge of the hole past its elastic limit. Moreover, when a remote uniaxial tension is applied vertically, the material at the top and bottom of the hole unloads even more. This secondary unloading could be ignored or perhaps avoided by a judicious choice of Γ , since the region involved does not include the neighborhood of anticipated crack initiation. But the initial unloading that occurs as the mandrel is removed affects the entire circumference of the hole and cannot be reasonably overlooked.

A numerical estimate of J (using stresses and displacements obtained from a finite element representation of the material around a cracked hole) was found to be path independent

* Large scale yielding here is taken to mean any plastic deformation that is not exclusively characteristic of the crack tip; e.g. plastic deformation influenced by boundaries other than the crack faces near the tip.

and in good agreement with the plane strain energy release rate available from Bowie's⁽³⁹⁾ analytical solution when no plastic deformation was involved. When the same model was used to simulate 2% cold work with subsequent 18 ksi remote tension, an attempted estimate of J (treating W as recoverable energy density) resulted in a path-dependent quantity defying interpretation.

Consequently, the J integral was abandoned as a potential fracture criterion with which to correlate the tests tabulated in Table 31. Alternatively, the following two approaches were employed in an effort to assess the apparent toughness appropriate to material near a 2% cold-worked open hole. Qualitatively, the results for aluminum and titanium can be discussed together.

The first approach consists of neglecting the residual stresses altogether in the calculation of K_I . Predictably, the computed apparent toughness was greater than the toughness obtained in the conventional test (Table 29); but the difference was least for the shortest crack length, where the effect of hole conditioning could reasonably be expected to be greatest. One possible explanation of this paradox relates to the fact that the crack was introduced prior to the cold-work operation. This means that the crack tips were probably blunted during the initial phase of the expansion. For the shorter cracks, however, subsequent expansion and unloading produced tangential stresses that would tend to press the crack faces together in a "resharpening" operation. Based on this argument, one might anticipate that the longer cracks remain more blunt and therefore would exhibit a higher apparent toughness. An area that needs further serious consideration is that addressing the importance of sequence in the cracking/cold-work operation.

The second approach acknowledges the residual stress field by superposing it with that due to remote loading in order to obtain tractions to remove from the prospective crack surface via a numerically generated Green's function⁽⁴⁰⁾. In strict accordance with the definitions of linear elastic fracture mechanics, such an approach is dubious at best; i.e. LEFM does not respond to situations in which the normal stress on the prospective crack surfaces is compressive while the extensional strain in the same direction is positive. Nonetheless, the apparent toughnesses computed in this manner were in general agreement with those obtained in conventional tests except for the shortest crack lengths. Here the apparent

toughness was substantially less. This may be attributed, in unknown fractions, to at least two sources. Firstly, the beneficial residual stress field may be largely lost due to relaxation--especially near the edge of an open cold-worked hole. This possibility needs rather immediate attention owing to the considerable impact it might have on life predictions. Secondly, reverse yielding is evident at the edge of the hole (see Figures 112 to 114), and an accurate determination of the stresses there requires a hysteresis data base sufficient to model the post-yield position and size of the yield surface. Moreover, reverse yielding intensifies the already formidable stress gradients near the edge of the hole and may require more sophisticated elements or refined modeling in this neighborhood.

4. CRACK GROWTH PREDICTIONS

Current methodologies for life predictions are based on a crack-growth-damage integration package that has a data base and analysis to interrelate the following elements: (a) initial crack geometry, (b) applied stress spectrum, (c) baseline crack growth rate and other material data, such as σ_y and K_{IC} , (d) stress intensity factor solution and (e) load-interaction model. In this section, the predicted number of cycles (or flights under the spectrum load) are compared with those counted in the test of aluminum and titanium specimens subjected to constant-amplitude, bomber and fighter spectrum loadings. There is no existing methodology which is capable of accounting for the interaction between the residual stresses created by the overload in the spectrum and that created during the cold-working operation or the installation of an interference-fit fastener. Therefore, no attempt was made to predict the crack growth from these types of fastener holes under spectrum loading.

The predicted results for cracks growing from an initial size, a_i , to a final size, a_f , are normalized by the corresponding test data and presented in Table 41 for constant amplitude loaded specimens and in Table 42 for spectrum loaded specimens. For specimens tested under spectrum loading, the predictions were made using the linear accumulation technique and three different retardation models included in the computer program, "CRACKGROWTH," available at the Lockheed-Georgia Company. These retardation models are the original and modified Willenborg et al models^(41, 42) and the Hsu model⁽⁴³⁾. The constant amplitude

crack growth rates presented in Figures 10 and 11 together with Forman's equation were used in the predictions. For corner cracks, the initial flaw shape was assumed to be quarter-circular. The final surface crack length observed during the test was used to determine the crack growth life of each test hole (except for specimen T-FS-1, in which the final dimension along the hole wall was used). As seen from the tables, most of the predictions are reasonably good. However, for spectrum loaded specimens, none of the existing models can consistently produce accurate predictions. Development of an improved load-interaction model and better understanding of the interdependence of the various parameters affecting the fatigue crack growth under flight-by-flight spectrum loading are necessary before adequate crack growth life predictions can be achieved for all load spectra.

SECTION VI

OVSERVATIONS AND CONCLUSIONS

Based on the analytical study conducted under this program, the following observations and conclusions have been made:

- (1) A Green's-function approach has been developed for estimating the stress intensity factors for straight through cracks emanating from any type of fastener hole. The approach consists of two steps: first, a nonlinear finite element solution for the elastic-plastic stress field appropriate to the unflawed hole is generated; next, a crack is introduced in this stress field by removing the tractions on the crack faces and computing the corresponding stress intensity factor using the Green's-function approach.
- (2) When the applied far-field stress exceeds about one third of the material yield strength, local plastic deformation begins at the edge of an open hole. The normalized stress intensity factors computed using the Green's-function approach is lower than the Bowie factor obtained for the purely elastic case. As local yielding proceeds, such normalized factors decrease as the far-field applied stress increases. When the crack length is longer than one radius of the hole, this plasticity effect becomes negligible.
- (3) For the cases where the cracks emanate from interference-fit fastener holes in both aluminum and titanium alloy plates subjected to constant amplitude far-field loading, the computed effective stress intensity factor ranges, $K_{\max} - K_{\min}$, are essentially constant and independent of the level of diametrical interference. However, the effective stress intensity factor ratio, $R_{\text{eff}} = K_{\min} / K_{\max}$, does depend upon the level of interference. For a crack length less than one radius, R_{eff} decreases rapidly as the amount of interference increases. When $a/r > 1$, R_{eff} remains almost constant as the amount of fastener hole interference increases.
- (4) By idealizing a crack emanating from an interference-fit fastener hole in a plate subjected to constant amplitude far-field loading as one emanating from a fastener

hole without residual stress and subjected to variable amplitude loading which produces the same ΔK_{eff} and R_{eff} , the predicted crack growth history correlates reasonably well with the test data.

- (5) For the cracks emanating from cold-worked fastener holes, the stress intensity factor corresponding to a given crack length increases as the amount of cold working decreases. The stress intensity factors at cracked cold-worked open and close tolerance fastener holes are practically the same. However, with a small amount of fastener load transfer, the corresponding stress intensity factor increases significantly. The computed stress intensity factors correlate excellently with test data reduced from the testing of aluminum and titanium materials with large initial crack lengths.
- (6) Theoretically speaking, if the crack length is smaller than the compressive zone resulting from the cold-work operation and the application of the maximum cyclic load, the crack will not propagate under constant amplitude cyclic loading. However, the experimental data negates such a conclusion. It is suspected that the relaxation of residual compressive strains due to cold working occurs, and after a period of fatigue cycling, the net hoop stress reverts to tension upon the reapplication of the maximum cyclic load. The existing methodology is not capable of taking such relaxation into account.
- (7) The Green's-function approach developed here can be easily extended to study cracks originating at any other fastener-hole combination.
- (8) The approximate stress intensity factor for a quarter-elliptical crack emanating from the corner of any fastener hole can be derived from the corresponding thru crack solution. The computed stress intensity factors show good agreement with the data reduced from testing.
- (9) The stress intensity factor for a double semi-elliptical embedded crack originating at open hole has been derived from the modification of a surface flaw solution. The correlation between the computed stress intensity factors and those reduced from tests using the fatigue crack growth method of calibrating K is good.

- (10) Current methods of predicting crack growth under flight-by-flight spectrum loading can not be easily extended to predict the growth of cracks from pre-conditioned fastener holes (such as cold-worked and interference-fit fastener holes). This is due to a lack of understanding of the interaction between the residual stresses created due to pre-conditioning and the application of an overload.

Based on the experimental program conducted, some of the observations and conclusions made may be summarized as follows:

- (1) Fatigue lives of unflawed fastener holes having about 10% of fastener load transfer can be increased through the use of interference-fit fasteners. The fatigue life of a cold-worked hole is comparable with that of a close tolerance fastener hole if each has the same amount of fastener load transfer.
- (2) Both corner cracks and embedded flaws are the most common types of natural cracks initiated due to fatigue cycling. The shapes of these natural cracks are respectively very close to quarter- and semi-elliptical. These shapes have been assumed in most of the analyses. Surface flaws near a fastener hole having a high level of interference fit are also possible origins of natural cracks. This is true because the peak tensile stresses (during both loading and unloading) are located some distance away from the hole wall.
- (3) With a preconditioned fastener hole (such as diametrical interference or cold working), the crack growth rate, in general, is significantly lower than that of a straight reamed hole without preconditioning.
- (4) For corner cracks emanating from straight reamed holes, both with and without cold working, the growth rate along the hole wall is larger than the corresponding rate on the plate surface. Hence, the final flaw shape ratios, a/c , are greater than 1 in all the cases observed here. For similar cracks at interference-fit fastener holes without fastener load transfer, the final flaw shape is close to quarter-circular which implies that the growth rates are practically the same on both the hole wall and plate surfaces. However, with a small amount of load transfer at the interference-fit fastener holes, the final crack dimension on the hole wall is much less than that on the plate surface.

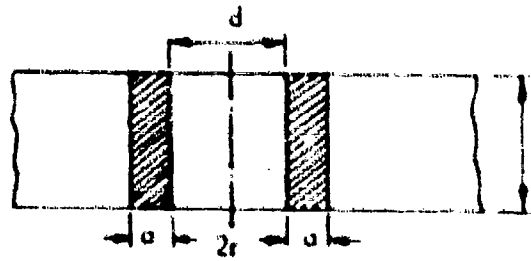
- (5) Data scatter is large in the tests of cracks emanating from cold-worked and interference-fit fastener holes. For the same type of far-field loading, such scatter decreases rapidly as the crack length increases. For a given initial crack size, if the applied load is too low (resulting in the effective ΔK being smaller than or close to ΔK threshold), one may anticipate that the growth behavior of such a crack would be essentially the same as that of a fatigue test without an intentional flaw.
- (6) The effect of 6 to 10 percent fastener load transfer on crack growth rates is more significant for cold-worked holes than close tolerance fastener holes. This effect is practically negligible at interference-fit fastener holes.
- (7) Data scatter obtained from the fighter spectrum tests is larger than that corresponding to the bomber spectrum tests, while the results of constant amplitude tests show the least scatter.
- (8) For initially intermediate and large cracks emanating from interference-fit fastener holes subjected to the same type of far-field loading, within the levels of interference studied here, their associated growth rates are practically the same for each level of interference. However, for small initial cracks, the crack growth rates decrease as the amount of interference increases.
- (9) For cracks originating at cold-worked fastener holes, the crack growth rates decrease as the amount of cold working increases.
- (10) For a given load spectrum and fastener-hole condition, the equivalent "threshold" crack length can be established from the testing of small initial cracks, from which a qualitative comparison between different types of fastener holes can be made. The equivalent threshold crack length is spectrum dependent.
- (11) The beneficial effect of the residual strains (created during the installation of interference-fit fasteners or during the cold-working operation) on retarding the fatigue crack growth is most significant when the crack length is small. The benefit decays as the crack length increases.

SECTION VII

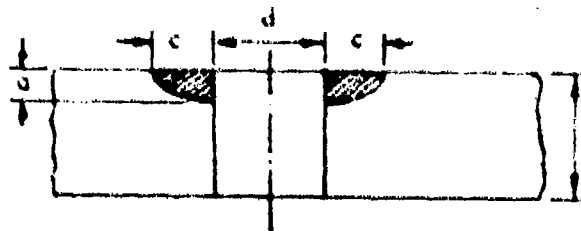
RECOMMENDATIONS

Based on the study conducted for this program, it was found that certain desirable information could not be obtained from the material available. The subjects listed under this section might be considered for inclusion in future Air Force R&D programs.

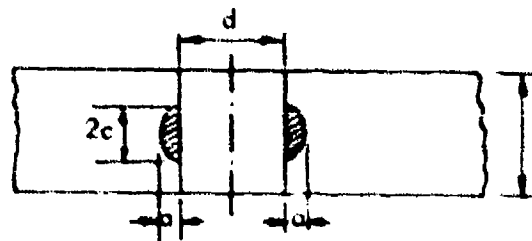
- (1) The beneficial effect of the cold-working operation on the fatigue and crack growth characteristics has been demonstrated based on test data generated mostly under tension-tension loading. The interactions between both overloads and compressive loads in a spectrum with the residual compressive hoop stresses around a fastener hole resulting from the cold-working operation should be investigated in more detail. Limited data available to date seems to indicate that they might negate such beneficial effects.
- (2) It is suspected that the residual compressive hoop stresses resulting from the cold-working operation may be relaxed significantly, even under constant amplitude tension-tension fatigue loading. An investigation should be conducted to answer why an initial crack--much smaller than the compressive zone resulting from the cold-working operation and the application of the maximum cyclic load--grew under cyclic loads.
- (3) Only one constant amplitude load level was used in the tests of cold-worked and interference-fit fastener holes. Since the resultant local stresses around the hole are sensitive to the far-field applied load, more far-field load levels should be used in a future study. This future study is needed as an intermediate step toward developing the methodology for analyzing the crack growth behavior under spectrum loading for these types of fastener holes.
- (4) A parametric study should be conducted to establish the relationships between the crack growth characteristics, the amount of fastener hole pre-conditioning and the far-field applied loads. Such a study is needed to allow the selection of an optimum fastener system for critical locations in a structure.



(a) Single or Double Thru Cracks

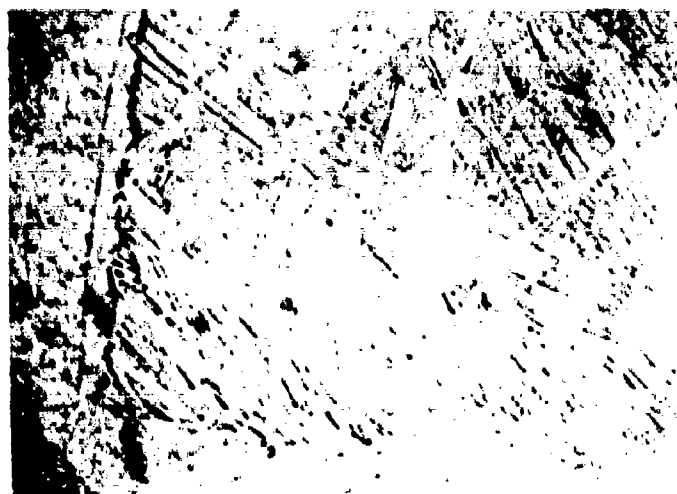


(b) Single or Double Quarter-Elliptical Part-Thru Cracks



(c) Single or Double Semi-Elliptical Part-Thru Cracks

Figure 1. Types of Cracks Considered in the Analytical Program



HNO₃ + HF ETCH

Ti-6Al-4V



KELLER'S ETCH

2219-T851

Figure 2. Photomicrographs of Test Materials - Mag. = 500X

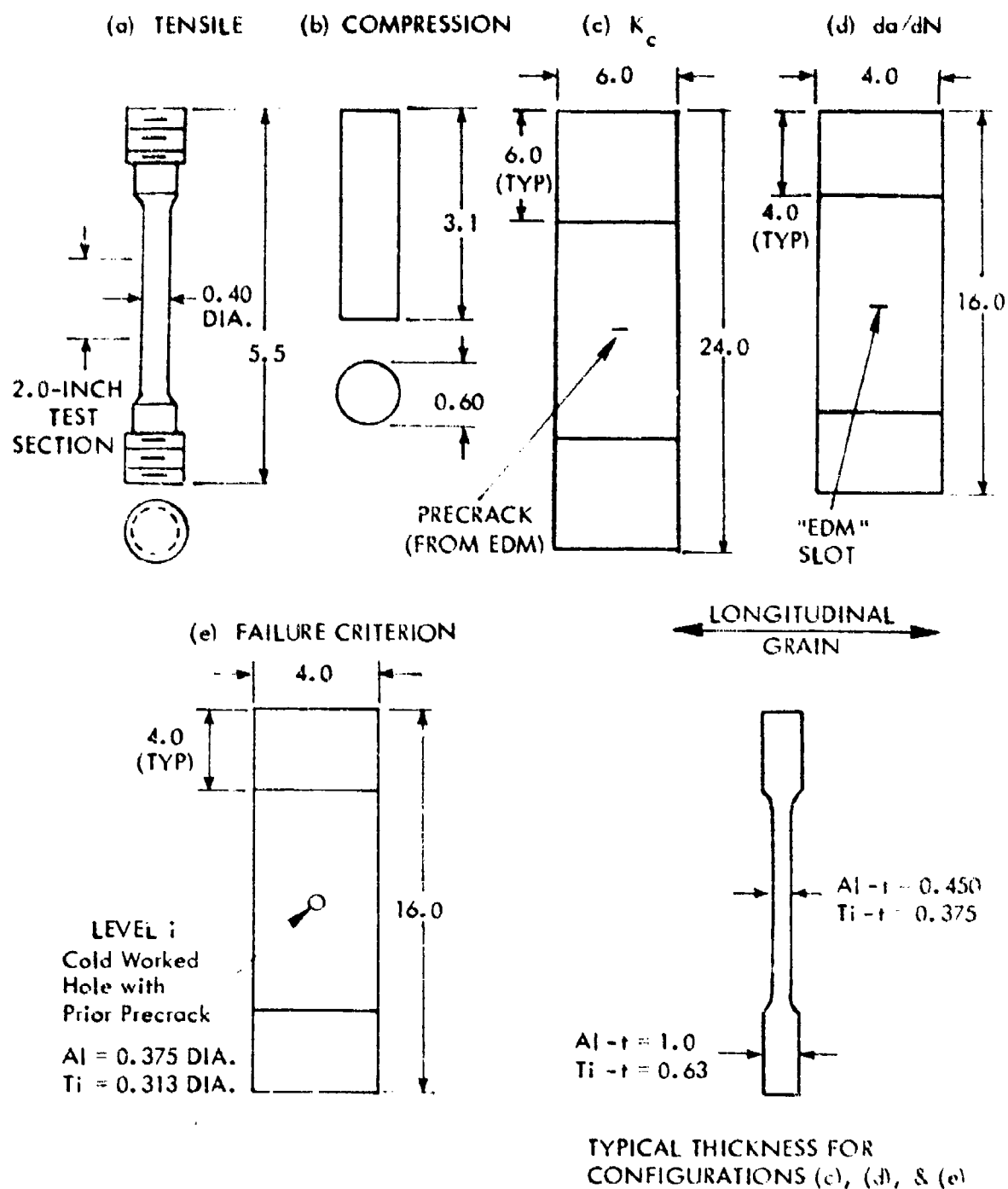


Figure 3. Test Specimen Configurations for Material Characterization and Failure Criterion Tests

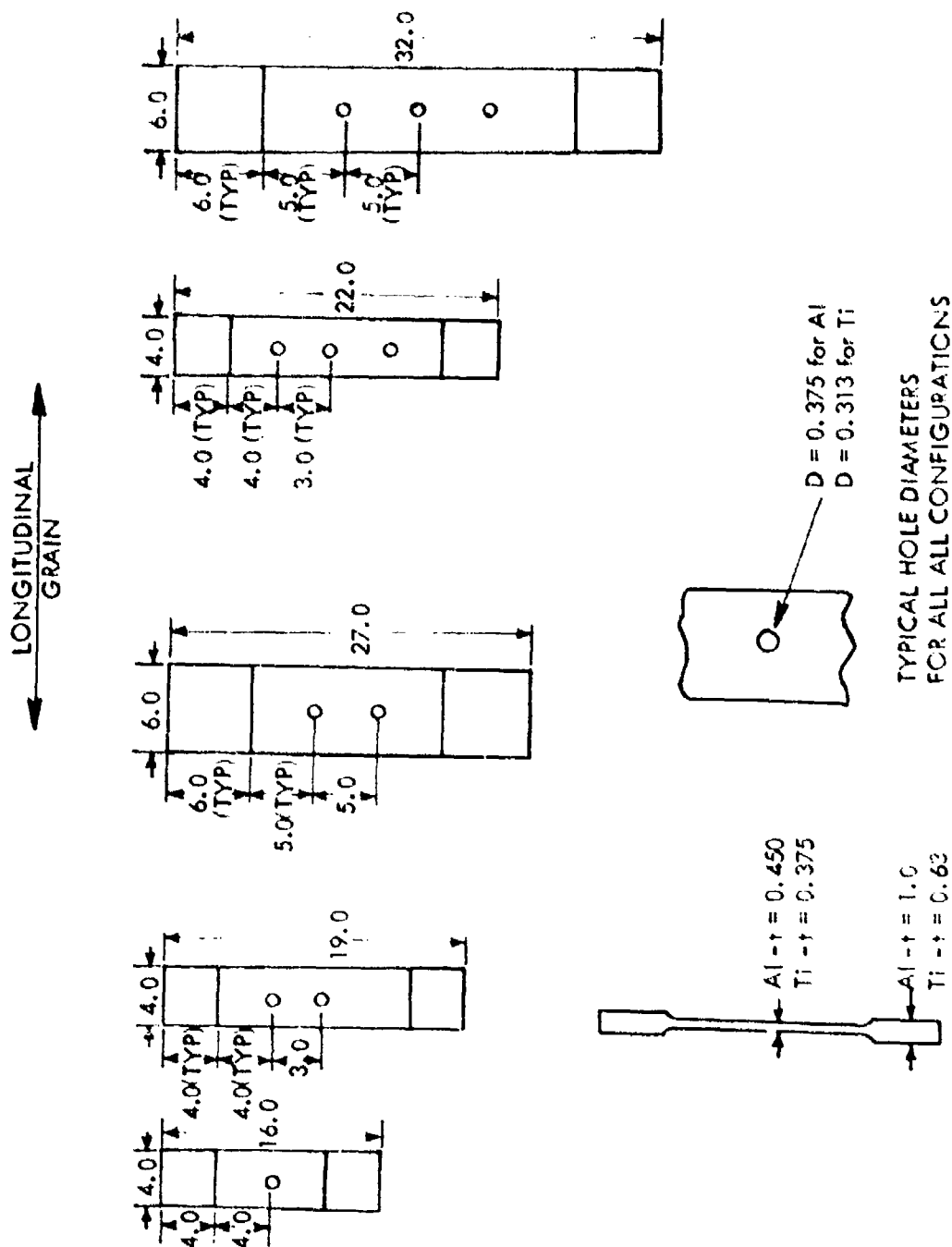


Figure 4. Test Specimen Configurations for Fatigue Tests with Interfacial Flaws

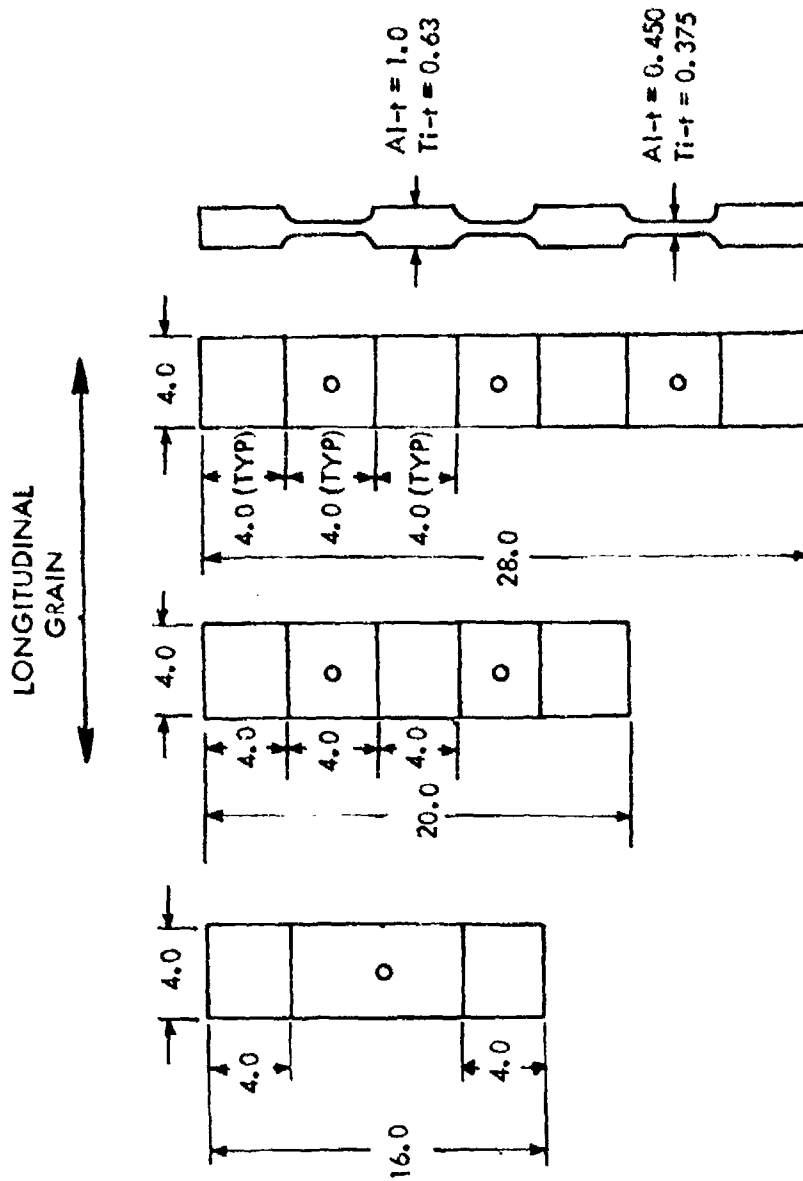


Figure 5. Test Specimen Configurations for Fatigue Tests
without Intentional Flaws

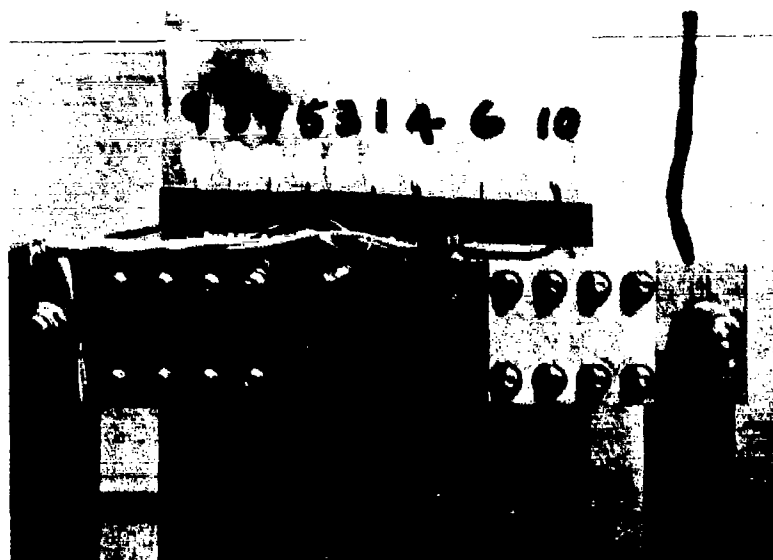


Figure 6. Detail of Fastener Load Transfer Arrangement

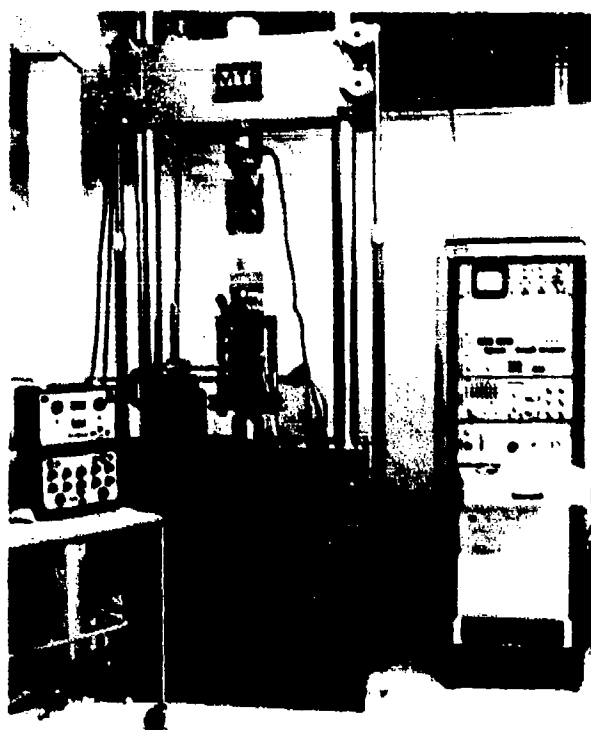


Figure 7. Detail of Test Setup

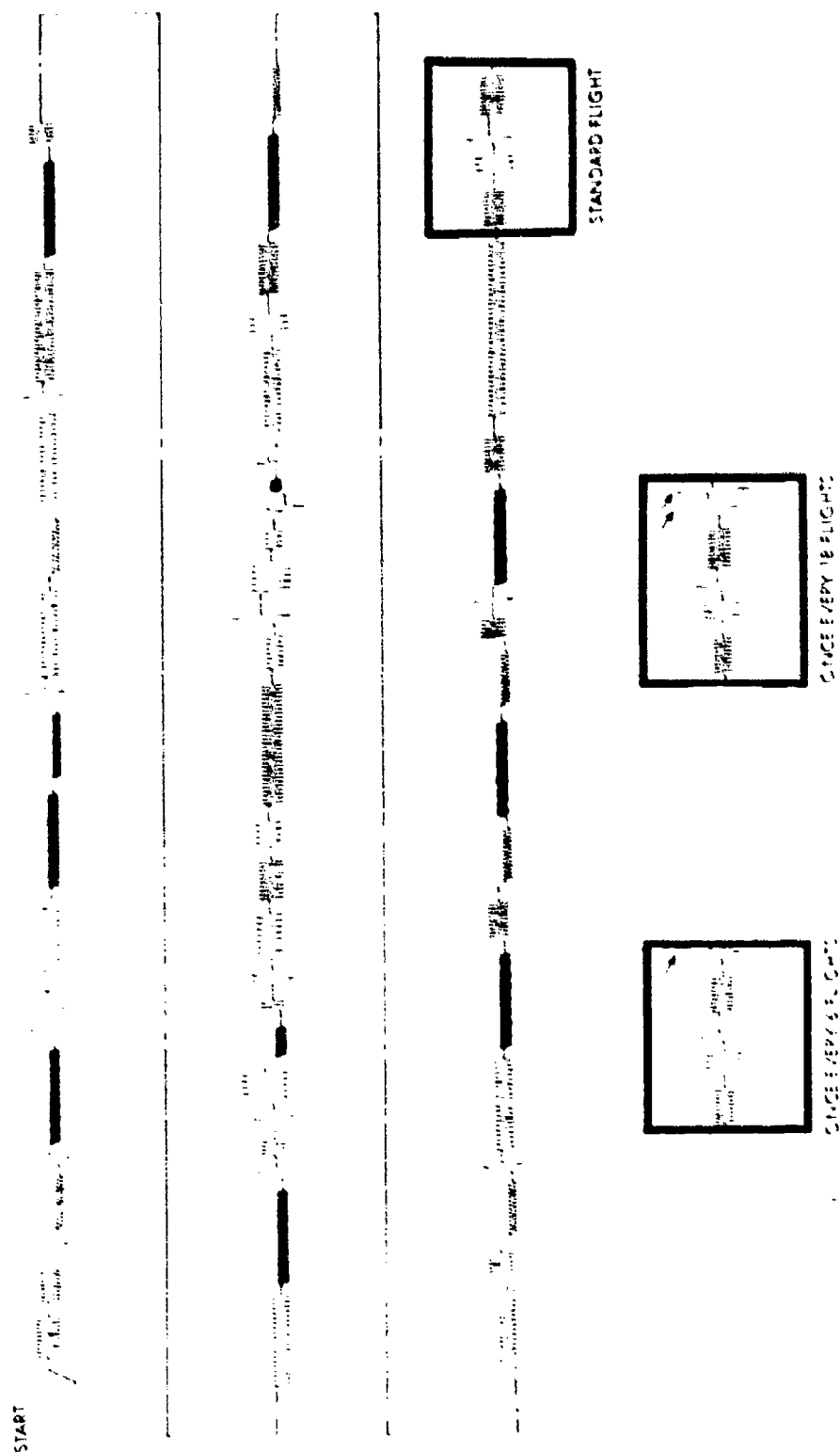


Figure 8. Fighter Spectrum

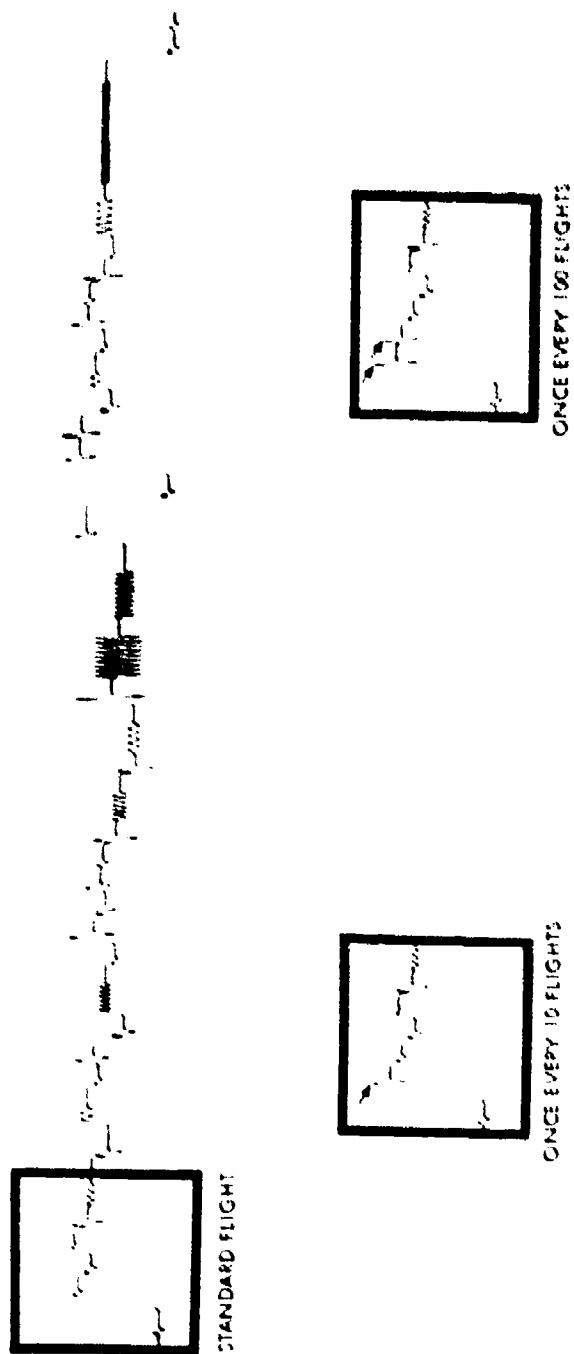
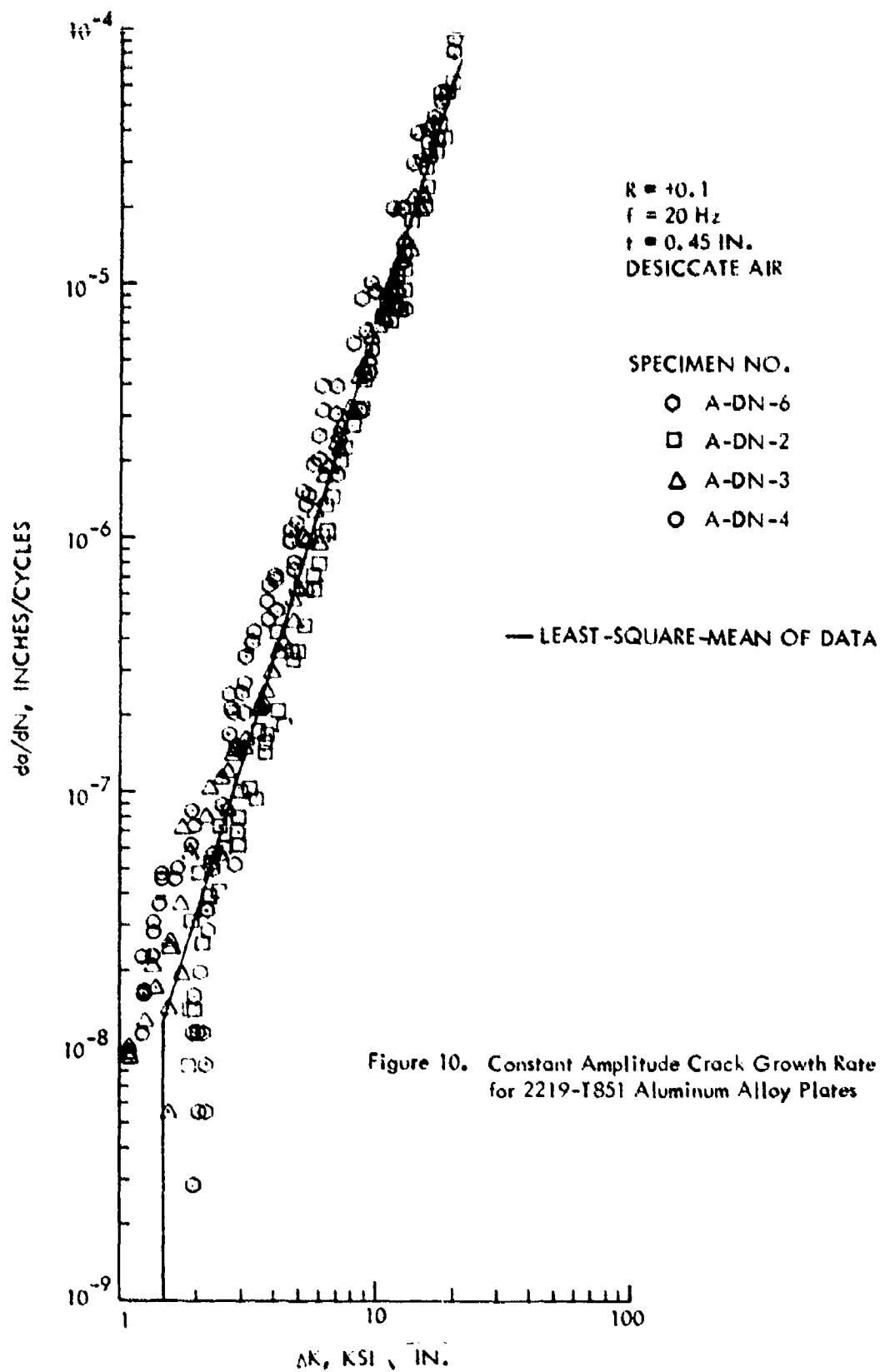


Figure 9. Bomber Spectrum



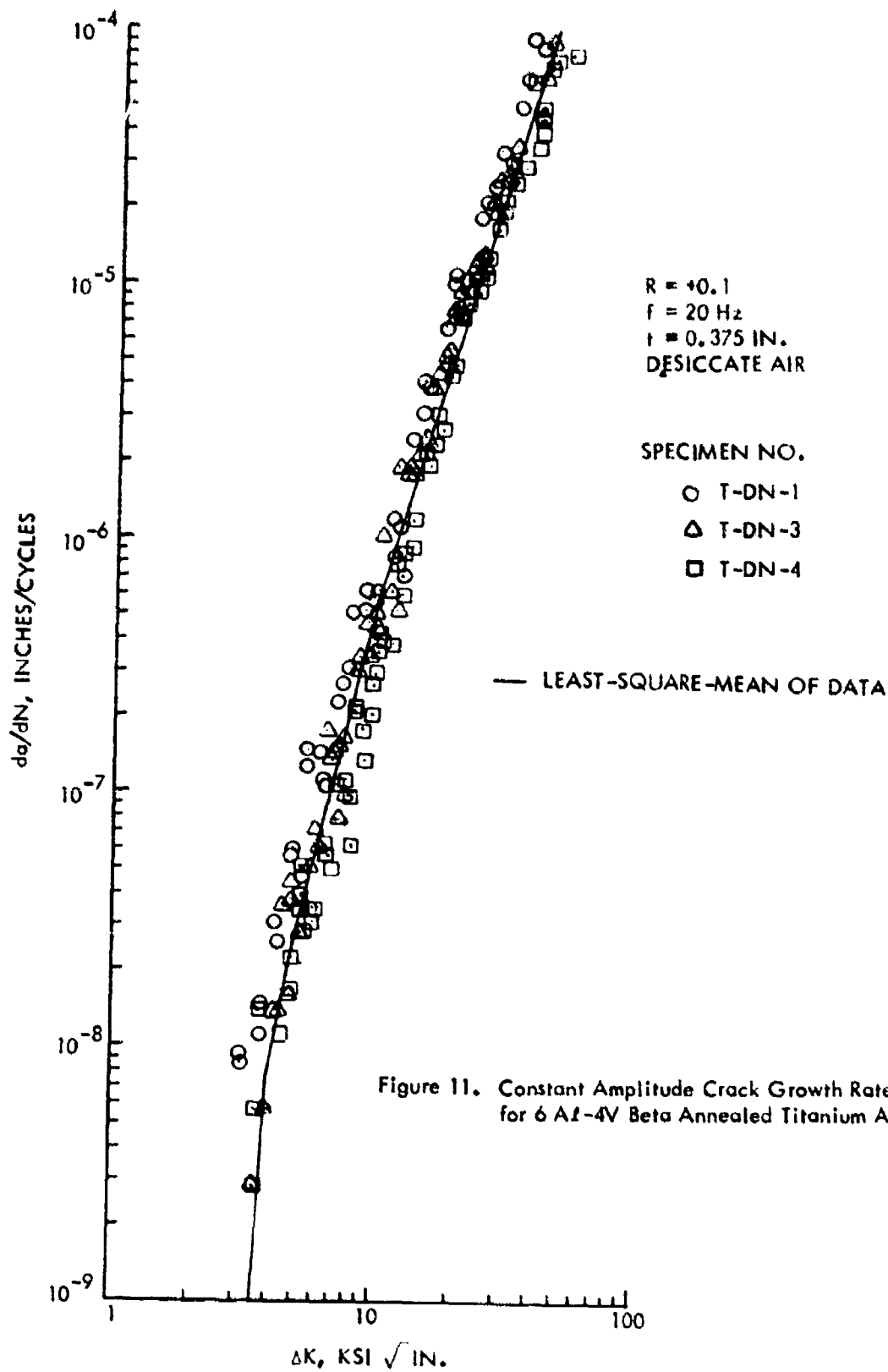


Figure 11. Constant Amplitude Crack Growth Rate Data for 6 Al-4V Beta Annealed Titanium Alloy Plates

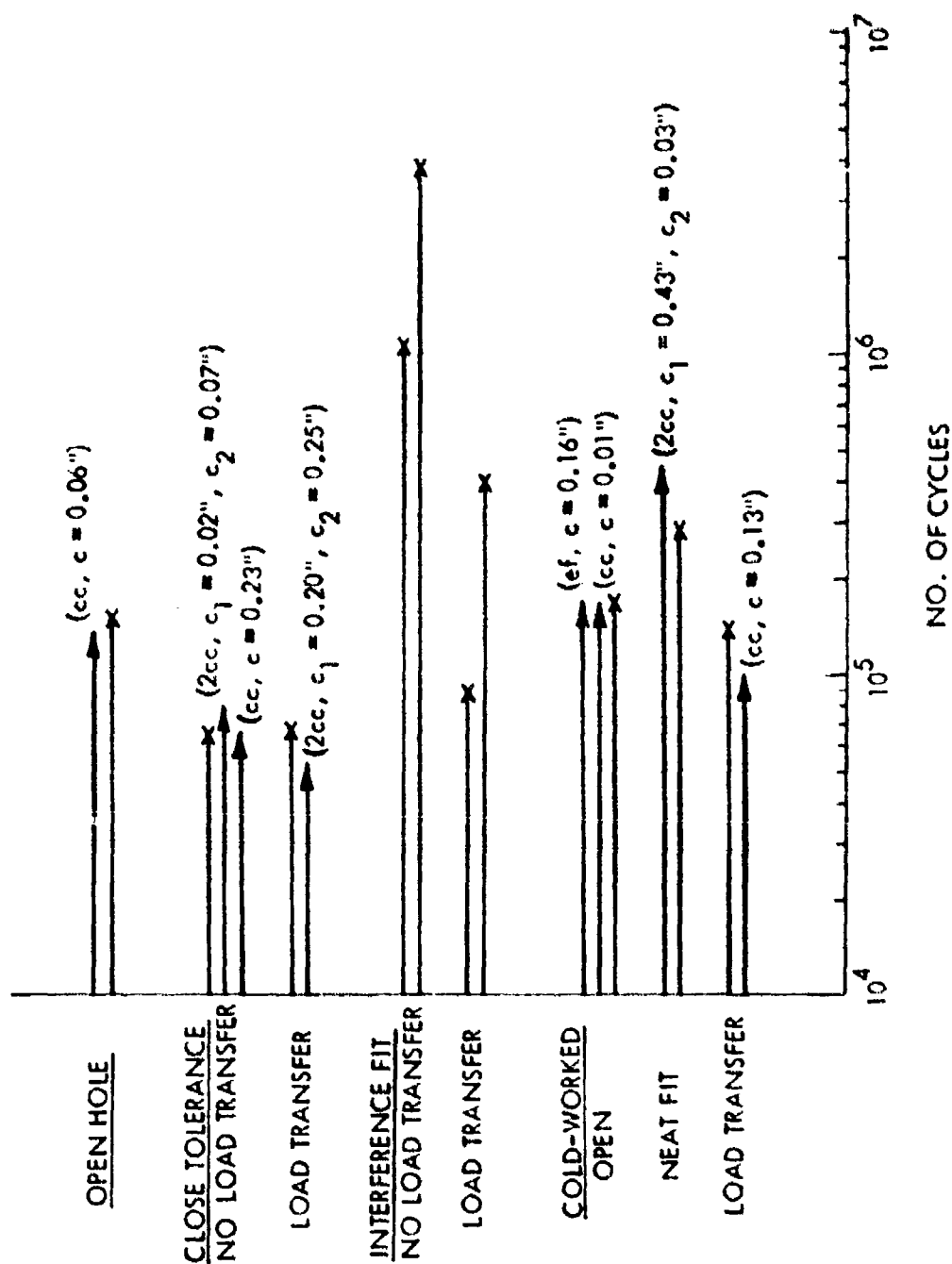


Figure 12. Fatigue Behavior of Various Types of Fastener Holes in 2219-T851 Aluminum Alloy Plates Subjected to Constant Amplitude Loading (18 Ksi and $R = 0.1$)



(a) Close Tolerance Fastener Hole with Fastener Load Transfer ($\sigma_b / \sigma_o \approx 1$)



(b) 0.0038 Inch Interference-Fit Fastener Hole with Fastener Load Transfer ($\sigma_b / \sigma_o \approx 1$)

Figure 13. Typical Surfaces of Natural Cracks Due to Constant Amplitude Fatigue Loading for 2219-T851 Aluminum Alloy

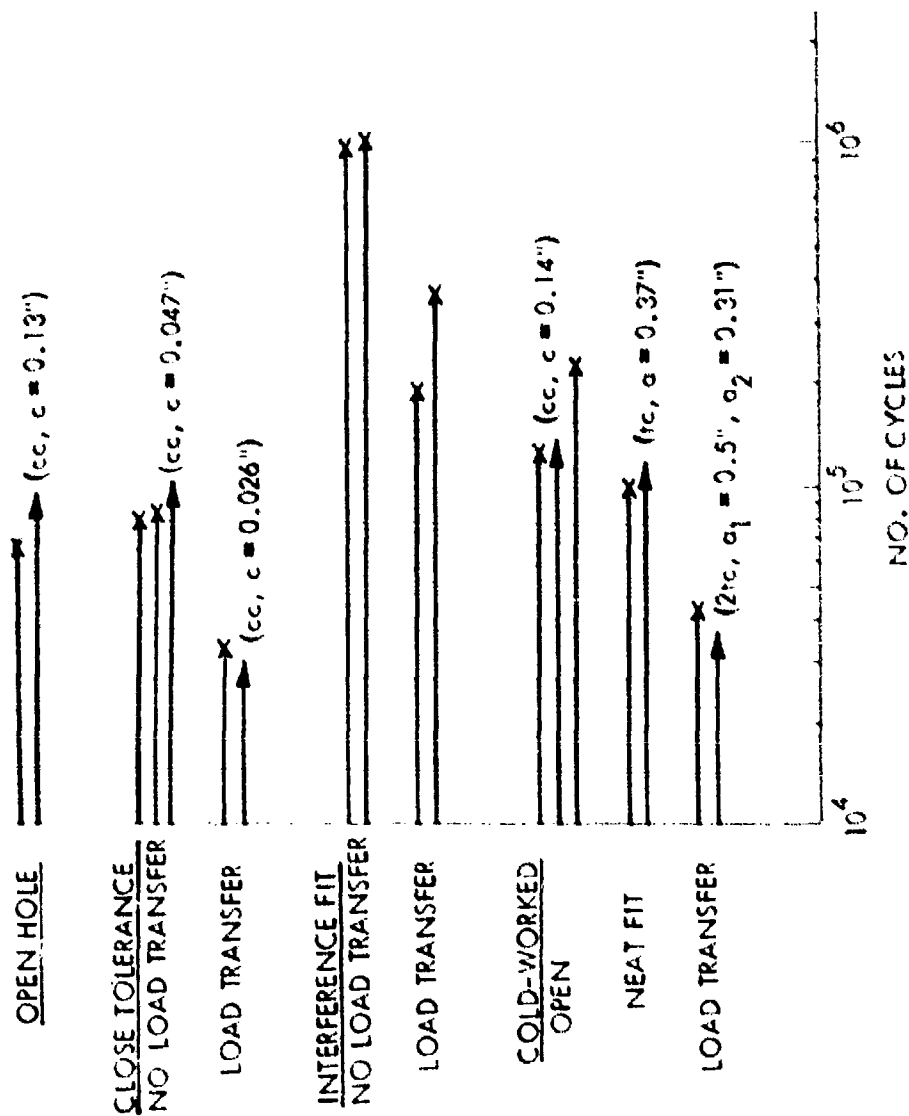


Figure 14. Fatigue Behavior of Various Types of Fastener Holes in 6A-4V Beta Annealed Titanium Plates Subjected to Constant Amplitude Loading (40 Ksi and $R = 0.1$)

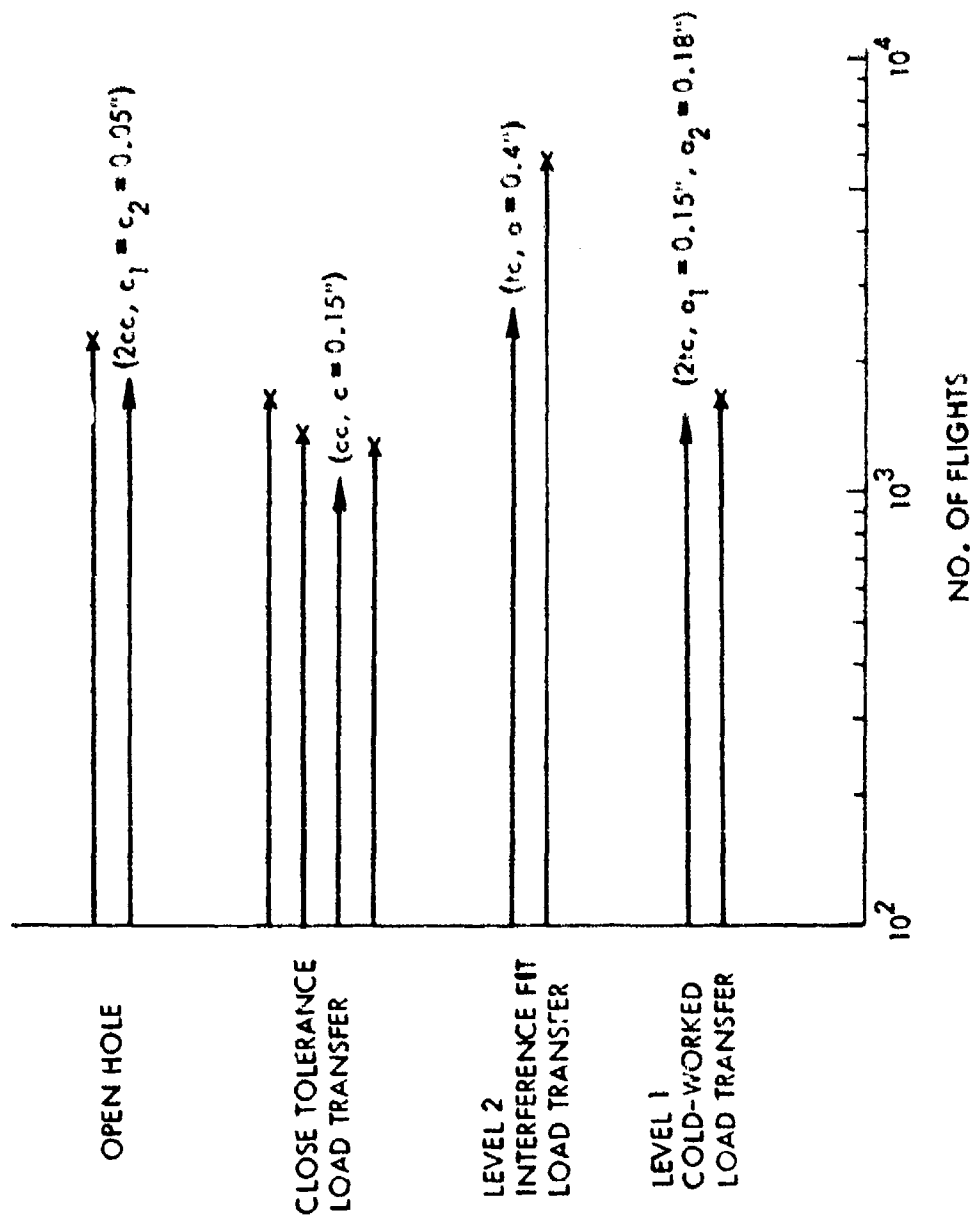


Figure 15. Fatigue Behavior of Various Types of Fastener Holes in 2219-T851 Aluminum Alloy Plates Subjected to Bomber Spectrum Loading

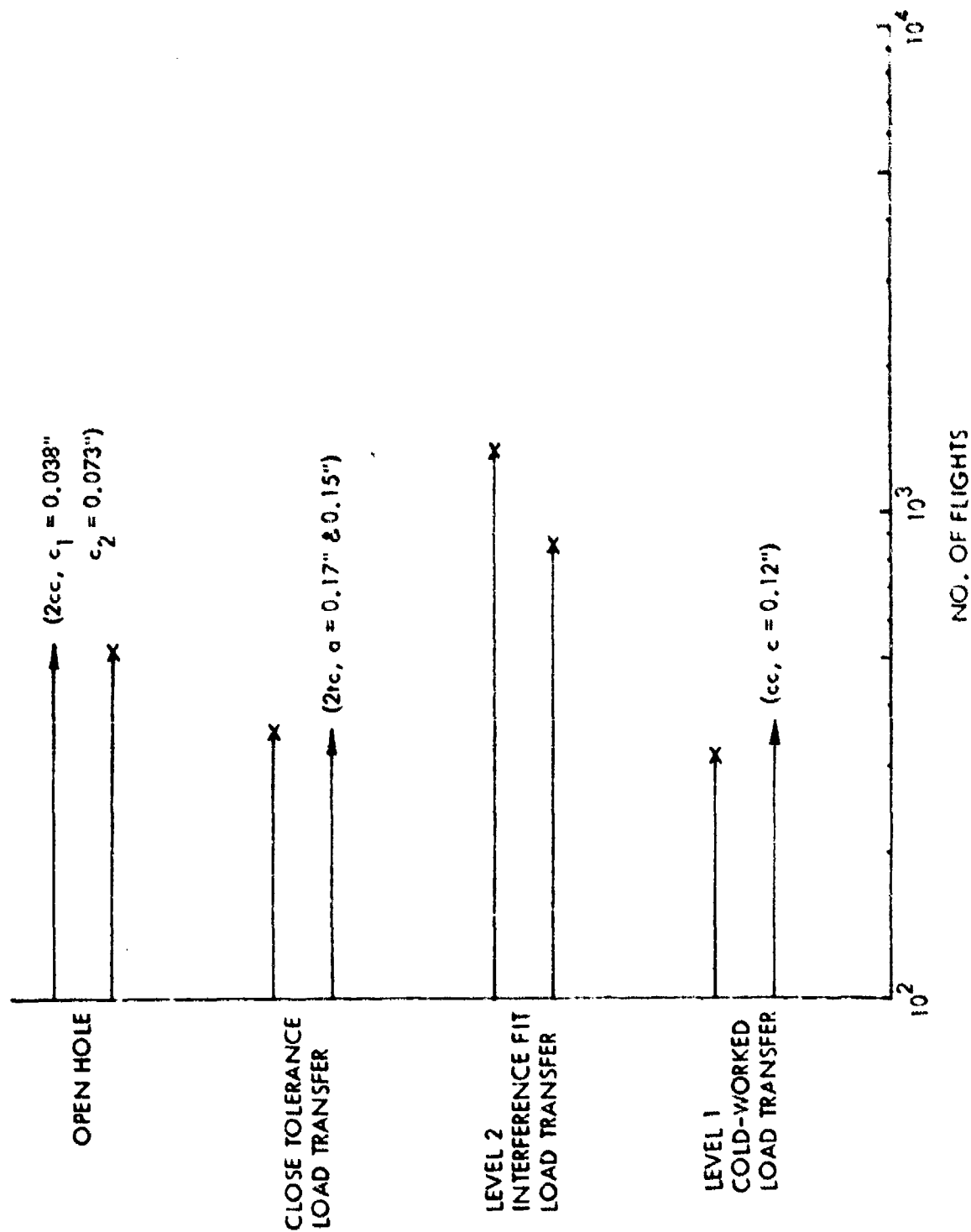


Figure 16. Fatigue Behavior of Various Types of Fastener Holes in 2219-T851 Aluminum Alloy Plates Subjected to Fighter Spectrum Loading



(a) Neat-Fit Hole with Fastener Load Transfer (Bomber)



(b) Cold-Worked Hole with Load Transfer (Bomber)



(c) Cold-Worked Hole with Load Transfer (Fighter)

Figure 17. Typical Surface of Natural Cracks Due to Spectrum Fatigue Loading for 2219-T851 Aluminum Alloy

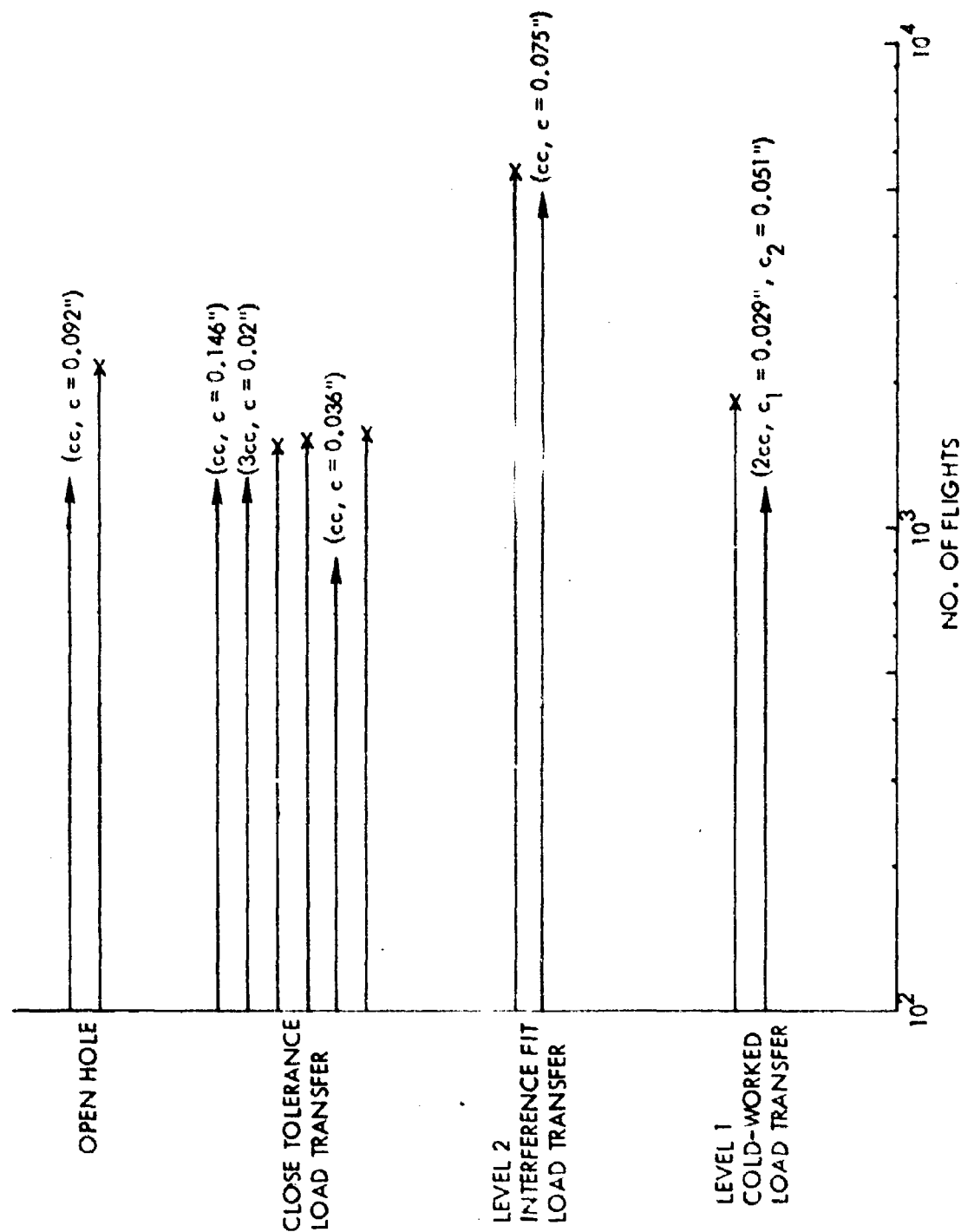


Figure 18. Fatigue Behavior of Various Types of Fastener Holes in 6Al-4V Beta Annealed Titanium Plates Subjected to Bomber Spectrum Loading

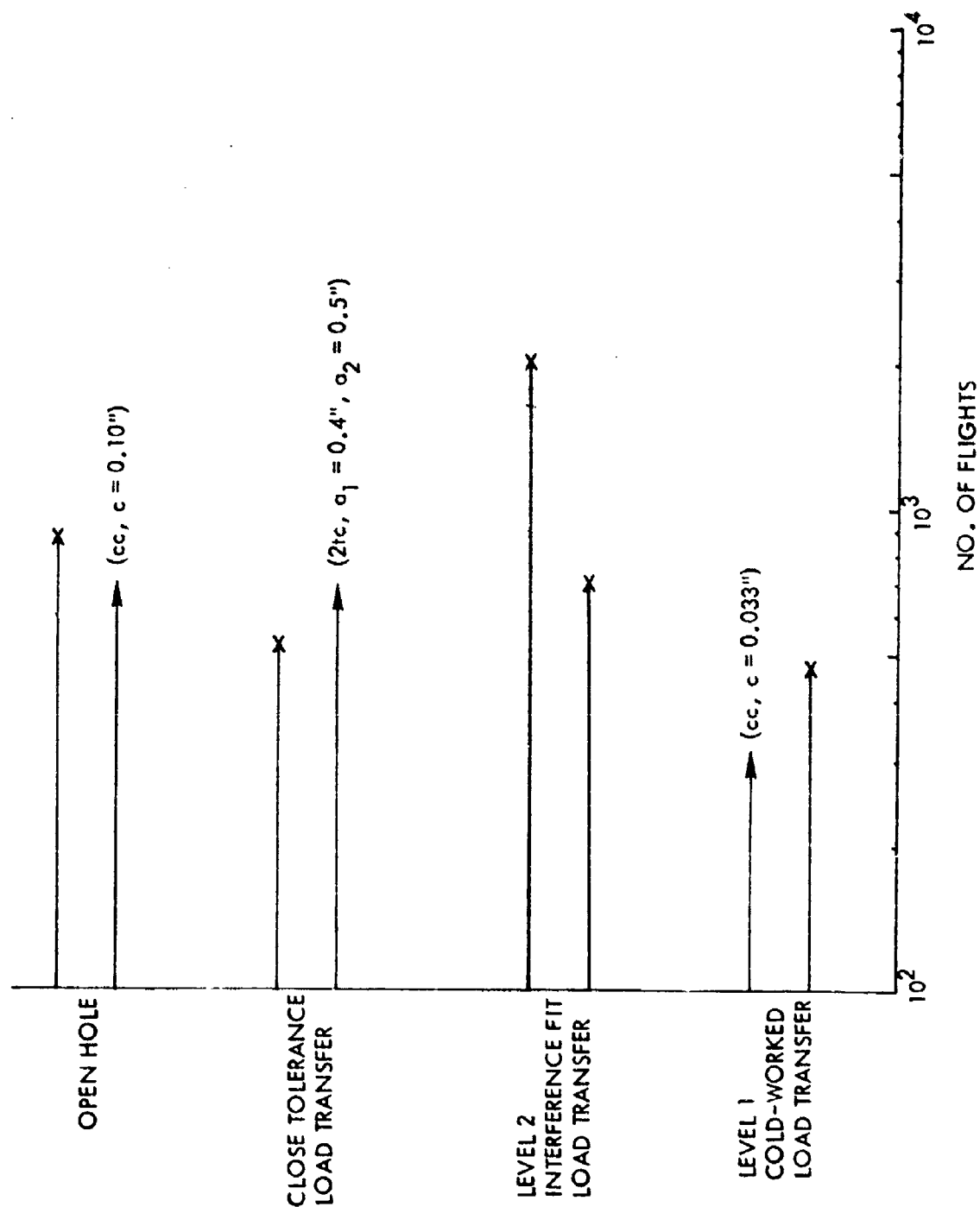


Figure 19. Fatigue Behavior of Various Types of Fastener Holes in 6Al-4V Beta Annealed Titanium Plates Subjected to Fighter Spectrum Loading

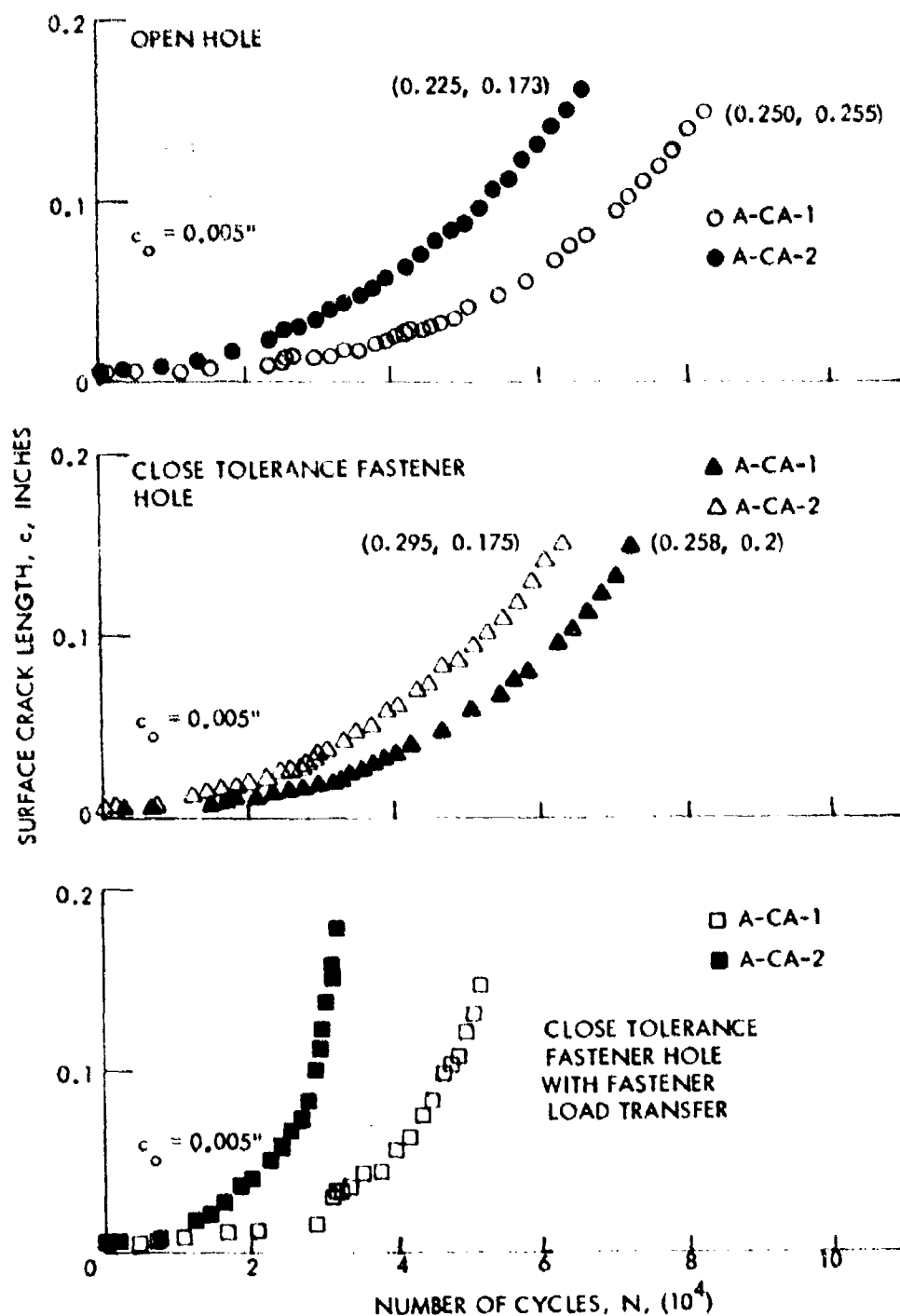


Figure 20. Growth Behavior of Small Corner Cracks from Open and Close Tolerance Fastener Holes with and without Fastener Load Transfer in 2219-T851 Aluminum Plates Subjected to 18 Ksi Constant Amplitude Loading

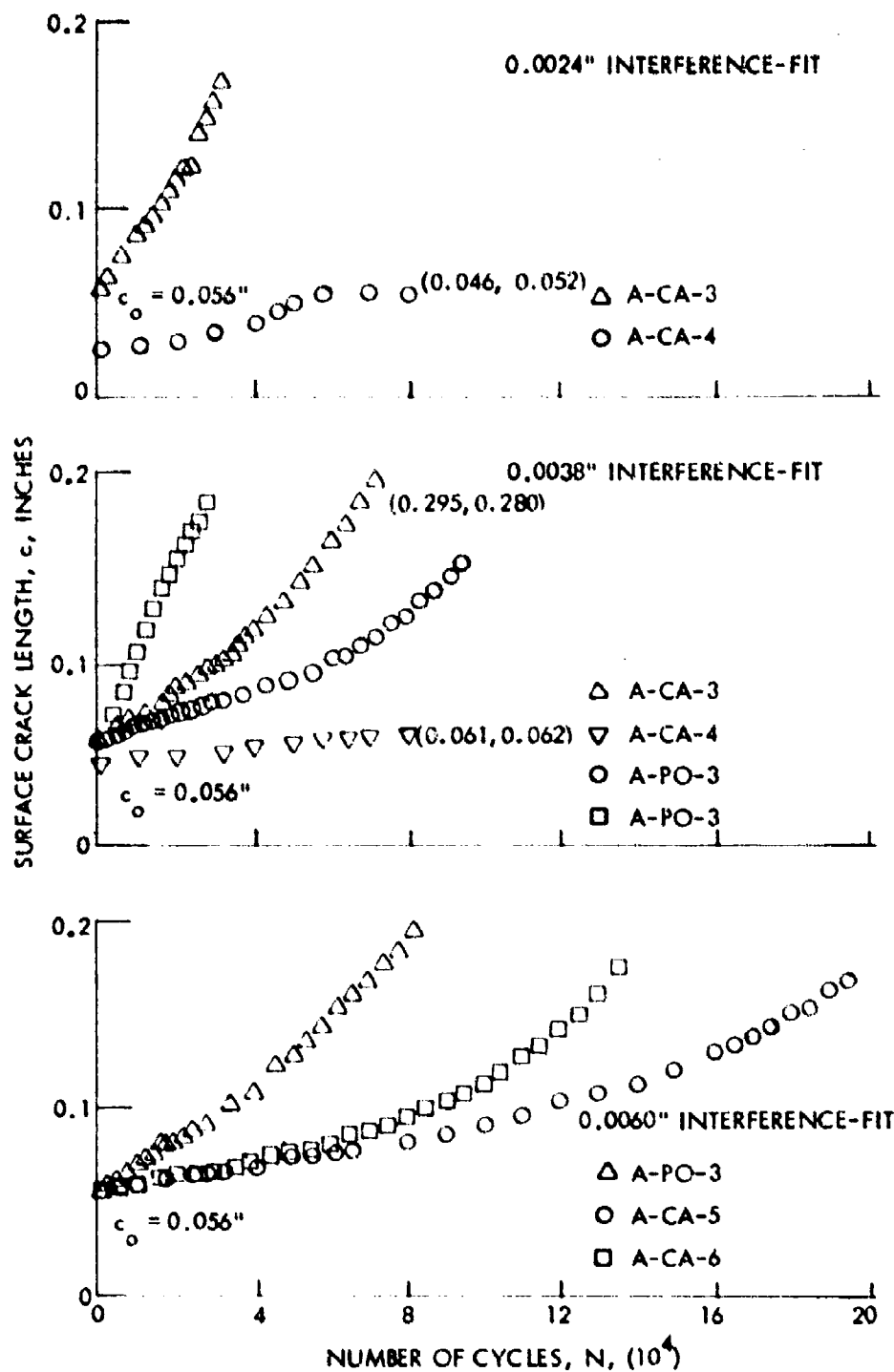


Figure 21. Growth Behavior of Intermediate Corner Cracks for Various Levels of Interference for Interference-Fit Fastener Holes in 2219-T851 Aluminum Plates Subjected to 18 ksi Constant Amplitude Loading

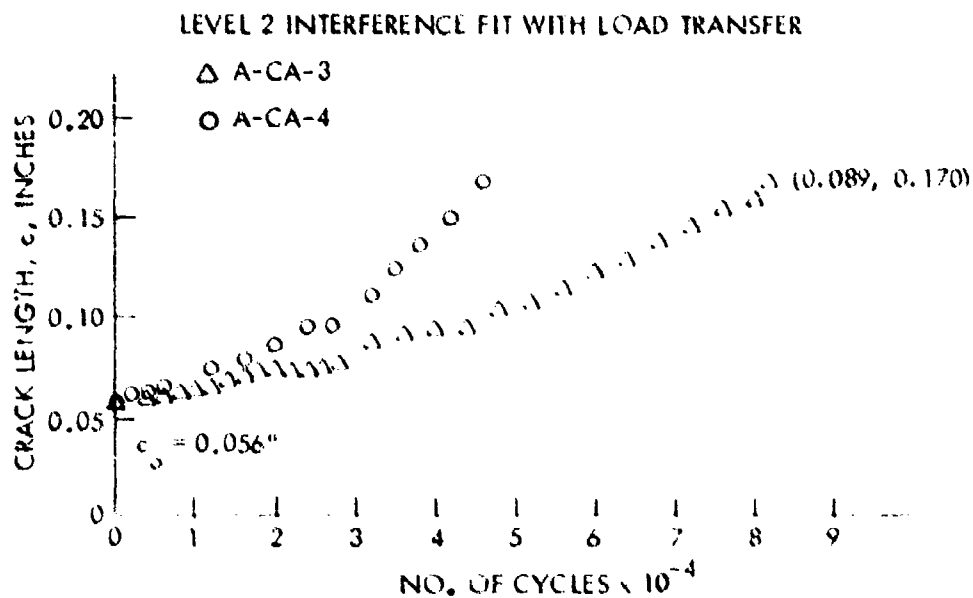
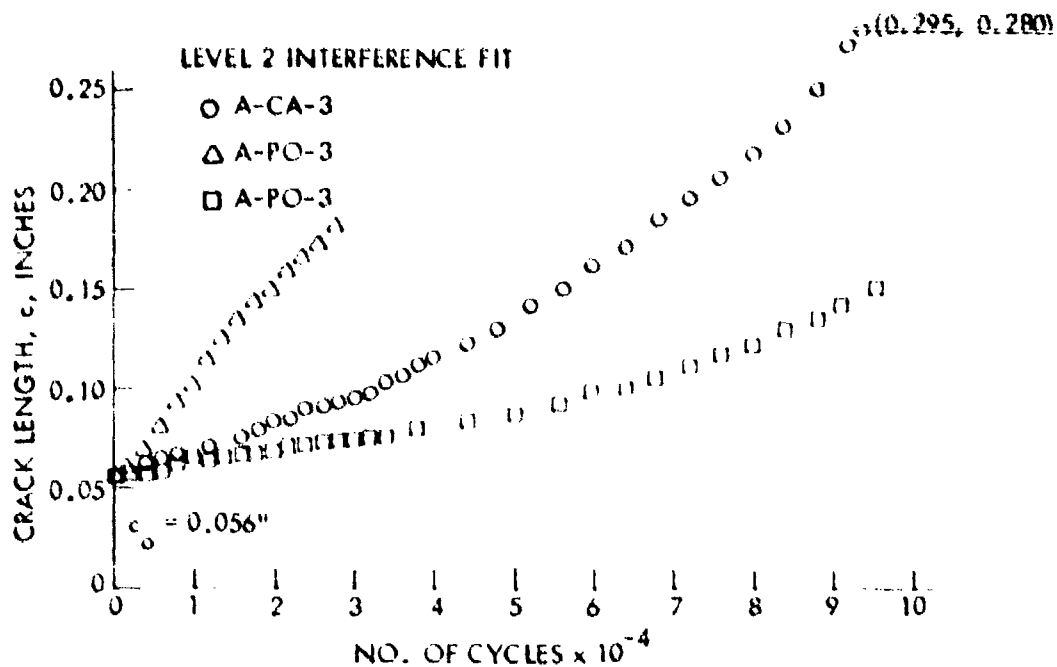


Figure 22. Growth Behavior of Intermediate Corner Cracks from Level 2 Interference-Fit Fastener Holes with and without Fastener Load Transfer in 2219-T851 Aluminum Alloy Plates Subjected to Constant Amplitude Loading ($\sigma = 18$ ksi, $R = 0.1$)

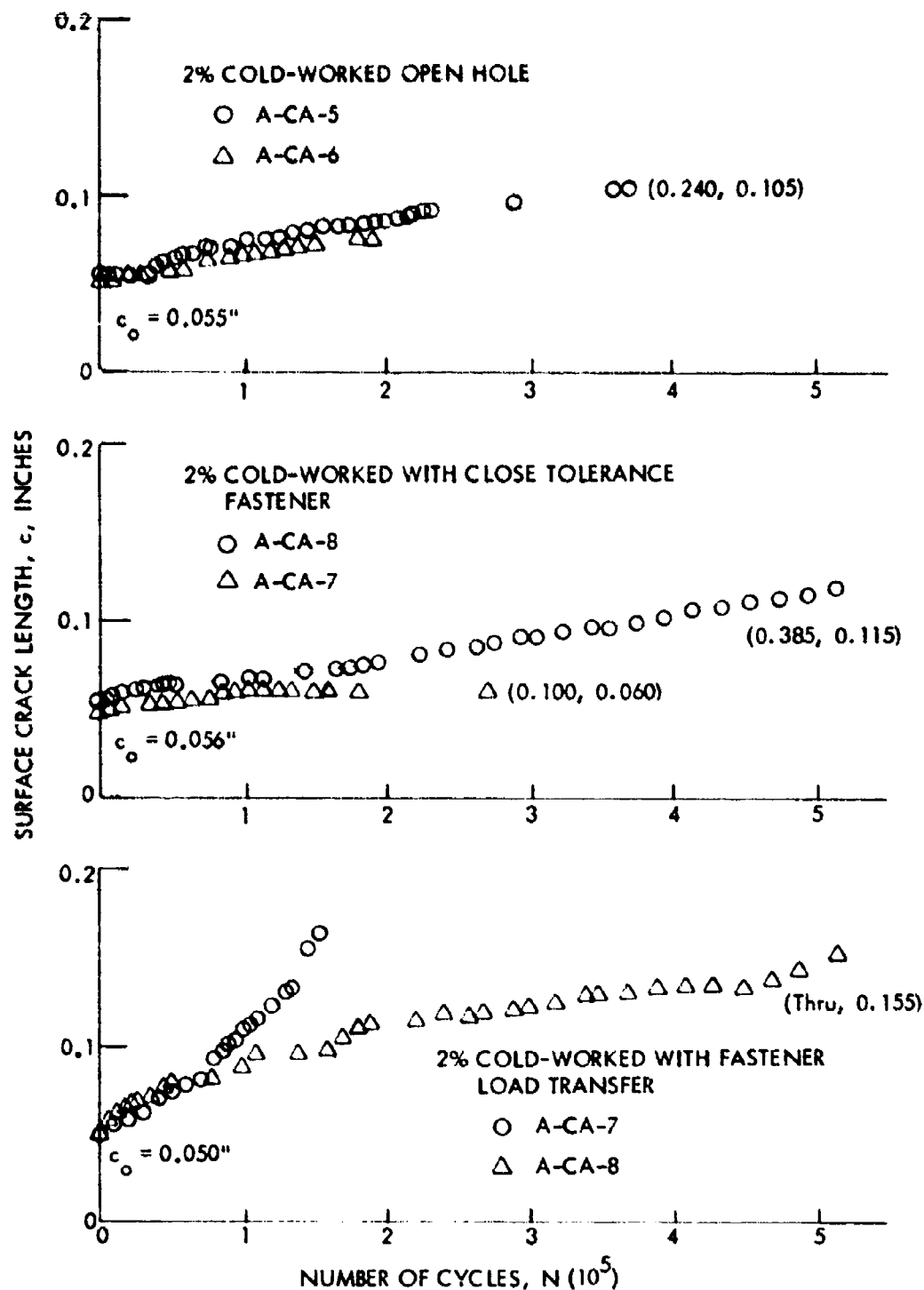


Figure 23. Growth Behavior of Intermediate Corner Cracks from Cold-Worked Fastener Holes with and without Load Transfer in 2219-T851 Aluminum Plates Subjected to 18 Ksi Constant Amplitude Loading

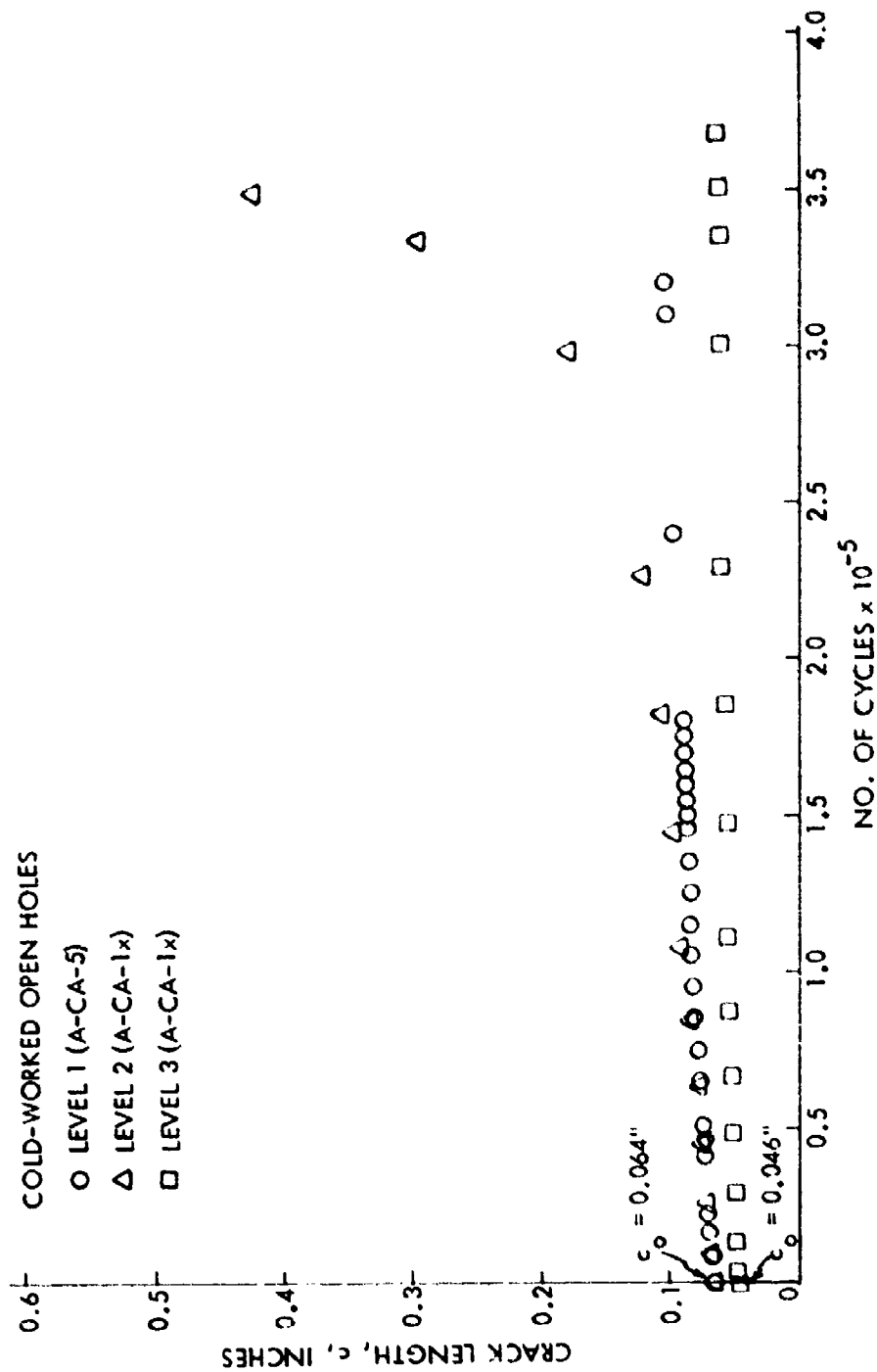


Figure 24. Comparison of Growth Behavior of Intermediate Corner Cracks for Various Levels of Cold Working for Open Holes in 2219-T851 Aluminum Alloy Plates Subjected to Constant Amplitude Loading ($\sigma = 18$ Ksi, $R = 0.1$)

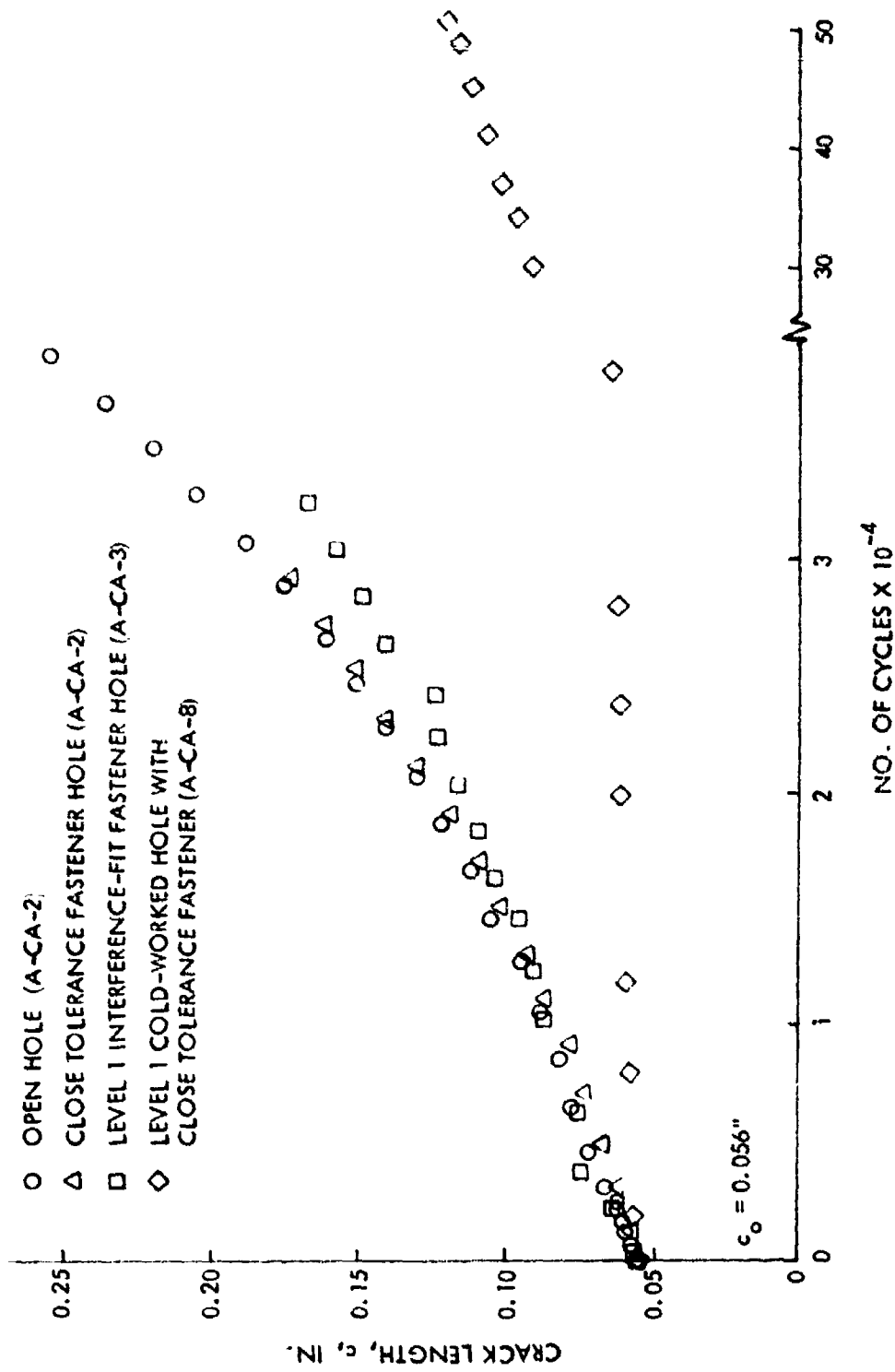
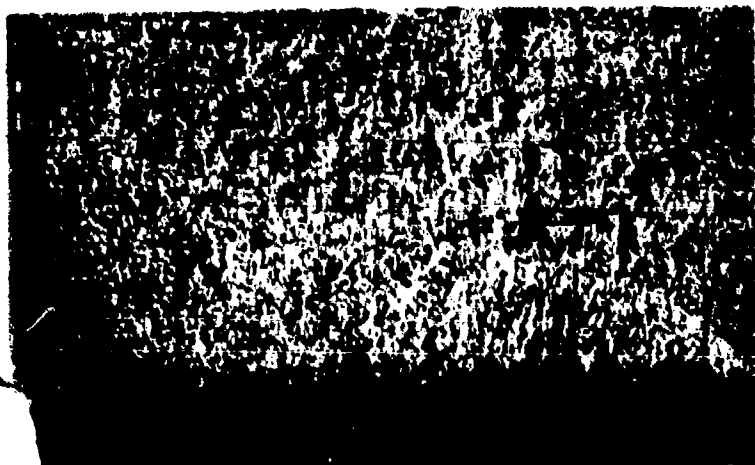


Figure 25. Comparison of Growth Behavior of Intermediate Corner Cracks from Various Types of Fastener Holes in 2219-T851 Aluminum Alloy Plates Subjected to Constant Amplitude Loading ($\sigma = 18$ KSI, $R = 0.1$)

ORIGINS OF INTENTIONAL CORNER CRACK



(a) OPEN HOLE



(b) NEAT-FIT HOLE



(c) NEAT-FIT HOLE HAVING
FASTENER LOAD TRANSFER

Figure 26. Surfaces of Corner Cracks Emanating from Various Types of Level 1 Cold-Worked Holes in 2219-T251 Aluminum Plates Subjected to Constant Amplitude Far-Field Loading ($\sigma_{max} = 18 \text{ ksi}$, $R = 0.1$)

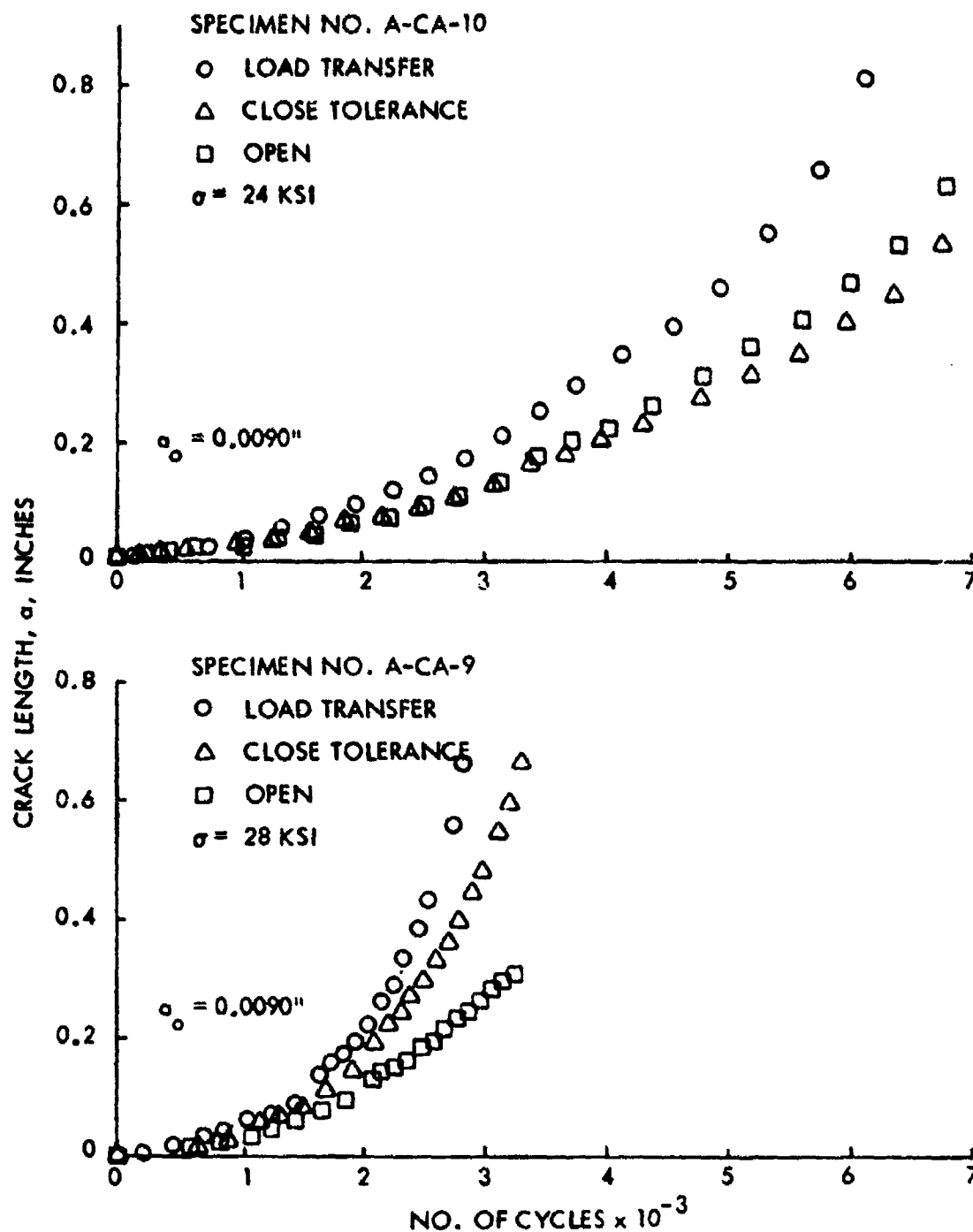


Figure 27. Growth Behavior of Small Thru Cracks from Open and Close Tolerance Fastener Holes in 2219-T851 Aluminum Alloy Plates Subjected to Constant Amplitude Loading

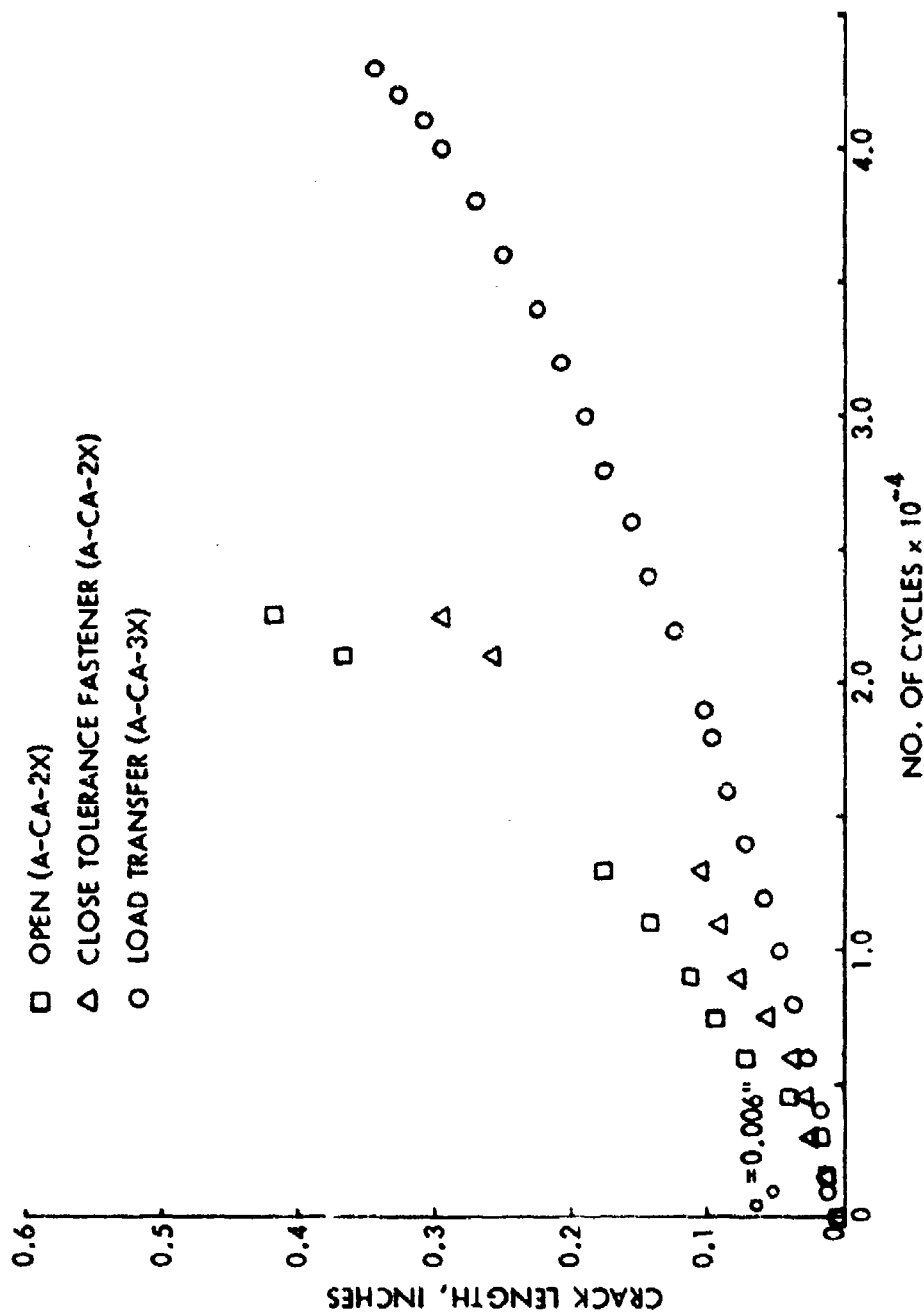


Figure 28. Growth Behavior of Small Thru Crack from an Open and Close Tolerance Fastener Holes in 2219-T851 Aluminum Alloy Plates Subjected to Constant Amplitude Loading ($\sigma = 18$ Ksi, $R = 0.1$)

SPECIMEN NO. A-CA-12

○ .0038 INTERFERENCE-FIT WITH LOAD TRANSFER

□ .0024 INTERFERENCE-FIT

△ .0038 INTERFERENCE-FIT

② 770,000 NO EXTENSION

③ 810,000 C = 0.55" FROM 0.0024" I. F. FASTENER HOLE

④ 822,000 UNIFORM THRU-CRACK FROM 0.0024" I. F. FASTENER HOLE

⑤ 835,500 FAILED FROM 0.0024" I. F. FASTENER HOLE

UNFLAMED FATIGUE TESTS:

—●— FATIGUE FAILED @ GRIP ($>10^6$)

—●— FATIGUE FAILED @ 852,466 AND 404,230

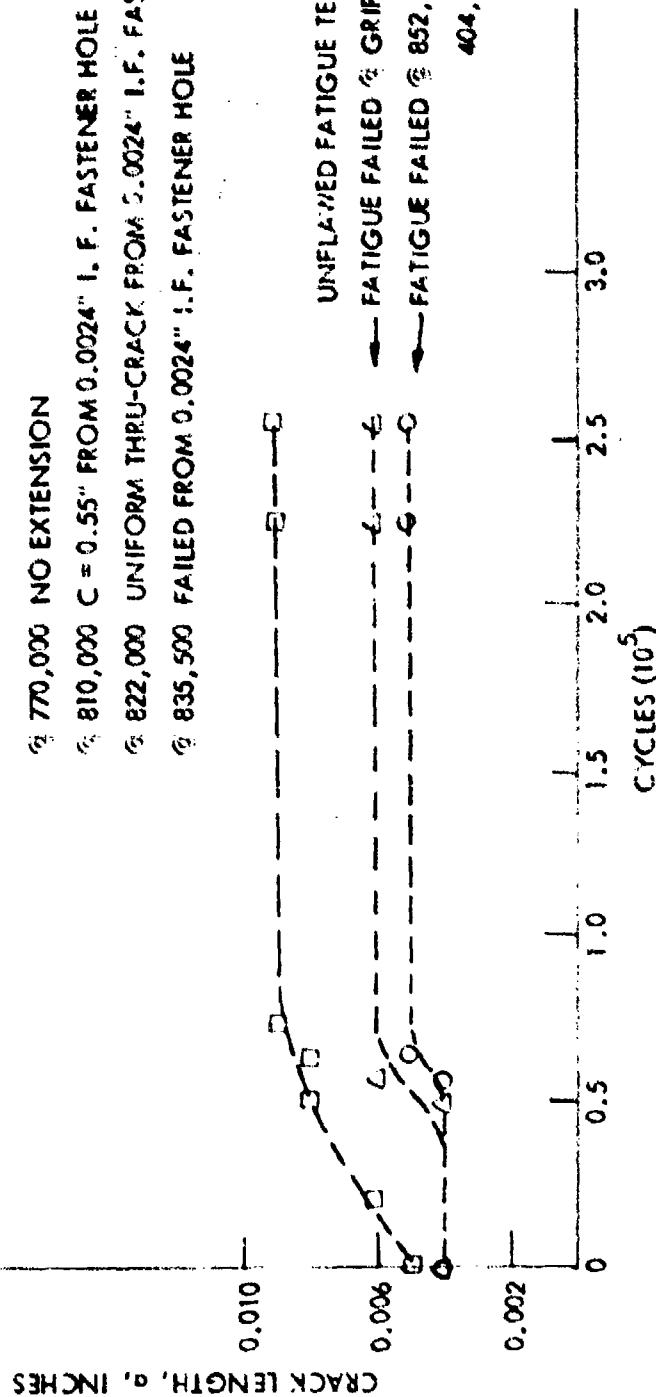


Figure 29. Growth Behavior of Small Thru Cracks from Interference-Fit Fastener Holes with and without Load Transfer in 2219-T851 Aluminum Plates Subjected to Constant Amplitude Loading ($q = 12$ Ksi and $P = 0.1$)

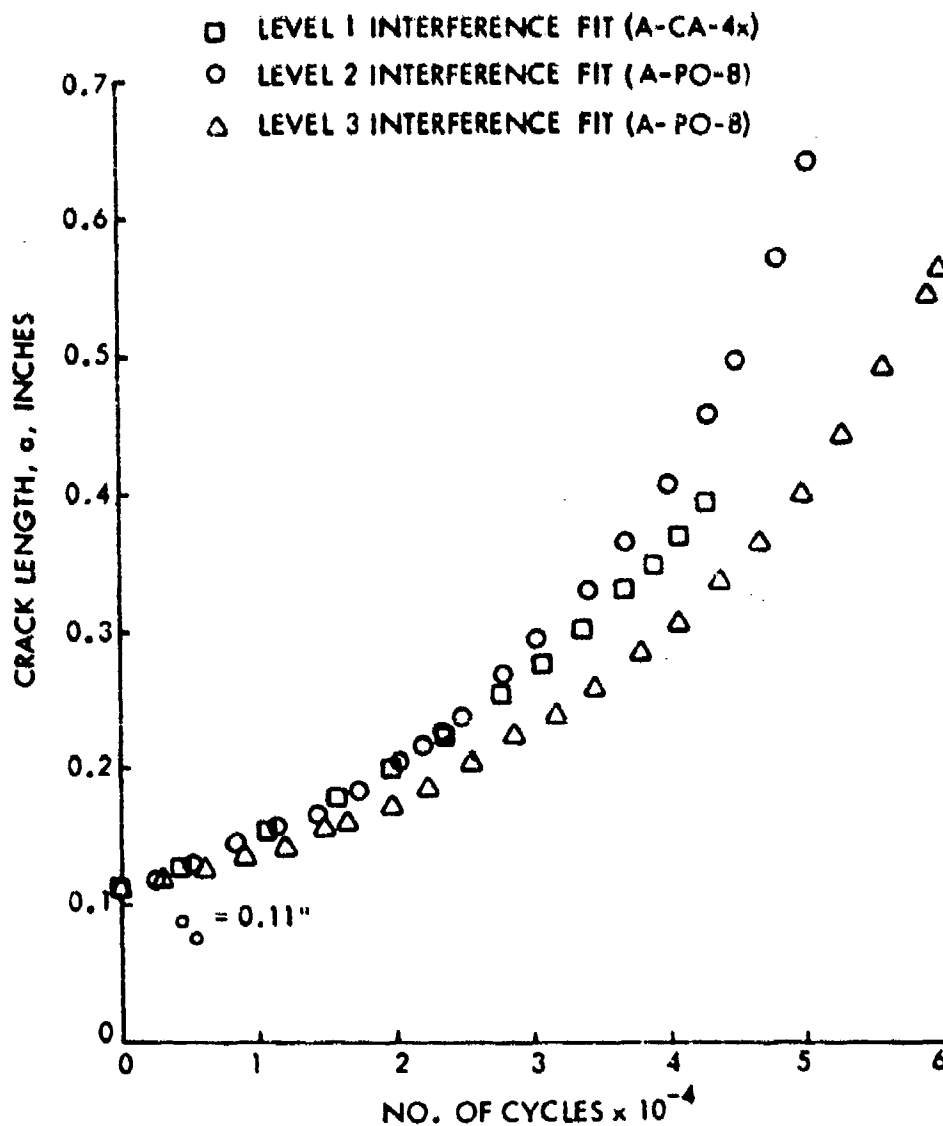


Figure 30. Growth Behavior of Intermediate Thru Cracks from Interference-Fit Fastener Holes for Various Levels of Interference in 2219-1351 Aluminum Alloy Plates Subjected to Constant Amplitude Loading ($\sigma = 18$ Ksi, $R = 0.1$)

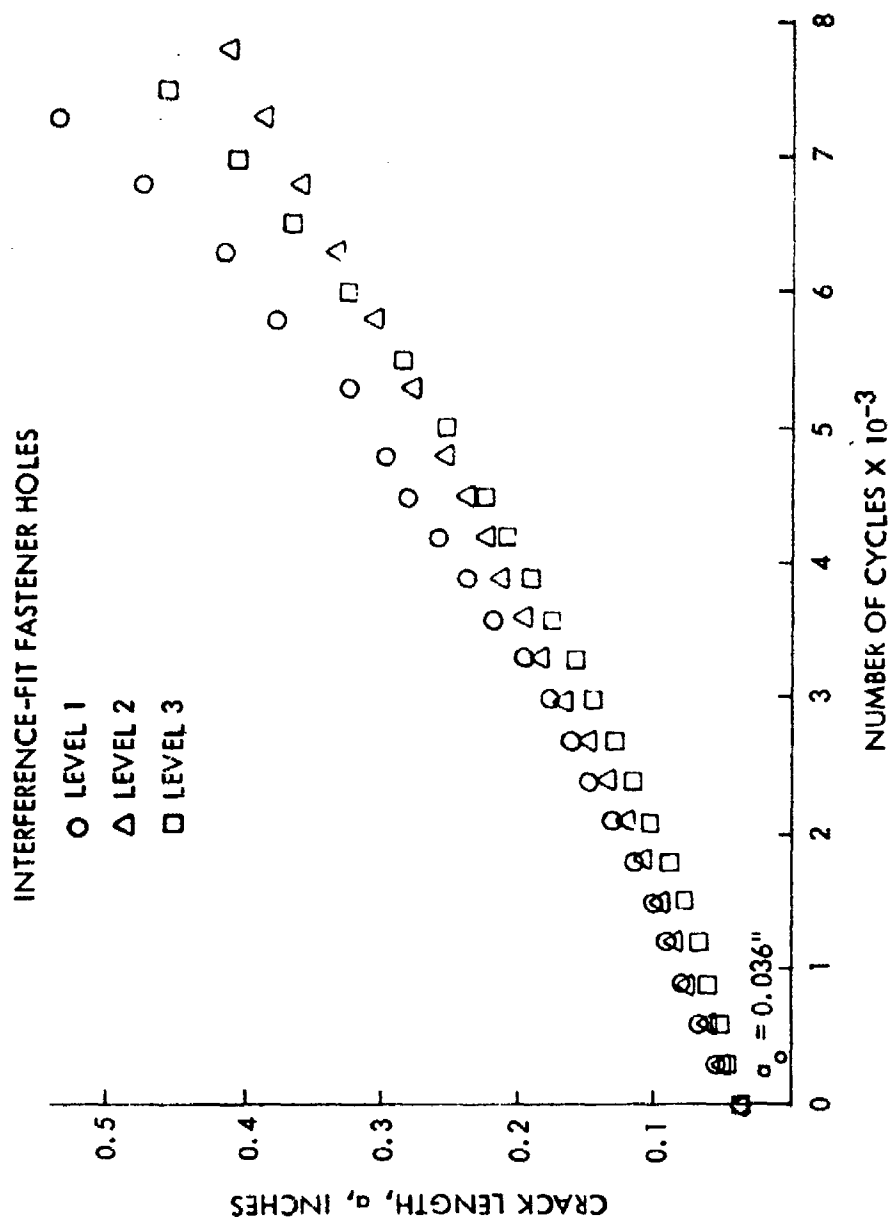


Figure 31. Growth Behavior of Thru Cracks from Interference-Fit Fastener Holes for Various Levels of Interference in 2219-T851 Aluminum Plates Subjected to Constant Amplitude Loading ($\sigma = 21$ Ksi, $R = 0.1$)

LEVEL 3 INTERFERENCE-FIT FASTENER HOLES

- A-CA-15
- △ A-CA-17
- A-CA-18

CRACK LENGTH, a , INCHES

0.6
0.5
0.4
0.3
0.2
0.1

$a_0 = 0.034$ "

NUMBER OF CYCLES $\times 10^{-3}$

2 4 6 8 10 12 14 16 18 20

Figure 32. Growth Behavior of Small and Intermediate Thru Cracks from Level 3 Interference-Fit Fastener Holes in 2219-T851 Aluminum Plates Subjected to Constant Amplitude Loading ($\sigma = 18$ KSI, $R = 0.1$)

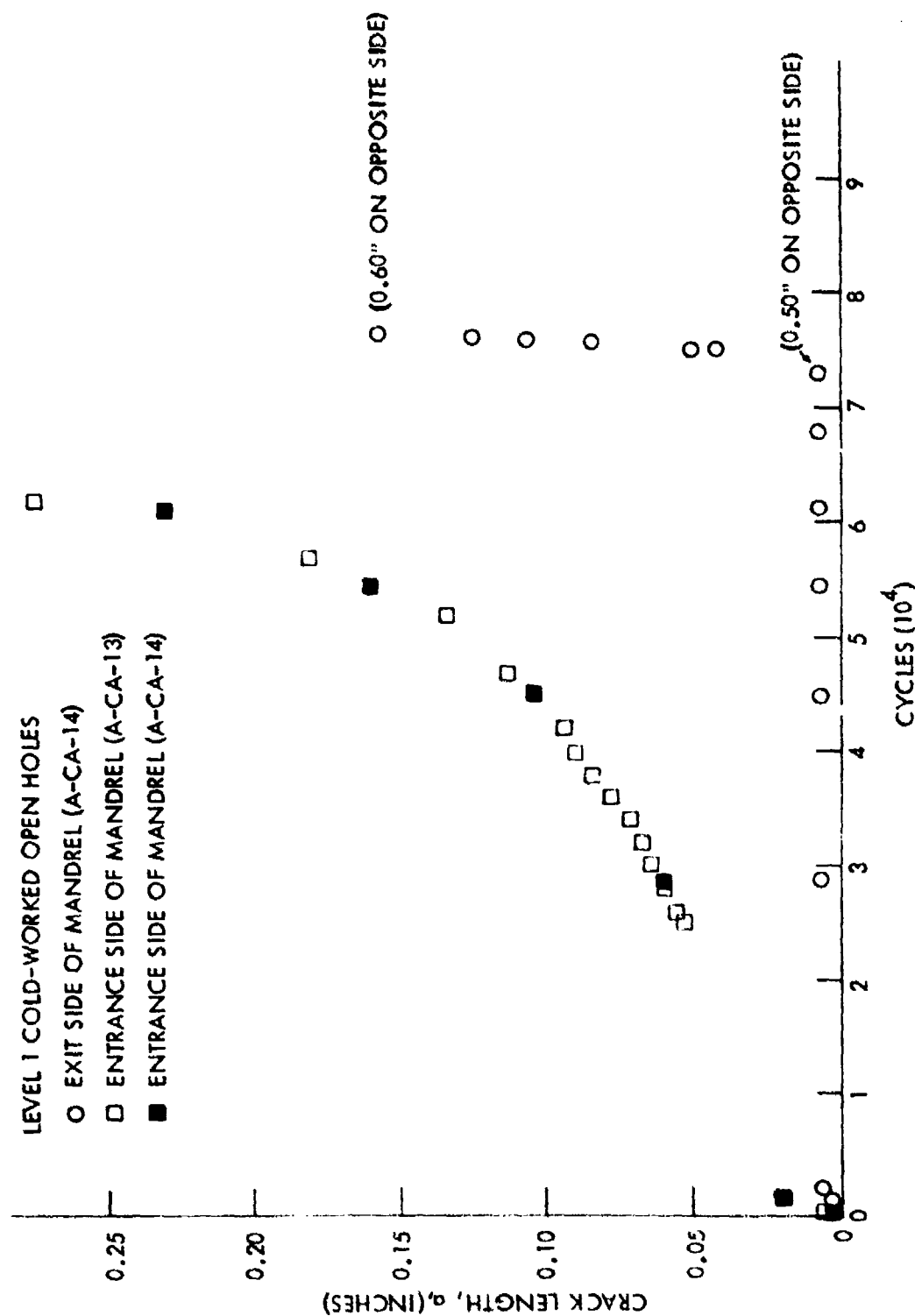


Figure 33. Growth Behavior of Small Thru Cracks from Cold-Worked Fastener Holes in 2219-T851 Aluminum Plates Subjected to Constant Amplitude Loading ($\sigma = 18$ Ksi and $R = 0.1$)

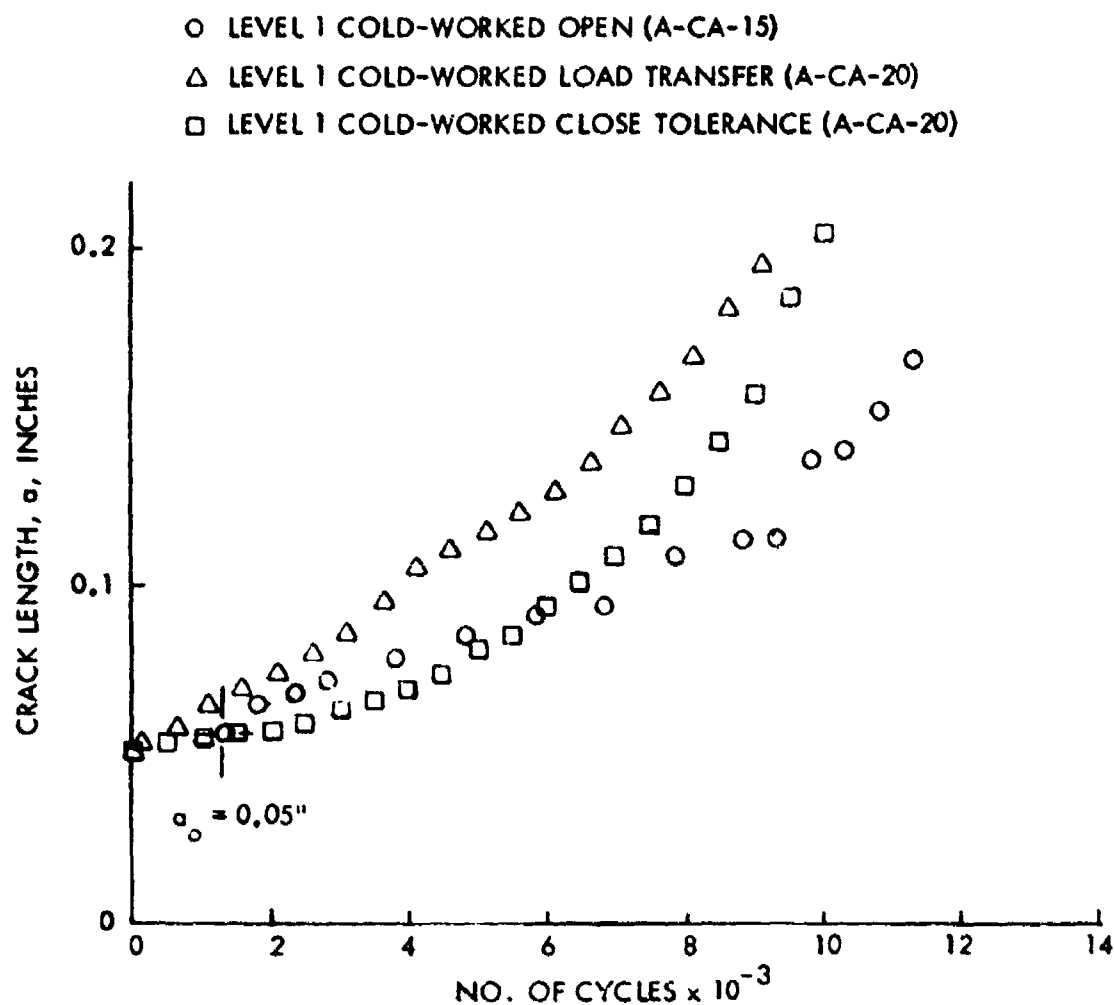


Figure 34. Growth Behavior of Intermediate Thru Cracks from Open and Filled Cold-Worked Fastener Holes in 2219-T851 Aluminum Alloy Plates Subjected to Constant Amplitude Loading ($\sigma = 18$ Ksi, $R = 0.1$)

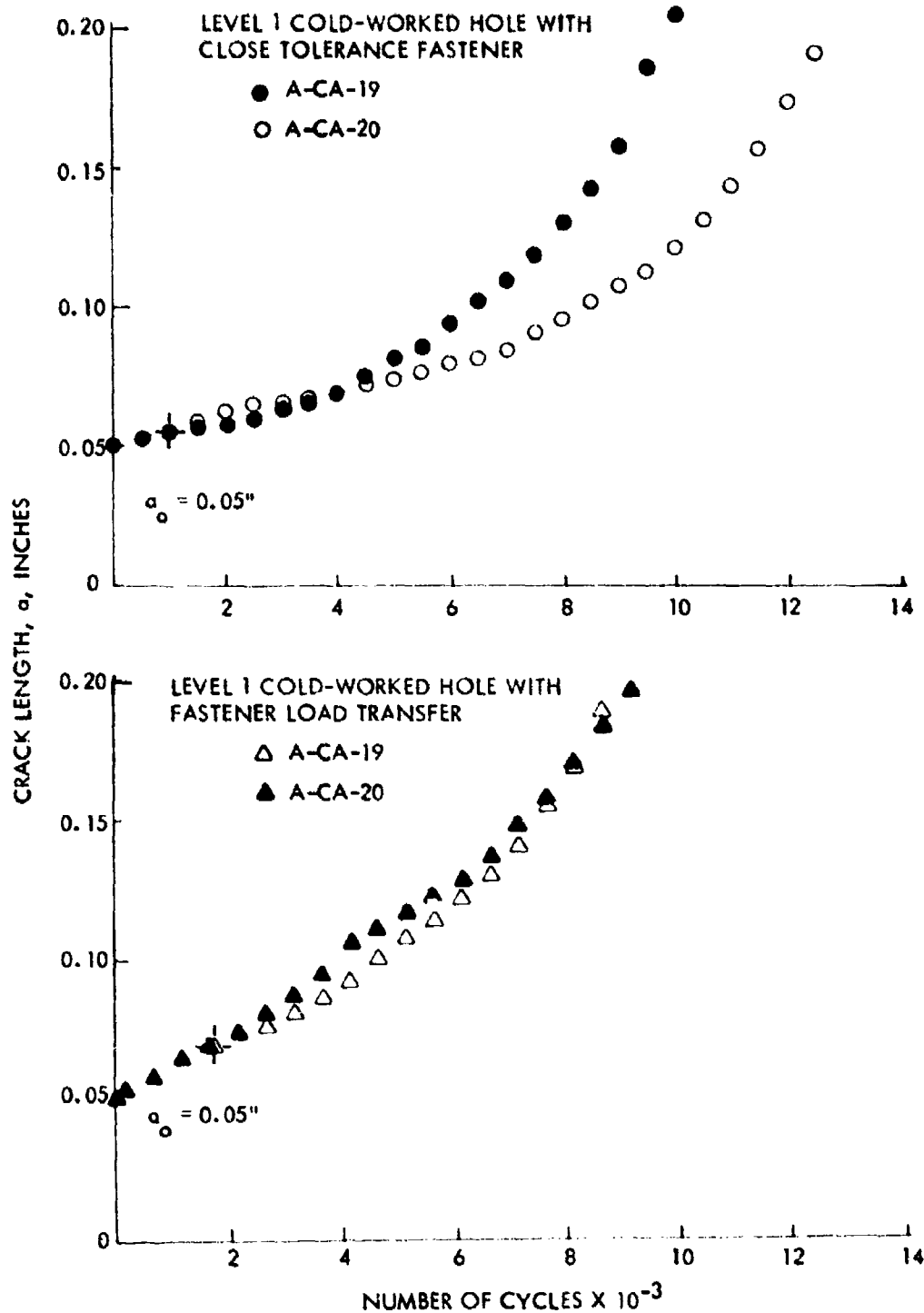


Figure 35. Growth Behavior of Intermediate Thru Cracks from Level 1 Cold-Worked Holes With and Without Fastener Load Transfer in 2219-T851 Aluminum Plates Subjected to Constant Amplitude Loading ($\sigma = 18$ Ksi, $R = 0.1$)

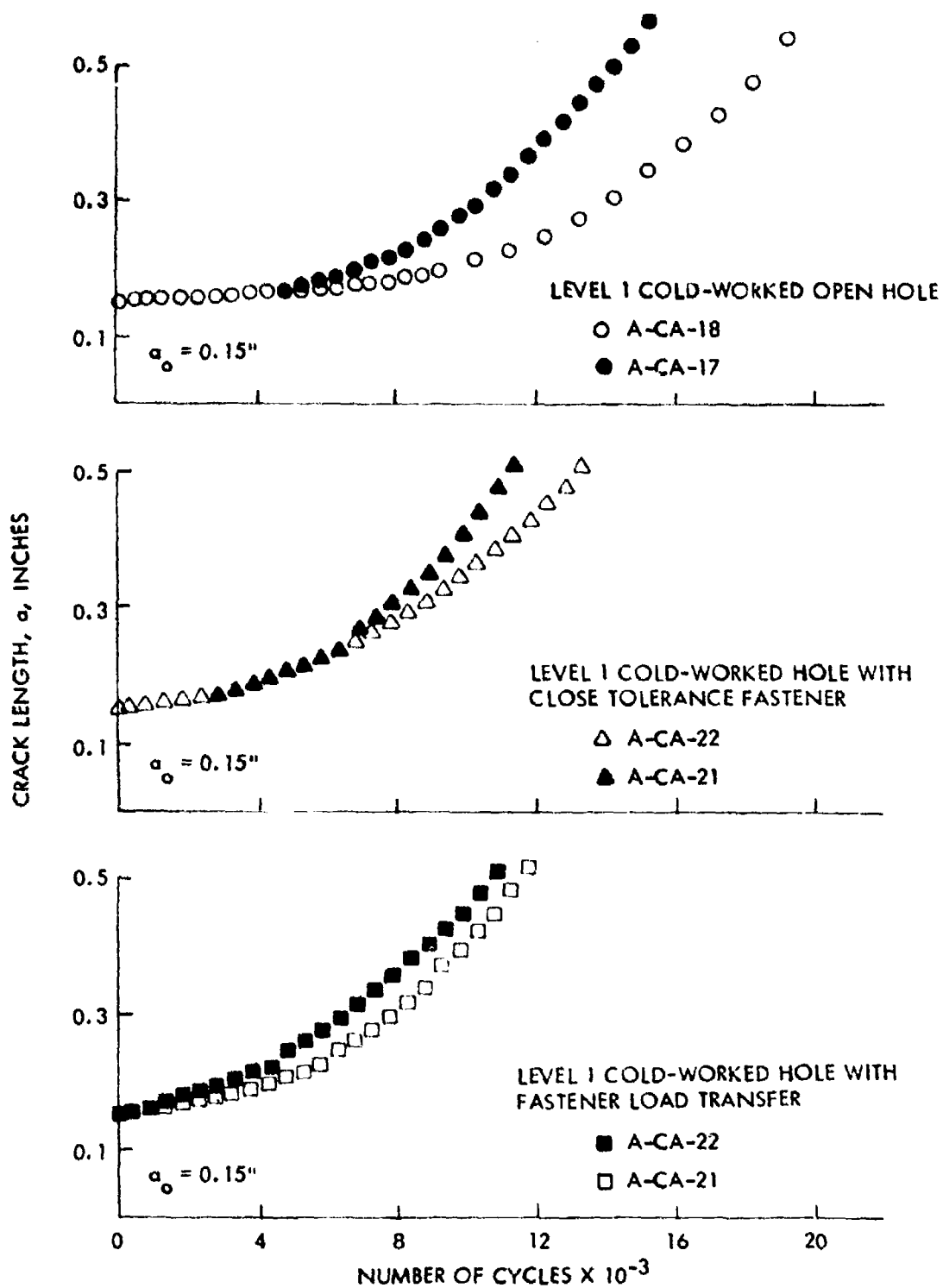


Figure 36. Growth Behavior of Large Thru Cracks from Level 1 Cold-Worked Holes in 2219-T851 Aluminum Plates Subjected to Constant Amplitude Loading ($\sigma = 18$ KSI, $R = 0.1$)

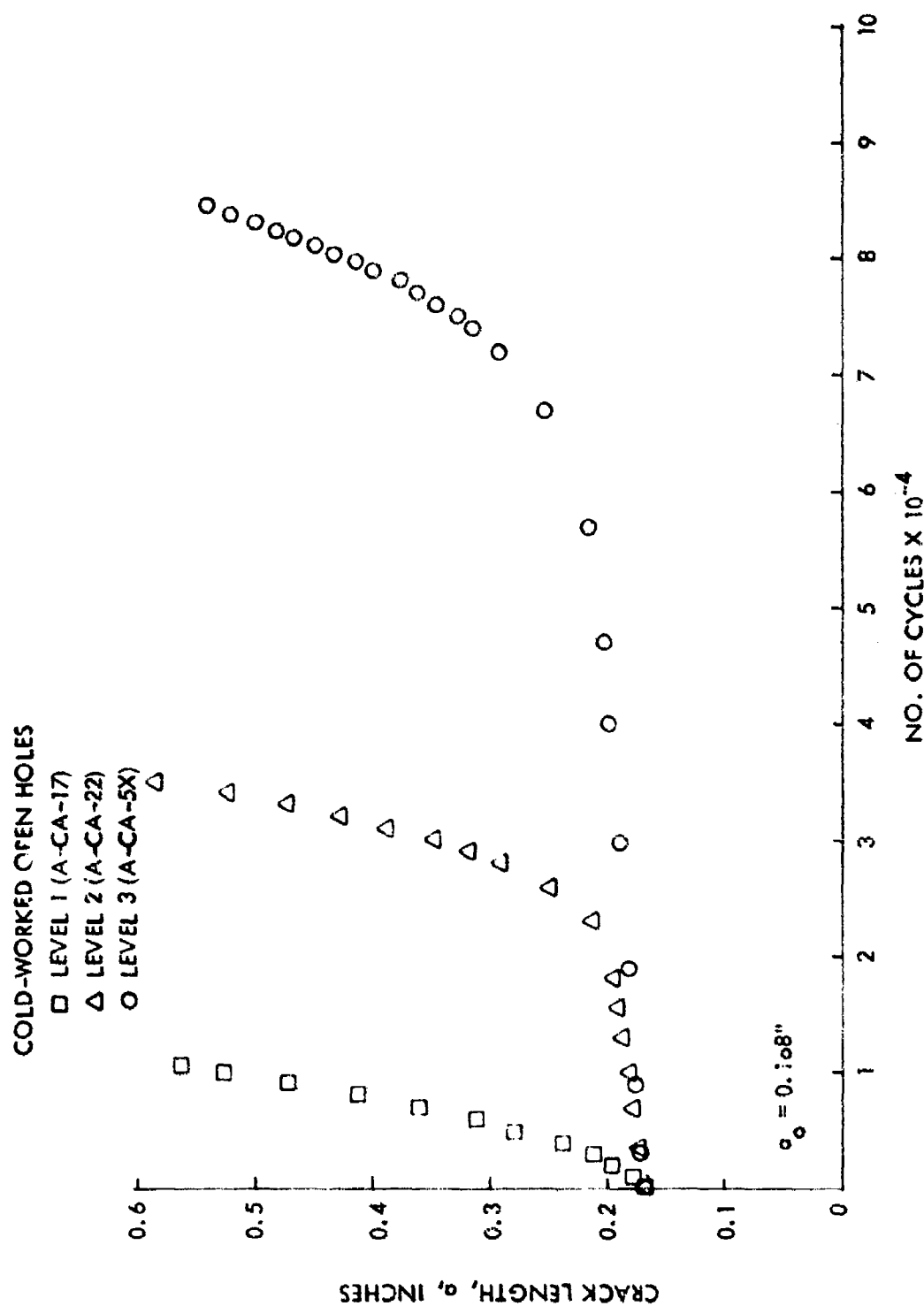


Figure 37. Growth Behavior of Large Thru Cracks from Cold-Worked Open Holes for Various Levels of Cold Working in 2219-T851 Aluminum Alloy Plates Subjected to Constant Amplitude Loading ($\sigma = 18$ Ksi, $R = 0.1$)

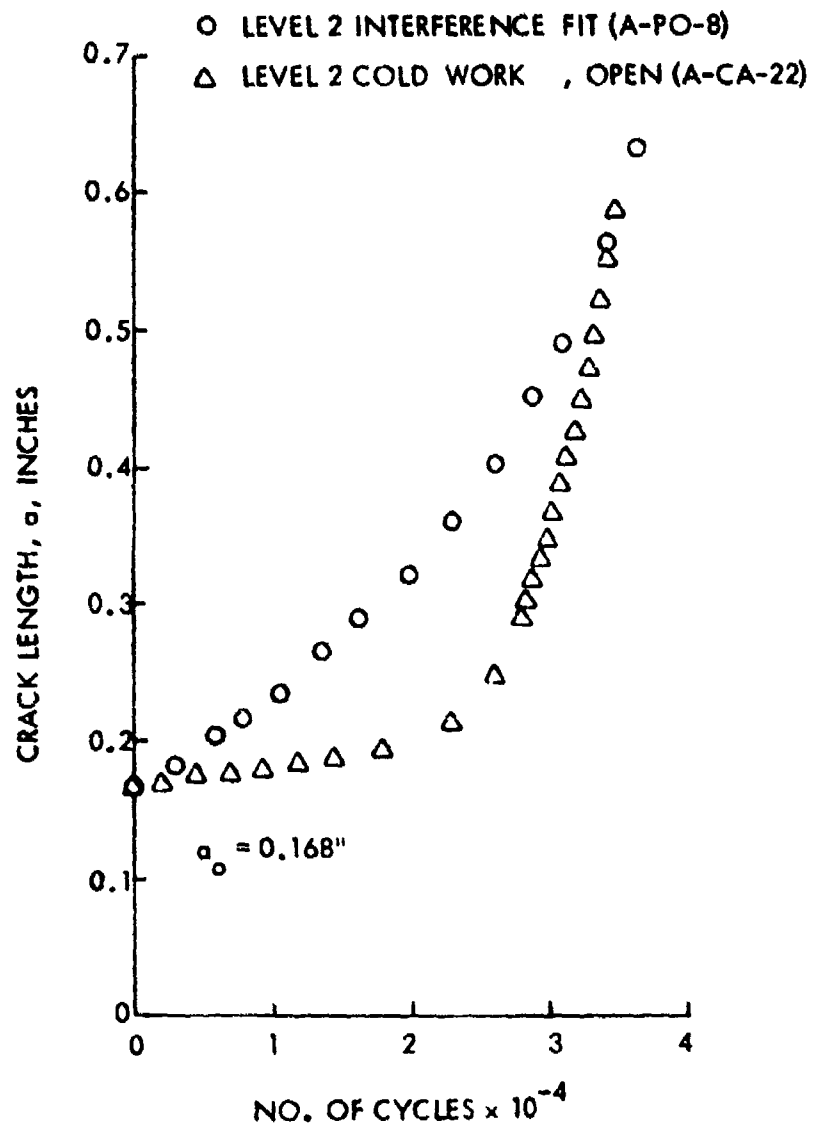


Figure 38. Comparison of Growth Behavior of Large Thru Cracks from Cold-Worked and Interference-Fit Fastener Holes in 2219-T851 Aluminum Alloy Plates Subjected to Constant Amplitude Loading ($\sigma = 18$ Ksi, $R = 0.1$)

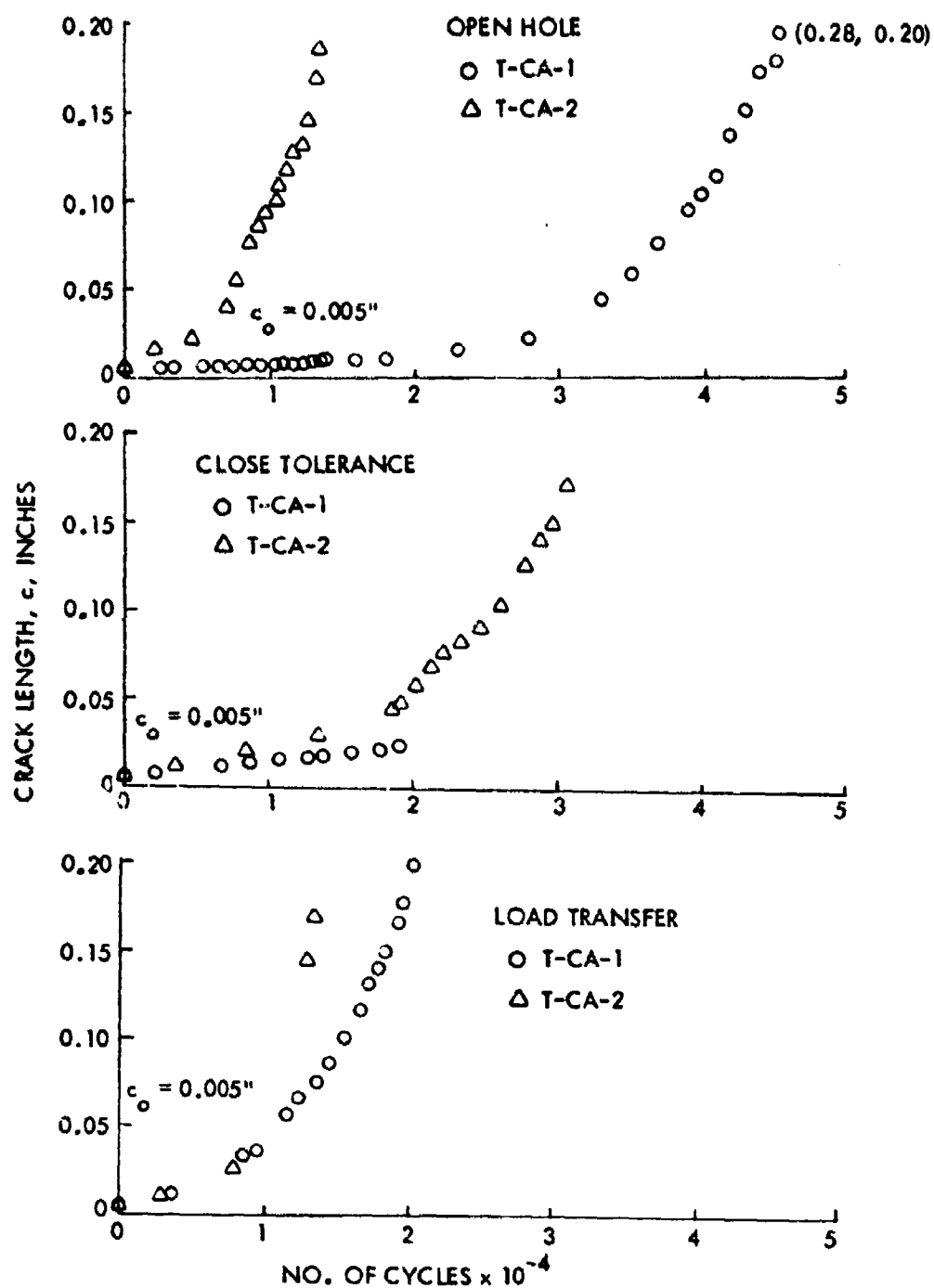


Figure 39. Growth Behavior of Small Corner Cracks from an Open and Close Tolerance Fastener Holes in 6Al-4V Beta Annealed Titanium Alloy Plates Subjected to Constant Amplitude Loading ($\sigma = 40$ Ksi, $R = 0.1$)

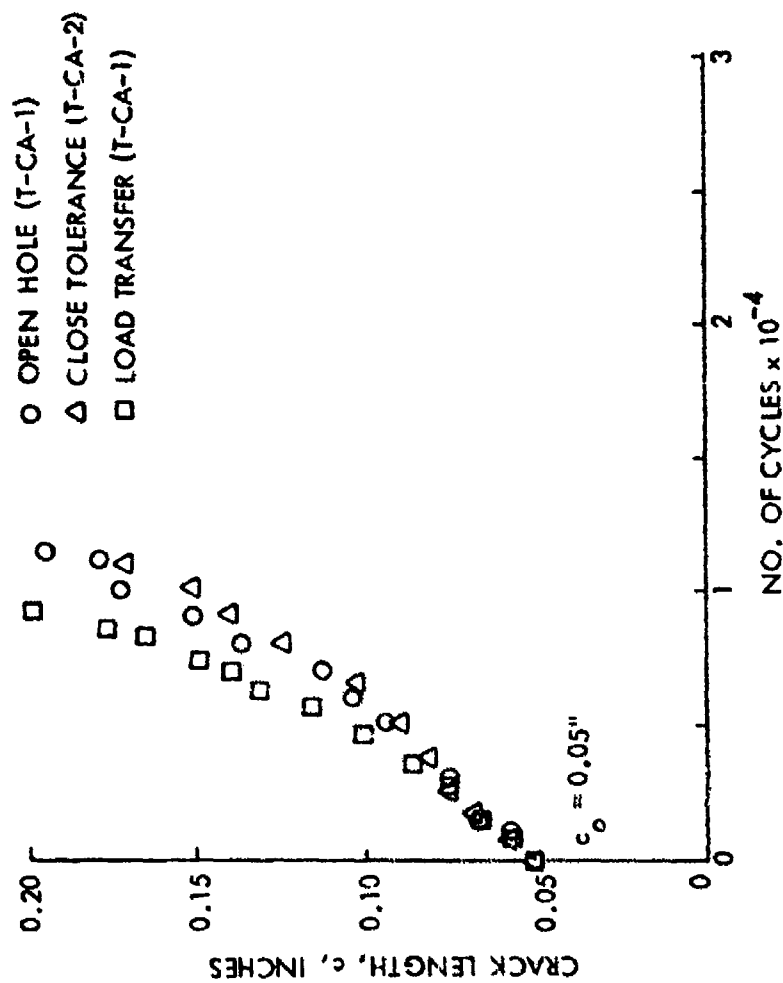


Figure 40. Growth Behavior of Intermediate Corner Cracks from an Open and Close Tolerance Fastener Holes in 6AL-4V Beta Annealed Titanium Alloy Plates Subjected to Constant Amplitude Loading ($\sigma = 40$ KSI, $R = 0.1$)

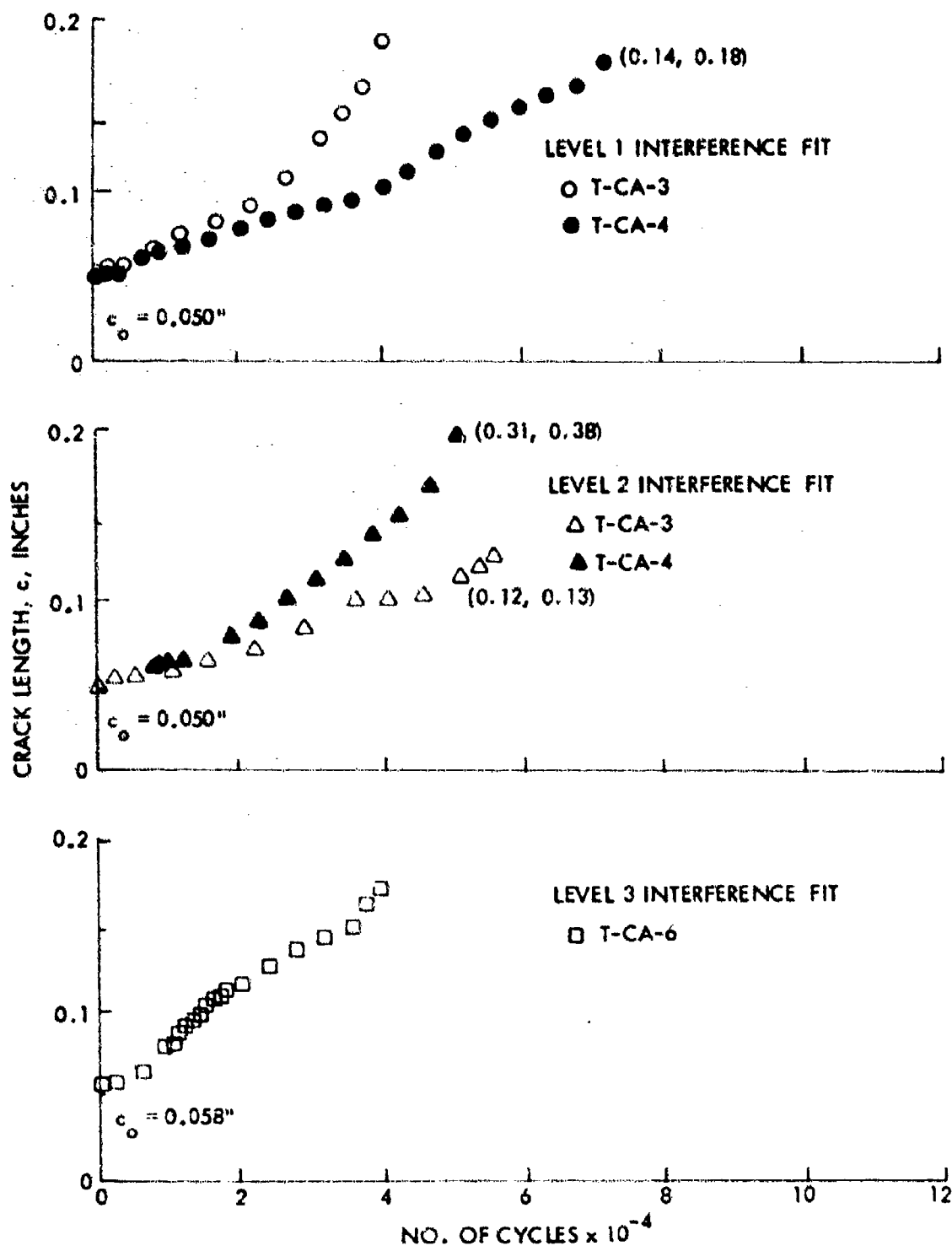


Figure 41. Growth Behavior of Intermediate Corner Cracks from Interference-Fit Fastener Holes for Various Levels of Interference in 6Al-4V Beta Annealed Titanium Plates Subjected to Constant Amplitude Loading ($\sigma = 40$ Ksi, $R = 0.1$)

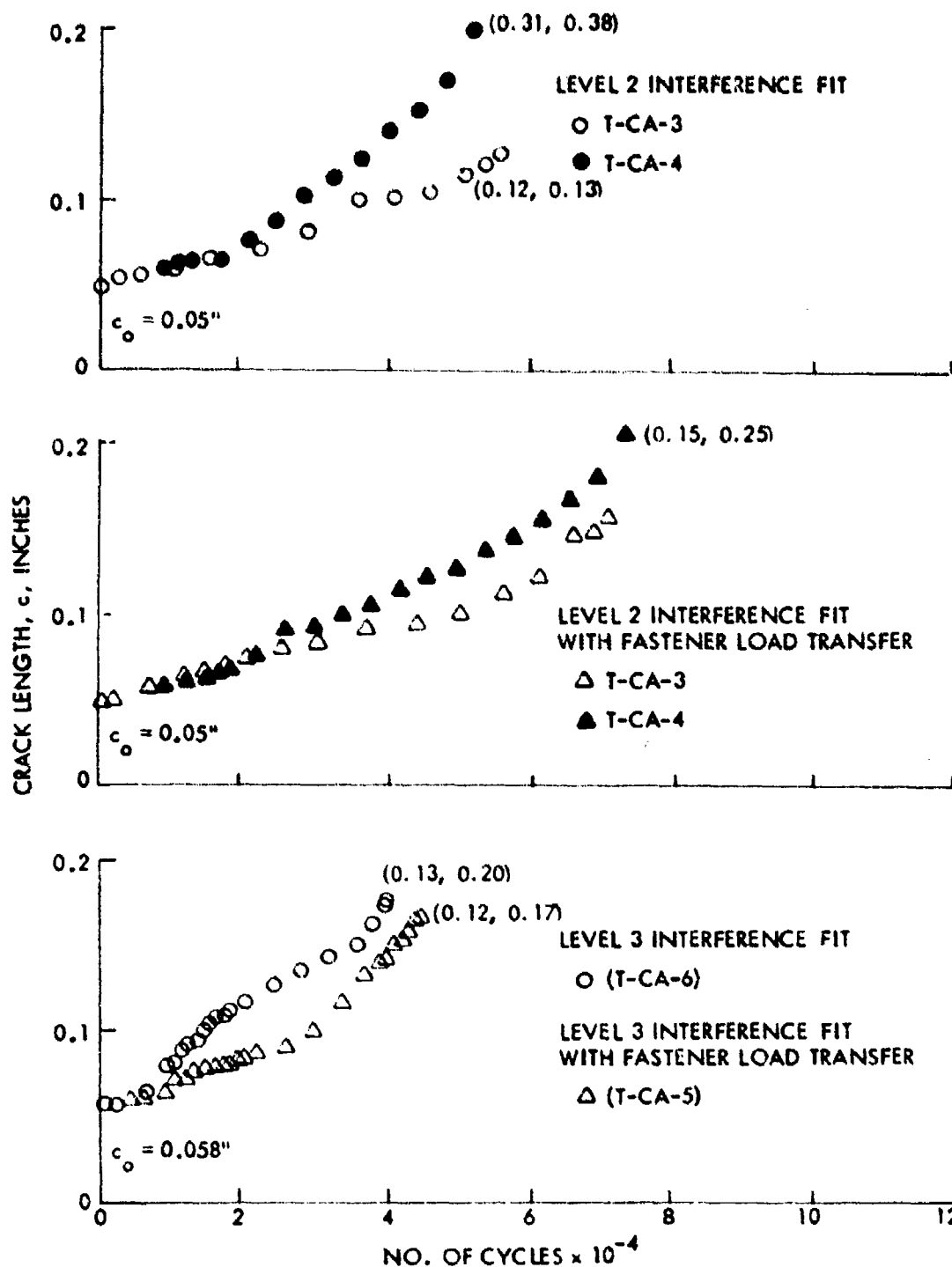


Figure 42. Growth Behavior of Intermediate Corner Cracks from Interference-Fit Fastener Holes with and without Fastener Load Transfer in 6Al-4V Beta Annealed Titanium Plates Subjected to Constant Amplitude Loading ($\sigma = 40$ Ksi, $R = 0.1$)

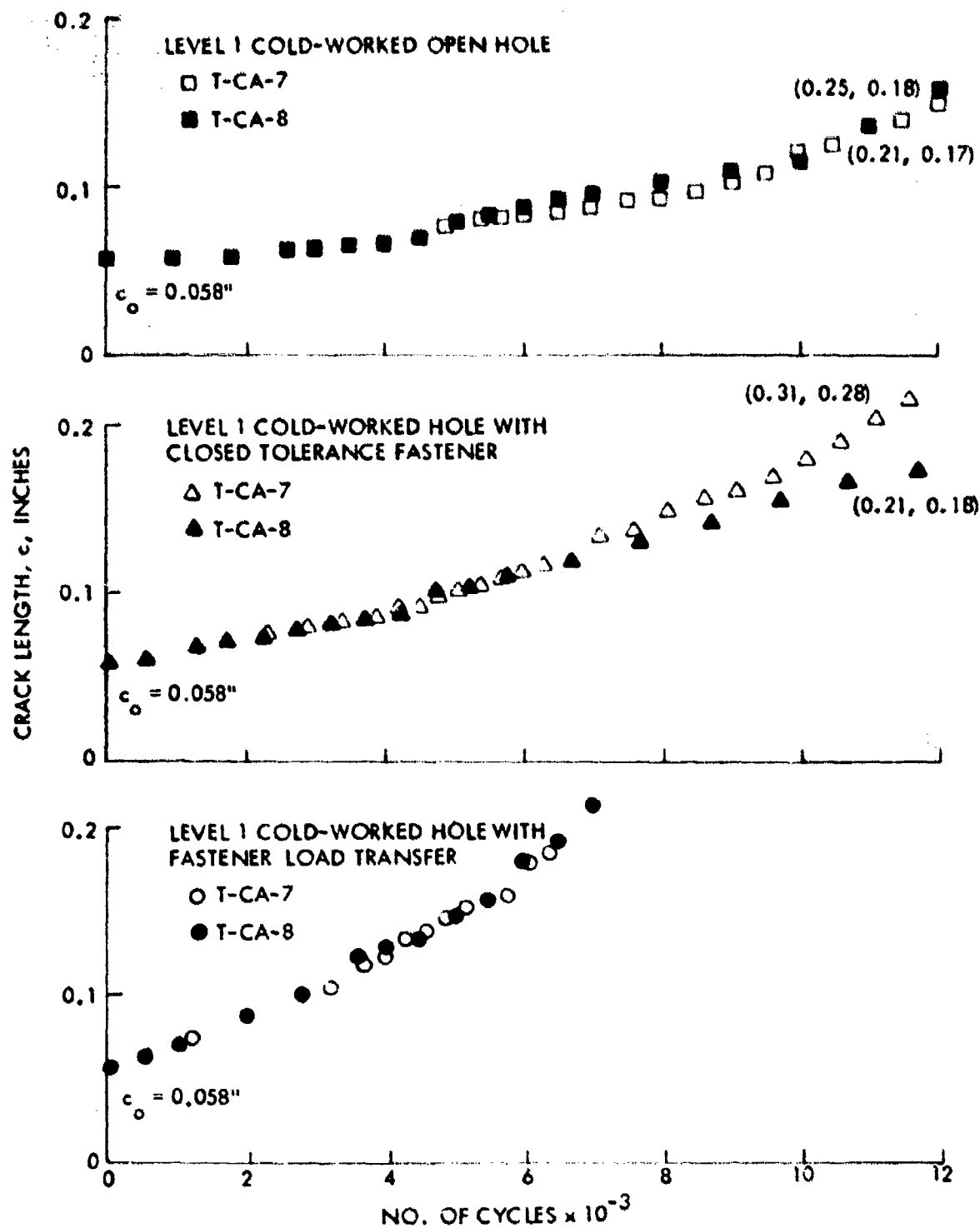


Figure 43. Growth Behavior of Intermediate Corner Cracks from Level 1 Cold-Worked Holes in 6Al-4V Beta Annealed Titanium Plates Subjected to Constant Amplitude Loading ($\sigma = 40$ Ksi, $R = 0.1$)

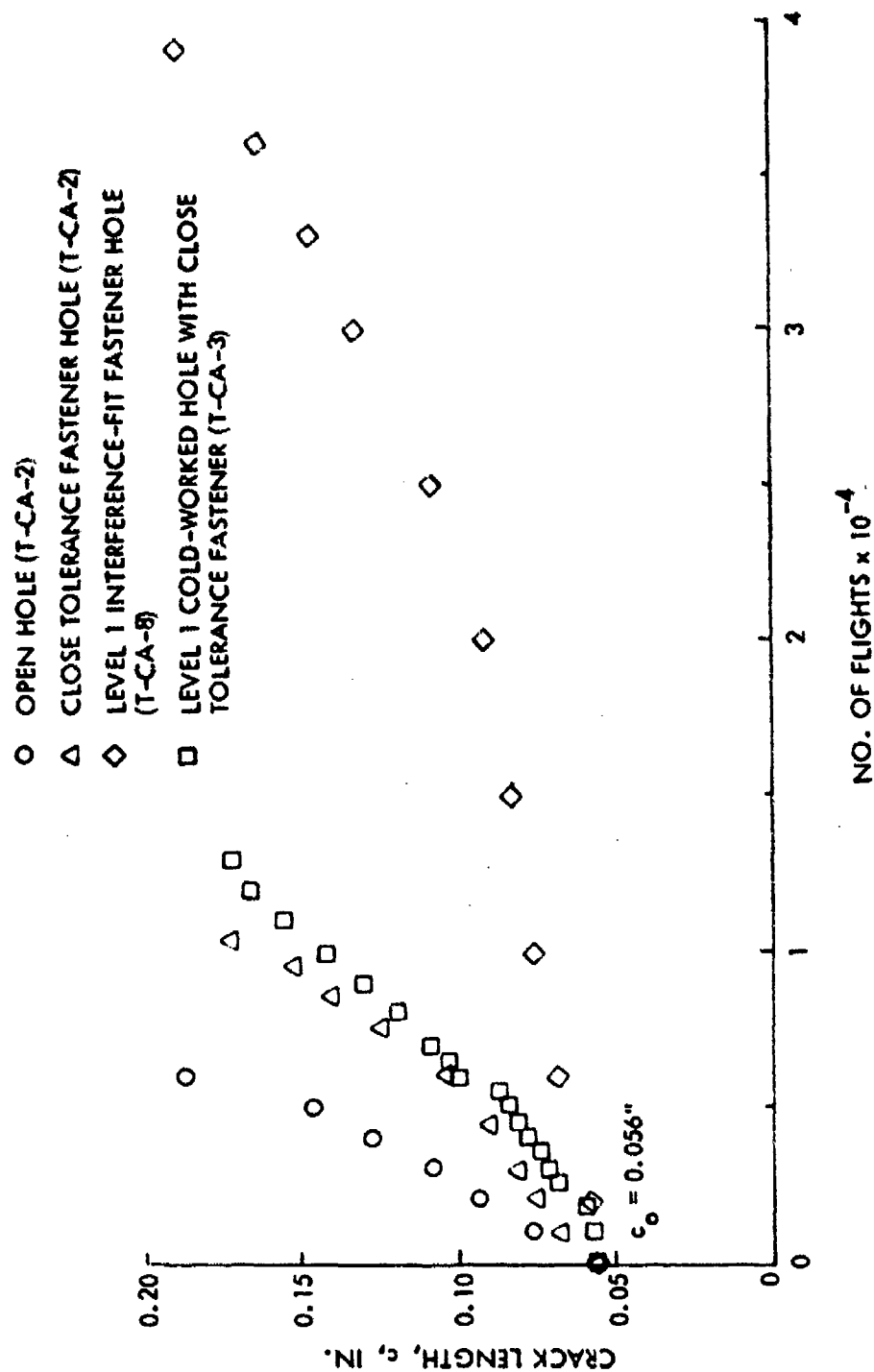


Figure 44. Comparison of Growth Behavior of Intermediate Corner Cracks from Various Types of Fastener Holes in 6Al-4V Beta Annealed Titanium Alloy Plates Subjected to Constant Amplitude Loading ($\sigma = 40$ KSI, $R = 0.1$)

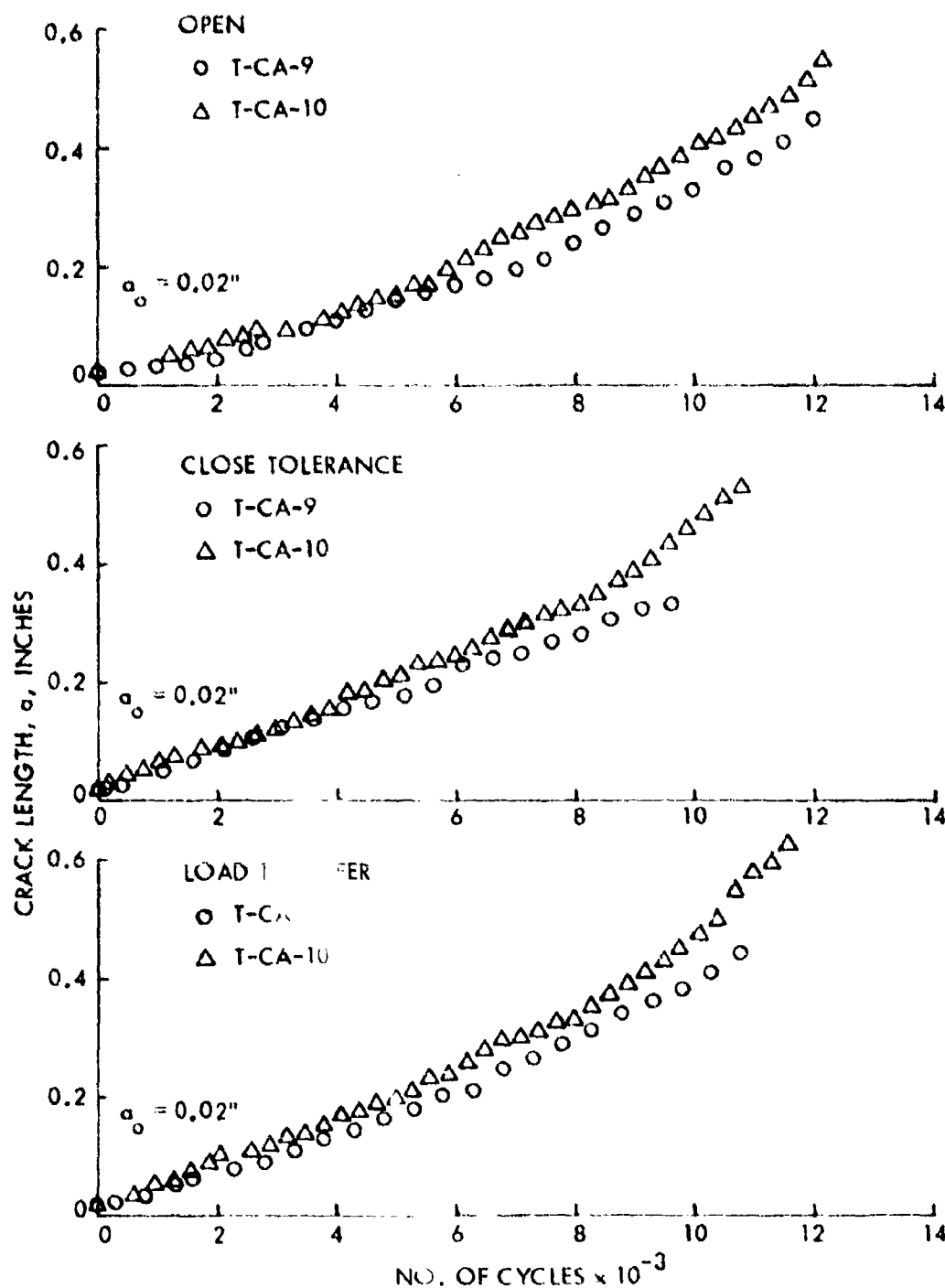


Figure 45 . Growth Behavior of Small Thru Cracks from Open and Close Tolerance Fastener Holes in 6Al-4V Beta Annealed Titanium Alloy Plates Subjected to Constant Amplitude Loading ($\sigma = 40$ Ksi, $R = 0.1$)

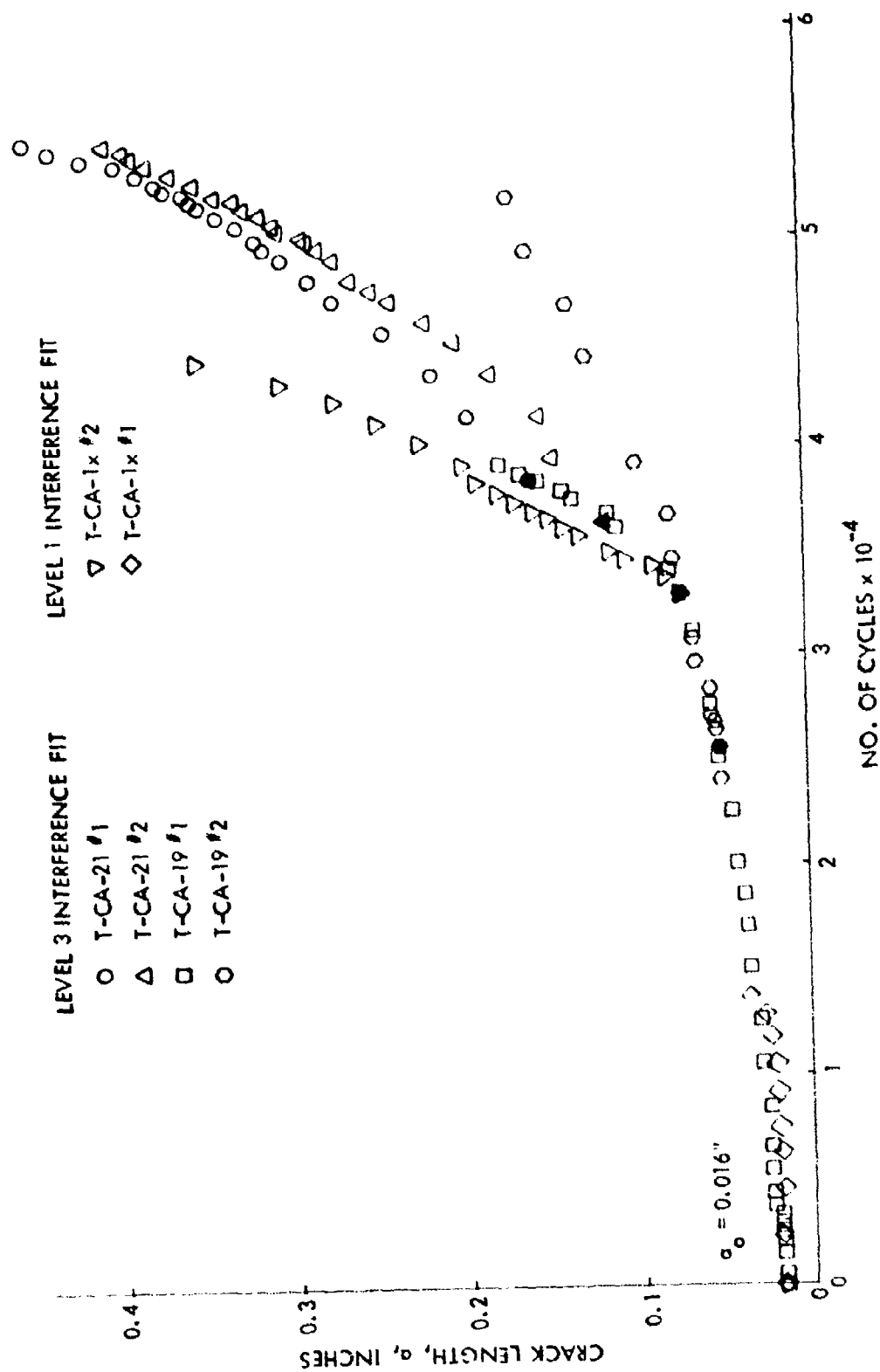


Figure 46. Growth Behavior of Small and Intermediate Thru Cracks from Interference-Fit Fastener Holes in 6Al-4V Beta Annealed Titanium Alloy Plates Subjected to Constant Amplitude Loading ($\sigma = 40$ Ksi, $R = 0.1$)

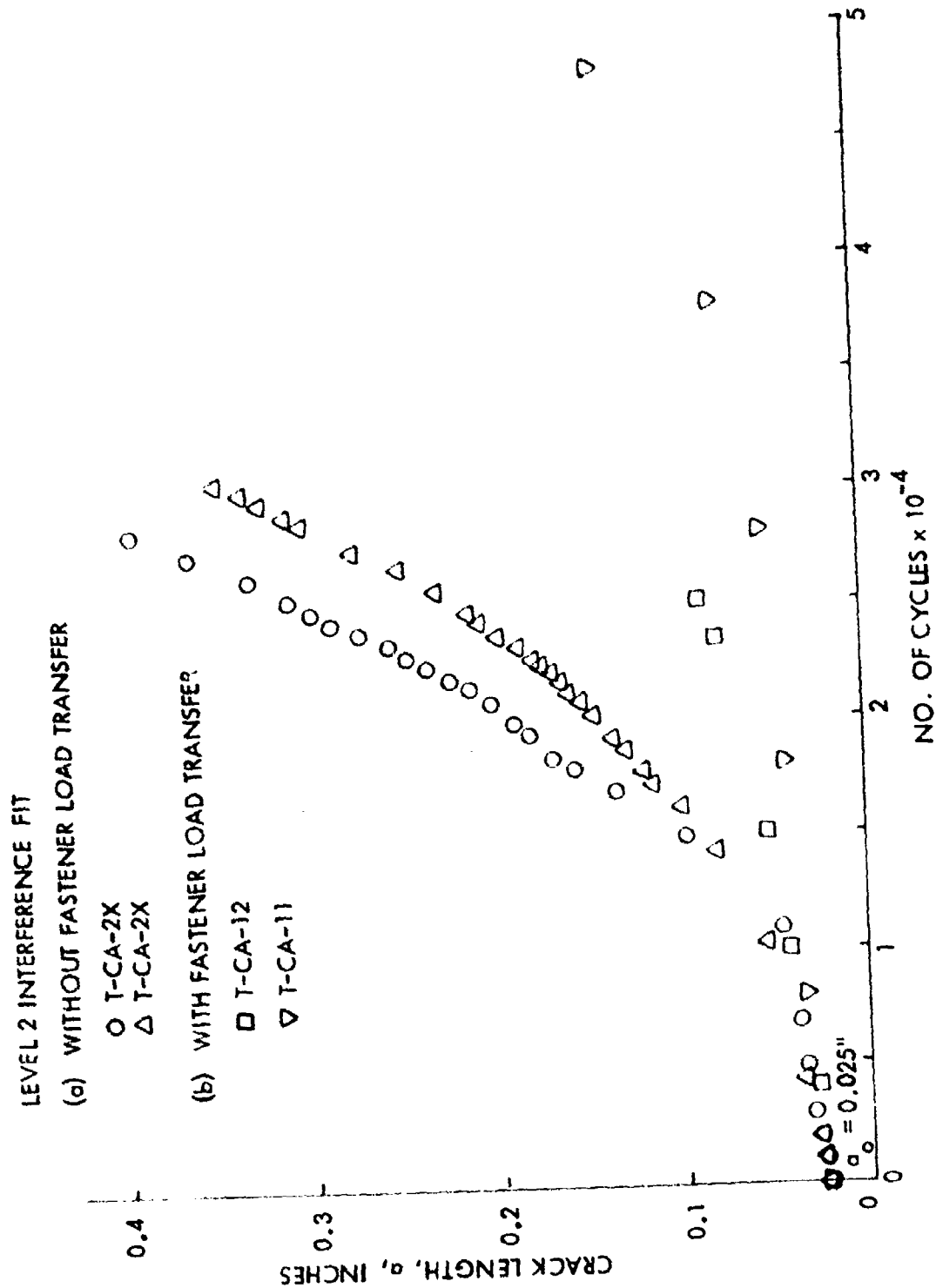


Figure 47. Growth Behavior of Small Thru Cracks from Level 2 Interference-Fit Fastener Holes with and without Fastener Load Transfer in 6Al-4V Beta Annealed Titanium Alloy Plates Subjected to Constant Amplitude Loading ($\sigma = 40$ Ksi, $R = 0.1$)

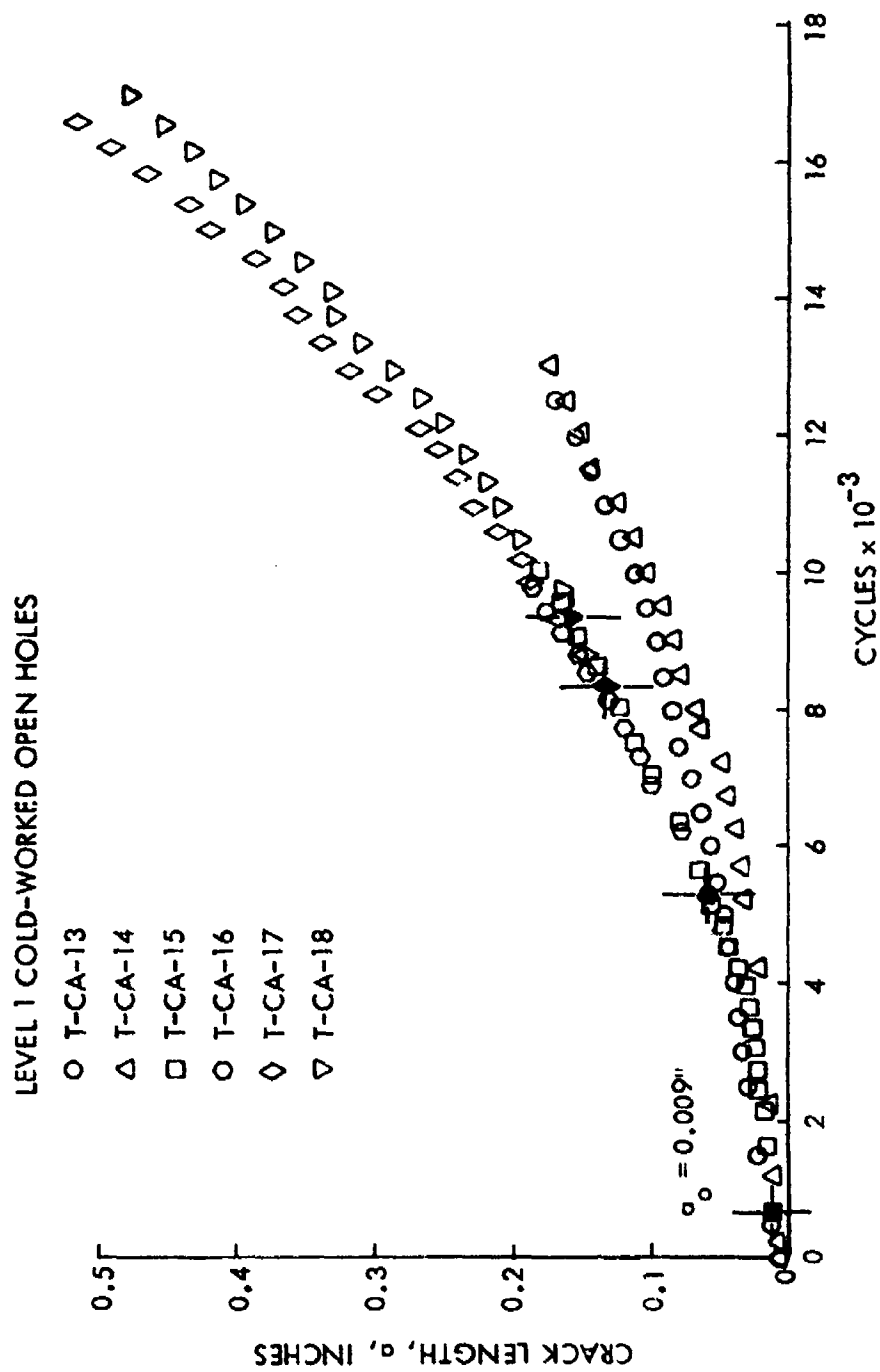


Figure 48. Growth Behavior of Thru Cracks from Level 1 Cold-Worked Open Holes in 6Al-4V Beta Annealed Titanium Alloy Plates Subjected to Constant Amplitude Loading

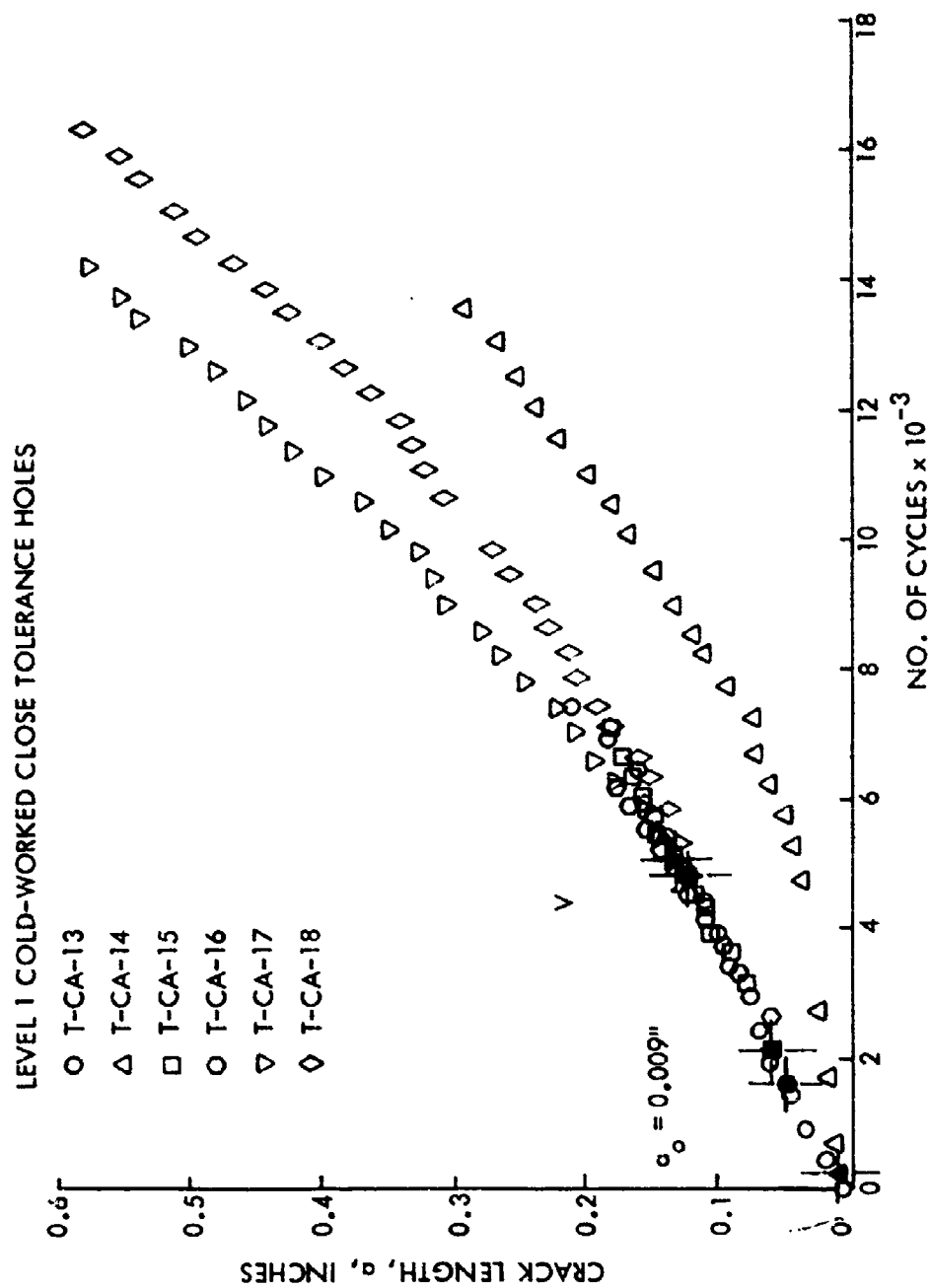


Figure 49. Growth Behavior of Small Thru Cracks from Level 1 Cold-Worked Filled Holes in 6Al-4V Beta Annealed Titanium Alloy Plates Subjected to Constant Amplitude Loading

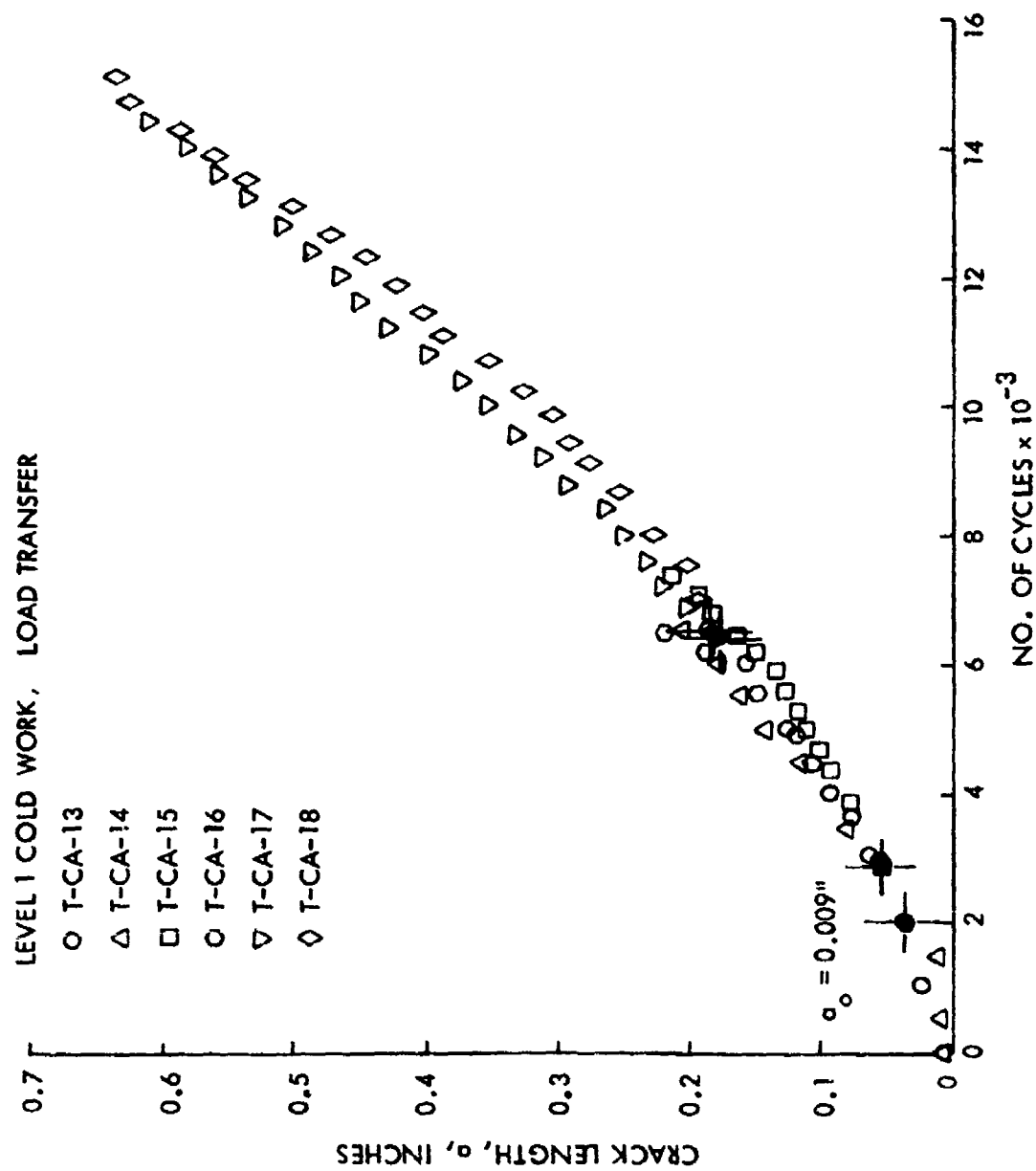


Figure 50. Growth Behavior of Small Thru Cracks from Level 1 Cold-Worked Loaded Holes in 6Al-4V Beta Annealed Titanium Alloy Plates Subjected to Constant Amplitude Loading

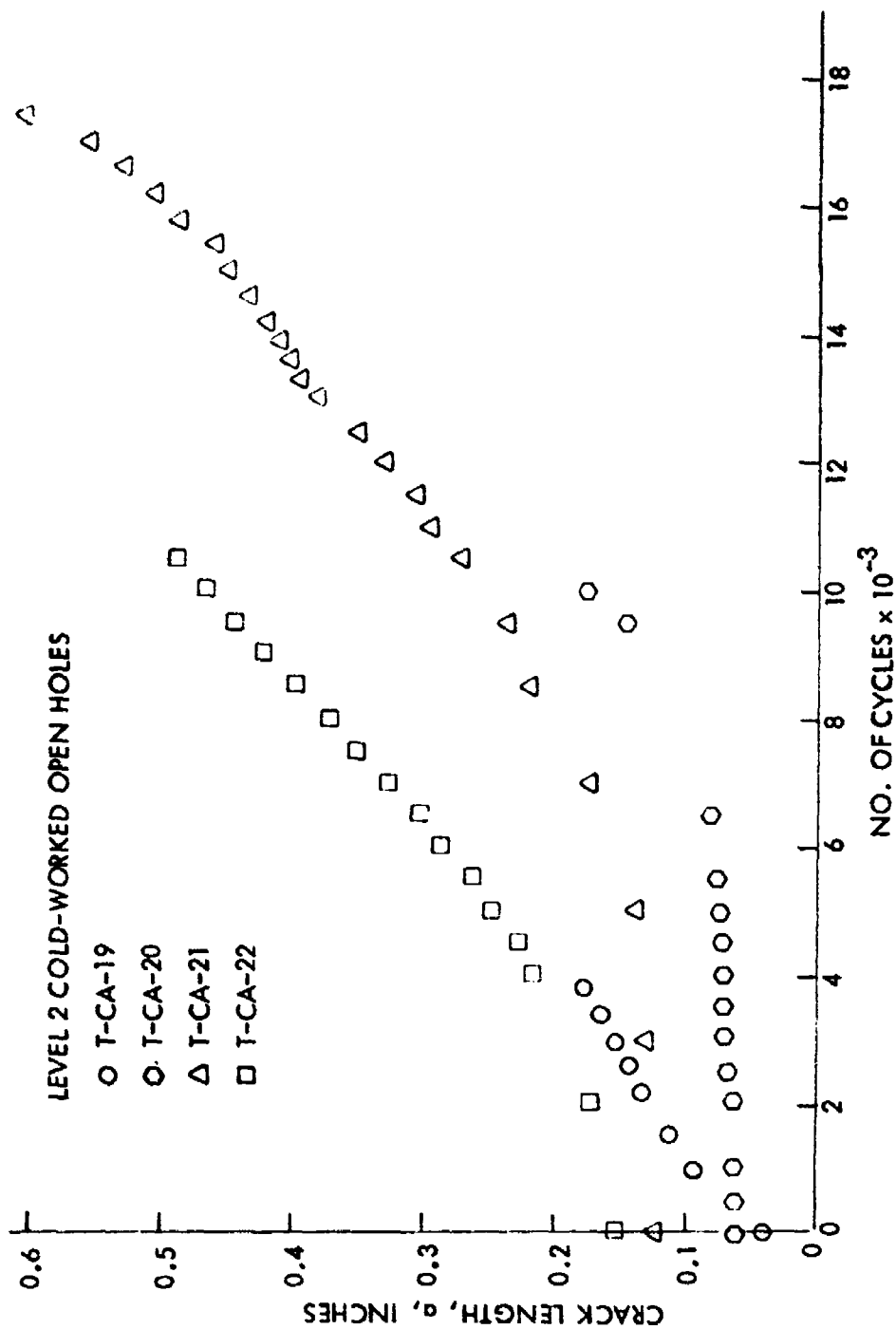


Figure 51 - Growth Behavior of Thru Cracks from Level 2 Cold-Worked Open Holes in 6Al-4V Beta Annealed Titanium Alloy Plates Subjected to Constant Amplitude Loading ($\sigma = 40$ Ksi, $R = 0.1$)

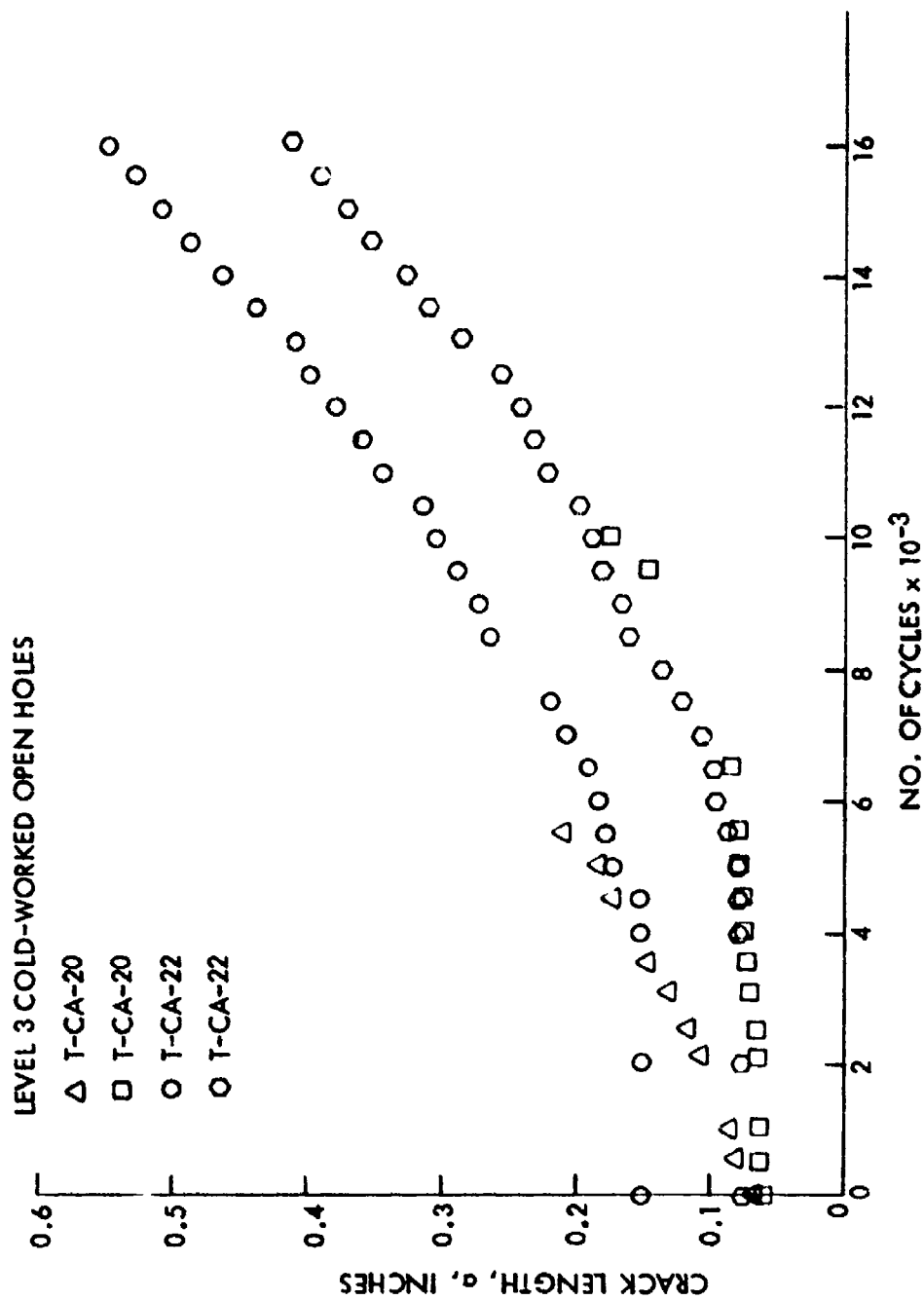


Figure 52. Growth Behavior of Thru Cracks from Level 3 Cold-Worked Open Holes in 6Al-4V Beta Annealed Titanium Alloy Plates Subjected to Constant Amplitude Loading ($\sigma = 40$ Ksi, $R = 0.1$)

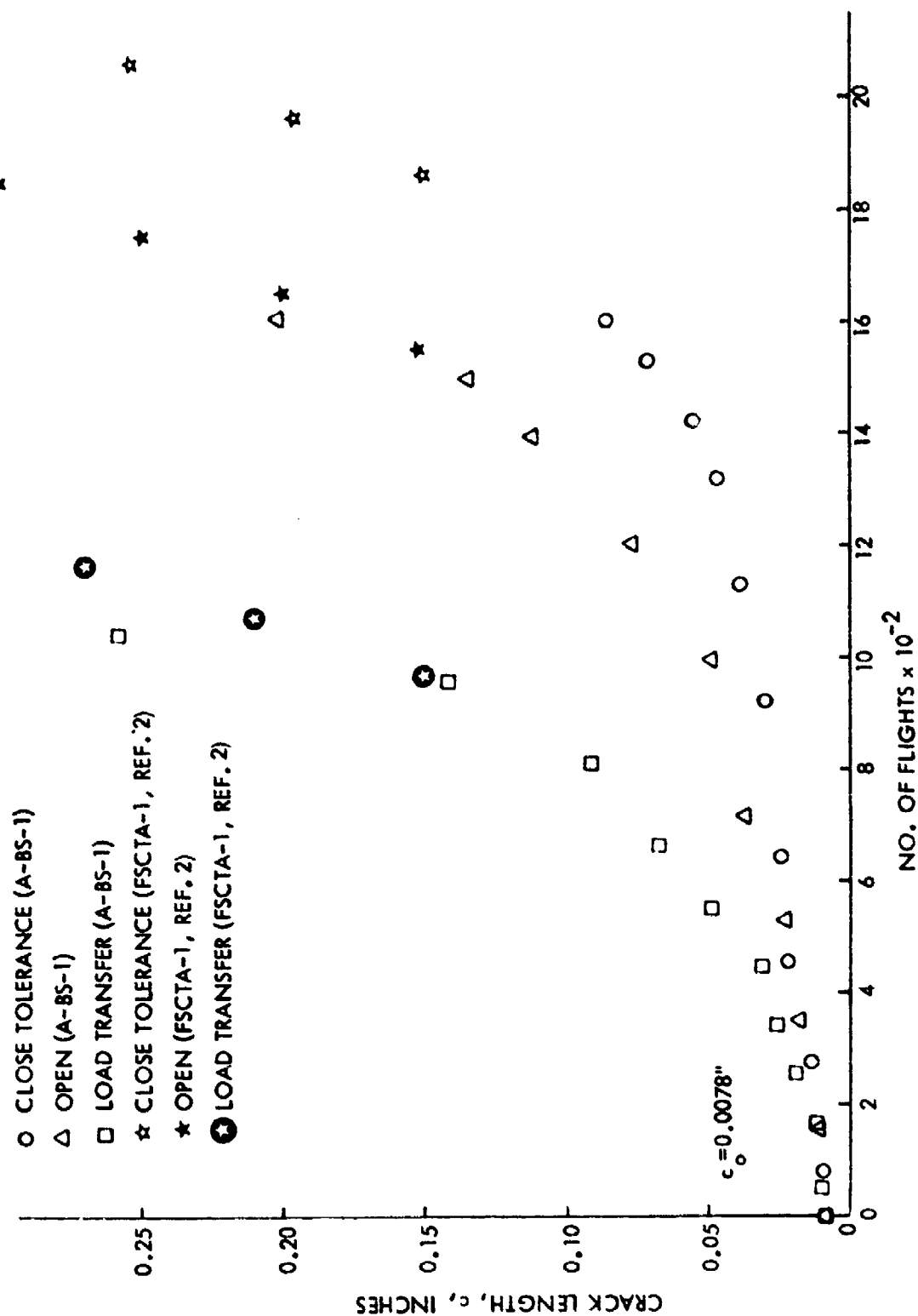


Figure 53. Crack Growth Behavior of Corner Cracks from Open and Close Tolerance Holes With and Without Fastener Load Transfer in 2219-T851 Aluminum Alloy Plates Subjected to Bomber Spectrum Loading

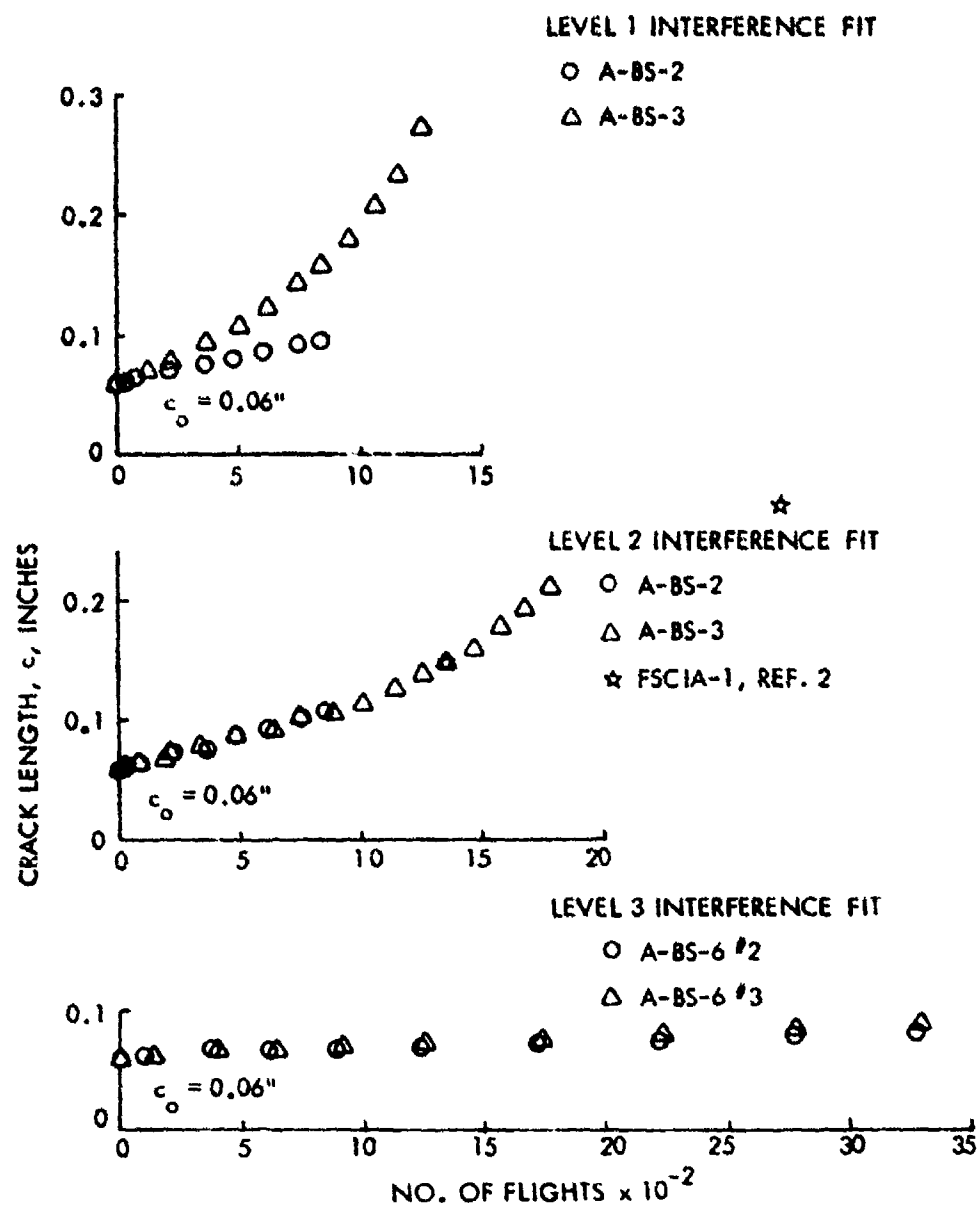


Figure 54. Growth Behavior of Intermediate Corner Cracks from Various Levels of Interference-Fit Fastener Holes in 2219-T851 Aluminum Alloy Plates Subjected to Bomber Spectrum Loading

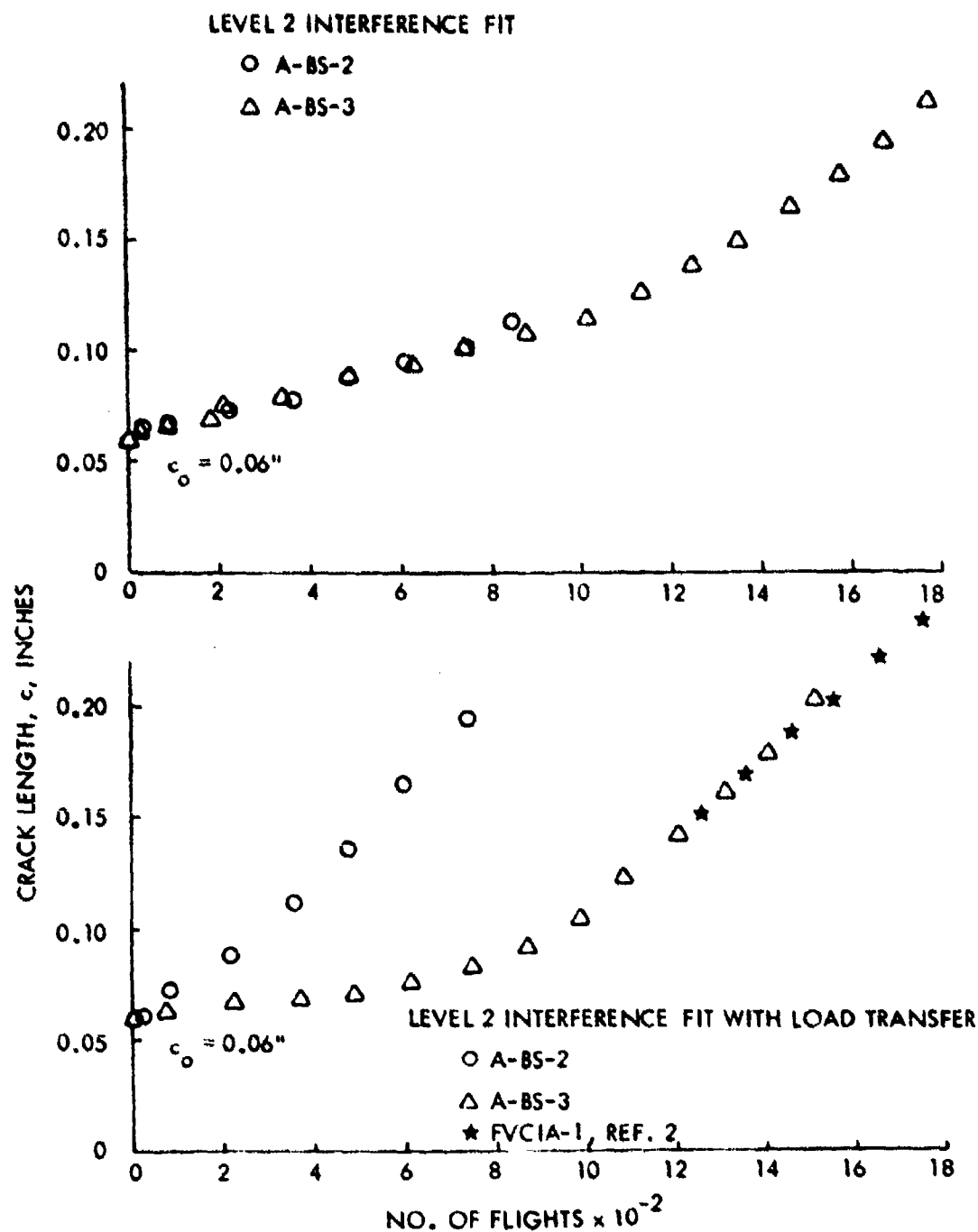


Figure 55. Growth Behavior of Intermediate Corner Cracks from Level 2 Interference-Fit Fastener Holes with and without Fastener Load Transfer in 2219-T851 Aluminum Alloy Plates Subjected to Bomber Spectrum Loading

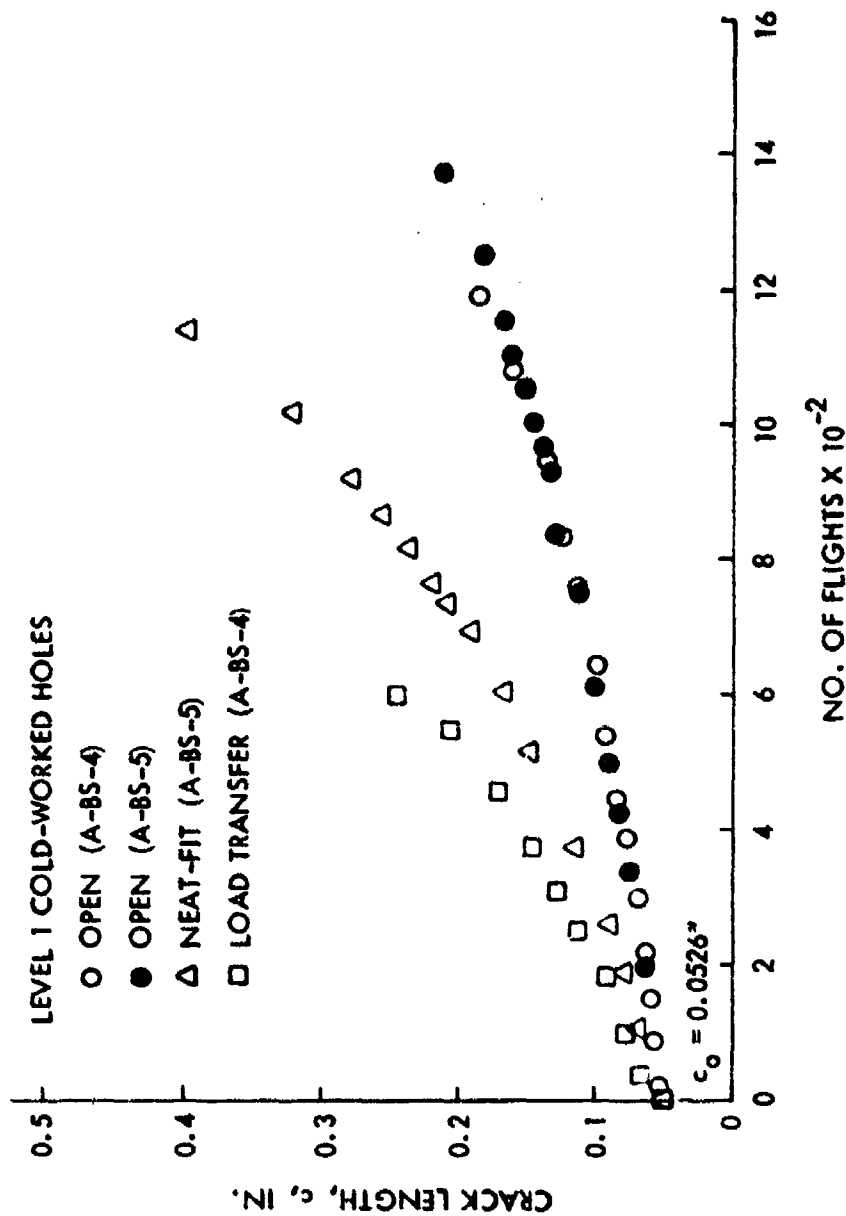


Figure 56. Growth Behavior of Intermediate Corner Cracks from Various Types of Level 1 Cold-Worked Holes in 2219-T851 Aluminum Alloy Plates Subjected to Bomber Spectrum Loading

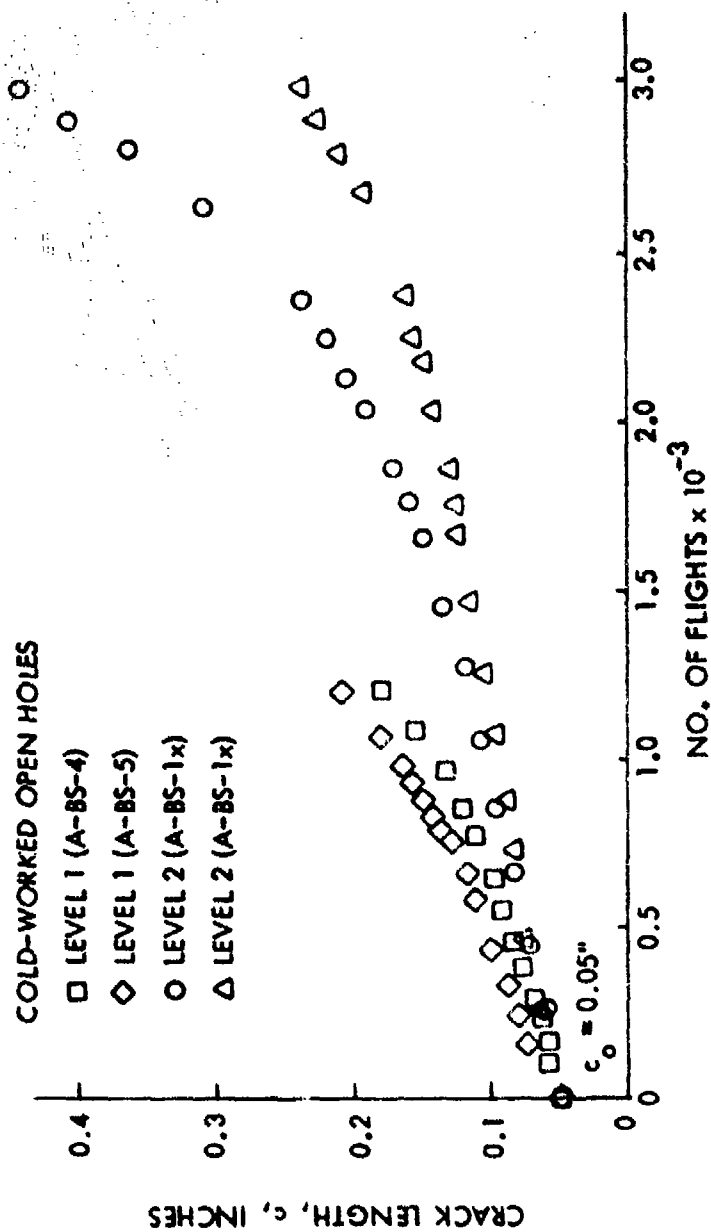


Figure 57. Growth Behavior of Intermediate Corner Cracks from Level 1 and Level 2 Cold-Worked Open Holes in 2219-T851 Aluminum Alloy Plates Subjected to Bomber Spectrum Loading

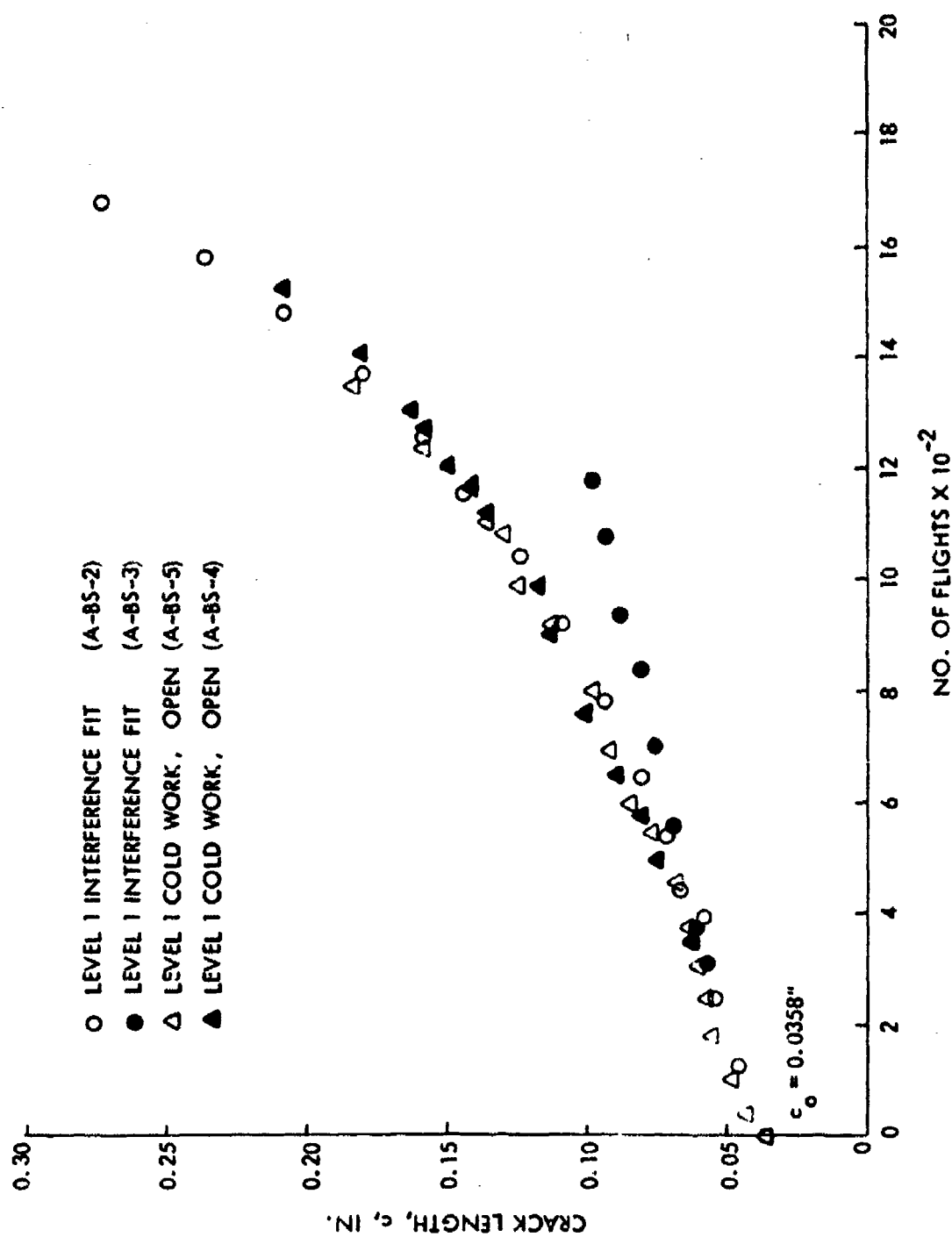


Figure 58. Comparison of Growth Behavior of Small Corner Cracks from Level 1 Cold-Worked and Interference-Fit Fastener Holes in 2219-T851 Aluminum Alloy Plates Subjected to Bomber Spectrum Loading

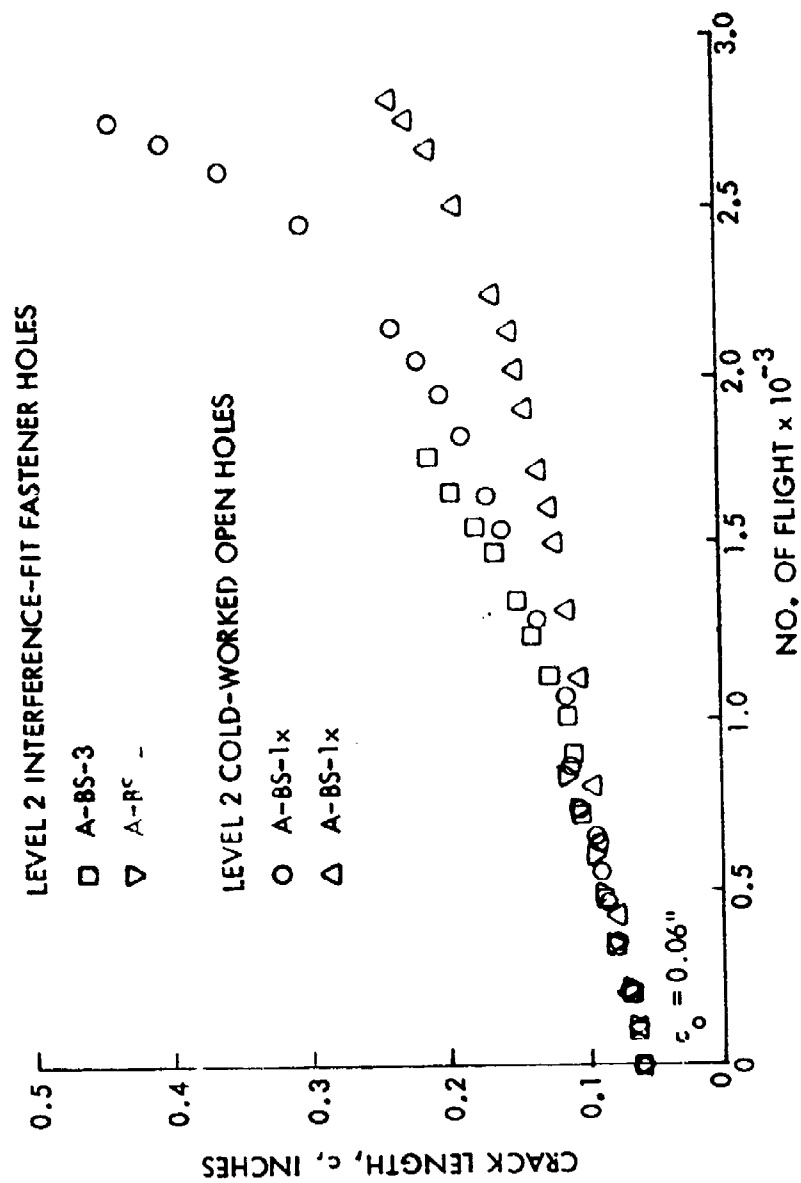


Figure 59. Comparison of Growth Behavior of Intermediate Corner Cracks from Level 2 Interference-Fit Fastener Holes and Level 2 Cold-Worked Open Holes in 2219-T851 Aluminum Alloy Plates Subjected to Bomber Spectrum Loading

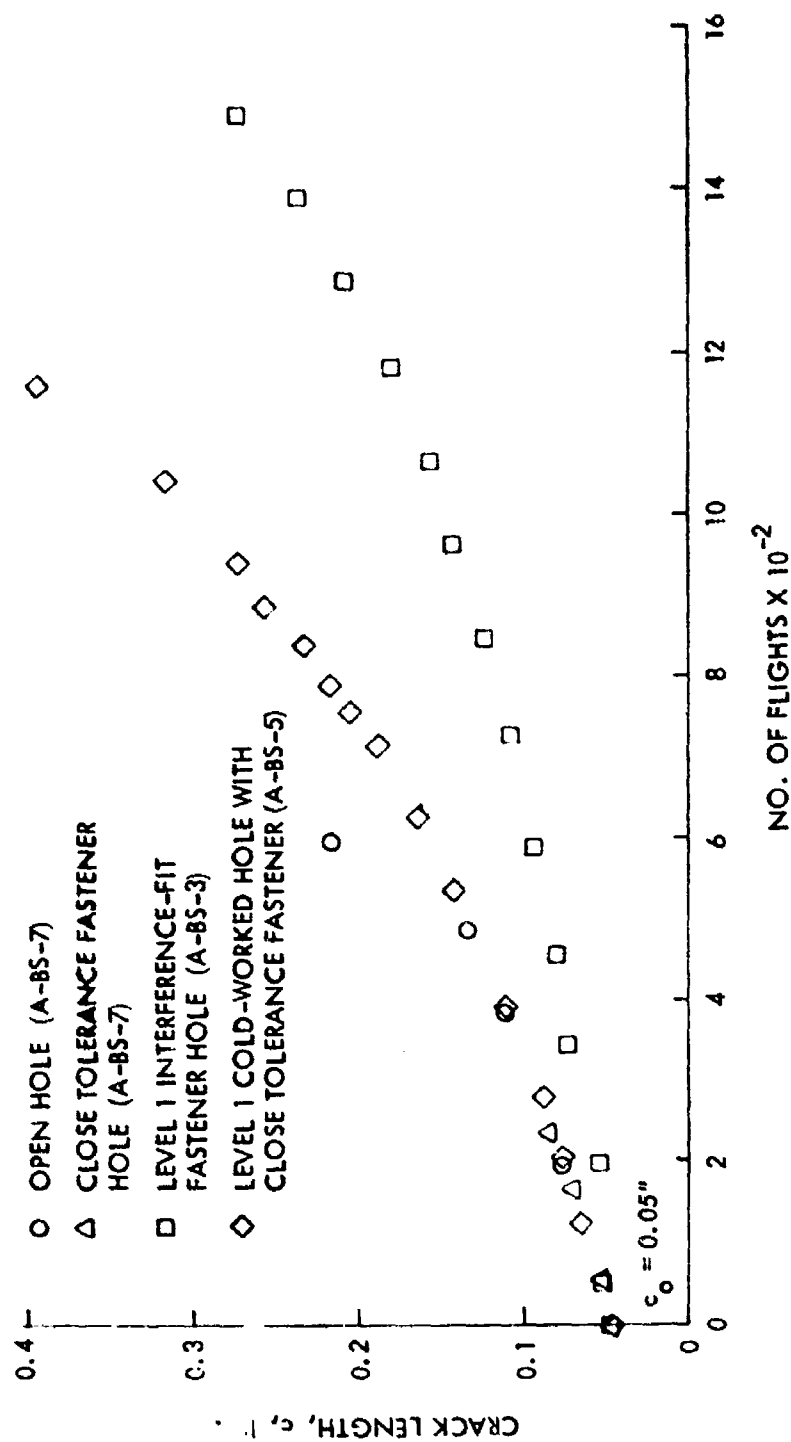


Figure 60 . Comparison of Growth Behavior of Intermediate Corner Cracks from Various Types of Fastener Holes in 2219-T851 Aluminum Alloy Plates Subjected to Bomber Spectrum Loading

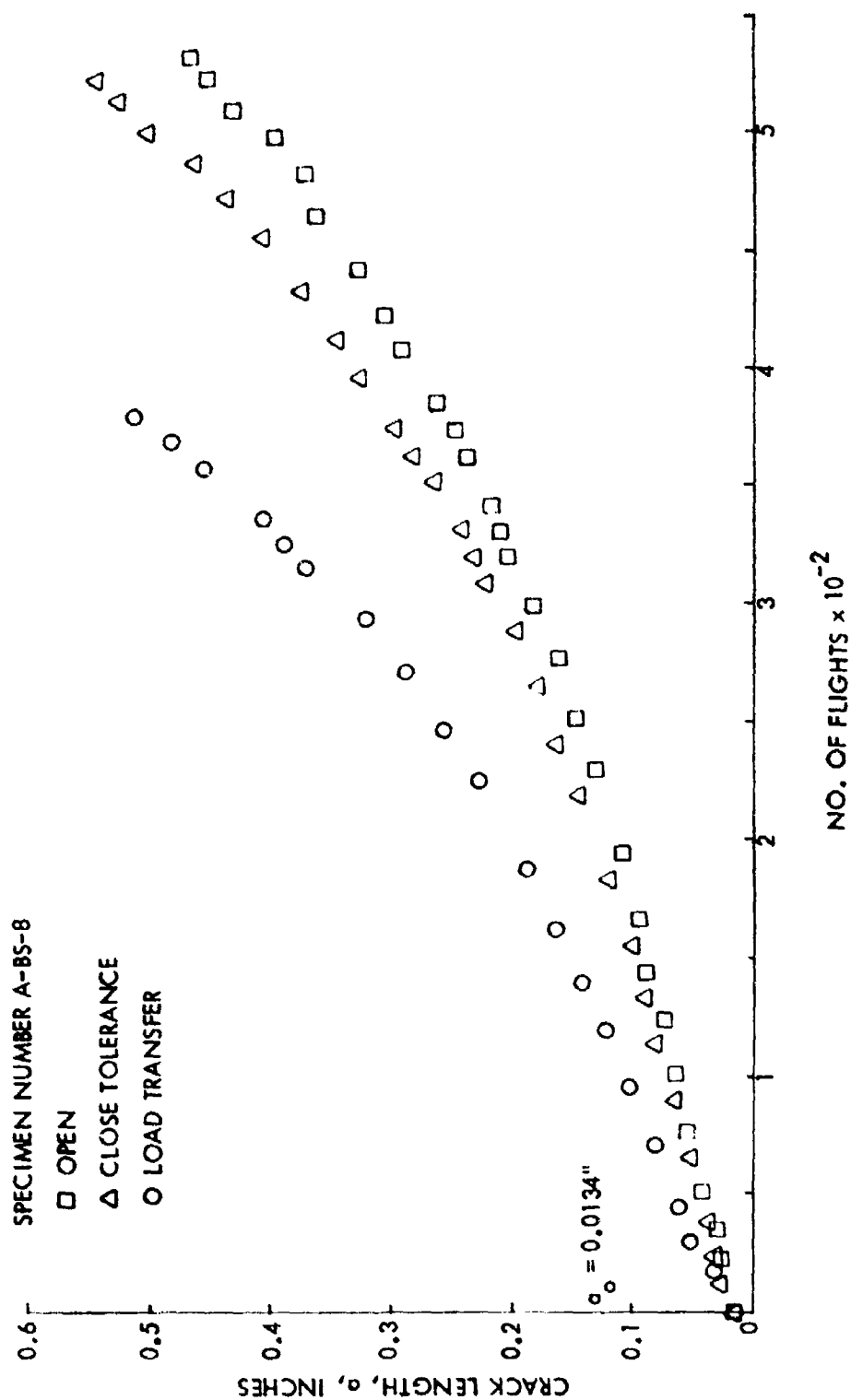


Figure 61. Growth Behavior of Small Thru Cracks from Open and Close-Tolerance Fastener Holes in 2219-T851 Aluminum Alloy Plates Subjected to Bomber Spectrum Loading

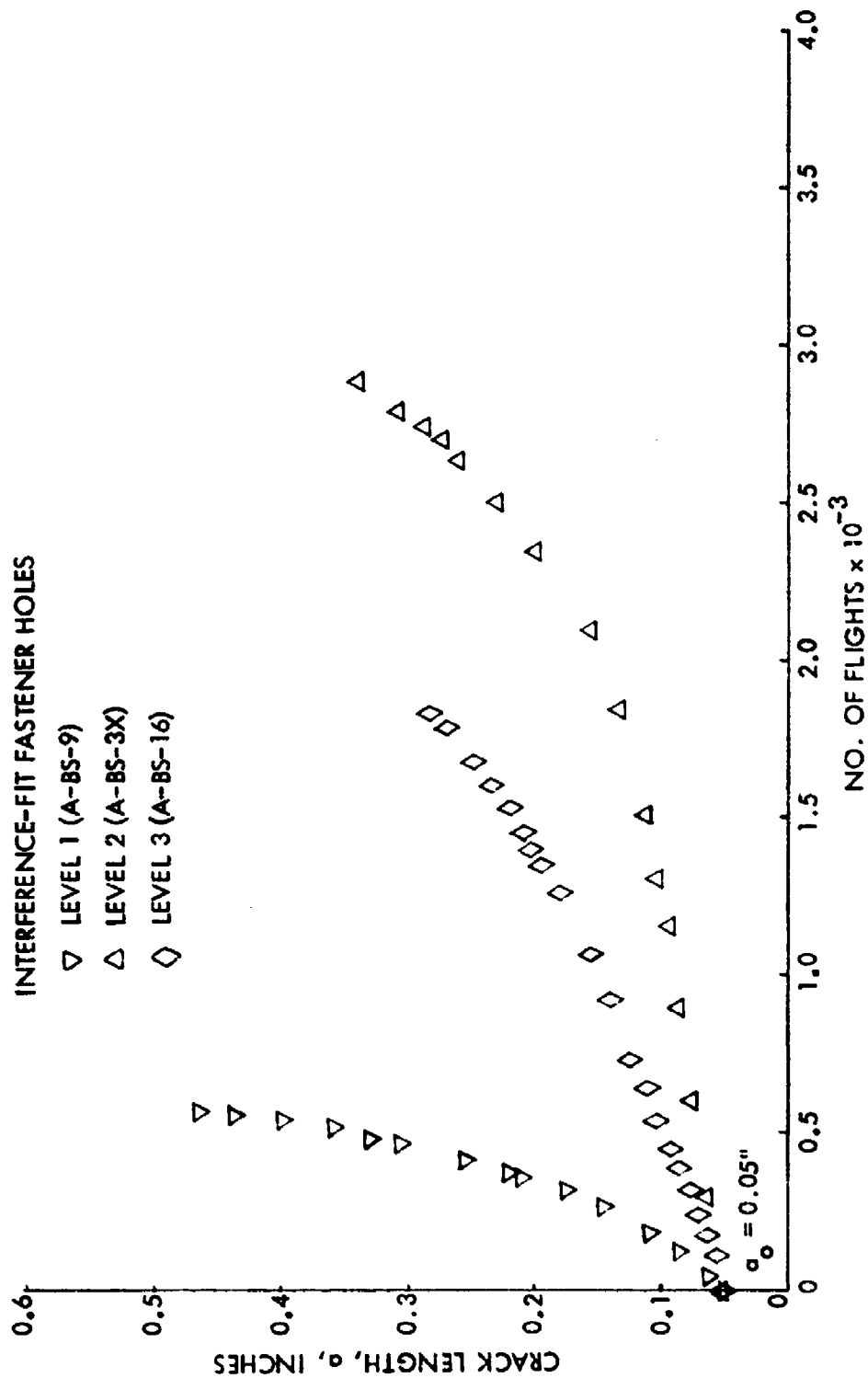


Figure 62. Growth Behavior of Intermediate Thru Cracks from Interference-Fit Fastener Holes for Various Levels of Interference in 2219-T851 Aluminum Alloy Plates Subjected to Bomber Spectrum Loading

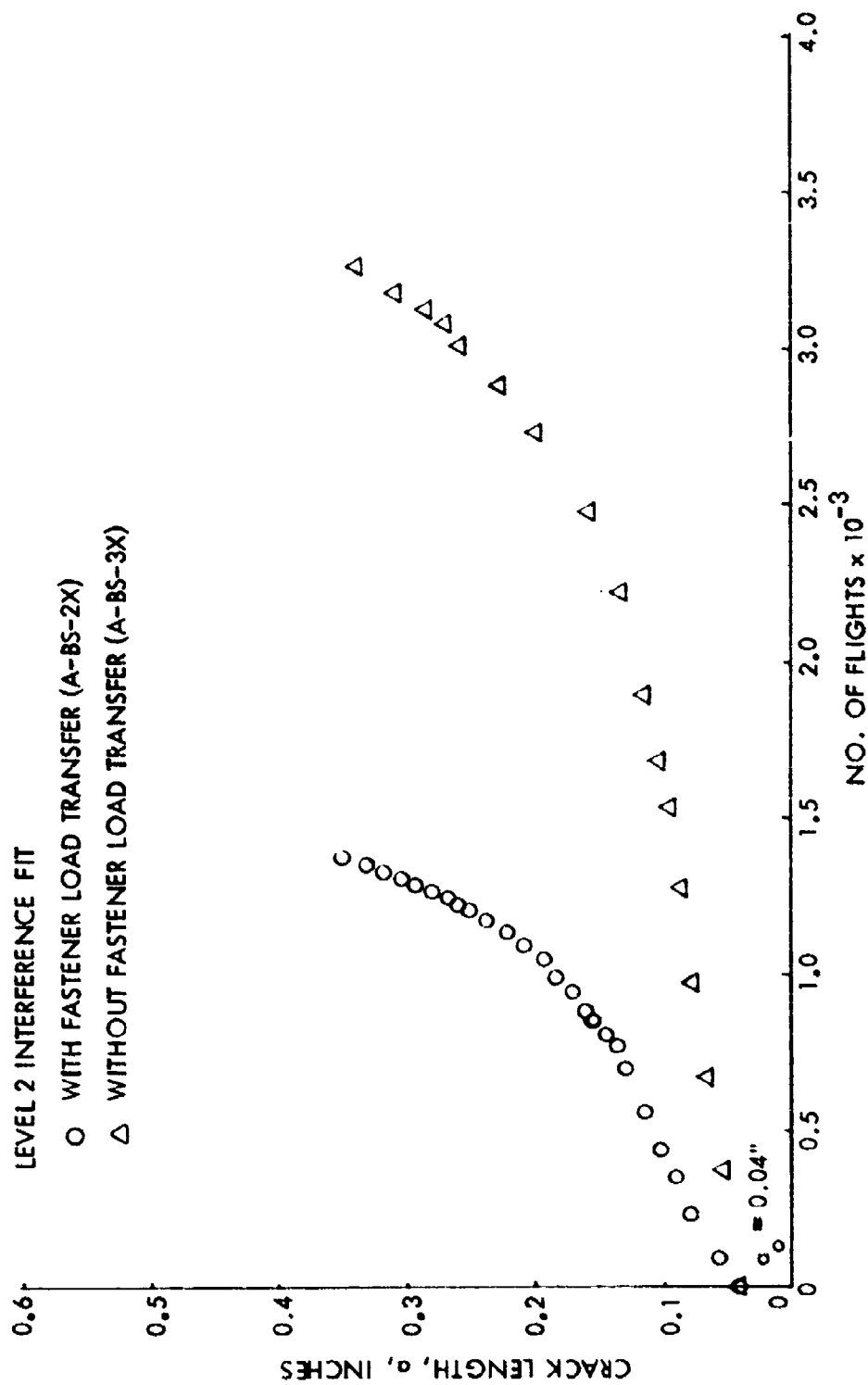


Figure 63 . Growth Behavior of Intermediate Thru Cracks from Level 2 Interference-Fit Fastener Holes with and without Fastener Load Transfer in 2219-T851 Aluminum Alloy Plates Subjected to Bomber Spectrum Loading

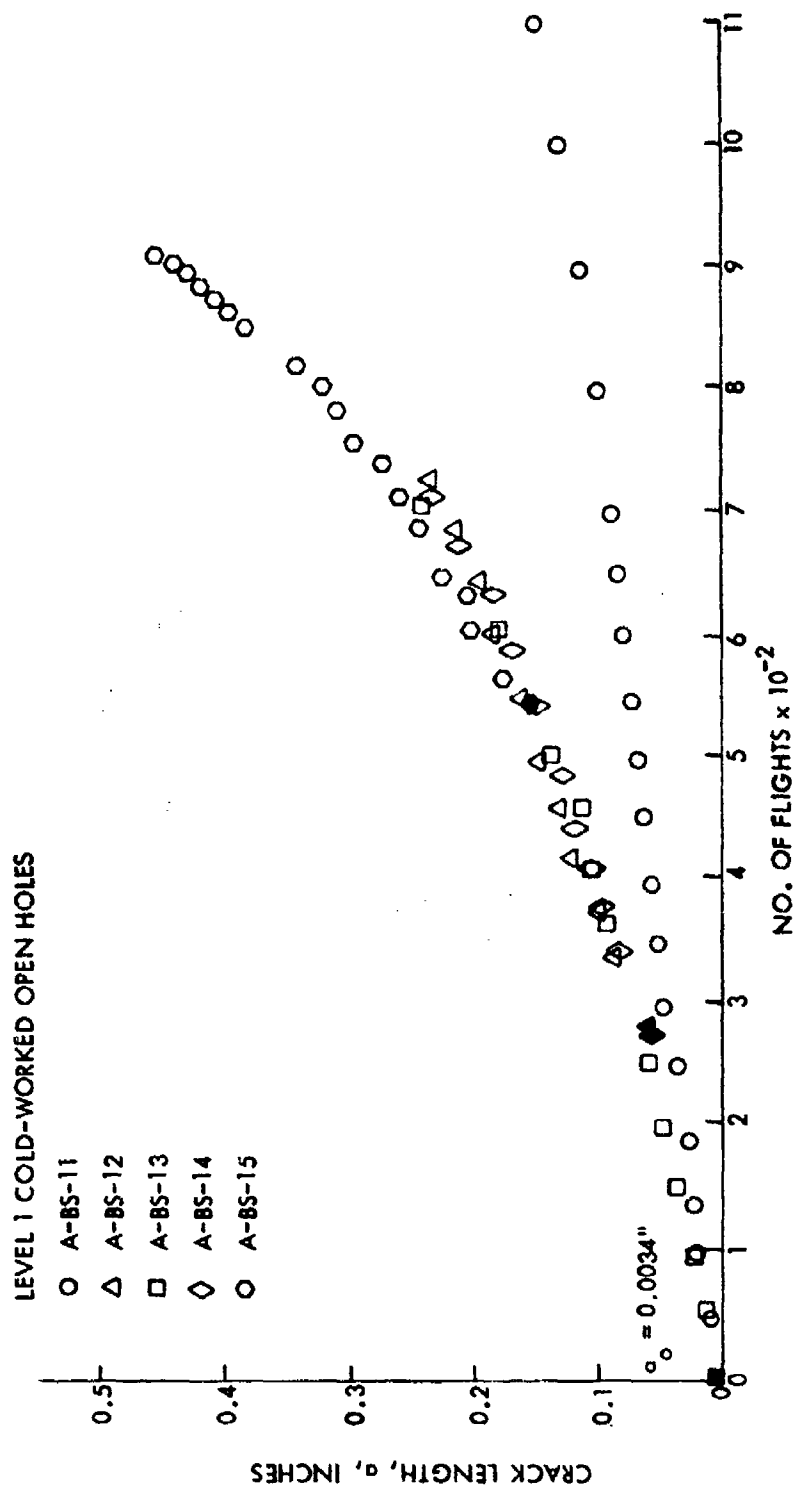


Figure 64. Growth Behavior of Thru Cracks from Level 1 Cold-Worked Open Holes in 2219-T851 Aluminum Alloy Plates Subjected to Bomber Spectrum Loading

LEVEL 1 COLD-WORKED HOLES WITH
CLOSE TOLERANCE FASTENERS

- A-BS-11
- △ A-BS-12
- A-BS-13
- ◇ A-BS-14
- A-BS-15

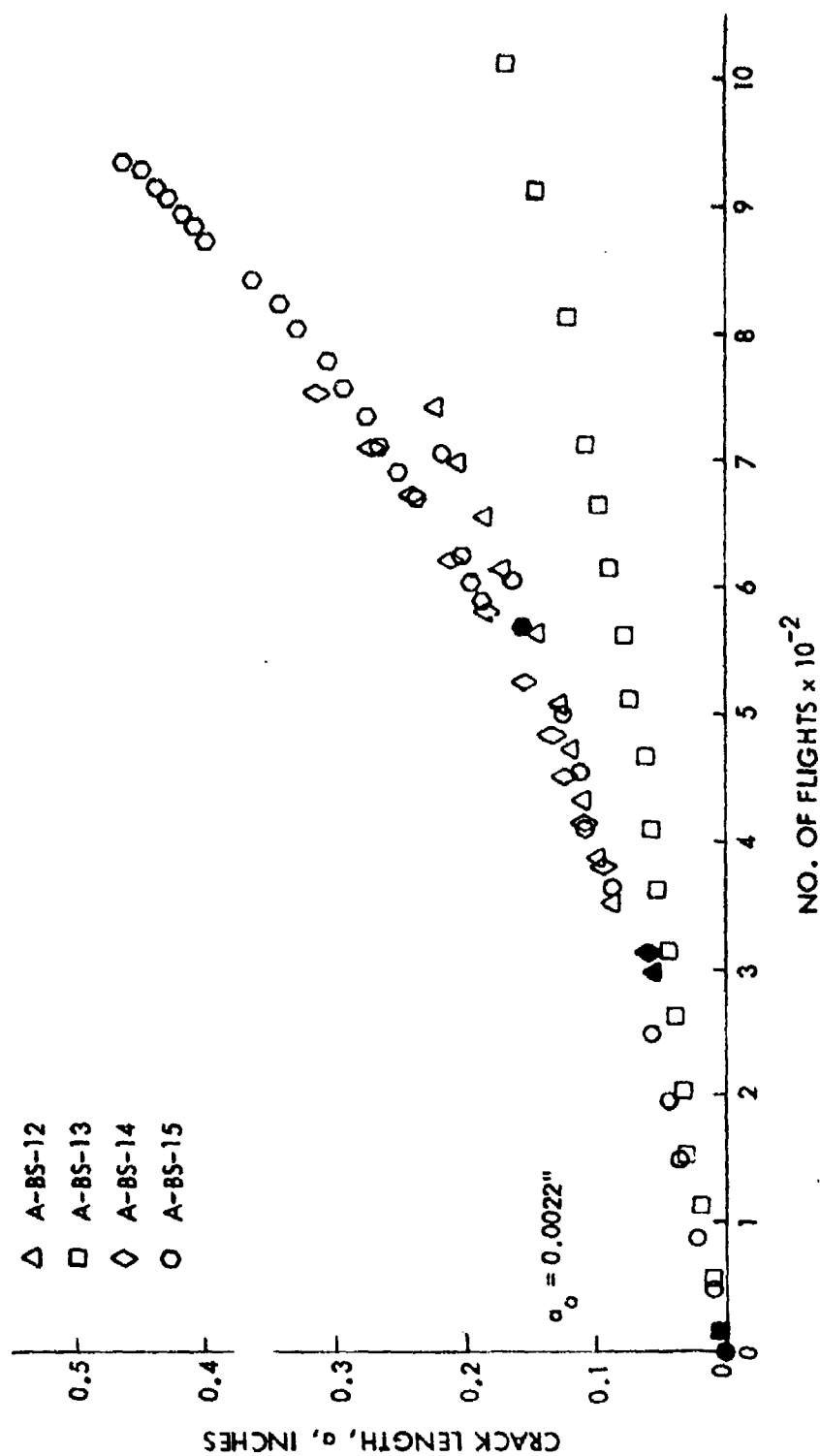


Figure 65. Growth Behavior of Thru Cracks from Level 1 Cold-Worked Filled Holes in 2219-T851 Aluminum Alloy Plates Subjected to Bomber Spectrum Loading

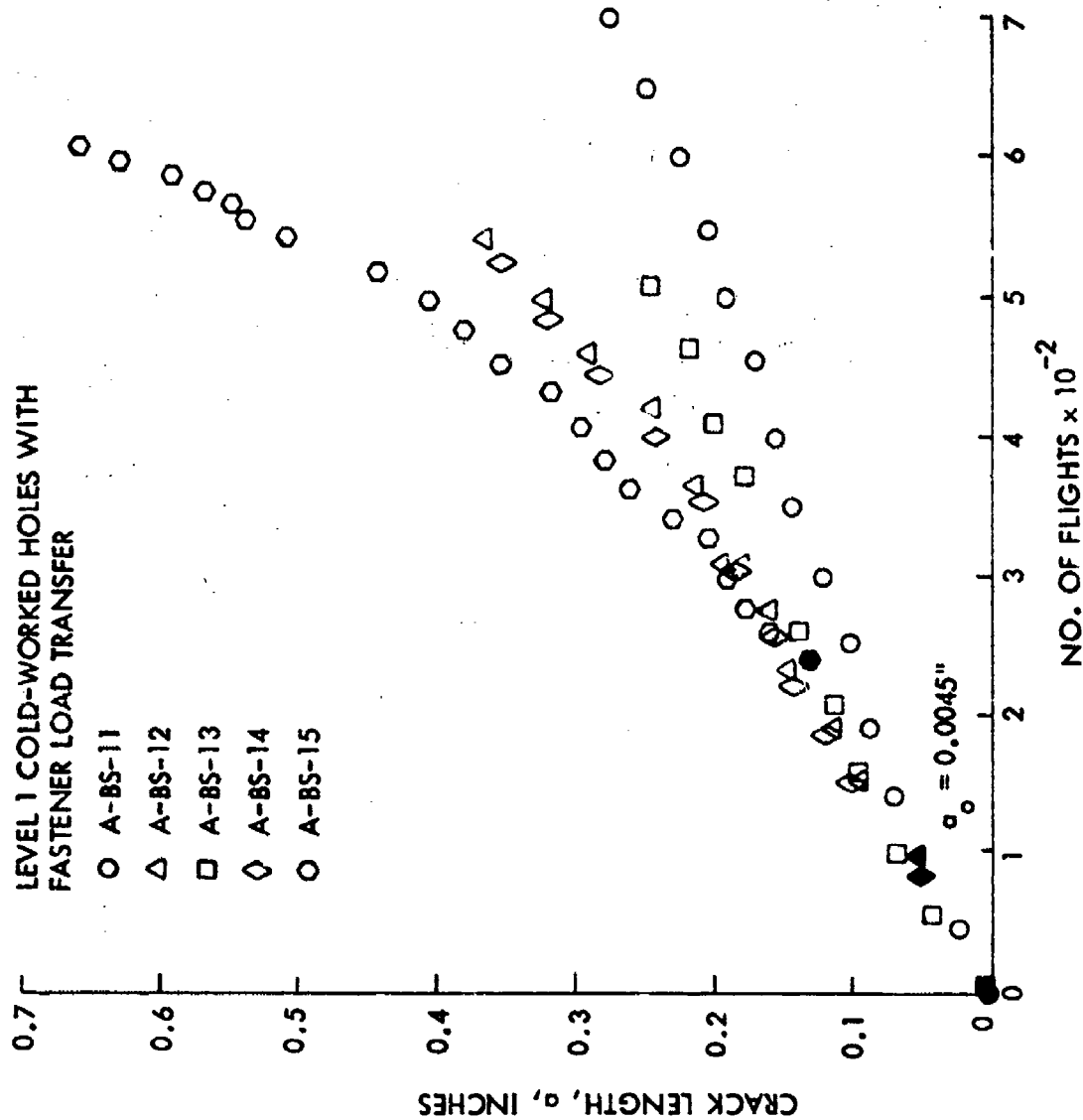


Figure 66. Growth Behavior of Thru Cracks from Level 1 Cold-Worked Holes Having Fastener Load Transfer in 2219-T851 Aluminum Alloy Plates Subjected to Bomber Spectrum Loading

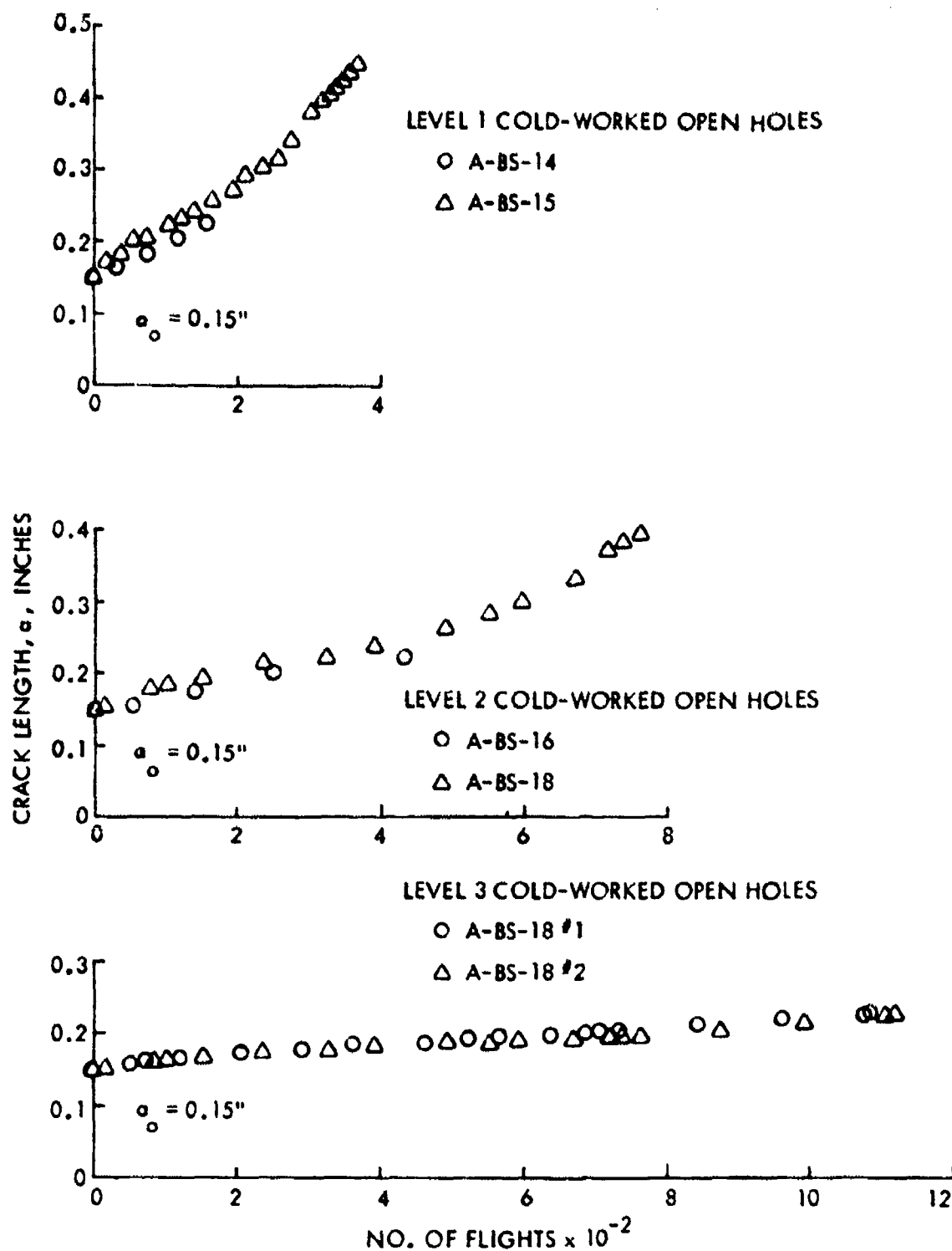


Figure 67. Growth Behavior of Large Thru Cracks from Cold-Worked Open Holes for Various Levels of Cold Working for 2219-T851 Aluminum Alloy Plates Subjected to Bomber Spectrum Loading

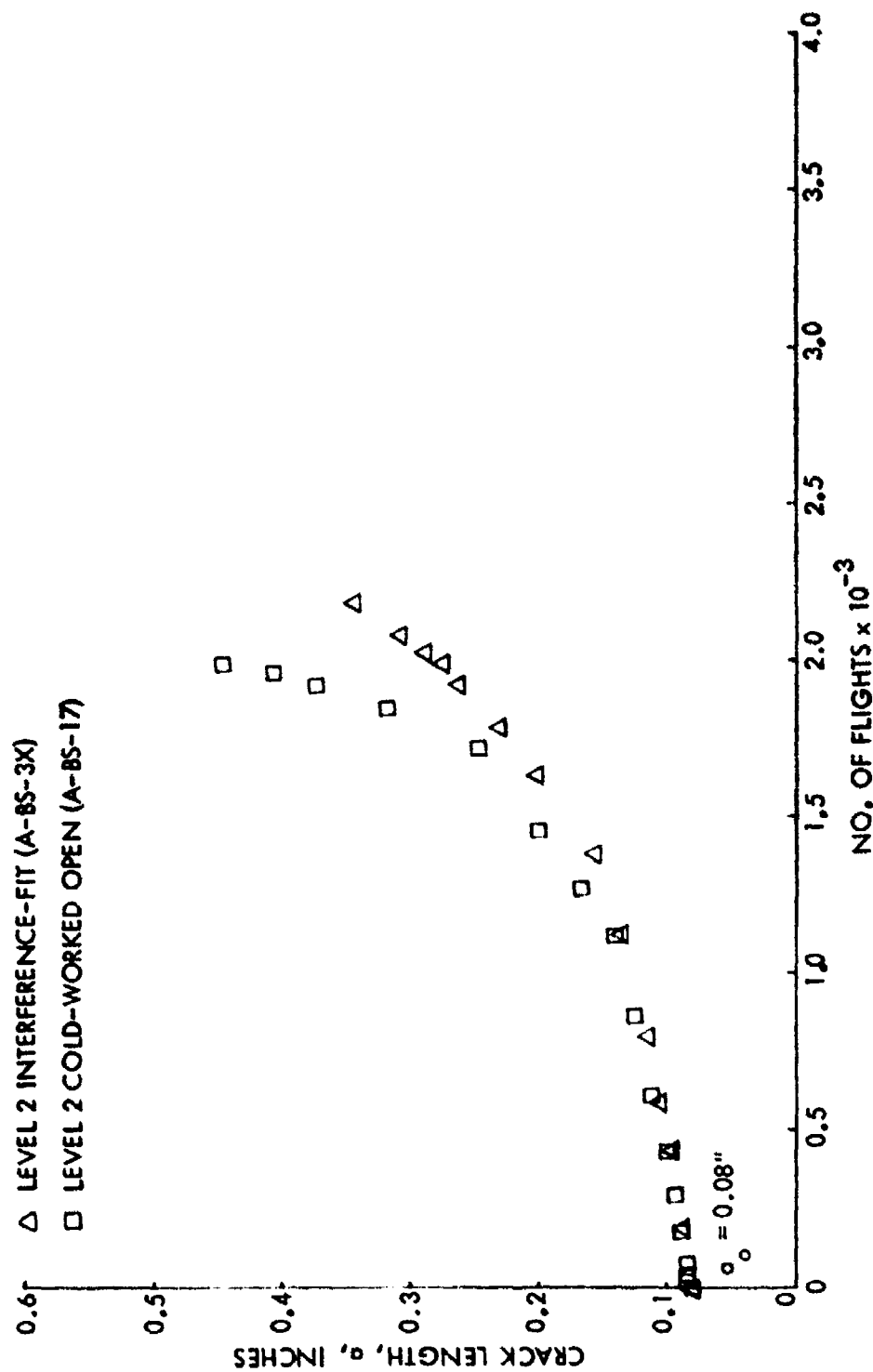


Figure 68. Comparison of Growth Behavior of Intermediate Thru Cracks from Level 2 Interference-Fit and Cold-Worked Fastener Holes in 2219-T851 Aluminum Alloy Plates Subjected to Bomber Spectrum Loading

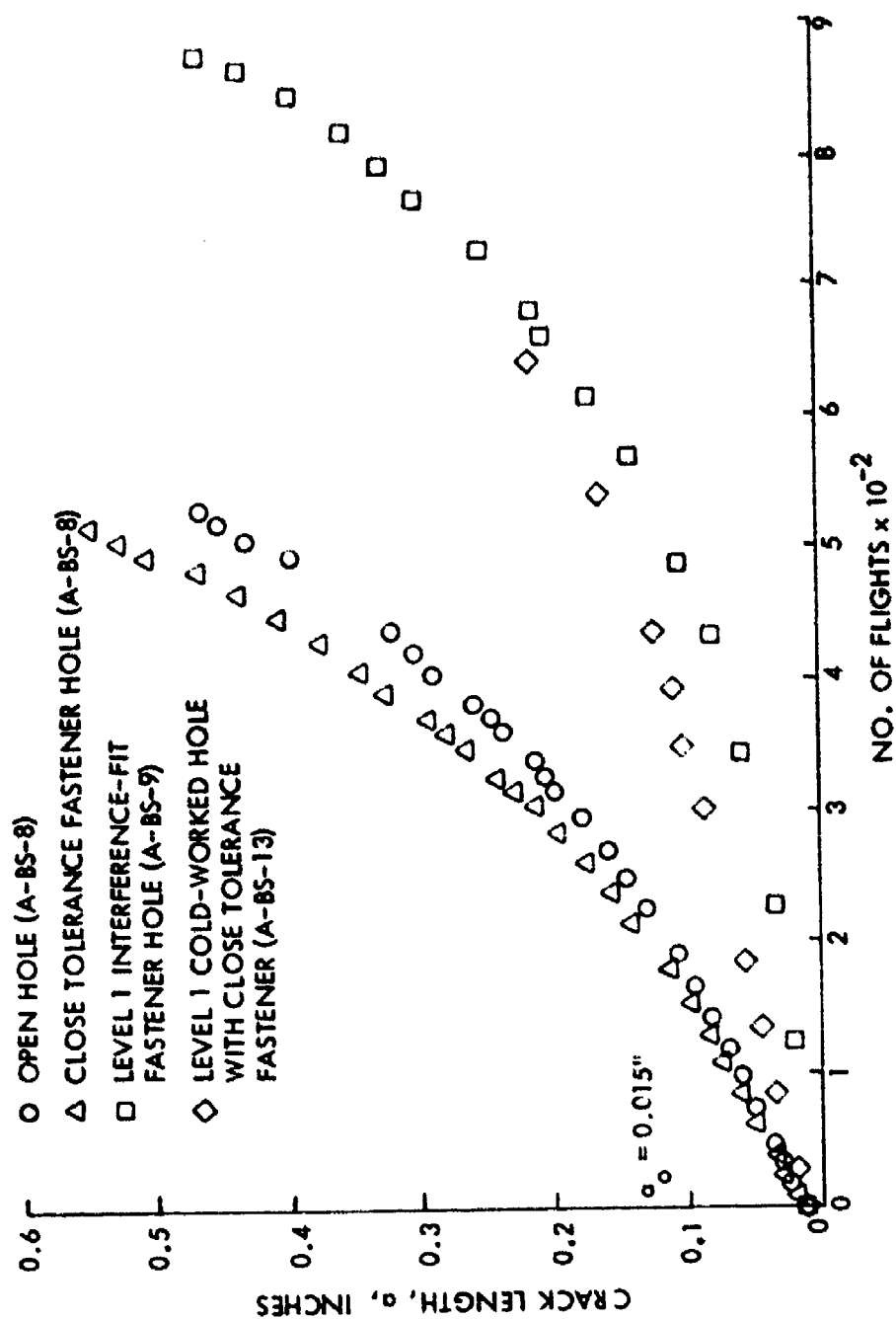


Figure 69. Comparison of Growth Behavior of Small Thru Cracks from Various Types of Fastener Holes in 2219-T851 Aluminum Alloy Plates Subjected to Bomber Spectrum Loading

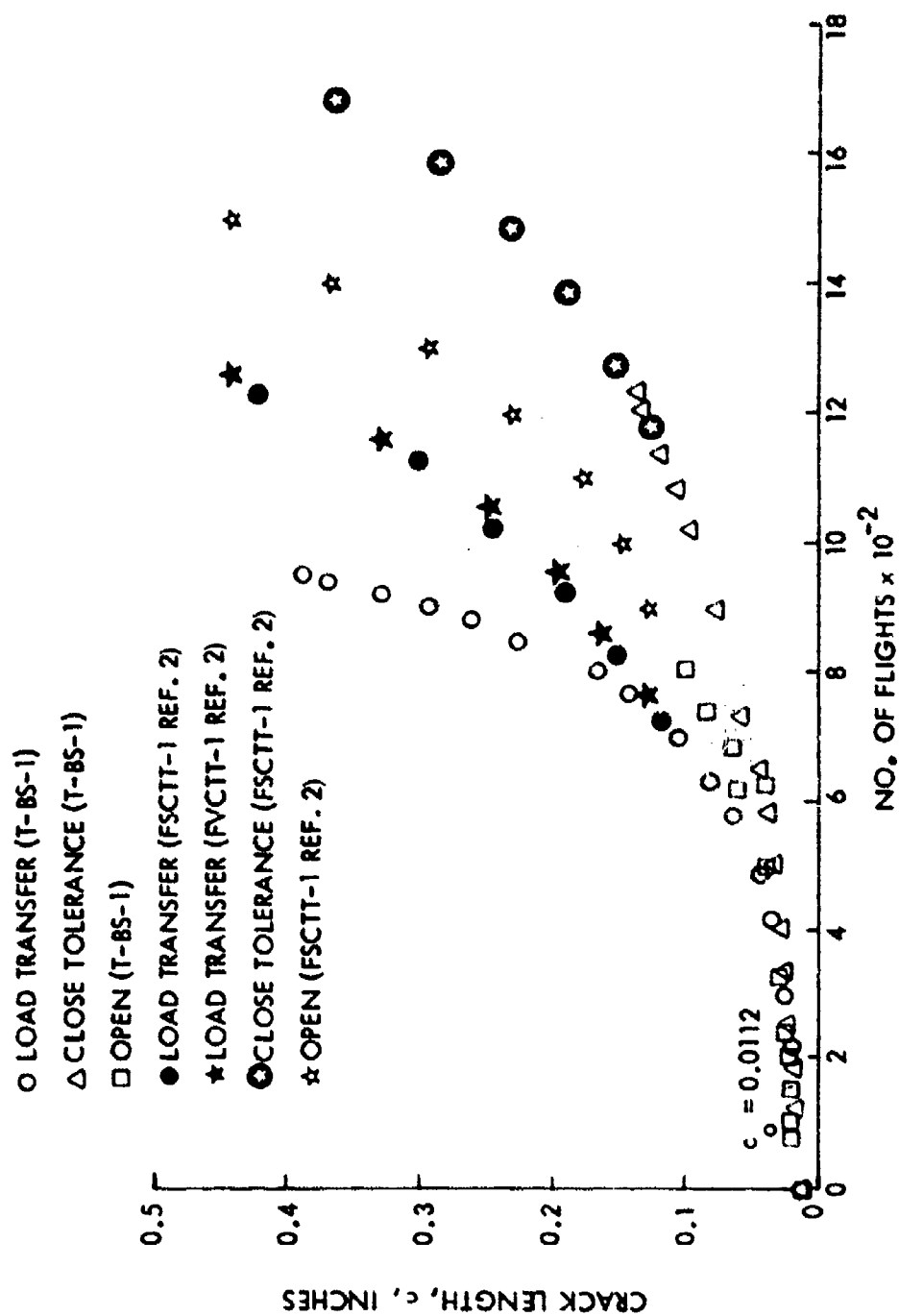


Figure 70. Growth Behavior of Corner Cracks from Open and Close Tolerance Holes in 6Al-4V Beta Annealed Titanium Alloy Plates Subjected to Bomber Spectrum Loading

LEVEL 1 INTERFERENCE FIT

- T-B5-2
- △ T-B5-3
- ☆ FSCIT-1 (REF. 2)
- ★ FSCIT-3 (REF. 2)

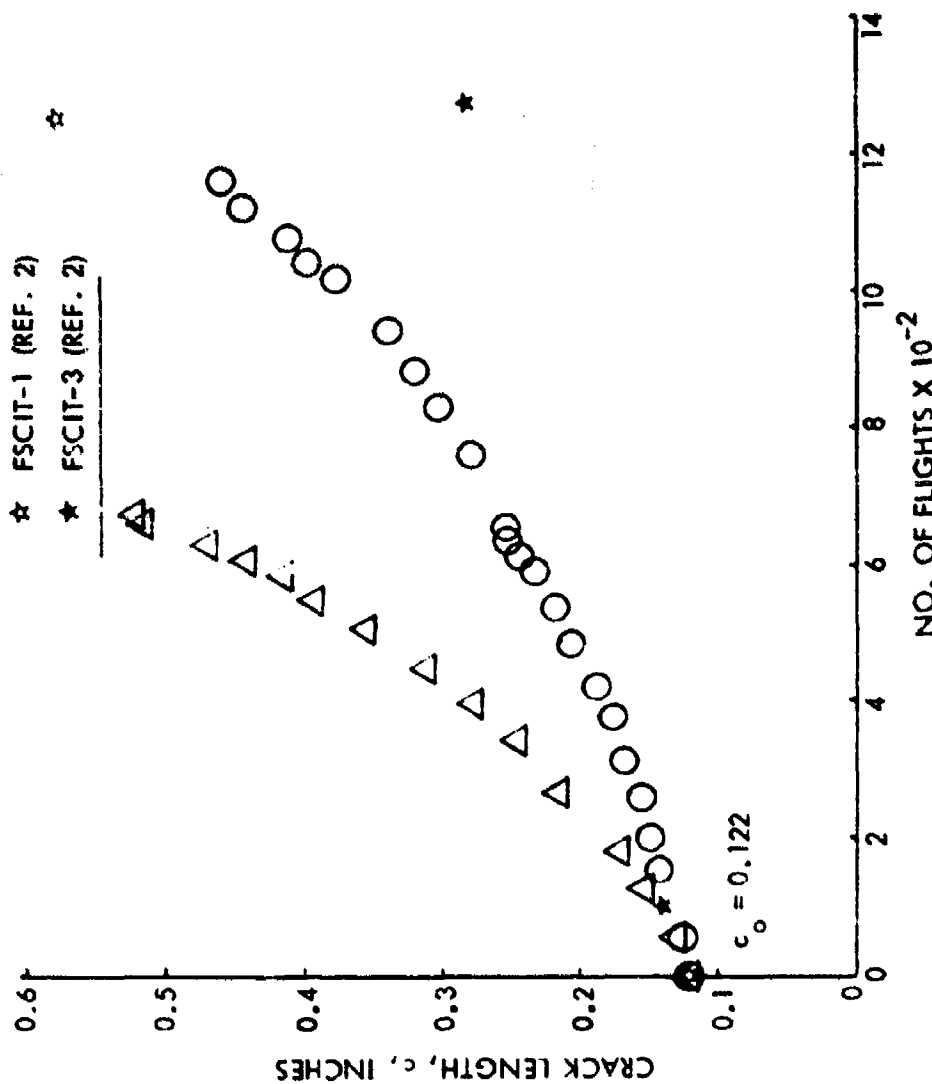


Figure 71. Growth Behavior of Intermediate Corner Cracks from Level 1 Interference-Fit Fastener Holes in 6Al-4V Beta Annealed Titanium Alloy Plates Subjected to Bomber Spectrum Loading

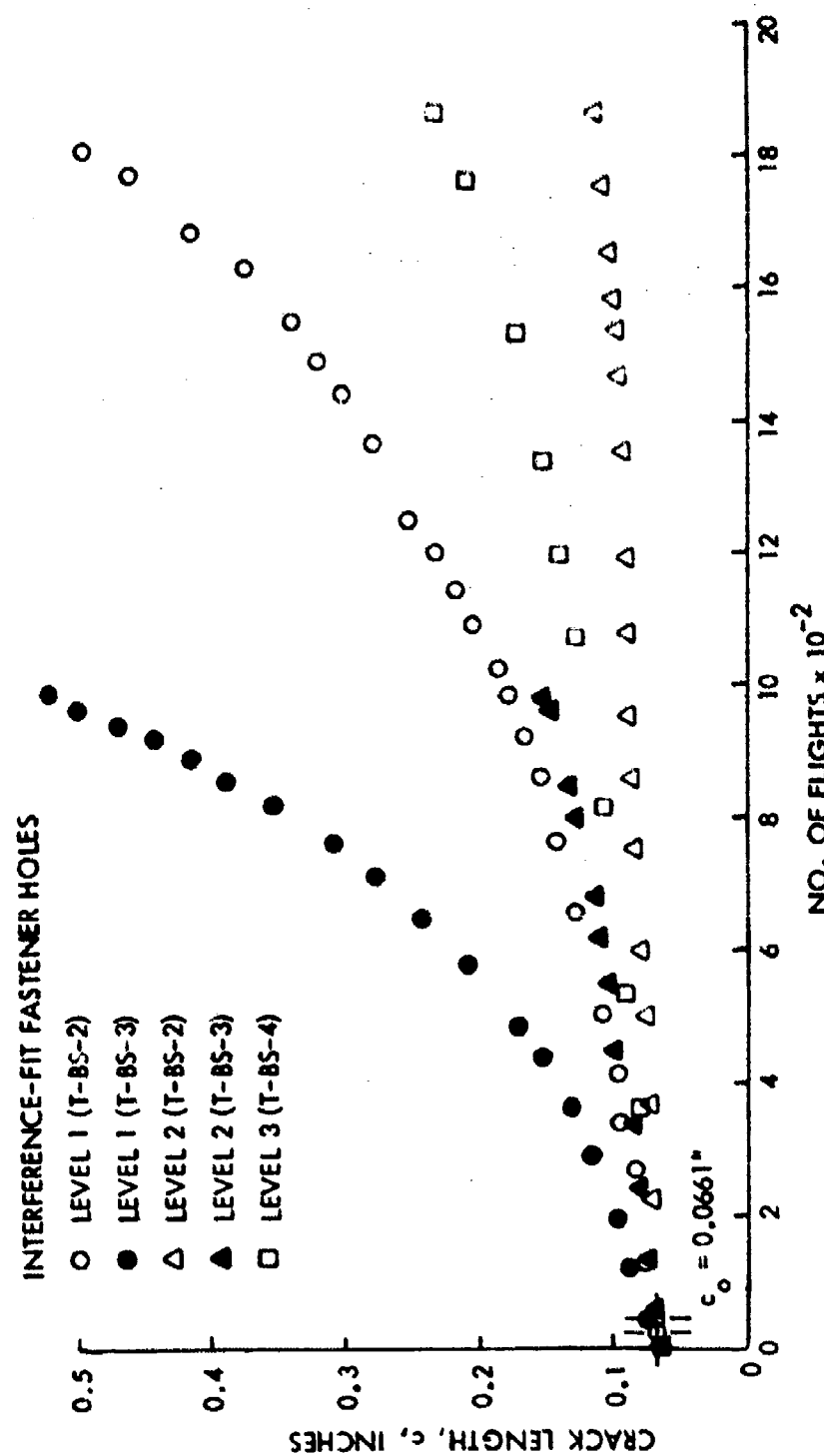


Figure 72. Growth Behavior of Intermediate Corner Cracks from Interference-Fit Fastener Holes for Various Levels of Interference in 6Al-4V Beta Annealed Titanium Alloy Plates Subjected to Bomber Spectrum Loading

LEVEL 1 COLD-WORKED FASTENER HOLES

- OPEN (T-BS-6)
- OPEN (T-BS-7)
- △ CLOSE TOLERANCE (T-BS-6)
- ▲ CLOSE TOLERANCE (T-BS-7)
- LOAD TRANSFER (T-BS-6)
- LOAD TRANSFER (T-BS-7)

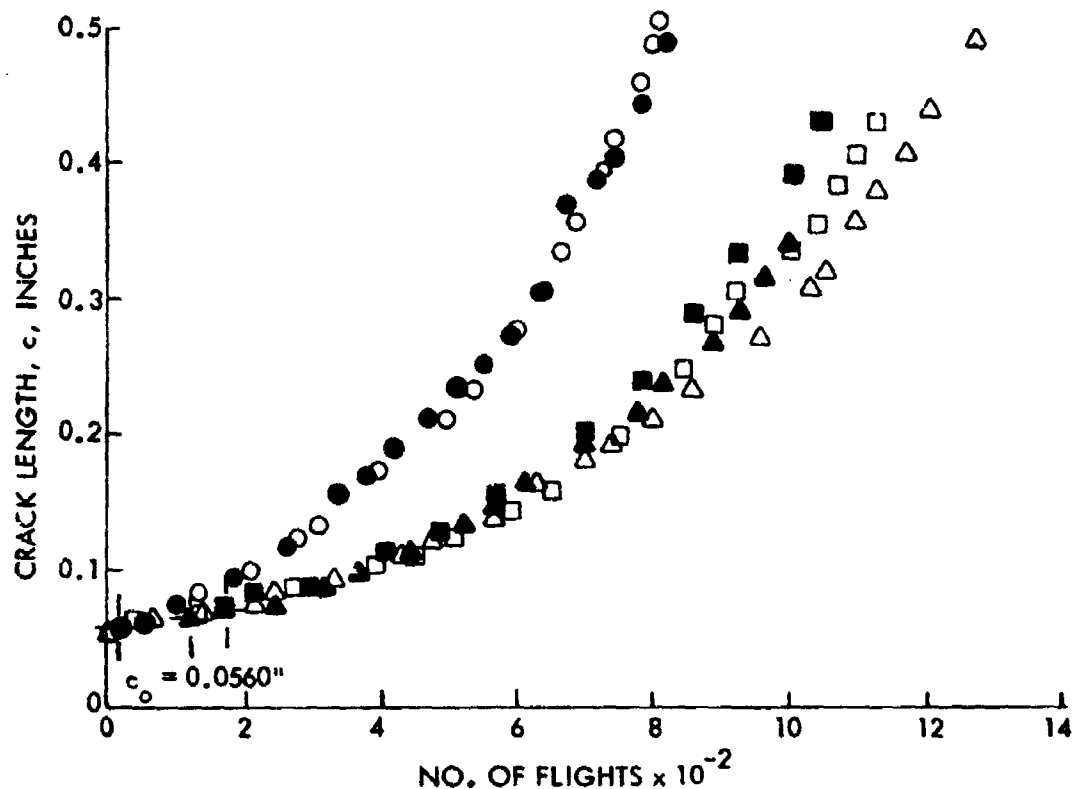


Figure 73. Growth Behavior of Intermediate Corner Cracks from Level 1 Cold-Worked Fastener Holes in 6Al-4V Beta Annealed Titanium Alloy Plates Subjected to Bomber Spectrum Loading

COLD-WORKED OPEN HOLES

- LEVEL 1 (T-BS-6)
- LEVEL 1 (T-BS-7)
- △ LEVEL 2 (T-BS-4)
- ▲ LEVEL 2 (T-BS-5)
- LEVEL 3 (T-BS-5)
- LEVEL 3 (T-BS-5)

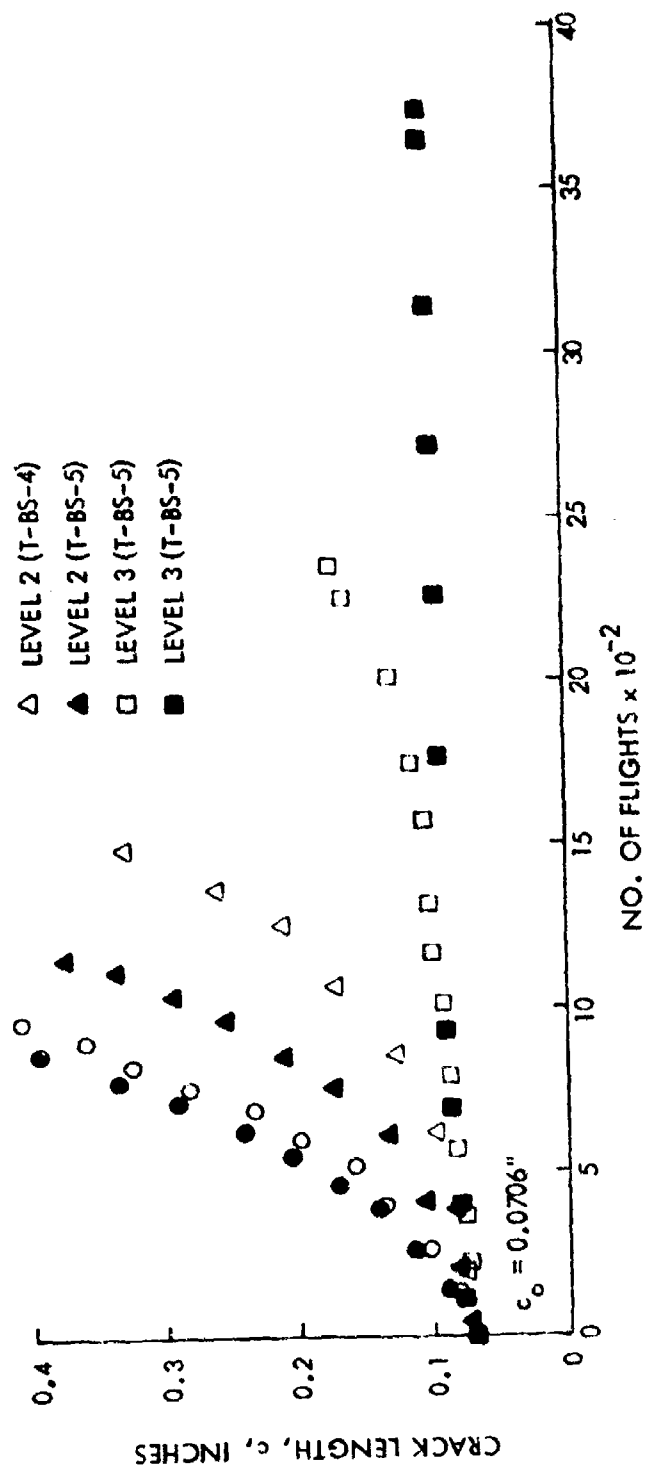


Figure 74. Growth Behavior of Intermediate Corner Cracks from Cold-Worked Open Holes for Various Levels of Cold Working in 6Al-4V Beta Annealed Titanium Alloy Plates Subjected to Bomber Spectrum Loading

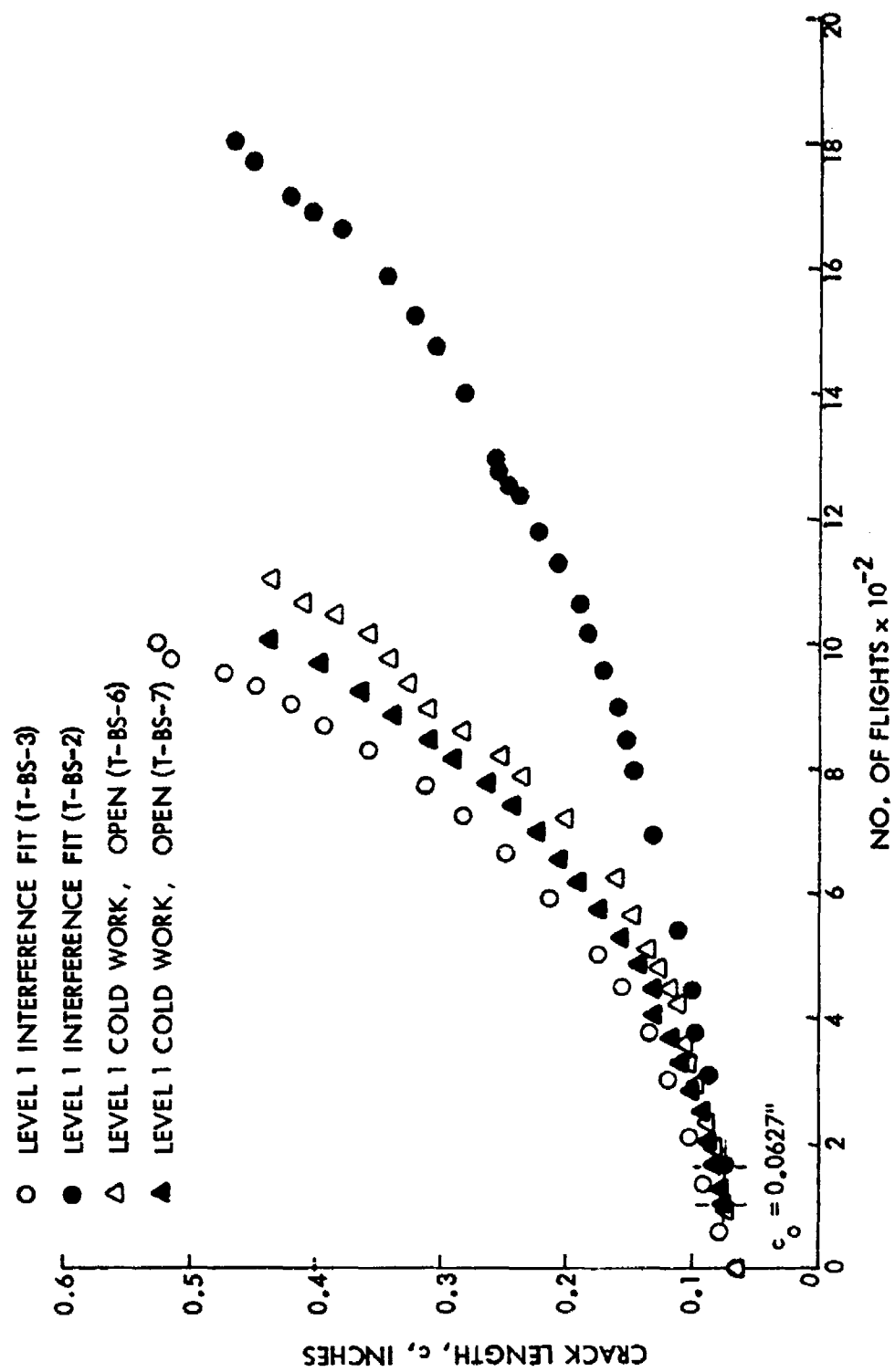


Figure 75. Comparison of Growth Behavior of Intermediate Corner Cracks from Level 1 Cold-Worked and Interference-Fit Fastener Holes in 6Al-4V Beta Annealed Titanium Alloy Plates Subjected to Bomber Spectrum Loading

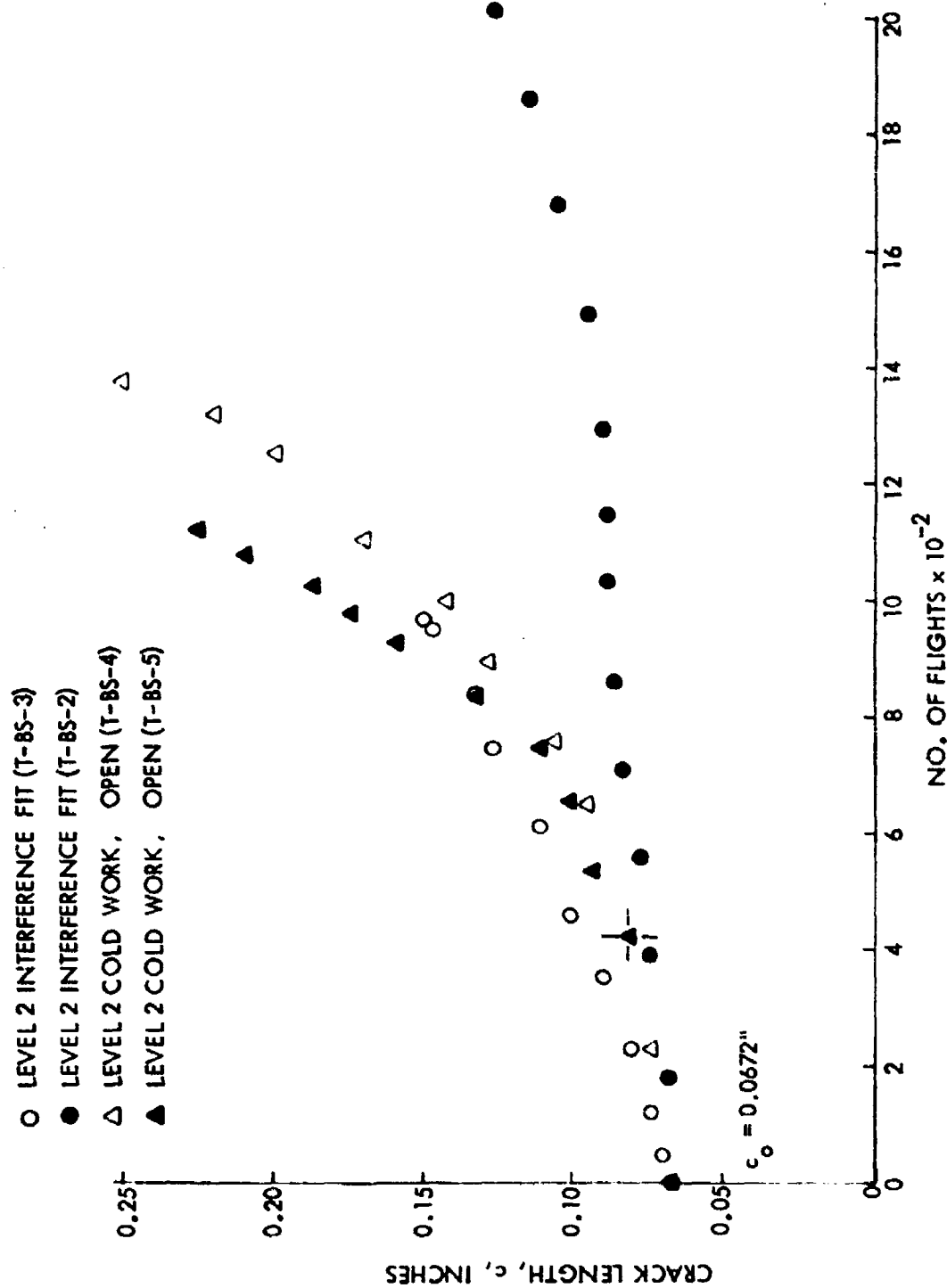


Figure 76. Comparison of Growth Behavior of Intermediate Corner Cracks from Level 2 Cold-Worked and Interference-Fit Fastener Holes in 6Al-4V Beta Annealed Titanium Alloy Plates Subjected to Bomber Spectrum Loading

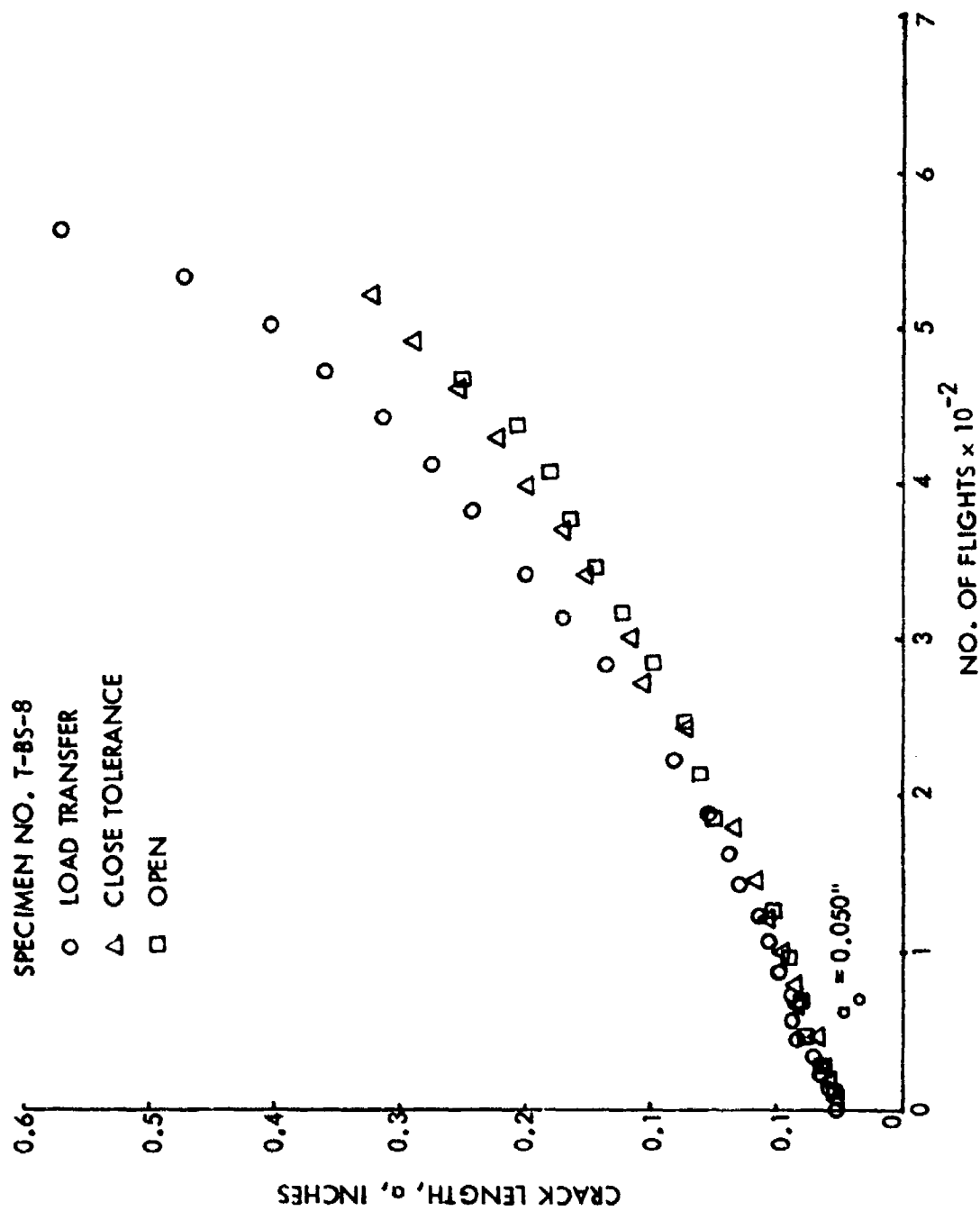


Figure 77. Growth Behavior of Small Thru Cracks from Open and Close Tolerance Fastener Holes in 6Al-4V Beta Annealed Titanium Alloy Plates Subjected to Bomber Spectrum Loading

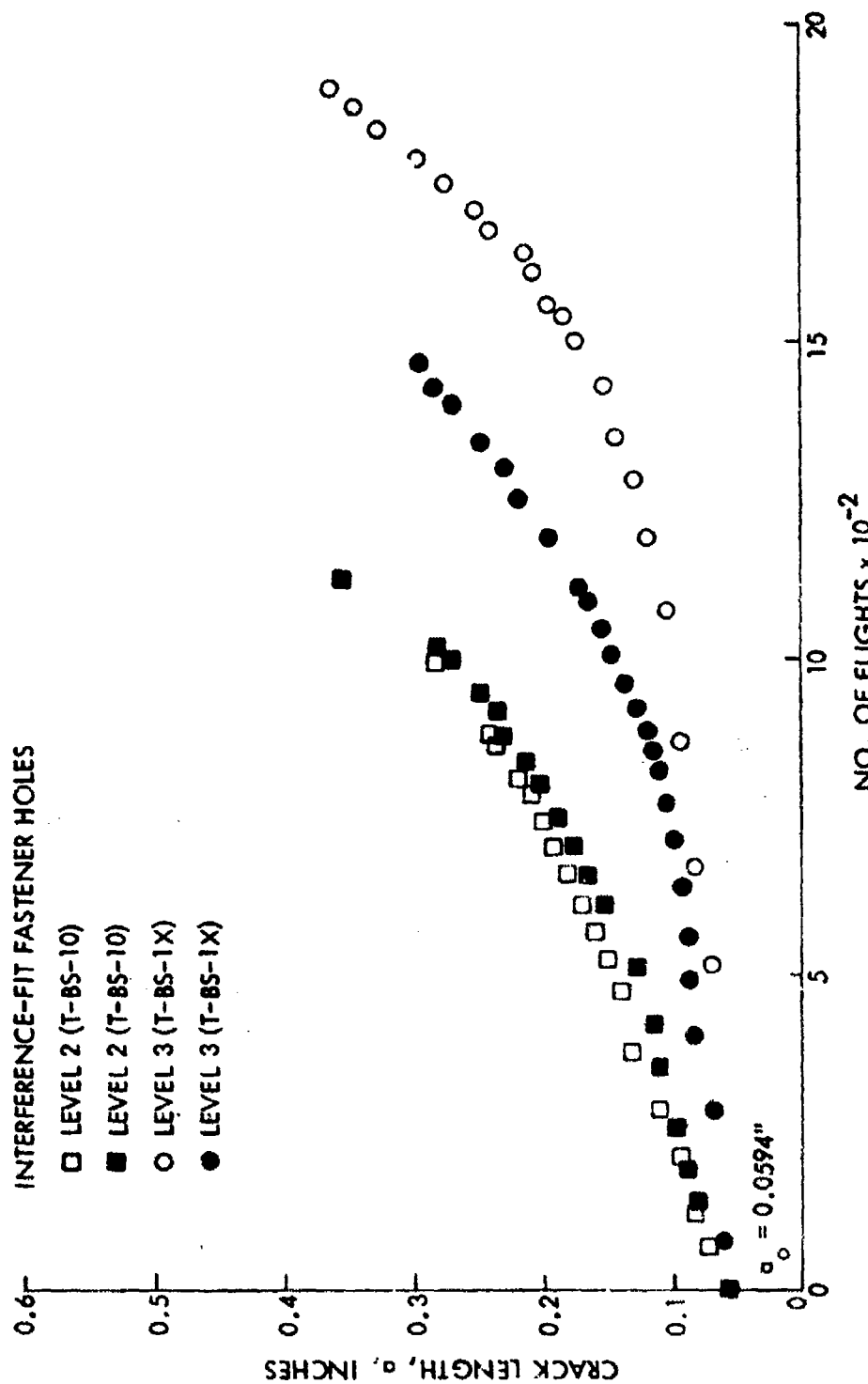


Figure 78. Growth Behavior of Intermediate Thru Cracks from Interference-Fit Fastener Holes for Various Levels of Interference in 6Al-4V Beta Annealed Titanium Alloy Plates Subjected to Bomber Spectrum Loading

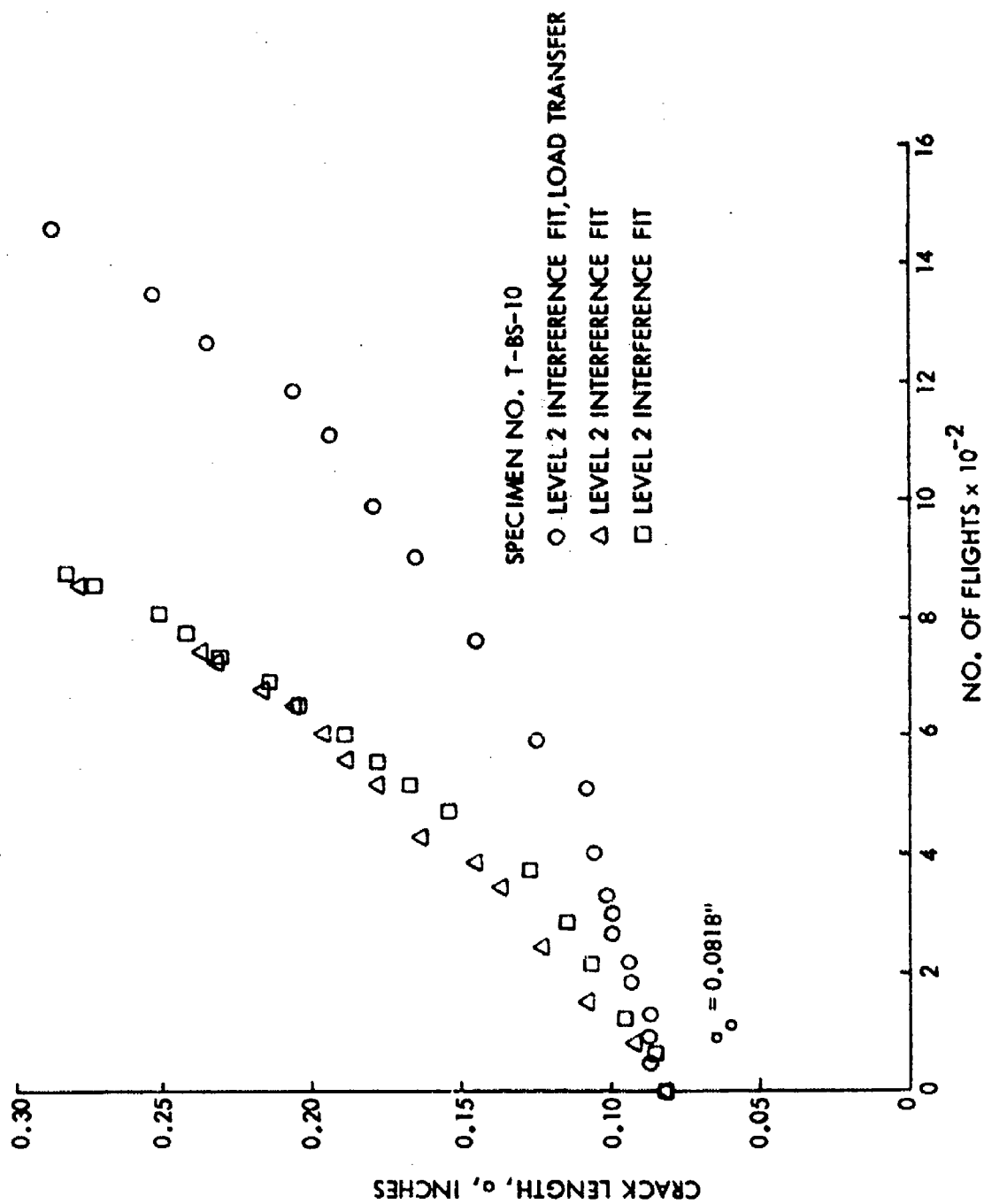


Figure 79. Growth Behavior of Intermediate Thru Cracks From Level 2 Interference-Fit Holes in 6Al-4V Beta Annealed Titanium Alloy Plates Subjected to Bomber Spectrum Loading

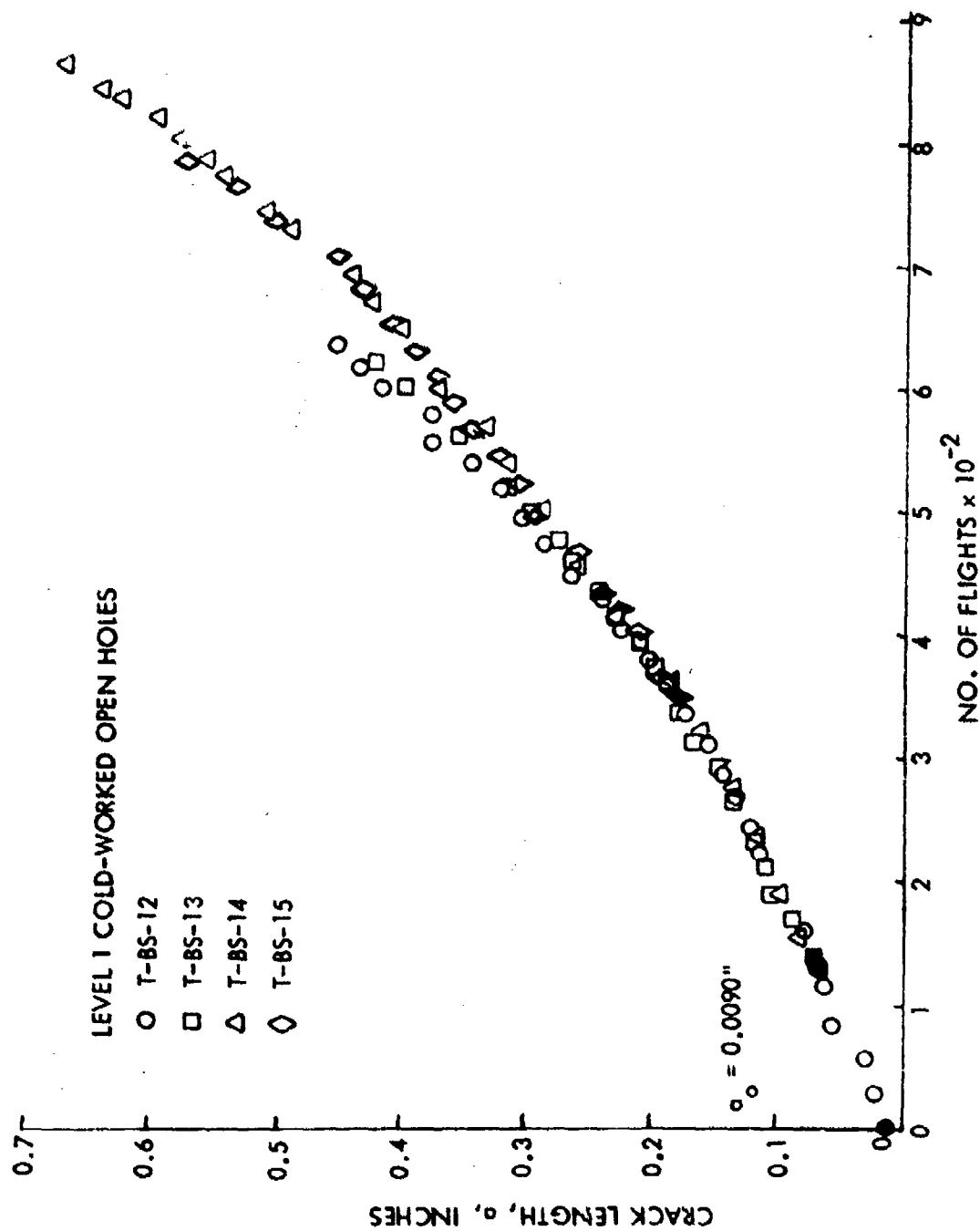


Figure 80. Growth Behavior of Thru Cracks from Cold-Worked Open Holes in 6Al-4V Beta Annealed Titanium Alloy Plates Subjected to Bomber Spectrum Loading

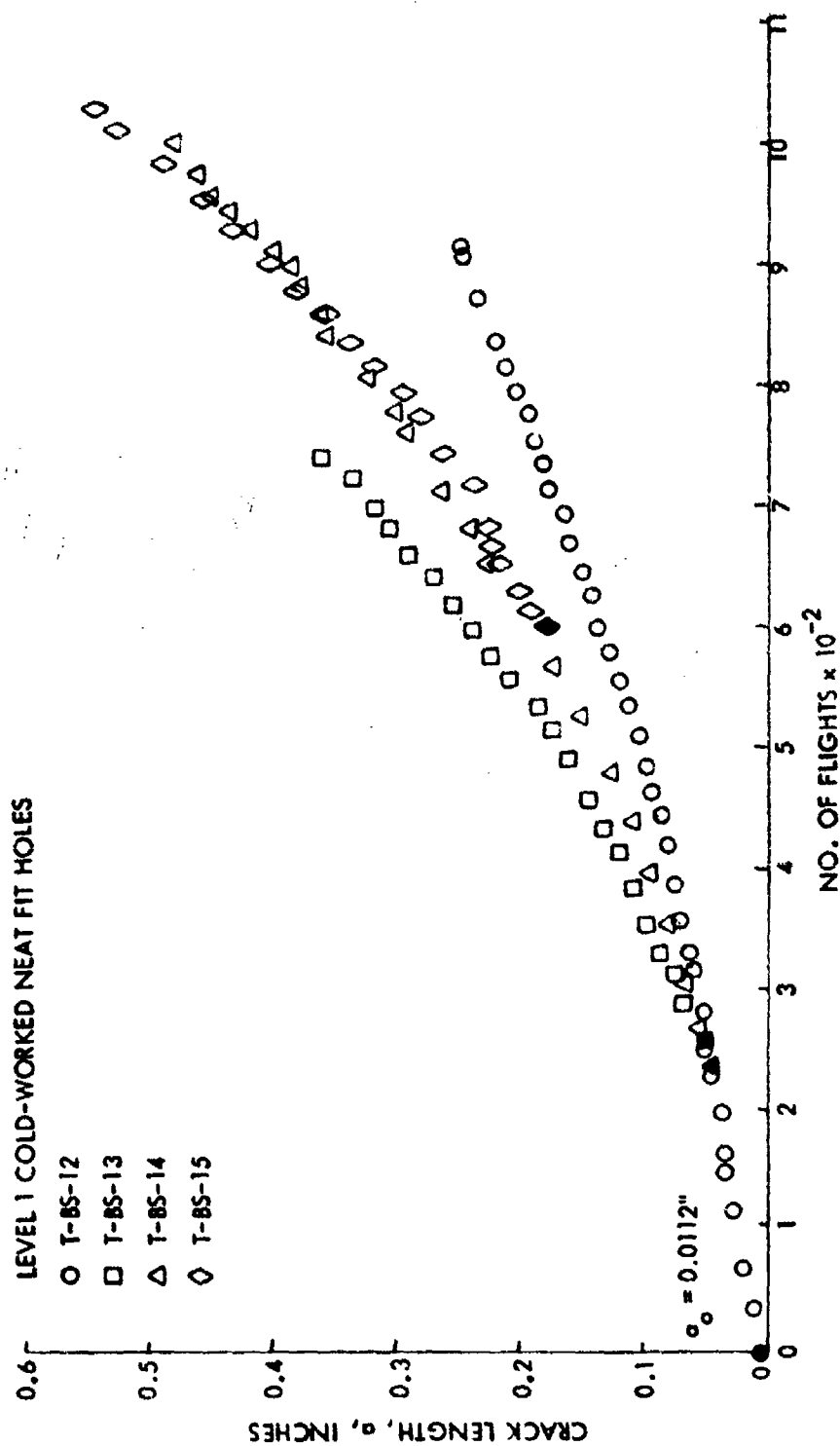


Figure 81. Growth Behavior of Thru Cracks from Level 1 Filled Cold-Worked Fastener Holes in 6Al-4V Beta Annealed Titanium Alloy Plates Subjected to Bomber Spectrum Loading

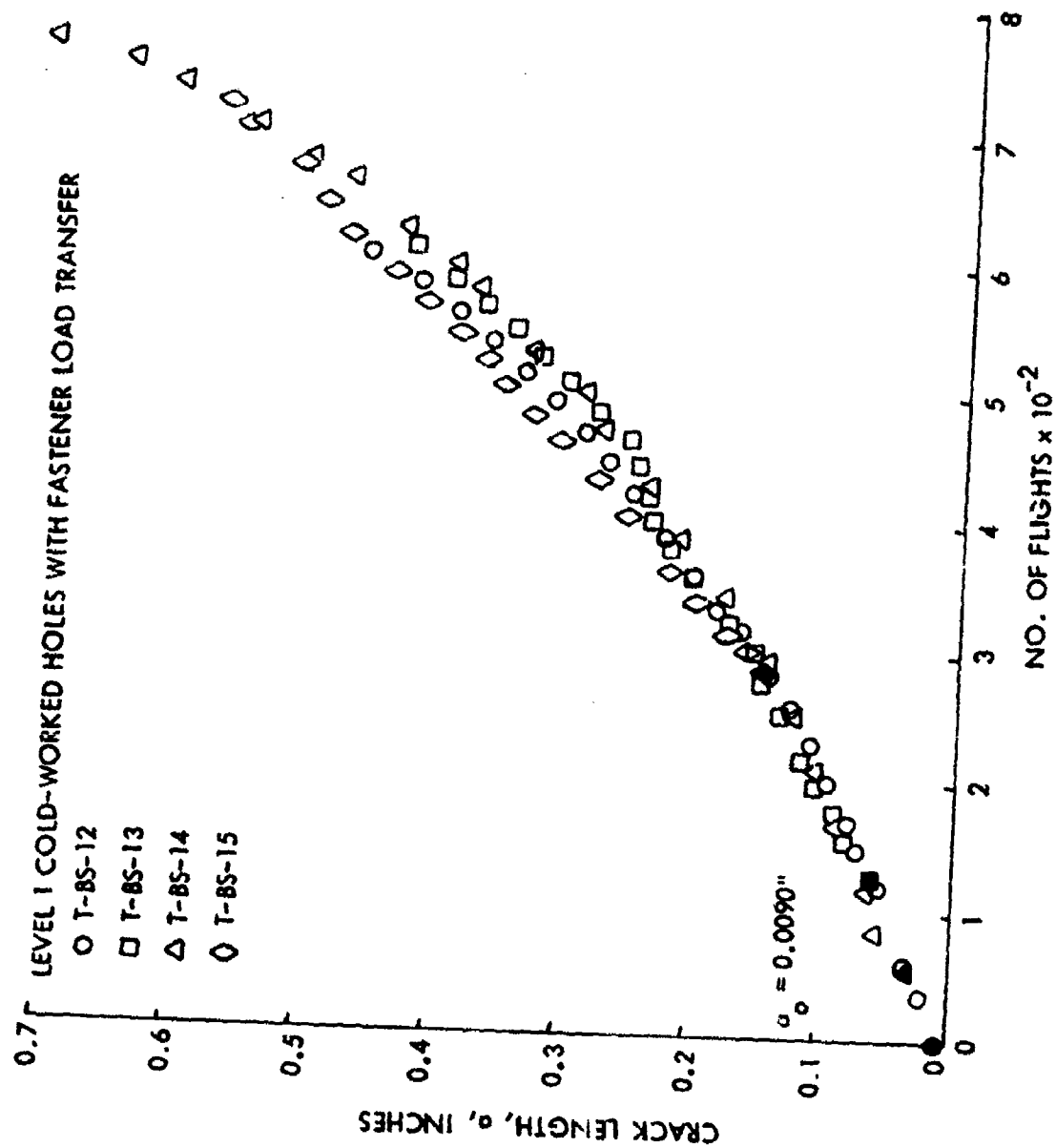


Figure 82. Growth Behavior of Thru Cracks from Level 1 Loaded Cold-Worked Fastener Holes in 6Al-4V Beta Annealed Titanium Alloy Plates Subjected to Bomber Spectrum Loading

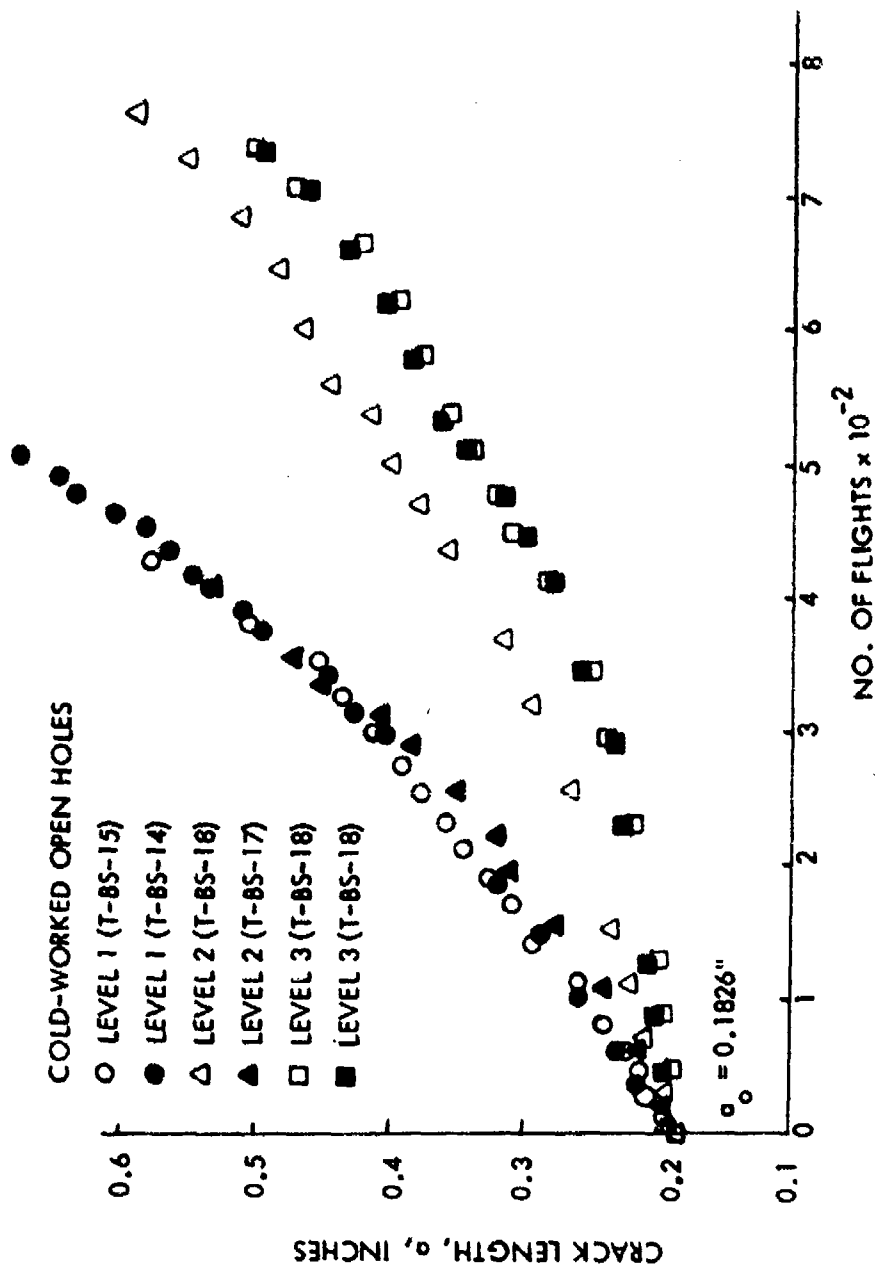


Figure 83. Growth Behavior of Large Thru Cracks from Cold-Worked Holes for Various Levels of Cold Working in 6Al-4V Beta Annealed Titanium Alloy Plates Subjected to Bomber Spectrum Loading

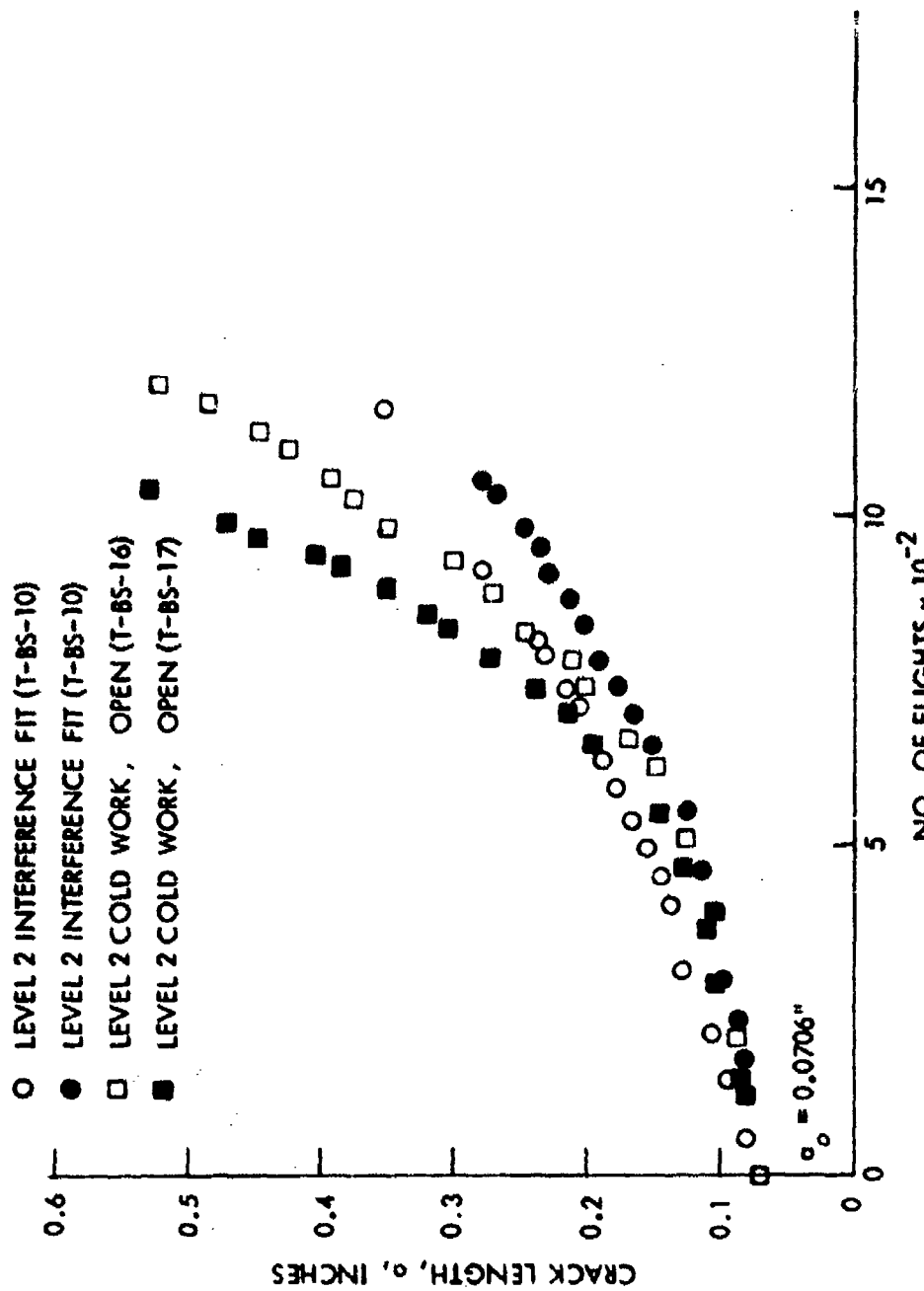


Figure 84. Comparison of Growth Behavior of Intermediate Thru Cracks from Level 2 Interference-Fit Fastener Holes and Cold-Worked Open Holes in 6Al-4V Beta Annealed Titanium Alloy Plates Subjected to Bomber Spectrum Loading

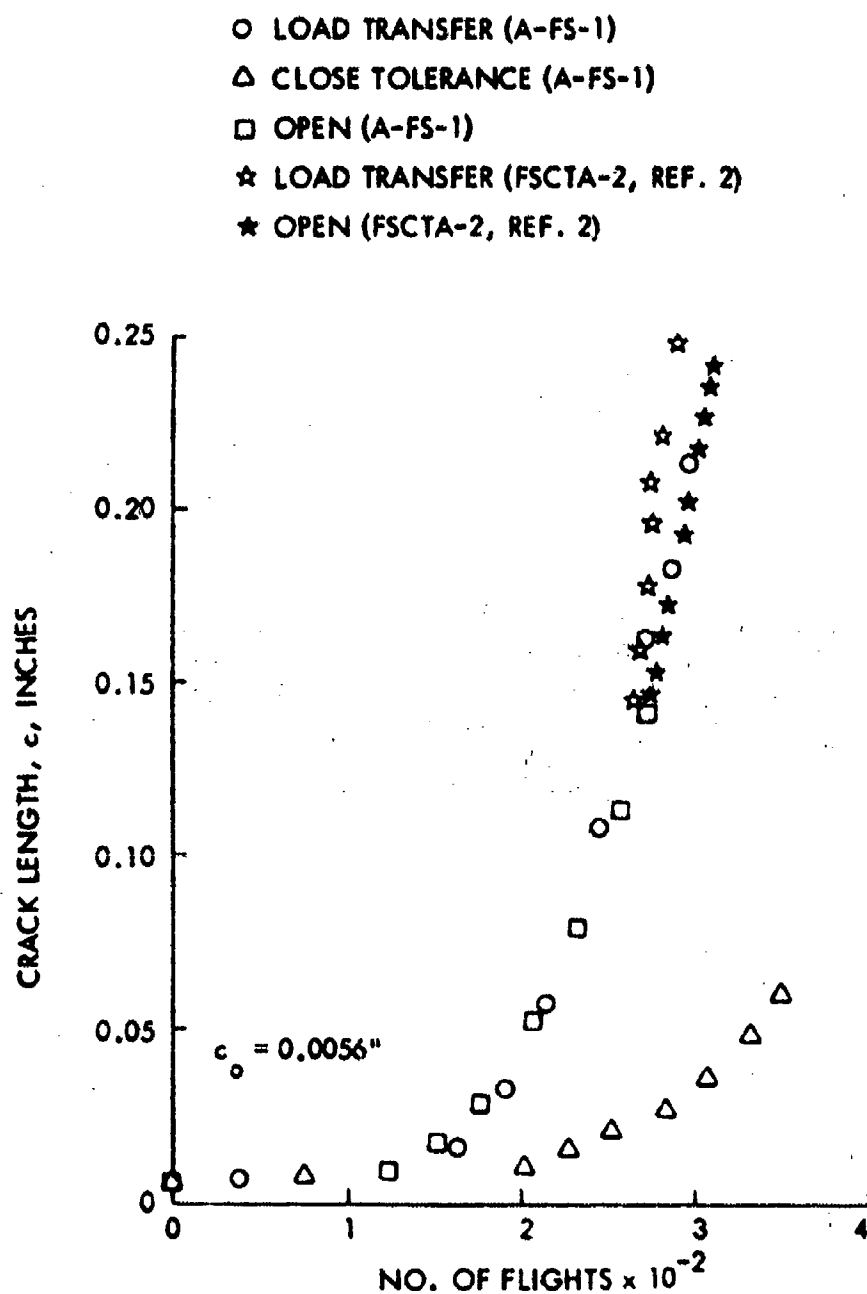


Figure 85. Growth Behavior of Corner Cracks from Open and Close Tolerance Fastener Holes in 2219-T851 Aluminum Alloy Plates Subjected to Fighter Spectrum Loading

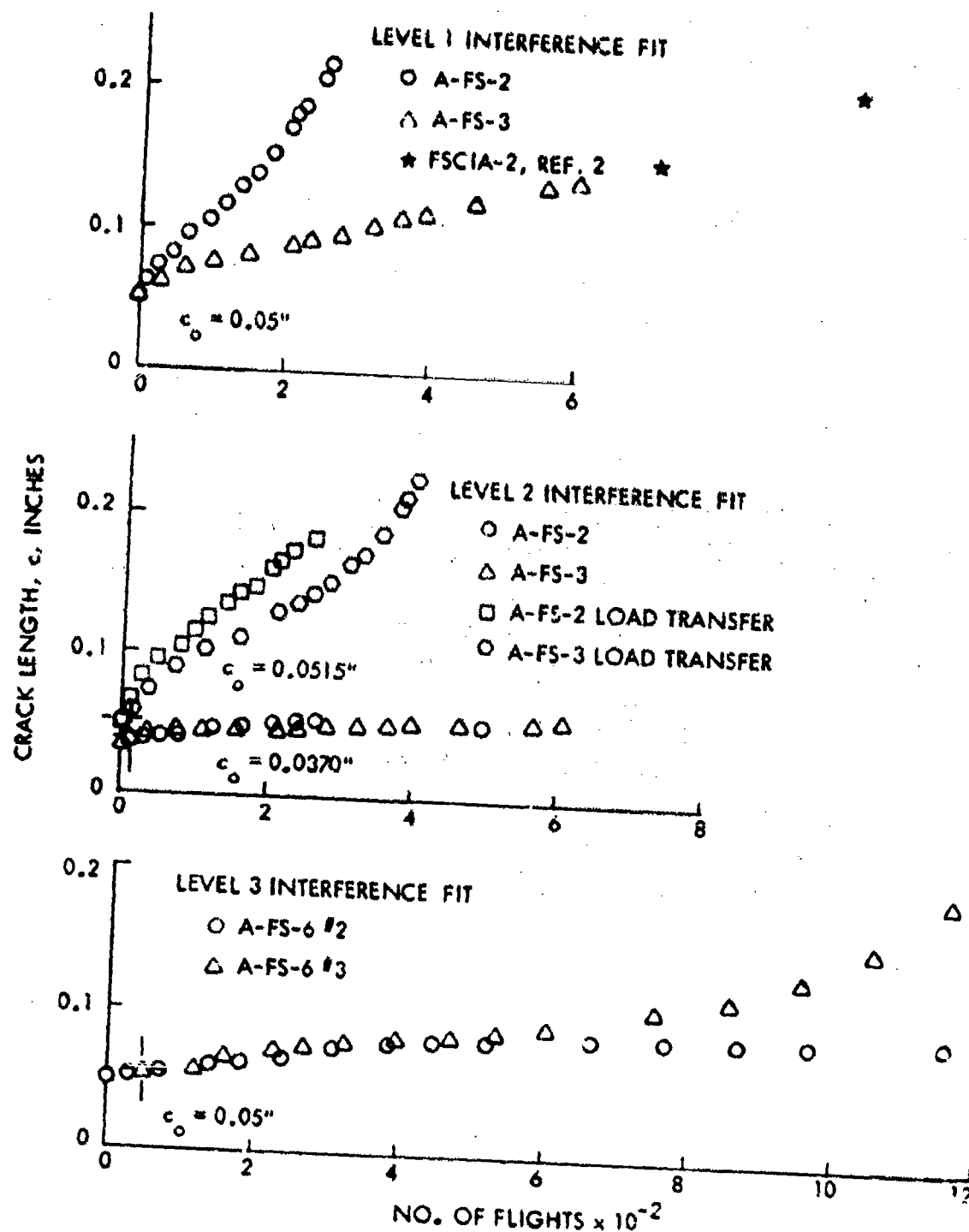


Figure 86. Growth Behavior of Small and Intermediate Corner Cracks from Interference-Fit Fastener Holes for Various Levels of Interference in 2219-T83 Aluminum Alloy Plates Subjected to Fighter Spectrum Loading

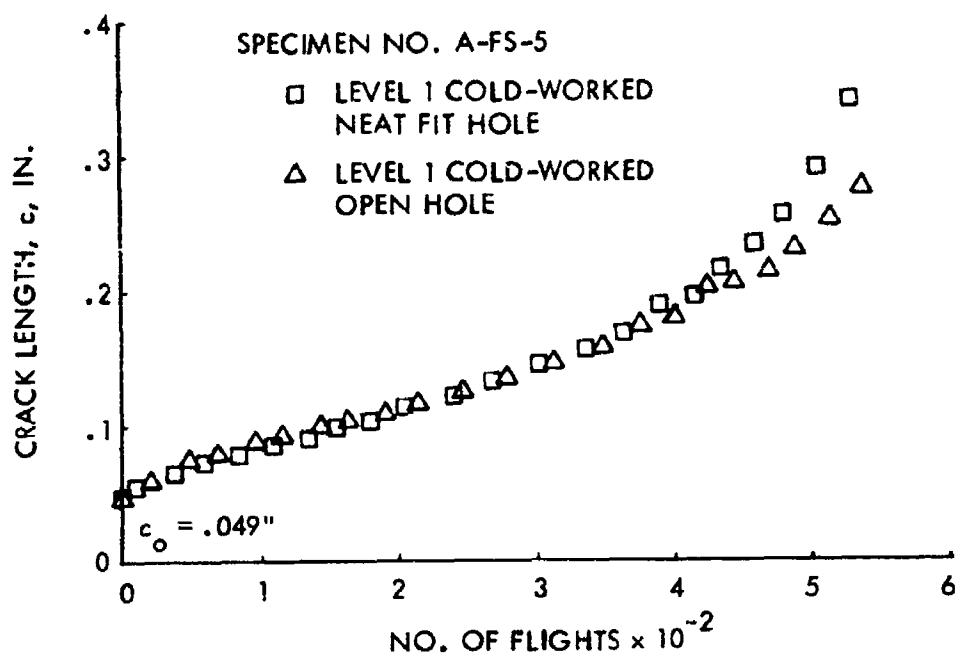
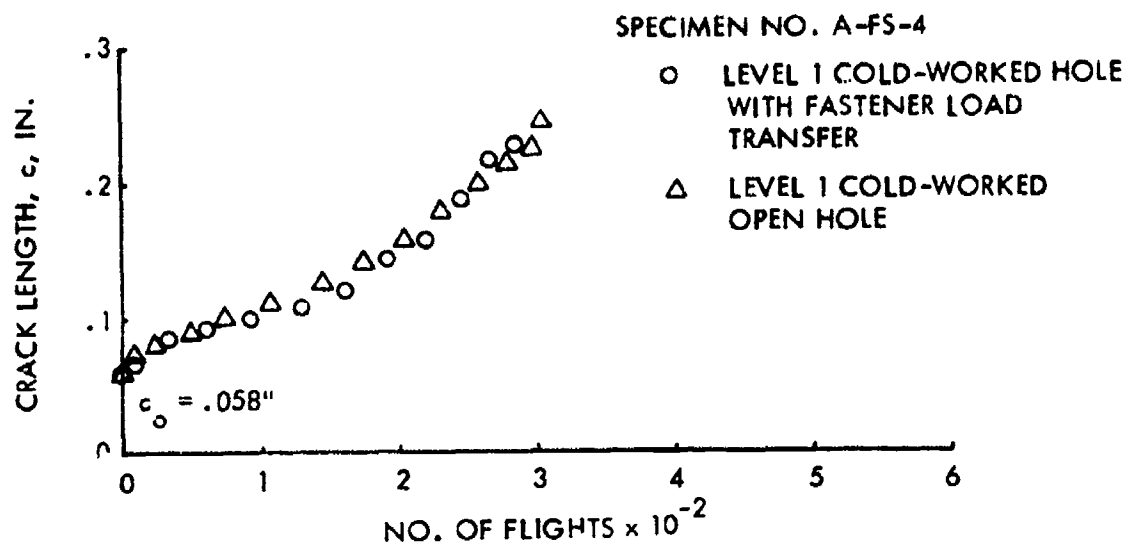


Figure 87. Growth Behavior of Intermediate Corner Cracks from Level 1 Cold-Worked Holes in 2219-T851 Aluminum Alloy Plates Subjected to Fighter Spectrum Loading

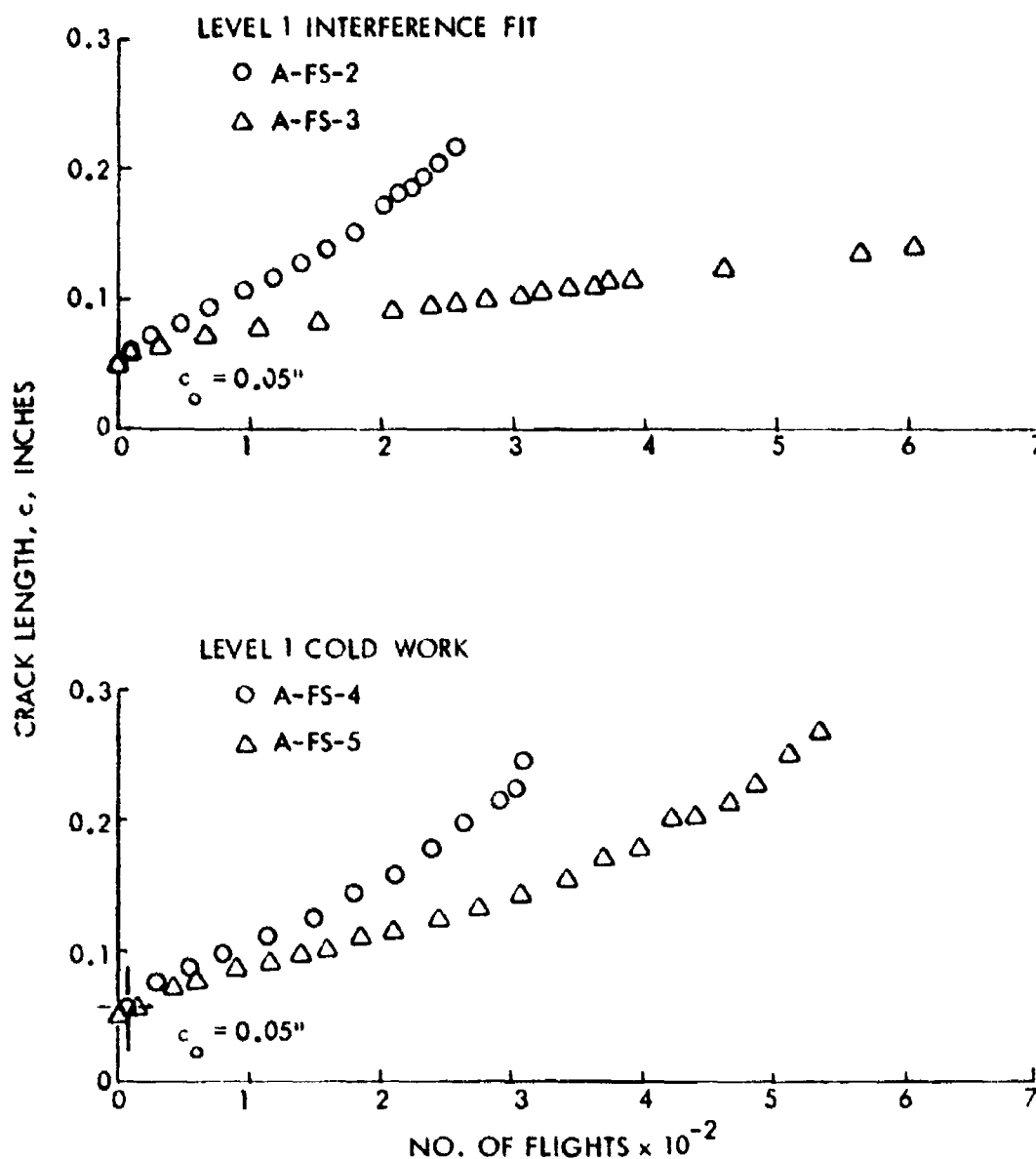


Figure 88. Comparison of Growth Behavior of Intermediate Corner Cracks from Level 1 Cold-Worked and Interference-Fit Fastener Holes in 2219-T851 Aluminum Alloy Plates Subjected to Fighter Spectrum Loading

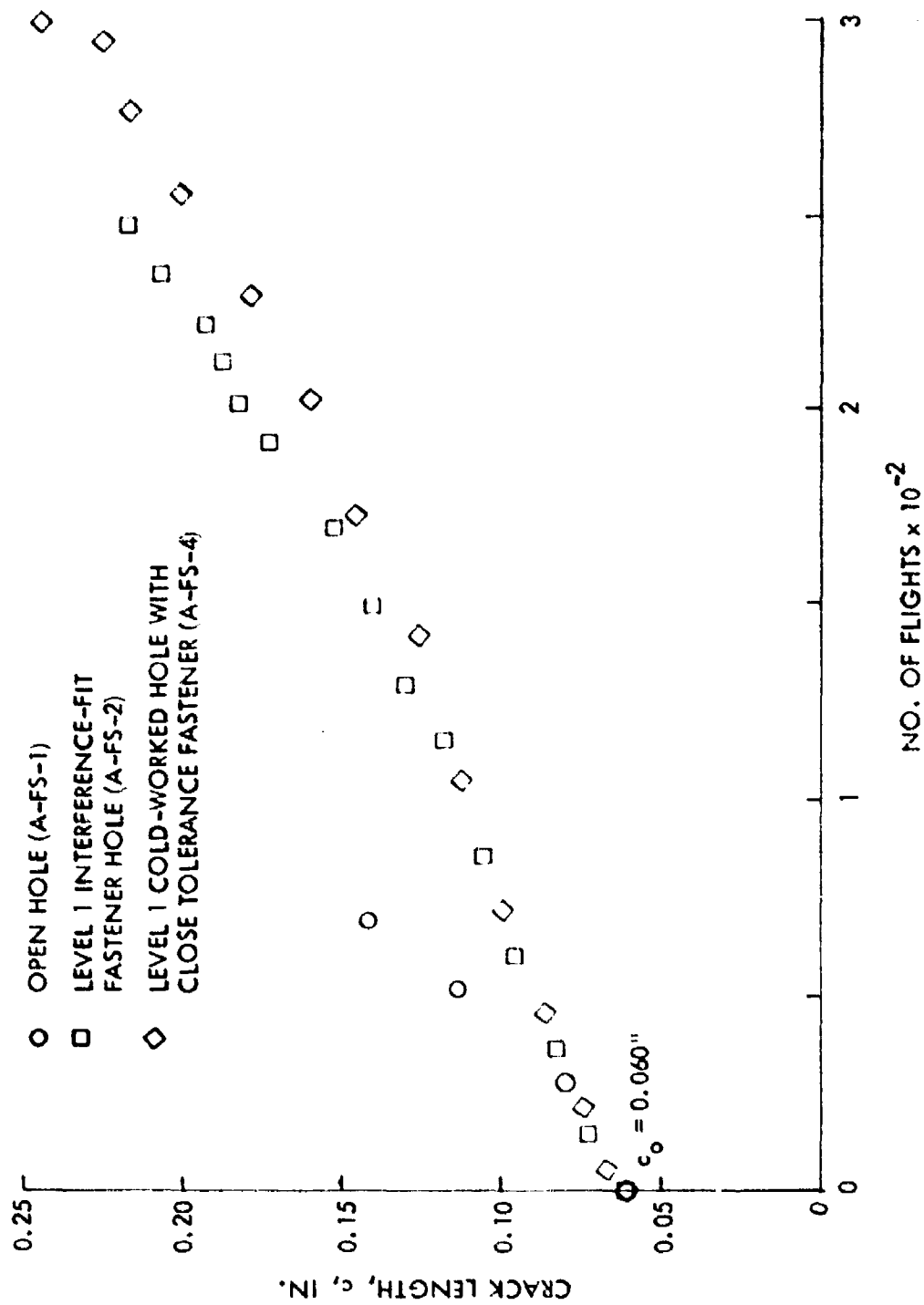


Figure 89. Comparison of Growth Behavior of Intermediate Corner Cracks from Various Types of Fastener Holes in 2219-T851 Aluminum Alloy Plates Subjected to Fighter Spectrum Loading

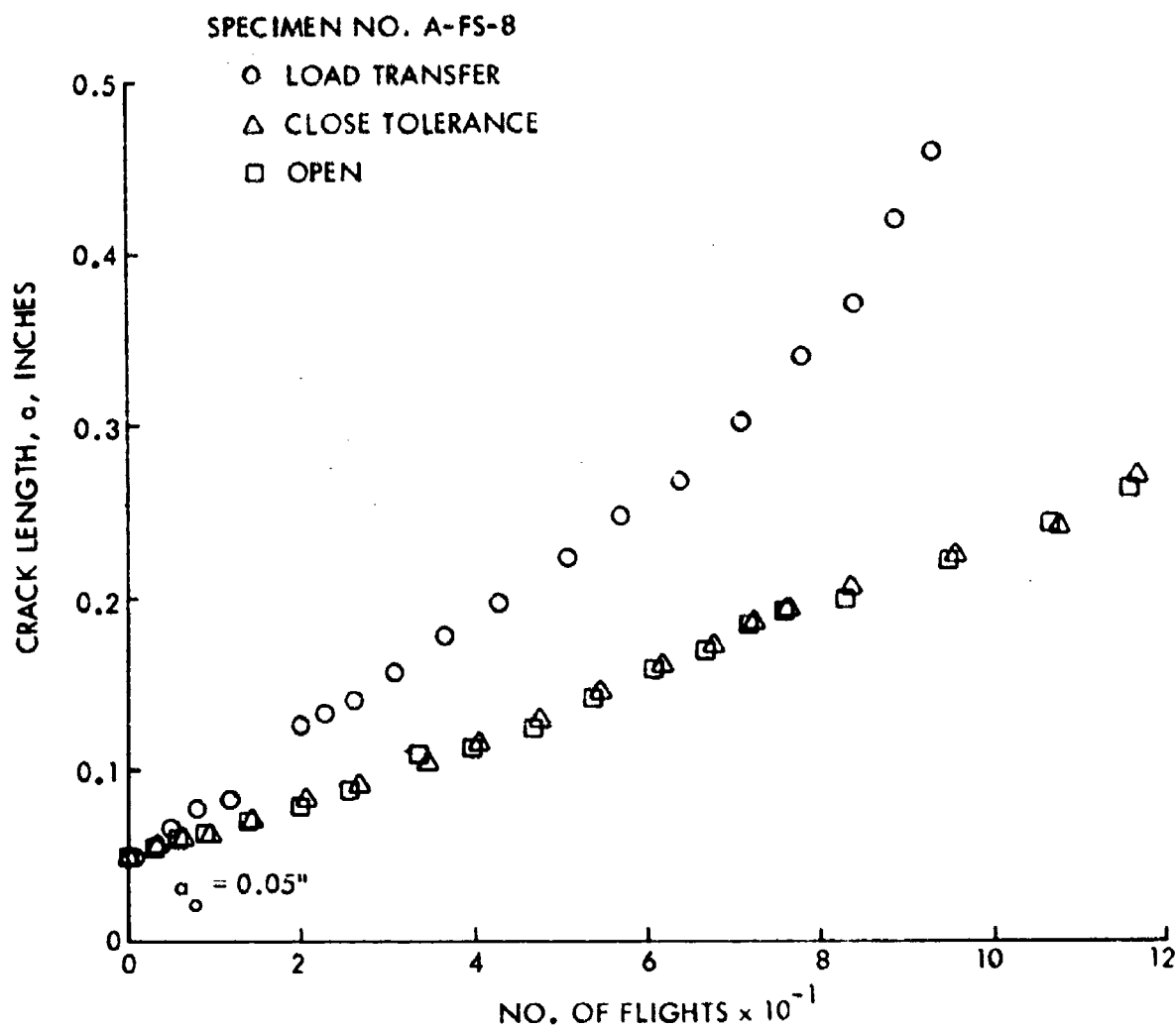


Figure 90. Growth Behavior of Intermediate Thru Cracks from Open and Close Tolerance Fastener Holes in 2219-T851 Aluminum Alloy Plates Subjected to Fighter Spectrum Loading

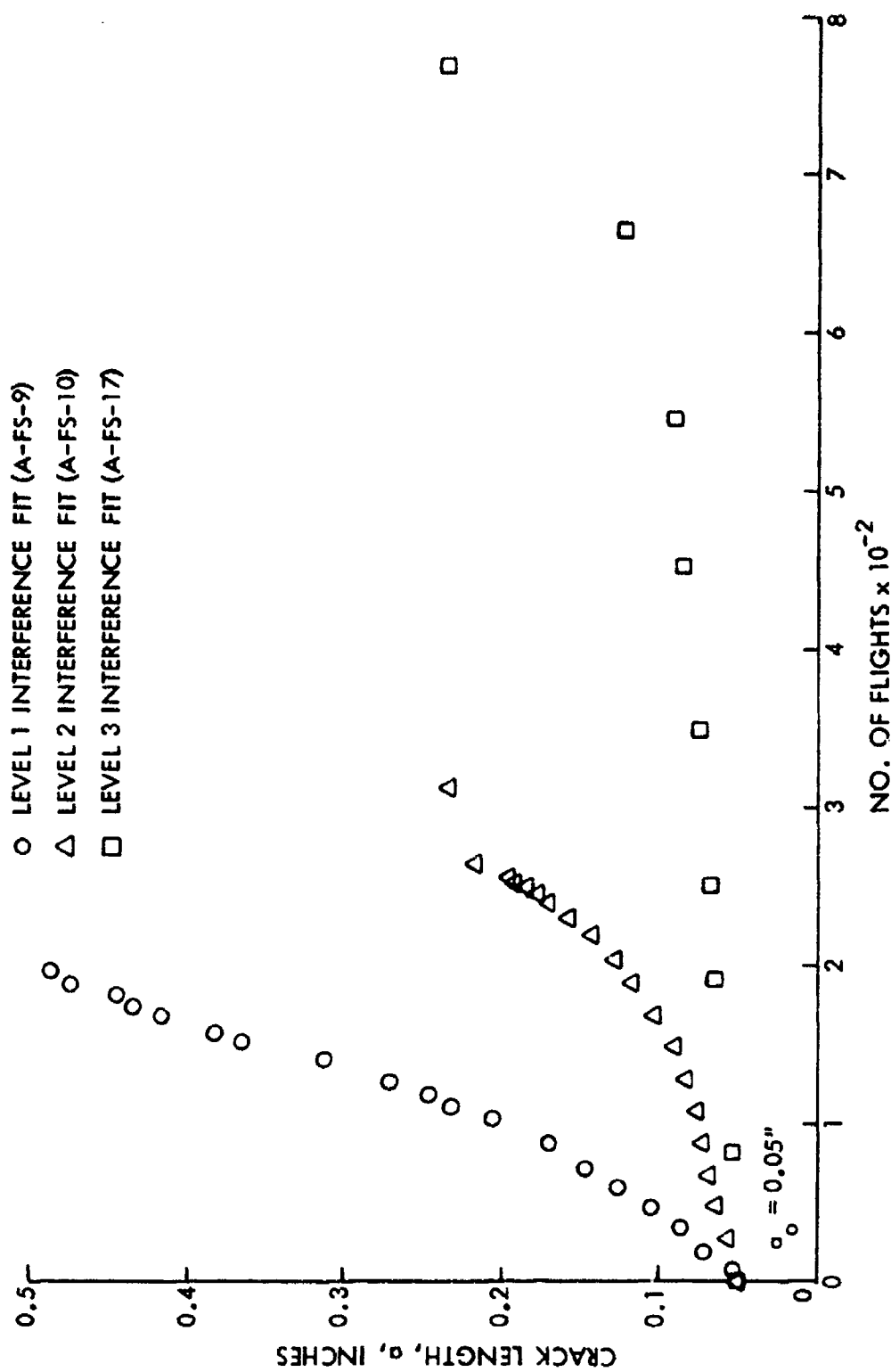


Figure 91. Growth Behavior of Intermediate Thru Cracks from Interference-Fit Fastener Holes for Various Levels of Interference in 2219-T851 Aluminum Alloy Plates Subjected to Fighter Spectrum Loading

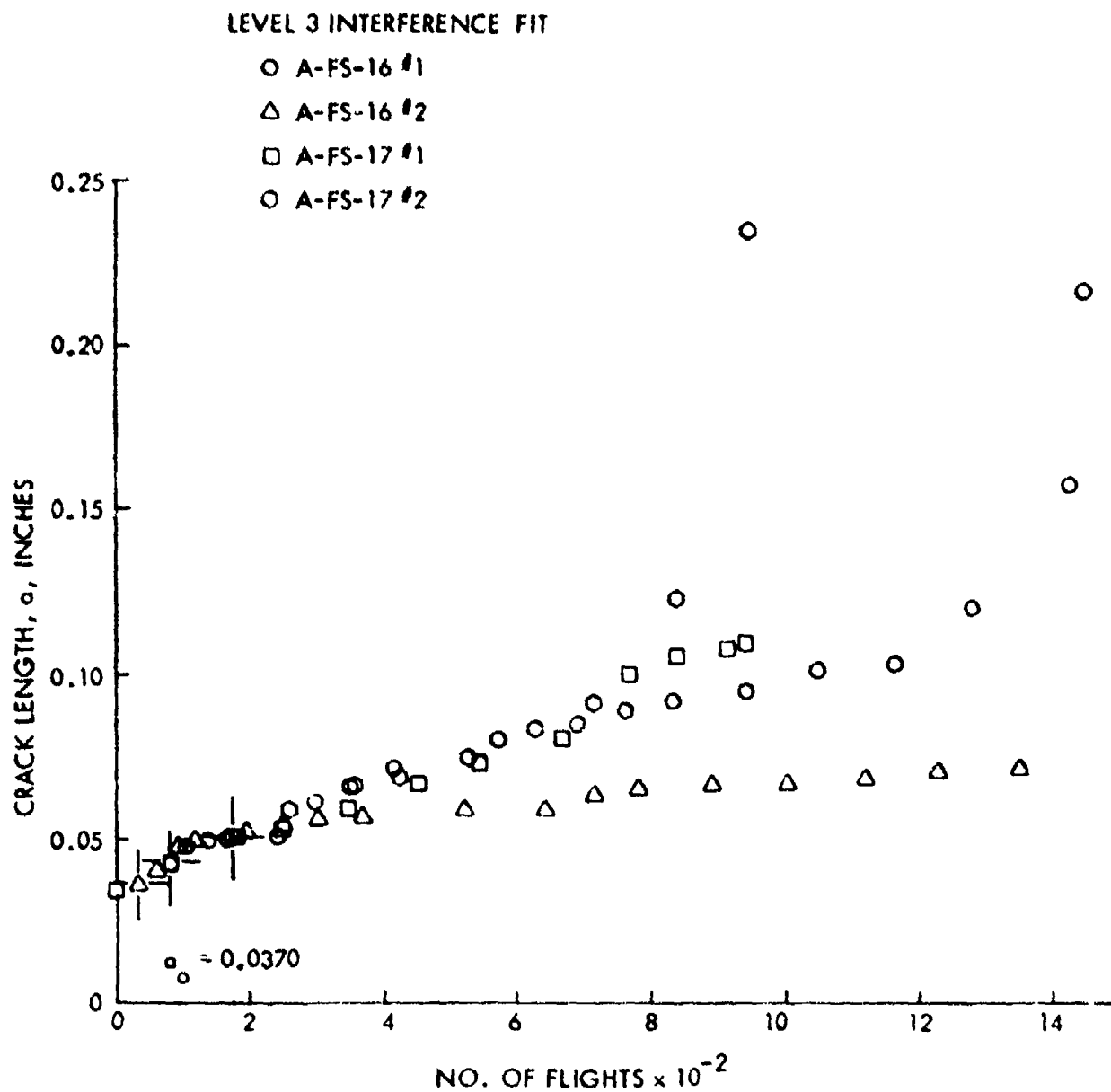


Figure 92. Growth Behavior of Small Thru Cracks from Level 3 Interference-Fit Fastener Holes in 2219-T851 Aluminum Alloy Plates Subjected to Fighter Spectrum Loading

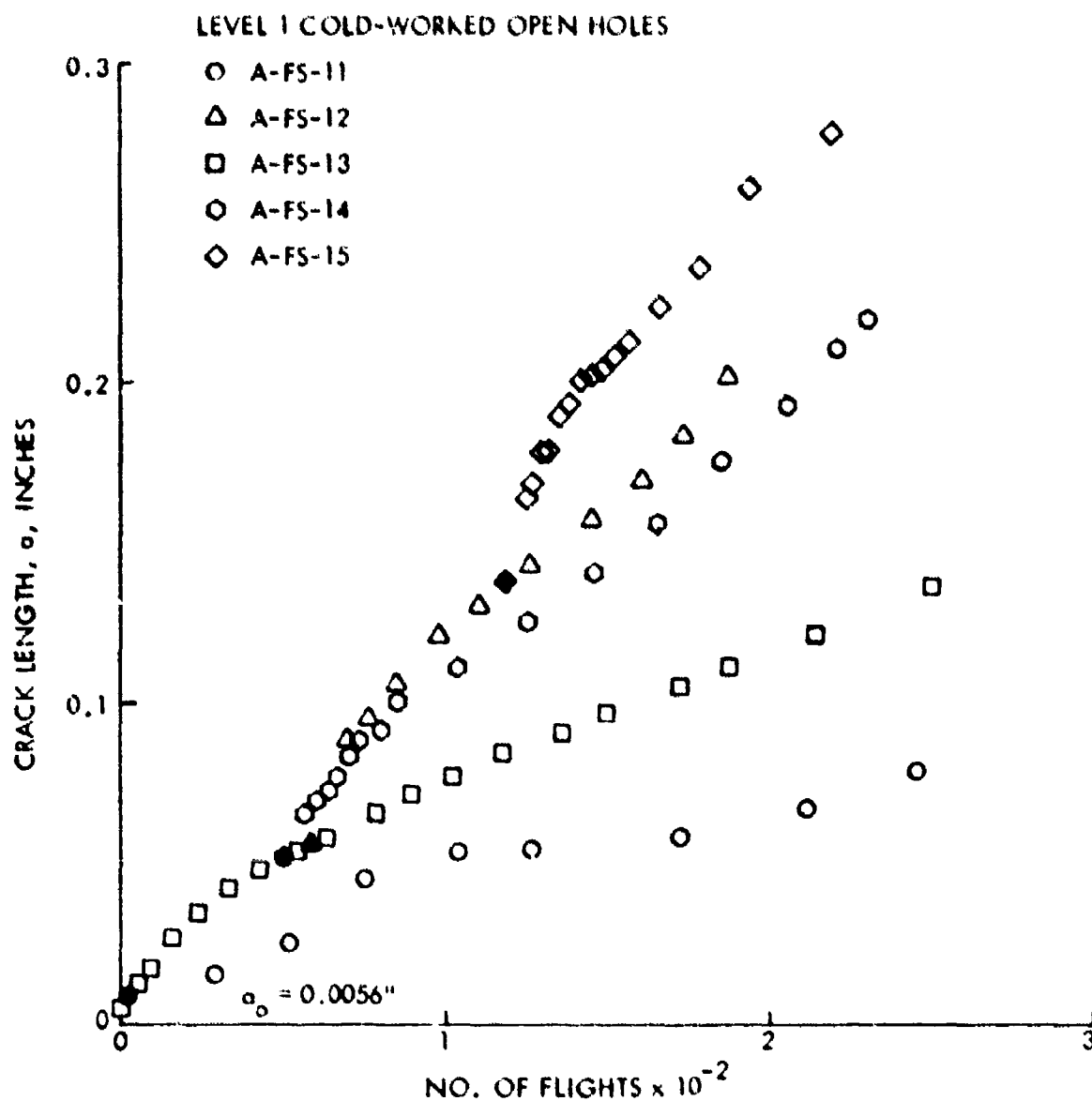
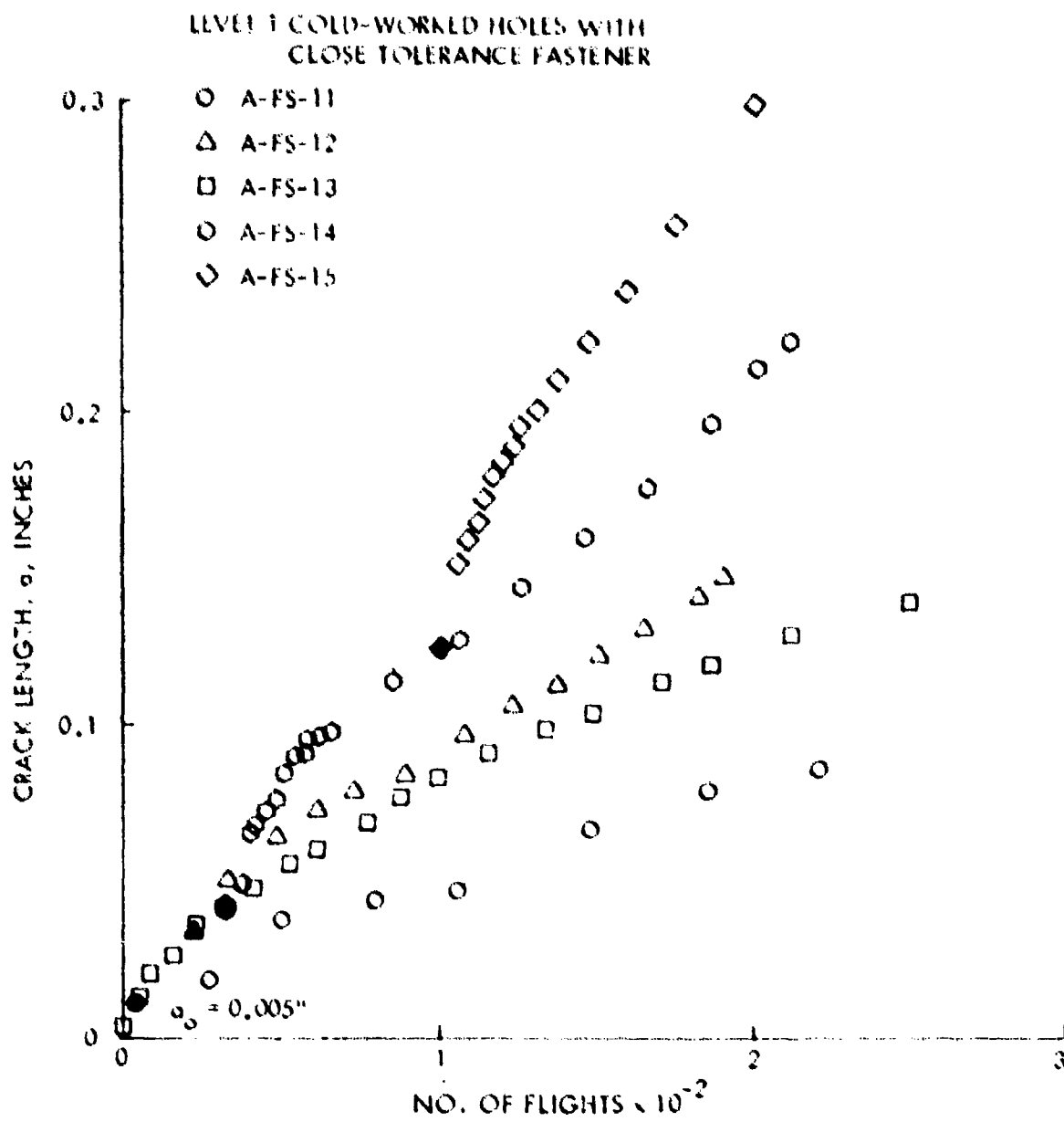


Figure 93. Growth Behavior of Thru Cracks from Level 1 Cold-Worked Open Holes in 2219-T851 Aluminum Alloy Plates Subjected to Fighter Spectrum Loading



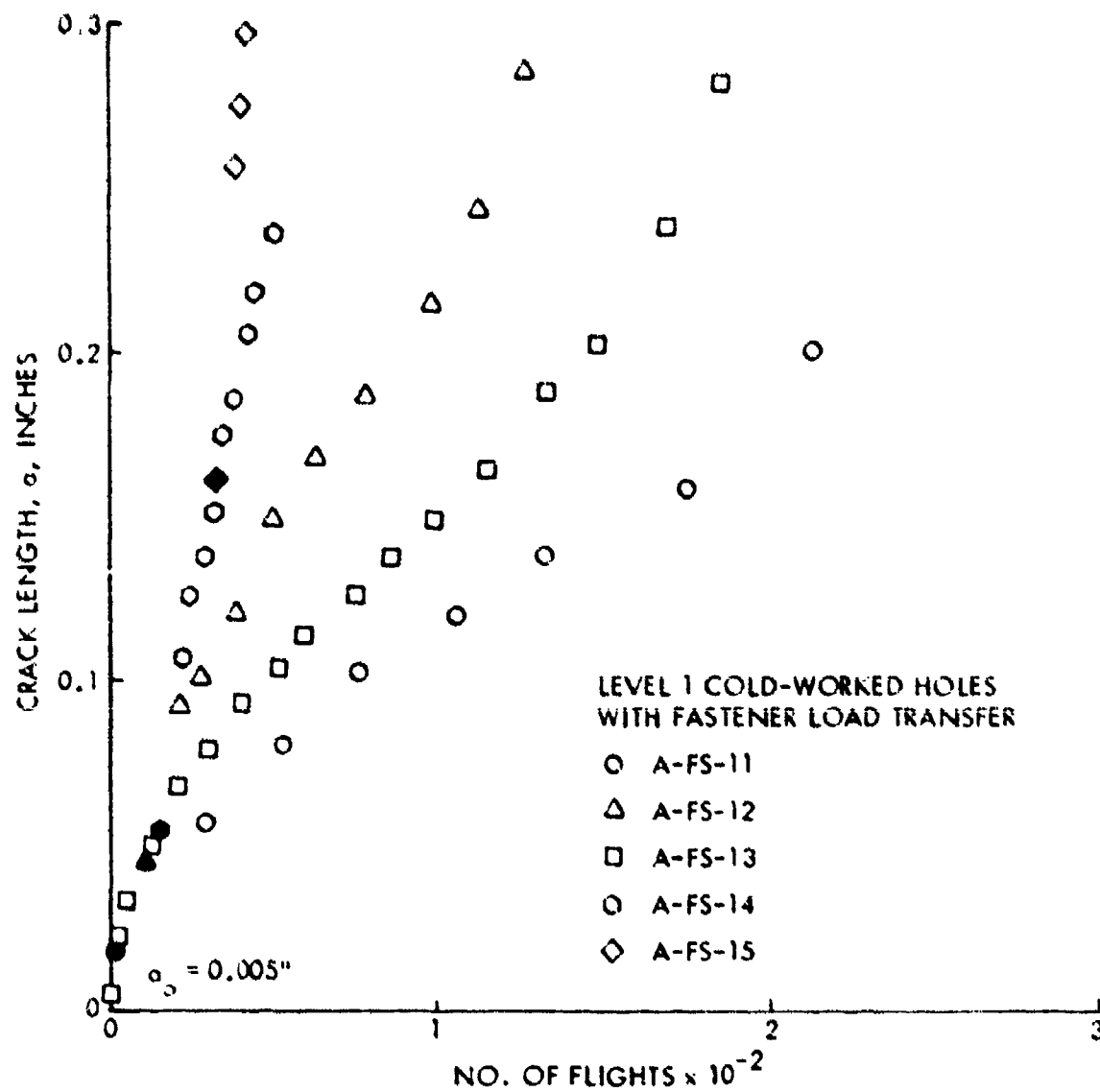


Figure 95. Growth Behavior of Thru Cracks from Level 1 Cold-Worked Holes with Fastener Load Transfer in 2219-T851 Aluminum Alloy Plates Subjected to Fighter Spectrum Loading

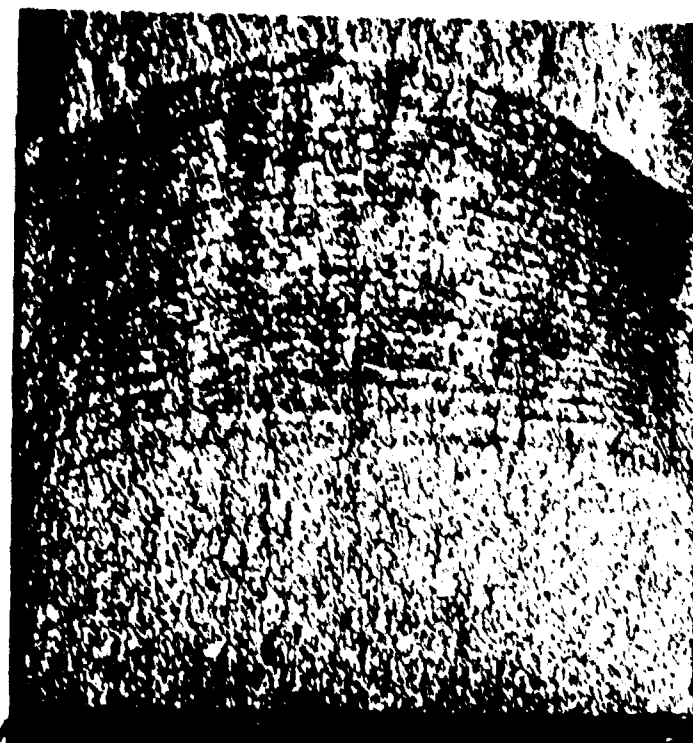
EDGE OF FASTENER HOLE



(a) SMALL CRACK



(b) INTERMEDIATE CRACK



(c) LARGE CRACK

Figure 26. Typical Crack Surfaces of Tensile Cracks (Having Various Initial Crack Lengths) Emerging from Level 1 Cold-Worked Open Holes Subjected to Tensile Loading

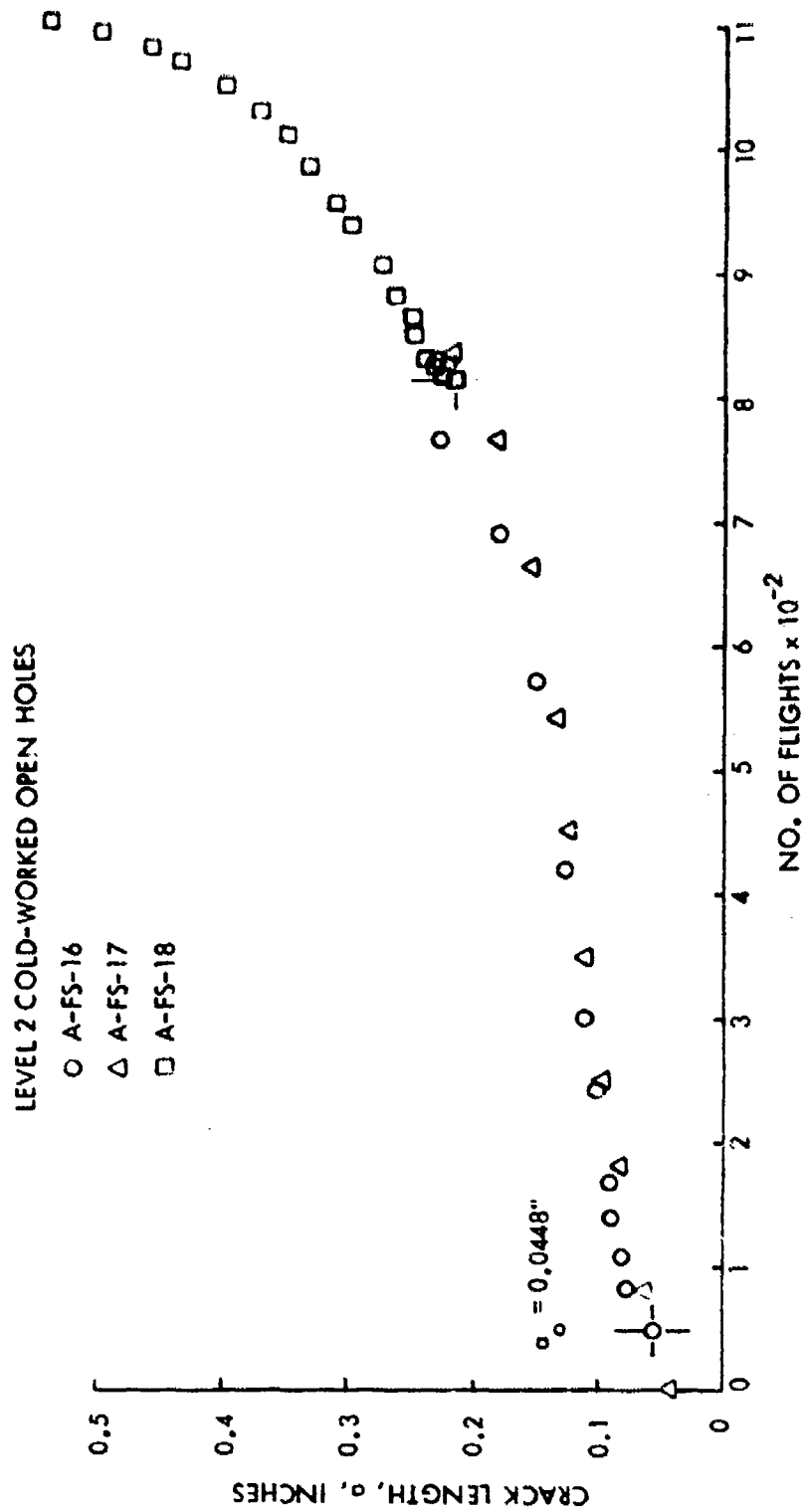


Figure 97. Growth Behavior of Thru Cracks from Level 2 Cold-Worked Open Holes in 2219-T851 Aluminum Alloy Plates Subjected to Fighter Spectrum Loading

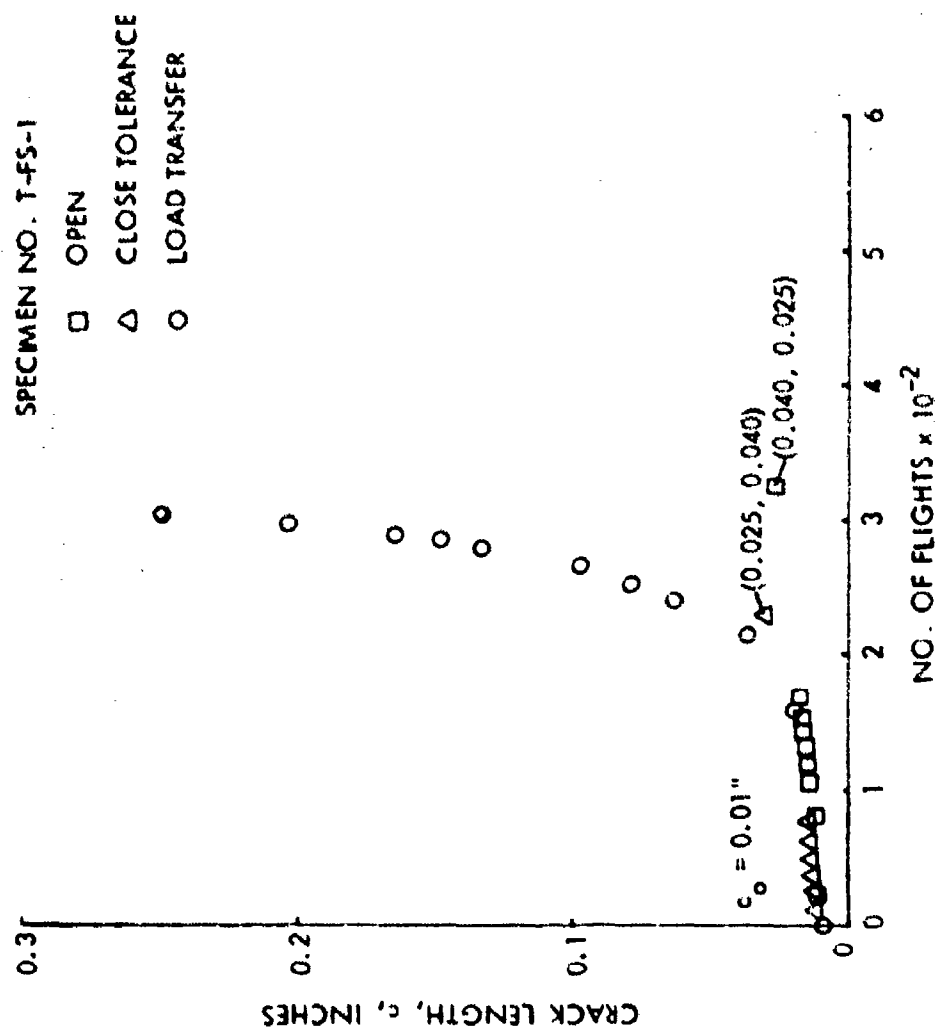


Figure 98. Growth Behavior of Small Corner Cracks from an Open and Close Tolerance Fastener Holes in 6AL-4V Beta Annealed Titanium Alloy Plates Subjected to Fighter Spectrum Loading

INTERFERENCE-FIT FASTENER HOLES

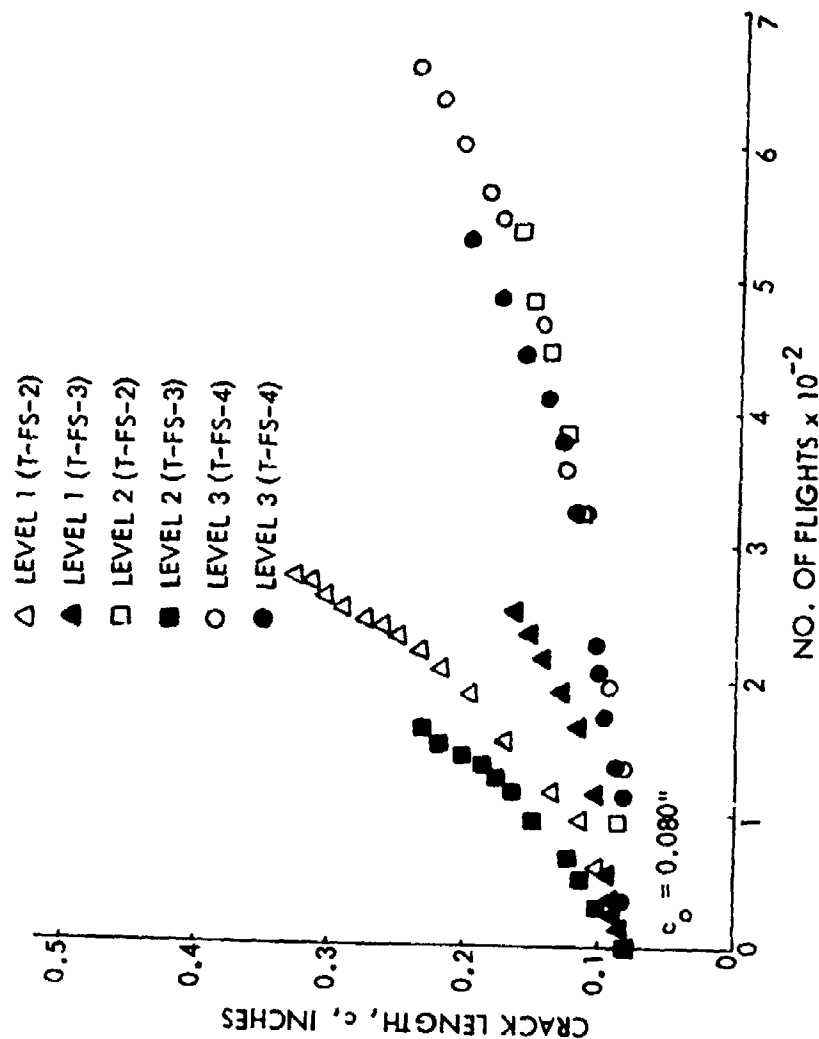


Figure 99. Growth Behavior of Intermediate Corner Cracks from Interference-Fit Fastener Holes for Various Levels of Interference in 6Al-4V Beta Annealed Titanium Alloy Plates Subjected to Fighter Spectrum Loading

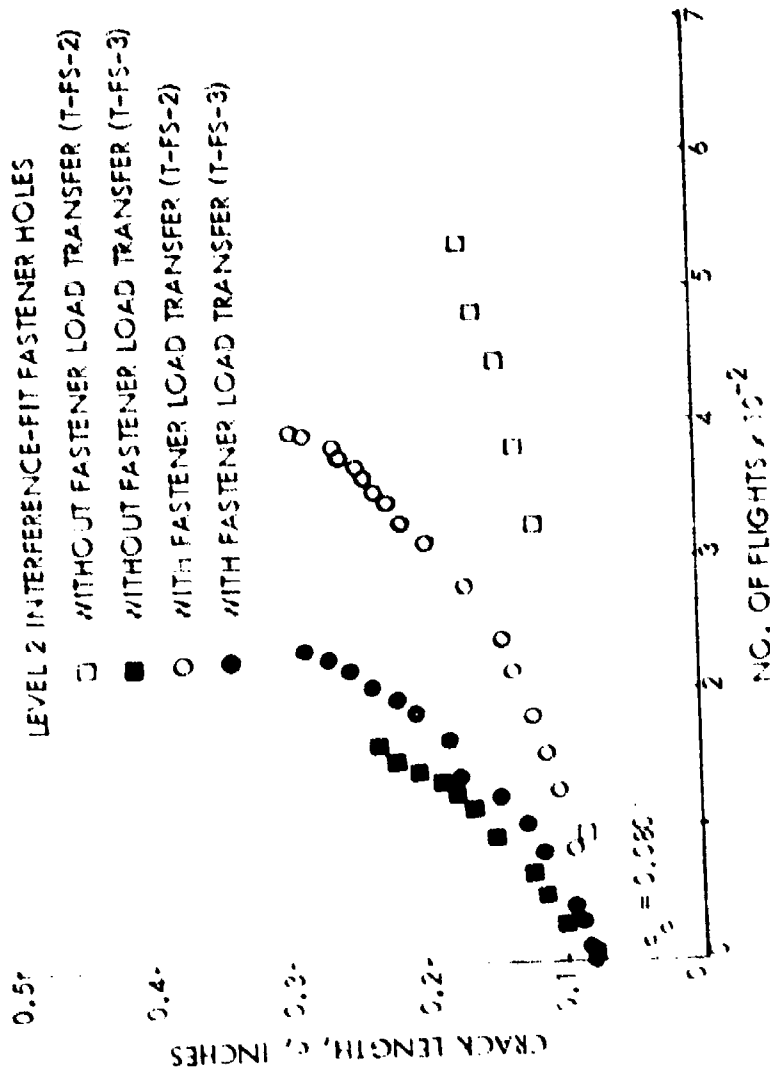


Figure 156. Growth Behavior of Intermediate Corner Cracks from Level 2 Interference-Fit Fastener Holes with and without Fastener Load Transfer in 6AL-4V Beta Annealed Titanium Alloy Plates Subjected to Fighter Spectrum Loading

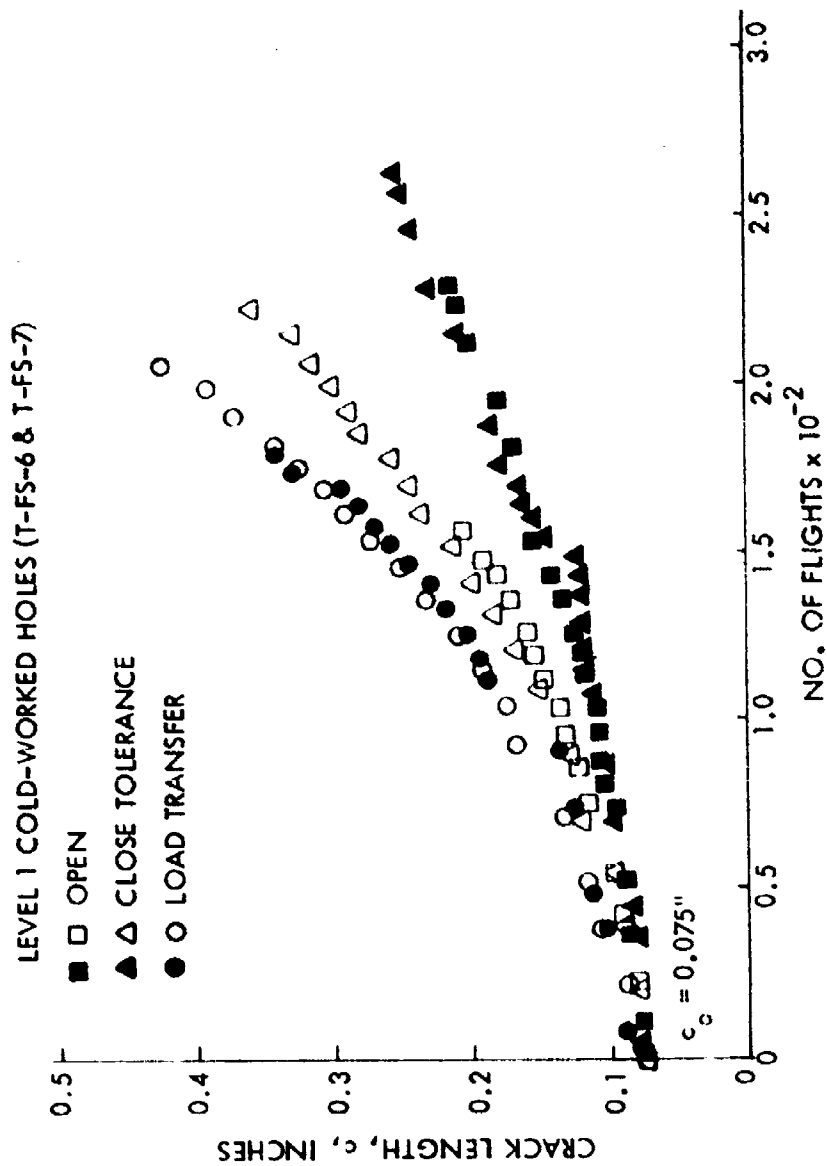


Figure 101. Growth Behavior of Intermediate Corner Cracks from Various Types of Level 1 Cold-Worked Holes in 6Al-4V Beta Annealed Titanium Alloy Plates Subjected to Fighter Spectrum Loading

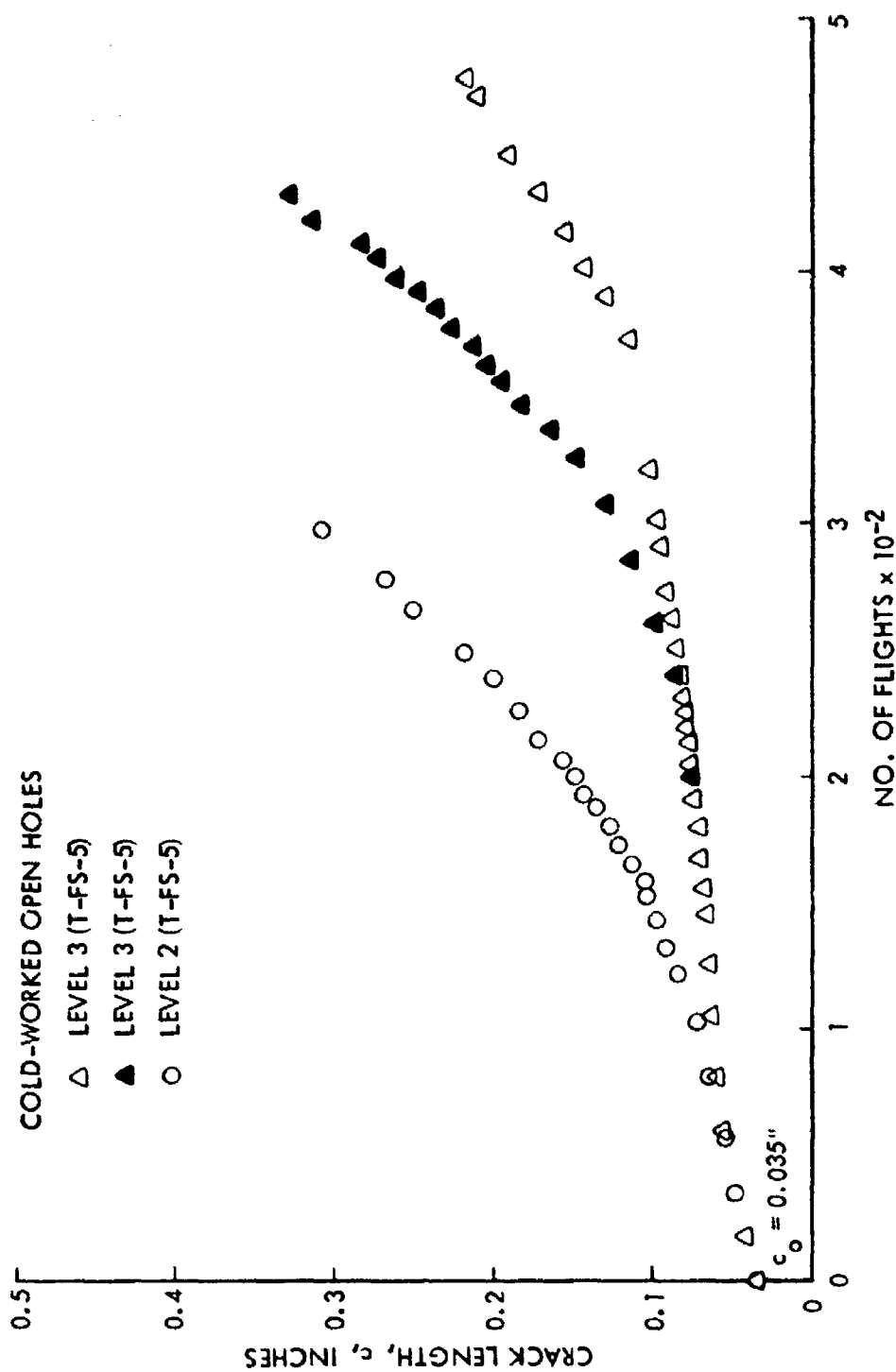


Figure 102. Growth Behavior of Small Corner Cracks from Cold-Worked Open Holes for Various Levels of Cold Working in 6Al-4V Beta Annealed Titanium Alloy Plates Subjected to Fighter Spectrum Loading

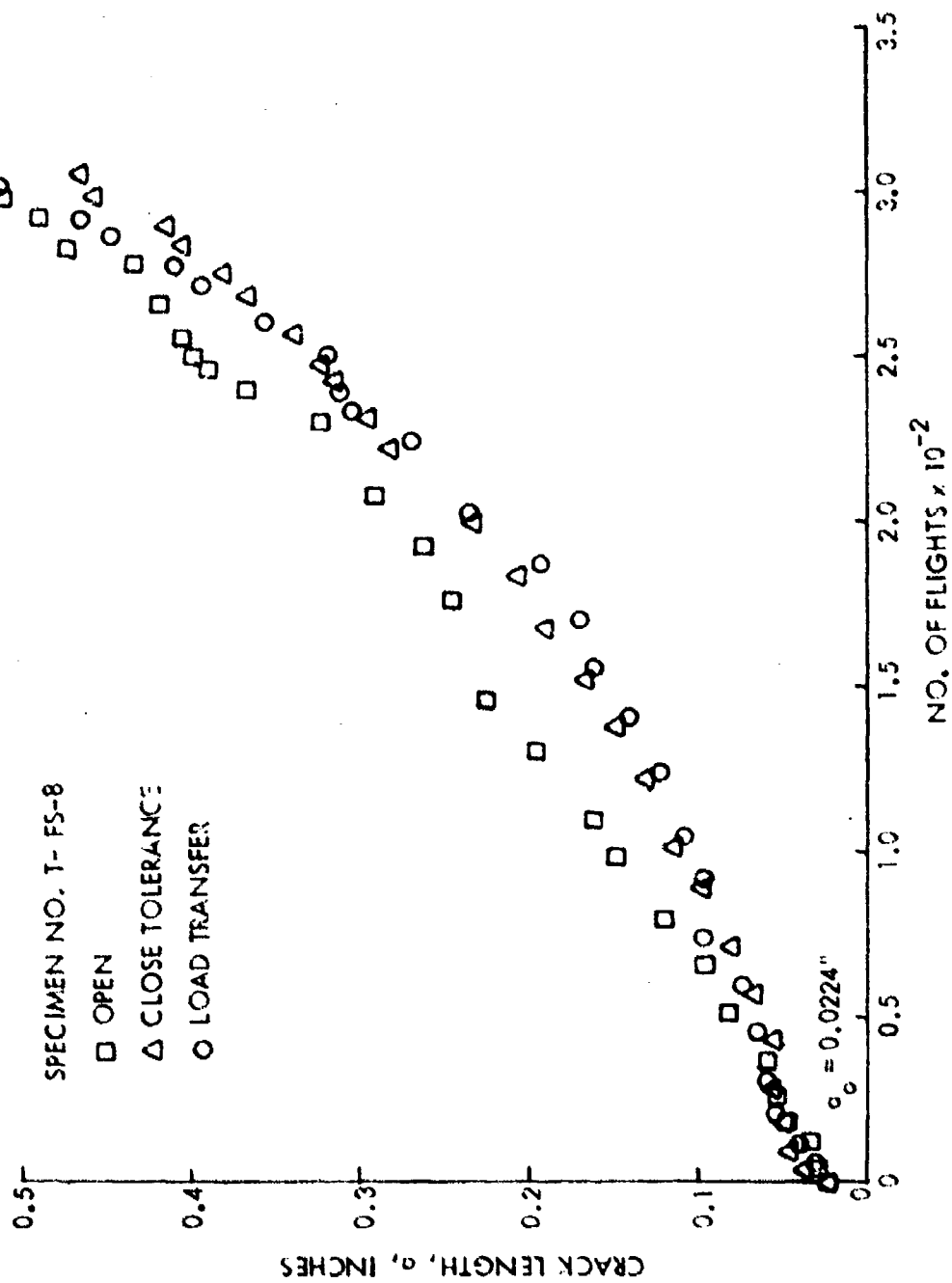


Figure 100. Growth Behavior of Small Thru Cracks from an Open and Close Tolerance Fastener Holes in 6Al-4 / Beta Annealed Titanium Alloy Plates Subjected to Fighter Spectrum Loading

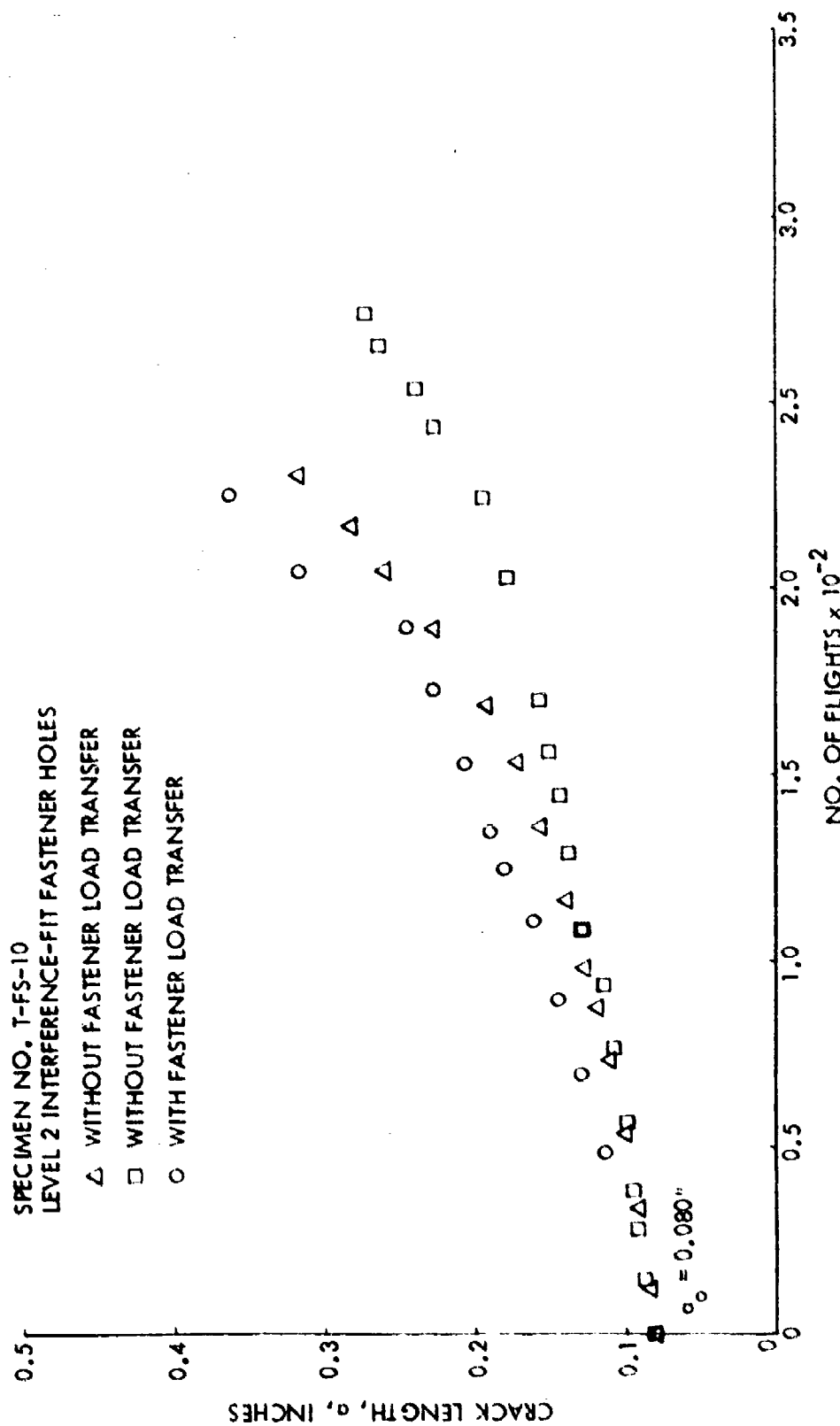


Figure 104. Growth Behavior of Intermediate Thru-Cracks from Level 2 Interference-Fit Fastener Holes with and without Fastener Load Transfer in 6AL-4V Beta Annealed Titanium Alloy Plates Subjected to Fighter Spectrum Loading

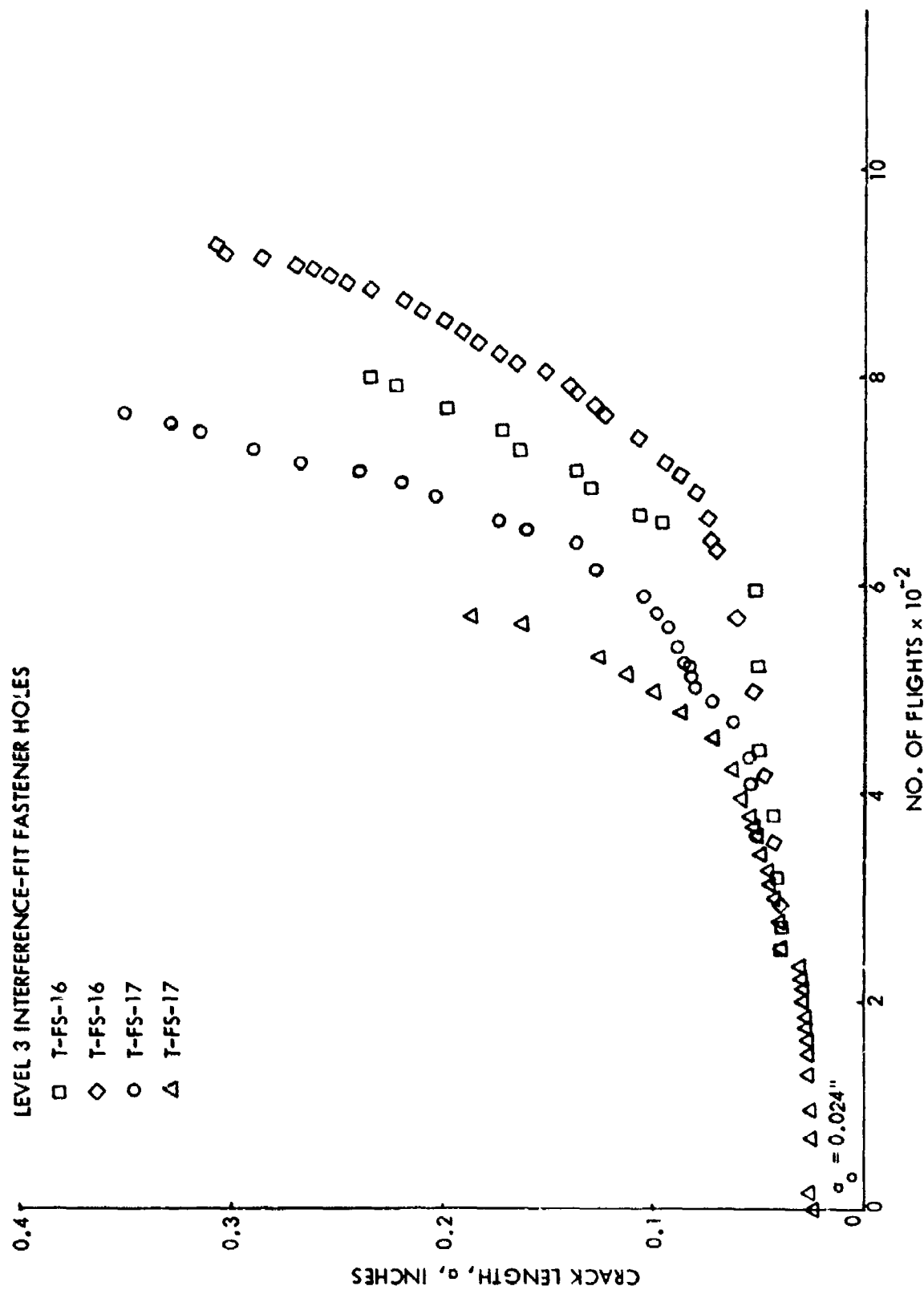


Figure 105. Growth Behavior of Small and Intermediate Thru Cracks from Level 3 Interference-Fit Fastener Holes in 6AL-4V Beta Annealed Titanium Alloy Plates Subjected to Fighter Spectrum Loading

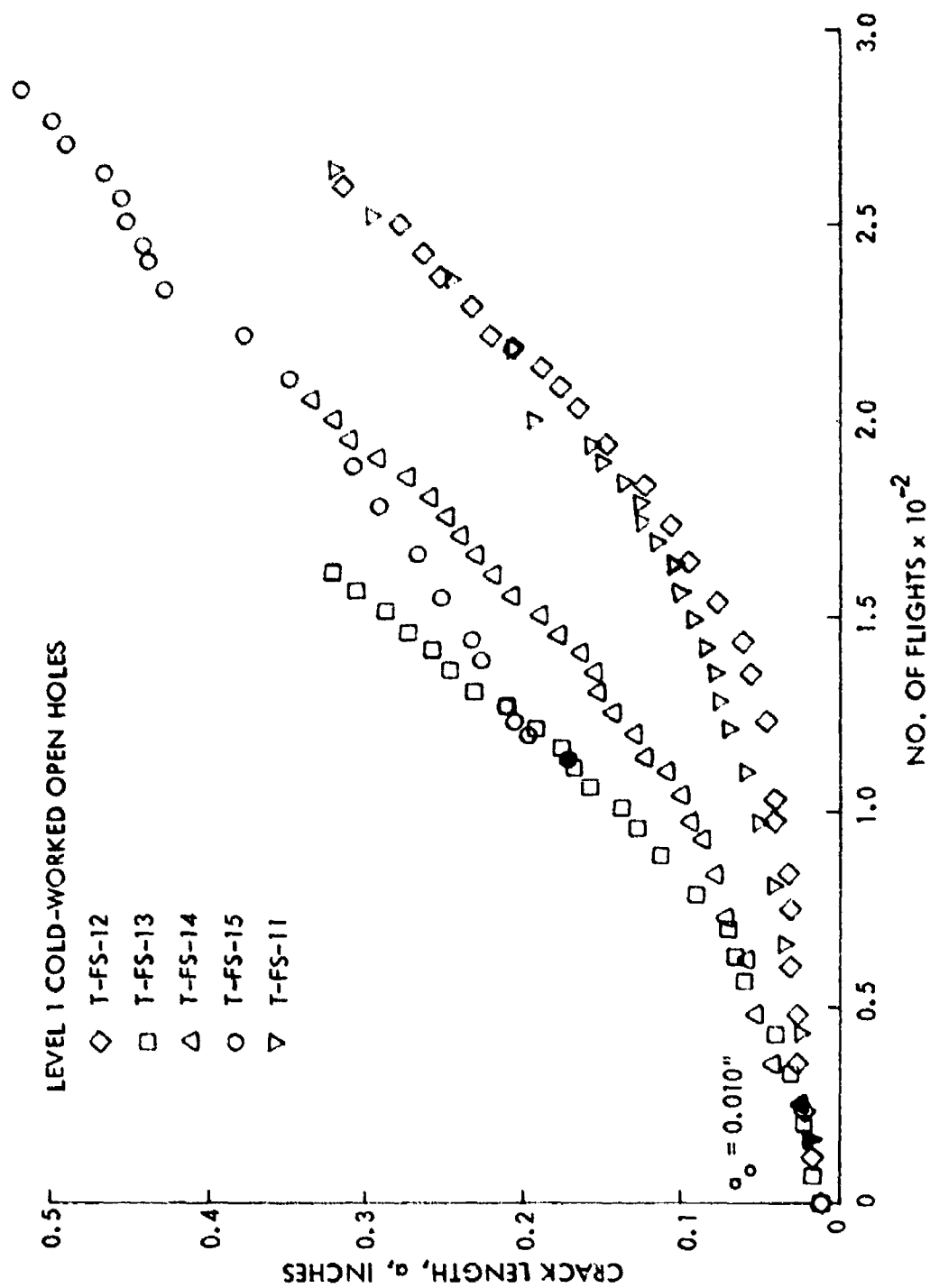


Figure 106. Growth Behavior of Small to Large Thru Cracks from Level 1 Cold-Worked Open Holes in 6Al-4V Beta Annealed Titanium Alloy Plates Subjected to Fighter Spectrum Loading

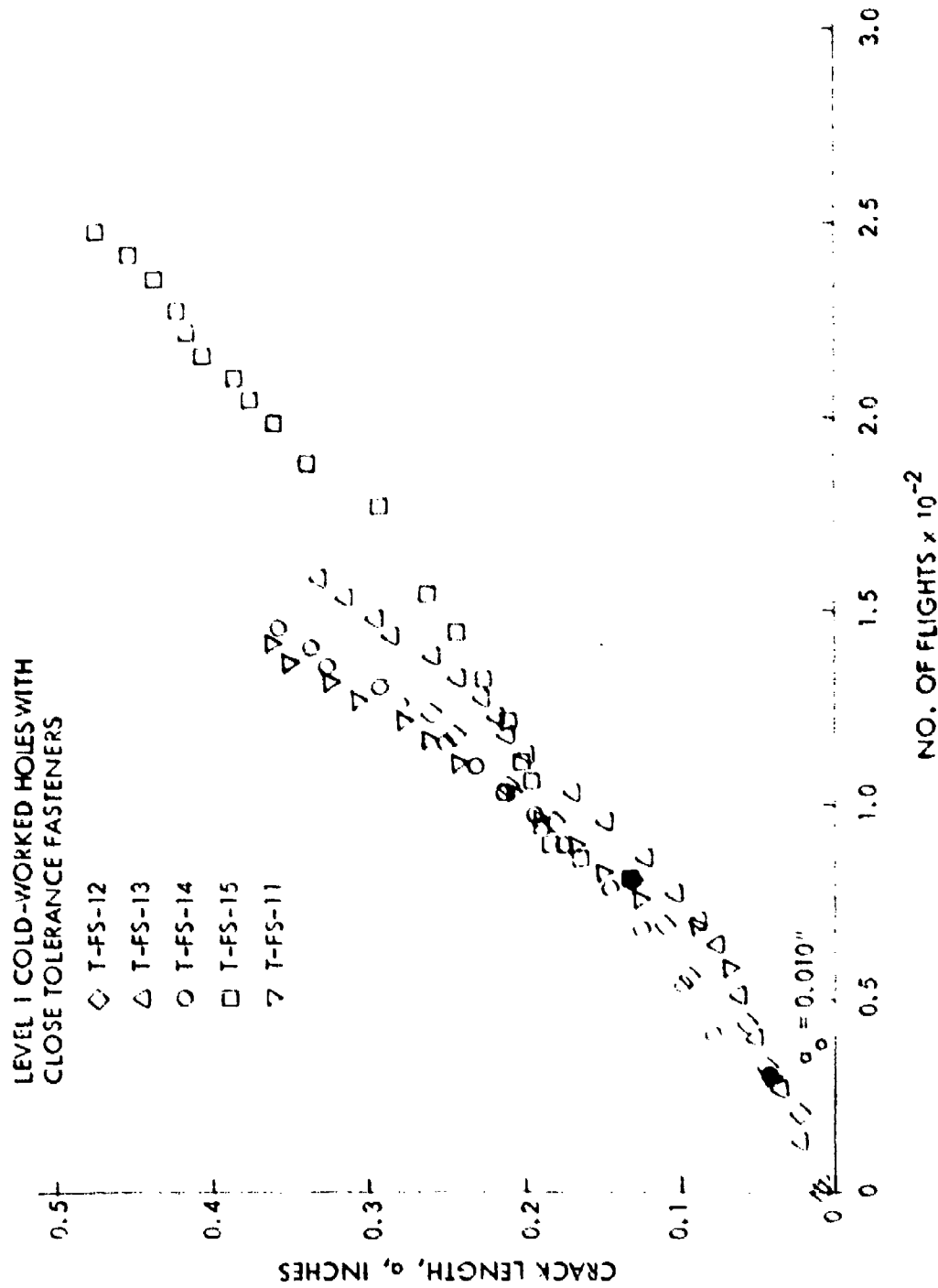


Figure 107. Growth Behavior of Small to Large Thru Cracks from Level 1 Cold-Worked Filled Holes in 6Al-4 / Beta Annealed Titanium Alloy Plates Subjected to Fighter Spectrum Loading

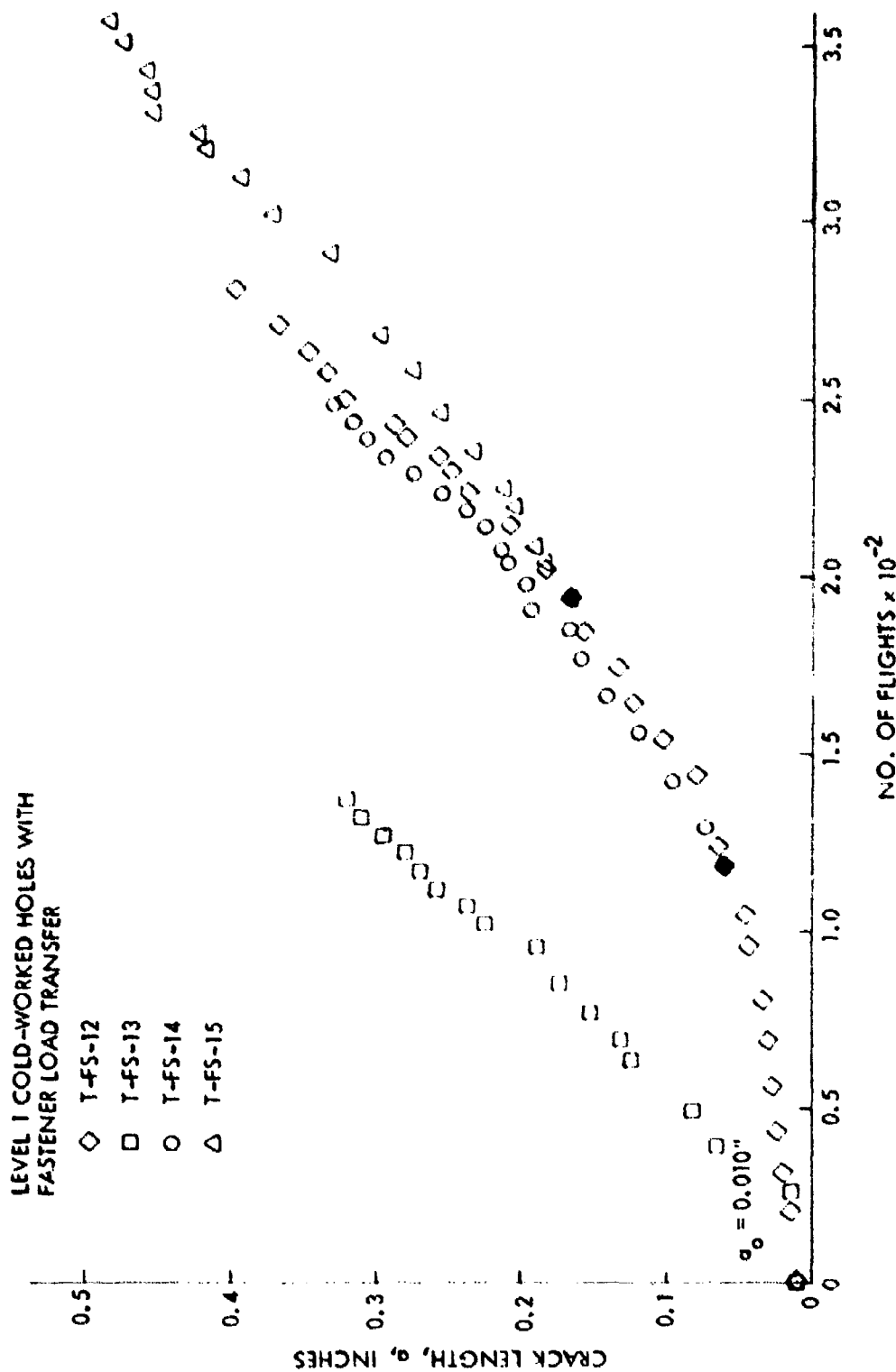


Figure 108. Growth Behavior of Small to Large Thru Cracks from Level I Cold-Worked Holes With Fastener Load Transfer in 6AL-4V Beta Annealed Titanium Alloy Plates Subjected to Fighter Spectrum Loading

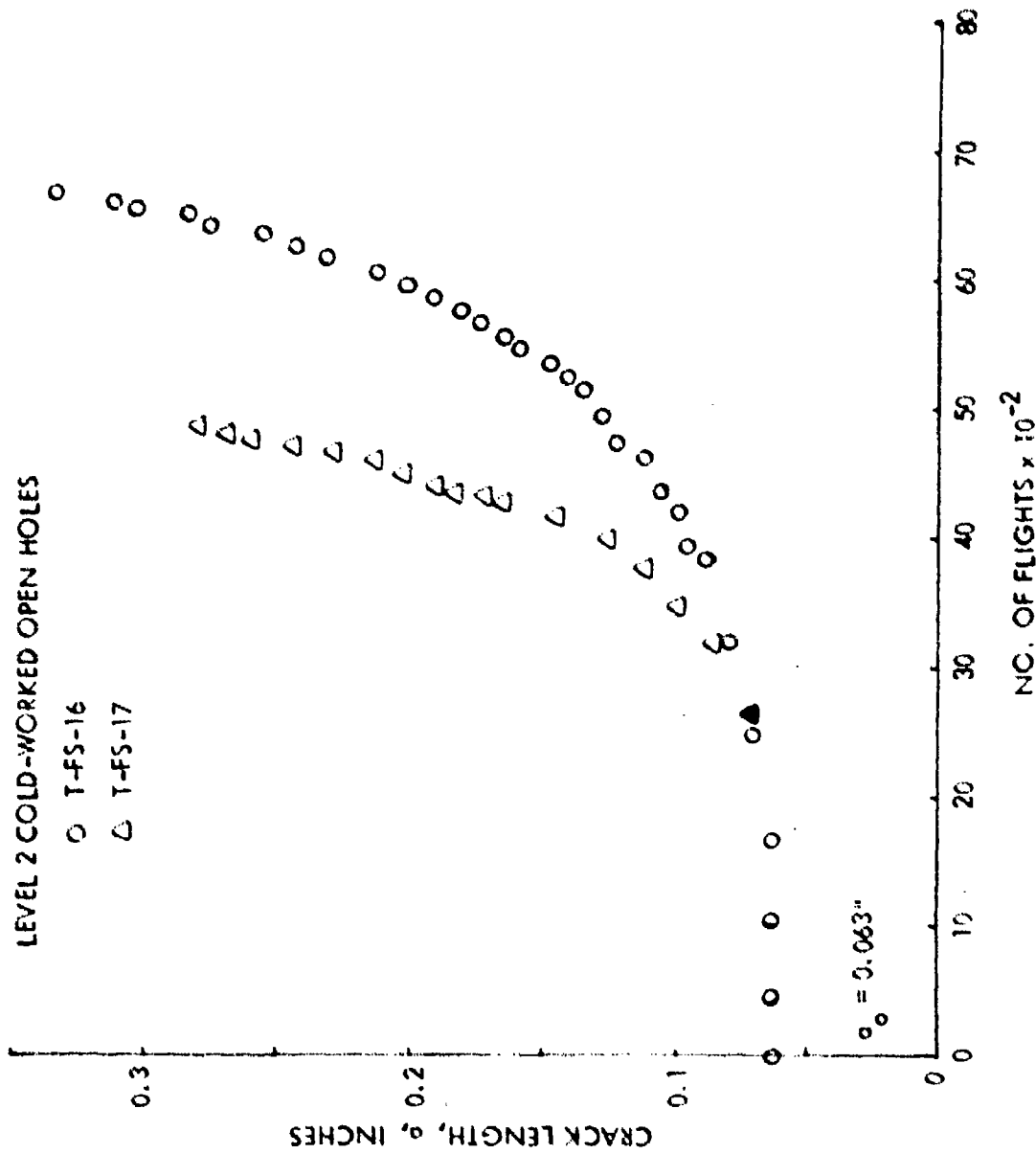


Figure 109. Growth Behavior of Intermediate Thru Cracks from Level 2 Cold-Worked Open Holes in 6Al-4V Beta Annealed Titanium Alloy Plates Subjected to Fighter Spectrum Loading

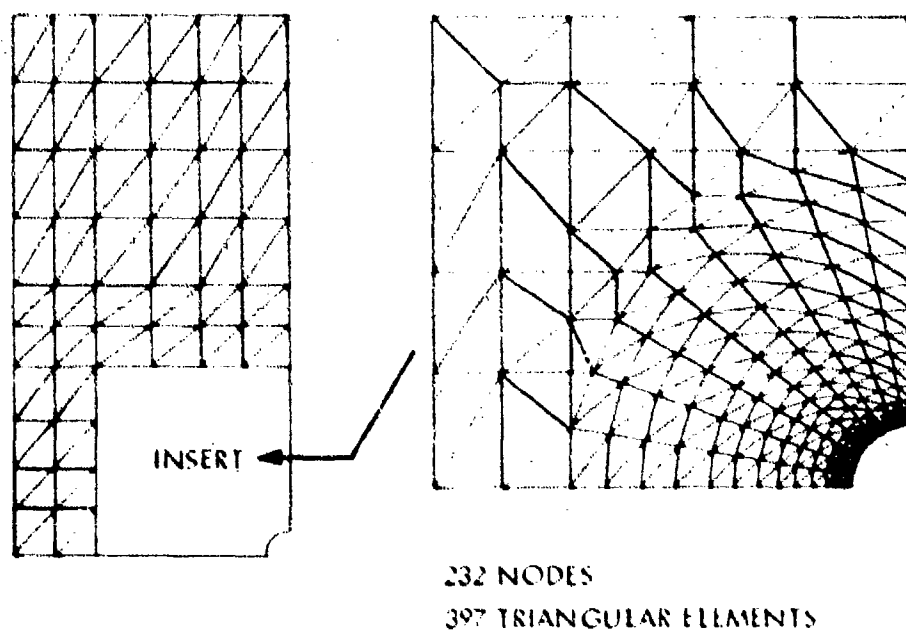


Figure 110. Finite Element Model

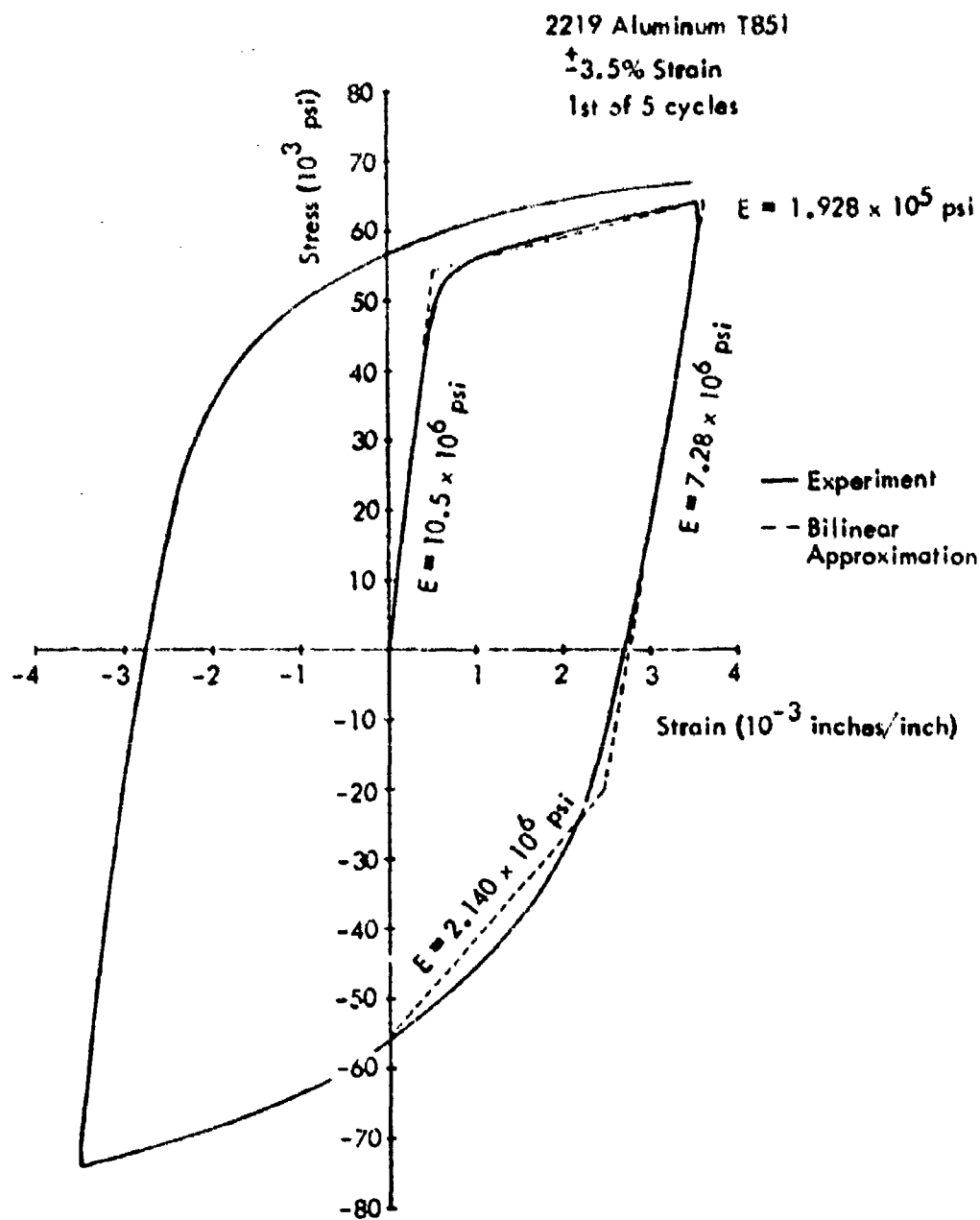


Figure 111. Cyclic Stress-Strain Curve

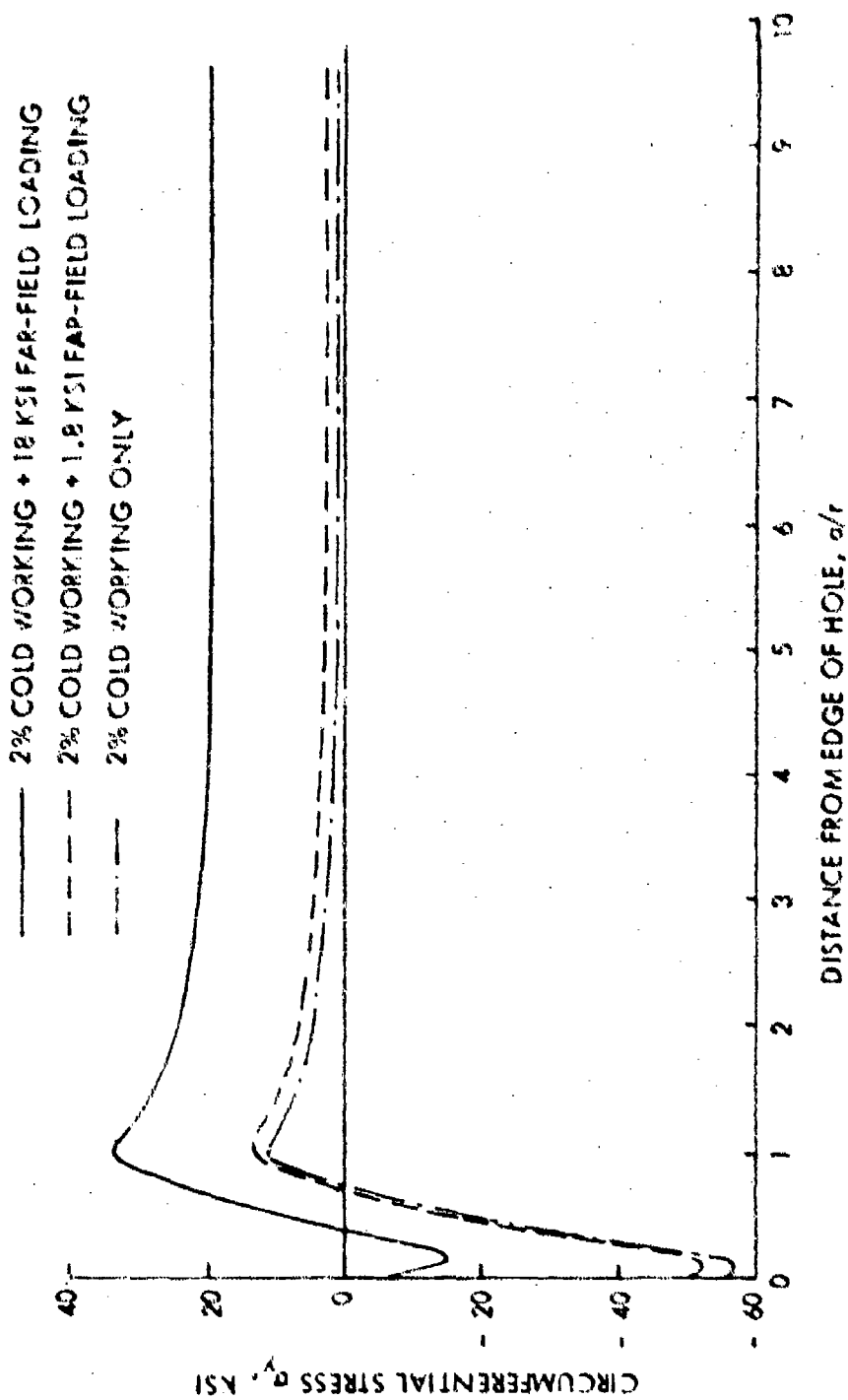


Figure 112. Unflamed Stress Distribution Along the r -Axis in 2219-T851 Aluminum Plate Caused by 2% Cold Working and Subsequent Far-Field Loading

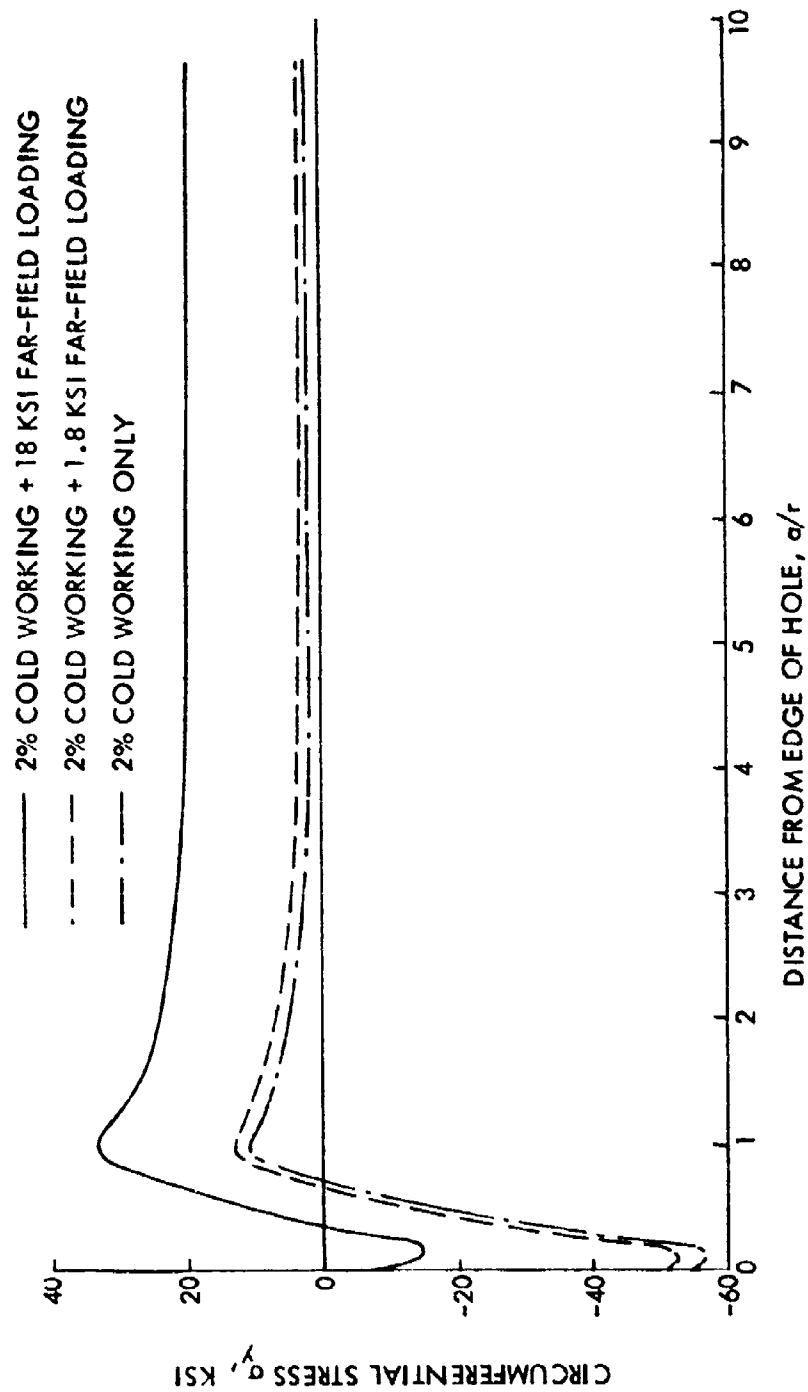


Figure 113. Stress Distribution Along the x-Axis in 2219-T851 Aluminum Plate Caused by 2% Cold Working and Subsequent Far-Field Loading ($a_i = 0.0125"$)

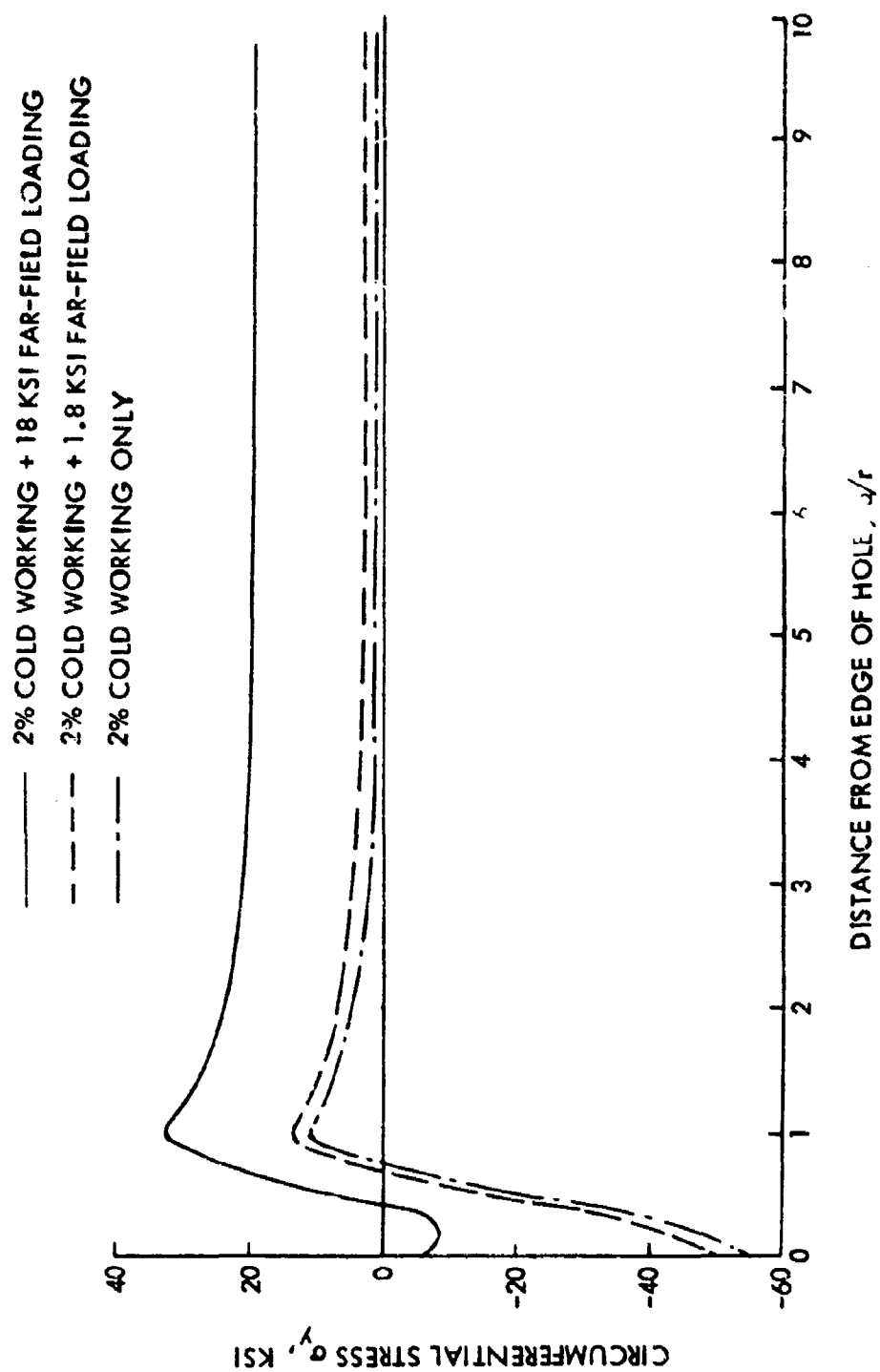


Figure 114. Stress Distribution Along the x-Axis in 2219-T851 Aluminum Plate
 Caused by 2% Cold Working and Subsequent Far-Field Loading
 ($\alpha_1 = 0.0525$)

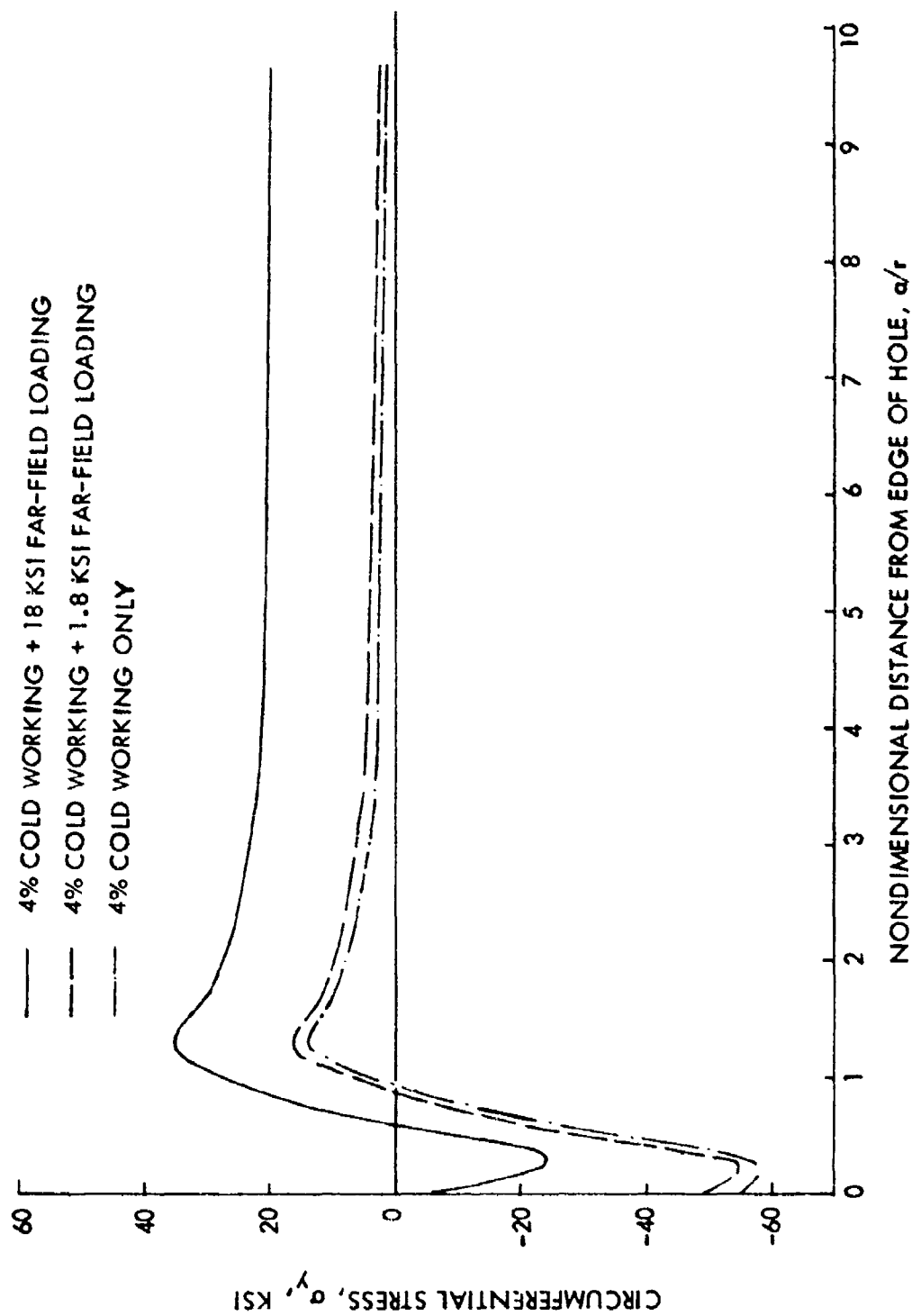


Figure 115. Unflawed Stress Distribution Along the x-Axis in 2219-T851 Aluminum Alloy Plate Caused by 4% Cold Working and Subsequent Far-Field Loading

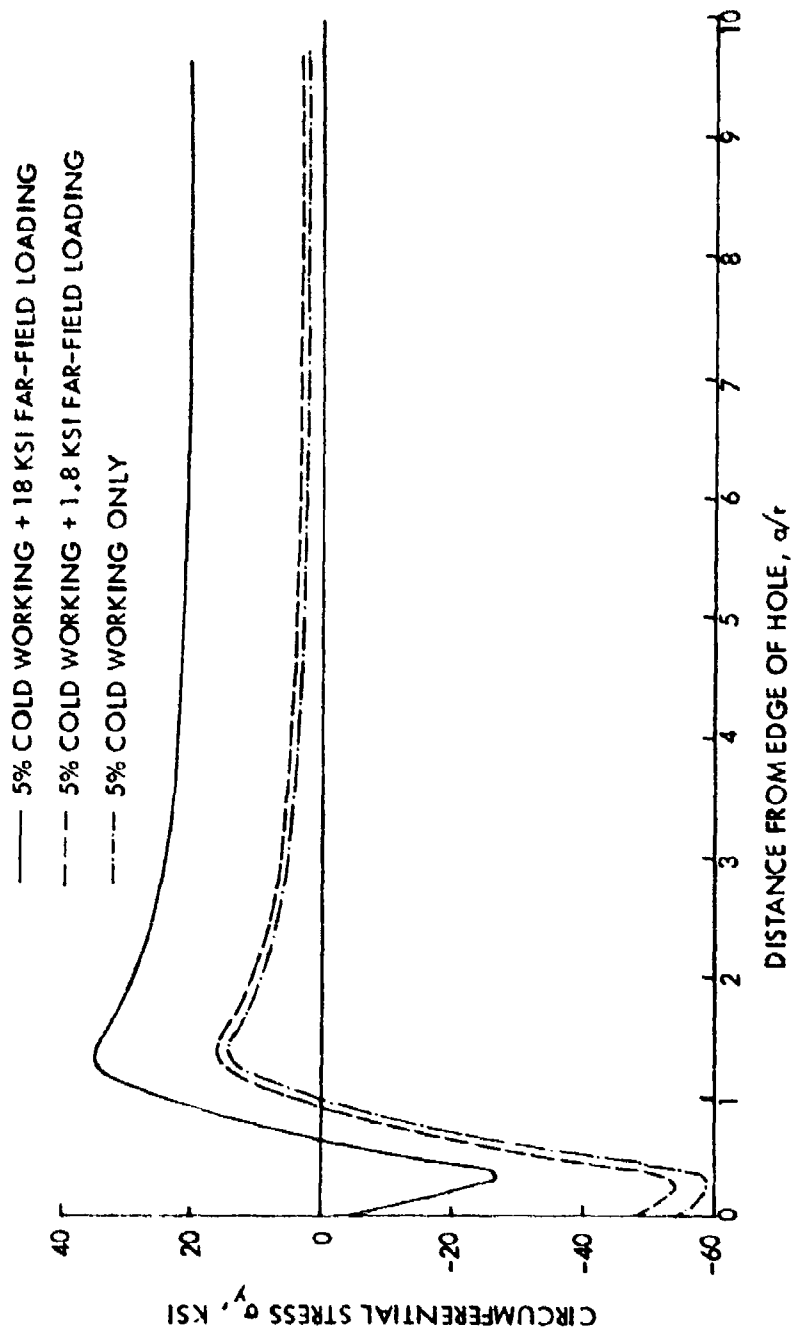


Figure 116. Unflawed Stress Distribution Along the x-Axis in 2219-T851 Aluminum Plate Caused by 5% Cold Working and Subsequent Far-Field Loading

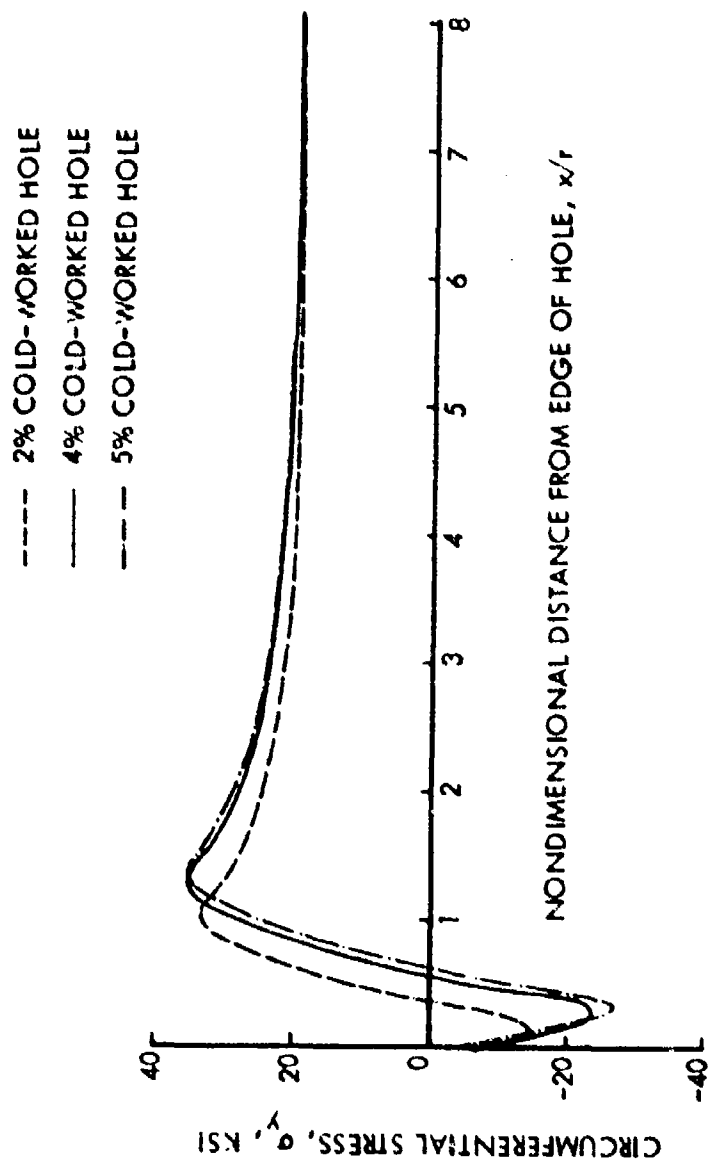


Figure 117 Unflawed Stress Distribution Along the x-Axis in 2219-T851 Aluminum Plates Caused by 2%, 4%, and 5% Cold-Working and Subsequent 18 Ksi Far-Field Loading

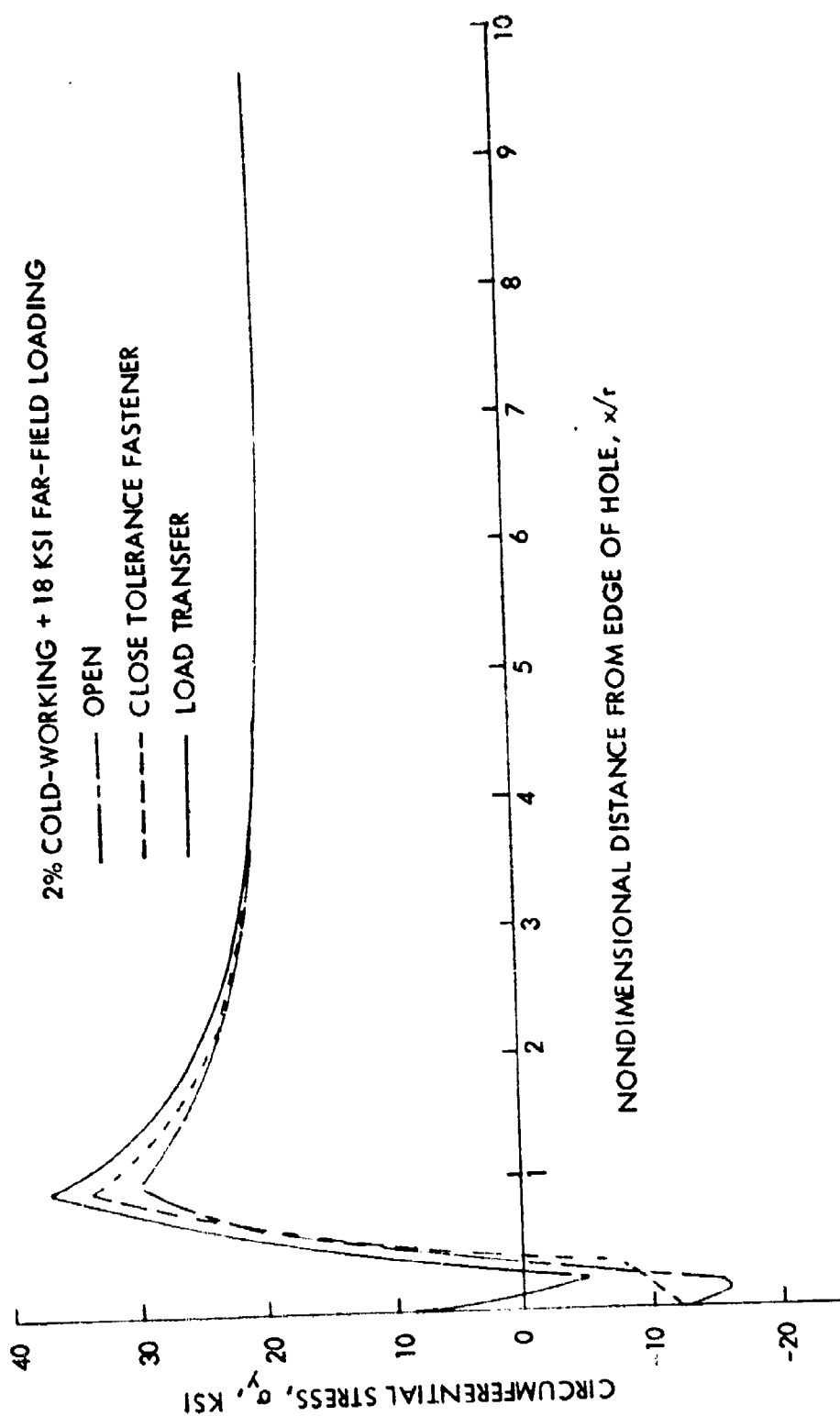


Figure 118. Unflawed Stress Distribution Along the X-Axis at Various Types of 2% Cold-Worked Holes in 2219-T851 Aluminum Plates Subjected to 18 Ksi Far-Field Loading

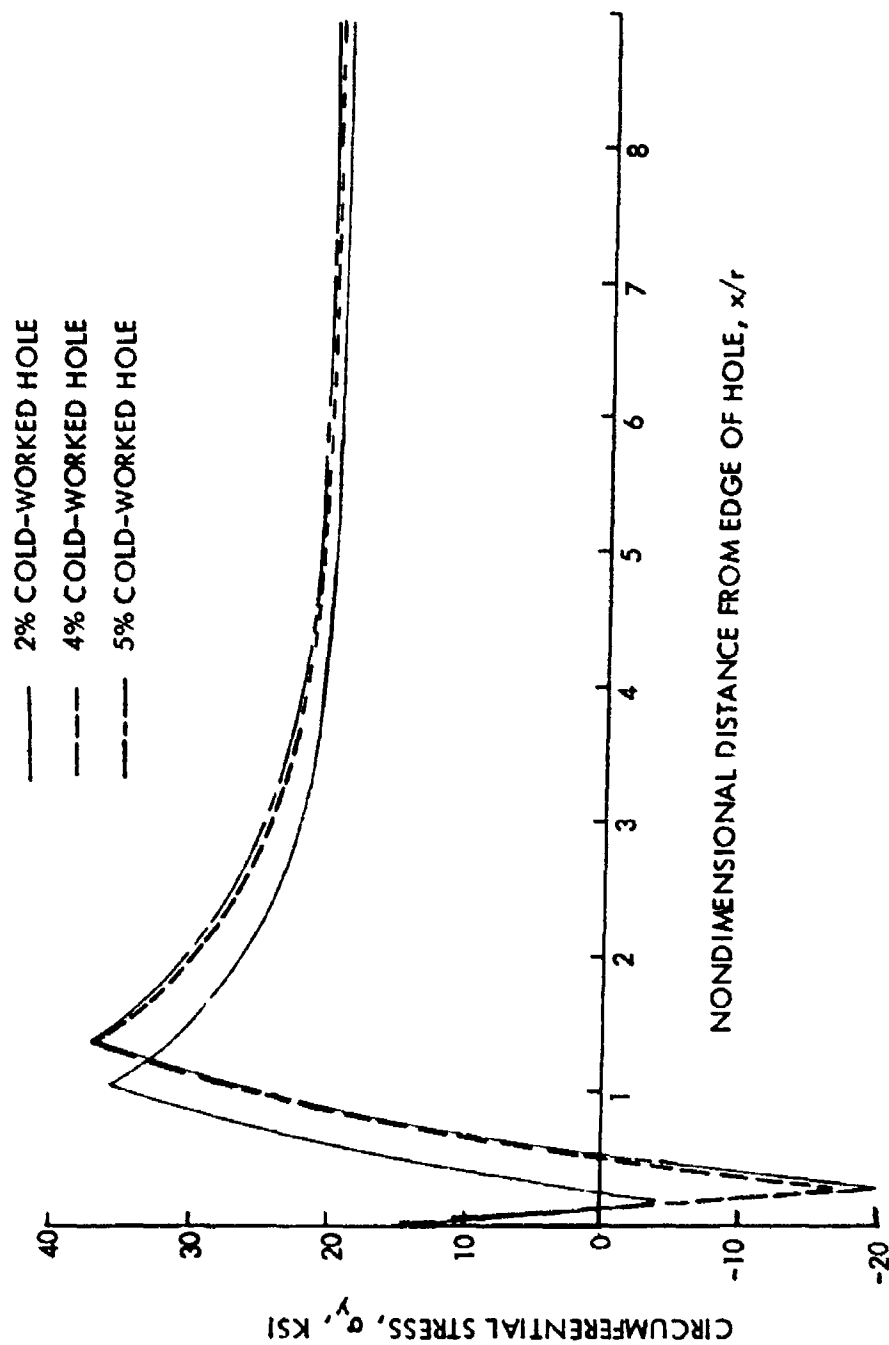


Figure 119. Unflawed Stress Distribution Along the x-Axis in 2219-T851 Aluminum Plates Caused by 2%, 4% and 5% Cold Working and Subsequent 18 Ksi Far-Field Loading and 10% Fastener Load Transfer

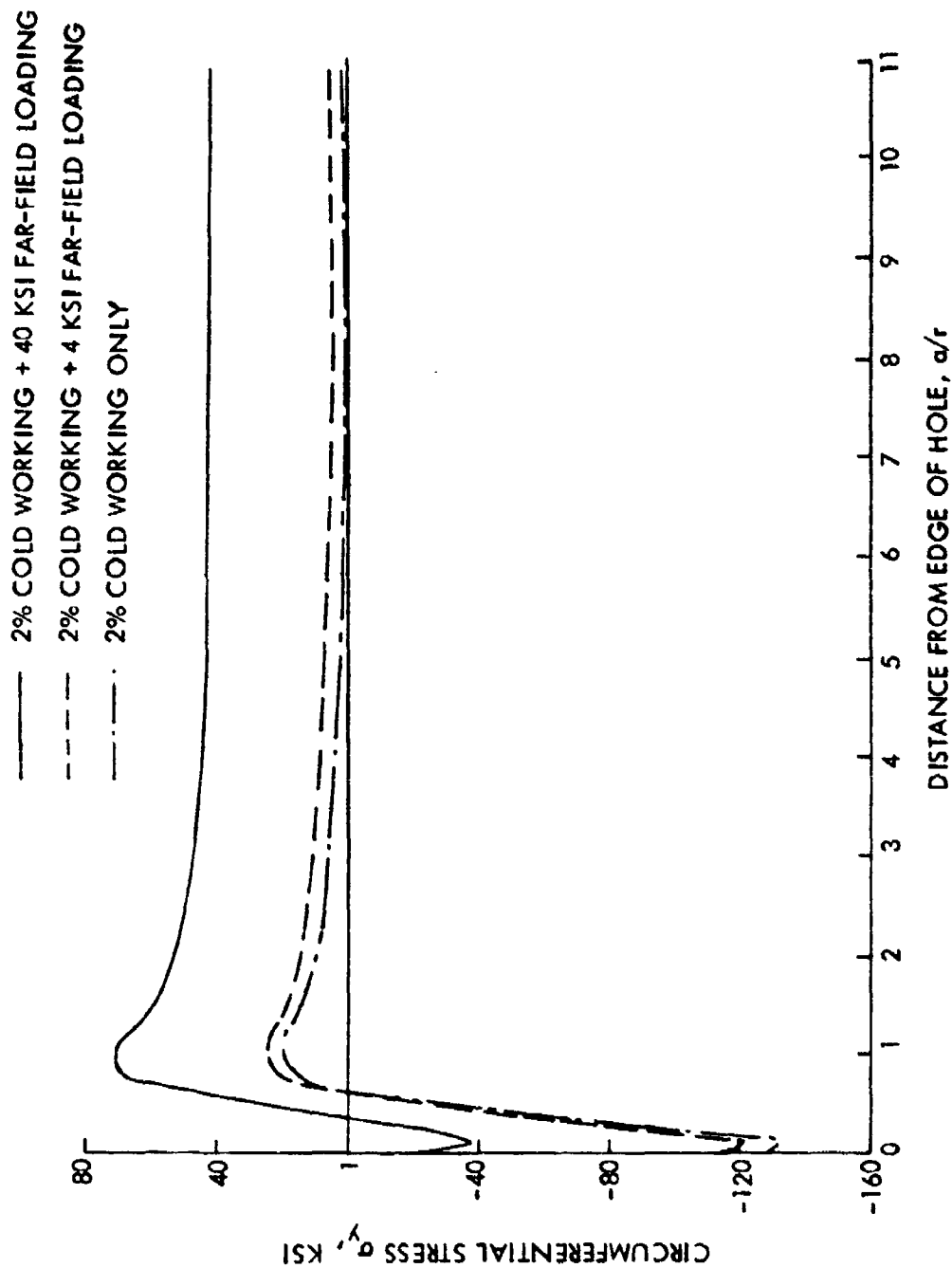


Figure 120. Unflowed Stress Distribution Along the x-Axis in 6Al-4V Beta Annealed Titanium Plate Caused by 2% Cold Working and Subsequent Far-Field Loading

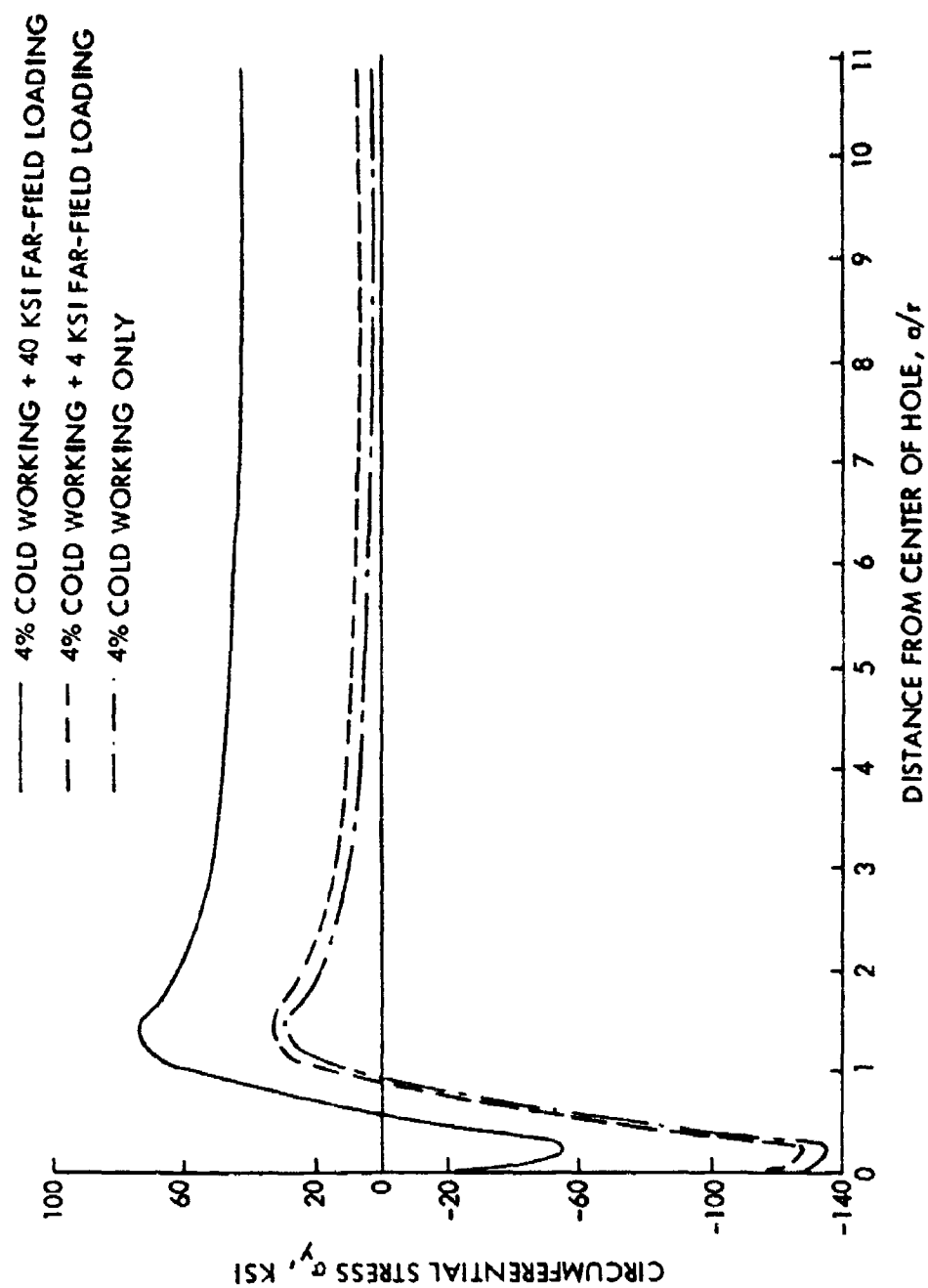


Figure 121. Unflowed Stress Distribution Along the x-Axis in 6Al-4V Beta Annealed Titanium Plate Caused by 4% Cold Working and Subsequent Far-Field Loading

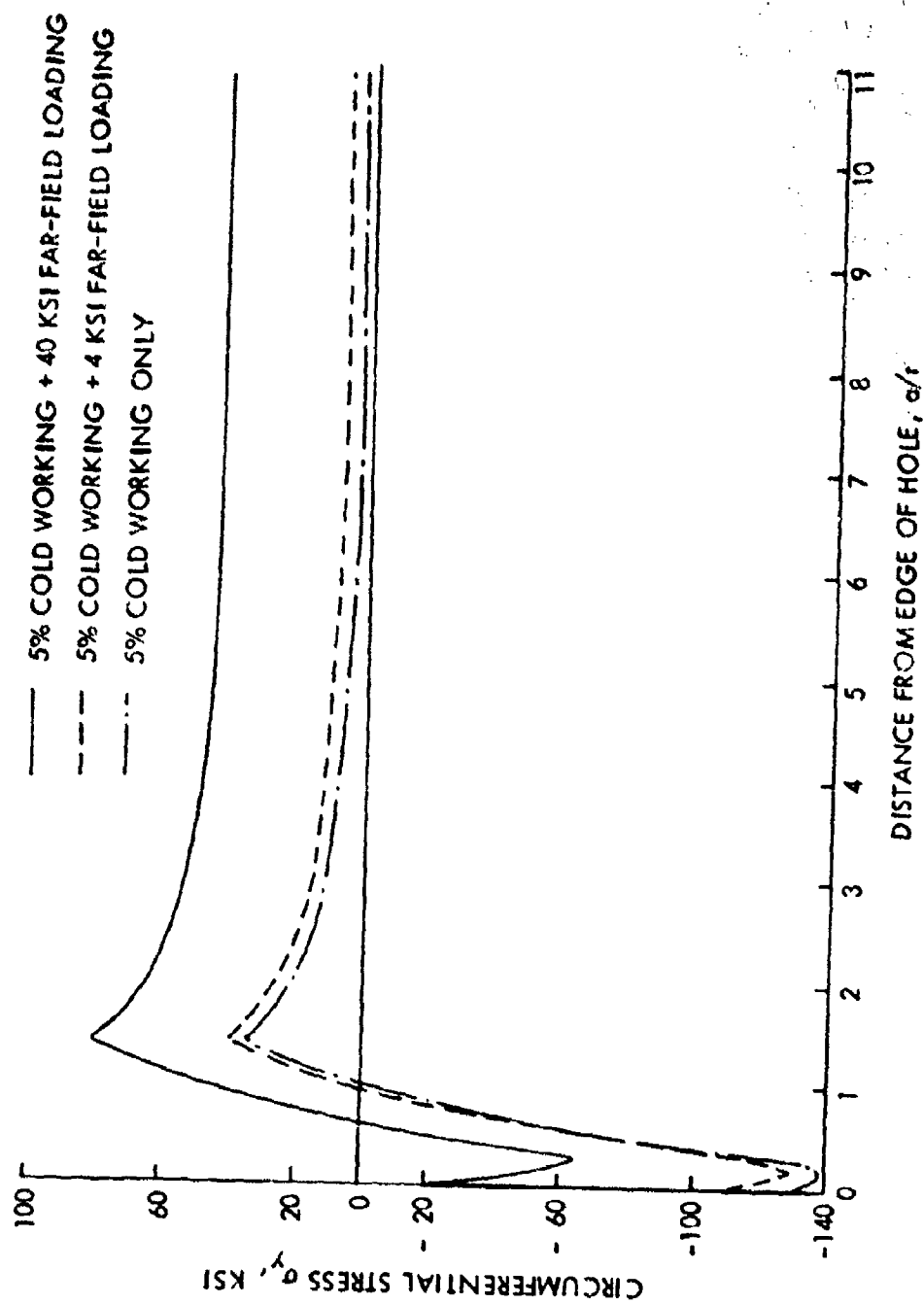


Figure 122. Unflawed Stress Distribution Along the x -Axis in 6A -4/ Beta Annealed Titanium Plate Caused by 5% Cold Working and Subsequent Far-Field Loading

2% COLD WORKING + 40 KSI FAR-FIELD LOADING

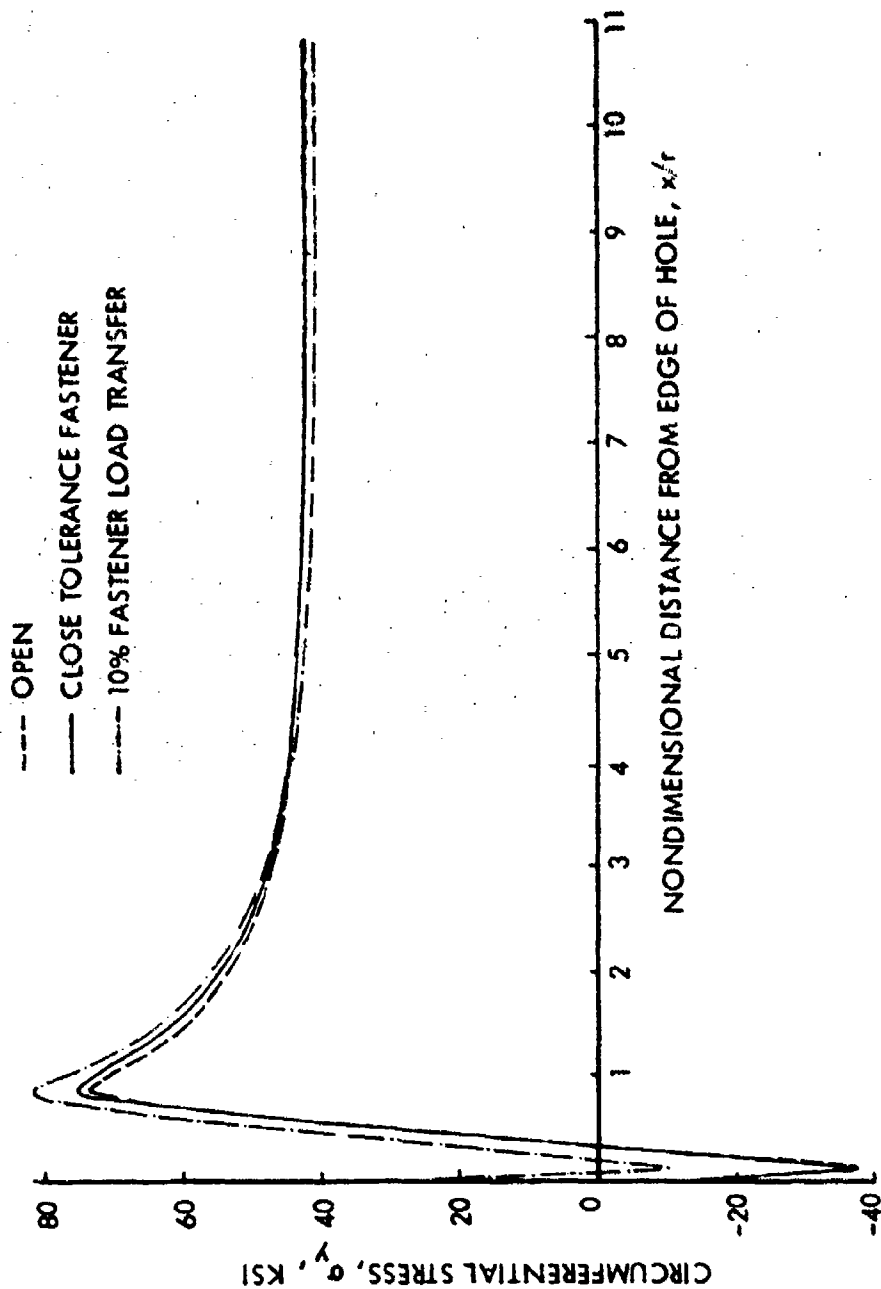


Figure 123 Unflawed Stress Distribution Along the x-Axis at 2% Cold-Worked Holes with and without Fastener Load Transfer in 6AL-4V Beta Annealed Titanium Plates Caused by 40 KSI Far-Field Loading

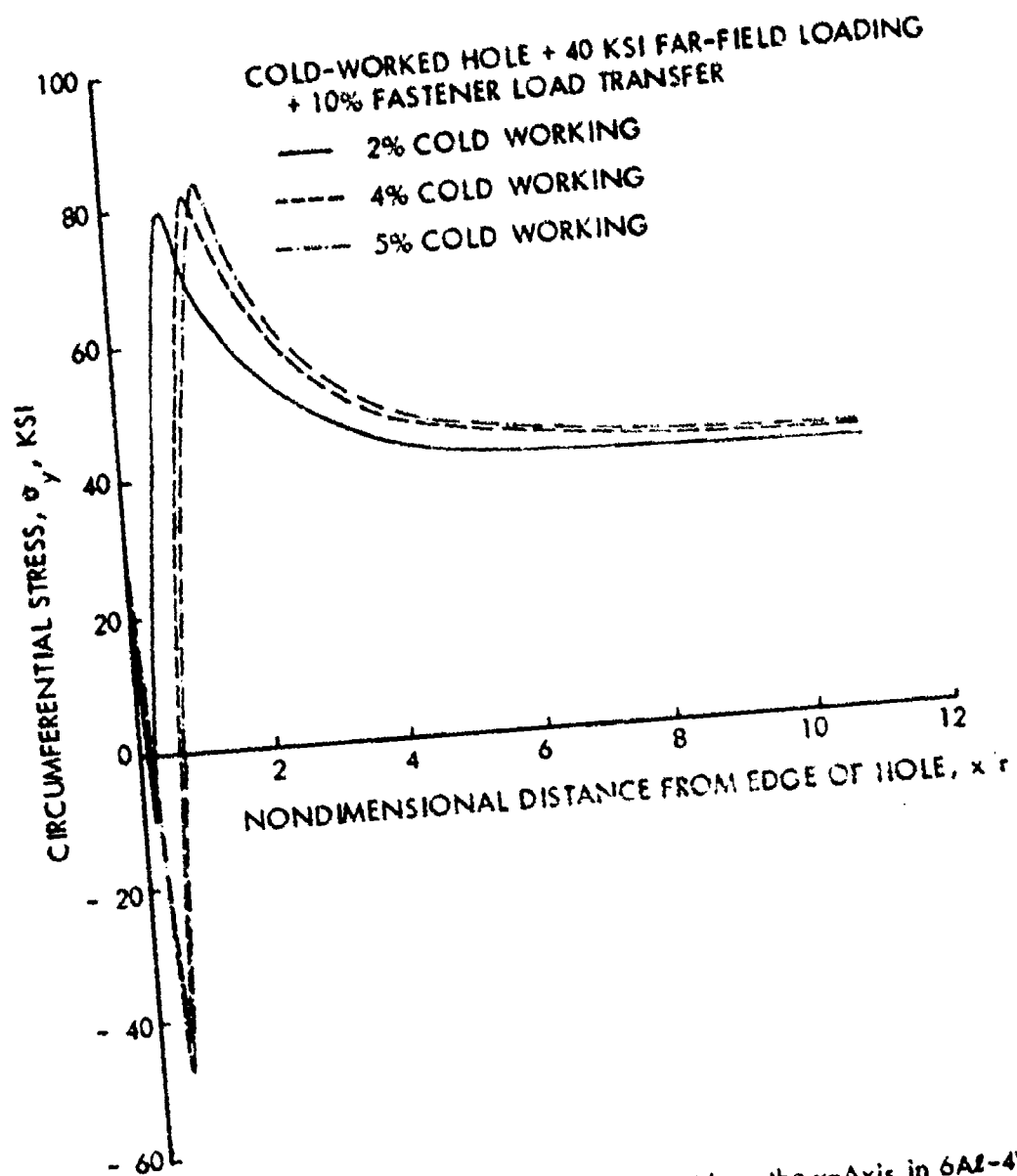


Figure 124 Unflawed Stress Distribution Along the x-Axis in 6Al-4V Beta Annealed Titanium Plates Caused by 2%, 4% and 5% Cold Working and Subsequent 40 Ksi Far-Field and 10% Fastener Loads

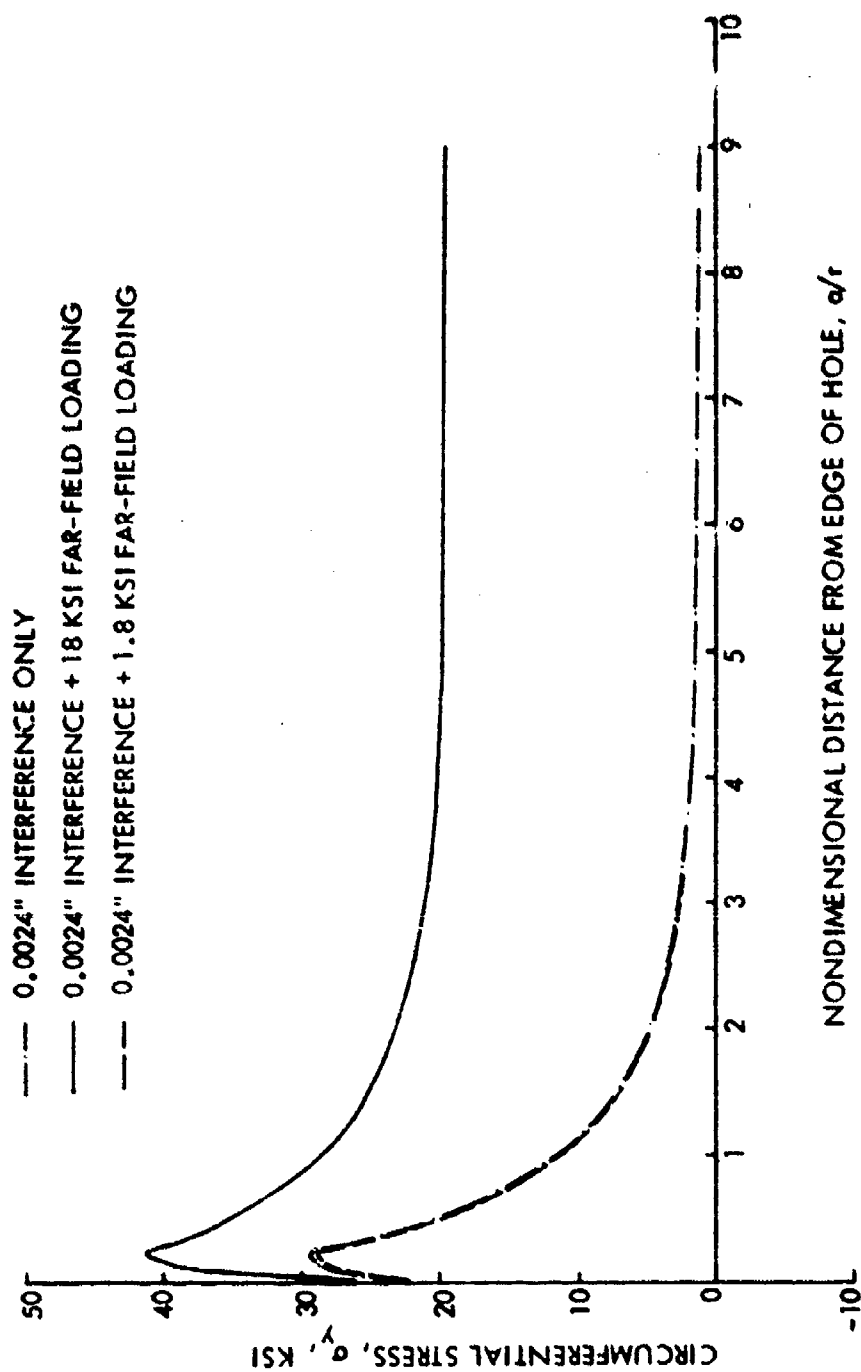


Figure 125. Unflawed Stress Distribution Along the y -Axis in 2219-T851 Aluminum Alloy Plate Caused by 0.0024 Inches Diametrical Interference and Subsequent Far-Field Loading

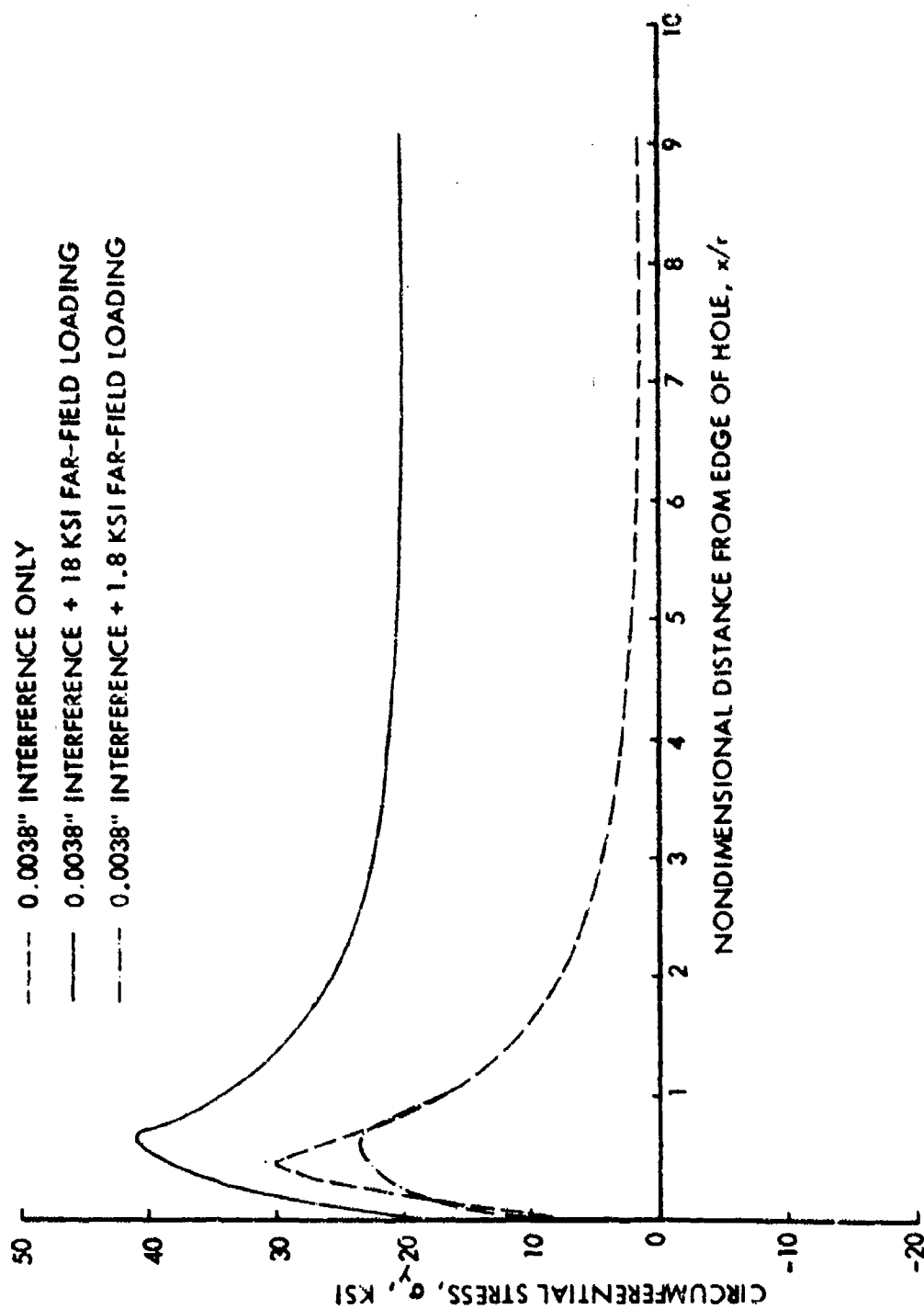


Figure 126. Unflawed Stress Distribution Along the x -Axis in 2219-T851 Aluminum Alloy Plate Caused by 0.0038 Inches Diametrical Interference and Subsequent Far-Field Loading

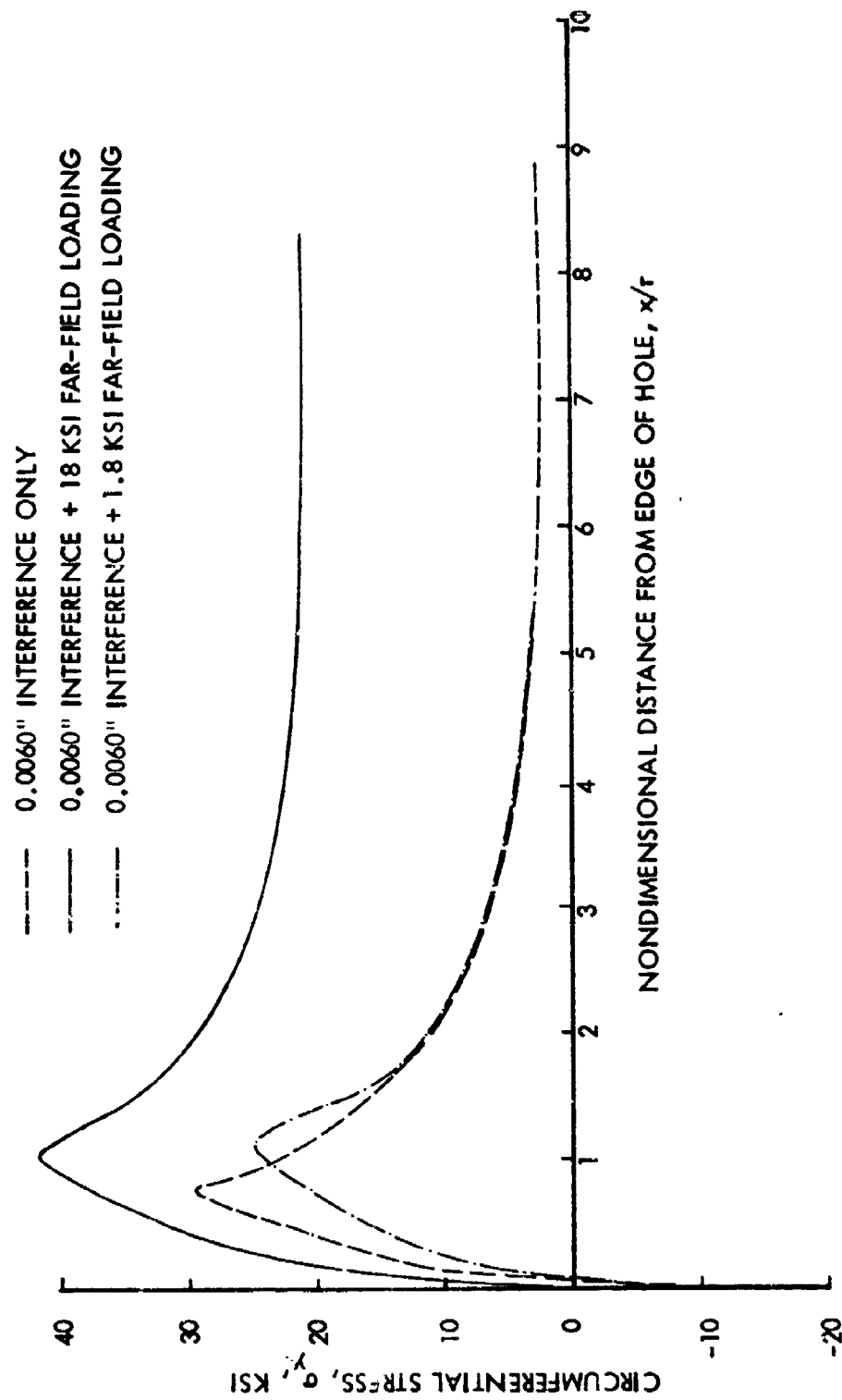


Figure 127. Unflowed Stress Distribution Along the x-Axis in 2219-T851 Aluminum Alloy Plate Caused by 0.0060 Inches Diametrical Interference and Subsequent Far-Field Loading

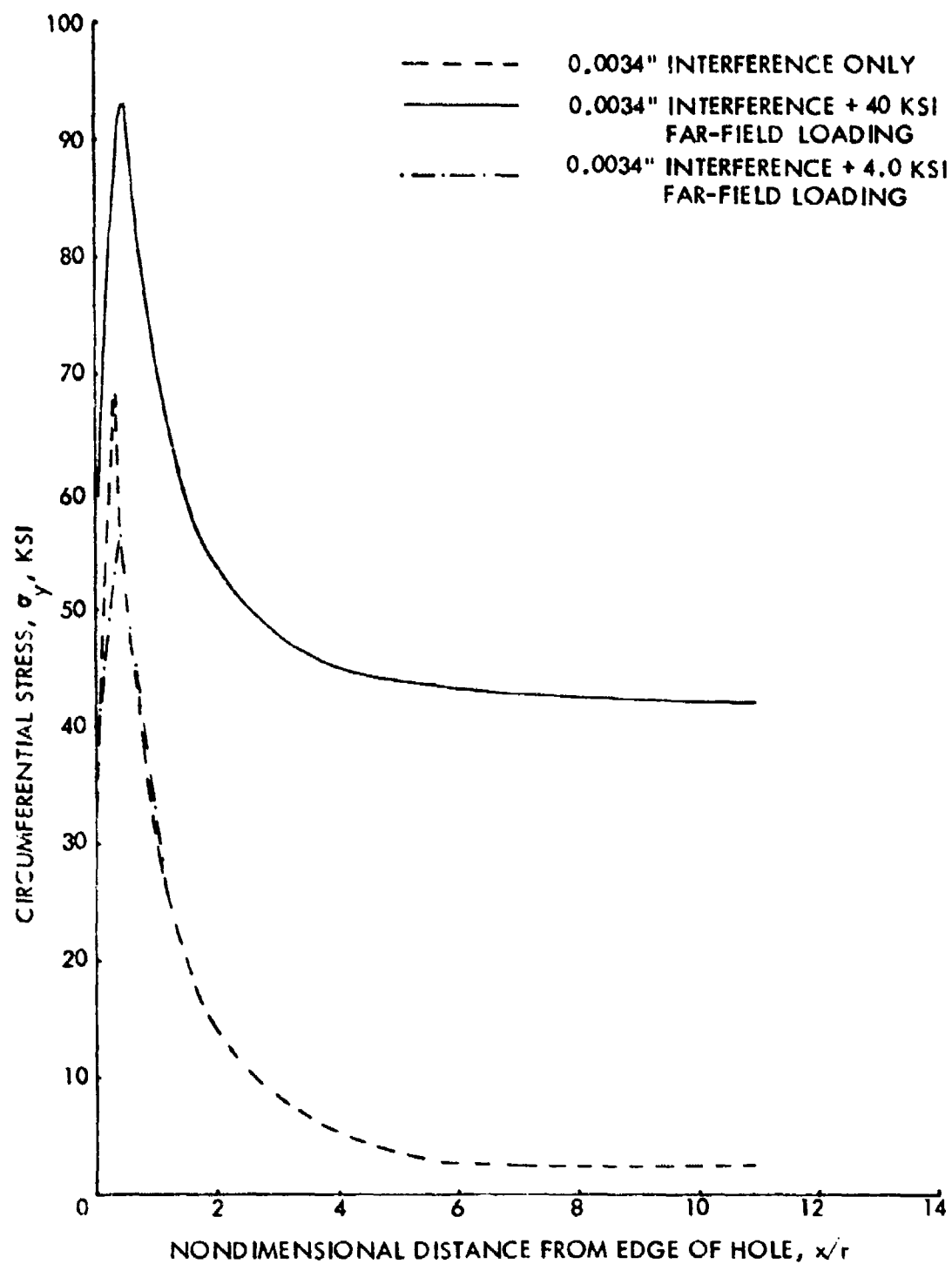


Figure 128. Unflawed Stress Distribution Along the x-Axis in 6Al-4V Beta Annealed Titanium Plate Caused by 0.0034 Inches Diametrical Interference and Subsequent Far-Field Loading

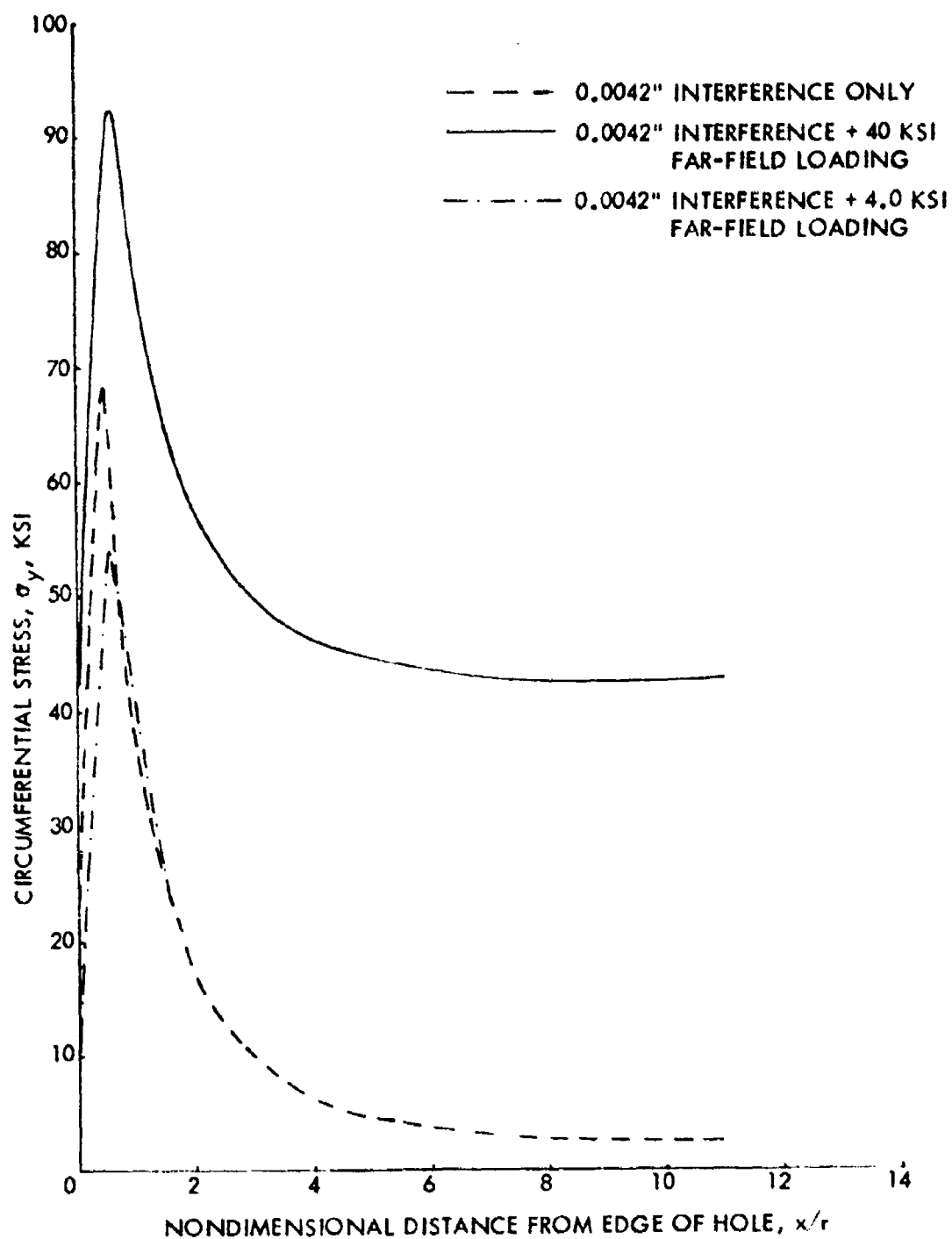


Figure 129. Unflawed Stress Distribution Along the x-Axis in 6Al-4V Beta Annealed Titanium Plate Caused by 0.0042 Inches Diametrical Interference and Subsequent Far-Field Loading

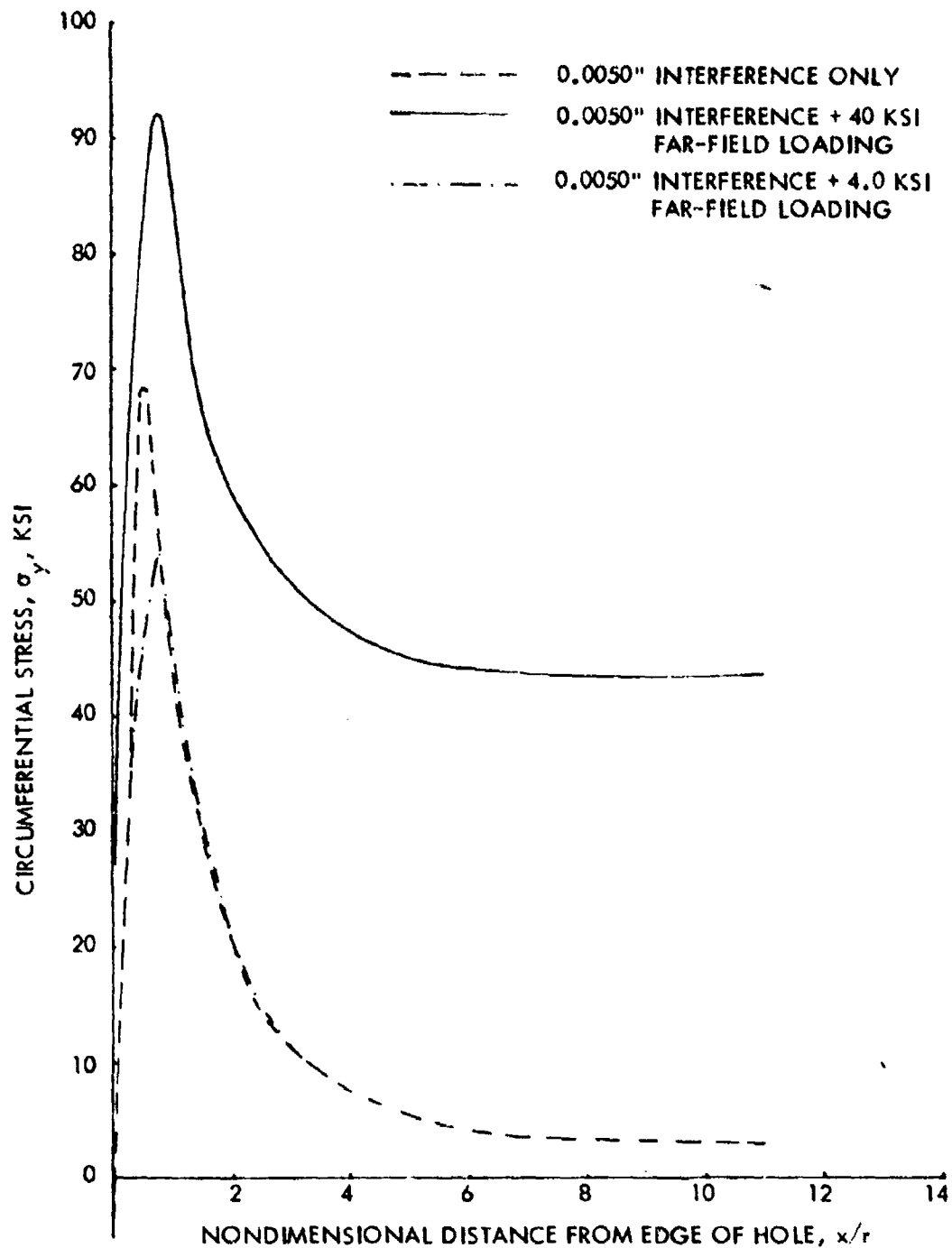


Figure 130. Unflawed Stress Distribution Along the x-Axis in 6Al-4V Beta Annealed Titanium Plate Caused by 0.0050 Inches Diametrical Interference and Subsequent Far-Field Loading

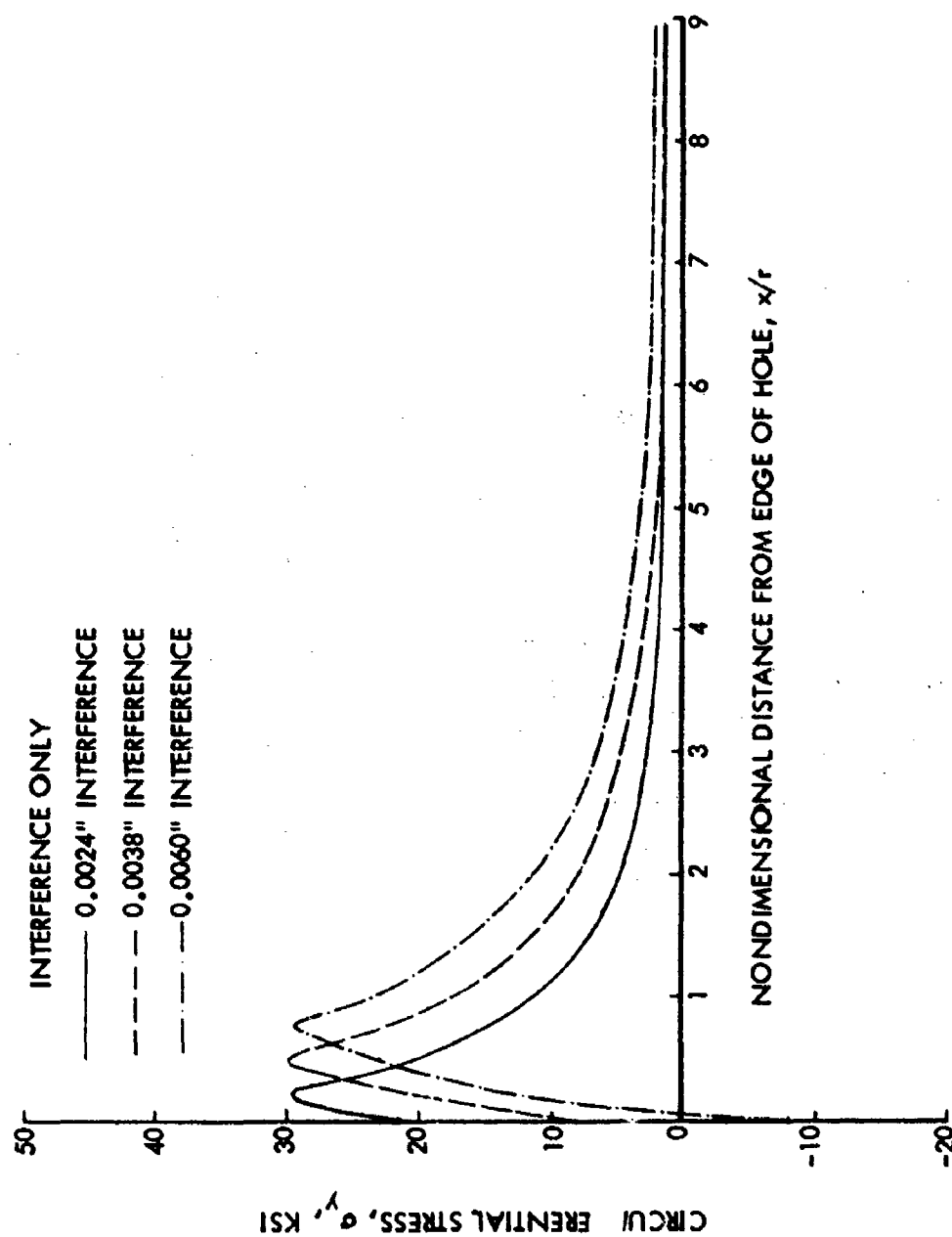


Figure 131 Unflawed Stress Distribution Along the x-Axis in 2219-T851 Aluminum Alloy Plates Due to the Installation of Three Different Levels of Interference-Fit Fastener

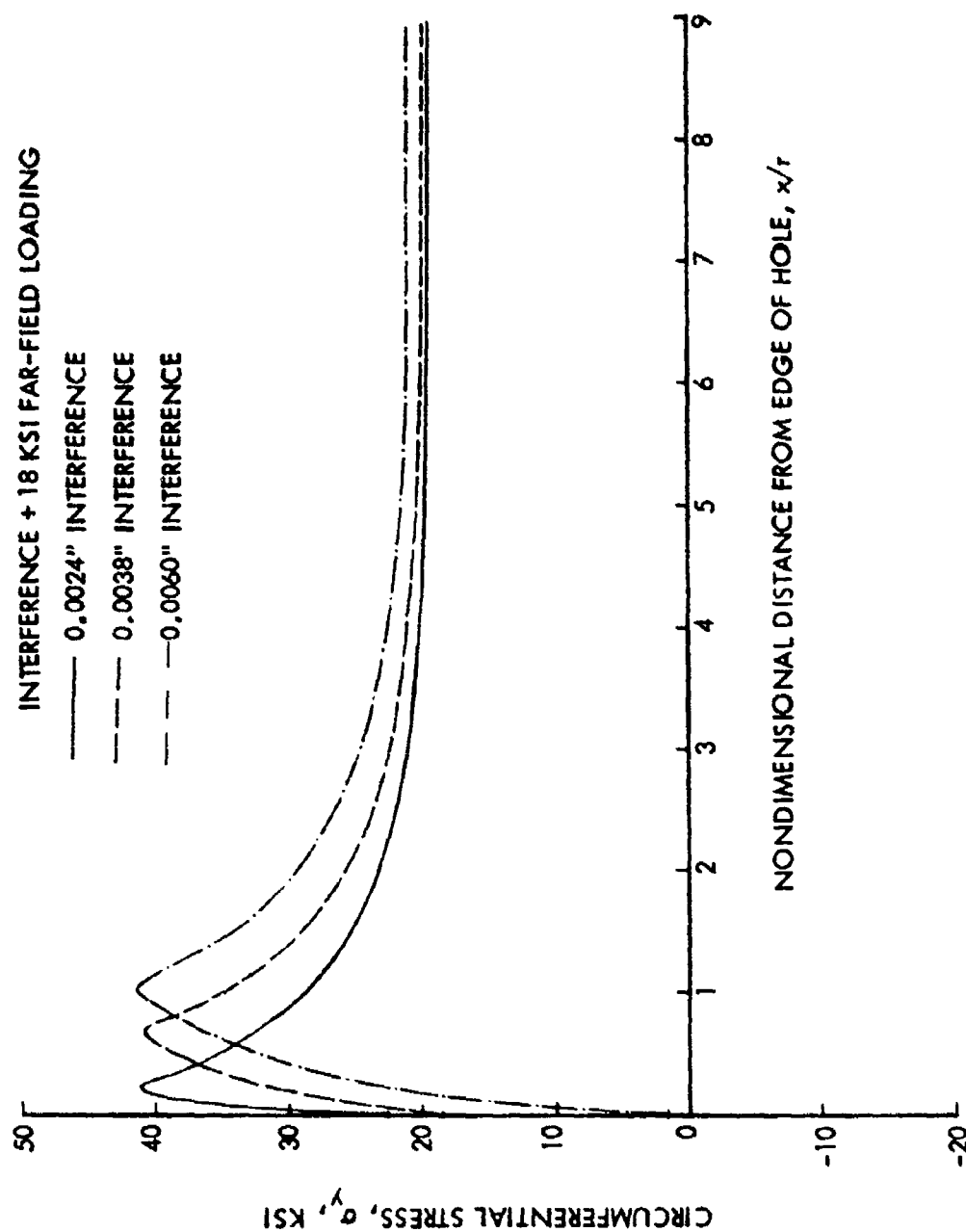


Figure 132 Unflawed Stress Distribution Along the x-Axis in 2219-T851 Aluminum Alloy Plates Due to the Application of 18 Ksi Far-Field Loading for Three Different Levels of Interference-Fit Fastener Holes

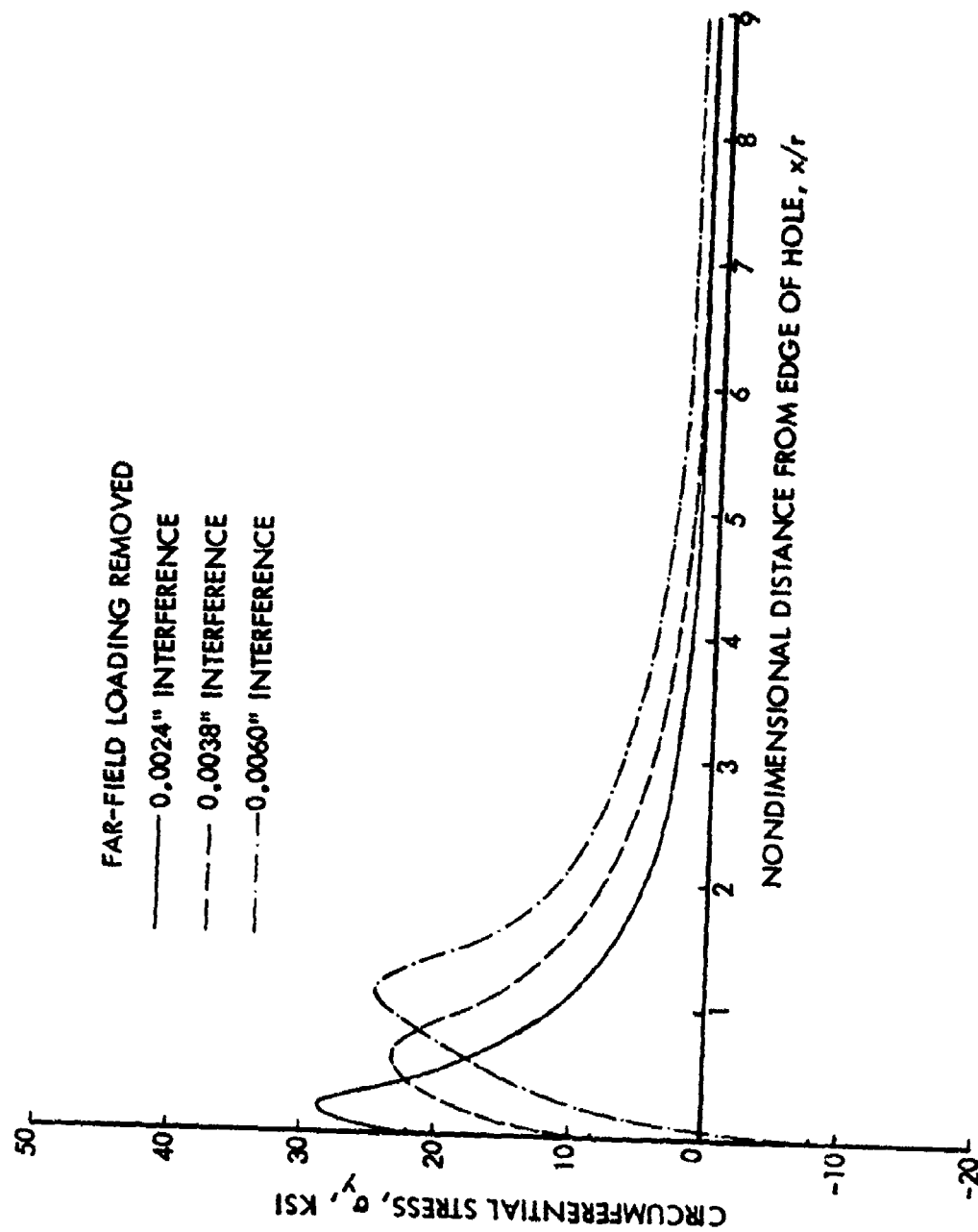


Figure 133 Unflawed Stress Distribution Along the x-Axis in 2219-T851 Aluminum Alloy Plates After Removal of the Far-Field Loading for Three Different Levels of Interference-Fit Fastener Holes

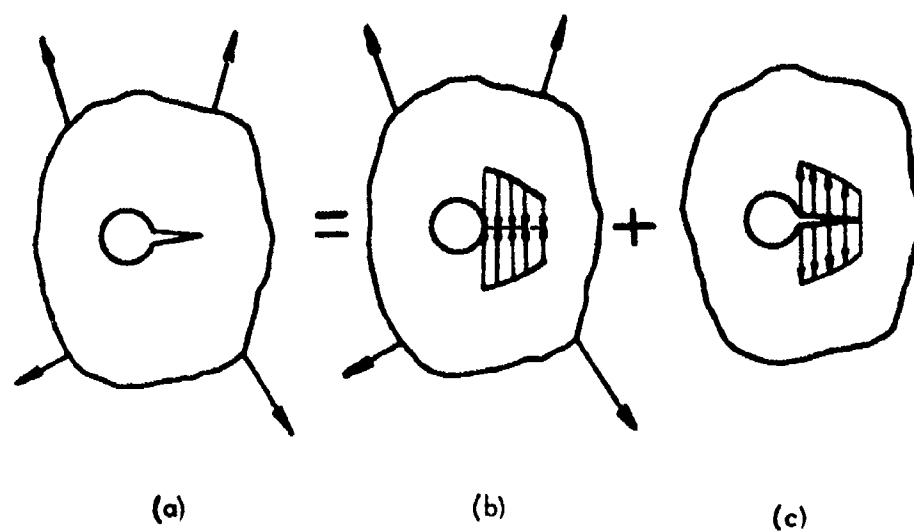


Figure 134 Schematic of Linear Superposition Method

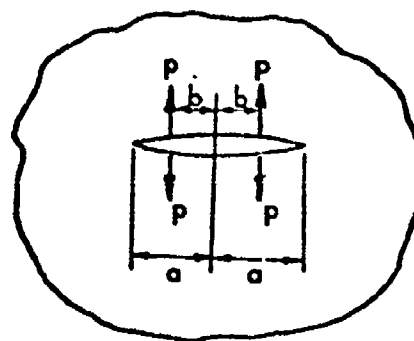


Figure 135 A Straight Crack Subjected to Two Pairs of Concentrated Forces on the Crack Surfaces

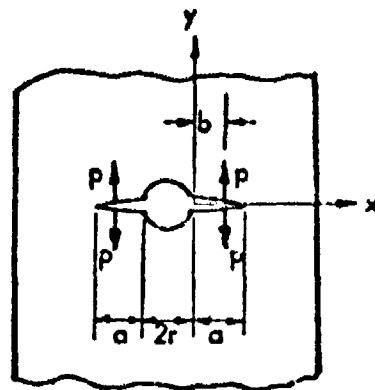


Figure 136 A Double Radial Crack Emanating from a Circular Hole
Subjected to Two Pairs of Concentrated Forces on the Crack Surfaces

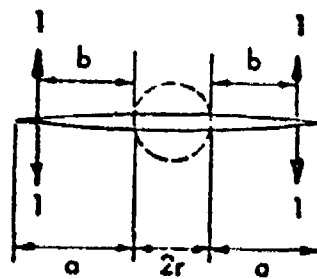


Figure 137 Idealization of the Hole as a Portion of a Straight Crack
When the Applied Forces Are Close to the Crack Tip

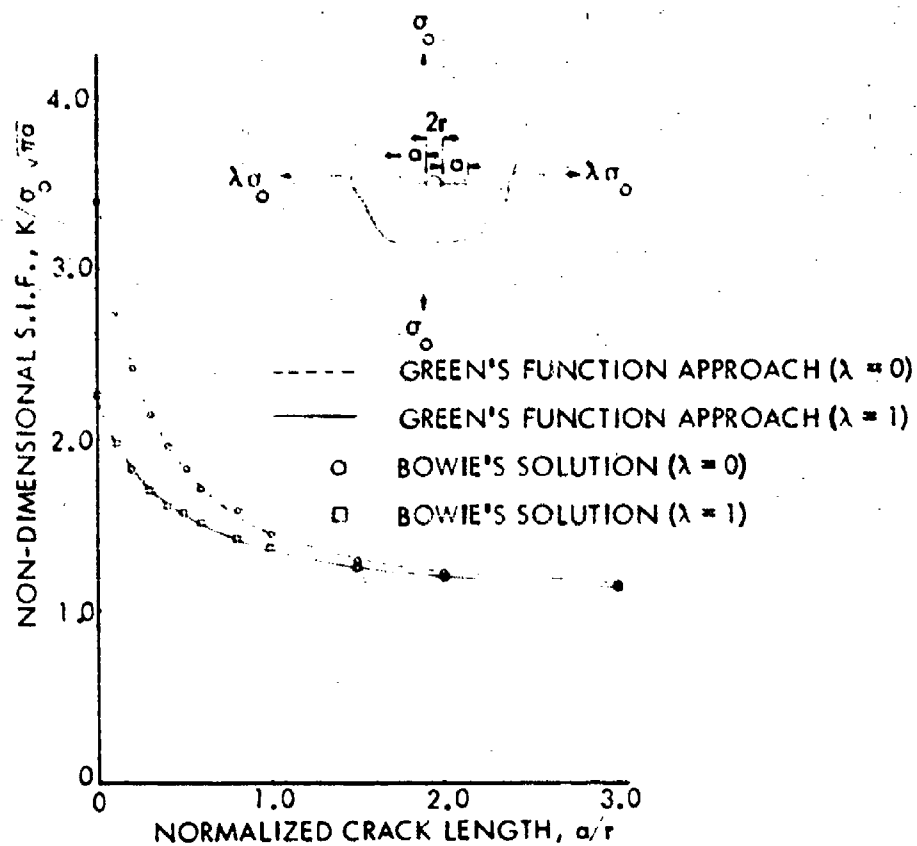


Figure 138 Normalized Stress Intensity Factors for a Double Crack Emanating from an Open Hole

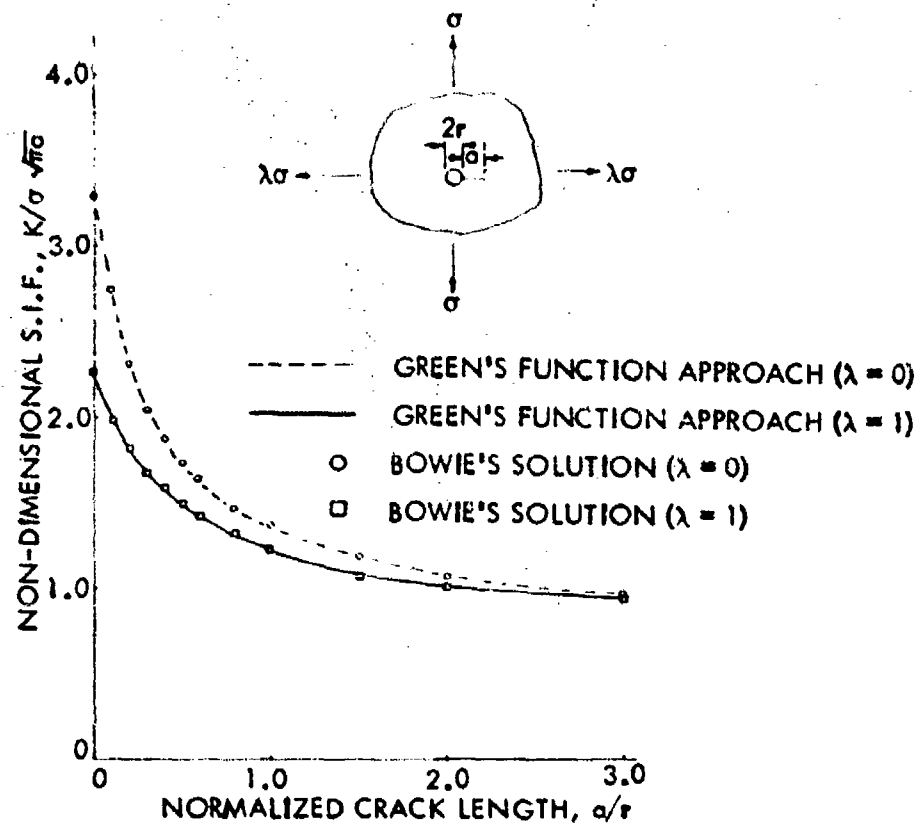


Figure 139 Normalized Stress Intensity Factors for a Single Crack Emanating from an Open Hole

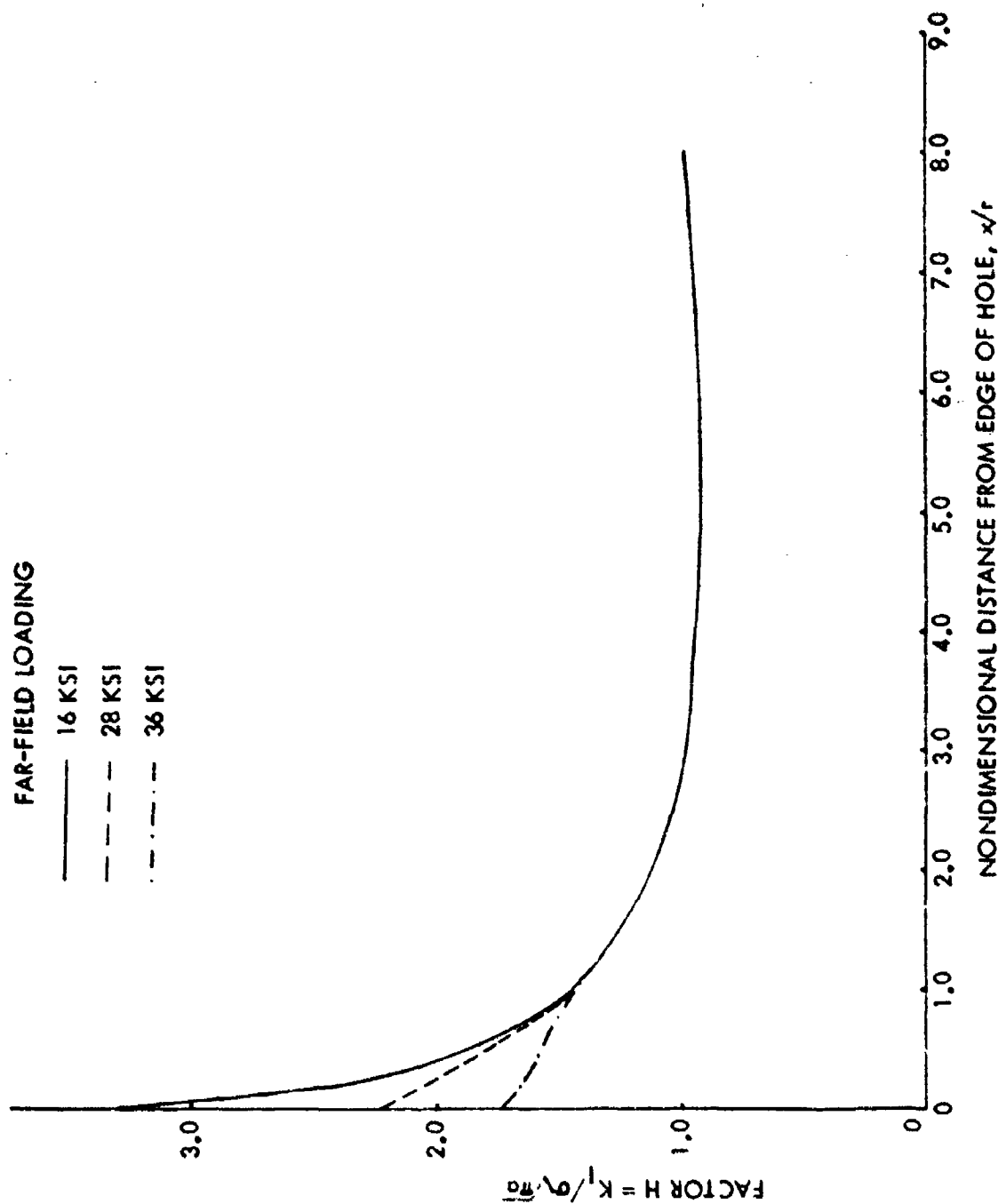


Figure 140. Normalized Stress Intensity Factors for Thru Cracks from an Open Hole in 2219-T851 Aluminum Plates Subjected to High Far-Field Loading (Accounting for Plasticity Effect)

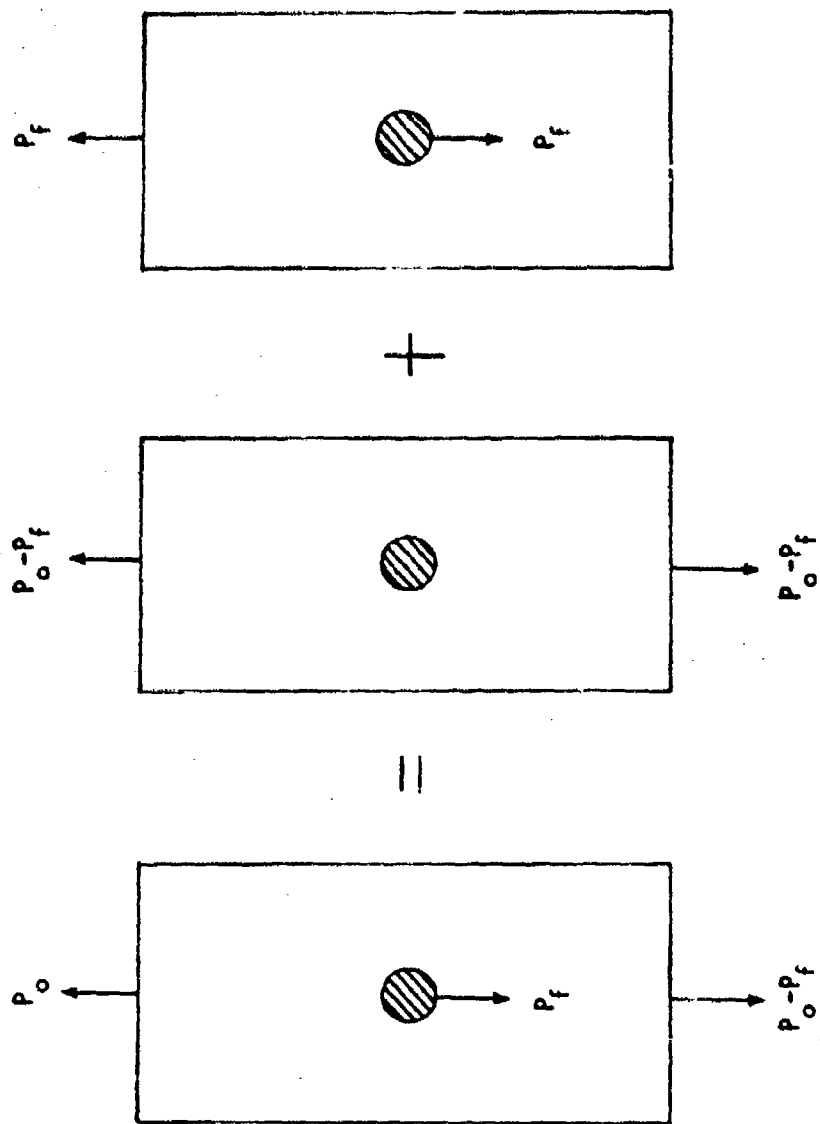


Figure 141 Illustration of Superposition Method

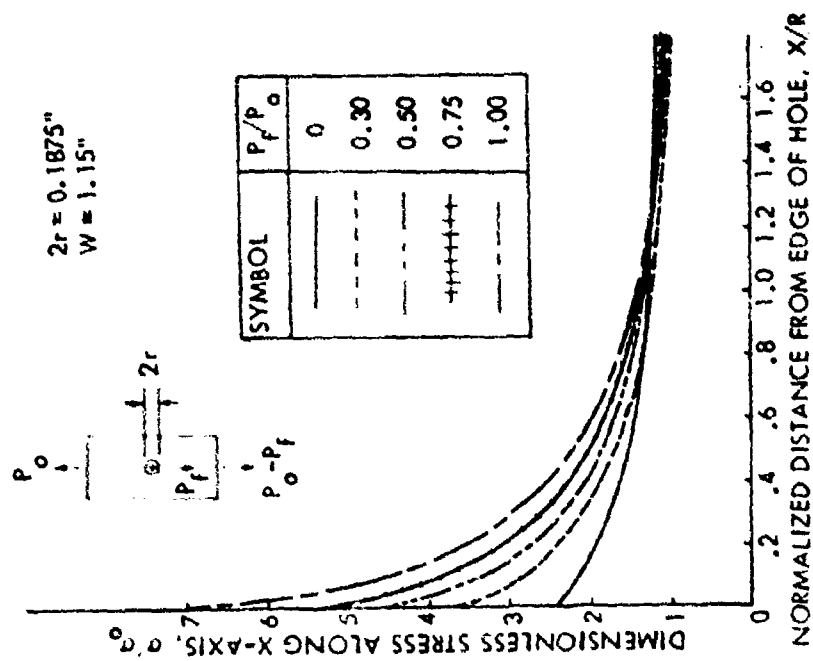


Figure 142 Normalized Unflawed Stress Distribution Along x-Axis in the Plate with Various Amounts of Fastener Load Transfer

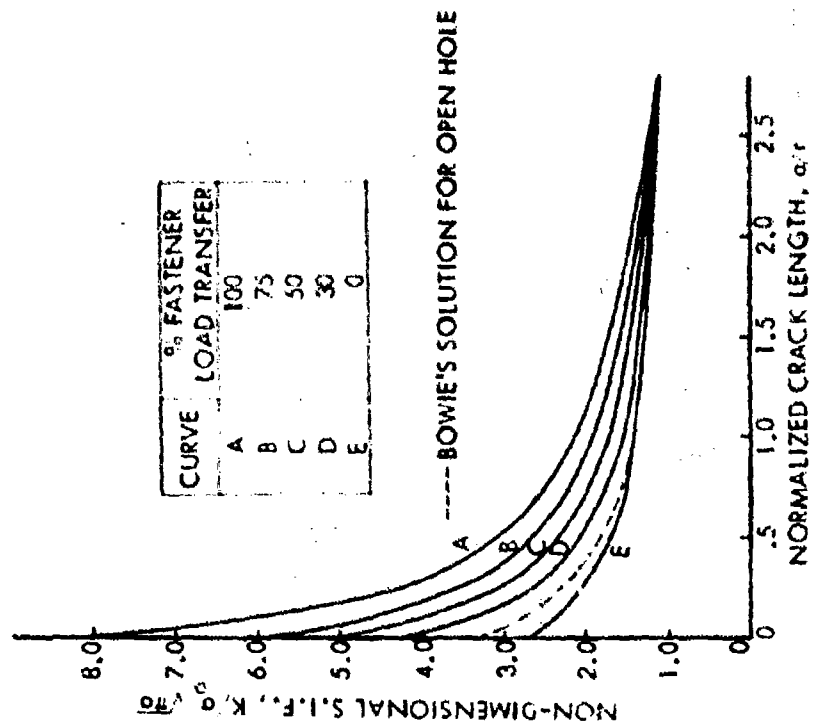


Figure 143 Normalized Stress Intensity Factors for a Double Crack Emanating from Neat-Fit Hole with Fraction of Fastener Load Transfer

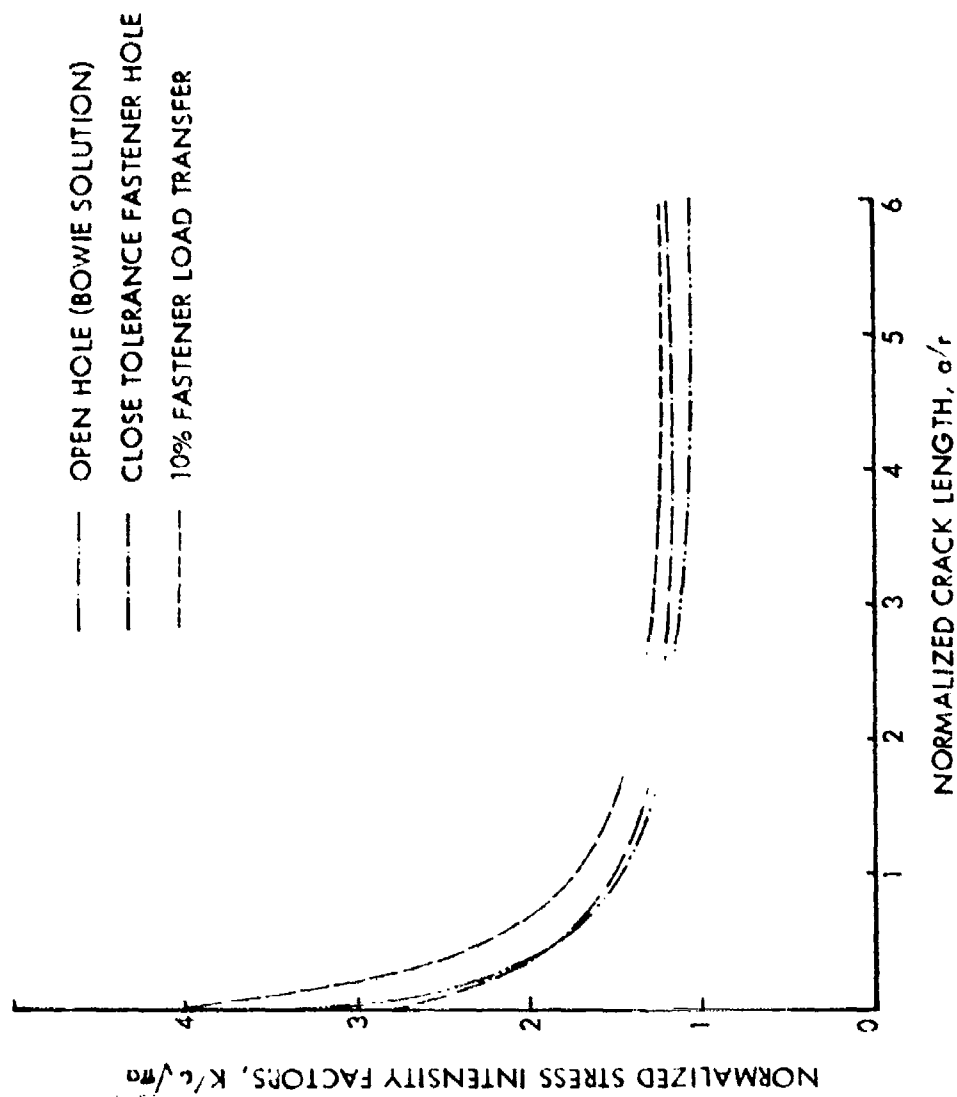


Figure 144. Normalized Stress Intensity Factors for Double Thru Cracks Emanating from an Open and Close Tolerance Fastener Holes With and Without Fastener Load Transfer in 2219-T851 Aluminum Plates

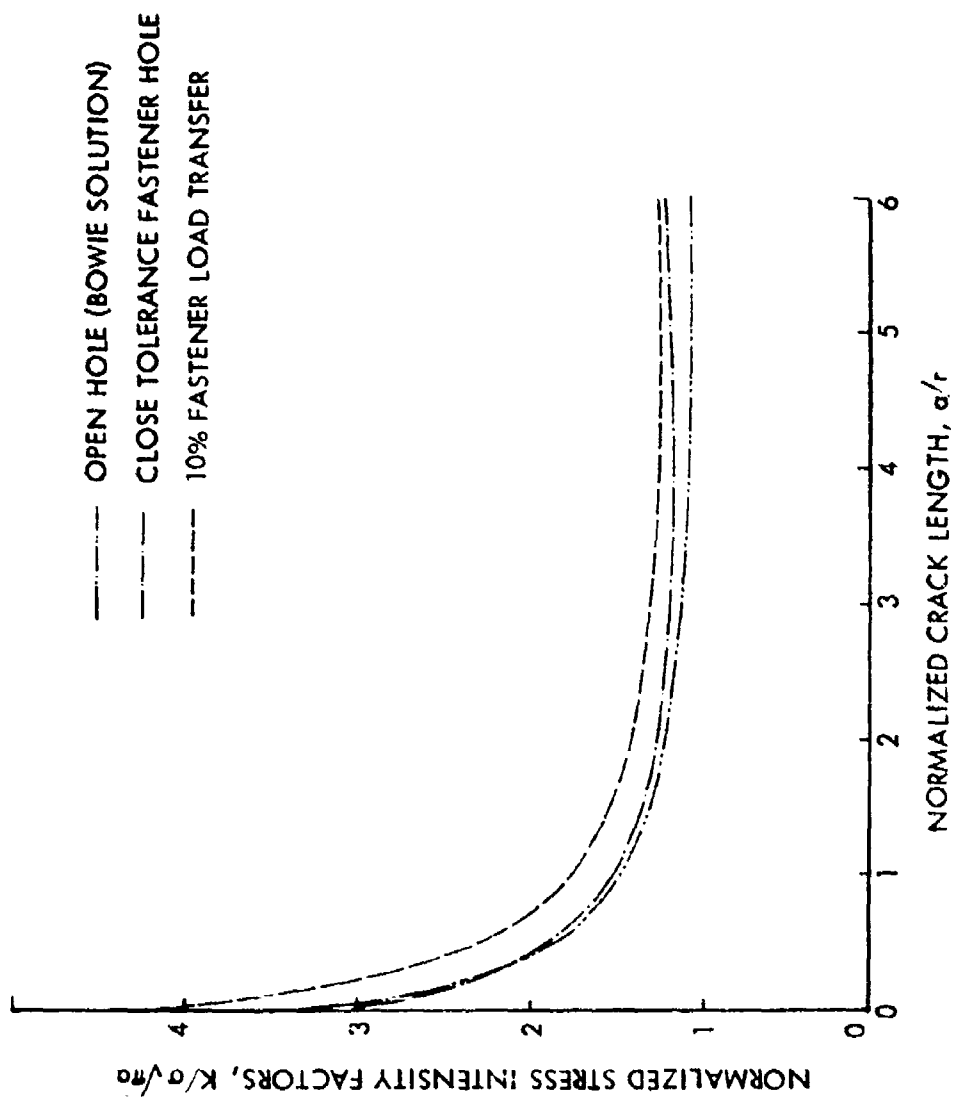


Figure 145. Normalized Stress Intensity Factors for Double Thru Cracks Emanating from an Open and Close Tolerance Fastener Holes With and Without Fastener Load Transfer in 6A-4V Beta Annealed Titanium Plates

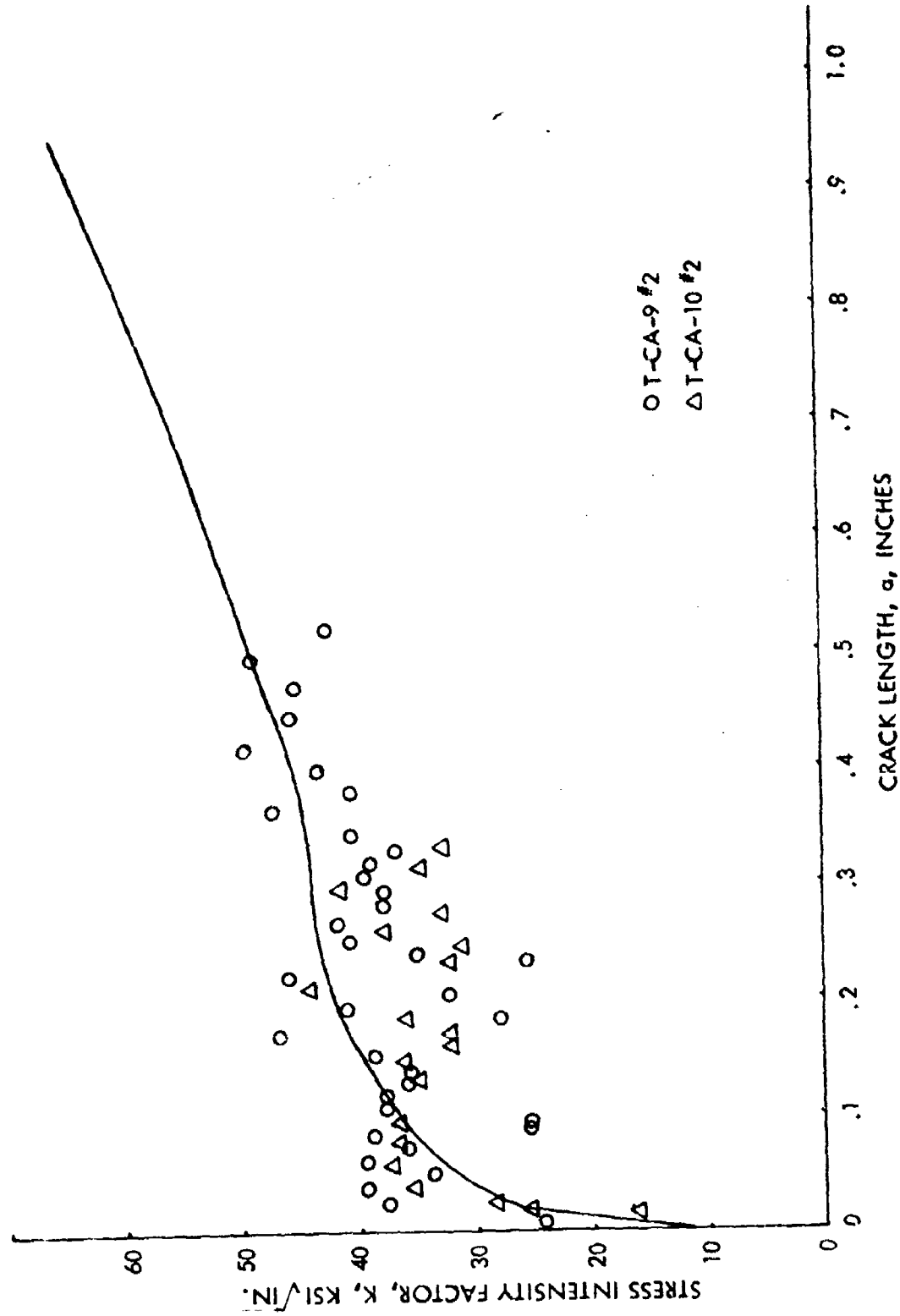


Figure 146 Stress Intensity Factors for a Single Thru Crack Emanating from a Close Tolerance Fastener Hole in 6Al-4V BA Titanium Plate Subjected to 40 Ksi Far-Field Loading

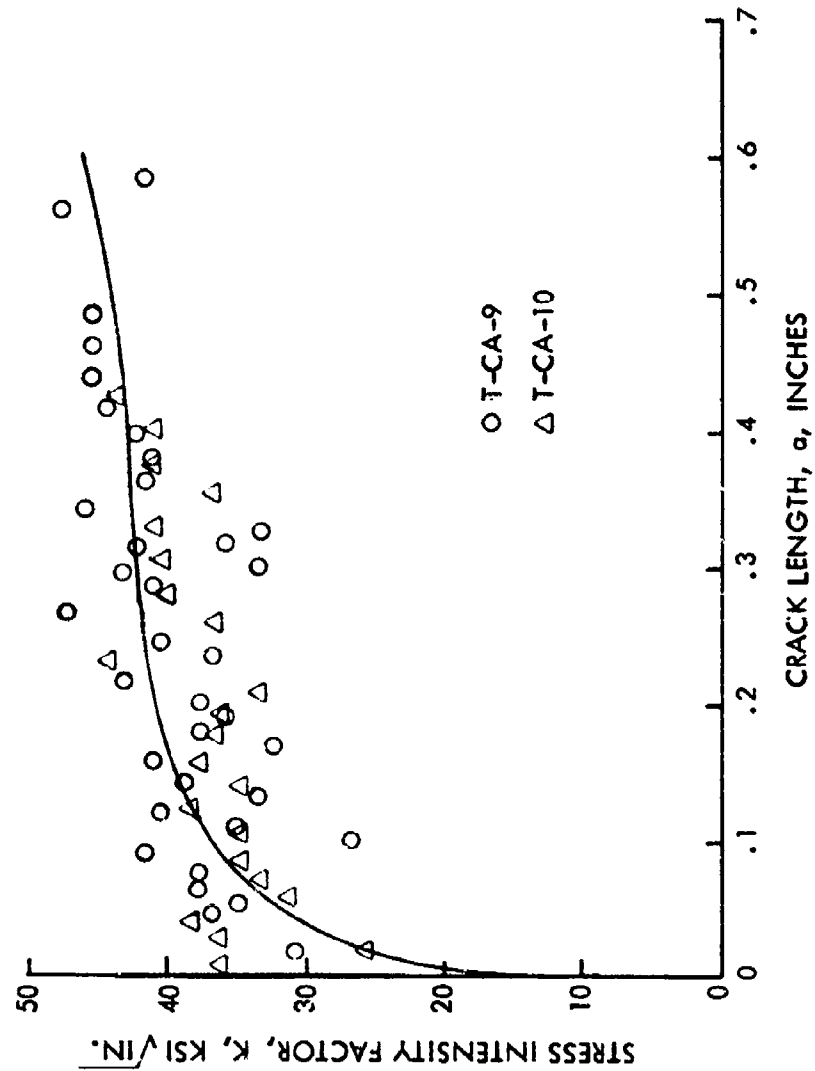


Figure 147 Stress Intensity Factors for a Single Thru Crack Emanating from a Close Tolerance Fastener Hole Having 10% Fastener Load Transfer in 6Al-4V β A Titanium Plate Subjected to 40 Ksi Far-Field Loading

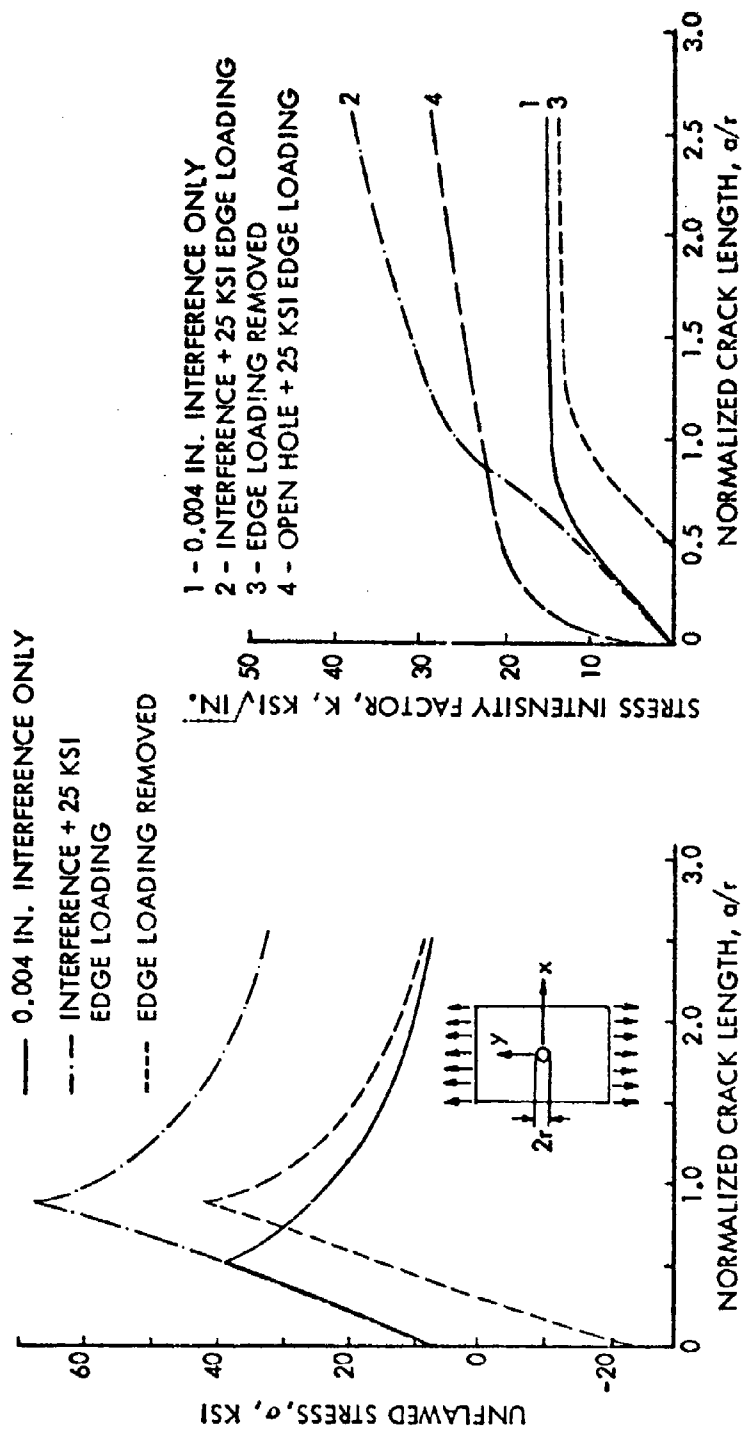


Figure 148 Stress σ at $y = 0$ in an Aluminum Plate with a Steel Interference-Fit Fastener Caused by Interference, Edge Loading and Unloading

Figure 149 Stress Intensity Factors for a Double Crack Emanating from an Interference-Fit Fastener Hole

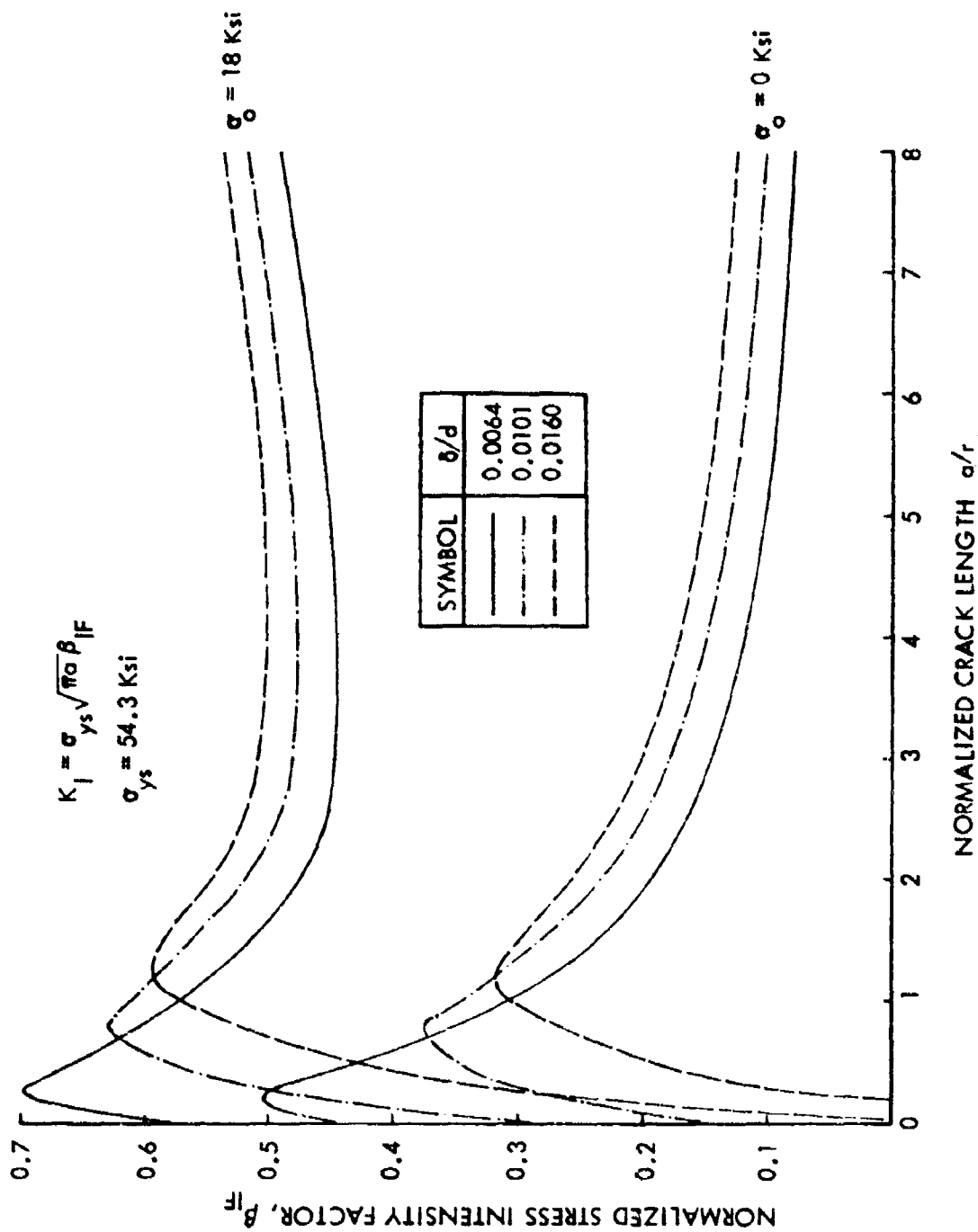


Figure 150. Normalized Stress Intensity Factors for Double Thru Cracks Emanating from Interference-Fit Fastener Holes in 2219-T851 Aluminum Plates Subjected to 18 Ksi Far-Field Loading and Subsequent Unloading

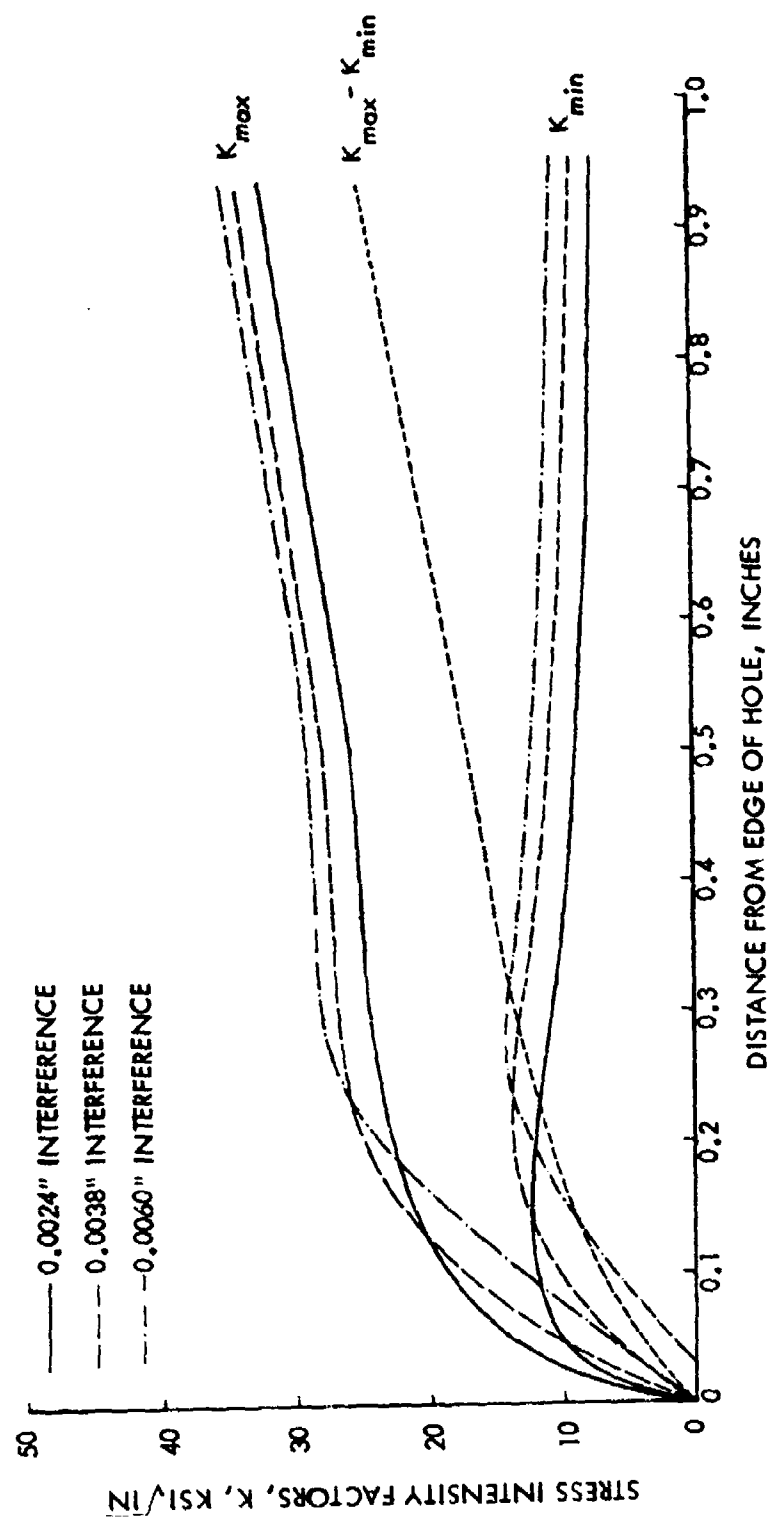


Figure 151. Stress Intensity Factors for Single Thru Cracks Emanating from Interference-Fit Fastener Holes for Various Levels of Interference in 2219-T851 Aluminum Alloy Plates Subjected to 18 Ksi Far-Field Loading and Subsequent Unloading

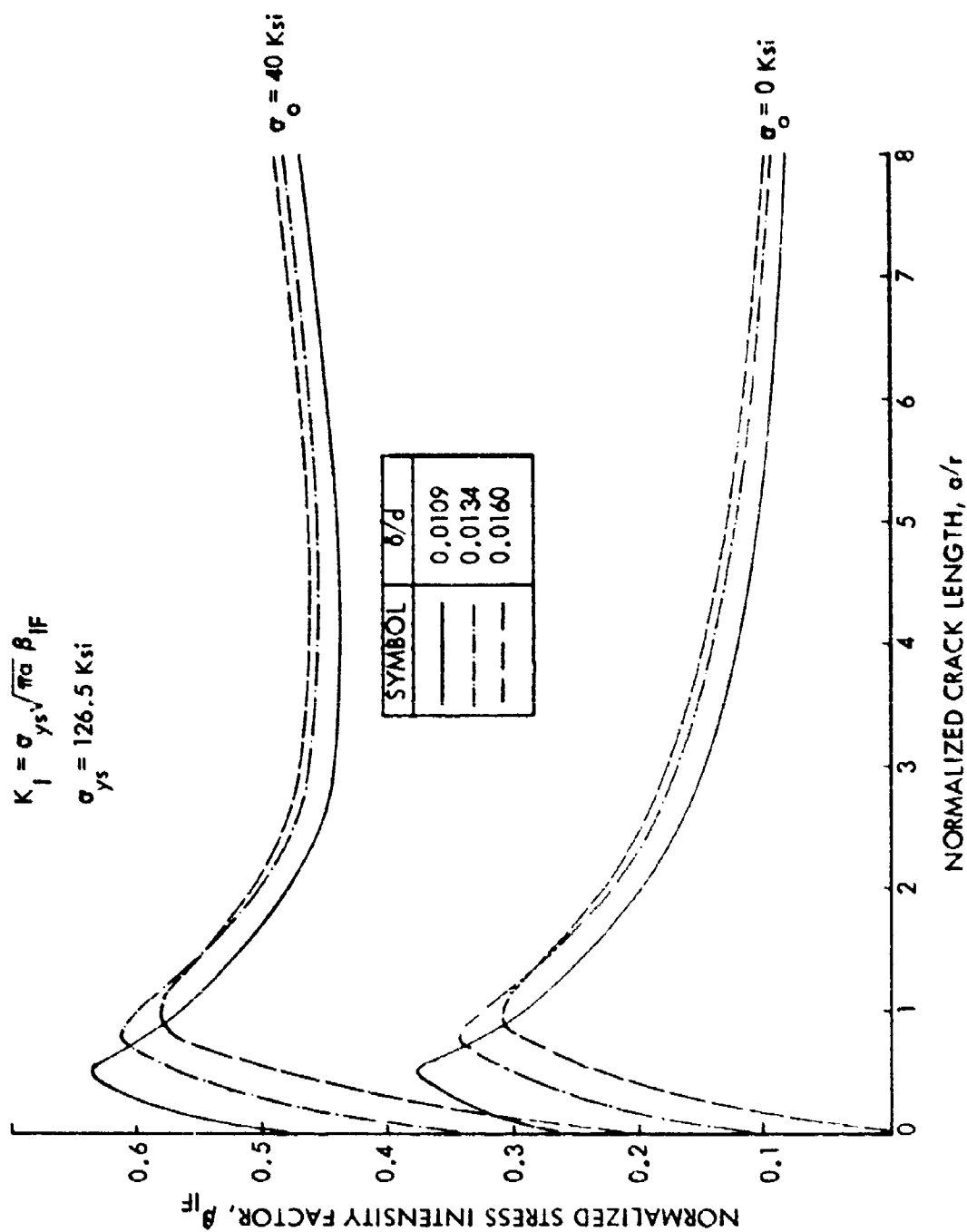


Figure 152. Normalized Stress Intensity Factors for Double Thru Cracks Emanating from Interference-Fit Fastener Holes in 6Al-4V Beta Annealed Titanium Plates Subjected to 40 Ksi Far-Field Loading and Subsequent Unloading

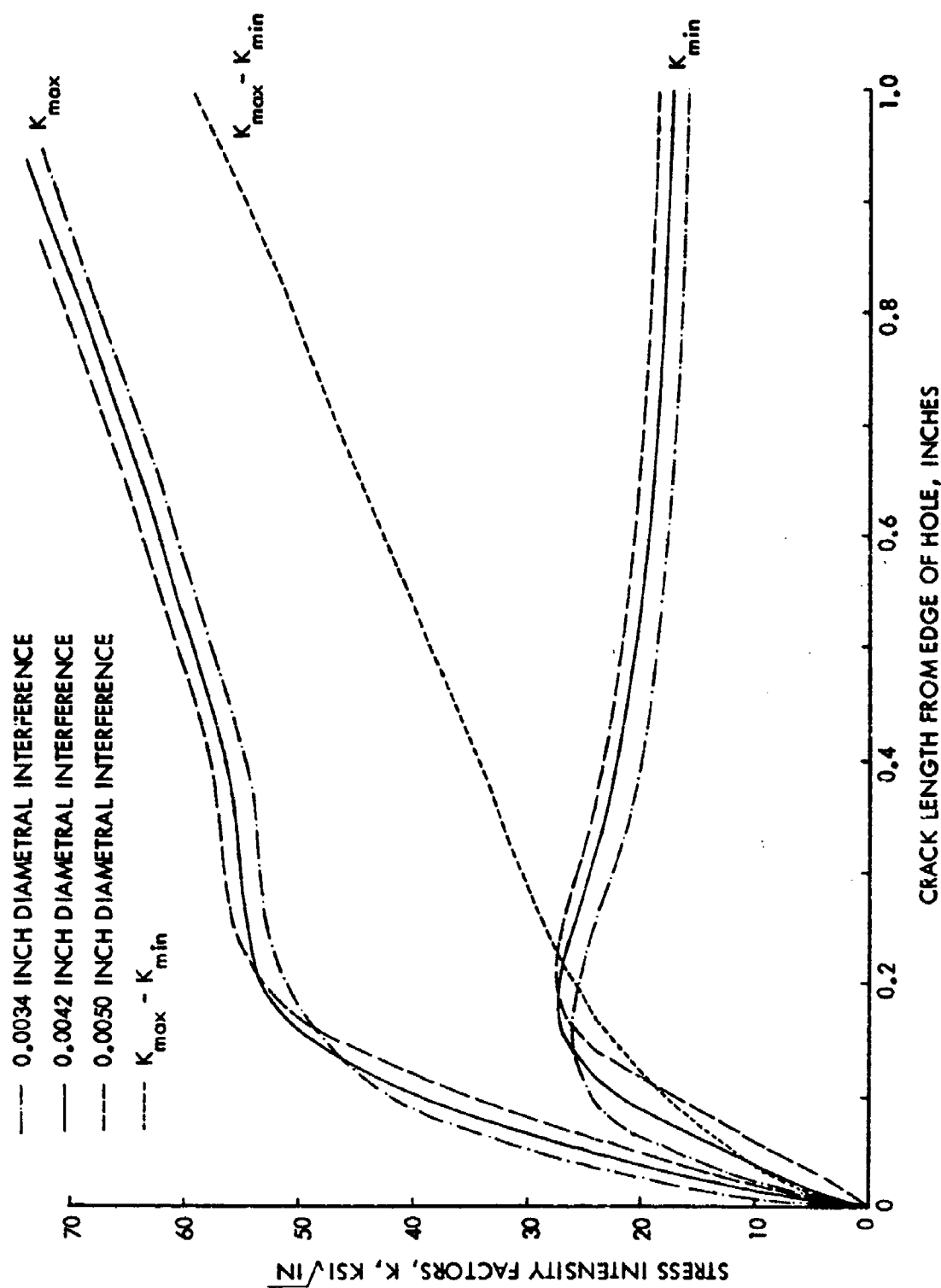


Figure 153. Stress Intensity Factor for Single Thru Cracks Emanating from Interference-Fit Fastener Holes for Various Levels of Interference in 6Al-4V Beta Annealed Titanium Plates Subjected to 40 Ksi Far-Field Loading and Subsequent Unloading

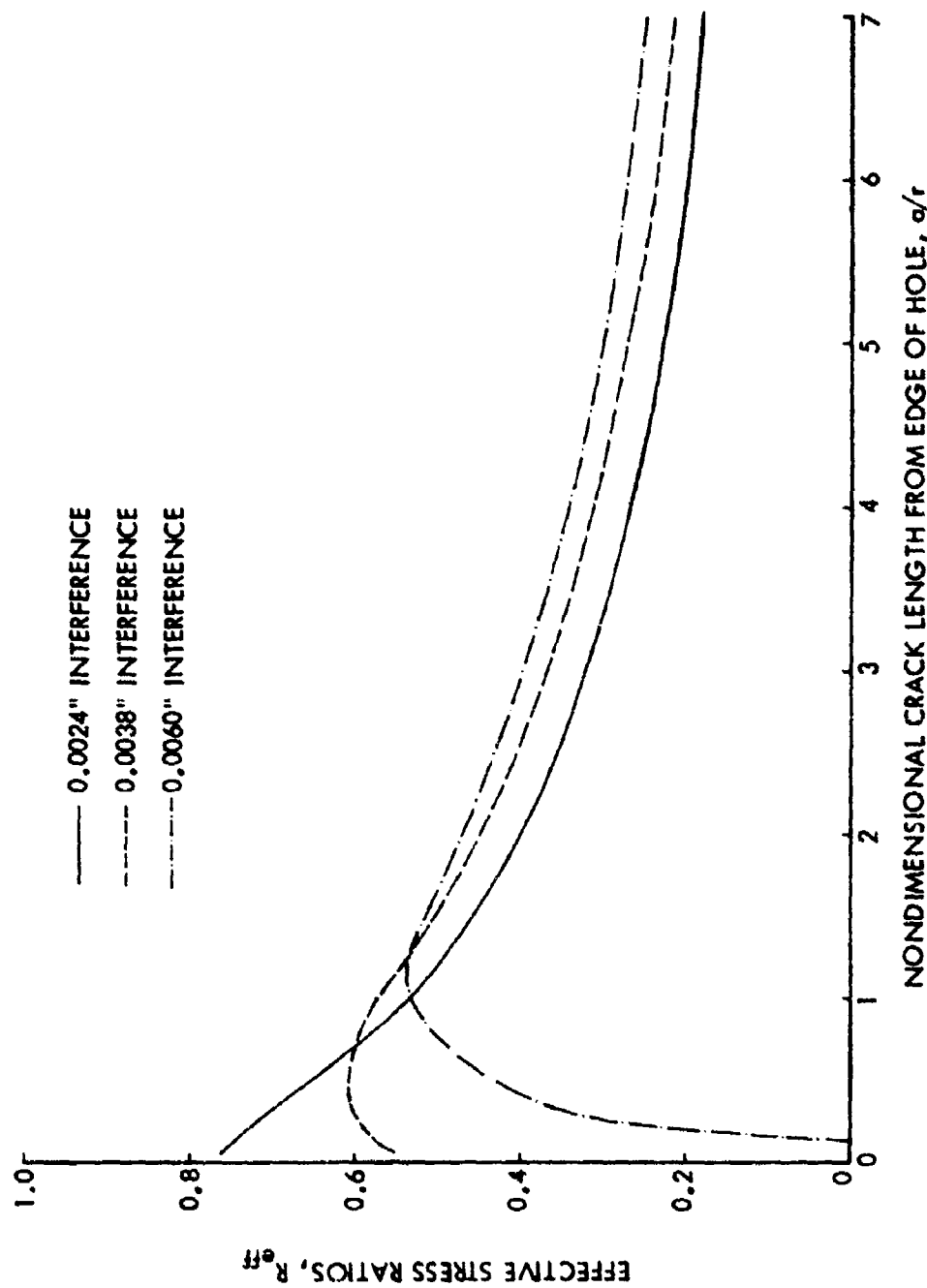


Figure 154. Effective Stress Intensity Factor Ratios for Single Thru Cracks Emanating from Interference-Fit Fastener Holes for Various Levels of Interference in 2219-T851 Aluminum Plates Subjected to Constant Amplitude 18 Ksi and $R = +0.1$ Far-Field Loading

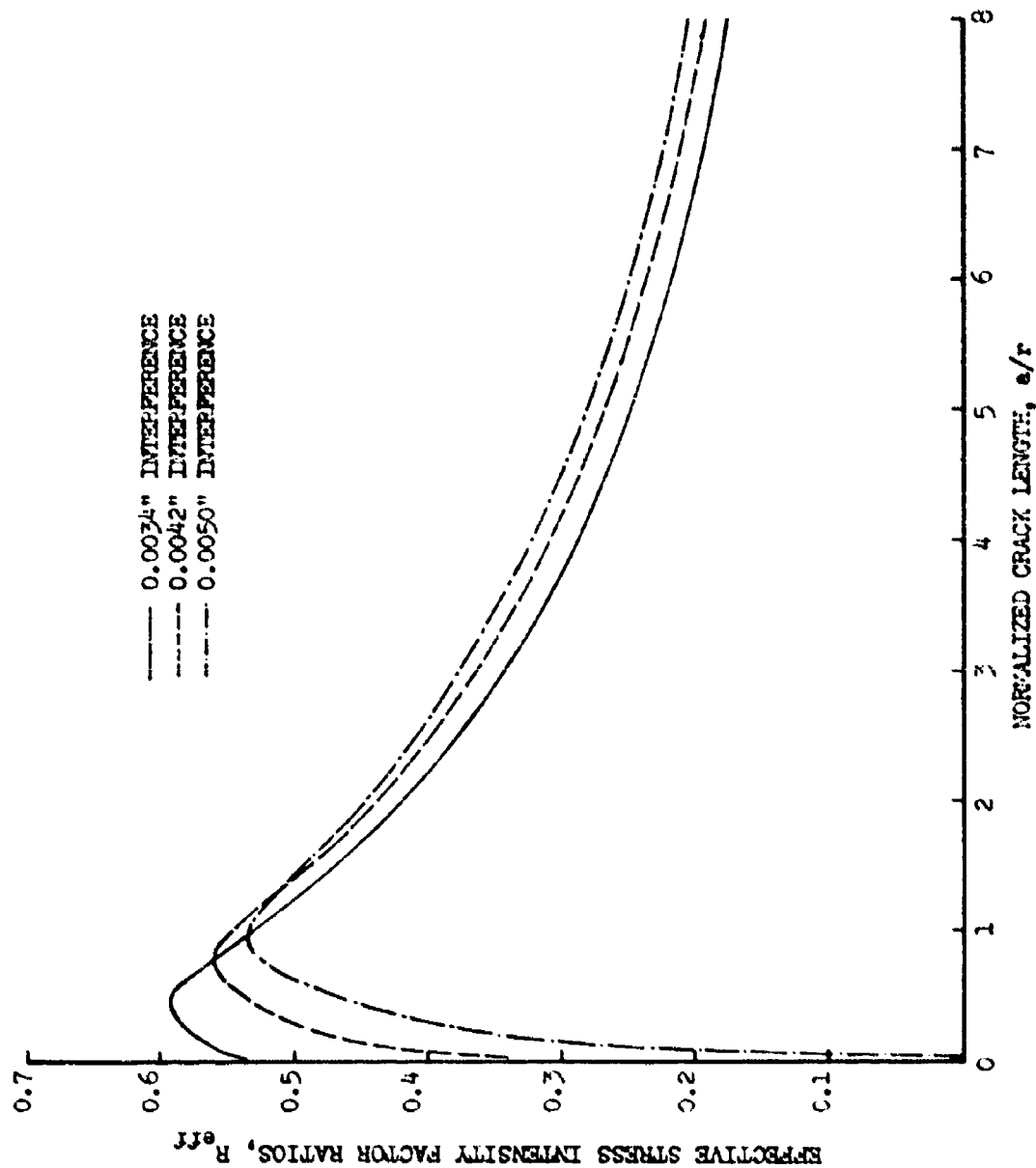


Figure 155. Effective Stress Intensity Factor Ratios for Single Thru Cracks Emanating from Interference-Fit Fastener Holes for Various Levels of Interference in 6Al-4V Beta Annealed Titanium Plates Subjected to Constant Amplitude 40 Ksi and $R = +0.1$ Far-Field Loading

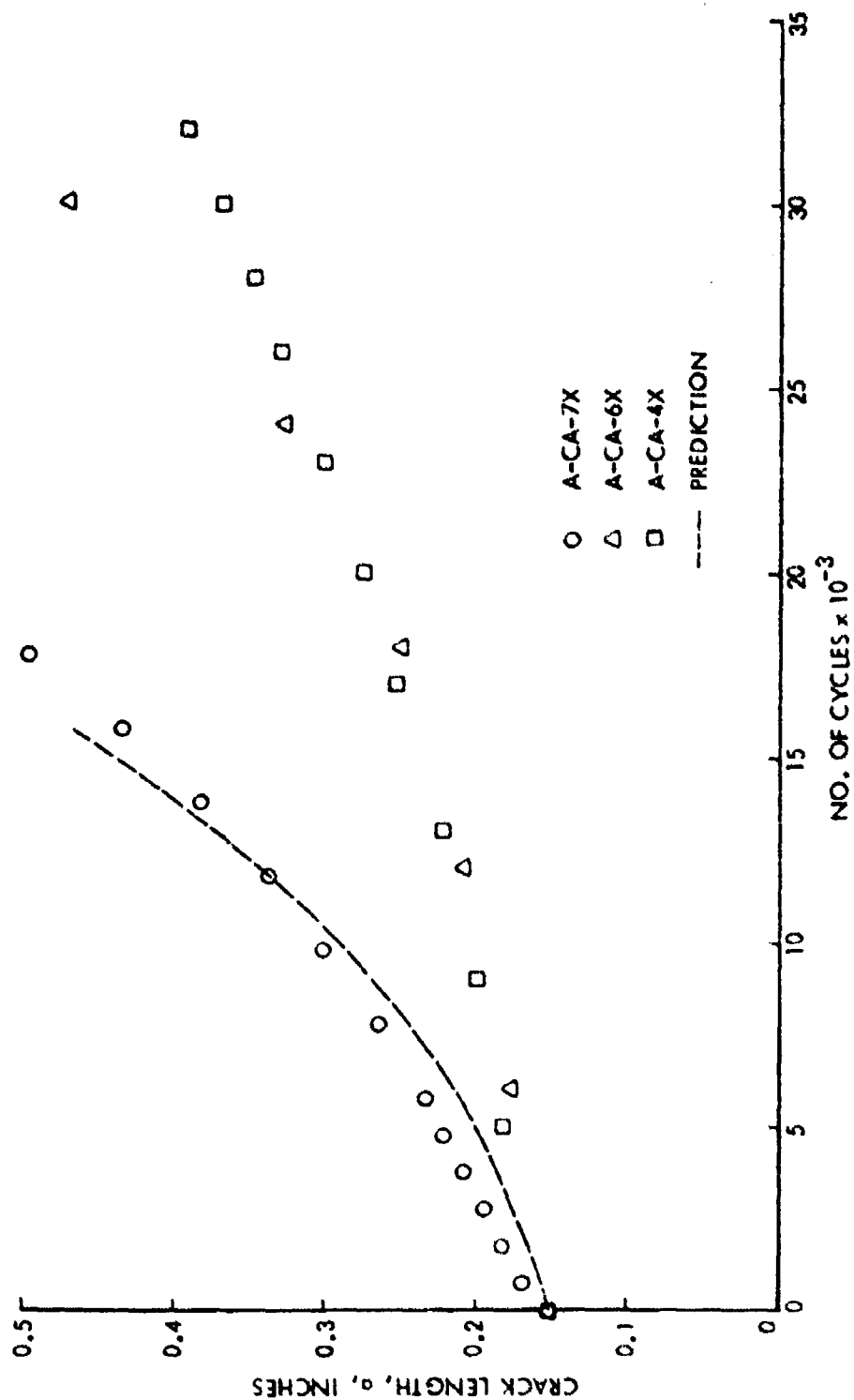


Figure 156 Crack Growth from 0.0024 Inch Diametrical Interference-Fit Fastener Holes in 2219-T851 Aluminum Alloy Plates Subjected to Constant Amplitude Far-Field Loading ($\sigma = 18$ Ksi and $R = 0.1$)

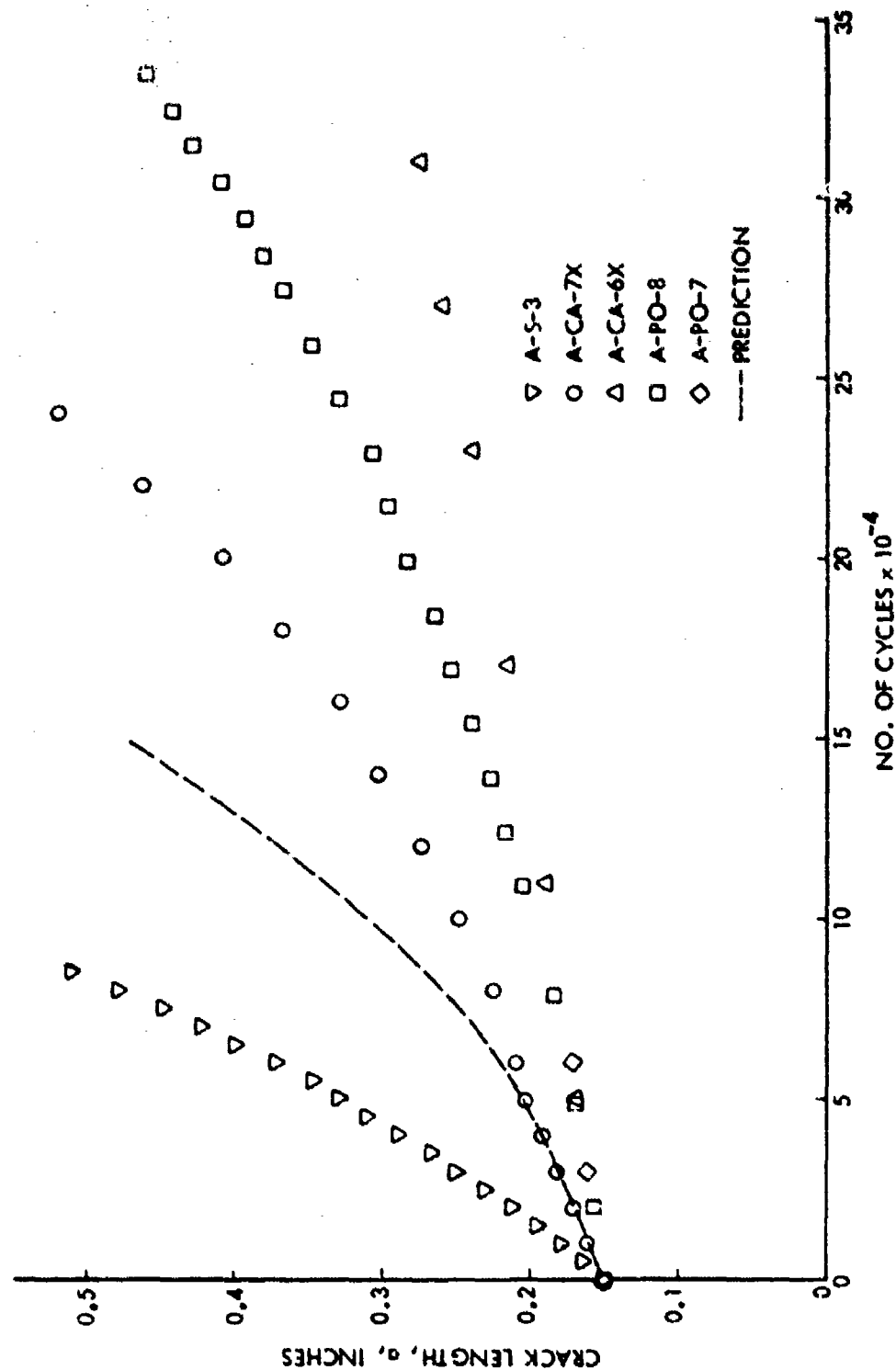


Figure 157 Crack Growth from 0.0038 Inch Diametrical Interference-Fit Fastener Holes in 2219-T8S1 Aluminum Alloy Plates Subjected to Constant Amplitude Far-Field Loading ($\sigma = 18$ Ksi and $R = 0.1$)

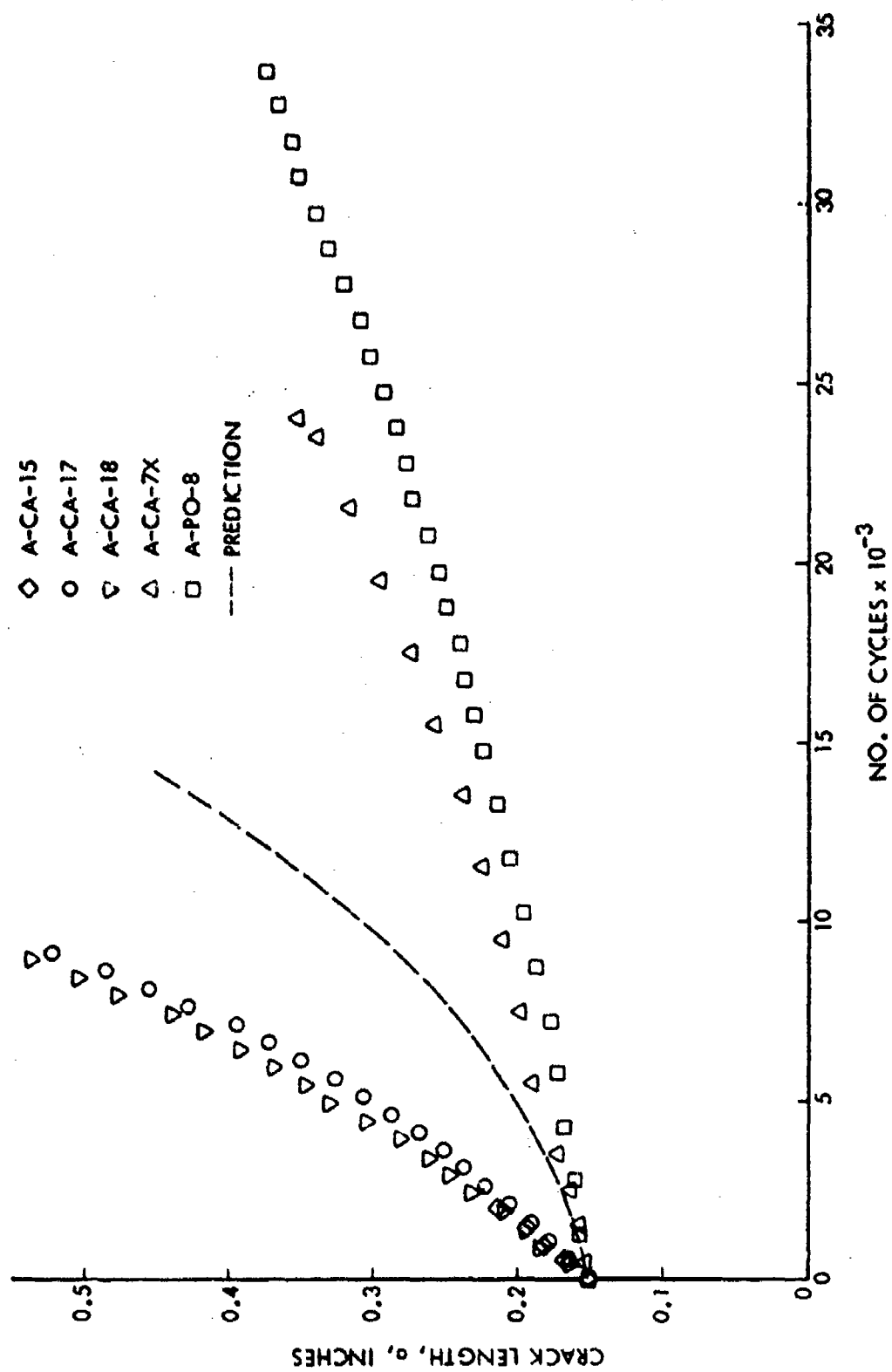


Figure 158 Crack Growth from 0.0060 Inch Diametrical Interference-Fit Fastener Holes in 2219-T851 Aluminum Alloy Plates Subjected to Constant Amplitude Far-Field Loading ($\sigma = 18$ Ksi and $R = 0.1$)

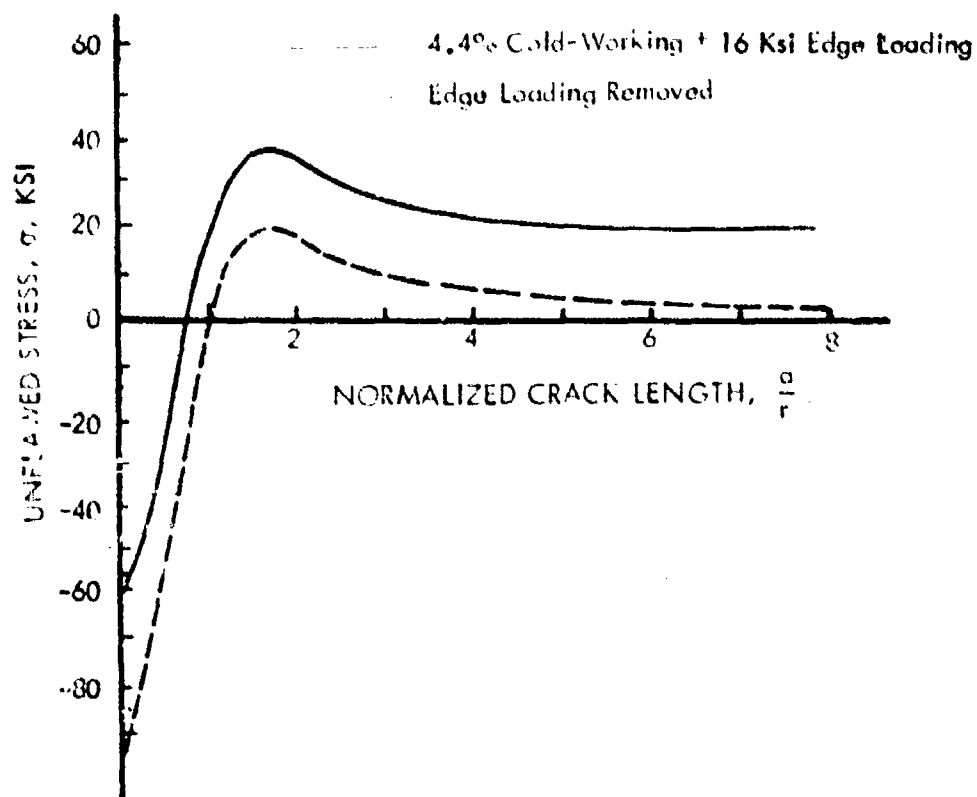


Figure 159 Stress at the Region of 4.4% Cold-Worked Hole in 7075-T6 Aluminum Plate Carried by 16 Ksi Edge Loading and Subsequent Unloading

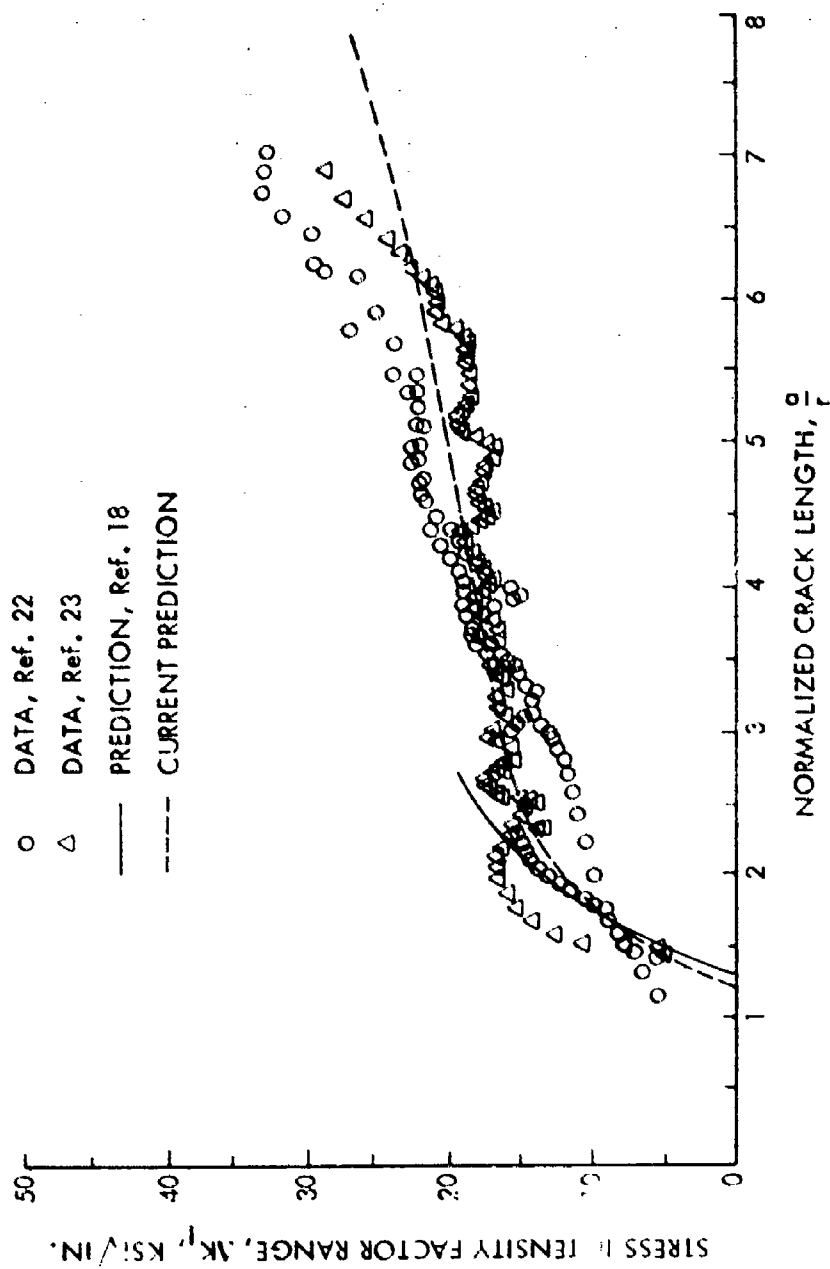


Figure 160. Stress Intensity Factors for a Single Thru Crack Emanating from Cold-Worked Hole

$$K_I = \sigma_{ys} \sqrt{\pi a} \beta_{CW}$$

$$\sigma_{ys} = 54.3$$

$$\sigma_o = 18 \text{ Ksi}$$

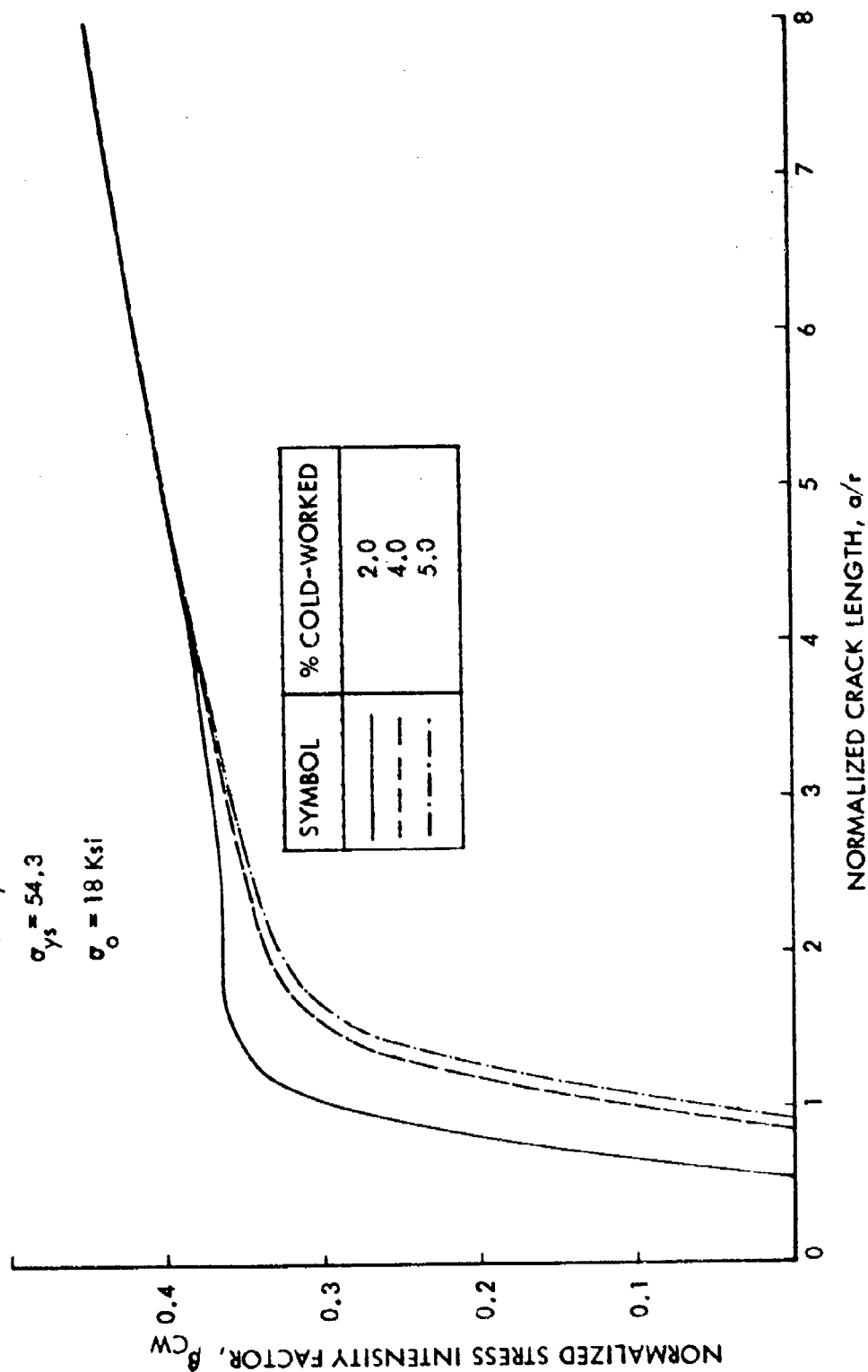


Figure 161. Normalized Stress Intensity Factors for Double Thru Cracks Emanating from Cold-Worked Open Holes in 2219-T851 Aluminum Plates Subjected to 18 Ksi Far-Field Loading

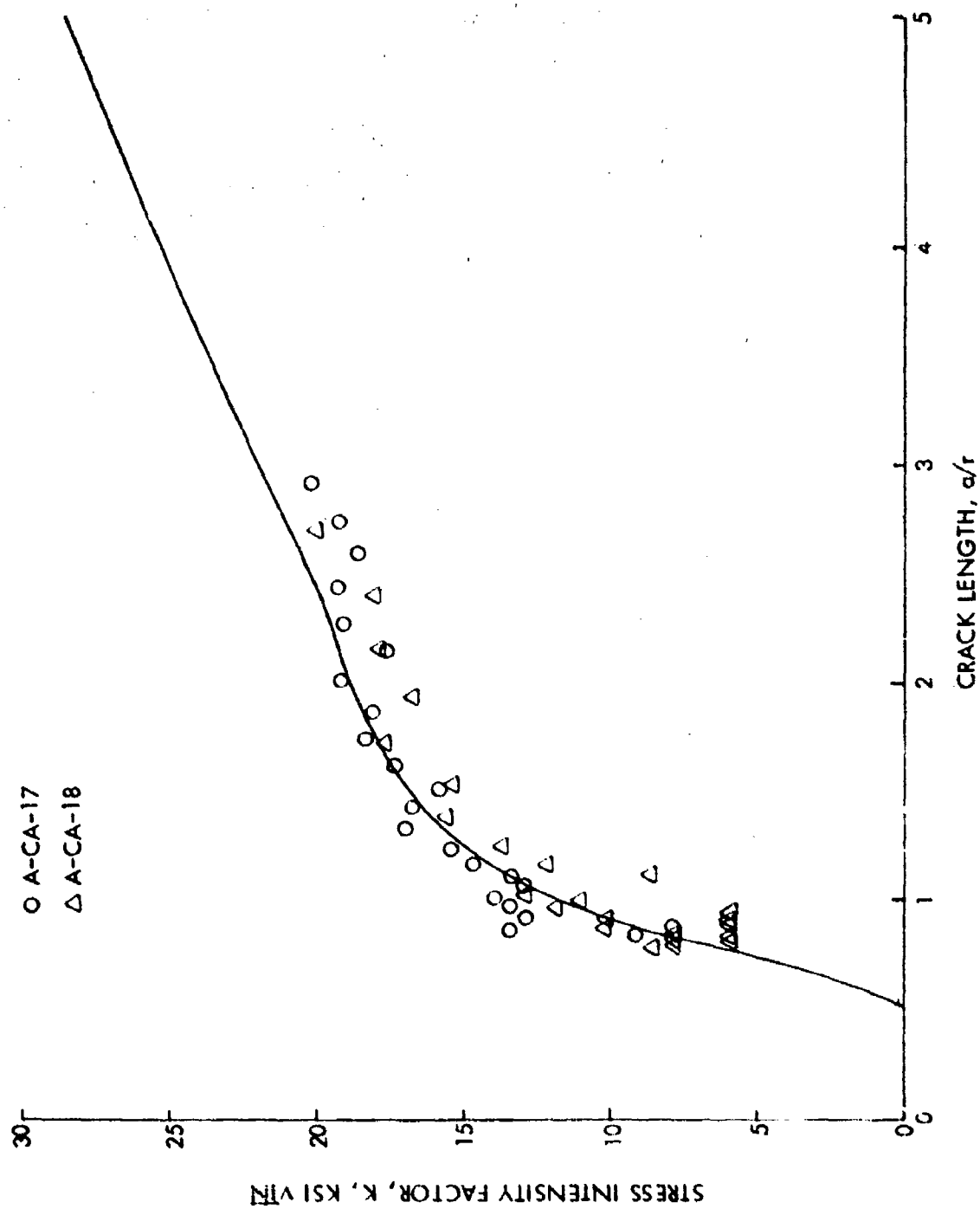


Figure 162. Stress Intensity Factors for a Single Thru Crack Emulating from Level 1 Cold-Worked Open Hole in 2219-T851 Aluminum Plate Subjected to Uniform Far-Field Loading

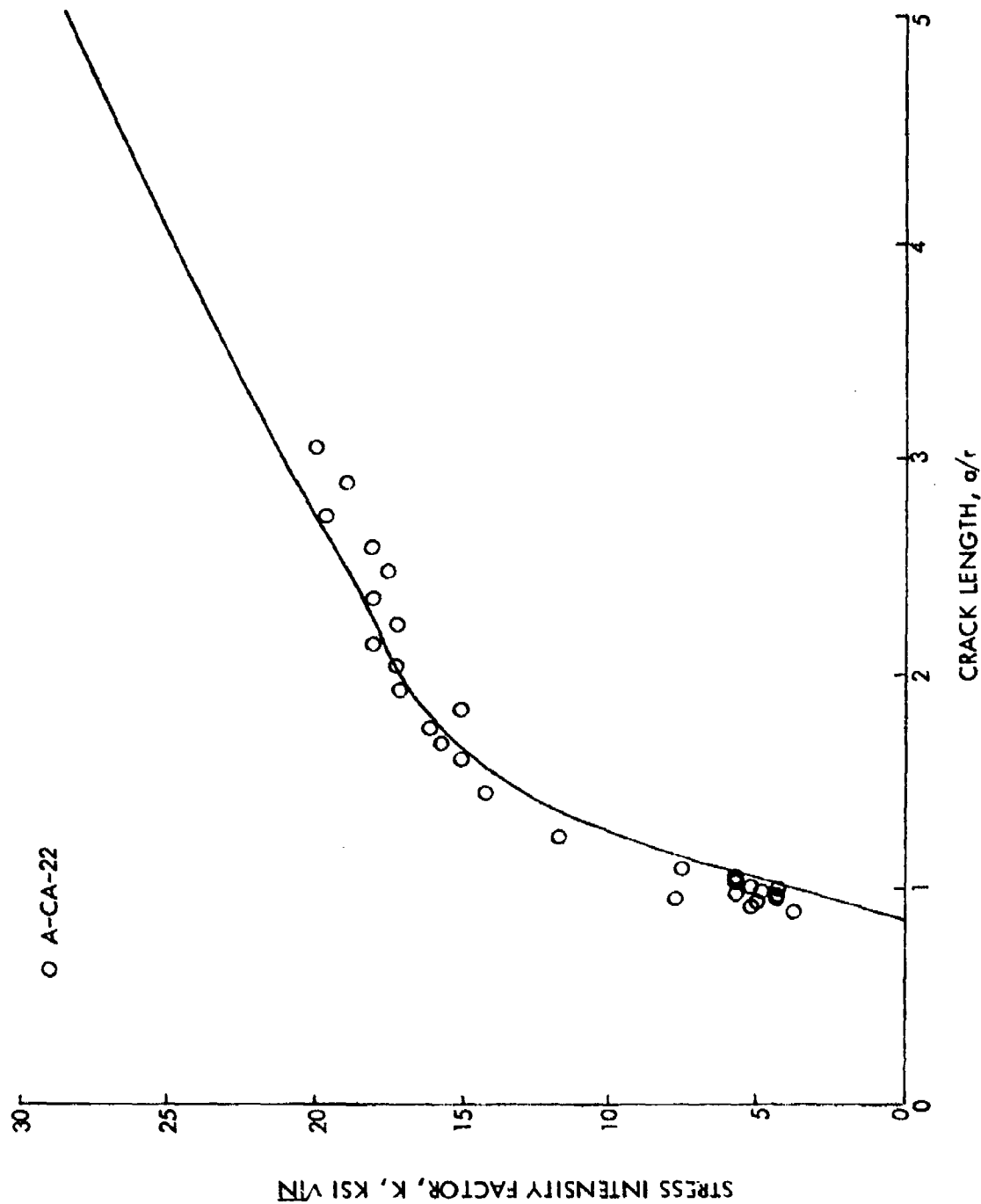


Figure 163. Stress Intensity Factors for a Single Thru Crack Emanating from Level 2 Cold-Worked Open Hole in 2219-T851 Aluminum Plate Subjected to Uniform Far-Field Loading ($\sigma = 18$ Ksi)

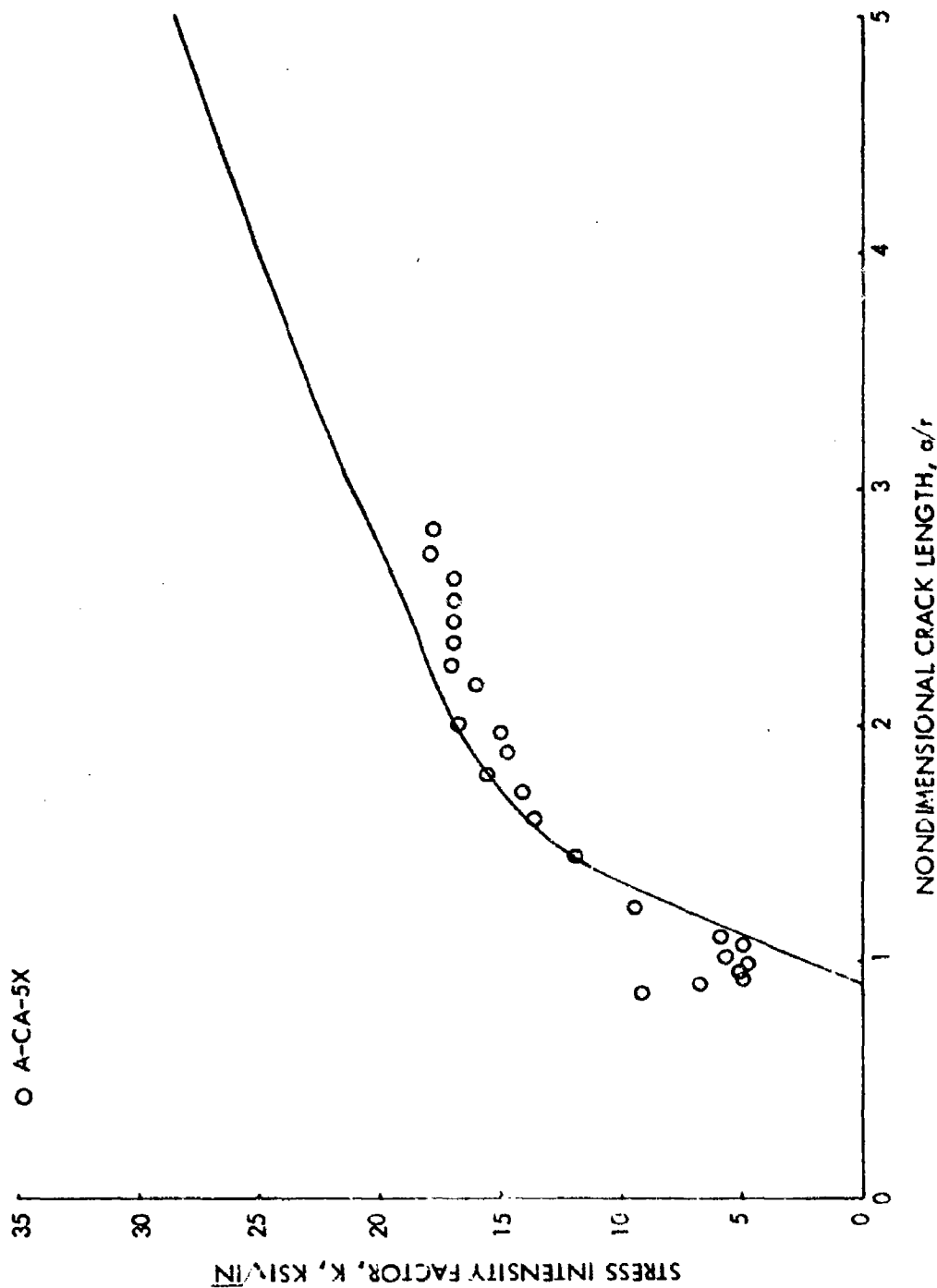


Figure 164. Stress Intensity Factors for a Single Thru Crack Emanating from Level 3 Cold-Worked Open Hole in 2219-T851 Aluminum Plate Subjected to Uniform Far-Field Loading (18 Ksi)

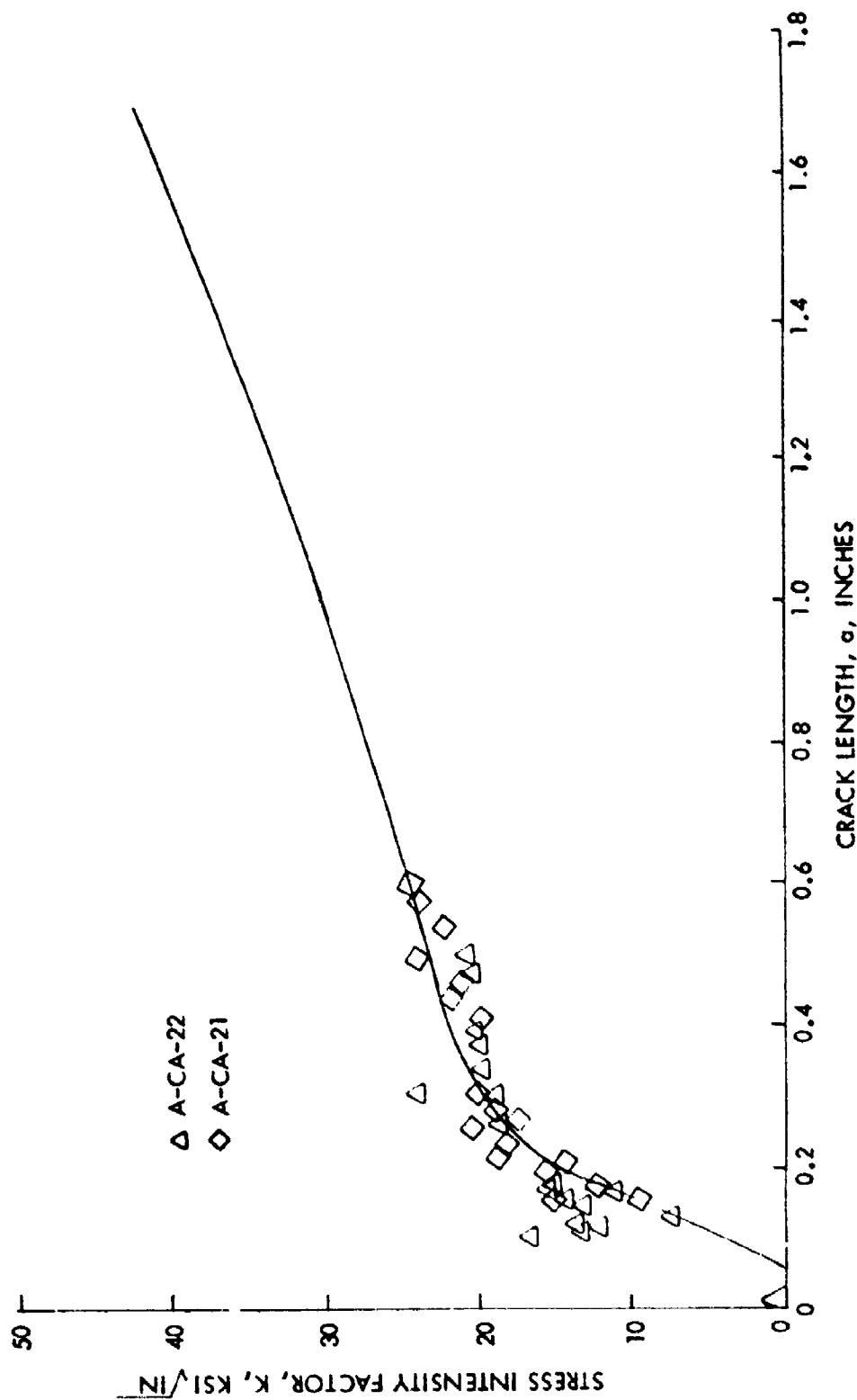


Figure 165. Stress Intensity Factors for a Single Thru Crack Emanating from Level 1 Cold-Worked Hole in 2219-T851 Aluminum Plate Subjected to 18 Ksi Far-Field Loading and 10% Fastener Load Transfer

$$K_I = \sigma_{ys} \sqrt{\pi a} \beta_{CW}$$

$$\sigma_{ys} = 126.5 \text{ Ksi}$$

$$\sigma_o = 40 \text{ Ksi}$$

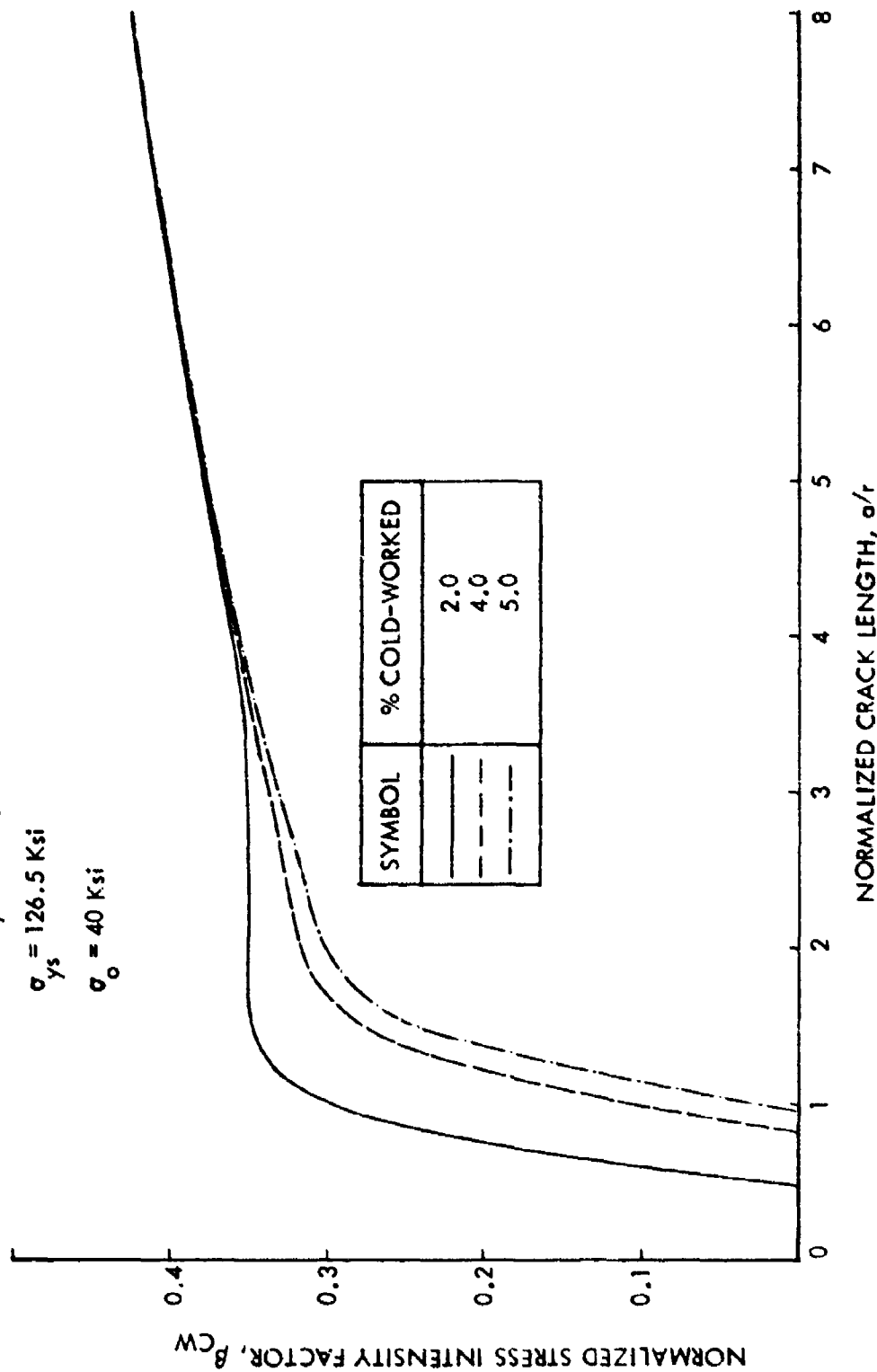


Figure 166. Normalized Stress Intensity Factors for Double Thru Cracks Emanating from Cold-Worked Open Holes in 6Al-4V Beta Annealed Titanium Plates Subjected to 40 Ksi Far-Field Loading

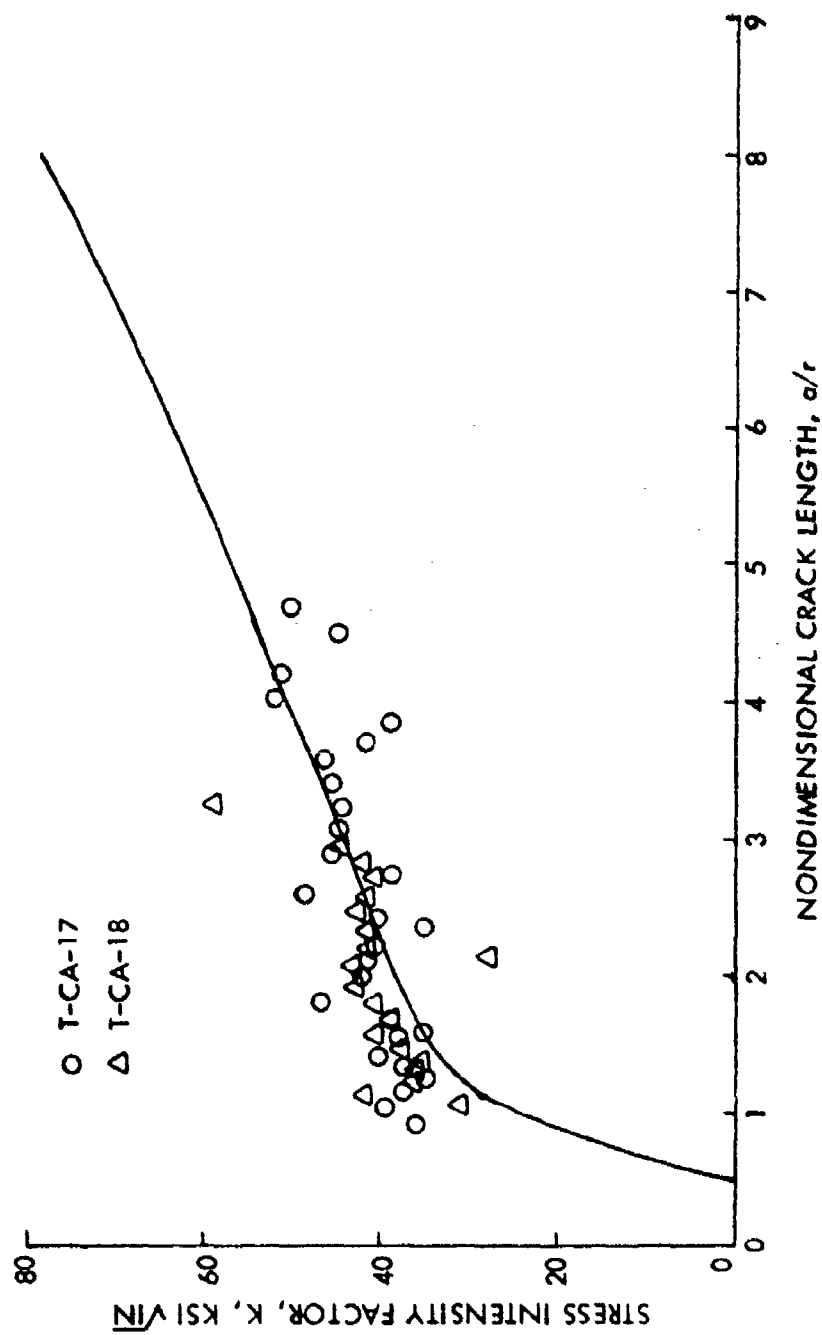


Figure 167. Stress Intensity Factors for a Single Thru Crack Emanating from Level 1 Cold-Worked Open Hole in 6Al-4V Beta Annealed Titanium Alloy Plate Subjected to Uniform Far-Field Loading

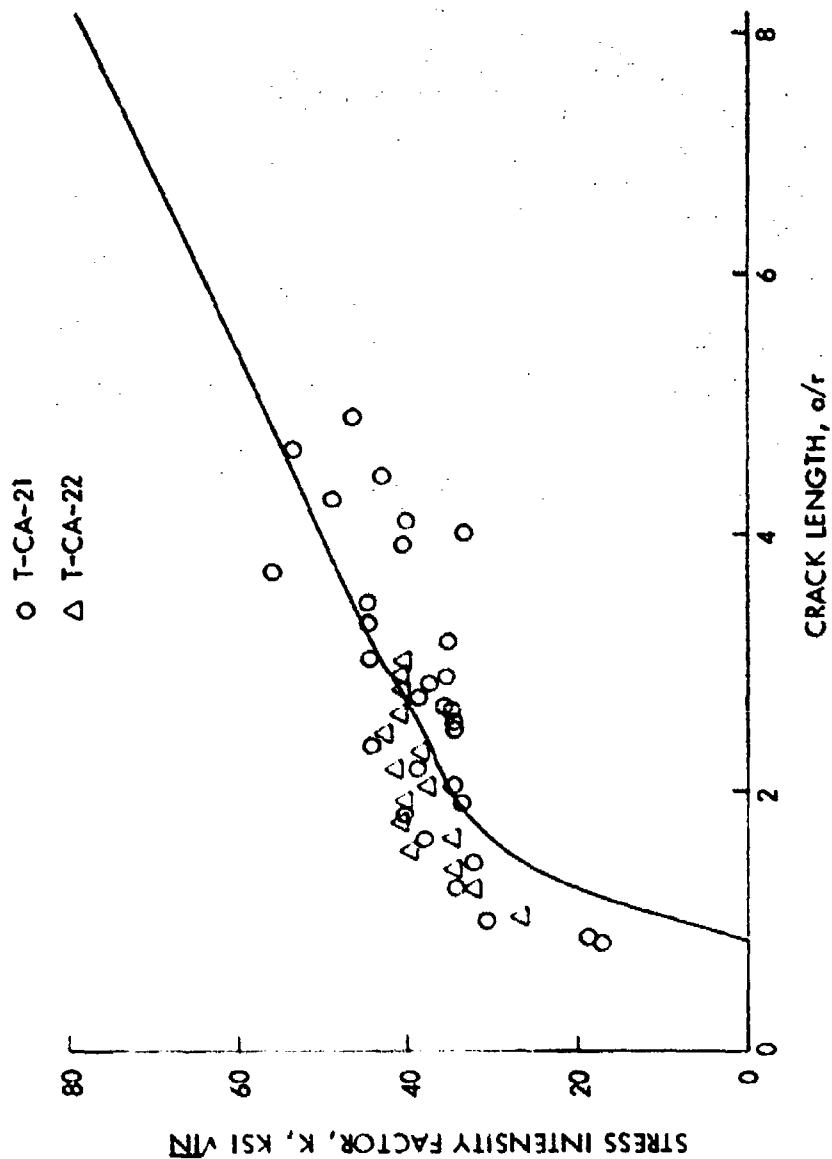


Figure 168 Stress Intensity Factors for a Single Thru Crack Emanating from Level 2 Cold-Worked Open Hole in 6Al-4V Beta Annealed Titanium Plate Subjected to 40 Ksi Uniform Far-Field Loading

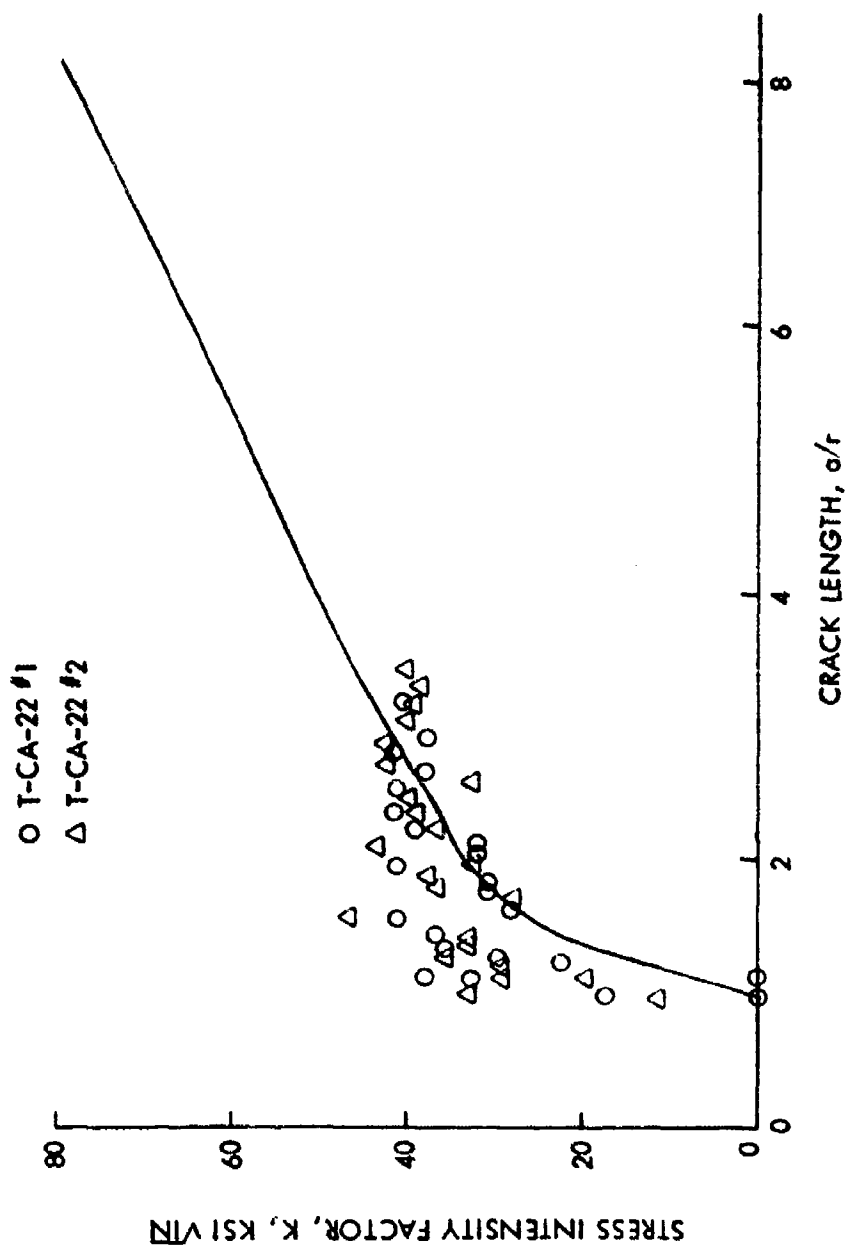


Figure 169 Stress Intensity Factor for a Single Thru Crack Emanating from Level 3 Cold-Worked Hole in 6Al-4V Beta Annealed Titanium Plate Subjected to 40 Ksi Uniform Far-Field Loading

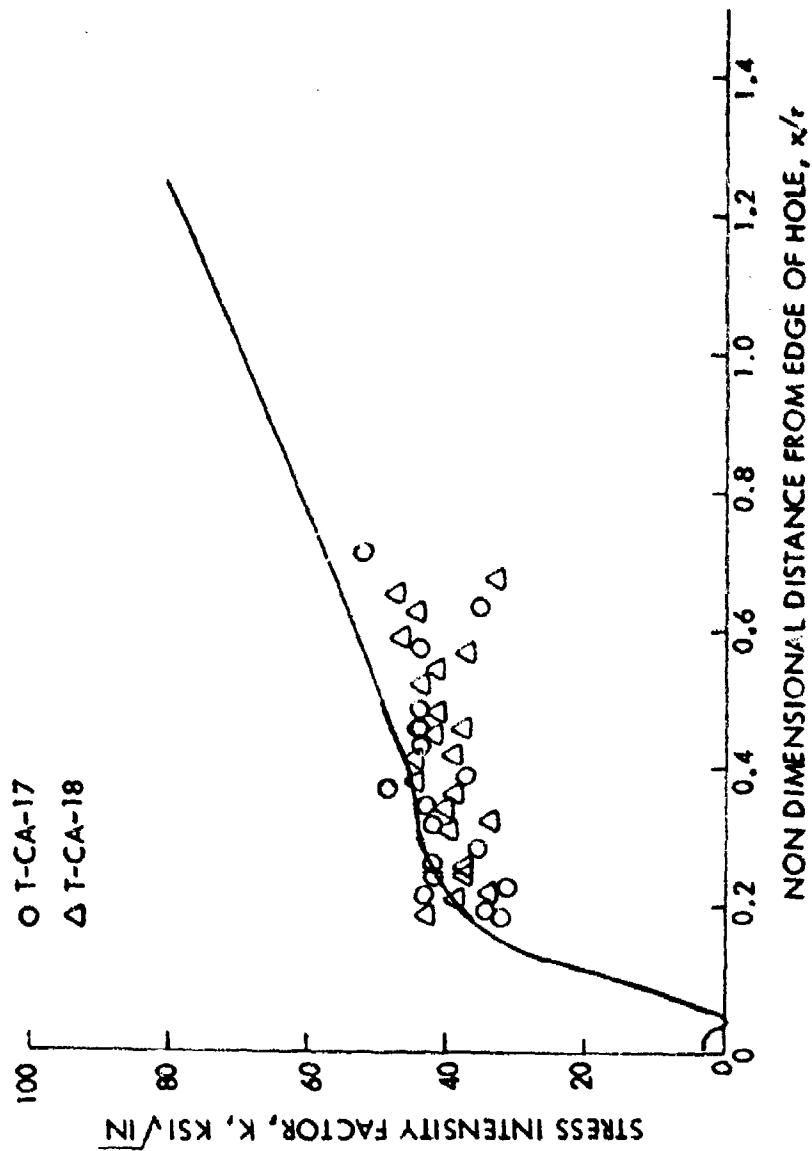


Figure 170. Stress Intensity Factor for a Single Thru Crack Emanating from Level I Cold-Worked Hole in 6Al-4V Beta Annealed Titanium Plate Subjected to 18 Ksi Far-Field Loading and 7% Fastener Load Transfer

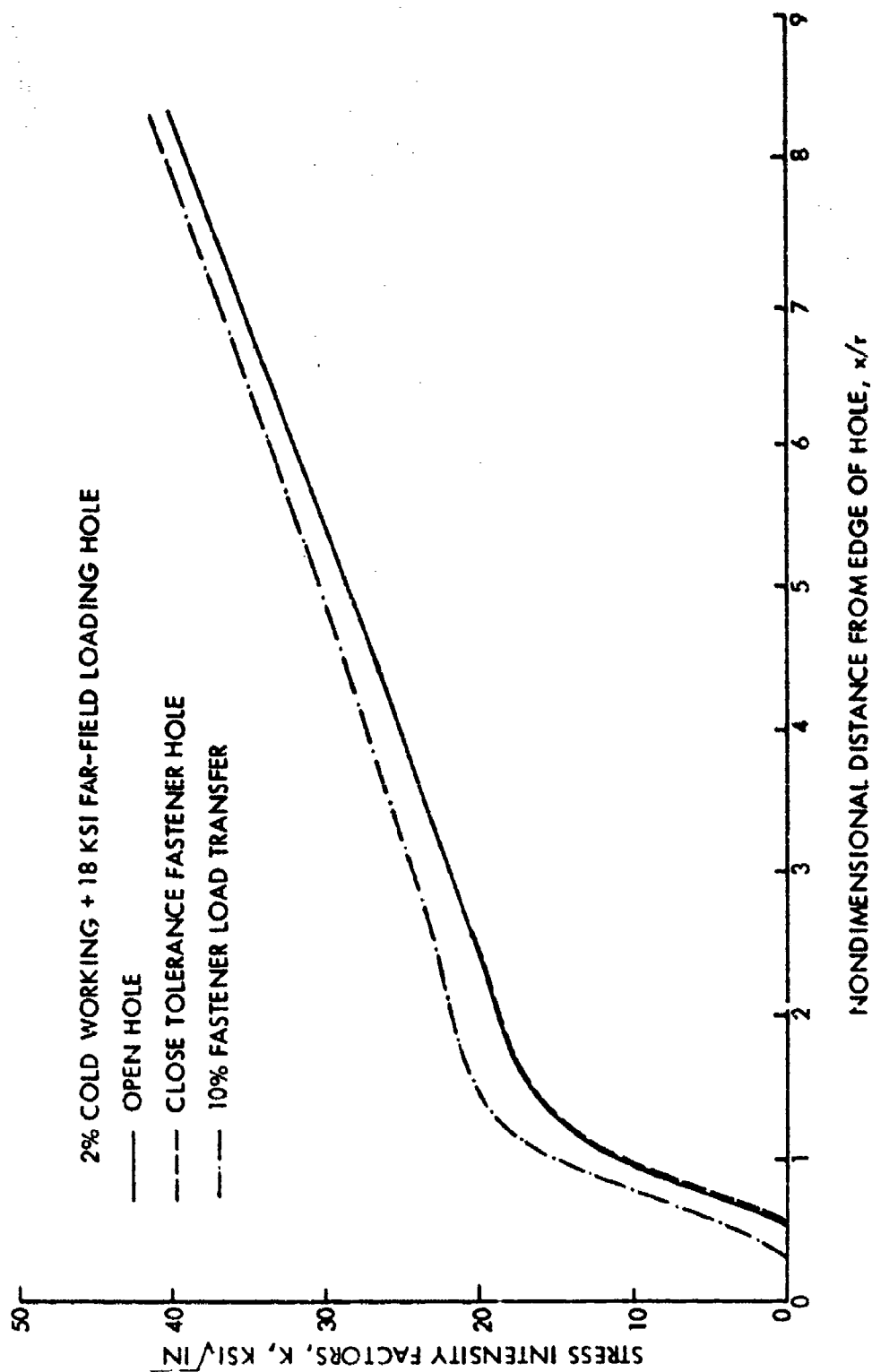


Figure 171. Stress Intensity Factors for Single Thru Cracks Emanating from Various Types of Level 1 Cold-Worked Holes in 2219-T851 Aluminum Plates Subjected to 18 Ksi Far-Field Loading

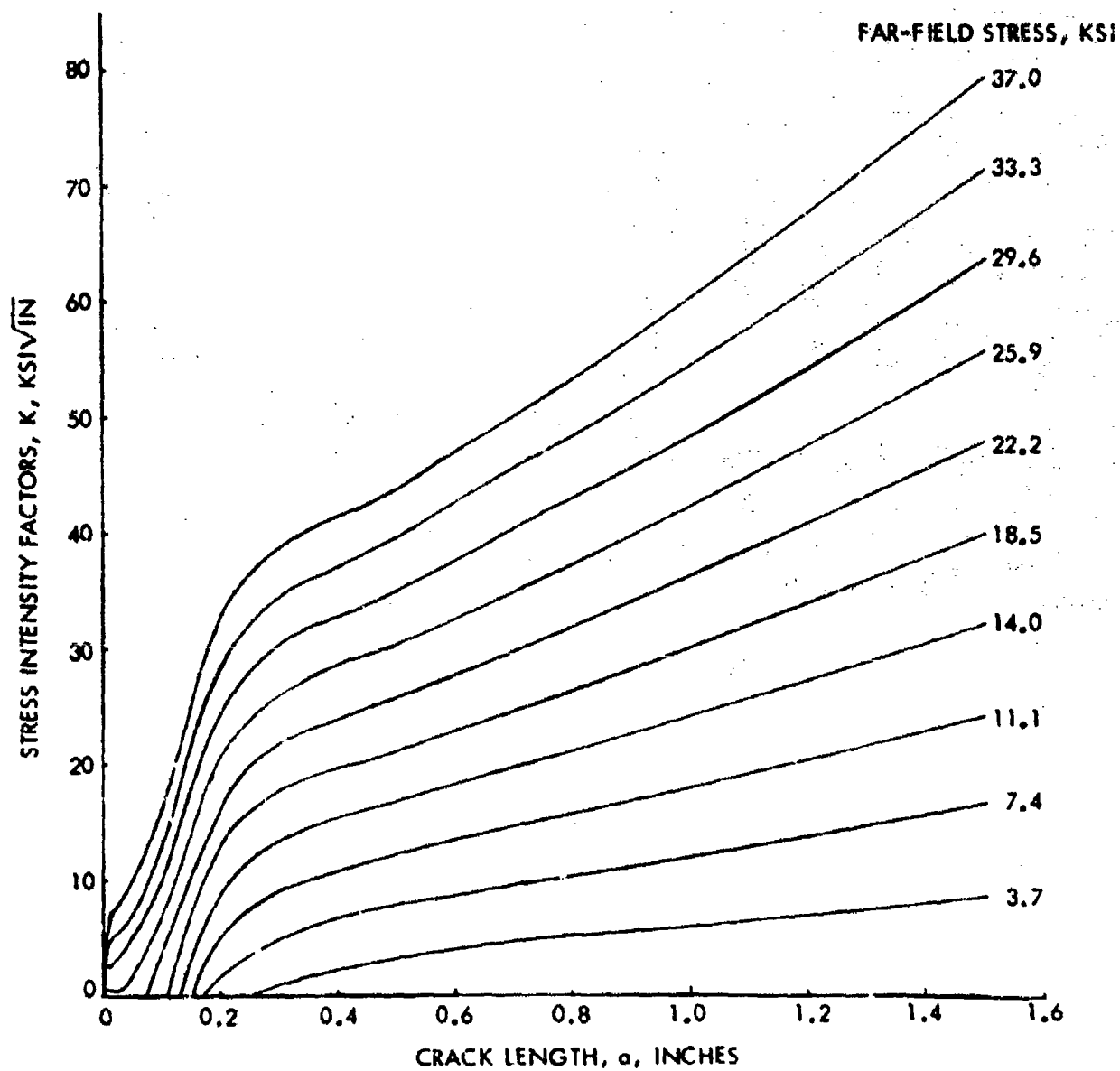


Figure 172. Stress Intensity Factors for a Single Thru Crack Emanating from Level 1 Cold-Worked Hole in 2219-T851 Aluminum Plate Subjected to Various Levels of Far-Field Loading

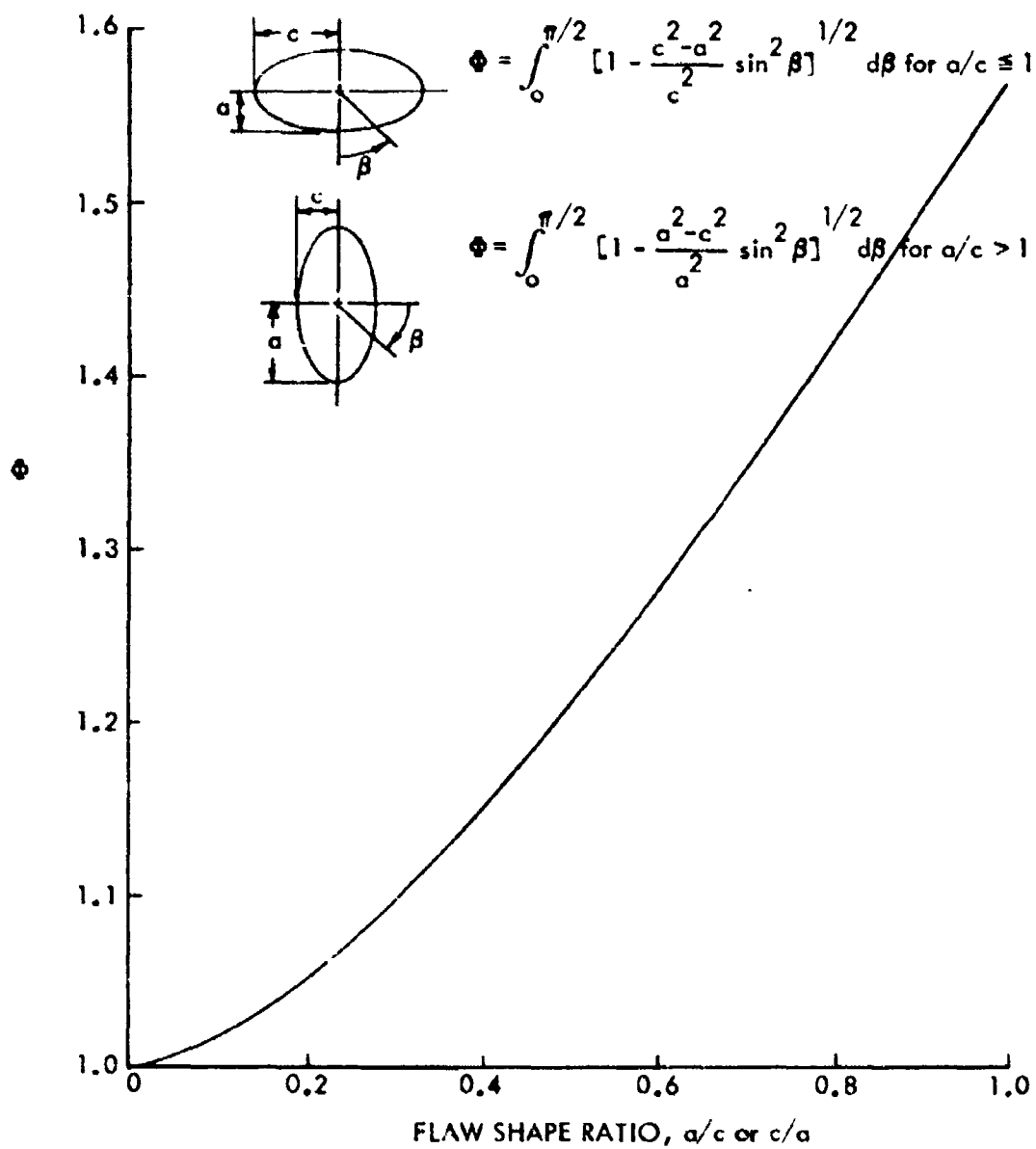


Figure 173 Flow Shape Parameter Φ

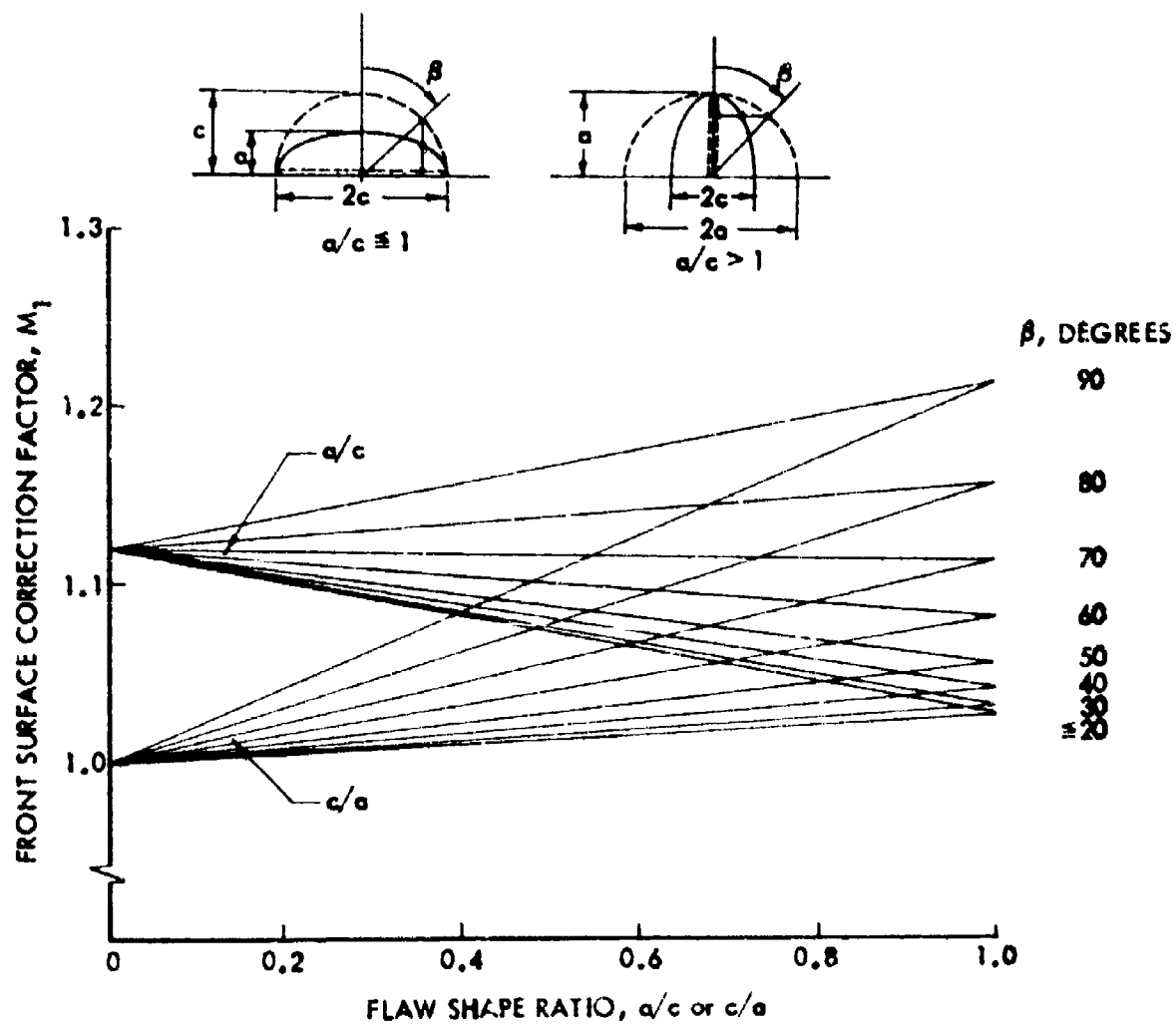


Figure 174 Front Free Surface Correction Factors, M_1

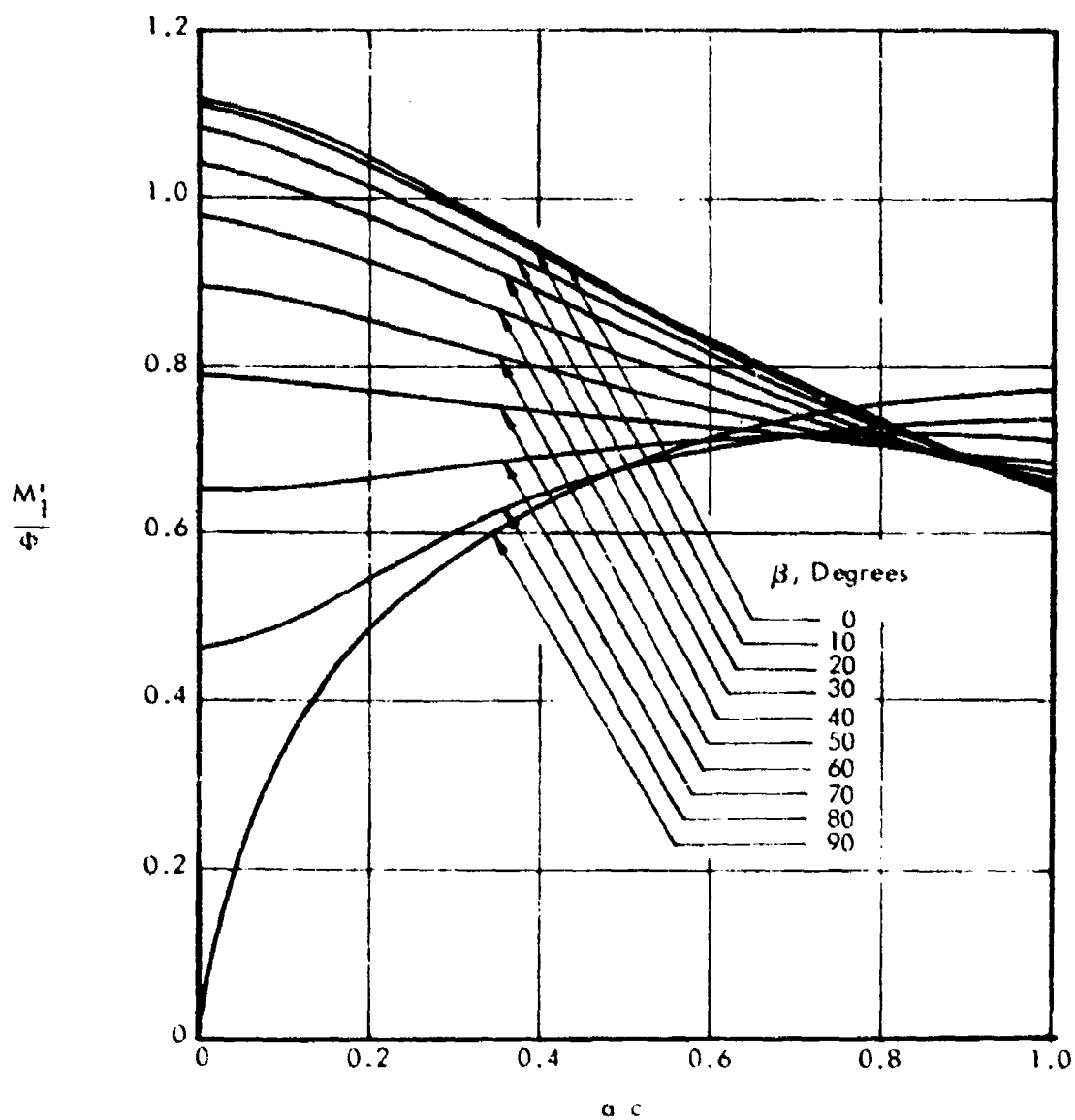


Figure 175. Factor $M_1' \Phi$ For $a/c \leq 1$

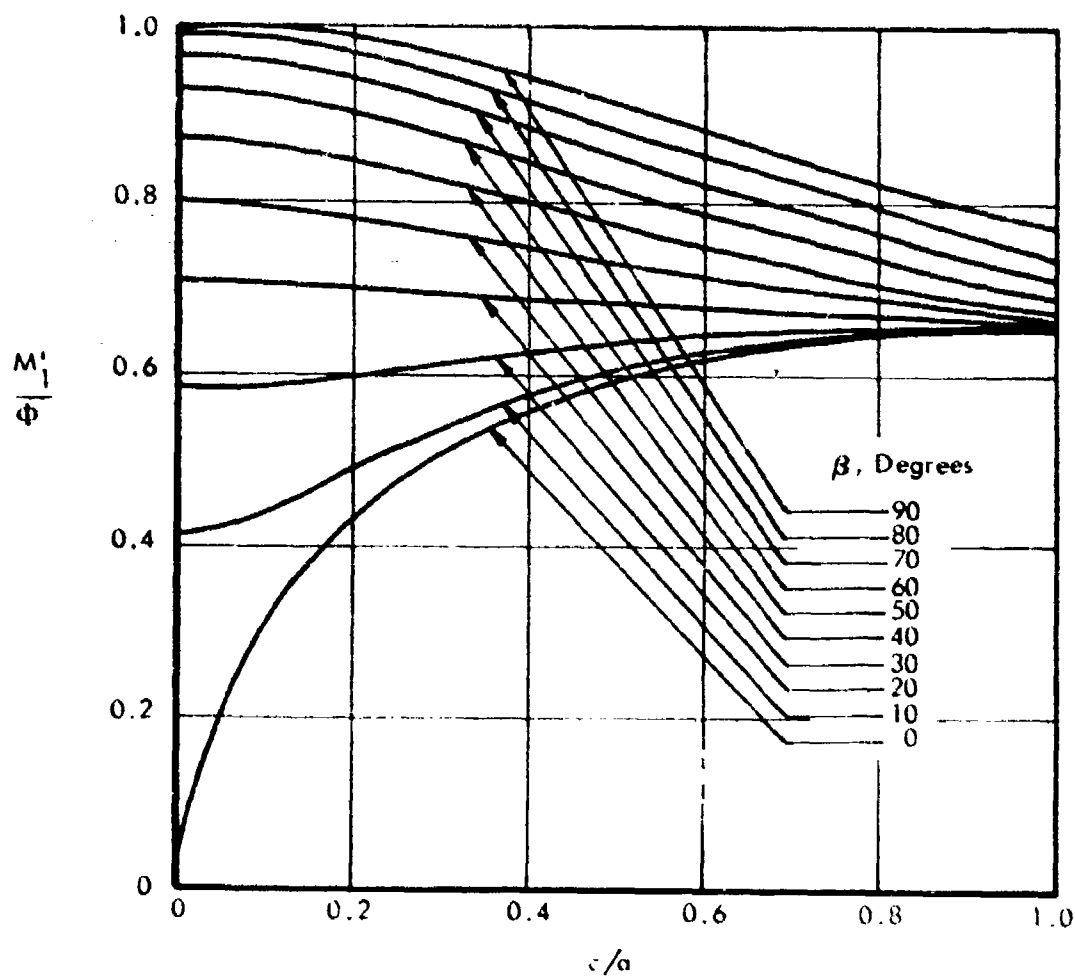
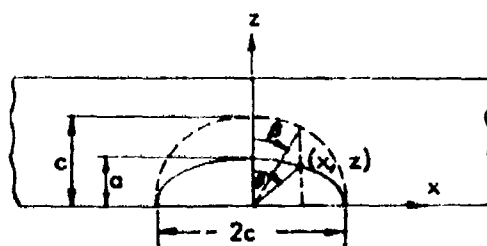


Figure 176. Factor M_1/Φ For $a/c \geq 1$



$$x = c \sin \beta$$

$$z = a \cos \beta$$

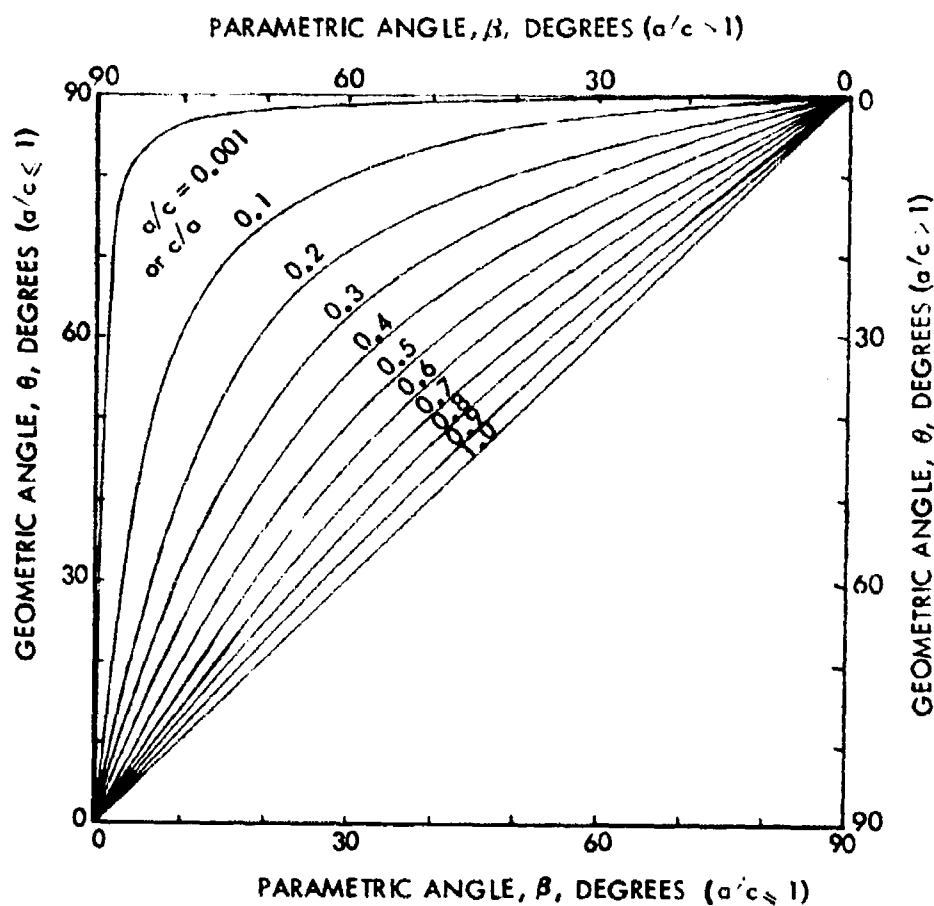


Figure 177 Relationship Between Parametric Angle β and Geometric Angle θ

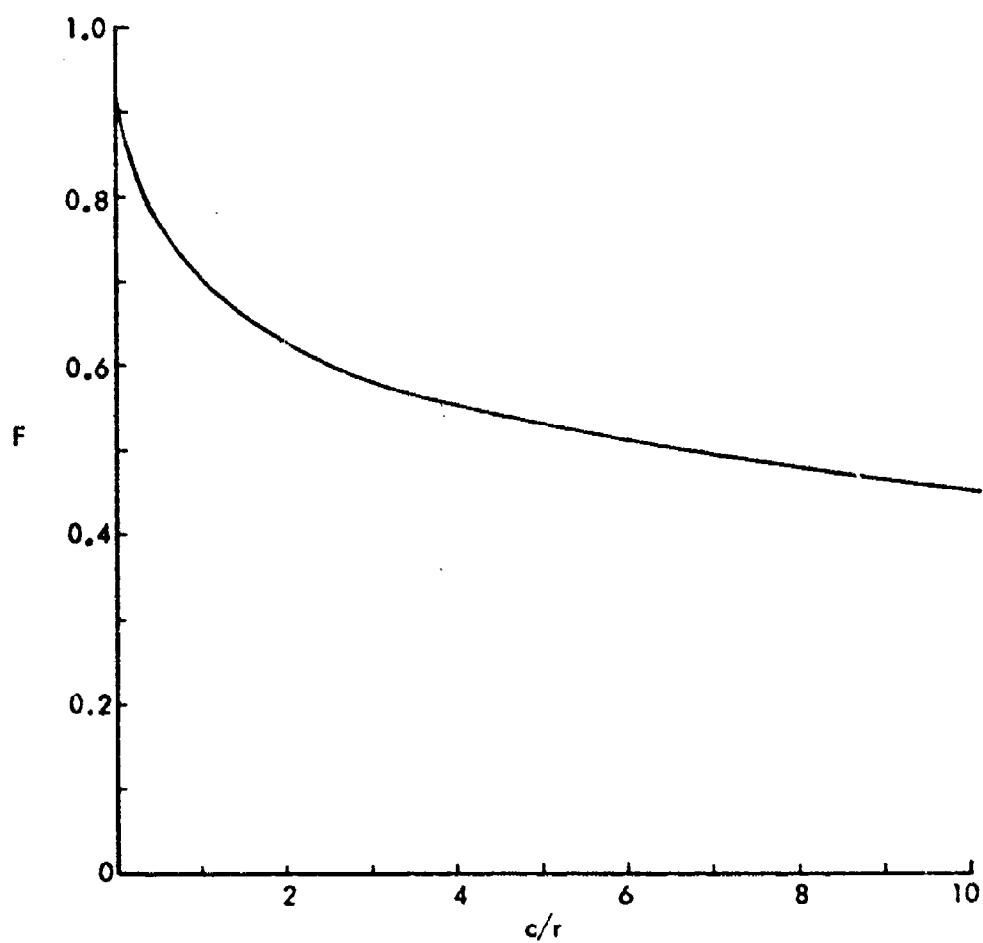


Figure 178 Nondimensional Factor F at the Edge of a Hole

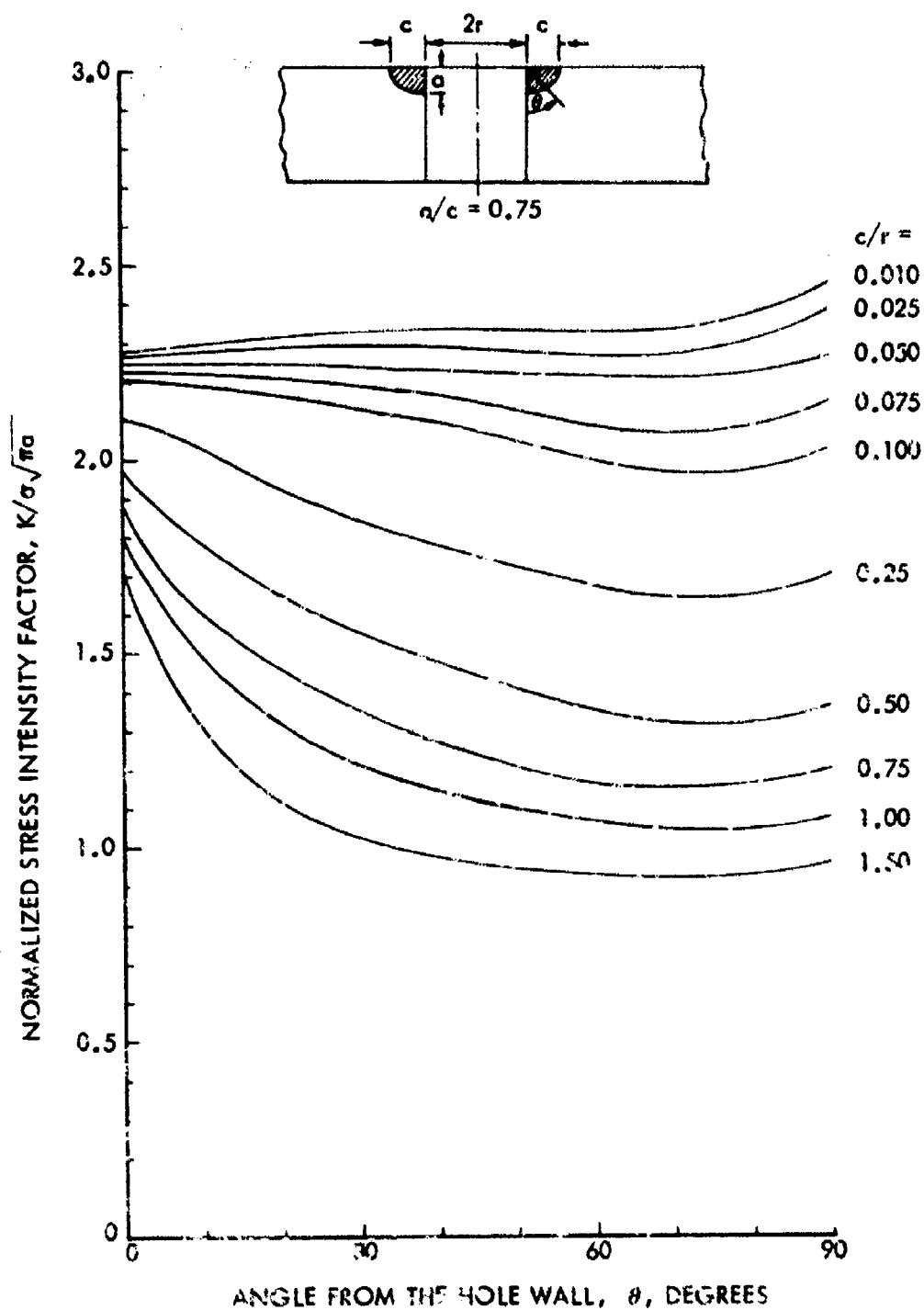


Figure 179 Normalized Stress Intensity Factors Along the Periphery of a Double Corner Crack Emanating from an Open Hole ($a/c = 0.75$)

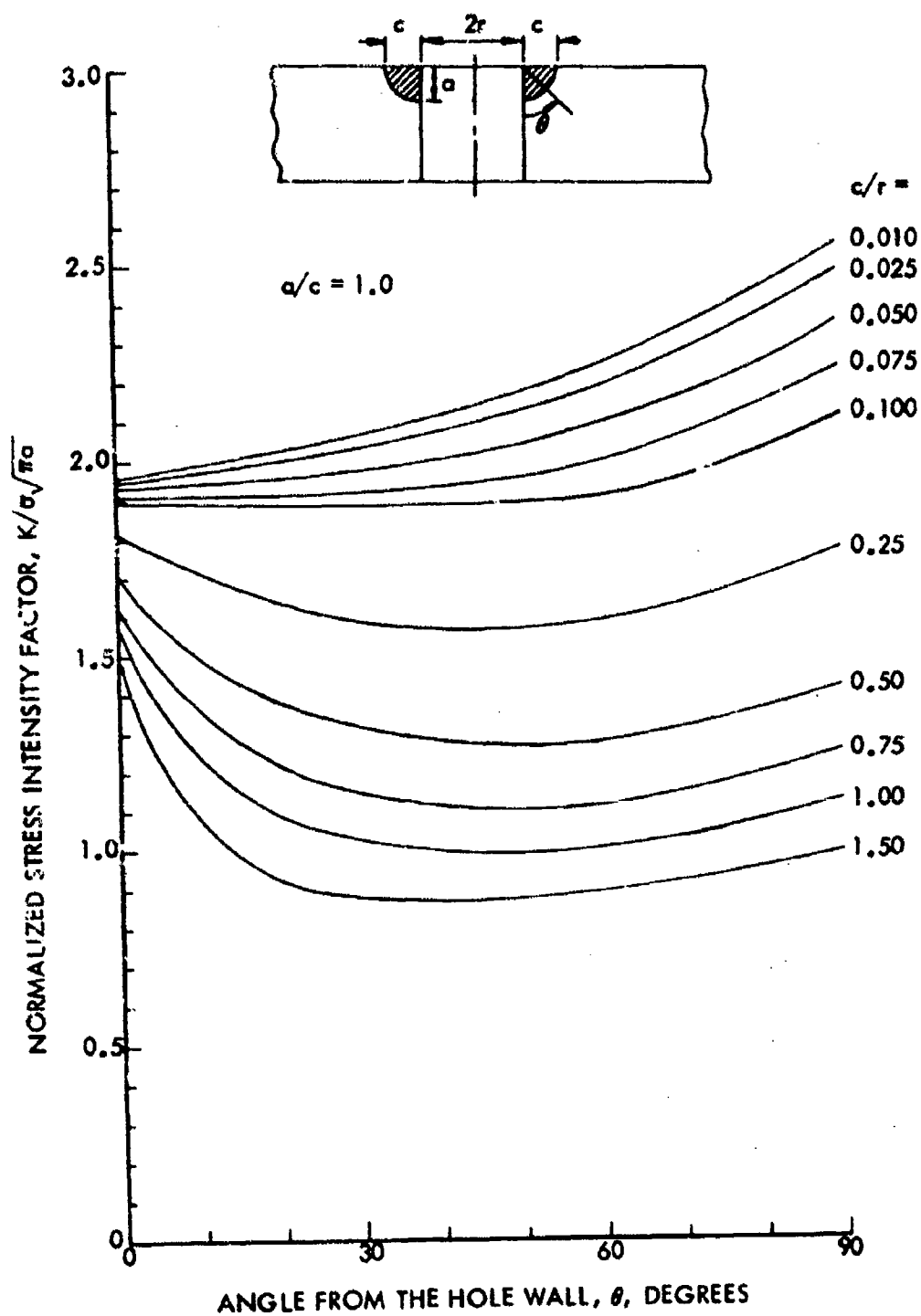


Figure 180 Normalized Stress Intensity Factors Along the Periphery of a Double Corner Crack Emanating from an Open Hole ($a/c = 1.0$)

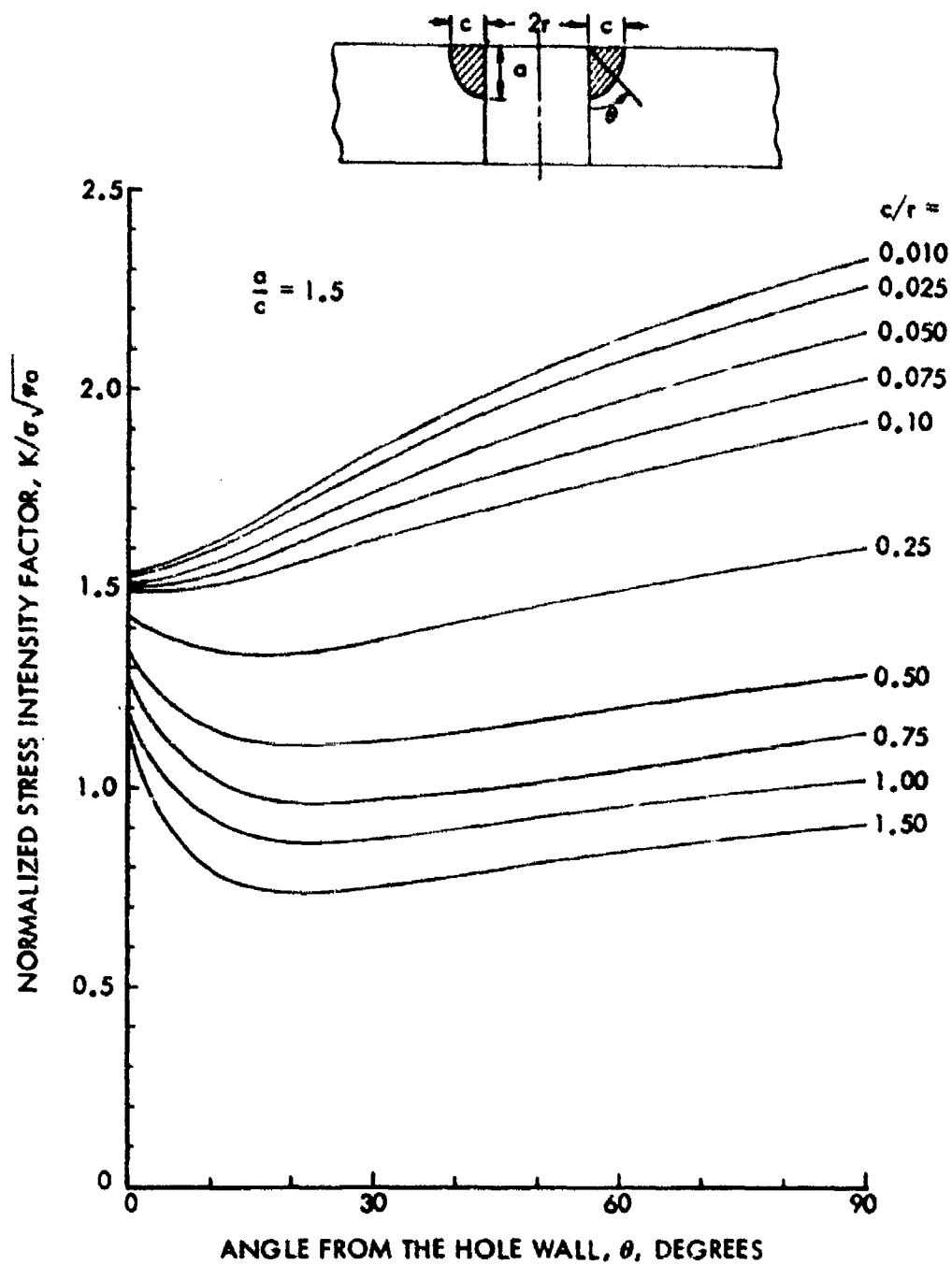


Figure 181 Normalized Stress Intensity Factors Along the Periphery of a Double Corner Crack Emanating from an Open Hole ($a/c = 1.5$)

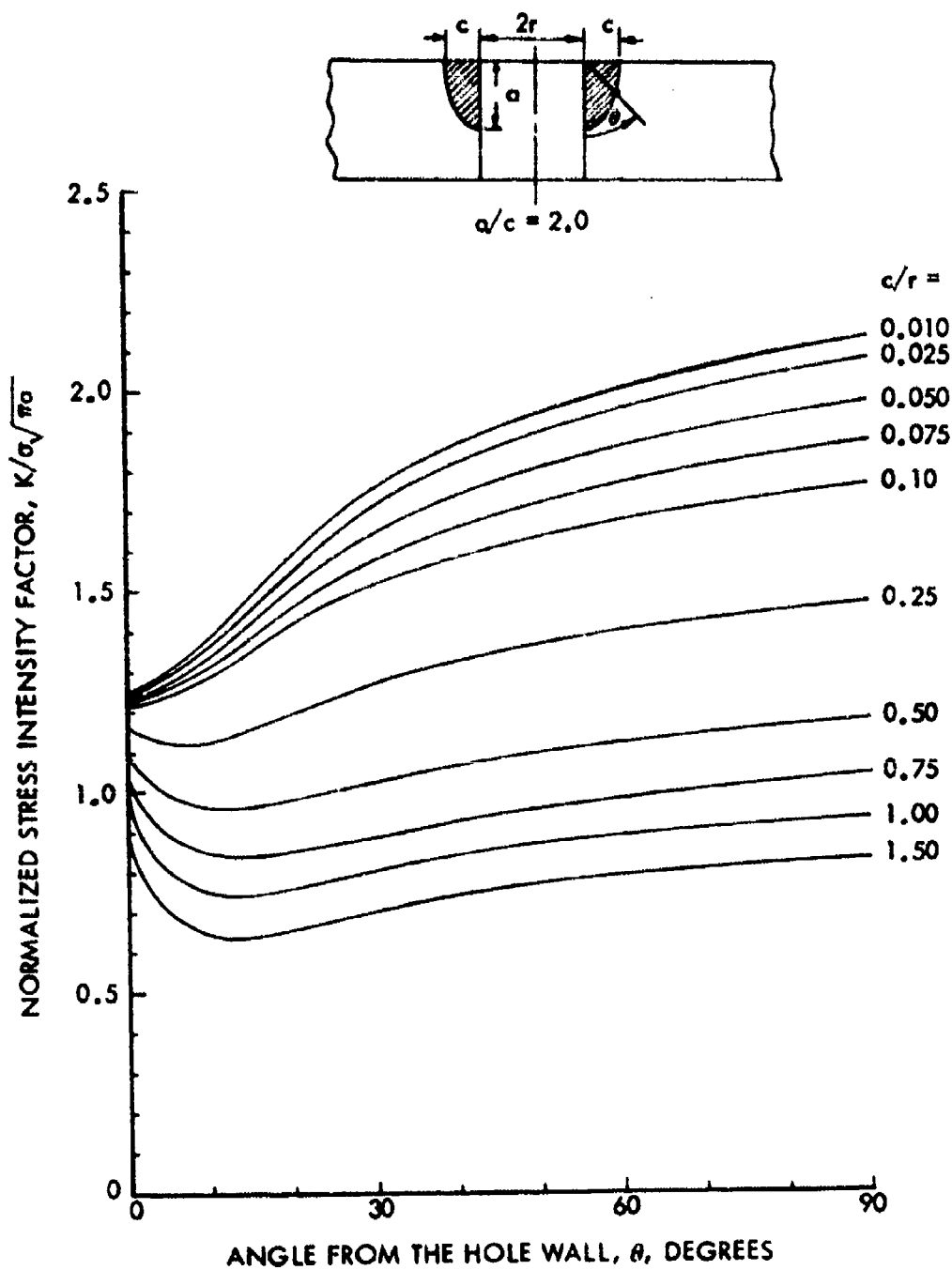


Figure 182 Normalized Stress Intensity Factors Along the Periphery of a Double Corner Crack Emanating from an Open Hole ($a/c = 2.0$)

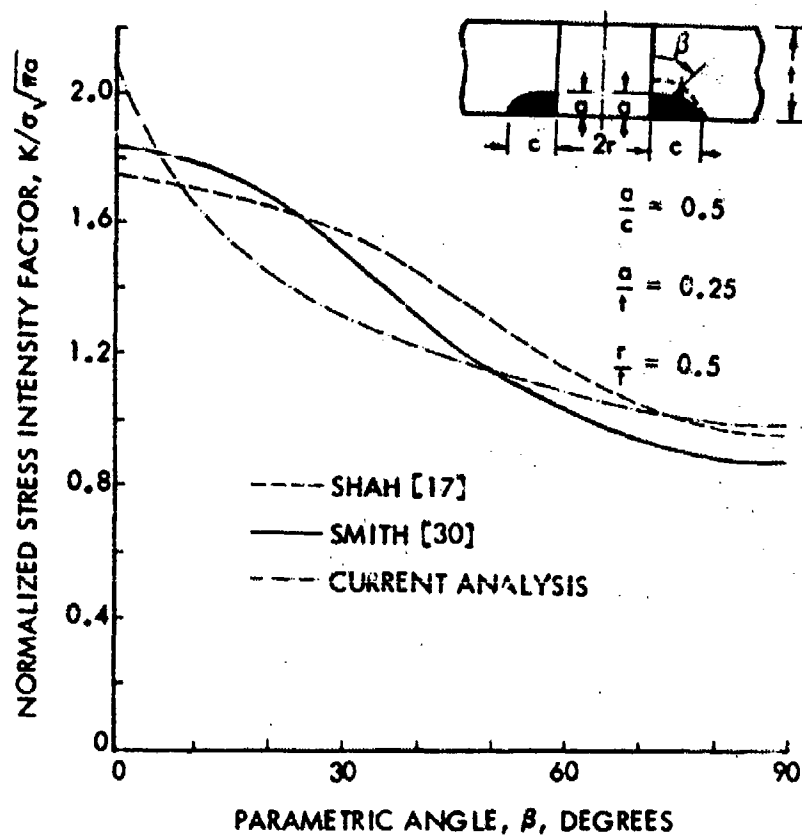


Figure 183 Comparisons of the Normalized Stress Intensity Factors for Double Corner Crack Emanating from an Open Hole

— Kobayashi et. al. [28]

- - - - - Shah [17]

- · - · - Current Analysis

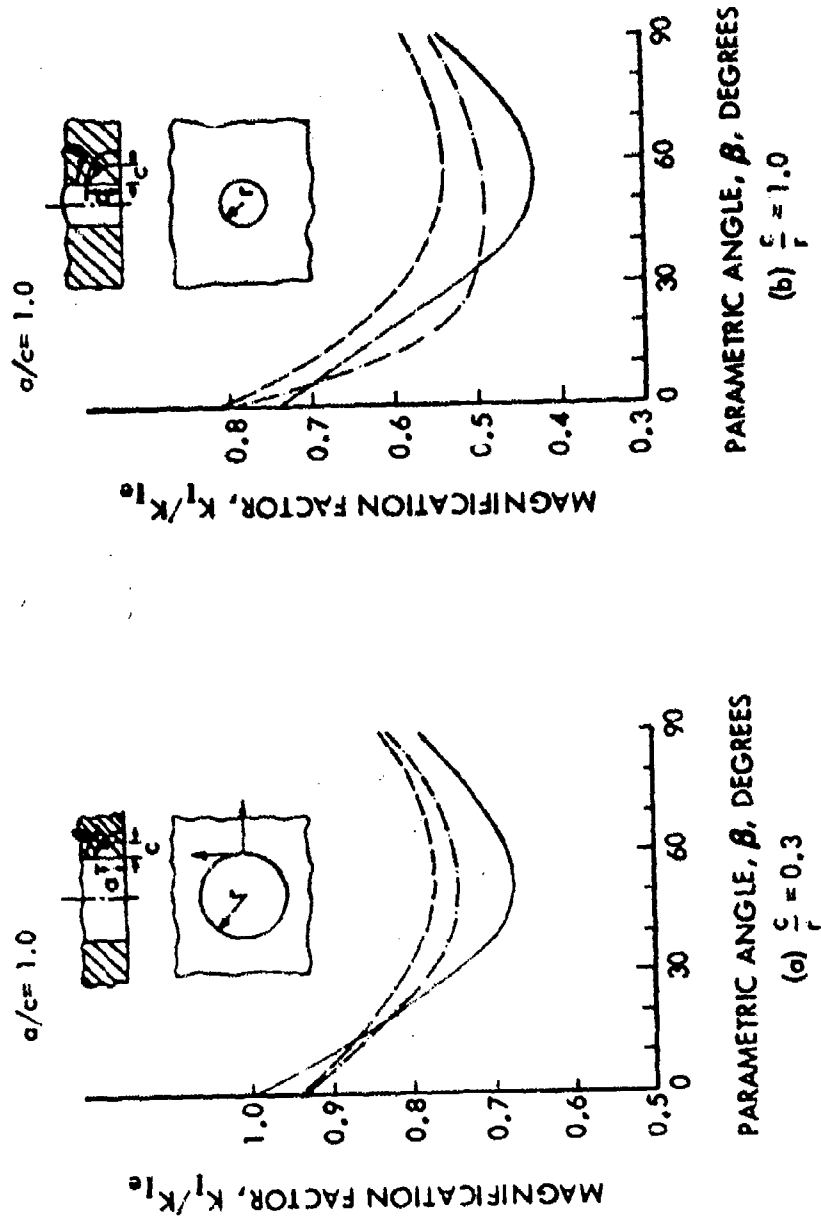


Figure 184 Comparisons of Estimated Magnification Factors for a Single Quarter-Ellipse Corner Crack Emanating from an Open Hole

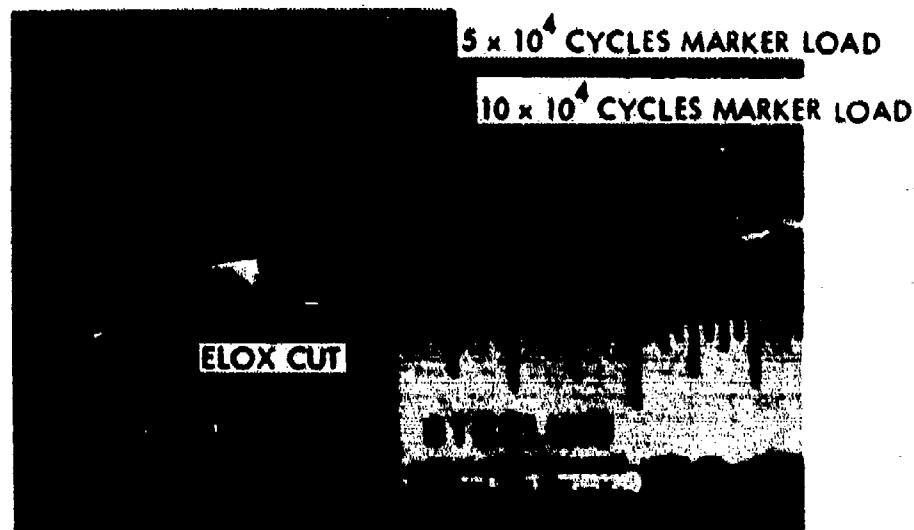


Figure 185 Fracture Surface of Test Specimen No. 1

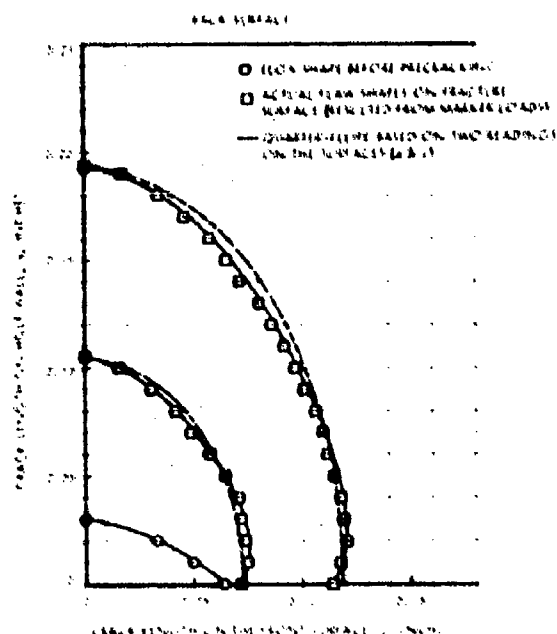


Figure 186 Change of Flaw Shape on Fracture Surface of Corner Crack Specimen (Test No. 1)

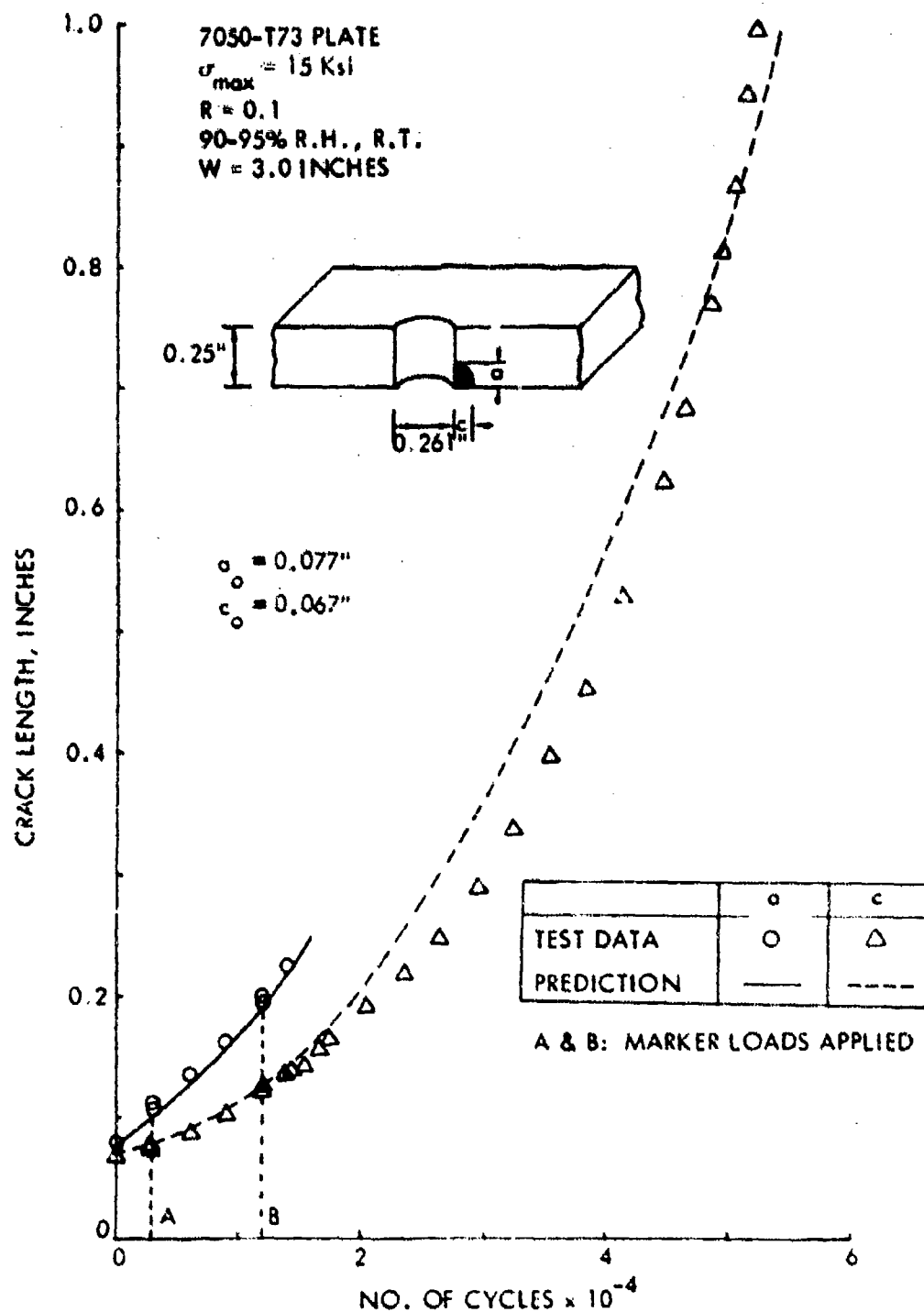


Figure 187 Correlation of Data and Prediction for a Corner Crack Emanating from an Open Hole in 7050-T73 Aluminum Plate Subjected to Constant Amplitude Loading (Test Specimen No. 1)

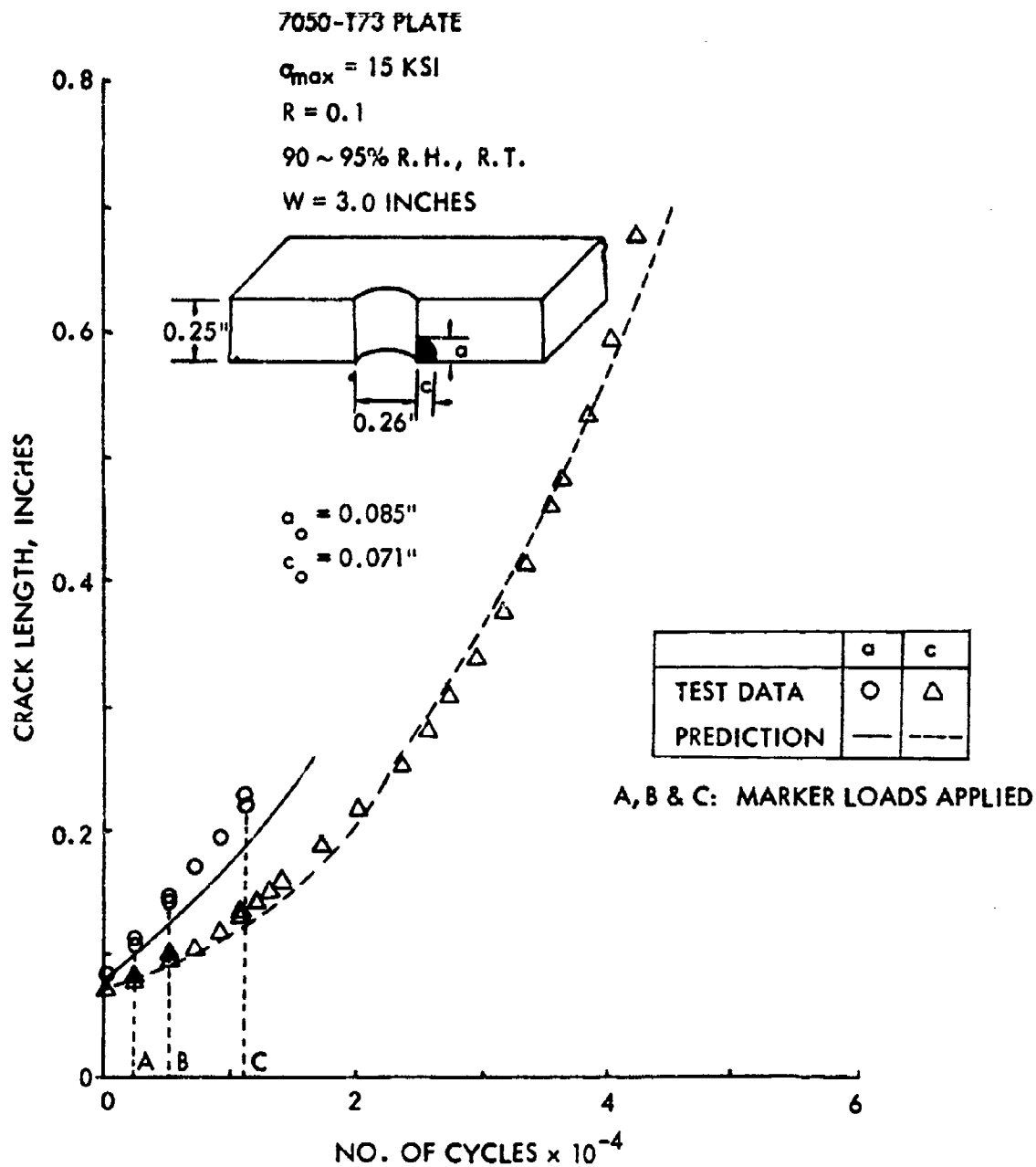


Figure 188 Correlation of Data and Prediction for a Corner Crack Emanating from an Open Hole in 7050-T73 Aluminum Plate Subjected to Constant Amplitude Loading (Test Specimen No. 2)

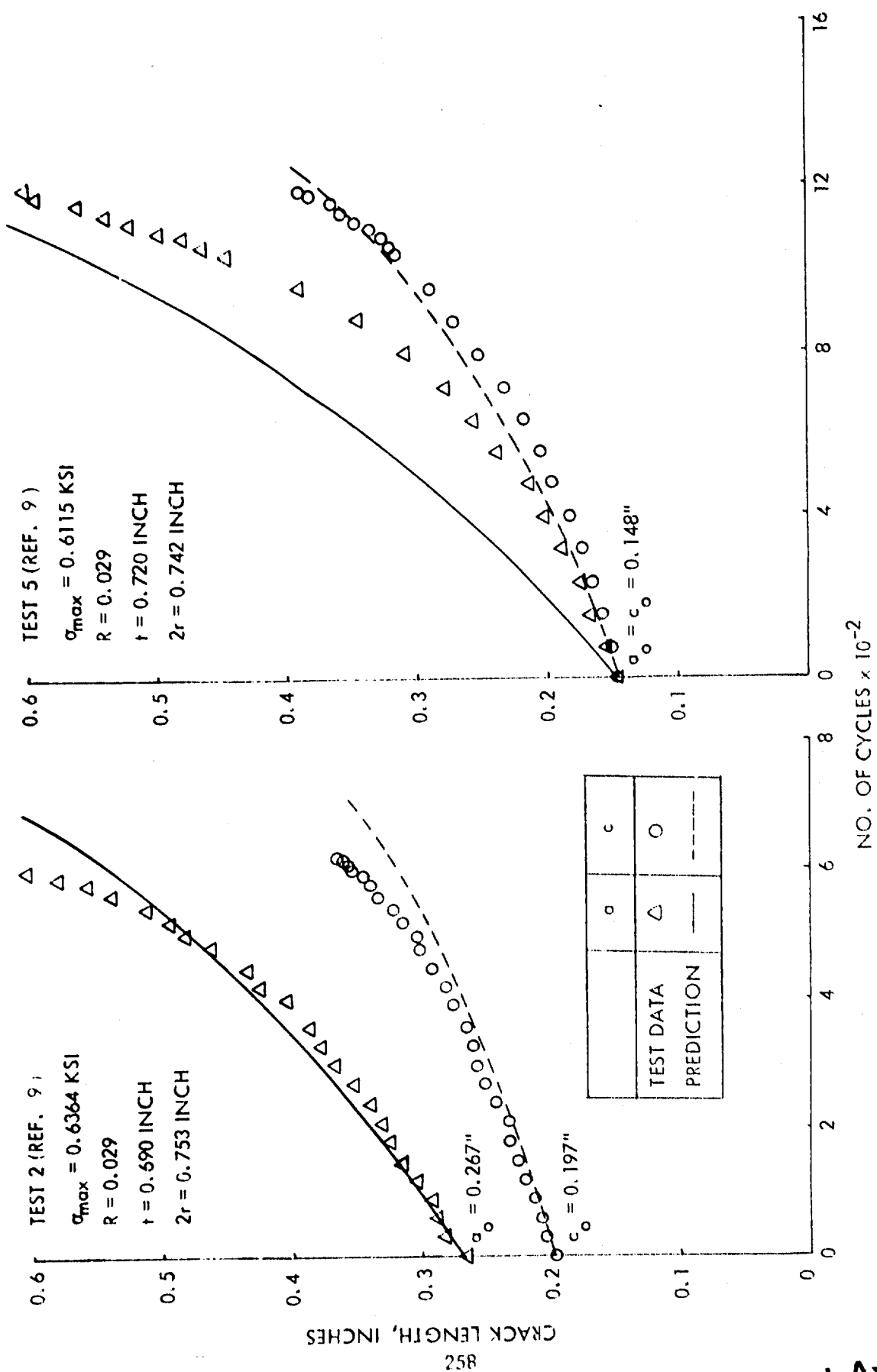


Figure 129 Correlations of Data and Predictions for Corner Cracks Emanating from Open Holes in PMMA Polymer Plates Subjected to Constant Amplitude Loading

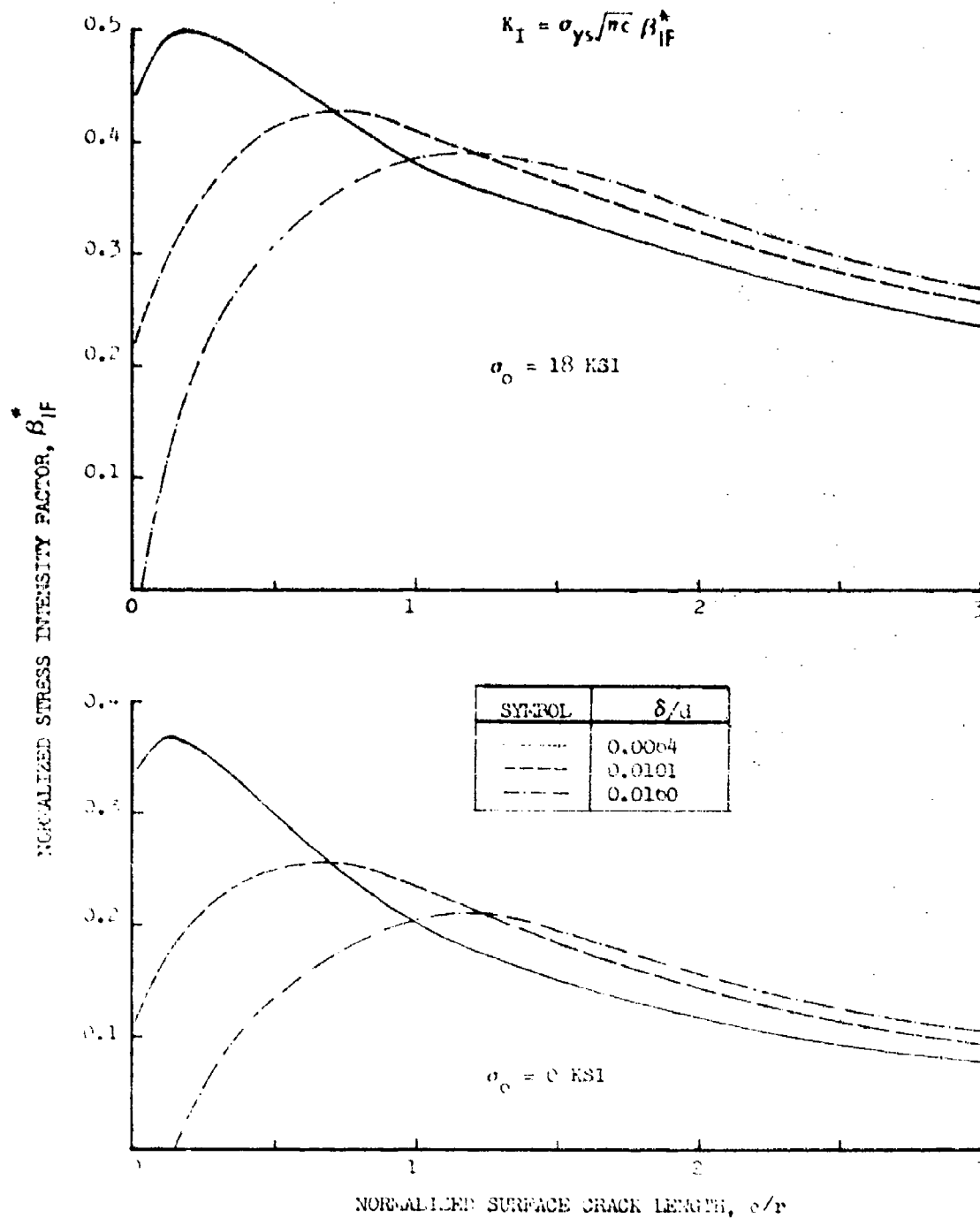


Figure 190 Normalized Stress Intensity Factors at the Intersection of Plate Surface and the Border of Single Corner Cracks Emanating from Interference-Fit Fastener Holes for Various Levels of Interference in 2219-T851 Aluminum Plates Subjected to Constant Amplitude Far-Field Loading ($\alpha c = 0.75$)

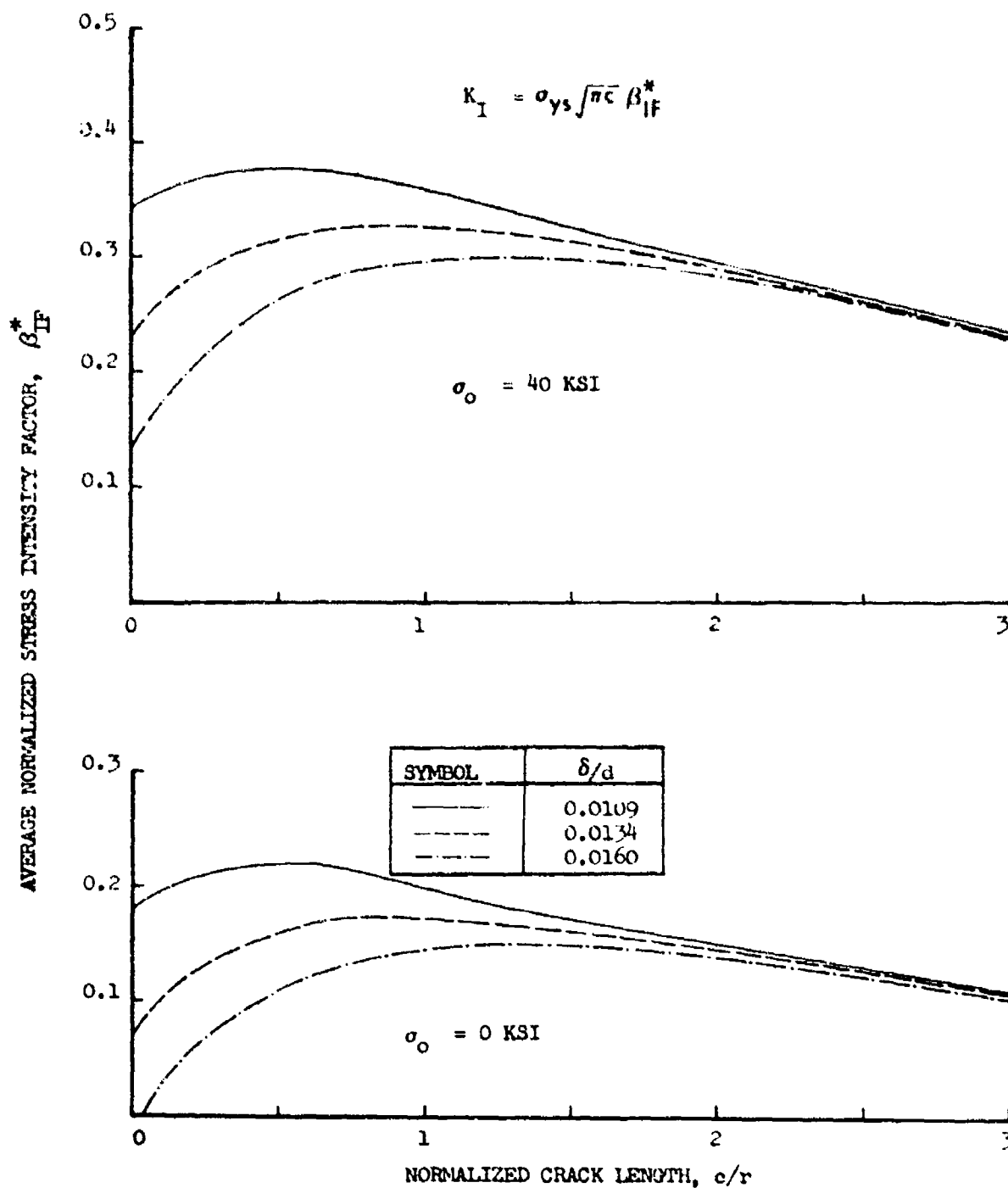


Figure 191 Normalized Stress Intensity Factors at the Intersection of Plate Surface and the Border of Single Corner Cracks Emanating from Interference-Fit Fastener Holes for Various Levels of Interference in 6Al-4V Beta Annealed Titanium Plates Subjected to Constant Amplitude Far-Field Loading ($a/c = 0.75$)

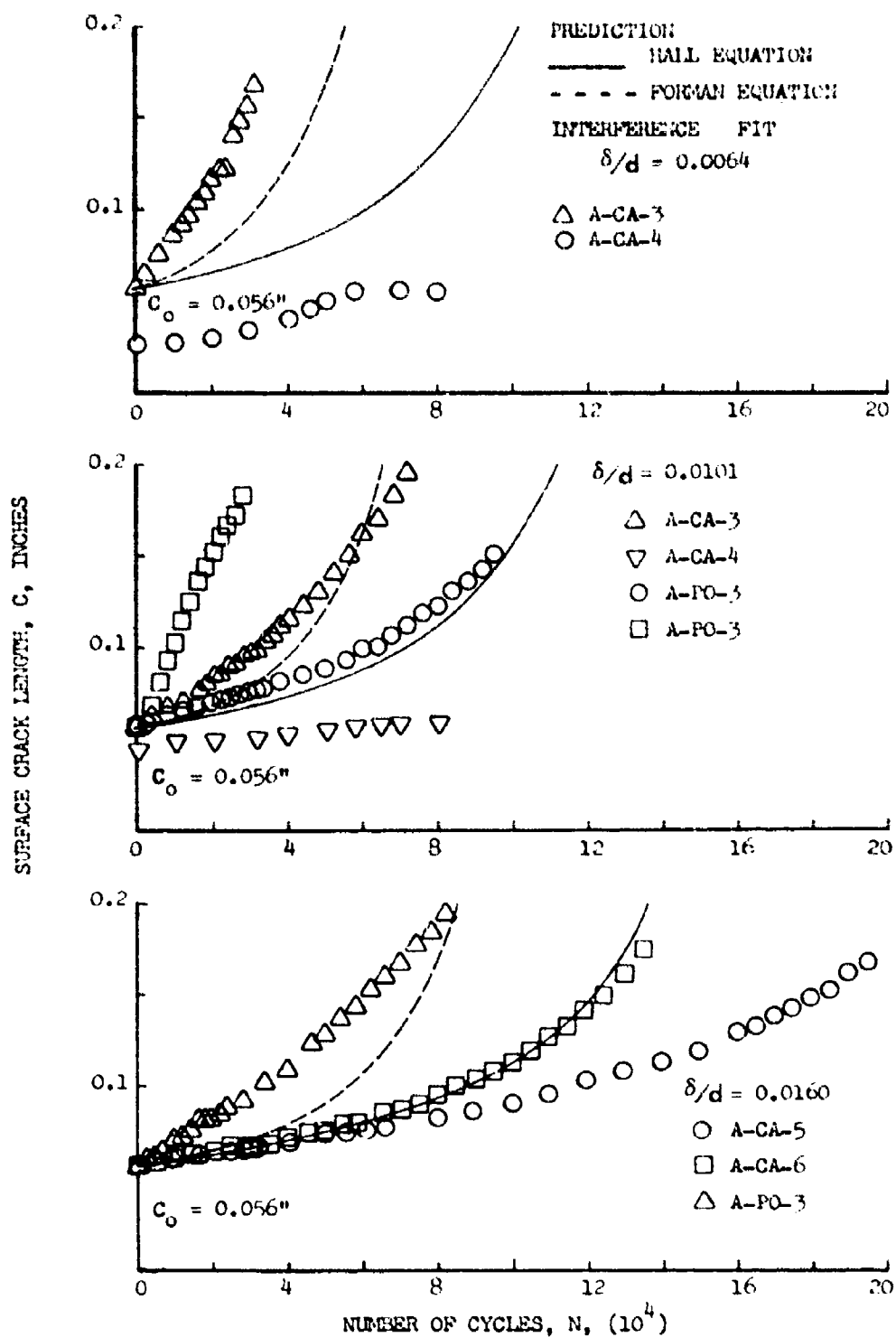


Figure 192 Correlation of Data and Predictions for Corner Cracks Emanating from Interference - Fit Fastener Holes in 2219-T851 Aluminum Plates Subjected to Constant Amplitude Loading ($\sigma_0 = 18$ KSI and $R = 0.1$)

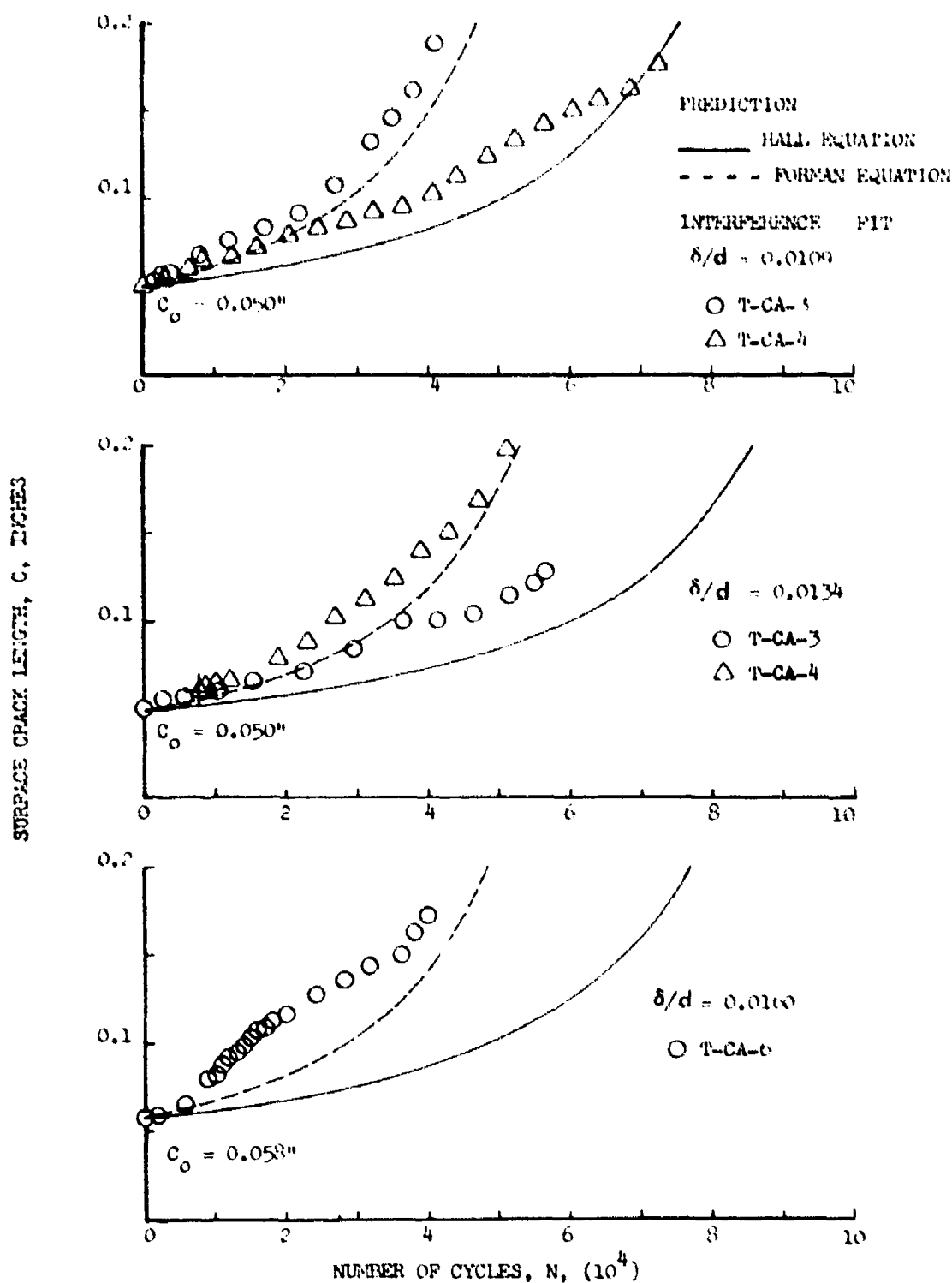
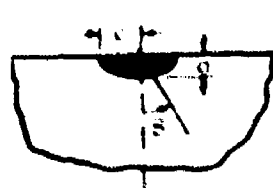
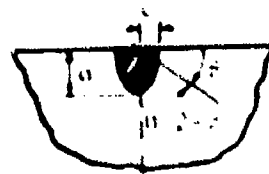


Figure 193 Correlation of Data and Predictions for Corner Cracks Emanating from Interference - Fit Fastener Holes in α Al-4V Beta Annealed Titanium Plates Subjected to Constant Amplitude Loading ($\sigma_0 = 40$ KSI and $R = 0.1$)



a c



a c

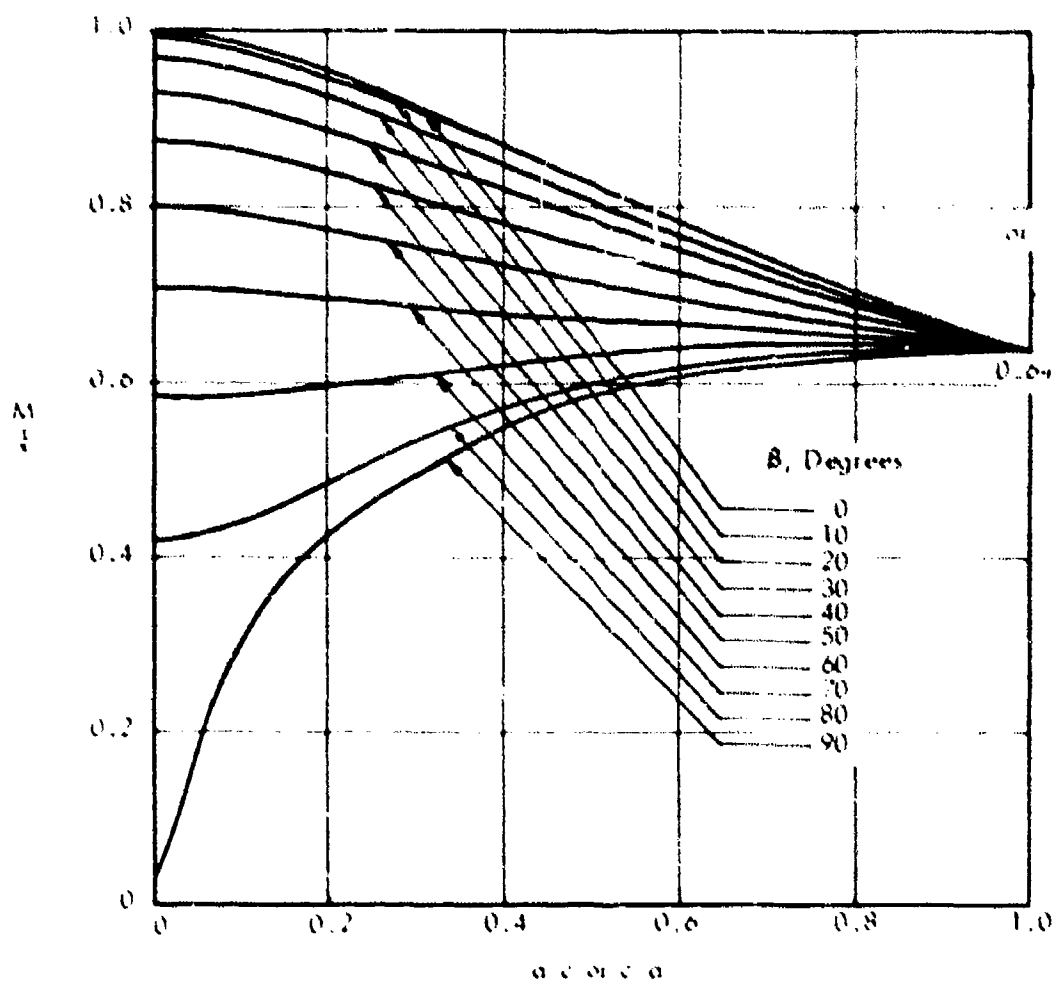
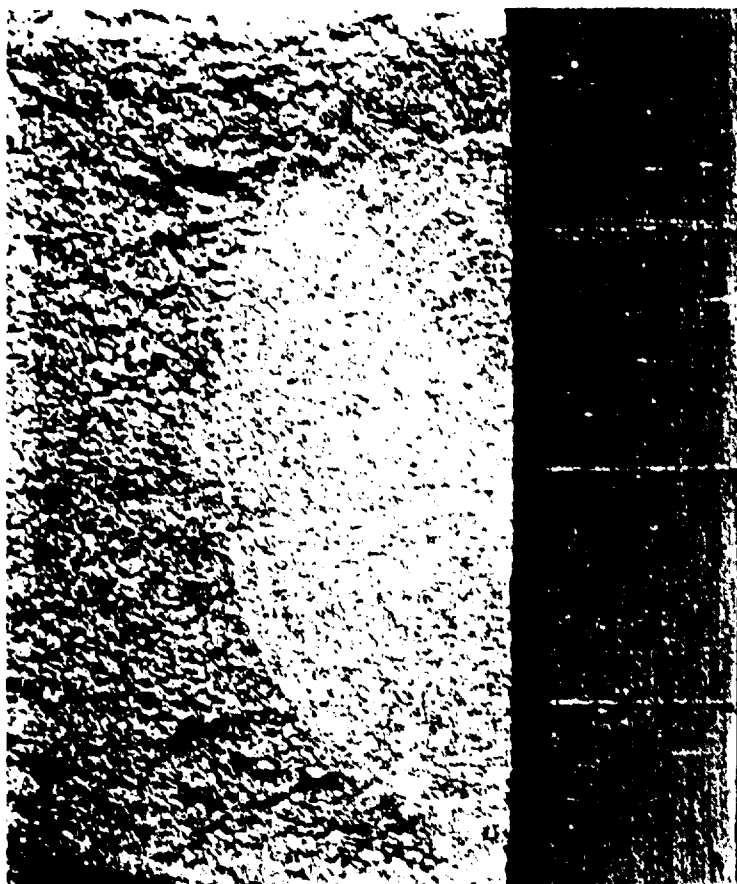
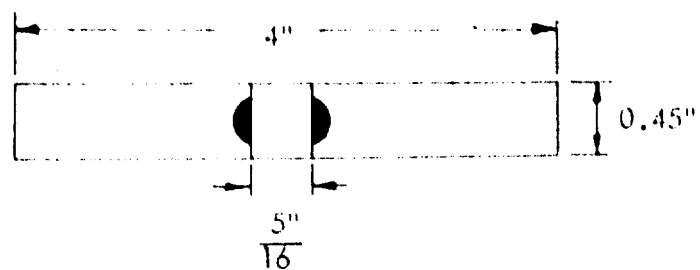


Figure 194 Flow Shape Factor, $M/4$



MAG. = 100X

Figure 195. Crack Surface of a Double Embedded Crack at Open Hole in 7075-T651 Aluminum Plate Subjected to Constant Amplitude Loading ($\sigma_{\max} = 15$ Ksi, $R = 0.1$)

TABLE 1 - SUMMARY OF FATIGUE AND CRACK GROWTH TEST HOLES AND TEST SPECIMENS

MATERIAL	LOADING CONDITION	FASTENER-HOLE CONDITION	NUMBER OF TEST HOLES			NUMBER OF TEST SPECIMENS					
			FATIGUE (UNFLAWED)	CORNER CRACK	THRU CRACK	FATIGUE (UNFLAWED)	CORNER CRACK	THRU CRACK	TOTAL		
2219-T851 Aluminum	Constant Amplitude	SR	7	6	9	15	3	2	4	6	
		TL	4	11	24	35	2	8	17	25	
		CW	7	12	24	36	3				
		Sub-Total	18	29	57	86	8	10	21	31	
	Spectrum Loading	SR	10	8	6	14	6	3	2	5	
		TL	4	18	27	45	2	11	24	35	
		CW	4	10	40	50	4				
		Sub-Total	18	36	73	109	14	14	26	40	
	6Al-4V βA Titanium	Constant Amplitude	SR	7	6	6	12	3	2	2	4
			TL	4	10	14	24	2	6	15	21
CW			7	8	28	36	3				
Sub-Total			18	24	48	72	8	8	17	25	
Spectrum Loading	SR	12	6	6	12	8	2	2	4		
	TL	4	16	19	35	4	12	19	31		
	CW	4	20	36	56	4					
	Sub-Total	20	42	61	103	16	14	21	35		
2219-T851 Al	6Al-4V βA Ti	Total	36	65	130	195	22	24	47	71	
			38	66	109	175	24	22	38	60	
Grand Total			74	131	239	370	46	46	85	131	

SR = Straight Reamed

TL = Taper-Lock (Interference-Fit Fastener)

CW = Cold-Worked

Best Available Copy

TABLE 2 - SUMMARY OF MATERIAL CHARACTERIZATION AND FAILURE CRITERION TESTS

MATERIAL	TENSILE	COMPRESSION		K_c	da/dN	da/dN THRESHOLD	FAILURE CRITERION	MICROSTRUCTURE
	T		T					
Ti-6Al-4V β Annealed	3		3	3	3	3	3	1
2219-T851	3		3	3	3	3	3	1
SPECIMEN CONFIGURATION FIGURE NO.	3(a)		3(b)	3(c)	3(d)	3(d)	3(e)	

T = Transverse Grain

For K_c , da/dN , and failure criterion tests, flaws will be in T-L direction.

TABLE J - SUMMARY OF CONSTANT AMPLITUDE FATIGUE TESTS ON
2219-1851 ALUMINUM SPECIMENS WITH $\sigma_o = 18$ ksi and R = 0.1

Hole Condition	Cold Work Level	Fastener		Test Hole	Cycles Applied	Remarks	Test Hole Number
		Type	Interference Inch				
Open	-	None	-	-	#1 133,840	cc, c = 0.060"	A-CAF-1-2
	-	None	-	-	#2 148,400	Fail *	A-CAF-2-2
Close Tolerance	-	CT	-	0	#1 53,200	cc, c = 0.21" Fail = 66200	A-CAF-3-1
	-	CT	-	0	#2 80,210	2cc, c ₁ = 0.02" * c ₂ = 0.07"	A-CAF-3-2
	-	CT	-	0	#3 60,300	cc, c = 0.04 & c = 0.23 = 66200	A-CAF-3-3
	-	CT	-	0.98	#1 68,570	Fail **	A-CAF-1-1
	-	CT	-	0.97	#2 52,450	2cc, c ₁ = 0.20" ** c ₂ = 0.25"	A-CAF-2-1
	-	CT	-	0.97	#2 52,450	2cc, c ₁ = 0.20" ** c ₂ = 0.25"	A-CAF-2-1
Interference Fit	-	TL	0.0038	0	#1 1,051,070	Failed in Grip	A-CAF-4-2
	-	TL	0.0038	0	#2 3,741,020	Failed in Grip	A-CAF-5-2
	-	TL	0.0038	1.00	#1 85,240	Fail **	A-CAF-4-1
	-	TL	0.0038	1.07	#2 404,230	Fail **	A-CAF-5-1
Cold Worked	2.2%	None	-	-	#1 167,200	EF	A-CAF-6-1
	2.2%	None	-	-	#2 165,700	cc, c = 0.01	A-CAF-6-2
	2.2%	None	-	-	#3 164,400	Fail *	A-CAF-6-3
	2.2%	CT	-	0	#2 436,060	2cc, c ₁ = 0.43" c ₂ = 0.03"	A-CAF-7-2
	2.2%	CT	-	0	#2 275,250	Fail *	A-CAF-8-2
	2.2%	CT	-	1.08	#1 136,630	Fail **	A-CAF-7-1
	2.2%	CT	-	1.02	#1 96,500	cc, c = 0.13	A-CAF-8-1

cc = Corner Crack

2cc = Two Corner Cracks

CT = Close Tolerance

EF = Embedded Flaw

TL = Taper Lok

* = Two corner cracks located on the same side of the fastener hole. When the crack surface was opened, a large embedded flaw was found.

** = Started from embedded flaw.

+ = Started from a corner crack.

++ = Crack originated on the surface away from hole.

TABLE 4 - SUMMARY OF CONSTANT AMPLITUDE FATIGUE TESTS ON
6AA-4V BETA ANNEALED TITANIUM SPECIMENS WITH $\sigma_a = 40$ ksi and $R = 0.1$

Hole Condition	Cold Work Level	Fastener			Test Hole	Cycles Applied	Remarks	Test Hole Number
		Type	Interference Inch	Load Transfer σ_b / σ_o				
Open	-	None	-	-	#1	76,590	Fail *	T-CAF-1
	-	None	-	-	#2	93,320	cc, c = 0.13"	T-CAF-2
Close Tolerance	-	CT	-	0	#1	100,200	cc, c = 0.047"	T-CAF-3-1
	-	CT	-	0	#2	83,320	Fail *	T-CAF-3-2
	-	CT	-	0	#3	80,790	Fail *	T-CAF-3-3
	-	CT	-	1.07	#1	33,420	Fail *	T-CAF-1
	-	CT	-	1.08	#2	30,320	cc, c = 0.026"	T-CAF-2
Interference Fit	-	TL	0.0042	0	#1	981,790	Fail In Grip	T-CAF-4-2
	-	TL	0.0042	0	#2	1,014,380	Fail *	T-CAF-5-2
	-	TL	0.0042	1.08	#1	187,310	Fail *	T-CAF-4-1
	-	TL	0.0042	0.97	#2	357,070	Fail *	T-CAF-5-1
Cold Worked	1.6%	None	-	-	#1	122,790	Fail *	T-CAF-6-1
				-	#2	133,010	cc, c = 0.14"	T-CAF-6-2
				-	#3	226,520	Fail *	T-CAF-6-3
	1.6%	CT	-	0	#2	99,670	Fail *	T-CAF-7-2
				0	#2	110,520	1c, a = 0.37" +	T-CAF-8-2
	1.6%	CT	-	1.05	#1	41,960	Fail * $a_1 = 0.5"$ +	T-CAF-7-1
				0.95	#1	36,670	2tc, $a_2 = 0.31"$	T-CAF-8-1

cc = Corner Crack

CT = Close Tolerance

2cc = Two Corner Cracks

TL = Taper Lok

* Started from corner cracks.

1c = Thru Crack

* Started from embedded flaw.

2tc = Two Thru Cracks

TABLE 5 - SUMMARY OF INITIAL CRACKS (OR ORIGINS) OF ALL
CONSTANT AMPLITUDE FATIGUE TESTS ON BOTH
ALUMINUM AND TITANIUM SPECIMENS

HOLE CONDITION	CORNER CRACK		EMBEDDED FLAW	OTHERS	TOTAL
	SINGLE	DOUBLE			
(a) 2219-T851 ALUMINUM					
Open	2	0	0	0	2
Close Tolerance	2	2	1	0	5
Interference Fit	0	0	1	1*	2
Cold Worked	4	1	2	0	7
Total	8	3	4	1	16
(b) 6Al-4V BETA ANNEALED TITANIUM					
Open	2	0	0	0	2
Close Tolerance	2	0	3	0	5
Interference Fit	3	0	0	0	3
Cold Worked	4	1	2	0	7
Total	11	1	5	0	17

* Crack originated on the surface away from hole.

TABLE 6 - SUMMARY OF SPECTRUM FATIGUE TESTS ON 2219-TB51 ALUMINUM SPECIMENS

(a) BOMBER SPECTRUM

HOLE CONDITION	FASTENER LOAD TRANSFER, σ_b/σ_o	NO. OF FLIGHTS APPLIED	REMARKS	TEST HOLE NUMBER
Open	NA	2264	Fail (A-BSE-1 #2
		1850	2cc, $c_1 = c_2 = 0.05"$	A-BSE-2 #2
Close-Tolerance	0.99	1663	Fail *	A-BSE-1 #1
	1.0	1060	cc, $c = 0.15"$	A-BSE-6
	1.12	1373	Fail *	A-BSE-2 #1
	1.02	1295	Fail *	A-BSE-5
Interference-Fit (0.0030")	1.01	2685	1c, $a = 0.4"$ (A-BSE-3
	1.01	5982	Fail (A-BSE-4
Cold-Worked (2.2%)	0.96	1493	2cc, $a = 0.15"$ and $0.18"$ **	A-BSE-7
	0.89	1636	Fail *	A-BSE-8

(b) FIGHTER SPECTRUM

HOLE CONDITION	FASTENER LOAD TRANSFER, σ_b/σ_o	NO. OF FLIGHTS APPLIED	REMARKS	TEST HOLE NUMBER
Open	NA	532	2cc, $c_1 = 0.038"$ $c_2 = 0.013"$	A-FSE-1 #2
		519	Fail *	A-FSE-2 #2
Close-Tolerance	1.03	354	Fail *	A-FSE-1 #1
	0.91	356	2cc, $a = 0.1"$ & $0.15"$ **	A-FSE-2 #1
Interference-Fit (0.0038")	1.03	1327	Fail (A-FSE-3
	1.03	858	Fail (A-FSE-4
Cold-Worked (2.2%)	1.01	317	Fail (A-FSE-1X
	1.00	271	cc, $c = 0.12"$	A-FSE-2X

(c) Corner Crack

2cc Two Corner Cracks

(d) Dirc Crack

2cc Two Dirc Cracks

* Started from embedded flaw

(Started from corner crack

** Started from double embedded flaw

(Started from double corner crack

Best Available Copy

TABLE 7 - SUMMARY OF INITIAL CRACKS (OR ORIGINS) OF ALL
SPECTRUM FATIGUE TESTS ON 2219-T851 ALUMINUM
SPECIMENS

HOLE CONDITION	CORNER CRACK		EMBEDDED FLAW	OTHERS	TOTAL
	SINGLE	DOUBLE			
(a) BOMBER SPECTRUM					
Open	1	1	0	0	2
Close Tolerance	1	0	3	0	4
Interference Fit	2	0	0	0	2
Cold Worked	0	0	2	0	2
Total	4	1	5	0	10
(b) FIGHTER SPECTRUM					
Open	0	1	1	0	2
Close Tolerance	0	0	2	0	2
Interference Fit	0	2	0	0	2
Cold Worked	2	0	0	0	2
Total	2	3	3	0	8

TABLE B - SUMMARY OF SPECTRUM FATIGUE TESTS ON 6Al-4V BETA ANNEALED TITANIUM SPECIMENS

(a) BOMBER SPECTRUM

HOLE CONDITION	FASTENER LOAD TRANSFER, σ_b/σ_o	NO. OF FLIGHTS APPLIED	REMARKS	TEST HOLE NUMBER
Open	NA	1277	cc, c = 0.092"	T-BSF-1 #2
		2170	Fail	T-BSF-2 #2
Close-Tolerance	1.00	1248	cc, c = 0.146"	T-BSF-1 #1
	1.00	1272	3cc, $c_1 = c_2 = c_3 = 0.02"$	T-BSF-3
	1.00	1497	Fail *	T-BSF-2 #1
	1.0	1536	Fail ++	T-BSF-5
	1.0	1873	cc, c = 0.036"	T-BSF-6
	1.0	1542	Fail ++	T-BSF-4
Interference-Fit (0.0042")	1.00	5407	Fail +	T-BSF-7
	1.00	3964	cc, c = 0.075"	T-BSF-8
Cold-Worked (1.6%)	1.00	1807	Fail ++	T-BSF-1X
	1.00	1214	2cc, $c_1 = 0.029"$, $c_2 = 0.051"$	T-BSF-2X

(b) FIGHTER SPECTRUM

HOLE CONDITION	FASTENER LOAD TRANSFER, σ_b/σ_o	NO. OF FLIGHTS APPLIED	REMARKS	TEST HOLE NUMBER
Open	None	867	Fail ++	T-FSF-2 #2
		701	cc, c = 0.10"	T-FSF-1 #2
Close-Tolerance	1.00	526	Fail *	T-FSF-2 #1
	1.00	701	2tc, $a_1 = 0.4"$, $a_2 = 0.5"$ *	T-FSF-1 #1
Interference-Fit (0.0042")	1.00	2056	Fail ++	T-FSF-3
	1.00	714	Fail ++	T-FSF-4
Cold-Worked (1.6%)	1.00	313	cc, c = 0.033"	T-FSF-1X
	1.00	466	Fail +	T-FSF-2X

cc - Corner Crack

tc - Through Crack

* - Started from embedded flaw

+ - Started from corner crack

++ - Started from double corner crack

2cc - Two Corner Cracks


3cc - Three Corner Cracks (two located on the same side of the fastener hole)

Best Available Copy

TABLE 9 - SUMMARY OF INITIAL CRACKS (OR ORIGINS) OF ALL
SPECTRUM FATIGUE TESTS ON 6Al-4V BETA ANNEALED
TITANIUM SPECIMENS

HOLE CONDITION	CORNER CRACK		EMBEDDED FLAW	OTHERS	TOTAL
	SINGLE	DOUBLE			
(a) BOMBER SPECTRUM					
Open	2	0	0	0	2
Close Tolerance	2	3	1	0	6
Interference Fit	2	0	0	0	2
Cold Worked	0	2	0	0	2
Total	6	5	1	0	12
(b) FIGHTER SPECTRUM					
Open	1	1	0	0	2
Close Tolerance	0	0	2	0	2
Interference Fit	0	2	0	0	2
Cold Worked	2	0	0	0	2
Total	3	3	2	0	8

TABLE 10 - SUMMARY OF CRACK GROWTH OF PART-THRU CRACKS FROM FASTENER
HOLE TESTS FOR 2219-T851 ALUMINUM ALLOY PLATES SUBJECTED TO
CONSTANT AMPLITUDE LOADING

CRACK GEOMETRY	SPECIMEN NO.	TEST HOLE NO.	HOLE CONDITION	FASTENER		FLAW SIZES, IN.		σ_{max} KSI R = +0.1	NO. OF CYCLES APPLIED	REMARKS	RAW DATA IN VOL. II TABLE NO.
				TYPE	LOADED	INITIAL	FINAL				
	A-CA-1	1	Reamed	CT	Yes	0.004	0.168	18	54,500	(1)	1
		2		CT	None	0.003	0.199		94,500		
		3		None	None	0.003	0.176		94,500		
	A-CA-2	1	Reamed	CT	Yes	0.003	0.179	18	44,000	(1)	2
		2		CT	None	0.003	0.172		79,500		
		3		None	None	0.004	0.255		79,500		
	A-CA-3	1	Reamed	TL #2	Yes	0.048	0.168	18	94,000	(1)	3
		2		TL #1	None	0.038	0.168		38,000		
		3		TL #2	None	0.056	0.280		94,000		
	A-CA-4	1	Reamed	TL #2	Yes	0.037	0.168	18	54,000	(1),(2)	4
		2		TL #1	None	0.025	0.054		79,900		
		3		TL #2	None	0.043	0.058		79,900		
	A-CA-5	1	Reamed	TL #3	None	0.054	0.168	18	230,000	(1)	5
		2	CW #3	None	None	0.054	0.059		370,000		
		3	CW #1	None	None	0.055	0.105		370,000		
	A-CA-6	1	Reamed	TL #3	None	0.055	0.175	18	140,000	(1)	6
		2	CW #3	None	None	0.054	0.055		190,000		
		3	CW #1	None	None	0.052	0.075		190,000		
	A-CA-7	1	CW #1	CT	Yes	0.047	0.165	18	160,000	(1),(2)	7
		2	CW #1	CT	None	0.048	0.060		270,000		
		3	CW #2	None	None	0.045	0.045		270,000		
	A-CA-8	1	CW #1	CT	Yes	0.040	0.152	18	515,000	(2)	8
		2	CW #1	CT	None	0.056	0.120		515,000		
		3	CW #2	None	None	0.039	0.067		515,000		
	A-PO-3	1	Reamed	TL #2	None	0.056	0.151	18	95,310	(1)	9
		2		TL #2	None	0.054	0.183		28,000		
		3		TL #3	None	0.043	0.205		95,310		
	A-CA-1a	1	CW #2	None	None	0.059	0.430	18	350,000	(2)	10
		2	CW #3	None	None	0.046	0.062		367,200		

(1) Crack at this test hole was intentionally retarded after application of number of cycles shown.

(2) Specimen failed through this test hole.

(3) Numbers following "#" indicate level of cold work or interference. (Tables 14 and 15)

TABLE 11 - SUMMARY OF CRACK GROWTH OF THREE CRACKS FROM FASTENER HOLE TESTS
FOR 2219-T83 ALUMINUM ALLOY PLATES SUBJECTED TO CONSTANT AMPLITUDE
LOADING



CRACK GEOMETRY	SPECIMEN NO.	TEST HOLE NO.	HOLE CONDITION	FASTENER		FLAW SIZES, IN.		σ_{max} KSI R = +0.1	NO. OF CYCLES APPLIED	REMARKS	RAW DATA IN VOL. II TABLE NO.
				TYPE	LOADED	INITIAL	FINAL				
	A-CA-9	1	Reamed	CT	Yes	0.0061	0.6656	28	3,400		11
		2		CT	None	0.0080	0.6644		3,400		
		3		None	None	0.0067	0.3130		3,400		
	A-CA-10	1	Reamed	CT	Yes	0.0034	0.8147	24	6,400		12
		2		CT	None	0.0079	0.5379		6,800		
		3		None	None	0.0090	0.6328		6,800		
	A-CA-11	1	Reamed	TL #2	Yes						(3)
		2		TL #1	None						
		3		TL #2	None						
	A-CA-12	1	Reamed	TL #2	Yes	0.004	0.005	18	255,000		13
		2		TL #1	None	0.005	0.009		255,000		
		3		TL #2	None	0.004	0.006		255,000		
	A-CA-13	1	Reamed	TL #3	None	0.006	0.650	18	90,000	(1)	14
		2	CW #1	None	None	0.005	0.464		67,000	(1), (2)	
		3	CW #3	None	None	0.006	0.007		100,000		
	A-CA-14	1	Reamed	TL #3	None	0.004	0.018	18	92,600		15
		2	CW #1	None	None	0.003	0.157		76,600	(1), (2)	
		3	CW #3	None	None	0.006	0.006		92,600		
	A-CA-15	1	Reamed	TL #3	None	0.034	0.213	18	10,000	(1)	16
		2	CW #1	None	None	0.057	0.168		10,000	(1)	
		3	CW #3	None	None	0.067	0.073		80,000		
	A-CA-16	1	Reamed	TL #1	None	0.035	0.627	21	7,800		17
		2		TL #2	None	0.036	0.408		7,800		
		3		TL #3	None	0.026	0.454		7,800		
	A-CA-17	1	Reamed	TL #3	None	0.103	0.522	18	11,500	(1)	18
		2	CW #1	None	None	0.155	0.563		11,500	(1)	
		3	CW #3	None	None	0.149	0.151		46,500		
	A-CA-18	1	Reamed	TL #3	None	0.104	0.536	18	10,500	(1), (2)	19
		2	CW #1	None	None	0.146	0.540		21,000	(1)	
		3	CW #3	None	None	0.144	0.150		56,000		
	A-CA-19	1	CW #1	CT	Yes	0.057	0.222	18	8,500	(1), (2)	20
		2	CW #1	CT	None	0.080	0.192		12,000	(1)	
		3	CW #2	None	None	0.056	0.063		37,200		
	A-CA-20	1	CW #1	CT	Yes	0.041	0.230	18	11,000	(1)	21
		2	CW #1	CT	None	0.041	0.205		14,000	(1)	
		3	CW #2	None	None	0.073	0.077		71,200		
	A-CA-21	1	CW #1	CT	Yes	0.136	0.561	18	13,500	(1)	22
		2	CW #1	CT	None	0.157	0.591		10,000	(1)	
		3	CW #2	None	None	0.125	0.146		53,500		

TABLE 11. SUMMARY OF CRACK GROWTH OF THREE CRACKS FROM FASTENER HOLE TESTS
FOR 2219-T83 ALUMINUM ALLOY PLATES SUBJECTED TO CONSTANT AMPLITUDE
LOADING (Continued)

CRACK GEOMETRY	SPECIMEN NO.	TEST HOLE NO.	HOLE CONDITION	FASTENER		FLAW SIZES, IN.		σ_{max} KSI R = 60:1	NO. OF CYCLES APPLIED	REMARKS	RAW DATA IN VOL. II TABLE NO.
				TYPE	LOADED	INITIAL	FINAL				
	A-C-A-22	1	CW #1	C1	Yes	0.093	0.379	18	18,000	(1)	23
		2	CW #1	C1	None	0.125	0.538		18,000	(1)	
		3	CW #2	None	None	0.168	0.587		35,000		
	A-P-C-7	1	Reamed	11 #2	None	0.011	0.170	18	484,000	(1)	24
		2	Reamed	11 #2	None	0.006	0.006		524,000		
		3	Reamed	11 #3	None	0.002	0.002		524,000		
	A-P-C-8	1	Reamed	11 #2	None	0.110	0.641	18	50,000	(1)	25
		2	Reamed	11 #3	None	0.093	0.565		68,000		
	A-C-A-25	1	Reamed	None	None	0.006	0.419	18	22,500		26
		2	Reamed	C1	None	0.006	0.297		22,500		
	A-C-A-35	1	Reamed	C1	Yes	0.034	0.345	18	43,000		27
	A-C-A-45	1	Reamed	11 #1	None	0.011	0.391	18	72,000	(1)	28
		2	Reamed	11 #1	None	0.013	0.081		85,800		
	A-C-A-55	1	CW #3	None	None	0.159	0.541	18	87,600	(2)	29
		2	CW #3	None	None	0.141	0.151		87,600		
	A-C-A-65	1		11 #1	None	0.055	0.653	18	64,000	(1), (2)	30
		2	Reamed	11 #2	None	0.056	0.276		68,570		
		3		11 #3	None	0.056	0.150		68,570		
	A-C-A-75	1		11 #1	None	0.144	0.697	18	22,000	(1), (2)	31
		2	Reamed	11 #2	None	0.149	0.602		26,450		
		3		11 #3	None	0.147	0.351		26,450		

- (1) Crack at this test hole was intentionally retarded after application of number of cycles shown.
 (2) Specimen failed through this test hole.
 (3) Equipment malfunctioned resulting in the loss of specimen.
 (4) Numbers following "#1" indicate level of cold work or interference (Tables 14 and 15).

Best Available Copy

TABLE 12. SUMMARY OF CRACK GROWTH OF FAST THROUGH CRACKS FROM FASTENER HOLES
TESTS 7, 8, 9, 10, 11, 12, 13, 14, 15, 16, 17, 18, 19, 20, 21, 22, 23, 24, 25, 26, 27, 28, 29, 30, 31, 32, 33, 34, 35, 36, 37, 38, 39, 40, 41, 42, 43, 44, 45, 46, 47, 48, 49, 50, 51, 52, 53, 54, 55, 56, 57, 58, 59, 60, 61, 62, 63, 64, 65, 66, 67, 68, 69, 70, 71, 72, 73, 74, 75, 76, 77, 78, 79, 80, 81, 82, 83, 84, 85, 86, 87, 88, 89, 90, 91, 92, 93, 94, 95, 96, 97, 98, 99, 100, 101, 102, 103, 104, 105, 106, 107, 108, 109, 110, 111, 112, 113, 114, 115, 116, 117, 118, 119, 120, 121, 122, 123, 124, 125, 126, 127, 128, 129, 130, 131, 132, 133, 134, 135, 136, 137, 138, 139, 140, 141, 142, 143, 144, 145, 146, 147, 148, 149, 150, 151, 152, 153, 154, 155, 156, 157, 158, 159, 160, 161, 162, 163, 164, 165, 166, 167, 168, 169, 170, 171, 172, 173, 174, 175, 176, 177, 178, 179, 180, 181, 182, 183, 184, 185, 186, 187, 188, 189, 190, 191, 192, 193, 194, 195, 196, 197, 198, 199, 200, 201, 202, 203, 204, 205, 206, 207, 208, 209, 210, 211, 212, 213, 214, 215, 216, 217, 218, 219, 220, 221, 222, 223, 224, 225, 226, 227, 228, 229, 230, 231, 232, 233, 234, 235, 236, 237, 238, 239, 240, 241, 242, 243, 244, 245, 246, 247, 248, 249, 250, 251, 252, 253, 254, 255, 256, 257, 258, 259, 260, 261, 262, 263, 264, 265, 266, 267, 268, 269, 270, 271, 272, 273, 274, 275, 276, 277, 278, 279, 280, 281, 282, 283, 284, 285, 286, 287, 288, 289, 290, 291, 292, 293, 294, 295, 296, 297, 298, 299, 300, 301, 302, 303, 304, 305, 306, 307, 308, 309, 310, 311, 312, 313, 314, 315, 316, 317, 318, 319, 320, 321, 322, 323, 324, 325, 326, 327, 328, 329, 330, 331, 332, 333, 334, 335, 336, 337, 338, 339, 340, 341, 342, 343, 344, 345, 346, 347, 348, 349, 350, 351, 352, 353, 354, 355, 356, 357, 358, 359, 360, 361, 362, 363, 364, 365, 366, 367, 368, 369, 370, 371, 372, 373, 374, 375, 376, 377, 378, 379, 380, 381, 382, 383, 384, 385, 386, 387, 388, 389, 390, 391, 392, 393, 394, 395, 396, 397, 398, 399, 400, 401, 402, 403, 404, 405, 406, 407, 408, 409, 410, 411, 412, 413, 414, 415, 416, 417, 418, 419, 420, 421, 422, 423, 424, 425, 426, 427, 428, 429, 430, 431, 432, 433, 434, 435, 436, 437, 438, 439, 440, 441, 442, 443, 444, 445, 446, 447, 448, 449, 450, 451, 452, 453, 454, 455, 456, 457, 458, 459, 460, 461, 462, 463, 464, 465, 466, 467, 468, 469, 470, 471, 472, 473, 474, 475, 476, 477, 478, 479, 480, 481, 482, 483, 484, 485, 486, 487, 488, 489, 490, 491, 492, 493, 494, 495, 496, 497, 498, 499, 500, 501, 502, 503, 504, 505, 506, 507, 508, 509, 510, 511, 512, 513, 514, 515, 516, 517, 518, 519, 520, 521, 522, 523, 524, 525, 526, 527, 528, 529, 530, 531, 532, 533, 534, 535, 536, 537, 538, 539, 540, 541, 542, 543, 544, 545, 546, 547, 548, 549, 550, 551, 552, 553, 554, 555, 556, 557, 558, 559, 560, 561, 562, 563, 564, 565, 566, 567, 568, 569, 570, 571, 572, 573, 574, 575, 576, 577, 578, 579, 580, 581, 582, 583, 584, 585, 586, 587, 588, 589, 590, 591, 592, 593, 594, 595, 596, 597, 598, 599, 600, 601, 602, 603, 604, 605, 606, 607, 608, 609, 610, 611, 612, 613, 614, 615, 616, 617, 618, 619, 620, 621, 622, 623, 624, 625, 626, 627, 628, 629, 630, 631, 632, 633, 634, 635, 636, 637, 638, 639, 640, 641, 642, 643, 644, 645, 646, 647, 648, 649, 650, 651, 652, 653, 654, 655, 656, 657, 658, 659, 660, 661, 662, 663, 664, 665, 666, 667, 668, 669, 670, 671, 672, 673, 674, 675, 676, 677, 678, 679, 680, 681, 682, 683, 684, 685, 686, 687, 688, 689, 690, 691, 692, 693, 694, 695, 696, 697, 698, 699, 700, 701, 702, 703, 704, 705, 706, 707, 708, 709, 710, 711, 712, 713, 714, 715, 716, 717, 718, 719, 720, 721, 722, 723, 724, 725, 726, 727, 728, 729, 730, 731, 732, 733, 734, 735, 736, 737, 738, 739, 740, 741, 742, 743, 744, 745, 746, 747, 748, 749, 750, 751, 752, 753, 754, 755, 756, 757, 758, 759, 760, 761, 762, 763, 764, 765, 766, 767, 768, 769, 770, 771, 772, 773, 774, 775, 776, 777, 778, 779, 780, 781, 782, 783, 784, 785, 786, 787, 788, 789, 790, 791, 792, 793, 794, 795, 796, 797, 798, 799, 800, 801, 802, 803, 804, 805, 806, 807, 808, 809, 810, 811, 812, 813, 814, 815, 816, 817, 818, 819, 820, 821, 822, 823, 824, 825, 826, 827, 828, 829, 830, 831, 832, 833, 834, 835, 836, 837, 838, 839, 840, 841, 842, 843, 844, 845, 846, 847, 848, 849, 850, 851, 852, 853, 854, 855, 856, 857, 858, 859, 860, 861, 862, 863, 864, 865, 866, 867, 868, 869, 870, 871, 872, 873, 874, 875, 876, 877, 878, 879, 880, 881, 882, 883, 884, 885, 886, 887, 888, 889, 890, 891, 892, 893, 894, 895, 896, 897, 898, 899, 900, 901, 902, 903, 904, 905, 906, 907, 908, 909, 910, 911, 912, 913, 914, 915, 916, 917, 918, 919, 920, 921, 922, 923, 924, 925, 926, 927, 928, 929, 930, 931, 932, 933, 934, 935, 936, 937, 938, 939, 940, 941, 942, 943, 944, 945, 946, 947, 948, 949, 950, 951, 952, 953, 954, 955, 956, 957, 958, 959, 960, 961, 962, 963, 964, 965, 966, 967, 968, 969, 970, 971, 972, 973, 974, 975, 976, 977, 978, 979, 980, 981, 982, 983, 984, 985, 986, 987, 988, 989, 990, 991, 992, 993, 994, 995, 996, 997, 998, 999, 1000.

TEST NUMBER	SPECIMEN NO.	TEST HOLE NO.	HOLE CONSTITUTION	FASTENER		FLAW SIZE IN		σ_{max} KSI ($R = 60,1$)	NO. OF CYCLES APPLIED	REMARKS	RAW DATA IN TABLE No. 11	
				TYPE	LOADED	INITIAL	FINAL					
T.C.A. 1	1	1	Round	CT	Yes	0.001	0.189		40,000	(1)		
		2		CT	None	0.001	0.022	40	61,000		32	
		3		None	None	0.000	0.197		61,000			
T.C.A. 2	1	1	Round	CT	Yes	0.001	0.150		40,000	(1)		
		2		CT	None	0.001	0.172	40	42,000	(1)	33	
		3		None	None	0.001	0.187		61,000			
T.C.A. 3	1	1	Round	TL P2	Yes	0.046	0.157		91,650			
		2		TL P1	None	0.050	0.188	40	41,000	(1), (2)	34	
		3		TL P2	None	0.037	0.127		91,650			
T.C.A. 4	1	1	Round	TL P2	Yes	0.059	0.251		75,000			
		2		TL P1	None	0.049	0.176	40	75,000		35	
		3		TL P2	None	0.054	0.198		51,000	(1)		
T.C.A. 5	1	1	Round	TL P1	Yes	0.080	0.166		39,130			
		2		TL P1	None	0.035	0.037	40	39,130		36	
		3		CW P2	None	0.040	0.228		14,800	(1), (2)		
T.C.A. 6	1	1	Round	TL P1	Yes	0.043	0.095		40,440			
		2		TL P1	None	0.058	0.196	40	40,440		37	
		3		CW P2	None	0.047	0.227		18,000	(1), (2)		
T.C.A. 7	1	1	Round	CW P1	CT	Yes	0.075	0.185		5,000	(1)	
		2		CW P2	CT	None	0.063	0.272	40	12,800		38
		3		CW P1	None	None	0.057	0.174		12,800		
T.C.A. 8	1	1	Round	CW P1	CT	Yes	0.050	0.213		7,000	(1)	
		2		CW P1	CT	None	0.058	0.172	40	14,000		39
		3		CW P1	None	None	0.050	0.179		14,000		


(1) Crack at this test hole was instantaneously retarded after application of number of cycles shown.

(2) Specimen failed through this test hole.

(3) Numbers following "P" indicate level of cold work or interference (Tables 14 and 15).


Best Available Copy

TABLE 13 - SUMMARY OF CRACK GROWTH OR THRU CRACKS FROM FASTENER HOLE TESTS
FOR 6AL-4V BETA ANNEALED TITANIUM ALLOY PLATES SUBJECTED TO CONSTANT
AMPLITUDE LOADING

CRACK GEOMETRY	SPECIMEN NO.	TEST HOLE NO.	HOLE CONDITION	FASTENER		FLAW SIZES, IN.		σ_{max} KSI $R = 60:1$	NO. OF CYCLES APPLIED	REMARKS	RAW DATA IN VOL. II TABLE NO.
				TYPE	LOADED	INITIAL	FINAL				
	T-CA-9	1	Retained	CT	Yes	0.003	0.627	40	12,600		40
		2		CT	None	0.001	0.329		12,600		
		3		None	None	0.013	0.345		12,600		
	T-CA-10	1	Retained	CT	Yes	0.002	0.447	40	12,000		41
		2		CT	None	0.008	0.336		12,000		
		3		None	None	0.020	0.451		12,000		
	T-CA-11	1	Retained	TL #2	Yes	0.011	0.345	40	136,500	(1), (2)	42
		2		TL #1	None	0.006	0.007		170,500		
		3		TL #1	None	0.004	0.007		170,500		
	T-CA-12	1	Retained	TL #2	Yes	0.011	0.088	40	70,210	(2)	43
		2		TL #1	None	0.011	0.011		70,210		
		3		TL #1	None	0.010	0.010		70,210		
	T-CA-13	1	CW #1	CT	Yes	0.003	0.186	40	5,000	(1)	44
		2	CW #1	CT	None	0	0.211		12,500		
		3	CW #1	None	None	0.009	0.168		12,500		
	T-CA-14	1	CW #1	CT	Yes	0.004	0.205	40	5,500	(1)	45
		2	CW #1	CT	None	0.013	0.296		13,300		
		3	CW #1	None	None	0.006	0.171		13,300		
	T-CA-15	1	CW #1	CT	Yes	0.056	0.216	40	4,500	(1)	46
		2	CW #1	CT	None	0.064	0.177		4,500		
		3	CW #1	None	None	0.011	0.183		9,400		
	T-CA-16	1	CW #1	CT	Yes	0.037	0.216	40	4,500		47
		2	CW #1	CT	None	0.050	0.177		4,500		
		3	CW #1	None	None	0.059	0.187		4,500		
	T-CA-17	1	CW #1	CT	Yes	0.178	0.982	40	11,400		48
		2	CW #1	CT	None	0.119	0.579		11,400		
		3	CW #1	None	None	0.132	0.749		11,400		
	T-CA-18	1	CW #1	CT	Yes	0.177	0.682	40	9,200		49
		2	CW #1	CT	None	0.135	0.573		9,200		
		3	CW #1	None	None	0.158	0.586		9,200		
	T-CA-19	1	Retained	TL #3	None	0.048	0.171	40	27,500	(1)	50
		2	Retained	TL #3	None	0.016	0.177		36,000		
		3	CW #2	None	None	0.040	0.176		3,800		
	T-CA-20	1	CW #3	None	None	0.071	0.209	40	5,500	(1)	51
		2	CW #3	None	None	0.084	0.171		5,500		
		3	CW #2	None	None	0.065	0.175		10,000		
	T-CA-21	1	Retained	TL #3	None	0.160	0.631	40	21,200		52
		2	Retained	TL #3	None	0.117	0.455		21,200		
		3	CW #2	None	None	0.123	0.780		21,200		
	T-CA-22	1	CW #3	None	None	0.174	0.509	40	16,000		53
		2	CW #3	None	None	0.150	0.547		16,000		
		3	CW #2	None	None	0.152	0.498		10,500		

Best Available Copy

TABLE 13 - SUMMARY OF CRACK GROWTH OF THRU CRACKS FROM FASTENER HOLE TESTS
FOR 6A2-4V BETA ANNEALED TITANIUM ALLOY PLATES SUBJECTED TO CONSTANT
AMPLITUDE LOADING (Continued)

CRACK GEOMETRY	SPECIMEN NO.	TEST HOLE NO.	HOLE CONDITION	FASTENER		FLAW SIZES, IN.		σ_{max} KSI R = +0.1	NO. OF CYCLES APPLIED	REMARKS	RAW DATA IN VOL. II TABLE NO.
				TYPE	LOADED	INITIAL	FINAL				
	T-S-3	1	CW #2	None	None	0.034	0.170	40	18,900	(1)	54
		2	CW #2	None	None	0.015	0.165		5,500		
	T-CA-1a	1	Reamed	TL #1	None	0.013	0.035	40	13,700		55
		2		TL #1	None	0.011	0.352		13,700		
	T-CA-2a	1	Reamed	TL #2	None	0.019	0.390	40	29,500	(1)	56
		2		TL #2	None	0.017	0.342		32,500		

- (1) Crack at this test hole was intentionally retarded after application of number of cycles shown.
(2) Specimen failed through this test hole.
(3) Specimen failed in the grip.
(4) Numbers following "#" indicate level of cold work or interference (Tables 14 and 15).

Best Available Copy

TABLE 14 - DIMENSIONS DURING COLD-WORKING OPERATION.

MATERIAL	COLD-WORKED LEVEL	INITIAL HOLE DIAMETER, D _i INCH	MANDREL DIAMETER INCH	SLEEVE HALL THICKNESS INCH	TOTAL EXPANSION DIAMETER INCH	ΔD INCH	% EXPANSION (ΔD/D _i)	DIAMETER AFTER RELAXATION INCH	DIAMETER AFTER FINAL BEAMING INCH
2213-1851* Aluminum	1	0.366	0.354	0.010	0.374	0.008	2.2	0.369	0.3750
	2	0.361	0.354	0.010	0.374	0.013	3.6	0.368	0.3750
	3	0.355	0.354	0.010	0.374	0.019	5.4	0.366	0.3750
6A1-61/B Anodized Titanium	1	0.308	0.297	0.008	0.313	0.005	1.6	0.310	0.3125
	2	0.301	0.297	0.008	0.313	0.012	4.0	0.306	0.3125
	3	0.298	0.297	0.008	0.313	0.015	5.0	0.303	0.3125

* Levels 2 and 3 are comparable with the previous program.

Level 1 was chosen arbitrarily in 0.005" diameter increment.

* The percentages of diametrical expansions used in the analyses are 2.0, 4.0, and 6.0% for both aluminum and titanium materials.


Best Available Copy

TABLE 15 - DIMENSIONS OF INTERFERENCE-FIT FASTENER HOLES

MATERIAL	INTERFERENCE-FIT LEVEL	TAPERED HOLE DIAMETER * D _i , INCHES (NUT SIDE)	ΔD INCH	% EXPANSION (ΔD/D _i)
2219-T851 Aluminum	1	0.375	0.0024	0.64
	2	0.375	0.0038	1.01
	3	0.375	0.0060	1.60
6AL-4V β Annealed Titanium	1	0.3125	0.0034	1.09
	2	0.3125	0.0042	1.34
	3	0.3125	0.0050	1.60

* Slope of Taper-Lok fastener is 1/4-in. per foot on the diameter.

TABLE 10 - SUMMARY OF CRACK GROWTH IN PART-THREE CRACKS FROM FASTENER HOLE TESTS FOR 2219-T35 ALUMINUM ALLOY PLATES SUBJECTED TO BOMBING SPECTRUM LOADING

CRACK GROWTH	SPECIMEN NO.	TEST FLIGHT NO.	HOLE CONDITION	FASTENER TYPE	FASTENER LOADED	FLAW SIZES, IN. INITIAL	FLAW SIZES, IN. FINAL	SPECTRUM	NO. OF FLIGHTS APPLIED	REMARKS	RAW DATA INCL. OF II TABLE NO.
	A-BS-1	1	Retained	CT	Yes	0.0056	0.2587	Bomber	1,130	(2)	57
		2		CT	None	0.0034	0.0470		1,130		
		3		None	None	0.0056	0.0504		1,130		
	A-BS-2	1	Retained	TL #2	Yes	0.0582	0.1938	Bomber	762	(1), (2)	58
		2		TL #1	None	0.0580	0.0963		865		
		3		TL #2	None	0.0571	0.1131		865		
	A-BS-3	1	Retained	TL #2	Yes	0.0459	0.2027	Bomber	1,801		59
		2		TL #1	None	0.0269	0.2722		1,801		
		3		TL #2	None	0.0560	0.2117		1,801		
	A-BS-4	1	CW #1	CT	Yes	0.0526	0.2419	Bomber	509	(1), (2)	60
		2	CW #1	None	None	0.0358	0.1826		1,350		
	A-BS-5	1	CW #1	CT	None	0.0470	0.3942	Bomber	1,220		61
		2	CW #1	None	None	0.0616	0.2072		1,220		
	A-BS-6	1	Retained	TL #3	None	0.0426	0.0526	Bomber	3,507	(3)	62
		2		TL #3	None	0.0582	0.0818		3,507		
		3		TL #3	None	0.0582	0.0896		3,507		
	A-BS-7	1	Retained	CT	None	0.0067	0.0851	Bomber	1,781		63
		2		None	None	0.0078	0.2016		1,781	(2)	
	A-BS-14	1	CW #2	None	None	0.0404	0.4424	Bomber	2,987		64
		2	CW #2	None	None	0.0404	0.2374		7,507		

(1) Crack at this fast hole was intentionally retarded after application of number of flights shown.


(2) Specimen failed through this fast hole.

(3) Specimen failed in the grip.

(4) Numbers following "#2" indicate level of cold work or interference (Tables 14 and 15).

Best Available Copy

TABLE 12- SUMMARY OF CRACK GROWTH OF THRU CRACKS FROM FASTENER HOLE TESTS
FOR 2219-T851 ALUMINUM ALLOY PLATES SUBJECTED TO BOMBER SPECTRUM
LOADING

CRACK GEOMETRY	SPECIMEN NO.	TEST HOLE NO.	HOLE CONDITION	FASTENER		FLAW SIZES, IN.		SPECTRUM	NO. OF FLIGHTS APPLIED	REMARKS	RAW DATA IN VOL. II TABLE NO.
				TYPE	LOADED	INITIAL	FINAL				
	A-BS-8	1	Reamed	CT	Yes	0,0101	0,5130	Bomber	385	(1)	65
		2		CT	None	0,0090	0,5477		532		
		3		None	None	0,0134	0,4659		532		
	A-BS-9	1	Reamed	TL #2	Yes	0,0045	0,0403	Bomber	2,505	(1), (2)	66
		2		TL #1	None	0,0045	0,4659		1,040		
		3		TL #1	None	0,0045	0,0370		2,505		
	A-BS-10	1	Reamed	TL #2	Yes	0,0022	0,0022	Bomber	2,480	(2)	67
		2		TL #2	None	0,0056	0,0090		2,480		
		3		TL #2	None	0,0045	0,0045		2,480		
	A-BS-11	1	CW #1	CT	Yes	0,0045	0,2755	Bomber	700	(1), (2)	68
		2	CW #1	CT	None	0,0067	0,2822		1,264		
		3	CW #1	None	None	0,0034	0,1814		1,264		
	A-BS-12	1	CW #1	CT	Yes	0,0531	0,3651	Bomber	442		69
		2	CW #1	CT	None	0,0593	0,2262		442		
		3	CW #1	None	None	0,0543	0,2307		442		
	A-BS-13	1	CW #1	CT	Yes	0,0056	0,2464	Bomber	501	(1)	70
		2	CW #1	CT	None	0,0022	0,2184		707		
		3	CW #1	None	None	0,0034	0,2374		707		
	A-BS-14	1	CW #1	CT	Yes	0,0513	0,3506	Bomber	440		71
		2	CW #1	CT	None	0,0617	0,3170		440		
		3	CW #1	None	None	0,0545	0,2285		440		
	A-BS-15	1	CW #1	CT	Yes	0,1276	0,6567	Bomber	368		72
		2	CW #1	CT	None	0,1595	0,4647		368		
		3	CW #1	None	None	0,1496	0,4499		368		
	A-BS-16	1	Reamed	TL #3	None	0,0336	0,0874	Bomber	1,840	(1), (2)	73
		2	Reamed	TL #3	None	0,0381	0,2834		1,840		
		3	CW #2	None	None	0,0493	0,2262		917		
	A-BS-17	1	Reamed	TL #3	None	0,0448	0,0784	Bomber	2,120	(1), (2)	74
		2	Reamed	TL #3	None	0,0246	0,0246		2,120		
		3	CW #2	None	None	0,0616	0,4458		2,023		
	A-BS-18	1	CW #3	None	None	0,1370	0,2310	Bomber	1,140	(1), (2)	75
		2	CW #3	None	None	0,1470	0,2290		1,140		
		3	CW #2	None	None	0,1400	0,3990		785		
	A-BS-2X	1	Reamed	TL #2	Yes	0,0372	0,3506	Bomber	1,407		76
	A-BS-3X	1	Reamed	TL #2	None	0,0146	0,0235	Bomber	3,958	(2)	77
		2	Reamed	TL #2	None	0,0246	0,3405		3,794		


(1) Crack at this test hole was intentionally retained after application of number of flights shown.

(2) Specimen failed through this test hole.

(3) Numbers following "#" indicate level of cold work or interference (Tables 14 and 15).

Best Available Copy

TABLE 10 SUMMARY OF CRACK GROWTH OF PART THRU CRACKS FROM FASTENER TO HOLE
TESTS FOR 2219-T851 ALUMINUM ALLOY PLATES SUBJECTED TO FIGHTER
SPECTRUM LOADING

CRACK GEOMETRY	SPECIMEN NO.	TEST HOLE NO.	HOLE CONDITION	FASTENER		FLAW SIZES IN.		SPECTRUM	NO. OF FLIGHTS APPLIED	REMARKS	RAW DATA IN VOL. II TABLE NO.
				TYPE	LOADED	INITIAL	FINAL				
	A-FX-1	1	Reamed	CT	Yes	0,0045	0,2139		331	(2)	
		2		CT	None	0,0056	0,0605	Fighter	340		78
		3		None	None	0,0045	0,1411		340		
	A-FX-2	1	Reamed	TL #2	Yes	0,0515	0,1048		257	(1)	
		2		TL #1	None	0,0504	0,2184	Fighter	257	(1), (2)	79
		3		TL #2	None	0,0392	0,0538		486		
	A-FX-3	1	Reamed	TL #2	Yes	0,0538	0,2251		395	(1), (2)	
		2		TL #1	None	0,0470	0,1400	Fighter	607		80
		3		TL #2	None	0,0370	0,0571		607		
	A-FX-4	1	CW #1	CT	Yes	0,0403	0,2262		297	(2)	
		2	CW #1	None	None	0,0582	0,2453	Fighter	301		81
	A-FX-5	1	CW #1	CT	None	0,0414	0,3416		537		
		2	CW #1	None	None	0,0406	0,2744	Fighter	537		82
	A-FX-6	1	Reamed	TL #3	None	0,0426	0,0603		1,693		
		2		TL #3	None	0,0470	0,1154	Fighter	1,693		83
		3		TL #3	None	0,0549	0,2240		1,191	(1), (2)	


(1) Crack of this test hole was intentionally retarded after application of number of flights shown.

(2) Specimen failed through this test hole.

(3) Numbers following "#" indicate level of cold work or interference (Tables 14 and 15).

Best Available Copy


TABLE IV SUMMARY OF CRACK GROWTH OF THROUGH CRACKS FROM FASTENER HOLE TESTS FOR 2219-T83 ALUMINUM ALLOY PLATES SUBJECTED TO FIGHTER SPECTRUM LOADING

CRACK GEOMETRY	SPECIMEN NO.	TEST HOLE NO.	HOLE CONDITION	FASTENER		FLAW SIZE IN.		SPECTRUM	NO. OF FLIGHTS APPLIED	REMARKS	RAW DATA IN VOL. II TABLE NO.
				TYPE	LOADED	INITIAL	FINAL				
	A-FS-8	1	Reamed	C1	Yes	0.0134	0.4592	Fighter	98	(1), (2)	84
		2		C1	None	0.0067	0.2722		138		
		3		None	None	0.0146	0.2654		138		
	A-FS-9	1	Reamed	TL #2	Yes	0.0123	0.1322	Fighter	385		85
		2		TL #1	None	0.0023	0.4850		233	(1), (2)	
		3		TL #1	None	0.0023	0.0224		385		
	A-FS-10	1	Reamed	TL #2	Yes	0.0045	0.2274	Fighter	373	(1), (2)	86
		2		TL #2	None	0.0078	0.0112		432		
		3		TL #2	None	0.0067	0.2352		395	(1)	
	A-FS-11	1	CW #1	C1	Yes	0.0045	0.2016	Fighter	235	(2)	87
		2		C1	None	0.0045	0.0862		270		
		3		None	None	0.0067	0.0784		270		
	A-FS-12	1	CW #1	C1	Yes	0.0470	0.2867	Fighter	115	(1), (2)	88
		2		C1	None	0.0336	0.1478		160		
		3		None	None	0.0549	0.2016		143	(1)	
	A-FS-13	1	CW #1	C1	Yes	0.0011	0.2822	Fighter	188	(1), (2)	89
		2		C1	None	0.0045	0.1389		250		
		3		None	None	0.0056	0.1366		250		
	A-FS-14	1	CW #1	C1	Yes	0.0560	0.2363	Fighter	35	(1)	90
		2		C1	None	0.0426	0.2206		180		
		3		None	None	0.0515	0.2229		180		
	A-FS-15	1	CW #1	C1	Yes	0.1613	0.4861	Fighter	38	(1), (2)	91
		2		C1	None	0.1266	0.3987		145		
		3		None	None	0.1366	0.3349		145		
	A-FS-16	1	Reamed	TL #3	None	0.0426	0.2173	Fighter	1,403	(1)	92
		2		TL #3	None	0.0370	0.0717		1,621		
		3		None	None	0.0560	0.2251		782	(1)	
	A-FS-17	1	Reamed	TL #3	None	0.0347	0.1098	Fighter	943		93
		2		TL #3	None	0.0504	0.2352		766	(1)	
		3		None	None	0.0448	0.2150		836	(1), (2)	
	A-FS-18	1	CW #3	None	None	0.1030	0.1904	Fighter	342		94
		2		None	None	0.1075	0.1982		342		
		3		None	None	0.1949	0.5343		291	(1), (2)	
	A-FS-19	1	Reamed	TL #1	None	0.0112	0.2845	Fighter	932	(1), (2)	95
		2		TL #1	None	0.0134	0.0538		1,020		
	A-FS-20	1	Reamed	TL #2	None	0.0078	0.3472	Fighter	1,571		96
		2		TL #2	None	0.0101	0.0336		1,571		

- (1) Crack at this test hole was intentionally retarded after application of number of flights shown.
 (2) Specimen failed through this test hole.
 (3) Numbers following "#3" indicate level of cold work or interference (Tables 14 and 15).

Best Available Copy

TABLE 20 - SUMMARY OF CRACK GROWTH OF PART-THRU CRACKS FROM FASTENER HOLE TESTS FOR 6A1-4V BETA ANNEALED TITANIUM ALLOY PLATES SUBJECTED TO BUMPER SPECTRUM LOADING


CRACK GEOMETRY	SPECIMEN NO.	TEST HOLE NO.	HOLE CONDITION	FASTENER		FLAW SIZES, IN.		SPECTRUM	NO. OF FLIGHTS APPLIED	REMARKS	RAW DATA IN VOL. II TABLE NO.
				TYPE	LOADED	INITIAL	FINAL				
	1-B5-1	1		CT	Yes	0.0011	0.3875		1,234	(1), (2)	97
		2	Reamed	CT	None	0.0023	0.1366	Bumper	1,817		
		3		None	None	0.0045	0.0997		1,817		
	1-B5-2	1		TI #2	Yes	0.0482	0.4962		1,307	(1), (2)	98
		2	Reamed	TI #1	None	0.0616	0.4962	Bumper	1,854	(1)	
		3		TI #2	None	0.0672	0.2106		2,623		
	1-B5-3	1		TI #2	Yes	0.0661	0.5118		1,238	(1), (2)	99
		2	Reamed	TI #1	None	0.0627	0.5230	Bumper	1,000	(1)	
		3		TI #2	None	0.0459	0.1512		1,511		
	1-B5-4	1	Reamed	TI #3	Yes	0.0594	0.5665		2,770	(1), (2)	100
		2	Reamed	TI #3	None	0.0504	0.4334	Bumper	2,770	(1)	
		3	CW #2	None	None	0.0459	0.3293		2,884		
	1-B5-5	1	CW #3	None	None	0.0459	0.1754		3,744		101
		2	CW #3	None	None	0.0708	0.1030	Bumper	3,744		
		3	CW #2	None	None	0.0426	0.3761		2,715	(1), (2)	
	1-B5-6	1	CW #1	CT	Yes	0.0560	0.5063		807	(1), (2)	102
		2	CW #1	CT	None	0.0482	0.5522	Bumper	1,400		
		3	CW #1	None	None	0.0336	0.4357		1,400		
	1-B5-7	1	CW #1	CT	Yes	0.0493	0.6709		900		103
		2	CW #1	CT	None	0.0583	0.3427	Bumper	900		
		3	CW #1	None	None	0.0706	0.4334		900		

(1) Crack at this test hole was intentionally retarded after application of number of flights shown.

(2) Specimen failed through this test hole.


(3) Numbers following "#" indicate level of cold work or interference (Tables 14 and 15).

TABLE 21 - SUMMARY OF CRACK GROWTH OF THREE CRACKS FROM FASTENER HOLE TESTS FOR 6AL-4V BETA ANNEALED TITANIUM ALLOY PLATES SUBJECTED TO BOMBER SPECTRUM LOADING

CRACK GEOMETRY	SPECIMEN NO.	TEST HOLE NO.	HOLE CONDITION	FASTENER		FLAW SIZES, IN.		SPECTRUM	NO. OF FLIGHTS APPLIED	REMARKS	RAW DATA IN VOL. II TABLE NO.
				TYPE	LOADED	INITIAL	FINAL				
	T-85-8	1	Reamed	CT	Yes	0.0045	0.8747	Bomber	610		104
		2		CT	None	0.0157	0.4245		610		
		3		None	None	0.0045	0.3528		610		
	T-85-9	1	Reamed	TL #2	Yes			Bomber		(3)	
		2		TL #1	None						
		3		TL #1	None						
	T-85-10	1	Reamed	TL #2	Yes	0.0540	0.2867	Bomber	1,929	(1)	105
		2		TL #2	None	0.0594	0.7800		984		
		3		TL #2	None	0.0818	0.3552		984		
	T-85-11	1	CW #1	CT	Yes	0.0638	0.4245	Bomber	481		106
		2	CW #1	CT	None	0.0504	0.2573		481		
		3	CW #1	None	None	0.0728	0.4745		481		
	T-85-12	1	CW #1	CT	Yes	0.0090	0.4581	Bomber	626	(1), (2)	107
		2	CW #1	CT	None	0.0112	0.2475		971		
		3	CW #1	None	None	0.0090	0.4547		838		
	T-85-13	1	CW #1	CT	Yes	0.0045	0.4402	Bomber	720		108
		2	CW #1	CT	None	0.0034	0.3517		720		
		3	CW #1	None	None	0.0034	0.4133		720		
	T-85-14	1	CW #1	CT	Yes	0.0325	0.8266	Bomber	734	(1), (2)	109
		2	CW #1	CT	None	0.0448	0.4794		758		
		3	CW #1	None	None	0.0672	0.7247		758		
	T-85-15	1	CW #1	CT	Yes	0.1456	0.5712	Bomber	430		110
		2	CW #1	CT	None	0.1781	0.5443		430		
		3	CW #1	None	None	0.1781	0.5746		430		
	T-85-16	1	Reamed	TL #3	None	0.0325	0.0661	Bomber	1,780	(1), (2)	111
		2	Reamed	TL #3	None	0.0213	0.0269		1,780		
		3	CW #2	None	None	0.0493	0.5197		1,323		
	T-85-17	1	Reamed	TL #3	None	0.0414	0.0795	Bomber	1,534	(1), (2)	112
		2	Reamed	TL #3	None	0.0291	0.0638		1,534		
		3	CW #2	None	None	0.0795	0.5298		918		
	T-85-18	1	CW #3	None	None	0.1714	0.4984	Bomber	758		113
		2	CW #3	None	None	0.1714	0.4642		758		
		3	CW #2	None	None	0.1826	0.5869		758		
	T-85-1a	1	Reamed	TL #3	None	0.050	0.3600	Bomber	1,942	(1)	114
		2		TL #3	None	0.0380	0.3100		2,349		

- (1) Crack at this test hole was intentionally retarded after application of number of flights shown.
 (2) Specimen failed through this test hole.
 (3) Equipment malfunctioned resulting in the loss of specimen.
 (4) Numbers following "#-" indicate level of cold work or interference (Tables 14 and 15).

TABLE 22. SUMMARY OF CRACK GROWTH OF PART-THIRD CRACKS FROM FASTENER HOLE TESTS FOR 6AL-4V BETA ANNEALED TITANIUM ALLOY PLATES SUBJECTED TO FIGHTER SPECTRUM LOADING

CRACK GEOMETRY	SPECIMEN NO.	TEST HOLE NO.	HOLE CONDITION	FASTENER		FLAW SIZES, IN.		SPECTRUM	NO. OF FLIGHTS APPLIED	REMARKS	RAW DATA IN VOL. II TABLE NO.
				TYPE	LOADED	INITIAL	FINAL				
	T-FS-1	1	Reamed	C1	Yes	0.0101	0.2487	Fighter	506	(1), (2)	115
		2		C1	None	0.0034	0.0280		500		
		3		None	None	0.0056	0.0269		500		
	T-FS-2	1	Reamed	TL #2	Yes	0.0717	0.2934	Fighter	418	(1), (2)	116
		2		TL #1	None	0.0403	0.3293		418	(1)	
		3		TL #2	None	0.0470	0.1680		1,146		
	T-FS-3	1	Reamed	TL #2	Yes	0.0616	0.3282	Fighter	305	(1)	117
		2		TL #1	None	0.0549	0.1680		502		
		3		TL #2	None	0.0358	0.2610		305	(1)	
	T-FS-4	1	Reamed	TL #3	Yes	0.0672	0.2475	Fighter	203	(1)	118
		2	Reamed	TL #3	None	0.0560	0.3405		1,150	(1)	
		3	CW #2	None	None	0.0571	0.3002		1,711		
	T-FS-5	1	CW #3	None	None	0.0616	0.3270	Fighter	253	(1), (2)	119
		2	CW #3	None	None	0.0336	0.2162		479		
		3	CW #2	None	None	0.0246	0.3058		324	(1)	
	T-FS-6	1	CW #1	C1	Yes	0.0650	0.4272	Fighter	220	(1)	120
		2	CW #1	C1	None	0.0739	0.3618		220	(1)	
		3	CW #1	None	None	0.0515	0.2912		265		
	T-FS-7	1	CW #1	C1	Yes	0.0650	0.3439	Fighter	189	(1), (2)	121
		2	CW #1	C1	None	0.0695	0.2554		276		
		3	CW #1	None	None	0.0638	0.2162		276		


(1) Crack at this test hole was intentionally retarded after application of number of flights shown.

(2) Specimen failed through this test hole.

(3) Numbers following "#-" indicate level of cold work or interference (Tables 14 and 15).

Best Available Copy

TABLE 23 - SUMMARY OF CRACK GROWTH OF THRU CRACKS FROM FASTENER HOLE TESTS FOR 6A1-4V BETA ANNEALED TITANIUM ALLOY PLATES SUBJECTED TO FIGHTER SPECTRUM LOADING

CRACK GEOMETRY	SPECIMEN NO.	TEST HOLE NO.	HOLE CONDITION	FASTENER		FLAW SIZES, IN.		SPECTRUM	NO. OF FLIGHTS APPLIED	REMARKS	RAW DATA IN VOL. II TABLE NO.
				TYPE	LOADED	INITIAL	FINAL				
	T-FS-8	1	Reamed	CT	Yes	0.0034	0.5522	Fighter	317	(1)	122
		2		CT	None	0.0101	0.4659		317		
		3		None	None	0.0157	0.5096		296		
	T-FS-9	1	Reamed	TL #2	Yes	0.0056	0.0056	Fighter	325		123
		2		TL #1	None	0.0045	0.0045		325		
		3		TL #1	None	0.0090	0.0090		325		
	T-FS-10	1	Reamed	TL #2	Yes	0.0806	0.3629	Fighter	226	(1), (2)	124
		2		TL #2	None	0.0695	0.3170		269		
		3		TL #2	None	0.0638	0.2722		370		
	T-FS-11	1	CW #1	CT	Yes	-	-	Fighter	-	(4)	125
		2	CW #1	CT	None	0.0067	0.3584		200		
		3	CW #1	None	None	0.0079	0.3203		270		
	T-FS-12	1	CW #1	CT	Yes	0.0045	0.7565	Fighter	123	(1)	126
		2	CW #1	CT	None	0.0090	0.3987		279		
		3	CW #1	None	None	0.0079	0.3147		279		
	T-FS-13	1	CW #1	CT	Yes	0.0112	0.3338	Fighter	156	(1)	127
		2	CW #1	CT	None	0.0023	0.3214		125		
		3	CW #1	None	None	0.0079	0.3203		166		
	T-FS-14	1	CW #1	CT	Yes	0.0370	0.3528	Fighter	115	(1)	128
		2	CW #1	CT	None	0.056	0.3147		125		
		3	CW #1	None	None	0.0246	0.3338		180		
	T-FS-15	1	CW #1	CT	Yes	0.1210	0.4514	Fighter	171		129
		2	CW #1	CT	None	0.1658	0.4850		171		
		3	CW #1	None	None	0.1702	0.5197		171		
	T-FS-16	1	Reamed	TL #3	None	0.0347	0.2352	Fighter	618	(1)	130
		2	Reamed	TL #3	None	0.0269	0.3069		773		
		3	CW #2	None	None	0.0403	0.3304		761		
	T-FS-17	1	Reamed	TL #3	None	0.0482	0.3551	Fighter	421	(1), (2)	131
		2	Reamed	TL #3	None	0.0235	0.1826		566		
		3	CW #2	None	None	0.0638	0.2800		234		
	T-FS-18	1	CW #3	None	None			Fighter		(3)	
		2	CW #3	None	None						
		3	CW #2	None	None						

- (1) Crack at this test hole was intentionally retarded after application of number of flights shown.
 (2) Specimen failed through this test hole.
 (3) Equipment malfunctioned resulting in the loss of specimen.
 (4) This hole was reamed too large for cold-working and consequently was not tested.
 (5) Numbers following "#" indicate level of cold work or interference (Tables 14 and 15).

Best Available Copy

TABLE 24 - SUMMARY OF ANALYTICAL PROGRAM

NUMBER	FASTENER-HOLE CONDITION	LOADING CONDITION
1	Open Hole	Remote
2	Close-Tolerance Fastener	Remote
3	Close-Tolerance Fastener	Remote + Fastener
4	Interference-Fit Fastener	None
5	Interference-Fit Fastener	Remote
6	Interference-Fit Fastener	Remote + Fastener
7	Open Cold-Worked Hole	None
8	Open Cold-Worked Hole	Remote
9	Filled Cold-Worked Hole	Remote
10	Filled Cold-Worked Hole	Remote + Fastener

TABLE 25 - CHEMICAL COMPOSITIONS OF TEST MATERIALS

ALLOY	ELEMENT	Si	Fe	Cu	Mn	Mg	Zn	Ti	Al	V	Sn
2219-T851	Measured, Percent	0.04	0.18	5.91	0.39	0.001	0.06	0.04	REM.	-	-
	Specification Range, Percent	0.2 max	0.3 max	5.8 6.8	0.2 0.4	0.02 max	0.01 max	0.02 0.10	REM.	-	-
Ti-6Al-4V	Measured, Percent	-	-	-	0	-	-	REM.	5.9	4.10	0
	Specification Range, Percent	-	-	-	-	-	-	REM.	5.75 6.75	3.5 4.5	-

TABLE 26 - MECHANICAL PROPERTIES OF MATERIALS

(a) TENSILE TESTS

MATERIAL	DIAMETER (IN.)	F _{TU} (KSI)	0.2% OFFSET F _{TY} (KSI)	ELONG. IN. 1 IN. (TI) 2 IN. (AL) (%)	REDUCTION IN AREA (%)	STRAIN AT FAILURE (IN./IN.)
2219-T831 Aluminum (1 in. Thick Plate)	0.4993	67.7	54.4	11.0	24.3	0.1377
	0.4018	67.0	54.6	11.0	23.6	0.1438
	0.5014	<u>67.6</u>	<u>54.1</u>	<u>12.0</u>	<u>21.1</u>	<u>0.1490</u>
		67.4	54.3	11.3	23.0	0.1435 (Avg.)
Ti-6Al-4V Beta Annealed (0.6 in. Thick Plate)	0.2518	135.5	125.6	12.5	23.4	0.1525
	0.2512	136.0	128.8	13.5	25.7	0.0969
	0.2516	<u>135.3</u>	<u>125.3</u>	<u>12.5</u>	<u>27.7</u>	<u>0.1235</u>
		135.6	126.5	12.8	25.6	0.1093 (Avg.)

(b) COMPRESSION TESTS

MATERIAL	DIAMETER (IN.)	0.2% OFFSET F _C (KSI)
2219-T831 Aluminum (1 in. Thick Plate)	0.7503	58.6
	0.7505	58.1
	0.7501	<u>58.6</u>
		58.4 (Avg.)
Ti-6Al-4V Beta Annealed (0.6 in. Thick Plate)	0.6009	137.9
	0.5960	137.3
	0.6006	<u>138.7</u>
		138.2 (Avg.)

TABLE 27 - SUMMARY OF TEST PROGRAM FASTENERS

Plate Alloy	Fastener Details				Part Number
	Type	Material	Head Configuration		
2219-T851 Aluminum Alloy	Taper-Lok (3/8 Dia.)	Alloy Steel	Protruding		TL410
	Close Tolerance (3/8 Dia.) Bolt	Alloy Steel	Protruding		NAST106
Ti-6Al-4V Beta Ann.	Taper-Lok (5/16 Dia.)	Ti-6Al-4V STA	Protruding		TLV-20
	Close Tolerance Hi-Lok (5/16 Dia.)	Ti-6Al-4V STA	Protruding		HLT410

TABLE 28 - FIGHTER SPECTRUM - STANDARD SEVERITY

LOAD LAYER	LOAD (% LIMIT)		CYCLES PER MISSION	LOAD LAYER	LOAD (% LIMIT)		CYCLES PER MISSION
	MAX	MIN			MAX	MIN	
1	63.2	17.5	10	34	103.1	5.8	1
2	55.3	17.5	9	35	70.8	3.4	5
3	70.8	3.4	1	36	47.0	16.4	4
4	28.9	13.2	13	37	46.5	-18.9	1
5	70.8	3.4	1	38	37.5	17.5	5
6	37.5	17.5	39	39	63.2	17.5	1
7	70.8	3.4	1	40	28.9	13.2	1
8	84.8	7.0	1	41	47.0	16.4	16
9	47.0	16.4	18	42	70.8	3.4	3
10	37.5	17.5	39	43	55.3	17.5	13
11	28.9	13.2	26	44	37.5	17.5	39
12	76.4	4.6	1	45	28.9	13.2	13
13	47.0	16.4	18	46	47.0	16.4	18
14	28.9	13.2	13	47	63.2	17.5	5
15	47.0	16.4	19	48	28.9	13.2	13
16	76.4	4.6	1	49	70.8	3.4	1
17	55.3	17.5	28	50	47.0	16.4	19
18	37.5	17.5	39	51	37.5	17.5	39
19	63.2	17.5	5	52	55.3	17.5	9
20	47.0	16.4	19	53	28.9	13.2	13
21	37.5	17.5	39	54	37.5	17.5	39
22	70.8	3.4	1	55	28.9	13.2	13
23	63.2	17.5	4	56	63.2	17.5	5
24	76.4	4.6	1	57	76.4	4.6	1
25	94.4	14.7	5	58	37.5	17.5	39
26	37.5	17.5	12	59	55.3	17.5	9
27	63.2	17.5	2	60	47.0	16.4	36
28	76.4	4.6	2	61	55.3	17.5	9
29	66.4	22.2	7	62	70.8	3.4	3
30	63.2	17.5	10	63	84.8	7.0	1
31	66.4	22.2	4	64	63.2	17.5	10
32	55.3	17.5	30	65	118.1	4.1	1 Every 6 Starting with 1st Mission
33	47.0	16.4	7	66	120.4	-14.2	1 Every 18 Starting with 18th Mission

ALLOY	LIMIT STRESS (KSI)
Al-2219-T851	30.9
Ti-6Al-4V 3 A	61.8

TABLE 29 - BOMBER SPECTRUM - STANDARD SEVERITY

LOAD LAYER	LOAD (% LIMIT)		CYCLES/ MISSION	LOAD LAYER	LOAD (% LIMIT)		CYCLES/ MISSION
	MAX	MIN			MAX	MIN	
1	-3	-15	1	23	34	0	1
2	100	58	1 Every 100	24	24	13	4
3	90	58	1 Every 10	25	72	8	1
4	68	58	1	26	56	11	9
5	58	45	1	27	38	19	10
6	69	65	1	28	99	53	1 Every 100
7	70	40	1	29	88	-12	1 Every 10
8	56	49	3	30	75	53	1
9	51	24	1	31	-3	-15	1
10	63	51	2	32	85	56	1
11	51	43	1	33	88	51	1
12	69	36	1	34	53	33	1
13	36	13	1	35	62	53	2
14	48	36	6	36	53	46	1
15	36	30	1	37	81	48	1
16	76	31	1	38	69	58	1
17	53	32	1	39	70	32	1
18	71	55	1 Every 10	40	45	40	1
19	62	33	1	41	59	43	5
20	51	40	1	42	55	46	29
21	55	13	1	43	-3	-15	1
22	38	23	6	44	-4	-14	1

ALLOY	LIMIT STRESS (KSI)
Al-2219-T851	33.6
Ti-6Al-4V 3 A	70.0

TABLE 30-- FRACTURE TOUGHNESS FOR 2219-T851 ALUMINUM
AND 6AL-4V β ANNEALED TITANIUM

Specimen Number	Width (in.)	Thickness (in.)	Total Crack Length (in.)	Gross Stress σ_o (Ksi)	Net Section Stress σ_n (Ksi)	σ_n / σ_y	K_{Ic} Ksi $\sqrt{\text{in.}}$
2219-T851 Aluminum							
A-K-1	6.009	0.4350	2.98	17.98	35.67	0.65	46.1
A-K-2	6.007	0.4515	3.00	18.36	36.68	0.68	47.4
A-K-3	6.009	0.4530	2.98	17.78	35.27	0.65	45.6
						Average	46.3
6AL-4V Beta Annealed Titanium							
T-K-1	6.006	0.3753	2.10	71.43	109.8	0.87	140.5
T-K-2	6.003	0.3740	2.10	71.49	109.9	0.87	140.6
T-K-3	6.005	0.3750	2.10	72.61	111.6	0.88	142.8
						Average	141.3

TABLE 31 - INITIAL AND FINAL DIMENSIONS OF CORNER CRACK TESTED SPECIMENS

(a) 2219-T851 ALUMINUM

Hole Condition	Fastener		Loading Condition	Initial Flaw			Final Flaw			Specimen Number
	Type	Loaded		a _i	c _i	(a/2c) _i	a _f	c _f	(a/2c) _f	
Reamed	None	None	CA	-	0.003	-	0.225	0.176	0.650	A-CA-1 #3
		↓	CA	-	0.004	-	0.350	0.255	0.686	A-CA-2 #3
	CT	Yes	CA (21)	0.168	0.146	0.575	0.412	0.390	0.528	FUCTA-1 *
		↓	CA (21)	0.174	0.144	0.604	0.406	0.349	0.582	FUCTA-1 *
	None	None	CA	-	0.003	-	0.358	0.199	0.899	A-CA-1 #2
		↓		-	0.003	-	0.295	0.172	0.858	A-CA-2 #2
		↓		-	-	-	0.030	0.025	0.600	A-CAF-3 #1
		↓		-	-	-	0.29	0.23	0.630	A-CAF-3 #2
CW #1	None			0.055	0.055	0.500	0.240	0.105	1.143	A-CA-5 #3
CW #2		↓		-	0.045	-	0.079	0.045	0.878	A-CA-7 #3
CW #2		↓		0.050	0.039	0.641	0.116	0.067	0.866	A-CA-8 #3
CW #3		↓		-	0.054	-	0.112	0.055	1.018	A-CA-6 #2
CW #1		↓	B	0.050	0.036	0.694	0.385	0.183	1.052	A-B5-4 #2
		↓	B	-	0.062	-	0.355	0.207	0.857	A-B5-5 #2
		↓	F	-	0.058	-	0.430	0.245	0.878	A-F5-4 #2
		↓	F	0.055	0.049	0.561	Thru	0.274	-	A-F5-5 #2
	CT		CA	-	0.048	-	0.100	0.060	0.822	A-CA-7 #2
	CT		CA	0.065	0.056	0.580	0.385	0.120	1.604	A-CA-8 #2

CA = Constant Amplitude

CW = Cold-Worked

- = Not clear or available

* = Data reported in Reference 2

B = Bomber

TL = Taper-Lok

F = Fighter

CT = Close Tolerance

TABLE 31 - INITIAL AND FINAL DIMENSIONS OF CORNER CRACK TESTED SPECIMENS (Cont'd)

(a) 2219-T851 ALUMINUM (Cont'd)

Hole Condition	Fastener		Loading Condition	Initial Flaw			Final Flaw			Specimen Number
	Type	Loaded		a _i	c _i	(a/2c) _i	a _f	c _f	(a/2c) _f	
CW #1	CT	None	CA	-	-	-	0.350	0.405	0.432	A-CAF-7 #2
		None	F	0.050	0.041	0.610	Thru	0.342	-	A-FS-5 #1
CW #3		Yes	CA	0.055	0.040	0.688	Thru	0.152	-	A-CA-8 #1
		None	CA (28)	0.176	0.150	0.587	0.267	0.188	0.710	FUCCA-1 *
CW #3		Yes	CA (28)	0.178	0.150	0.593	0.377	0.166	1.136	FUCCA-1 *
Reamed	TL #1	None	CA	-	0.025	-	0.046	0.054	0.426	A-CA-4 #2
			B	-	0.027	-	0.210	0.272	0.386	A-BS-3 #2
			CA (24)	0.156	0.145	0.538	0.276	0.321	0.430	FUCIA-1 *
		Yes		0.136	0.144	0.472	0.281	0.411	0.342	FUCIA-2 *
				0.160	0.138	0.580	0.403	0.460	0.438	FUCIA-1 *
	TL #2	None	CA	0.062	0.056	0.554	0.295	0.280	0.527	A-CA-3 #3
		None		0.028	0.043	0.326	0.061	0.058	0.526	A-CA-4 #3
		Yes		0.062	0.048	0.646	0.089	0.168	0.265	A-CA-3 #1
		None		0.065	0.056	0.580	0.065	0.151	0.215	A-PO-3 #1
	TL #3			0.055	0.043	0.640	0.185	0.205	0.451	A-PO-3 #3
	TL #2		B	0.075	0.056	0.670	0.160	0.212	0.377	A-BS-3 #3
	TL #3		F	0.050	0.043	0.581	0.060	0.068	0.441	A-FS-6 #1
	TL #3		F	-	0.047	-	0.075	0.115	0.326	A-FS-6 #2
	TL #2		CA (24)	0.144	0.130	0.554	0.273	0.364	0.375	FUCIA-2 *
	TL #2	Yes		0.160	0.139	0.576	0.343	0.490	0.350	FUCIA-2 *
	TL #3	None		0.151	0.140	0.539	0.175	0.188	0.465	FUCIA-1 *

CA = Constant Amplitude
CW = Cold-Worked
- = Not clear or available

* = Data reported in Reference 2
B = Bomber
TL = Taper-Lok

F = Fighter
CT = Close Tolerance

TABLE 31 - INITIAL AND FINAL DIMENSIONS OF CORNER CRACK TESTED SPECIMEN (Cont'd)

(b) 6AL-4V BETA ANNEALED TITANIUM

Hole Condition	Fastener Type	Fastener Loaded	Loading Condition	Initial Flow			Final Flow			Specimen Number
				a_i	ϵ_i	$(a/2c)_i$	a_f	ϵ_f	$(a/2c)_f$	
Reamed	None	None	CA	-	0.004	-	0.28	0.20	0.700	T-CA-1 #3
				-	0.003	-	Thru	0.187	-	T-CA-2 #3
				-	-	-	0.22	0.12	0.917	T-CAF-2 #2
			F	-	0.006	-	0.040	0.027	0.741	T-FS-1 #3
	CT		F	-	0.003	-	0.040	0.028	0.714	T-FS-1 #2
	None		CA (25)	0.114	0.124	0.460	0.300	0.285	0.526	FUCTT-1*
	CT		CA (25)	0.114	0.136	0.419	0.300	0.273	0.549	FUCTT-1*
	CT	Yes	CA (25)	0.128	0.138	0.464	0.276	0.257	0.537	FUCTT-1*
	TL #1	None	CA	-	0.049	-	0.14	0.18	0.389	T-CA-4 #2
	TL #2			-	0.037	-	0.12	0.13	0.462	T-CA-3 #3
	TL #3			-	0.035	-	0.052	0.037	0.703	T-CA-5 #2
	TL #3			-	0.058	-	0.13	0.20	0.325	T-CA-6 #2
	TL #2	Yes		-	0.046	-	0.112	0.157	0.357	T-CA-3 #1
	TL #2			-	0.059	-	0.15	0.25	0.300	T-CA-4 #1
	TL #3			-	0.043	-	0.10	0.095	0.526	T-CA-6 #1
	TL #2	None	B	-	0.067	-	0.180	0.211	0.427	T-BS-2 #3
	TL #3	Yes	CA	-	0.060	-	0.125	0.166	0.377	T-CA-5 #1
	TL #2	None	CA	-	0.054	-	0.31	0.38	0.408	T-CA-4 #3
	TL #1	None	F	-	0.055	-	0.15	0.17	0.441	T-FS-3 #2

CA = Constant Amplitude

CW = Cold-Worked

- = Not clear or available

* = Data reported in Reference 2

B = Bomber

TL = Taper-Lok

F = Fighter

CT = Close Tolerance

TABLE 31 - INITIAL AND FINAL DIMENSIONS OF CORNER CRACK TESTED SPECIMEN (Cont'd)
(b) 6AL-4V BETA ANNEALED TITANIUM(Cont'd)

Hole Condition	Fastener		Loading Condition	Initial Flow			Final Flow			Specimen Number
	Type	Loaded		a _i	c _i	(a/2c) _i	a _f	c _f	(a/2c) _f	
Reamed	TL #2	None	F	-	0.036	-	0.12	0.26	0.231	T-FS-3 #3
	TL #1		CA (50)	0.129	0.124	0.520	0.204	0.219	0.466	FUCIT-2 *
	TL #2		CA (50)	0.120	0.115	0.522	Thru	0.765	-	FUCIT-2 *
CW #1	None		CA	-	0.057	-	0.21	0.17	0.618	T-CA-7 #3
	None			-	0.056	-	0.25	0.18	0.694	T-CA-8 #3
	CT			-	0.063	-	0.31	0.27	0.574	T-CA-7 #2
	CT			-	0.056	-	0.21	0.17	0.618	T-CA-8 #2
	None			-	-	-	0.31	0.21	0.738	T-CAF-6 #2
	None		B	-	0.034	-	Thru	0.436	-	T-B5-6 #3
	CT		B	-	0.048	-	Thru	0.552	-	T-B5-6 #2
CW #2	None		B	-	0.046	-	0.370	0.329	0.562	T-B5-4 #3
CW #2			F	0.035	0.057	0.307	0.33	0.30	0.550	T-FS-4 #3
CW #1			F	-	0.064	-	0.27	0.22	0.614	T-FS-7 #3
CW #1				-	0.052	-	0.33	0.29	0.569	T-FS-6 #3
CW #3				-	0.034	-	0.25	0.22	0.568	T-FS-5 #2
CW #1	CT			-	0.070	-	0.31	0.26	0.596	T-FS-7 #2
CW #1	CT		CA (55)	0.128	0.123	0.520	0.258	0.134	0.963	FUCCT-1 *
CW #1	CT	Yes	CA (55)	0.130	0.112	0.580	0.351	0.134	1.310	FUCCT-1 *

* = Data reported in Reference 2
CA = Constant Amplitude
CW = Cold-Worked
- = Not clear or available
F = Fighter
B = Bomber
CT = Close Tolerance
TL = Taper-Lok

TABLE 32 - RESULTS OF FRACTURE TESTS ON FLAWED ALUMINUM
AND TITANIUM COLD-WORKED OPEN HOLES

SP. NO.	MATERIAL	WIDTH, IN.	THICK., IN.	HOLE DIA., IN.	CRACK LENGTH, IN.	MAX. LOAD, LBS.	DISPLACEMENT @ FAILURE IN. Δ	σ_c KSI
A-J-1	Al.	4.004	0.4443	0.375	0.045	78,000	0.018	43.8
A-J-2	Al.	4.005	0.4517	0.375	0.105	75,500	0.014	41.7
A-J-3	Al.	4.007	0.4475	0.375	0.160	75,000	0.014	41.8
T-J-1	Ti.	4.002	0.3759	0.313	0.065	174,500	0.034	116.0
T-J-2	Ti.	4.000	0.3758	0.313	0.130	170,500	0.031	113.4
T-J-3	Ti.	4.002	0.3758	0.313	0.160	168,500	0.030	112.0

Δ Measured between points 1-inch above and 1-inch below ζ of hole.

TABLE 33 - THRESHOLD CRACK LENGTHS FOR VARIOUS FASTENER-HOLE COMBINATIONS
IN 2219-T851 ALUMINUM PLATES SUBJECTED TO 18 KSI CONSTANT AMPLITUDE
FAR-FIELD LOADING

FASTENER-HOLE CONDITION	a_i IN.	a_f IN.	a_m IN.	ΔN CYCLES	$\frac{\Delta a}{dN} \times 10^6$ IN./CYCLE	ΔK ($R = 0.1$) KSI \sqrt{IN}	K_{max} KSI \sqrt{IN}	a_{th} IN.	SPECIMEN NO.
(a) Corner Cracks									
OPEN	0.003	0.007	0.0050	23000	0.174	3.2	3.6	0.00111	A-CA-1 #3
CT	0.003	0.006	0.0045	19000	0.158	3.1	3.4	0.00113	A-CA-1 #2
CT + LT	0.004	0.009	0.0065	13000	0.385	4.0	4.4	0.00097	A-CA-1 #1
TL #1	0.025	0.029	0.0270	24000	0.167	3.2	3.6	0.0060	A-CA-4 #2
TL #2	0.045	0.049	0.0470	30000	0.133	3.0	3.3	0.0125	A-CA-4 #3
TL #3	0.054	0.059	0.0565	44000	0.114	2.9	3.2	0.0159	A-CA-5 #1
CW #1	0.052	0.056	0.0540	20000	0.200	3.3	3.7	0.0114	A-CA-6 #3
CW #2	0.064	0.085	0.0745	83000	0.253	3.5	3.9	0.0142	A-CA-1X #1
CW #3	0.046	0.062	0.0540	367000	0.044	2.2	2.5	0.0250	A-CA-1X #2
(b) Thru Cracks									
OPEN	0.006	0.012	0.0090	1500	4.0	8.5	9.4	0.00029	A-CA-2X #1
CT	0.006	0.011	0.0085	1500	3.3	8.0	8.9	0.00031	A-CA-2X #2
CT + LT	0.004	0.011	0.0075	2000	3.8	8.3	9.3	0.00026	A-CA-3X #1
TL #1	0.016	0.020	0.0180	24000	0.17	3.2	3.6	0.0040	A-CA-4X #2
TL #2	0.011	0.018	0.0145	365000	0.019	1.8	2.0	0.0105	A-PO-7 #1
TL #3	0.034	0.036	0.0350	2500	0.800	5.1	5.7	0.0031	A-CA-15 #1
CW #1	0.053	0.056	0.0545	5000	0.60	4.6	5.1	0.0061	A-CA-13 #2
CW #2	0.056	0.063	0.0595	37200	0.19	3.3	3.7	0.0126	A-CA-19 #3
CW #3	0.141	0.146	0.1435	22000	0.23	3.4	3.8	0.0287	A-CA-5X #2

TABLE 34- THRESHOLD CRACK LENGTHS FOR VARIOUS FASTENER-HOLE COMBINATIONS
IN 6Al-4V BETA ANNEALED TITANIUM PLATES SUBJECTED TO 40 KSI CONSTANT
AMPLITUDE FAR-FIELD LOADING

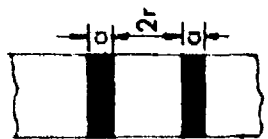
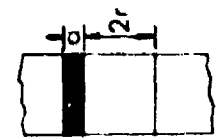
FASTENER-HOLE CONDITION	a_i IN.	a_f IN.	a_m IN.	N CYCLES	$\frac{da}{dN} \times 10^6$ IN./CYCLE	$\frac{\Delta K}{(R=0.1)}$ KSI \sqrt{IN}	K_{max} KSI \sqrt{IN}	a_m IN.	SPECIMEN NO.
(a) Corner Cracks									
OPEN	0.004	0.008	0.006	28,200	0.14	7.1	7.9	0.00132	T-CA-2 #3
CT	0.003	0.011	0.007	49,600	0.16	7.3	8.1	0.00146	T-CA-1 #2
CT + LT	0.003	0.011	0.007	14,000	0.57	10.1	11.2	0.00076	T-CA-2 #1
TL #1	0.050	0.058	0.054	4,000	2.00	14.5	16.1	0.0029	T-CA-3 #2
TL #2	0.054	0.062	0.058	8,000	1.0	12.0	13.3	0.0045	T-CA-4 #3
TL #3	0.058	0.065	0.0615	6,000	1.2	12.5	13.9	0.0044	T-CA-6 #2
CW #1	0.057	0.063	0.060	2,800	2.1	14.8	16.4	0.0031	T-CA-7 #3
CW #2	0.047	0.061	0.054	6,000	2.3	15.0	16.7	0.0027	T-CA-6 #3
(b) Thru Cracks									
OPEN	0.020	0.024	0.022	500	8.0	21.5	23.9	0.00053	T-CA-10 #3
CT	0.008	0.048	0.028	3,500	11.4	23.6	26.2	0.00056	T-CA-10 #2
CT + LT	0.019	0.024	0.0215	500	10.0	23.0	25.6	0.00045	T-CA-10 #1
TL #1	0.013	0.035	0.024	13,700	1.60	13.6	15.1	0.0014	T-CA-1X
TL #2	0.019	0.037	0.028	8,000	2.30	15.0	16.7	0.0014	T-CA-2X
TL #3	0.019	0.038	0.0285	16,500	1.20	12.5	13.9	0.0020	T-CA-19 #2
CW #1	0.011	0.015	0.013	2,000	2.0	14.5	16.1	0.0007	T-CA-14 #3
CW #2	0.093	0.112	0.1025	1,000	19.0	27.5	30.6	0.0015	T-CA-19 #3
CW #3	0.078	0.083	0.0815	500	10.0	23.0	25.6	0.0017	T-CA-20 #1

TABLE 35 - GREEN'S FUNCTION FOR A DOUBLE CRACK EMANATING FROM AN OPEN HOLE IN AN INFINITE PLATE

$\frac{a/r}{x/a}$.20	.30	.40	.50	.60	.70	.80	.90	1.00	1.40	1.60	2.00	2.40	3.00
.00	.664	.629	.603	.595	.563	.575	.572	.554	.548	.571	.582	.594	.600	.611
.10	.676	.639	.615	.604	.582	.583	.586	.569	.563	.587	.596	.603	.603	.615
.20	.688	.645	.628	.617	.599	.596	.600	.589	.578	.604	.612	.613	.609	.624
.30	.699	.658	.646	.633	.621	.613	.623	.610	.598	.627	.630	.625	.619	.635
.40	.718	.679	.671	.656	.651	.639	.655	.639	.624	.656	.653	.642	.635	.664
.45	.740	.691	.689	.671	.673	.657	.674	.658	.643	.674	.665	.654	.647	.680
.50	.760	.708	.712	.689	.698	.681	.701	.682	.668	.692	.678	.670	.662	.699
.55	.781	.732	.739	.712	.730	.711	.733	.708	.699	.709	.695	.692	.679	.721
.60	.802	.764	.762	.746	.770	.752	.766	.739	.737	.730	.725	.721	.702	.753
.65	.840	.811	.793	.790	.814	.803	.808	.781	.786	.766	.760	.760	.729	.795
.70	.889	.868	.837	.838	.865	.867	.850	.827	.847	.812	.801	.811	.760	.842
.75	.960	.946	.907	.911	.913	.960	.912	.911	.929	.888	.859	.884	.817	.906
.80	1.071	1.089	1.044	1.030	.989	1.056	1.018	.995	1.021	.985	.955	.979	.904	.977
.85	1.234	1.254	1.245	1.211	1.141	1.252	1.177	1.187	1.192	1.130	1.130	1.120	1.042	1.101
.90	1.429	1.432	1.434	1.436	1.437	1.438	1.440	1.441	1.442	1.445	1.446	1.448	1.449	1.451

* For $x/a > 0.9$, $G(a/r, x/a) = \frac{1}{\pi} \left[\frac{4(1 + r/a)}{(1 - x/a)(1 + x/a + 2r/a)} \right]^{1/2}$

TABLE 36. SUMMARY OF STRESS INTENSITY FACTOR SOLUTIONS
FOR THRU-CRACKED FASTENER HOLES

CRACK GEOMETRY	HOLE CONDITION	FASTENER		STRESS INTENSITY FACTOR	β (FIG. NO.)	REMARKS
		Type (1)	% Load Transfer			
	Reamed	None	-	$K = \sigma_o \sqrt{\pi a} \beta_{OP}$	138	(2)
		CT	≥ 0	$K = \sigma_o \sqrt{\pi a} \beta_{CT}$	143-145	
	Reamed	TL	0	$K = \sigma_{ys} \sqrt{\pi a} \beta_{IF}$	150, 152	(3)
		TL	> 0	"	Not Shown	
	Cold-Worked	None	-	$K = \sigma_{ys} \sqrt{\pi a} \beta_{CW}$	161, 166	(4)
		CT	≥ 0	"	Not Shown	
	Each of Above	Each of Above	Each of Above	$K = \frac{B_1}{B_2} K$	-	
				one crack	two cracks	

(1) CT: Close Tolerance, TL: Taper-Lok

(2) Bowie Solution: B_1 for Single Crack, B_2 for Double Crack

(3) β_{IF} valid for specified material, far-field loading, and level of interference.

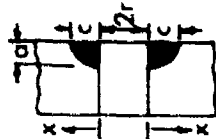
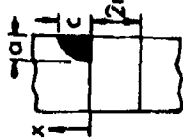
(4) β_{CW} valid for specified material, far-field loading, and level of cold working.

TABLE 37 - COMPARISON OF STRESS INTENSITY FACTOR SOLUTIONS FOR
CORNER CRACKS EMANATING FROM OPEN HOLES IN PLATES
LOADED IN TENSION NORMAL TO CRACK SURFACES
($a/c \equiv 1.4$, $r/r = 1.895$)

S.I.F. at Hole Wall, $K_A/\sigma_o\sqrt{\pi a}$							
a/t	c/r	Snow Data (32)	Gran (25)	Hsu/Liu (26)	Hall/Finger (24)	Shah (17)	Fujimoto (33)
0.3	0.42	1.39	2.60	1.79*	1.22	1.38	1.65
0.4	0.56	1.31	2.69	1.79	1.17	1.32	1.54
0.5	0.69	1.25	2.82	1.79	1.09	1.27	1.40
0.6	0.83	1.22	3.01	1.79	1.03	1.25	1.30
0.7	0.97	1.19	3.33	1.79	0.98	1.21	1.26
0.8	1.11	1.23	3.90	1.79	0.94	1.08	1.15
S.I.F. at Plate Surface, $K_C/\sigma_o\sqrt{\pi c}$							
0.3	0.42	1.58	1.34	1.57	1.44	1.52	1.58
0.4	0.56	1.46	1.21	1.44	1.38	1.41	1.45
0.5	0.69	1.41	1.13	1.32	1.29	1.26	1.35
0.6	0.83	1.35	1.06	1.24	1.22	1.18	1.25
0.7	0.97	1.36	1.02	1.18	1.16	1.08	1.19
0.8	1.11	1.36	0.99	1.14	1.11	1.08	1.14

* Factor $(\frac{c}{a})^{1/2}$ was omitted in References (32) and (33).

TABLE 38. SUMMARY OF STRESS INTENSITY FACTOR SOLUTIONS
FOR CORNER-CRACKED FASTENER HOLES

CRACK GEOMETRY	HOLE CONDITION	FASTENER		STRESS INTENSITY FACTOR	M'_1/ϕ (Fig. No.)	β (Fig. No.)	M_c	REMARKS
		Type (1)	% Load Transfer					
	Reamed	None	-	$K = \sigma_o \sqrt{\pi c} \beta_{OP} \frac{M'_1}{\phi} M_c$	175, 176	138	Eq. (27) & Fig. 178	(2), (3)
		CT	≥ 0	$K = \sigma_o \sqrt{\pi c} \beta_{CT} \frac{M'_1}{\phi} M_c$		143-145		
	Reamed	TL	0	$K = \sigma_{ys} \sqrt{\pi c} \beta_{IF} \frac{M'_1}{\phi} M_c$	175, 176	150, 152	Eq. (27) & Fig. 178	(2), (3), (4)
		TL	> 0	"		Not Shown		
	Cold-Worked	None	-	$K = \sigma_{ys} \sqrt{\pi c} \beta_{CW} \frac{M'_1}{\phi} M_c$	175, 176	161, 166	Eq. (27) & Fig. 178	(2), (3), (5)
		CT	≥ 0	"		Not Shown		
	Each of Above	Each of Above	Each of Above	$K = \frac{B_1}{B_2} K_{one crack} = \frac{K}{2} K_{two cracks}$	-	-	-	(6)

(1) CT: Close Tolerance, TL: Taper-Lok

(2) For $a/c \leq 1$, multiply K by $\sqrt{a/c}$

(3) For specific point on crack periphery, β is evaluation at normalized distance from edge of hole to that point (i.e., x/r).

(4) β_{IF} valid for specified material, far-field loading, and level of interference.

(5) β_{CW} valid for specified material, far-field loading, and level of cold working.


(6) Bowie factors B_1 and B_2 are evaluated at $x/r = \pi ac/4tr$.

TABLE 39 - COMPARISON OF STRESS INTENSITY FACTOR SOLUTIONS FOR A
DOUBLE SEMI-ELLIPTICAL EMBEDDED CRACK EMANATING FROM
AN OPEN HOLE IN 7075-T651 ALUMINUM ALLOY PLATE

CRACK LENGTH, IN.		a/c	c/r	LOCKHEED DATA *		SHAH (17)		PRESENT SOLUTION	
a	c			K_A	K_C	K_A	K_C	K_A	K_C
0.049	0.063	0.778	0.31		11.2	8.9	10.4	8.9	10.5
0.056	0.073	0.795	0.36	10.4	12.2	9.2	10.9	9.3	10.9
0.063	0.085	0.741	0.40	10.4	12.8	9.5	11.3	9.5	11.5
0.071	0.098	0.724	0.45	10.6	12.2	9.7	11.9	9.6	12.0
0.078	0.110	0.709	0.50	10.4	12.2	10.0	12.2	9.9	12.4
0.085	0.122	0.697	0.54	10.4	12.2	10.2	12.6	10.0	12.9
0.093	0.134	0.694	0.60	10.6	13.7	10.4	13.0	10.2	13.5
0.102	0.149	0.685	0.65	10.9	14.4	10.7	13.5	10.5	14.0
0.112	0.166	0.675	0.72	11.2	14.4	10.9	14.0	10.6	14.6
0.124	0.183	0.678	0.79	12.2					

* Data was reduced using the same procedure reported in Ref. 22.

TABLE 40. SUMMARY OF STRESS INTENSITY FACTOR SOLUTIONS
FOR EMBEDDED-CRACKED FASTENER HOLES

CRACK GEOMETRY	HOLE CONDITION	FASTENER		STRESS INTENSITY FACTOR	M/q (Fig. No.)	β (Fig. No.)	M_c	REMARKS
		Type (1)	% Load Transfer					
	Reamed	None CT	- ≥ 0	$K = \sigma_o \sqrt{\pi c} \beta_{OP} \frac{M}{\Phi} M_c$ $K = \sigma_o \sqrt{\pi c} \beta_{CT} \frac{M}{\Phi} M_c$	194	138 143-145	Eq. (27) & Fig. 178	(2), (3)
	Reamed	TL TL	0 > 0	$K = \sigma_{ys} \sqrt{\pi c} \beta_{IF} \frac{M}{\Phi} M_c$ "	194	150, 152 Not Shown	Eq. (27) & Fig. 178	(2), (3), (4)
	Cold-Worked	None CT	- ≥ 0	$K = \sigma_{ys} \sqrt{\pi c} \beta_{CW} \frac{M}{\Phi} M_c$ "	194	161, 166 Not Shown	Eq. (27) & Fig. 178	(2), (3), (5)
	Each of Above	Each of Above	Each of Above	$K_{one\ crack} = \frac{B_1}{B_2} K_{two\ cracks}$	-	-	-	(6)

(1) CT: Close Tolerance, TL: Taper-Lok

(2) For $a/c \leq 1$, multiply K by $\sqrt{a/c}$

(3) For specific point on crack periphery, β is evaluated at normalized distance from edge of hole to that point (i.e., x/r).

(4) β_{IF} valid for specified material, far-field loading, and level of interference.

(5) β_{CW} valid for specified material, far-field loading, and level of cold working.

(6) Bowie factors B_1 and B_2 are evaluated at $x/r = \pi a c / 2tr$.

TABLE 41 - CORRELATIONS OF TESTED AND PREDICTED CRACK GROWTH LIVES FOR CONSTANT AMPLITUDE LOADED SPECIMENS

MATERIAL	CRACK GEOMETRY	HOLE CONDITION	FASTENER		σ_u , KSI	TEST HOLE NUMBER	CRACK LENGTH, IN.		TEST LIFE CYCLES	PREDICTED CYCLES	PREDICTED TESTED
			TYPE (1)	ϕ , %			INITIAL	FINAL			
2219-T851 Aluminum	Thru Crack	Reamed	None	-	24	A-CA-10-3	0.009	0.330	6,180	5,390	0.87
			CT	0	-	A-CA-10-2	-	-	5,000	5,610	1.12
			CT	0.96	-	A-CA-10-1	-	-	3,950	7,440	0.65
			None	-	18	A-CA-2X-1	0.006	0.300	18,500	15,830	0.86
			CT	0	-	A-CA-2X-2	-	-	22,500	16,870	0.75
			TL #1	0	18	A-CA-7X-1	0.150	0.500	17,500	10,640	0.61
			TL #1	0	18	A-CA-6X-1	0.150	0.500	30,660	10,640	0.35
			TL #2	0	18	A-CA-3-1	0.150	0.500	8,340	9,000	1.08
			TL #2	0	18	A-CA-7X-2	0.150	0.500	23,340	9,000	0.39
			TL #3	0	18	A-CA-17-1	0.150	0.50	8,800	8,880	1.01
			TL #3	0	18	A-CA-7X-3	0.150	0.50	23,950	8,880	0.37
			CW #1	None	-	A-CA-21-2	0.20	0.50	6,500	11,180	1.72
			None	-	18	A-CA-18-2	0.20	0.50	9,400	11,180	1.19
			CW #2	None	-	A-CA-22	0.168	0.50	33,500	53,970	1.61
			CW #3	None	-	A-CA-5X-1	0.168	0.50	41,450	60,170	1.45
			CW #1	CT	1.02	A-CA-21-1	0.168	0.50	7,330	5,990	0.85
			CT	1.05	18	A-CA-22-1	0.168	0.50	7,500	5,990	0.80
	Corner Crack	Reamed	None	-	18	A-CA-1-3	0.005	0.150	87,650	31,230	0.38
			None	-	18	A-CA-2-3	0.005	0.150	64,000	31,230	0.49
			CT	0	18	A-CA-1-2	0.005	0.150	72,620	45,250	0.62
			CT	0	18	A-CA-2-2	0.005	0.150	63,000	45,250	0.72
			CT	0.99	18	A-CA-1-1	0.005	0.150	51,600	15,640	0.30
			CT	1.03	18	A-CA-2-1	0.005	0.150	33,500	15,640	0.47
			TL #1	0	18	A-CA-3-2	0.056	0.150	28,770	46,740	1.63
			TL #2	0	18	A-CA-3-3	0.056	0.150	56,000	57,040	1.02
			TL #2	0	18	A-PO-3-1	0.056	0.150	95,300	57,040	0.60
			TL #3	0	18	A-PO-3-3	0.056	0.150	60,670	75,430	1.24
			TL #3	0	18	A-CA-6-1	0.056	0.150	130,000	75,430	0.58
		Reamed	TL #1	0	40	T-CA-1X-2	0.05	0.30	10,900	17,600	1.61
			TL #2	0	40	T-CA-2X-1	0.05	0.30	13,890	19,560	1.41
			TL #2	0	40	T-CA-2X-2	0.05	0.30	19,320	19,560	1.01
			TL #3	0	40	T-CA-19-1	0.05	0.30	21,650	18,190	0.84
			TL #3	0	40	T-CA-19-2	0.05	0.30	14,530	18,190	1.25
		CW #1	None	-	40	T-CA-17-2	0.15	0.50	8,550	8,820	1.03
			None	-	40	T-CA-18-2	0.15	0.50	7,810	8,820	1.13
			None	-	40	T-CA-21-3	0.20	0.50	9,150	10,050	1.23
			None	-	40	T-CA-22-3	0.20	0.50	11,590	10,050	0.87
			None	-	40	T-CA-22-1	0.20	0.50	8,910	14,910	1.67
			None	-	40	T-CA-22-2	0.20	0.50	8,060	14,910	1.67
		CW #1	CT	1.10	40	T-CA-17-1	0.20	0.50	5,600	3,590	0.64
			CT	1.05	40	T-CA-18-1	0.20	0.50	6,000	3,590	0.60
	Corner Crack	Reamed	None	-	40	T-CA-1-3	0.005	0.150	42,900	21,700	0.51
			None	-	40	T-CA-2-3	0.005	0.150	12,680	21,700	1.71
			CT	0	40	T-CA-1-2	0.005	0.150	29,300	25,080	0.86
			CT	1.00	40	T-CA-1-1	0.005	0.150	18,500	9,470	0.51
			CT	1.01	40	T-CA-2-1	0.005	0.150	13,100	9,470	0.72
			TL #1	0	40	T-CA-3-2	0.05	0.150	35,800	39,960	1.12
		Reamed	TL #1	0	40	T-CA-4-2	0.05	0.150	60,850	39,960	0.66
			TL #2	0	40	T-CA-4-3	0.054	0.150	42,700	40,540	0.95
			TL #3	0	40	T-CA-6-2	0.058	0.196	40,440	47,950	1.18

(1) CT - Close Tolerance, TL - Taper-Lok, CW - Cold-Worked
 Numbers following ϕ indicate level of cold work or interference (Tables 14 and 15)

TABLE 42. CORRELATION OF TESTS AND MEDIAN CRACK GROWTH RATES FOR SPECIMENS LOADED SPECIMENS

MATERIAL	CRACK GEOMETRY	SPECTRUM TYPE	FASTENER-HOLE CONDITION	SPECIMEN NUMBER	CRACK LENGTH, IN.		TESTS LIFE Cycles	MEDIAN TESTED		
					INITIAL	FINAL		AREA	WIDE-BEAM	WIDE-BEAM
2124-T3 Aluminum	Corner Crack	Bumper	Crack	A-85-1/3	0.026	0.466	510	0.30	2.01	1.19
				A-85-1/2	0.027	0.548	510	0.75	0.96	1.11
				A-85-1/1	0.010	0.513	385	1.46	3.70	2.15
		Finger	Crack	A-85-1/3	0.018	0.265	133	0.25	2.32	0.55
				A-85-1/2	0.018	0.272	133	0.25	2.26	0.54
				A-85-1/1	0.022	0.459	93	0.35	3.29	0.83
	Corner Crack	Bumper	Crack	A-85-1/3	0.006	0.550*	1130	0.57	1.46	0.81
				A-85-1/2	0.006	0.547*	921	0.57	2.84	1.53
				A-85-1/1	0.006	0.142*	1010	1.51	2.61	1.45
		Finger	Crack	A-85-1/3	0.005	0.141*	343	0.75	2.73	0.64
				A-85-1/2	0.006	0.041*	343	0.26	2.52	0.68
				A-85-1/1	0.005	0.214*	343	0.33	3.41	0.80
6061-T6 Aluminum	Corner Crack	Bumper	Crack	T-85-1/3	0.019	0.333	561	0.34	2.43	1.51
				T-85-1/2	0.014	0.423	610	0.71	2.32	1.29
				T-85-1/1	0.019	0.674	594	1.31	3.35	1.96
		Finger	Crack	T-85-1/3	0.024	0.510	314	0.20	1.45	0.39
				T-85-1/2	0.0145	0.466	314	0.19	1.41	0.37
				T-85-1/1	0.012	0.552	314	0.24	1.75	0.46
	Corner Crack	Bumper	Crack	T-85-1/3	0.012	0.150*	303	0.38	2.24	1.25
				T-85-1/2	0.012	0.137*	1233	0.77	2.31	1.29
				T-85-1/1	0.019	0.227*	530	1.50	3.35	2.11
		Finger	Crack	T-85-1/3	0.012	0.240**	312	0.23	2.34	0.71
				T-85-1/2	0.0067	0.240**	312	0.27	2.29	0.69
				T-85-1/1	0.019	0.203*	130	0.56	5.32	1.39

CT = Crack Transfer
 CT = Crack Transfer
 * Dimension on the plate surface
 ** Dimension on the hole wall

REFERENCES

1. Gran, R. J., Orazio, F. D., Paris, P. C., Irwin, G. R., and Hertzberg, R., "Investigation and Analysis Development of Early Life Aircraft Structural Failures," AFFDL-TR-70-149, Air Force Flight Dynamics Laboratory, March 1971.
2. Hall, L. R., Shah, R. C., and Engstrom, W. L., "Fracture and Fatigue Crack Growth Behavior of Surface Flaws and Flaws Originating at Fastener Holes," AFFDL-TR-74-47, Air Force Flight Dynamics Laboratory, May 1974.
3. Hsu, T. M., and Markham, J. W., "Interaction Effects of Multiple Cracks," AIAA Journal, Vol. 15, No. 3, p.421, American Institute of Aeronautics and Astronautics, March 1977.
4. Salmon, M., Sandhu, R., and Berke, L., "An Application of the Finite-Element Method to Elastic-Plastic Problems of Plane Stress," AFFDL-TR-68-39, Air Force Flight Dynamics Laboratory, May 1970.
5. Allen, M., and Ellis, J. A., "Stress and Strain Distribution in the Vicinity of Interference-Fit Fasteners," AFFDL-TR-72-153, Air Force Flight Dynamics Laboratory, January 1973.
6. Bowie, O. L., "Analysis of an Infinite Plate Containing Radial Cracks Originating from the Boundary of an Internal Circular Hole," Journal of Mathematics and Physics, Vol. 35, pp. 60-71, 1956.
7. Bueckner, H. F., "A Novel Principle for the Computation of Stress Intensity Factors," Zeitschrift für Angewandte Mathematik und Mechanik, Vol. 50, pp. 529-545, 1970.
8. Bueckner, H. F., "Weight Functions for the Notched Bar," Zeitschrift für Angewandte Mathematik und Mechanik, Vol. 51, pp. 97-109, 1971.
9. Bueckner, H. F., "Field Singularities and Related Integral Representations," Chapter 5, Methods of Analysis and Solutions of Crack Problems, edited by G. C. Sih, Noordhoff International Publishing, 1973.
10. Bueckner, H. F., "The Weight Functions of the Configuration of Collinear Cracks," International Journal of Fracture, Vol. 11, 11. 71-83, 1975.
11. Rice, J. R., "Some Remarks on Elastic Crack-Tip Stress Fields," International Journal of Solids and Structures, Vol. 8, pp. 751-758, 1972.

REFERENCES (Continued)

12. Paris, P. C., McMeeking, R. M., and Tada, H., "The Weight Function Method for Determining Stress Intensity Factors," ASTM STP601, pp. 471-489, 1976.
13. Emery, A. F., Walker, G. E., Jr., and Williams, J. A., "A Green's Function for the Stress Intensity Factors of Edge Cracks and Its Applications to Thermal Stresses," Journal of Basic Engineering, Vol. 91, pp. 618-624, 1969.
14. Paris, P. C., and Sih, G. C., "Stress Analysis of Cracks," Fracture Toughness Testing and Its Applications, ASTM STP381, pp. 30-81, 1965.
15. Crews, J. H., and White, N. H., "Fatigue Crack Growth From a Circular Hole with and without High Prior Loading," NASA TND-6899, September 1972.
16. Schmidt, R. A., "An Approximate Technique for Obtaining Stress Intensity Factors for Some Difficult Planar Problems," ASME, ASM 13th Annual Symposium on Fracture and Flaws, Albuquerque, N. M., 1973.
17. Shah, R. C., "Stress Intensity Factors for Through and Part-Through Cracks Originating at Fastener Holes," ASTM STP590, pp. 429-459, 1976.
18. Grandt, A. F., "Stress Intensity Factors for Some Through-Cracked Fastener Holes," International Journal of Fracture, Vol. 11, pp. 283-294, 1975.
19. Aberson, J. A., and Anderson, J. M., "Cracked Finite-Element Proposed for NASTRAN," NASTRAN User's Colloquium, NASA TMX-2893, pp. 531-550, 1973.
20. Brombolich, L. J., "Elastic-Plastic Analysis of Stresses Near Fastener Holes," Eleventh Aerospace Sciences Meeting of American Institute of Aeronautics and Astronautics, Washington, D. C., January 1973.
21. Adler, W. F., and Dupree, D. M., "Stress Analysis of Cold-Worked Fastener Holes," Technical Report AFML-TR-74-44, Air Force Materials Laboratory, July 1974.
22. Grandt, A. F., Jr., and Hinnerichs, T. D., "Stress Intensity Factor Measurements for Flawed Fastener Holes," Proceedings of the Army Symposium on Solid Mechanics, Watertown, Ma., September 1974.
23. Cathey, W. N., "Determination of Stress Intensity Factors for Cold-Worked Fastener Holes in 7075 Aluminum Using the Crack Growth Methods," AFML-TR-74-283, Air Force Materials Laboratory, May 1975.

REFERENCES (Continued)

24. Hall, L. R., and Finger, R. W., "Fracture and Fatigue Growth of Partially Embedded Flaws," Proceedings of Air Force Conference on Fatigue and Fracture of Aircraft Structures and Materials, AFFDL-TR-70-144, Air Force Flight Dynamics Laboratory, September 1970.
25. Gran, R. J., Crazio, F. D., Paris, P. C., Irwin, G. R., and Hertzberg, R., "Investigation and Analysis Development of Early Life Aircraft Structural Failures," AFFDL-TR-70-149, Air Force Flight Dynamics Laboratory, March 1971.
26. Hsu, T. M., and Liu, A. F., "Stress Intensity Factors for Truncated Elliptical Cracks," presented at the Seventh National Symposium on Fracture Mechanics, College Park, Maryland, August 27-29, 1973.
27. Kobayashi, A. S., and Enetanya, A. N., "Stress Intensity Factor of a Corner Crack," Mechanics of Crack Growth, ASTM STP590, 1976.
28. Kobayashi, A. S., Polvanich, N., Emery, A. F., and Love, W. J., "Corner Crack at the Bore of a Rotating Disk," ASME paper no. 75-WA/GT-18.
29. Smith, F. W., Kobayashi, A. S., and Emery, A. F., "Stress Intensity Factors for Penny-Shaped Cracks, Part 1 - Infinite Solid," Journal of Applied Mechanics, Vol. 34, 1967.
30. Smith, F. W., and Kullgren, T. E., "Theoretical and Experimental Analysis of Surface Cracks Emanating from Fastener Holes," AFFDL-TR-76-104, Air Force Flight Dynamics Laboratory, February 1977.
31. McGowan, J. J., and Smith, C. W., "Stress Intensity Factors for Deep Cracks Emanating from the Corner Formed by a Hole Intersecting a Plate Surface," Mechanics of Crack Growth, ASTM STP590, 1976.
32. Snow, J. R., "A Stress Intensity Factor Calibration for Corner Flaws at an Open Hole," AFML-TR-74-282, Air Force Materials Laboratory, May 1975.
33. Fujimoto, W. T., "Determination of Crack Growth and Fracture Toughness Parameters for Surface Flaws Emanating from Fastener Holes," Proceedings of AIAA/ASME/SAE 17th Structures, Structural Dynamics, and Materials Conference, King of Prussia, Pa., May 5-7, 1976.

REFERENCES (Continued)

34. Tracey, D. M., "3-D Elastic Singular Element for Evaluation of K Along an Arbitrary Crack Front," International Journal of Fracture, Vol. 9, 1973.
35. Cruse, T. A., and Meyers, G. J., "Three-Dimensional Fracture Mechanics Analysis," Journal of the Structural Division, Transactions of ASCE, February 1977.
36. Forman, R. G., Kearney, V. E., and Engle, R. M., "Numerical Analysis of Crack Propagation in Cyclic-Loaded Structures," Journal of Basic Engineering, pp. 459-464, September 1967.
37. Kobayashi, A. S., "A Simple Procedure for Estimating Stress Intensity Factor in Region of High Stress Gradient," Significant of Defects in Welded Structures, Proceedings of the Japan-U.S. Seminar, Tokyo, 1973.
38. Rice, J. R., "A Path Independent Integral and the Approximate Analysis of Strain Concentration by Notches and Cracks," Transactions of the ASME Journal of Applied Mechanics, pp. 379-386, June 1968.
39. Shah, R. C., "Quarter or Semi-Circular Cracks Originating at Interference-Fit Fasteners," AIAA/ASME/SAE 17th Structures, Structural Dynamics and Materials Conference, King of Prussia, Pa., May 5-7, 1976.
40. Hsu, T. M., and Rudd, J. L., "Green's Function for a Thru-Crack Emanating from Fastener Holes," Proceedings of the Fourth International Conference on Fracture, Vol. 3, pp. 139-148, June 1977.
41. Willenborg, J., Engle, R. M., and Wood, H. A., "A Crack Growth Retardation Model Using an Effective Stress Concept," AFFDL Technical Memorandum 71-1-FBR, Air Force Flight Dynamics Laboratory, January 1971.
42. Gallagher, J. P., and Hughes, T. F., "Influence of Yield Strength on Overload Affected Fatigue Crack Growth Behavior in 4340 Steel," AFFDL-TR-74-27, Air Force Flight Dynamics Laboratory, July 1974.
43. Hsu, T. M., "Development of Load-Interaction Model," Lockheed-Georgia Report SMN 390, February 1976.